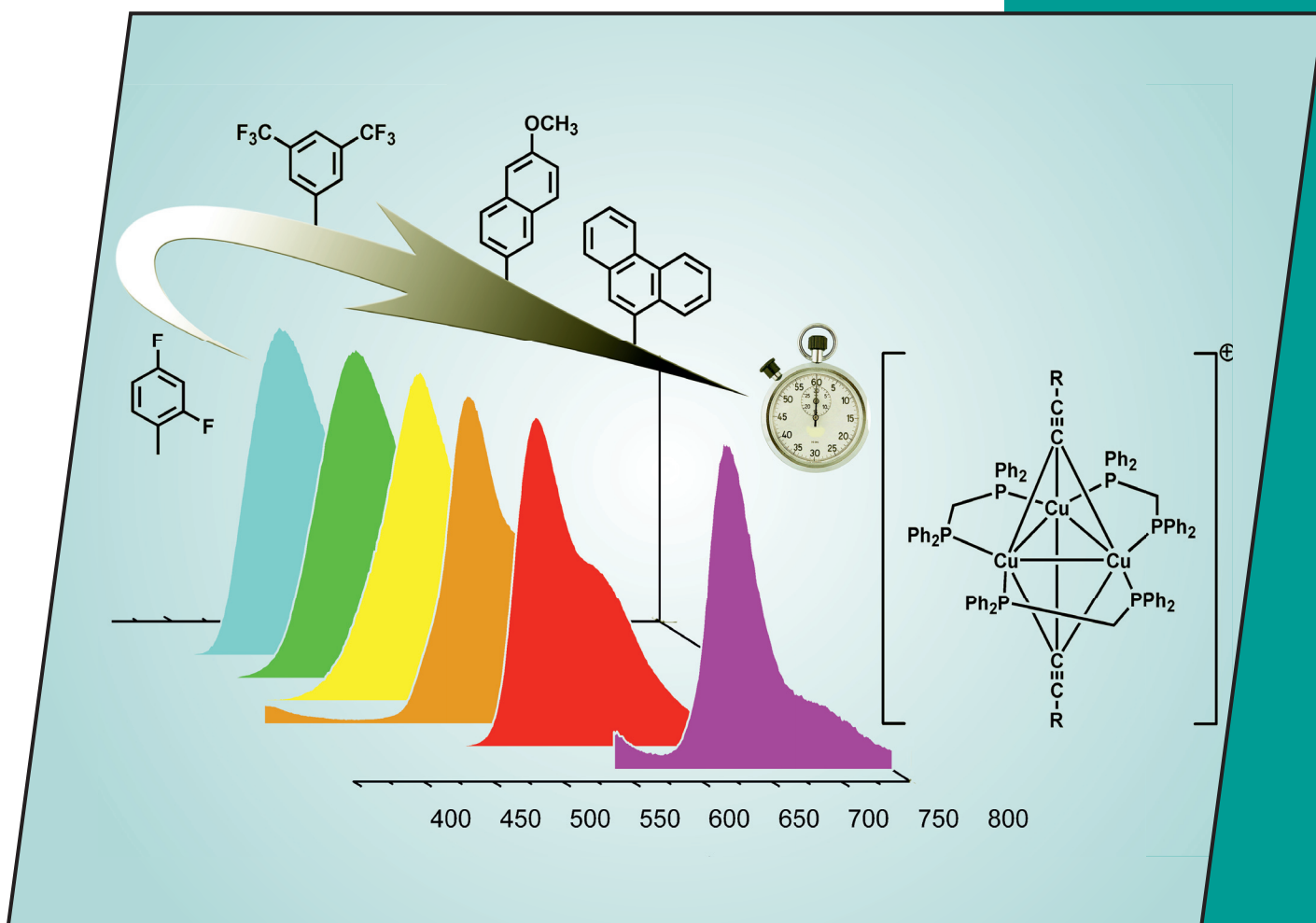


23/2010
2nd August Issue

EurJIC
European Journal of
Inorganic Chemistry



Cover Picture

Paolo Coppo et al.
Copper(I) Trinuclear Phosphorescent Complexes

Microreview

Natalia V. Belkova et al.
Study on Transition Metal Hydride Complexes

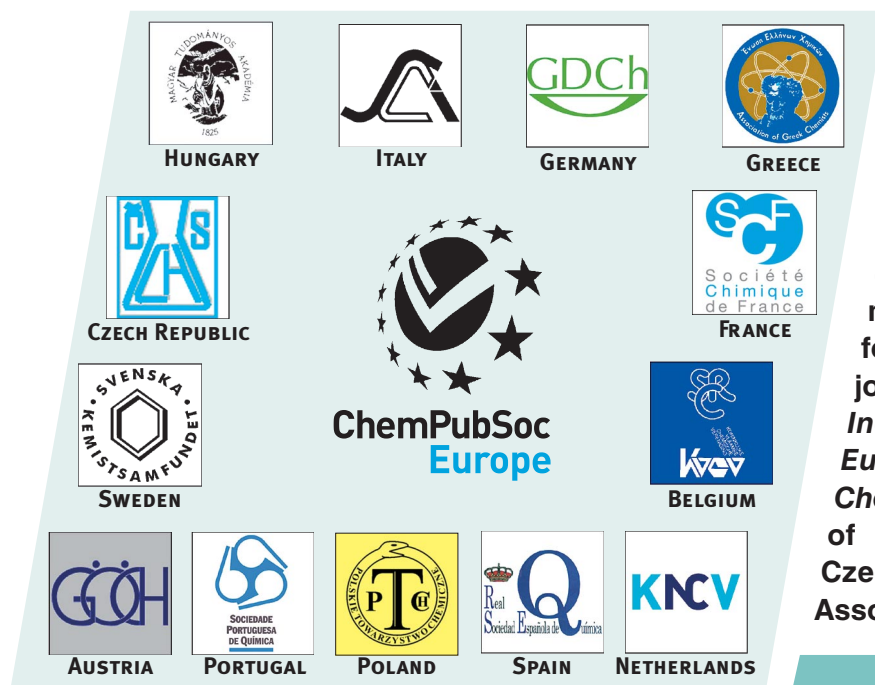
 **WILEY-VCH**

www.eurjic.org

A Journal of



ChemPubSoc
Europe

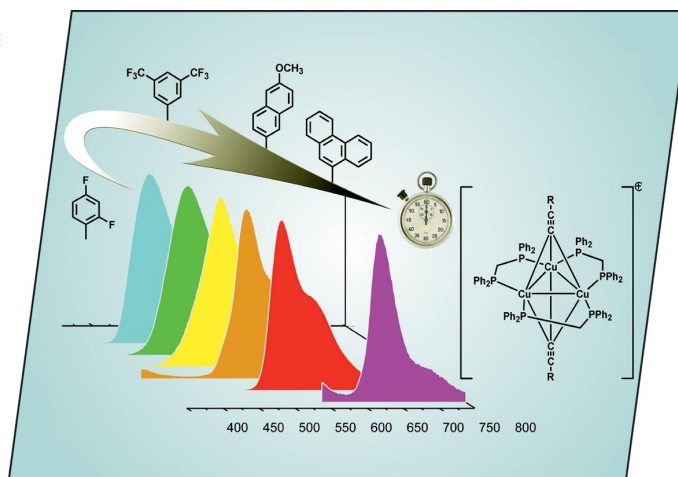


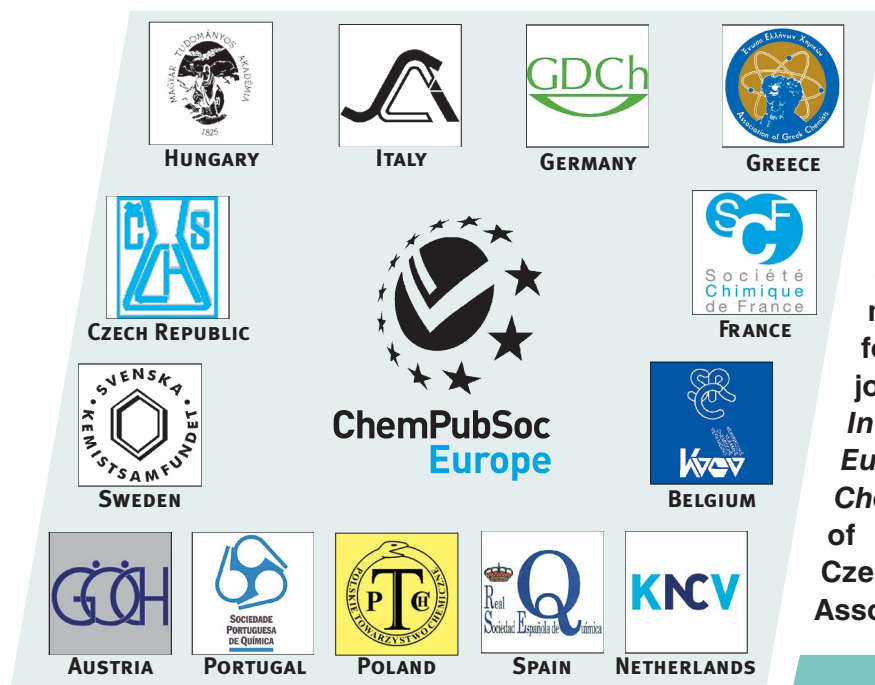
EurJIC is co-owned by 11 societies of ChemPubSoc Europe, a union of European chemical societies for the purpose of publishing high-quality science. All owners merged their national journals to form two leading chemistry journals, the *European Journal of Inorganic Chemistry* and the *European Journal of Organic Chemistry*. Three further members of ChemPubSoc Europe (Austria, Czech Republic and Sweden) are Associates of the two journals.

Other ChemPubSoc Europe journals are *Chemistry – A European Journal*, *ChemBioChem*, *ChemPhysChem*, *ChemMedChem*, *ChemSusChem* and *ChemCatChem*.

COVER PICTURE

The cover picture shows the emissions of the Cu^I coordination complexes presented in the Short Communication by P. Coppo et al. on p. 3567ff. The energy of the emission can be tuned within the visible region by careful selection of the alkynyl ligands. In addition, the lifetime of the excited state can be increased by up to two orders of magnitude, by coordination to highly conjugated alkynyl ligands. All complexes show good quantum yields of photoluminescence in de-gassed solutions.



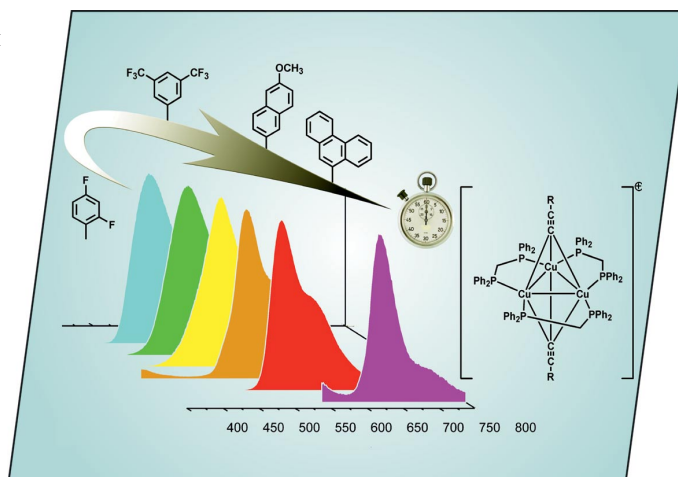


EurJIC is co-owned by 11 societies of ChemPubSoc Europe, a union of European chemical societies for the purpose of publishing high-quality science. All owners merged their national journals to form two leading chemistry journals, the *European Journal of Inorganic Chemistry* and the *European Journal of Organic Chemistry*. Three further members of ChemPubSoc Europe (Austria, Czech Republic and Sweden) are Associates of the two journals.

Other ChemPubSoc Europe journals are *Chemistry – A European Journal*, *ChemBioChem*, *ChemPhysChem*, *ChemMedChem*, *ChemSusChem* and *ChemCatChem*.

COVER PICTURE

The cover picture shows the emissions of the Cu^I coordination complexes presented in the Short Communication by P. Coppo et al. on p. 3567ff. The energy of the emission can be tuned within the visible region by careful selection of the alkynyl ligands. In addition, the lifetime of the excited state can be increased by up to two orders of magnitude, by coordination to highly conjugated alkynyl ligands. All complexes show good quantum yields of photoluminescence in de-gassed solutions.



CONTENTS

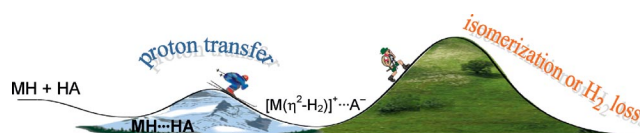
MICROREVIEW

Transition Metal Hydrides

N. V. Belkova,* L. M. Epstein,
E. S. Shubina 3555–3565

Dihydrogen Bonding, Proton Transfer and Beyond: What We Can Learn from Kinetics and Thermodynamics

Keywords: Transition metal hydrides / Dihydrogen bonding / Proton transfer / Kinetics / Thermodynamics



Low temperature assisted proton transfer and $\eta^2\text{-H}_2$ complexes transformations – knowing the kinetic and thermodynamic

relationships for different stages allows to govern better the reactivity of transition metal hydrides

SHORT COMMUNICATIONS

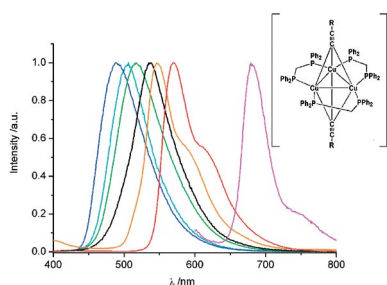
Phosphorescent Copper(I) Complexes

I. Andrés-Tomé, C. J. Winscom,
P. Coppo* 3567–3570



Copper(I) Trinuclear Phosphorescent Complexes with Tuneable Optical and Photophysical Properties

Keywords: Luminescence / Copper / OLEDs / Alkyne ligands / Phosphane ligands



Novel Cu^{I} trinuclear phosphorescent complexes carrying a range of conjugated alkyne ligands are reported. They show high quantum yields, tuneable colour and extended emission lifetime.

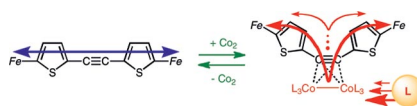
Tuneable Molecular Wires

Y. Tanaka, T. Koike,
M. Akita* 3571–3575



Reversible, Fine Performance Tuning of an Organometallic Molecular Wire by Addition, Ligand Replacement and Removal of Dicobalt Fragments

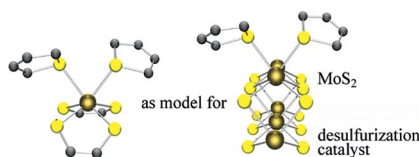
Keywords: Metal–metal interactions / Mixed-valent compounds / Molecular devices / Molecular wires / Organometallic compounds



The communication performance of a $\text{C}\equiv\text{C}$ -containing diiron molecular wire can be finely tuned in a reversible manner by coordination, removal and ligand exchange of dicobalt species. In contrast to the direct $\text{Fe}-\text{Fe}$ transition mechanism for the diiron wire, the communication mechanism of the dicobalt adducts involves indirect $\text{Fe}-\text{Co}-\text{Fe}$ electron transfer readily controlled by the ligand on the cobalt centres.

FULL PAPERS

A key industrial process is the removal of organic sulfur from petroleum, through hydrodesulfurization (HDS) on MoS_2 catalysts. HDS reactions of thiophenes are difficult to carry out and are not fully understood. We present new molecular models for the proposed active sites in HDS catalysis: bisdithiolene complexes containing 2,5-dihydrothiophene and tetrahydrothiophene.



Dithiolene Complexes as Catalyst Models

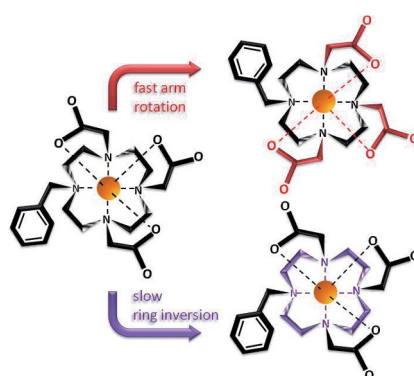
N. Nguyen, D. J. Harrison, A. J. Lough,
A. G. De Crisci, U. Fekl* 3577–3585

Molybdenum Dithiolene Complexes as Structural Models for the Active Sites of Molybdenum(IV) Sulfide Hydrodesulfurization Catalysts

Keywords: Molybdenum / Sulfur / Desulfurization / Heterogeneous catalysis

Lanthanide Complexes

A study on the solution structure and dynamics of $\text{Ln}^{\text{III}}(\text{do}3\text{a})$ complexes ($\text{H}_3\text{do}3\text{a}$ = 1,4,7,10-tetraazacyclododecane-1,4,7-triacetic acid) shows that the $\Delta(\lambda\lambda\lambda\lambda)$ conformation is favored over the $\Delta(\delta\delta\delta\delta)$ one. The energy barrier associated with the ring inversion is similar to that observed for $\text{Ln}^{\text{III}}(\text{dota})$ (H_4dota = 1,4,7,10-tetraazacyclododecane-1,4,7,10-tetraacetic acid) complexes, whereas the low energy barrier for the arm rotation is responsible for fast isomer interconversion.



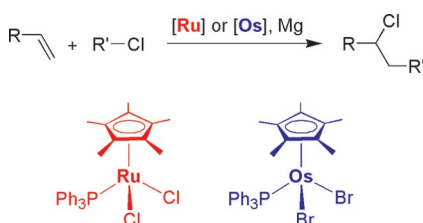
M. Regueiro-Figueroa, D. Esteban-Gómez,
A. de Blas, T. Rodríguez-Blas,*
C. Platas-Iglesias* 3586–3595

Structure and Dynamics of Lanthanide(III) Complexes with an *N*-Alkylated do3a Ligand ($\text{H}_3\text{do}3\text{a}$ = 1,4,7,10-Tetraazacyclododecane-1,4,7-triacetic Acid): A Combined Experimental and DFT Study

Keywords: Lanthanides / Macrocyclic ligands / Density functional calculations / X-ray diffraction

Radical Chemistry

The catalytic activity of the complexes $[\text{Cp}^*\text{OsBr}_2(\text{PPh}_3)]$ and $[\text{Cp}^*\text{RuCl}_2(\text{PPh}_3)]$ in conjunction with Mg has been evaluated for atom transfer radical addition (ATRA) reactions and for atom transfer radical cyclization (ATRC) reactions.

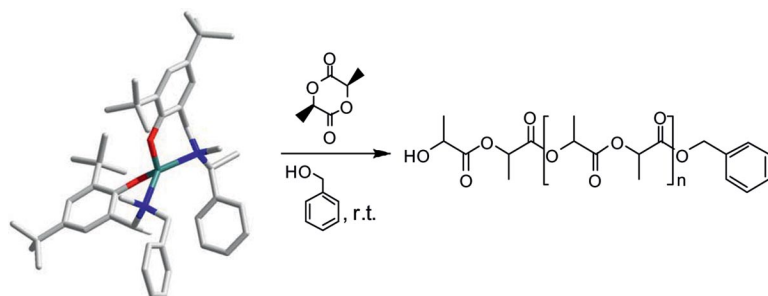


M. A. Fernández-Zúmel, G. Kiefer,
K. Thommes, R. Scopelliti,
K. Severin* 3596–3601

Ruthenium vs. Osmium Complexes as Catalysts for Atom Transfer Radical Addition Reactions

Keywords: ATRA / ATRC / Osmium / Radical reactions / Ruthenium

Lactide Polymerization



A series of homoleptic monomeric and dimeric magnesium aminophenolates have been synthesized in the direct reaction of MgBu_2 with aminophenols. When grafted with benzyl alcohol, the resulting com-

pounds revealed high activity in the ring-opening polymerization (ROP) of lactides to give linear polymers with a narrow polydispersity index (PDI).

J. Ejfler, K. Krauz-Dziedzic, S. Szafert,
L. B. Jerzykiewicz,
P. Sobota* 3602–3609

Synthesis, Characterization, and Catalytic Studies of (Aryloxo)magnesium Complexes

Keywords: Aminophenolates / Magnesium / Lactides / Polymerization / Structure elucidation

CONTENTS

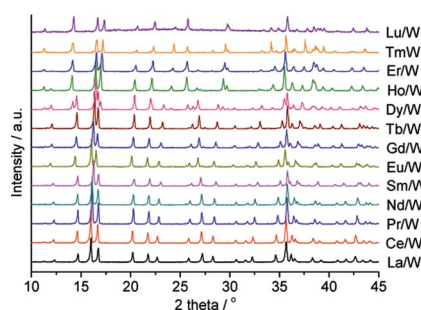
Octacyanometallates

A.-H. Yuan,* P. D. Southon, D. J. Price,
C. J. Kepert,* H. Zhou,
W.-Y. Liu 3610–3614



Syntheses, Crystal Structures, and the Phase Transformation of Octacyanometallate-Based $\text{Ln}^{\text{III}}-\text{W}^{\text{V}}$ Bimetallic Assemblies with Two-Dimensional Corrugated Layers

Keywords: Octacyanometallates / Lanthanides / Solid-state structures / Tungsten / Layered compounds / Phase / transformation



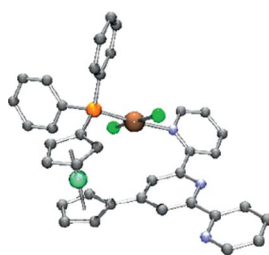
Two series of 4f–5d complexes, $\text{Ln}(\text{H}_2\text{O})_5[\text{W}(\text{CN})_8]$ ($\text{Ln} = \text{La}, \text{Pr}, \text{Nd}, \text{Eu}, \text{Gd}$) and $\text{Ln}(\text{H}_2\text{O})_4[\text{W}(\text{CN})_8]$ ($\text{Ln} = \text{Ho}, \text{Er}, \text{Tm}, \text{Lu}$), have been synthesized and characterized structurally. TGA and powder XRD results reveal the presence of the phase transformation in the $\text{Ln}-\text{W}$ system with increasing atomic number of the Ln^{III} atoms.

Heteromultimetallic Complexes

A. Hildebrandt, N. Wetzold, P. Ecorchard,
B. Walfort, T. Rüffer,
H. Lang* 3615–3627

Synthesis and Reaction Chemistry of Heterodi- and Heterotrimetallic Transition-Metal Complexes Based on 1-(Diphenylphosphanyl)-1'-terpyridylferrocene

Keywords: Heterometallic complexes / Metallocenes / Solid-state structures / Terpyridine / N,P ligands



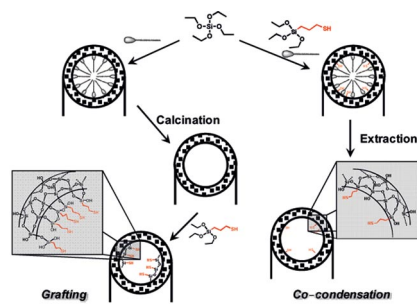
The synthesis of $[\text{Fe}(\eta^5\text{-C}_5\text{H}_4\text{PPh}_2)(\eta^5\text{-C}_5\text{H}_4\text{terpy})]$ (terpy = 2,2':6',2''-terpyridin-4'-yl) and its reaction towards diverse transition-metal compounds is described. The structure of seven molecules is reported. The use of $[\text{Fe}(\eta^5\text{-C}_5\text{H}_4\text{PPh}_2\text{Cl}_2\text{Pd})(\eta^5\text{-C}_5\text{H}_4\text{terpy})]$ and $[\text{Fe}(\eta^5\text{-C}_5\text{H}_4\text{PPh}_2\text{Cl}_2\text{Pd})(\eta^5\text{-C}_5\text{H}_4\text{-CH=CHC(O)(py)})]$ in the Heck–Mizoroki reaction is discussed.

Functionalised Mesoporous Silica

V. La Parola, A. Longo, A. M. Venezia,*
A. Spinella, E. Caponetti 3628–3635

Interaction of Gold with Co-Condensed and Grafted HMS-SH Silica: A ^{29}Si $\{^1\text{H}\}$ CP-MAS NMR Spectroscopy, XRD, XPS and Au L_{III} EXAFS Study

Keywords: Mesoporous materials / Silica / Inorganic-organic hybrid composites / Gold / Sulfur



The supporting capability of $-\text{SH}$ modified HMS is evaluated by depositing gold through incipient wet impregnation. The effect of the two support functionalisation procedures, co-condensation and grafting, is investigated by XRD, Au L_{III} EXAFS and XPS. A stronger interaction between gold and the thiol groups is achieved in the grafted-SH silica with consequent better gold dispersion.

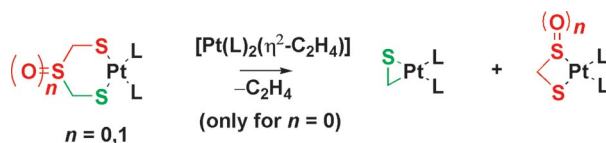
Fragmentation of Metallacycles

H. Petzold,* T. Weisheit, S. Bräutigam,
H. Görls, G. Mloston,*
W. Weigand* 3636–3641



Reactions of 1,2,4-Trithiolane and Its 4-S-Oxide with Diphosphane Pt^0 Complexes

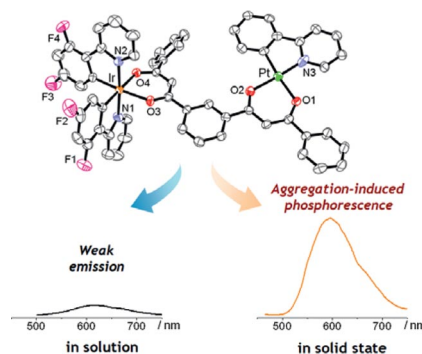
Keywords: 1,2,4-Trithiolanes / S ligands / Oxidative addition / Metallacycles / Reactive intermediates



The 1-platina-2,4,6-trithiane cycle was obtained by oxidative addition of a Pt^0 fragment into the sulfur–sulfur bond of 1,2,4-trithiolane and 1,2,4-trithiolane 4-S-oxide. Depending on the phosphane used for the

preparation of the ligand, either the six-membered platinacycle is isolated or thioformaldehyde is eliminated with subsequent ring contraction.

Dinuclear complexes $[\{\text{Ir}(\text{ppyFF})_2\}_2(\mu_2\text{-L})]$ (**4**) and $[\{\text{Ir}(\text{ppyFF})_2\}_2(\mu_2\text{-L})\{\text{Pt}(\text{ppy})\}]$ (**5**) [ppyFF = 2-(2,4-difluorophenyl)pyridine, ppy = 2-phenylpyridine, L = 1,3-bis(3-phenyl-3-oxopropanoyl)benzene] linked by bridging ligand L have been prepared. Although **4** and **5** exhibit weak emission in solution, an intense orange-red emission (i.e., aggregation-induced phosphorescence) is produced in the solid state.



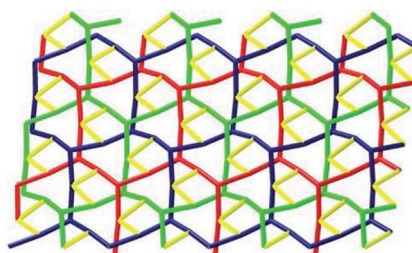
C. H. Shin, J. O. Huh, S. J. Baek,
S. K. Kim, M. H. Lee,*
Y. Do* 3642–3651

Dinuclear Iridium(III) Complexes Linked by a Bis(β-diketonato) Bridging Ligand: Energy Convergence versus Aggregation-Induced Emission

Keywords: Aggregation / Dimetallic complexes / Phosphorescence / Iridium / Platinum

Self-Catenated Networks

An unprecedented self-catenated 3D layer pillar framework formed by connecting 2D borromean layers through ferrocenyl bridges is presented. The complex can undergo a dehydrated and rehydrated process in a single-crystal-to-single-crystal manner without affecting the overall framework. The amorphous sample can further be regenerated by water to the crystalline material again.



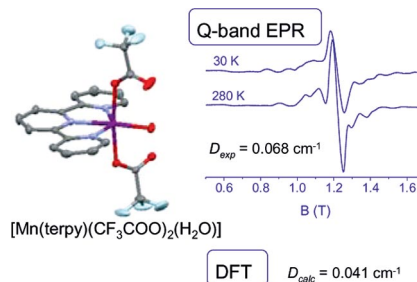
X. Shi, W. Wang, H. Hou,*
Y. Fan 3652–3657

A Hydroscopic Self-Catenated Net Formed by Borromean Layers Interlocked by Ferrocenyl Bridging Ligands

Keywords: Structure elucidation / Coordination polymers / Layered compounds / Cadmium / Bridging ligands / Adsorption / Reversible hydration

Electronic Structure

The electronic parameters of a series of six- and seven-coordinate mononuclear Mn^{II} complexes with only N/O-based ligands have been determined by X- and Q-band EPR spectroscopy and satisfactorily predicted by quantum chemistry using a DFT approach.

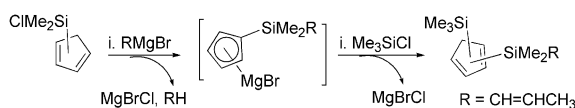


J. Rich, C. E. Castillo, I. R. M. Rodríguez,
C. Duboc,* M.-N. Collomb* ... 3658–3665

Investigation of the Zero-Field Splitting in Six- and Seven-Coordinate Mononuclear Mn^{II} Complexes with N/O-Based Ligands by Combining EPR Spectroscopy and Quantum Chemistry

Keywords: Manganese / EPR spectroscopy / Zero-field splitting / Electronic parameters / Density functional calculations

Disilylcyclopentadienyl Compounds



A protocol for alkylation and deprotonation of (halosilyl)cyclopentadiene derivatives through reaction with Grignard reagents has been used to synthesize mixed disilyl-substituted cyclopentadiene systems

tethered to alkene units. Corresponding Li, Zr, Mo and W (dimethylorganosilyl)(trimethylsilyl)cyclopentadienyl compounds are also reported and their behaviour is examined.

C. E. Petrisor, G. Chahboun,
M. A. E. Amrani, E. Royo,*
T. Cuenca* 3666–3674

Mixed Disilyl-Substituted Cyclopentadiene Derivatives and Corresponding Zirconium, Molybdenum and Tungsten Compounds

Keywords: Molybdenum / Tungsten / Zirconium / Cyclopentadienyl ligands

* Author to whom correspondence should be addressed.

Supporting information on the WWW (see article for access details).



On these pages, we feature a selection of the excellent work that has recently been published in our sister journals. If you are reading these pages on a

computer, click on any of the items to read the full article. Otherwise please see the DOIs for easy online access through Wiley InterScience.

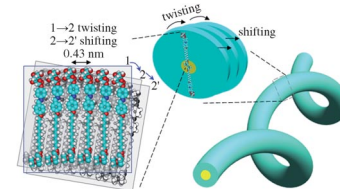


Self-Assembly

T.-F. Lin, R.-M. Ho,* C.-H. Sung, M.-S. Ho, C.-S. Hsu*

Twist Ferrocene Wires from Self-assembly of Chiral Rod–Coil Organometallics

Let's twist again! A chiral rod–coil organometallic material, FC11, has been synthesized and shows liquid-crystalline behavior. By taking advantage of the self-assembly of the chiral Schiff based rod–coil molecule that is end-capped with ferrocene, the self-assembled superstructure can serve as a template to form iron-rich spiral superstructures (see graphic).



Chem. Eur. J.
DOI: 10.1002/chem.201000772

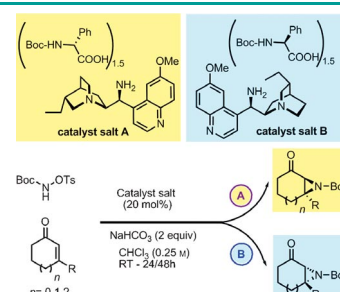


Organocatalysis

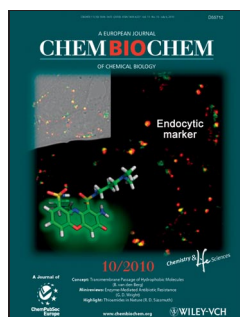
F. De Vincentiis, G. Bencivenni, F. Pesciaioli, A. Mazzanti, G. Bartoli, P. Galzerano, P. Melchiorre*

Asymmetric Catalytic Aziridination of Cyclic Enones

Access to aziridine antipodes: The first catalytic method for the asymmetric aziridination of cyclic enones is described (see scheme). The presented organocatalytic strategy is effective for a wide variety of substrates, thereby providing fast access to both of the antipodes of the aziridines with very high enantiomeric purity.



Chem. Asian J.
DOI: 10.1002/asia.201000040

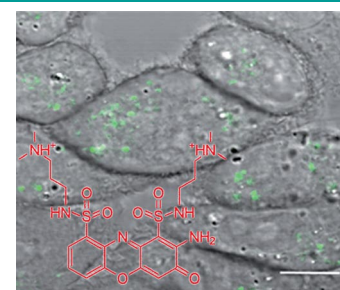


Biocatalysis

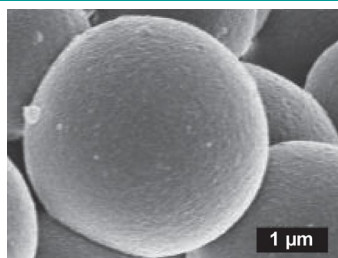
F. Bruyneel, L. D'Auria, O. Payen, P. J. Courtoy, J. Marchand-Brynaert*

Live-Cell Imaging with Water-Soluble Aminophenoxazinone Dyes Synthesised through Laccase Biocatalysis

Light 'em up: Water-soluble aminophenoxazinone dyes were used as valuable compounds in live-cell imaging. These heterocycles were produced by using an enzymatic synthetic strategy. Among the compounds tested, one in particular gave excellent results as an endocytic marker; it performed in a similar manner to Lucifer Yellow.



ChemBioChem
DOI: 10.1002/cbic.201000145



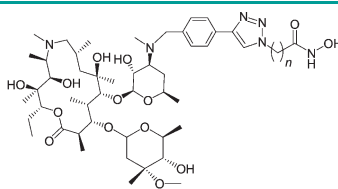
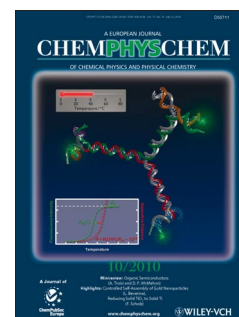
ChemPhysChem
DOI: 10.1002/cphc.201000188

Microfluidics

V. Chokkalingam, B. Weidenhof, M. Krämer, S. Herminghaus, R. Seemann, W. F. Maier*

Template-free Preparation of Mesoporous Silica Spheres through Optimized Microfluidics

Droplet-based microfluidics is used to perform sol–gel reactions. The chemicals are dispensed, mixed, and pre-processed inside a microfluidic device allowing for long operation times without any clogging. Using this approach and optimizing all reaction and processing parameters, mesoporous silica particles with a very high surface area of $820 \text{ m}^2 \text{ g}^{-1}$ and a narrow pore radius distribution of around 2.4 nm are obtained.



	IC ₅₀ values	
	7 (n=6)	16 (n=9)
HDAC1	13.9 nM	226.7 nM
pf-HDAC-1	29 nM	182 nM
<i>P. falciparum</i>	0.098 mg mL ⁻¹	0.883 mg mL ⁻¹
<i>L. donovani</i>	NA	3.54 mg mL ⁻¹

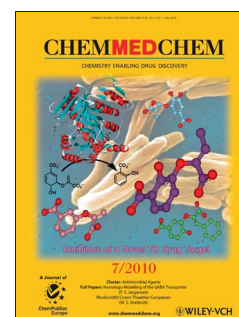
ChemMedChem
DOI: 10.1002/cmdc.201000087

Antiparasitic Agents

W. Guerrant, S. C. Mwakwari, P. C. Chen, S. I. Khan, B. L. Tekwani,* A. K. Oyelere*

A Structure–Activity Relationship Study of the Antimalarial and Antileishmanial Activities of Nonpeptide Macrocyclic Histone Deacetylase Inhibitors

Histone deacetylase inhibitors (HDACi) cause a diverse range of responses in biological systems. The depth of the antiparasitic capabilities of macrocyclic HDACi was determined against malarial and leishmanial pathogens. Antiparasitic activities of macrocyclic HDACi derived from macrolide skeletons are dependent on the length (*n*) of the spacer group that separates their zinc-binding and surface-recognition moieties. Antimalarial activities peak when *n* = 6, whereas antileishmanial activities are optimum when *n* = 8–9. This observation could facilitate the identification of other HDACi that are more selective for either parasite.



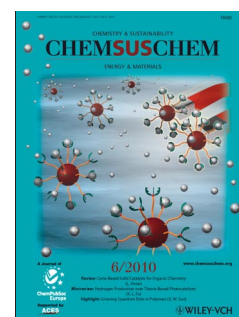
ChemSusChem
DOI: 10.1002/cssc.200900254

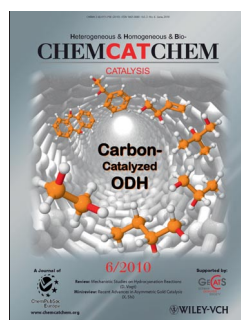
Aqueous-Phase Reforming

A. V. Kirilin, A. V. Tokarev, E. V. Murzina, L. M. Kustov, J.-P. Mikkola,* D. Yu. Murzin*

Reaction Products and Transformations of Intermediates in the Aqueous-Phase Reforming of Sorbitol

Aqueous-phase reforming of sorbitol over a Pt/Al₂O₃ catalyst is investigated. Parameters such as the sorbitol feed rate and temperature are studied. An analytical approach based on analysis of the gas and liquid phases as well as the total carbon content is developed to identify intermediates. The formation of the majority of identified compounds is explained, and a plausible reaction network for the conversion of sorbitol and transformation of intermediates is proposed.



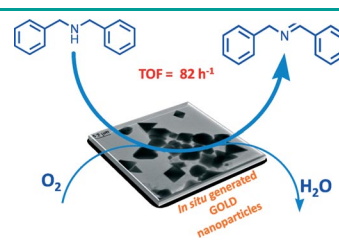


Gold Catalysis

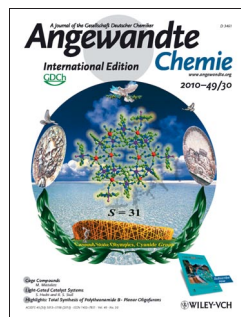
L. Aschwanden, T. Mallat, M. Maciejewski, F. Krumeich, A. Baiker*

Development of a New Generation of Gold Catalysts for Amine Oxidation

New gold dream: Outstandingly active Au/CeO₂ catalysts have been developed for the aerobic oxidation of amines to imines. The gold nanoparticles are generated in an organic medium in situ prior to the oxidation reaction. Various halogen-containing gold salts can be applied in the presence of nanoceria and the amine substrate acts as the reducing agent. A crucial point is the synergism between the vacuum-treated (200 °C) ceria and gold.



ChemCatChem
DOI: 10.1002/cctc.201000092

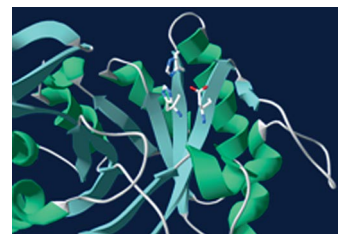


Artificial Metalloenzymes

J. Podtetenieff, A. Taglieber, E. Bill, E. J. Reijerse, M. T. Reetz*

An Artificial Metalloenzyme: Creation of a Designed Copper Binding Site in a Thermostable Protein

Guided by nature: A designed binding site comprising the His/His/Asp motif for Cu^{II} complexation has been constructed in a robust protein by site-specific mutagenesis (see picture). The artificial metalloenzyme catalyzes an enantioselective Diels–Alder reaction.



Angew. Chem. Int. Ed.
DOI: 10.1002/anie.201002106



Reaction Monitoring

E. Heller,* J. Klöckner, W. Lautenschläger, U. Holzgrabe*

Online Monitoring of Microwave-Enhanced Reactions by UV/Vis Spectroscopy

Fast microwave-enhanced reactions were monitored online by UV/Vis spectroscopy with a sensor in solution. This method is superior to slower methods (e.g. NMR, HPLC, TLC), because it is much faster and can also be performed in concentrated solutions.



Eur. J. Org. Chem.
DOI: 10.1002/ejoc.201000441

New Journal

Heterogeneous, Homogeneous and BioCatalysis

www.chemcatchem.org

FREE ONLINE ACCESS

In 2010 for all users from institutions that have registered

Ask your librarian to register for complimentary online access TODAY

www.interscience.wiley.com/newjournals

Founding Societies:

GESELLSCHAFT DEUTSCHER CHEMIKER

A journal of

Dihydrogen Bonding, Proton Transfer and Beyond: What We Can Learn from Kinetics and Thermodynamics

Natalia V. Belkova,^{*,[a]} Lina M. Epstein,^[a] and Elena S. Shubina^[a]

Keywords: Transition metal hydrides / Dihydrogen bonding / Proton transfer / Kinetics / Thermodynamics

Hydrogen bonding to transition metal hydride complexes and its role in the proton transfer process has been a subject of the authors' research interest in recent years. The present microreview analyzes the relationships of kinetic and thermodynamic parameters of dihydrogen bonding, $MH\cdots HA$, proton transfer, yielding $[M(\eta^2-H_2)]$ species, and

subsequent steps such as $[M(\eta^2-H_2)]$ to $[M(H)_2]$ isomerization or H_2 evolution on the basis of all data acquired so far. It aims at showing the factors that determine the stability of the species involved, the physico-chemical (thermodynamic and kinetic) origin of the effects observed, and, ideally, allow one to better govern the hydrides reactivity.

Introduction

Dihydrogen and dihydride complexes – $[M(\eta^2-H_2)]$ and $[M(H)_2]$ – of transition metals keep attracting the researchers' attention as is evidenced by the continuous appearance of numerous research papers and review articles. The most re-

cent reviews in the field cover different aspects of this chemistry like structure-NMR spectroscopic properties correlation,^[1] aqueous chemistry,^[2] or relevance to H_2 bioconversion in hydrogenases and hydrogen storage.^[3,4] Protonation of metal hydride complexes is generally recognised as the most common method of $[M(\eta^2-H_2)]$ preparation.^[3] Moreover, proton transfer involving transition metal hydrides and/or heterolytic splitting of dihydrogen are important steps in many catalytic processes,^[5] including ionic hydrogenation and reduction of H^+ to H_2 . Detailed studies of the mechanism of proton transfer to transition metal hydrides

[a] A. N. Nesmeyanov Institute of Organoelement Compounds, Russian Academy of Sciences, Vavilov Street 28, 119991 Moscow, Russia
Fax: +7-495-1355085
E-mail: nataliabelk@ineos.ac.ru



Natalia Belkova graduated from Chemistry Department of Moscow State University (MSU) in 1993 and received the PhD degree in 1997 with E. Shubina and L. Epstein. Her PhD work was awarded by Academia Europaea award for young scientists from Russia in 1997. After post-doctoral fellowship in St. Jude Childrens Research Hospital (Memphis, TN) she returned to A. N. Nesmeyanov Institute of Organoelement Compounds (INEOS) where she is senior researcher now.

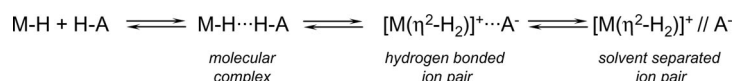


Lina Epstein received her Ph.D. degree at MSU (1967) and D.Sc. degree at INEOS (1985). She organized the Moscow Colloquium on Hydrogen Bonding (1975). In 1985–2000 she was head of the Spectroscopy Group in the lab of Prof. A. N. Nesmeyanov at INEOS. This group evolved into the Laboratory of Metal Hydrides at INEOS, where Prof. Epstein is now leading researcher.



Elena Shubina graduated from Chemistry Department of MSU (1974). She received her Ph.D. degree with L. Epstein in 1982 and completed the D.Sc. degree at INEOS in 1997. She was Visiting Professor at Université de Bourgogne, Dijon in 2001–2004. Prof. Shubina is head of the Metal Hydrides Laboratory at INEOS since 2001, member of organization committees for International Conferences on organometallic and coordination chemistry held in Russia and of the International Advisory Board for EuCOMC.

Their research interests lie in the field of physical organometallic, inorganic and coordination chemistry including structural properties relationships for metal complexes, intermolecular interactions, especially hydrogen bonds and proton transfer, molecular spectroscopy, theoretical studies.



Scheme 1. Mechanism of proton transfer to transition metal hydrides.

have firmly shown that, in spite of its apparent simplicity, the process involves several steps and proceeds via various hydrogen bonded intermediates of molecular or ionic type (Scheme 1).^[6–8] Properties of these hydrogen bonded complexes have been thoroughly discussed in several reviews as well,^[9–12] including those coming from our laboratory.^[7,8,13,14] The data begin to appear, confirming the importance of this phenomenon in catalytic reduction^[15–17] and hydrogen activation.^[18] In this contribution we focus on the relationships of kinetic and thermodynamic parameters of dihydrogen bonding, $\text{MH}\cdots\text{HA}$, proton transfer and subsequent steps such as $[\text{M}(\eta^2\text{-H}_2)]$ to $[\text{M}(\text{H})_2]$ isomerization or H_2 evolution with the emphasis on the experimental data and on factors that determine the stability of the species involved and allow one to better govern the overall reaction. Theoretical results will also be considered in conjunction with experimental work, providing more intimate mechanistic understanding.

Background

Since the results of the investigations mentioned above serve as a basis to understand the problems discussed in this paper, we begin this review by summarizing the salient points of those studies.

(i) The formation of a hydrogen bond between transition metal hydride and proton donor, $\text{MH}\cdots\text{HA}$, widely called a dihydrogen bond (DHB), is possible due to the partial negative charge born by a hydride ligand. These bonds are of medium to weak strength and their structural, electronic and spectroscopic features are similar to those of classical hydrogen bonds of the same energies.

(ii) Dihydrogen bond formation is exothermic (the associated enthalpy change, $\Delta H^\circ_{\text{DHB}}$, is negative varying from -2 to -8 kcal mol^{-1}).^[13] The entropy change, $\Delta S^\circ_{\text{DHB}}$, is negative as well varying from -5 to -25 e.u. Thus, the dihydrogen bond formation equilibrium is favoured at lower temperatures.

(iii) Analysis of the theoretical data shows a linear correlation between enthalpy values and $\text{H}\cdots\text{H}$ distances in dihydrogen bonded complexes of transition metal and main group element hydrides.^[7] Experimental estimation of the dihydrogen bond length is based on T_{1min} data, which decreases upon complexation.^[5,14,19,20] Sometimes, however, the relaxation is artificially increased by the presence of paramagnetic impurities or by undetected $[\text{M}(\eta^2\text{-H}_2)]^+$ complex, yielding overestimated $\text{H}\cdots\text{H}$ distances. Thus, the data acquired up to date confirm this qualitative trend but do not allow a solid correlation.

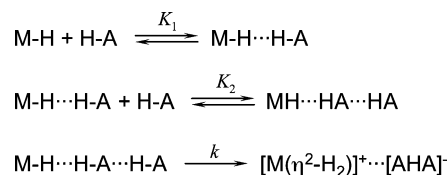
(iv) Hydrogen bond enthalpies for different systems (bases) should be compared with caution since they are a function of proton donor and solvent. Therefore, we use^[13,21] also a

basicity factor, E_j , which can be calculated using Equation (1)^[22] where E_j is the basicity factor of the proton acceptor, P_i is the acidity factor of the proton donor (both invariable), ΔH_{ij} is the formation enthalpy of the complex of interest, and ΔH_{11} is the hydrogen bonding enthalpy for the standard pair $\text{PhOH}/\text{Et}_2\text{O}$ ($P_1 = E_1 = 1.00$) in a given solvent.^[23]

$$E_j = \Delta H_{ij}/(\Delta H_{11}P_i) \quad (1)$$

(v) Dihydrogen bond formation is the first, incipient step of proton transfer reaction yielding cationic non-classical hydride complex, $[\text{M}(\eta^2\text{-H}_2)]^+$. In solvents of low to medium polarity, which are most commonly used (toluene, dichloromethane, THF), the non-classical species exists as a contact ion pair stabilized by the hydrogen bond between cation and anion. The anion is present in the homoconjugated form, $[\text{AHA}]^-$, as has been established by the experimental determination of the ion pair composition when $\text{HA} = 4\text{-nitrophenol}$.^[24–26] This results can be safely extended to other proton donors since most have a proven ability to form homoconjugated anions, even in polar media.^[27] Note, however, that a 1:1 ion pair composition has been determined for $[\text{Cp}^*\text{MH}_4(\text{dppe})]^+$ complexes ($\text{M} = \text{Mo}$,^[25] W ^[28]), which have a classical tetrahydrido structure. Interestingly, attempts to optimize corresponding hydrogen bonded ion pair structures with $[\text{A}]^-$ being alkoxide have been successful for classical $[\text{M}(\text{H})_2]^+$ cations but not for non-classical ones; $[\text{M}(\eta^2\text{-H}_2)]^+\cdots[\text{A}]^-$ ion pairs always return back to the neutral dihydrogen bonded structure whereas $[\text{M}(\eta^2\text{-H}_2)]^+\cdots[\text{AHA}]^-$ ion pairs give stable minima.^[25,26,29–31]

(vi) Experimental kinetic data support the participation of a second proton donor molecule in the proton transfer step.^[28,32] Therefore, the general reaction Scheme could be drawn as in Scheme 2.



Scheme 2. Kinetic model for proton transfer to transition metal hydride involving two proton donor molecules.

The resulting expression for the observed rate constant is represented in Equation (2).

$$k_{\text{obs}} = \frac{K_1 K_2 k [\text{HA}]^2}{1 + K_1 [\text{HA}] + K_1 K_2 [\text{HA}]^2} \quad (2)$$

The last term in the denominator (proportional to the 1:2 adduct) can reasonably be neglected to yield Equation (3). According to this model, the $[\text{HA}]$ dependence is a function

of the hydrogen-bonding equilibrium: under conditions in which the dominant species is free hydride, the expression simplifies to yield a second-order dependence on [HA], whereas a first-order behaviour is expected if the dominant species is the 1:1 adduct, [MH]...HA.

$$k_{obs} \sim \frac{K_1 K_2 k [HA]^2}{1 + K_1 [HA]} \quad (3)$$

These equations show that the two reaction steps are intimately connected: hydrogen bond formation, though extremely fast (diffusion controlled),^[33] should influence the kinetics of the second step – proton transfer itself. We consider this interrelationship in the next section.

Kinetics and Thermodynamics of Proton Transfer via Dihydrogen Bonded Complexes

The presence of several potential proton accepting ligands (like, e.g., carbonyl, nitrosyl or functional groups with basic nitrogen atoms) in the hydride complex opens the possibility of proton donor binding at these sites. They can be idle, like the nitrogen atom of the N(CH₂CH₂-PPh₂)₃ ligand in [κ³-N(CH₂CH₂PPh₂)₃]IrH₃,^[31] or compete with the basic hydride ligand.^[36] Thus, the nature of the hydrogen-bonded species formed upon interaction with proton donors indicates the more basic (bearing greater electron density), better accessible centre in the molecule.^[8] For example, the Mo–CO...HA hydrogen bond dominates in the interaction of [Cp*MoH(CO)(PMe₃)₂] with fluorinated alcohols, but only the MoH...HA species is the real intermediate of the proton transfer yielding the [Mo(η²-H₂)]⁺ product.^[37] Proton transfer to a carbonyl ligand is energetically much less favourable, if possible at all.^[37] The same situation is found for other carbonyl or nitrosyl hydrido complexes, like [CpRuH(CO)(PCy₃)]^[29] or [ReH₂(CO)(NO)(PR₃)₂].^[38,39] On the other hand, kinetically controlled protonation of basic nitrogen in PTA (1,3,5-triaza-7-phosphaadamantane) or pyridine can be regarded as an alternative lower energy pathway, where this functionality serves as a proton relay, ultimately delivering the proton to the hydride site^[40,41] or facilitating H/D exchange.^[42] Dihydrogen bonded species have been found involved in this process.^[40,41]

The observed linear correlation between the hydrogen bonding parameters (formation enthalpies or basicity factors) and those of the proton transfer step (enthalpies or pK_a) is an important feature of organic systems. For transition metal hydrides yielding cationic (η²-H₂) complexes, a similar correlation may also be found (Figure 1). The deviation of the [PP₃OsH₂]/CF₃CH₂OH system (point 7, Figure 1), for which quite a small value of ΔH°_{PT} was determined, could be related to the aperiodic trend in the pK_a values of (η²-H₂) ligands in this family of hydrides and longer (weaker) H–H bond in the osmium complex as compared to the ruthenium derivatives.^[43] Another important correlation may be found between the basicity factor E_j in

hydrogen bond^[7,21,22] and the overall protonation enthalpy [MH] + HA ↔ [M(η²-H₂)]⁺ (Figure 2), which quantitatively shows that the proton transfer is thermodynamically more favourable for more basic hydrides.

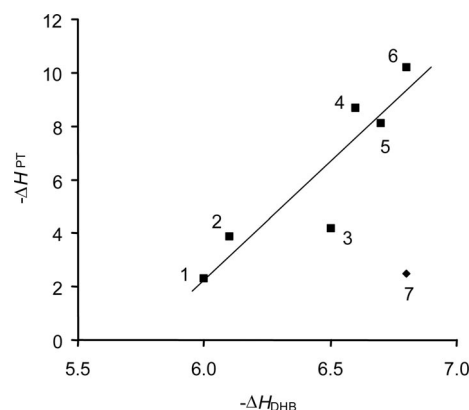


Figure 1. Correlation between the enthalpies (–ΔH°, kcal mol^{–1}) of dihydrogen bond formation (DHB) and proton transfer (PT). Data obtained in CH₂Cl₂ for the reaction of (CF₃)₃COH with [(triphos)-Re(CO)₂H]^[44] (1), (CF₃)₂CHOH with [Cp*FeH(dppe)]^[26] (3), [(triphos)Ru(CO)H₂]^[45] (4), [Cp*RuH(dppe)]^[24] (5), [RuH₂(dppm)₂]^[46] (6), and CF₃CH₂OH with [Cp*MoH₃(dppe)]^[25] (2), [PP₃OsH₂]^[47] (7).

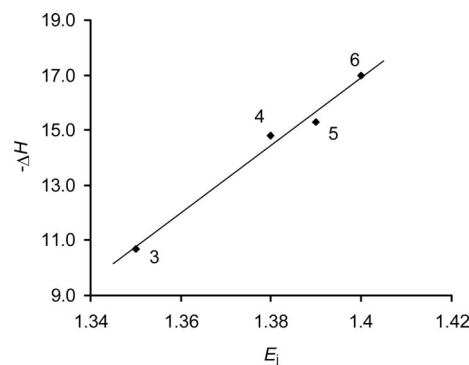


Figure 2. Correlation between the basicity factors E_j of hydride ligand and the enthalpies of their protonation (–ΔH°, kcal mol^{–1}) by (CF₃)₂CHOH in CH₂Cl₂ (sum of the two ΔH° values in Figure 1, points 3–6).

The data on proton transfer kinetics are still scarce. In most cases only activation free energies ΔG[‡] can be calculated from the published reaction rates (Table 1), which vary from 14 to 24 kcal/mol at 298 K. In other cases the activation free energy ΔG[‡] has been estimated to be in the 12–16 kcal mol^{–1} range in agreement with the observation of two separate NMR resonances for the MH...HA and the [M(η²-H₂)]⁺ complexes.^[44,45,48] Some of these systems have been investigated by stopped flow kinetics, i.e. [Cp*FeH(dppe)]^[26,32] and [Cp*MH₃(dppe)] (M = Mo,^[25] W^[28]), or by conventional mixing at low temperatures with IR or UV/Vis monitoring, i.e., [CpRuH(CO)(PCy₃)]^[29] and [Cp*MoH₃(dppe)].^[25] The number of data is rather limited but it does not preclude from deducing some trends.

Table 1. Hydrides basicity factors (E_j), dihydrogen bond formation enthalpies ($\Delta H^\circ_{\text{DHB}}$, kcal mol $^{-1}$) and the activation free energies at 298 K (ΔG^\ddagger_{298} , kcal mol $^{-1}$) of proton transfer step.

		E_j	ROH	P_1	Solvent	$\Delta H^\circ_{\text{DHB}}$	ΔG^\ddagger_{298}	Ref.
1	[WH(CO) $_2$ (NO)(PEt $_3$) $_2$]	0.87	PhOH	1.00	hexane	−5.0	23.6	[34]
2			(CF $_3$) $_2$ CHOH	1.05	hexane	−5.2	23.3	[34]
3			(CF $_3$) $_3$ COH	1.33	hexane	−6.4	21.9	[34]
4	[WH(CO) $_2$ (NO)(PMe $_3$) $_2$]	0.91	PhOH	1.00	hexane	−5.2	23.5	[34]
5			(CF $_3$) $_2$ CHOH	1.05	hexane	−5.6	22.9	[34]
6	[CpRuH(CO)(PCy $_3$)]	1.02	(CF $_3$) $_3$ COH	1.33	CH $_2$ Cl $_2$	−6.2	14.1 [a]	[35]
7					hexane	−7.6	16.7 [b]	[29]
8	[Cp*FeH(dppe)]	1.34	CF $_3$ CH $_2$ OH	0.89	CH $_2$ Cl $_2$	−5.9	21.3	[32]
9			(CF $_3$) $_2$ CHOH	1.05	CH $_2$ Cl $_2$	−6.5	16.5	[26,32]
10			(CF $_3$) $_3$ COH	1.33	CH $_2$ Cl $_2$	−8.3	14.5	[32]
11	[Cp*MoH $_3$ (dppe)]	1.45	CF $_3$ CH $_2$ OH	0.89	CH $_2$ Cl $_2$	−6.1	17.4	[25]
12			(CF $_3$) $_2$ CHOH	1.05	toluene	−6.1	16.1	[25]
13	[Cp*WH $_3$ (dppe)]	1.73	(CF $_3$) $_2$ CHOH	1.05	toluene	−7.3	14.2 [c]	[28]
14			(CF $_3$) $_3$ COH	1.33	toluene	−9.2	14.0 [c]	[28]
15			(CF $_3$) $_3$ COH	1.33	CH $_2$ Cl $_2$	−10.6	13.3 [d]	[28]
			(CF $_3$) $_3$ COH	1.33	CH $_2$ Cl $_2$		13.1 [e]	[28]

[a] At 200 K. [b] Calculated from $\Delta H^\ddagger = 11.0$ kcal mol $^{-1}$, $\Delta S^\ddagger = -19$ e.u. obtained in 200–240 K range. $\Delta G^\ddagger_{200\text{ K}} = 14.6$ kcal mol $^{-1}$. [c] At 293 K. [d] At 288 K. [e] At 283 K.

As can be seen from Table 1 the proton transfer barrier is particularly sensitive to the strength of the proton donor. For a given hydride the activation free energy at 298 K, ΔG^\ddagger_{298} , decreases with the increase of the proton donor strength (acidity factor P_1 ^[7,21,22]) (Figure 3). When dihydrogen-bonded adducts are present as observable intermediates in proton transfer to a transition metal hydride, the stronger the M–H \cdots HA interaction ($\Delta H^\circ_{\text{DHB}}$), the lower the proton transfer activation barrier (Figure 4). This experimental trend is also predicted by theoretical calculations.^[29,30,49] The calculation also show that an extreme increase of the dihydrogen bond strength leads to disappearance of the dihydrogen bond minimum and a spontaneous proton transfer.^[6,49,50]

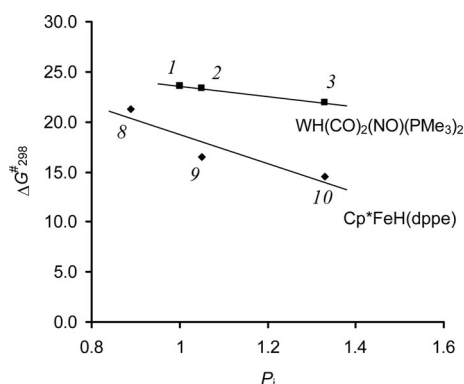


Figure 3. Correlations between the acidity factors P_1 of proton donors and the activation free energies ΔG^\ddagger_{298} (kcal mol $^{-1}$) for [WH(CO) $_2$ (NO)(PMe $_3$) $_2$] in hexane^[34] (1) and [Cp*FeH(dppe)] in CH $_2$ Cl $_2$.^[32] Numbers (in italic) correspond to the entry numbers in Table 1.

To date the activation enthalpy and entropy associated with the proton transfer step are known only for [Cp*FeH(dppe)]/(CF $_3$) $_2$ CHOH in CH $_2$ Cl $_2$ ($\Delta H^\ddagger =$

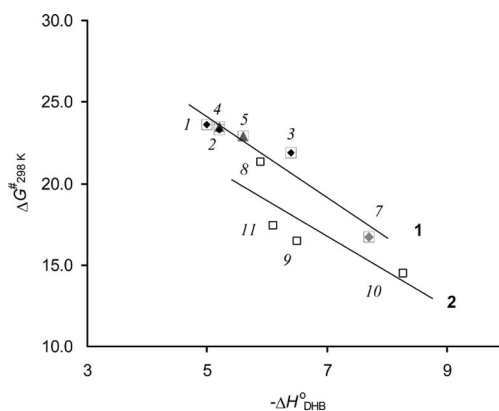


Figure 4. Correlation between the dihydrogen bond formation enthalpies ($-\Delta H^\circ_{\text{DHB}}$, kcal mol $^{-1}$) and the activation free energies ΔG^\ddagger_{298} (kcal mol $^{-1}$) in hexane (1, rhombi and triangles 1–7), dichloromethane (2, open squares 8–11). Numbers (printed in *italics*) correspond to the entry numbers in Table 1.

3.9 kcal mol $^{-1}$, $\Delta S^\ddagger = -40$ e.u.),^[26] for [Cp*MoH $_3$ (dppe)]/CF $_3$ CH $_2$ OH in CH $_2$ Cl $_2$ ($\Delta H^\ddagger = 12.3$ kcal mol $^{-1}$, $\Delta S^\ddagger = -15.7$ e.u.), and for [CpRuH(CO)(PCy $_3$)]/(CF $_3$) $_3$ COH in hexane ($\Delta H^\ddagger = 11.0$ kcal mol $^{-1}$, $\Delta S^\ddagger = -19$ e.u.).^[29] The proton transfer rate constant for the MH \cdots HA \rightarrow [M(η^2 -H $_2$)] $^+$ [AHA] $^-$ transformation grows as the temperature increases, as does the activation free energy ΔG^\ddagger . This appears to result from the substantial *negative* activation entropy, which indicates a highly ordered transition state for proton transfer. Indeed, DFT calculations show there is a strong interaction between the two tightly bonded units in the TS (Figure 5). The transition state can be regarded as an H $_2$ entity (H–H length ca. 0.9 Å) simultaneously bonded to both the [M] $^+$ and the [AHA] $^-$ units (M–H and H–O distances are ca. 1.6 and 1.4 Å, respectively).^[25,32,35] In the work of Ferafin et al. the proton transfer from CF $_3$ COOH to [ReH $_2$ (CO)(NO)(PR $_3$) $_2$] is reported as having positive ΔH^\ddagger

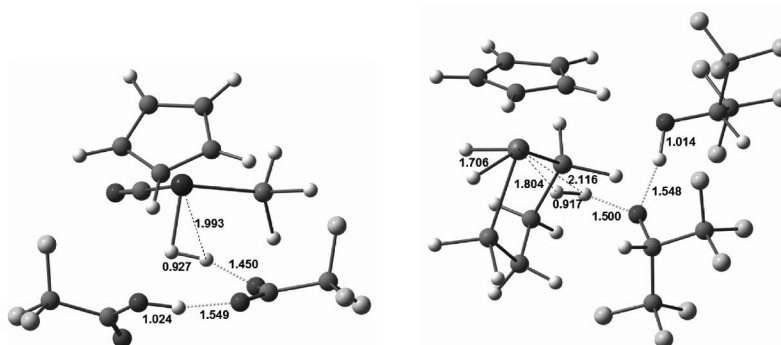


Figure 5. Transition states for proton transfer from two CF_3COOH molecules to $[\text{CpRuH}(\text{CO})(\text{PH}_3)]$ (left) or two $(\text{CF}_3)_2\text{CHOH}$ molecules to $[\text{CpMoH}_3(\text{dpe})]$ (right).

and ΔS^\ddagger .^[10,51] However, as admitted in the original paper, “it appears quite unusual that a second-order reaction is accompanied by a positive ΔS^\ddagger value”.^[51] A possible reason for this discrepancy is that the dihydrogen bond formation and the participation of two acid molecules have not been taken into account in the analysis of the data obtained under stoichiometric hydride/acid ratio [Scheme 2, Equations (2)–(3)].

Dihydrogen bonded complexes can be easily envisaged as intermediates of the intermolecular hydride-proton exchange. Though this phenomenon is well documented for transition metal hydrides, theoretical studies on this subject are practically absent.^[52] In the above mentioned work by Feracin et al. the transition state for the hydride-proton exchange in $[\text{ReH}_2(\text{CO})(\text{NO})(\text{PR}_3)_2]/\text{CF}_3\text{COOH}$ has been described at the EHT calculation level.^[51] It is seemingly similar to that of proton transfer (Figure 5), differing by longer H–H and H–O distances (of 1.2 and 1.6 Å, respectively). It is arguable that two processes follow the same reaction pathway and have similar reaction energy profiles (Figure 6). For weak proton donors (HA_1 in Figure 6) the transition state is too high and the ionic form $\{[\text{M}(\eta^2\text{-H}_2)]^+ \cdots [\text{A}]^-$ ion pair} is too close in energy to the TS to yield sufficient stability to the proton transfer product. However, these energy levels may still be accessible to allow the proton-hydride exchange. Facile rotation of $\eta^2\text{-H}_2$ ligand or 1,2-shift of A_1^- within the $(\eta^2\text{-H}_2)$ ligand completes the exchange mechanism. When the proton donor is too weak and the ion pair local minimum does not exist, all these events can occur in one concerted step (long-dashed line in Figure 6).^[53] Indeed, the intermolecular hydride-proton or isotope exchange is observed in the NMR spectra even when the dihydrogen bond is not strong enough to allow the proton transfer, e.g., for $[\text{Cp}^*\text{MoH}(\text{PMe}_3)_3]$ or $[\text{WH}(\text{CO})_2(\text{NO})(\text{PR}_3)_2]$ in the presence of CH_3OD .^[42,54,55]

As discussed above, when the proton donor is more acidic (HA_2 in Figure 6) the dihydrogen bond becomes stronger, the barrier for proton transfer $\{[\text{M}(\eta^2\text{-H}_2)]^+ \cdots [\text{A}]^-$ ion pair formation} decreases and the product ion pair is stabilized. Under these conditions equilibrium between the $[\text{M}(\eta^2\text{-H}_2)]^+ \cdots [\text{A}]^-$ and $\text{MH} \cdots \text{HA}$ states may be established, as in the case of $[\text{ReH}_2(\text{CO})(\text{NO})(\text{PR}_3)_2]/\text{CF}_3\text{COOH}$. In the

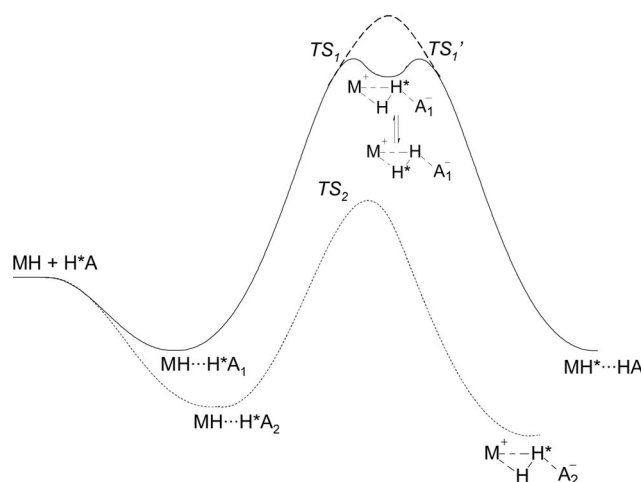


Figure 6. The reaction energy profiles for hydride-proton exchange (solid line) and proton transfer (dashed line).

limiting case of essentially quantitative proton transfer, dynamic equilibrium may still allow isotope exchange. For example, the non-classical species generated by the low temperature reaction of $[\text{Cp}^*\text{FeH}(\text{dppe})]$ with CF_3COOD was found to exist as a mixture of three isotopomers, HH, HD and DD.^[56]

Thus, as already predicted by Bakhmutov,^[10] the proton-hydride exchange rate may be a good probe for a proton transfer under conditions when partial proton transfer occurs. The activation enthalpy and entropy of intermolecular H/H (H/D) exchange reported for the $[\text{CpW}(\text{CO})_2(\text{PMe}_3)\text{-H}]/[(\text{CH}_3)_3\text{C}_6\text{H}_4\text{N}(\text{CH}_3)_2\text{D}]^+$ system^[57] yield an activation free energy comparable to those shown in Table 1: ΔG^\ddagger is $17.7 \text{ kcal mol}^{-1}$ at 200 K and increases to $21.2 \text{ kcal mol}^{-1}$ at 298 K. For the above-mentioned $[\text{ReH}_2(\text{CO})(\text{NO})(\text{PR}_3)_2]/\text{CF}_3\text{COOH}$ systems the activation enthalpies (positive values) and entropies (negative values)^[10] are lower and accordingly give lower activation free energies: ΔG^\ddagger varies from 8 to 10 kcal mol^{-1} at 200 K increasing by 1–2 kcal mol^{-1} at 298 K. These values are close to e.g. $\Delta G^\ddagger_{200} = 11.5 \text{ kcal mol}^{-1}$ calculated for $[\text{Cp}^*\text{FeH}(\text{dppe})]/(\text{CF}_3)_2\text{CHOH}$ and are in agreement with immediate proton transfer observed on the IR and NMR timescale.

Ion Pairing and Subsequent Transformations of $[M(\eta^2-H_2)]^+$ Complexes

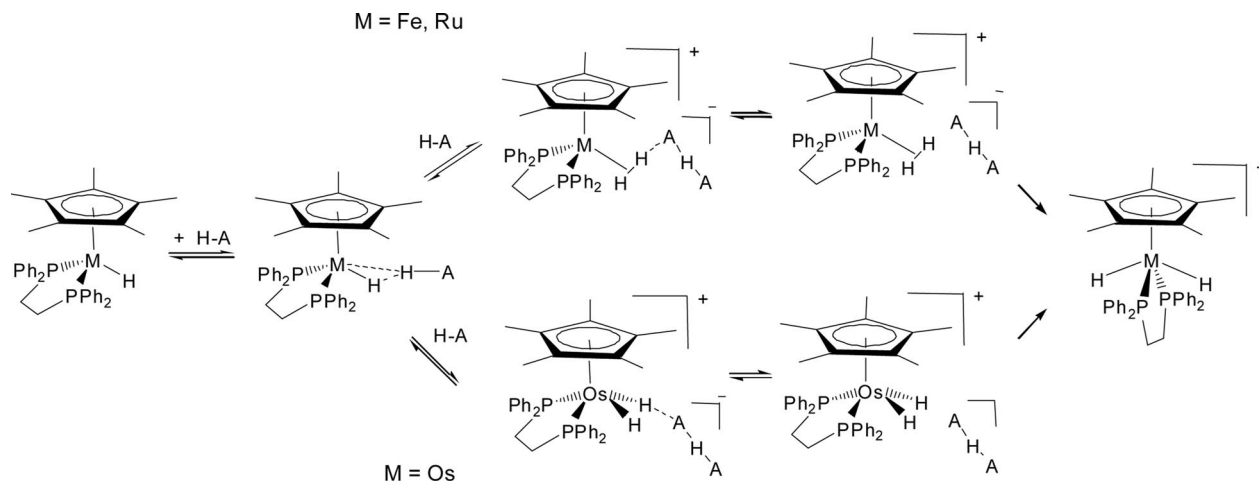
The negative enthalpy and entropy for the proton transfer step favour the protonation product as the temperature decreases. Hydrogen bonding between cation and anion is also thermodynamically more favourable at lower temperatures. Thus, lowering the temperature assists the proton transfer by shifting the tautomeric equilibrium $MH\cdots HA \leftrightarrow [M(\eta^2-H_2)]^+\cdots A^-$ to the right and prevents the hydrogen bonded ion pair dissociation. All this helps to stabilize the $[M(\eta^2-H_2)]^+$ complexes against isomerization into the classical form or to prevent H_2 evolution and formation of M-A species.

We have recently shown that the irreversible isomerization of the $[Cp^*M(\eta^2-H_2)(dppe)]^+$ complexes ($M = Fe,^{[32]} Ru,^{[24]}$) into their classical *trans*-dihydride isomers occurs upon dissociation of the $[M(\eta^2-H_2)]^+\cdots[AHA]^-$ ion pair (Scheme 3). This is qualitatively indicated by the dependence of the temperature at which the $[M(\eta^2-H_2)]^+ \rightarrow [M(H)_2]^+$ isomerization becomes observable on the counteranion nature: higher temperatures are necessary to induce the isomerization in the presence of more basic anions due to greater ion pair stability.^[32] At the same time the isomerization rate constant does not depend on the anion nature.^[24,32,56] The osmium congener, $[Cp^*OsH(dppe)]$, does not yield a non-classical cationic dihydride complex but rather a *cis*-dihydride tautomer as the kinetic protonation product, which then isomerizes to *trans*-dihydride upon warming (Scheme 3).^[58,59]

Variable temperature NMR studies allowed determining the activation parameters for the isomerization step. Despite the different structure of the intermediate $\{[M(\eta^2-H_2)]^+ \text{ for Fe and Ru, } cis-[M(H)_2]^+ \text{ for Os}\}$ the activation enthalpy values appeared identical, within experimental error, for all three metals ($\Delta H^\ddagger_{\text{isom}} = 21.6 \pm 0.8 \text{ kcal mol}^{-1}$ for Fe,^[56] $20.9 \pm 0.8 \text{ kcal mol}^{-1}$ for Ru,^[24] $21.5 \pm 1.0 \text{ kcal mol}^{-1}$ for Os^[59]). The activation entropy, $\Delta S^\ddagger_{\text{isom}}$, is small, positive and increasing on descending the group: $5 \pm 3 \text{ e.u.}$ for Fe,^[56]

$9 \pm 3 \text{ e.u.}$ for Ru,^[24] $12 \pm 4 \text{ e.u.}$ for Os.^[59] Similar data have been obtained for the irreversible isomerization of the related $[CpRu(\eta^2-H_2)(PPh_3)_2]^+$ complex ($\Delta H^\ddagger_{\text{isom}} = 16.1 \pm 1.8 \text{ kcal mol}^{-1}$, $\Delta S^\ddagger_{\text{isom}} = 3 \pm 8 \text{ e.u.}$).^[60] Note that the activation enthalpy of isomerization is greater than that of proton transfer. However, because of the opposite sign of the entropy terms, the activation free energy of isomerization decreases and that of proton transfer increases as the temperature increases. $\Delta G^\ddagger_{\text{isom}}$ is too high (too small isomerization rate constant) at low temperatures (below 230 K) for the reaction to occur even in the case of “non-coordinating” anions like BF_4^- . The non-classical to classical rearrangement is reversible in certain cases,^[60] for instance for complex $[CpRuH_2(dmdppe)]^+$, $dmdppe = (1,1\text{-dimethyl-2,2-diphenylphosphanyl})ethane$, for which $\Delta H^\circ = -0.92 \pm 0.07 \text{ kcal mol}^{-1}$ and $\Delta S^\circ = -4.5 \pm 0.3 \text{ e.u.}$ have been determined (the equilibrium is relatively insensitive to temperature changes).

An interesting ion pairing effect was shown by Basallote et al.:^[61] deprotonation of the dihydrogen complex *trans*- $[FeH(\eta^2-H_2)(dppe)_2]^+[BF_4]^-$ with an excess of NEt_3 to form *cis*- $[FeH_2(dppe)_2]$ is accelerated by added BF_4^- and PF_6^- and decelerated by BPh_4^- relative to the absence of added salt. Theoretical calculations have shown that the deprotonation occurs via intermediates with $Fe(\eta^2-H_2)\cdots N$ and $FeH\cdots HN$ hydrogen bonded intermediates, this being the microscopic reverse pathway of the protonation reaction depicted in Scheme 1. The experimentally derived ion pair formation constants, K_{ipX} , and the deprotonation rate constants, k_X , can be explained with the help of DFT calculations. The bulky BPh_4^- anion yields quite a stable ion pair [$K_{\text{ipBPh}_4} = (3.5 \pm 0.6) \times 10^2 \text{ M}^{-1}$ in acetone] and shields the η^2-H_2 ligand against NEt_3 , preventing deprotonation. The smaller anions BF_4^- and PF_6^- , on the other hand, could not provide such effective shielding in spite of similar ion pair stability. At the same time, they accompany the proton along the reaction, stabilising the positive charge and lowering the barrier for the Et_3NH^+ detachment process. Hence, the ion pair formation constants and the deprotonation rate

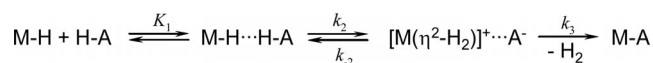


Scheme 3. Hydrogen bonding and proton transfer to $[Cp^*MH(dppe)]$ hydride complexes.

constants vary in the opposite direction ($K_{\text{ipBF}_4}/K_{\text{ipPF}_6} = 0.44$, $k_{\text{BF}_4}/k_{\text{PF}_6} = 1.63$), i.e. the less stable ion pair formed with BF_4^- gives faster reaction.^[61]

In many cases, however, basic anions ($\text{A}^- = \text{OR}^-$, OCOR^-) tend to displace H_2 out of the transition metal coordination sphere, yielding organyloxo products. This is the case for the protonation products of complexes $[(\text{triphos})\text{ReH}(\text{CO})_2]$,^[62] $[\text{Re}(\text{CO})\text{H}_2(\text{NO})(\text{PR}_3)_2]$,^[63] and $[\text{CpRuH}(\text{CO})(\text{PCy}_3)]$,^[64] for which the corresponding $[\text{M}(\eta^2\text{-H}_2)]^+$ cations could be isolated as $[\text{BF}_4]^-$ salts but evolved into $[\text{MA}]$ species in the presence of fluorinated alcohols or carboxylic acids. In contrast to the isomerization process, this reaction proceeds intramolecularly and does not require a hydrogen bonded ion pair dissociation.^[64]

The more recently published kinetic study of the $[\text{WH}(\text{CO})_2(\text{NO})(\text{PR}_3)_2]$ protonation is a special case,^[34] because this hydride complex does not give a detectable non-classical cation under any conditions,^[19,54] although the corresponding local minimum has been found by computational investigations.^[65] Under conditions suitable for proton transfer, H_2 evolution has been observed yielding the organyloxo complex $[\text{W}(\text{OR})(\text{CO})_2(\text{NO})(\text{PR}_3)_2]$ {Scheme 4, Equation (4)} with identical rates for the disappearance of the dihydrogen bonded adduct and for the organyloxo complex formation. However, this rate does not depend on the anion basicity (coordination ability) but correlates with the HA strength (Figure 3).^[34] This indicates that the proton transfer step is rate determining for this system. Thus, $k_3 \gg k_{-2}$ and Equation (4) for the rate constant k_{obs} transforms into just k_2 .



Scheme 4. Kinetic model for the reaction of $[\text{WH}(\text{CO})_2(\text{NO})(\text{PR}_3)_2]$ with proton donors.

$$k_{\text{obs}} = k_2 k_3 / (k_{-2} + k_3) \approx k_2 \quad (4)$$

The same trend may be expected for the related tungsten hydride $\text{WH}(\text{CO})(\text{NO})(\text{PMe}_3)_3$. Indeed, variable temperature IR and NMR studies^[66] on the interaction between this hydride and proton donors revealed dihydrogen bond

formation followed by H_2 evolution. The kinetics of the latter reaction was studied at 333 K in $[\text{D}_8]\text{toluene}$ by monitoring the disappearance of the starting hydride. The published data on the reaction half-life times, $t_{1/2}$, allow the calculation of the observed rate constants $k'_{\text{obs}} = \ln 2/t_{1/2}$, which in this case is expressed by Equation (5). The dihydrogen bond formation constant, K_1 , is extremely small at elevated temperatures (e.g., $K_1 = 0.06 \text{ L mol}^{-1}$ for complex with 3,4,5-trimethylphenol at 333 K) decelerating the reaction.

$$k'_{\text{obs}} = \frac{k_2 k_3}{k_{-2} + k_3} \cdot \frac{K_1 [\text{HA}]}{1 + K_1 [\text{HA}]} \sim k_2 K_1 [\text{HA}] \quad (5)$$

The rate constants and activation free energy for $[\text{WH}(\text{CO})(\text{NO})(\text{PMe}_3)_3]$ reaction with proton donors vary linearly with the HA acidity ($\text{p}K_{\text{a}}$) (Figure 7). The point belonging to $\text{CF}_3\text{CH}_2\text{OH}$ (not to $i\text{PrOH}$ as stated in the original article^[66]) falls off the trend for unknown reason. This trend confirms that the reaction rate-determining step is proton transfer and not organyloxo coordination, similarly to that was found for $[\text{WH}(\text{CO})_2(\text{NO})(\text{PMe}_3)_2]$ (see above).

Similarly to the above described tungsten systems, the non-classical isomer has not been detected experimentally for $[\text{Cp}^*\text{MoH}_4(\text{dppe})]^+$ but its facile accessibility from the tetrahydride protonation product is evidenced by the H_2 evolution at ambient temperature^[25,67,68] and confirmed theoretically.^[69] It appears that the nature of the solvent and the amount of excess acid determine the nature of the reaction product by delicately controlling the position of the proton transfer and ion pairing equilibria between $[\text{Cp}^*\text{MoH}_3(\text{dppe})]$ and $[\text{CF}_3\text{COOH}]$ (Scheme 5).^[70] The use of suitable solvent, temperature, and hydride/acid ratio conditions led to the selective formation of the dihydrido complex $[\text{Cp}^*\text{Mo}(\text{dppe})(\text{H})_2(\eta^1\text{-O}_2\text{CCF}_3)]$ as H_2 evolution product. The $[\text{Cp}^*\text{MoH}_4(\text{dppe})]^+\cdots[\text{OCOCF}_3]^-$ ion pair dissociation precludes the formation of the trifluoroacetato product leading to the non-specific H_2 loss/decomposition (see below). This system is the first one where activation parameters for the H_2 evolution process have been determined: $\Delta H^\ddagger_{\text{H}_2} = 31.8 \pm 0.5 \text{ kcal mol}^{-1}$ and $\Delta S^\ddagger_{\text{H}_2} = 36 \pm 2 \text{ e.u.}$ The reaction rate does not depend on the solvent

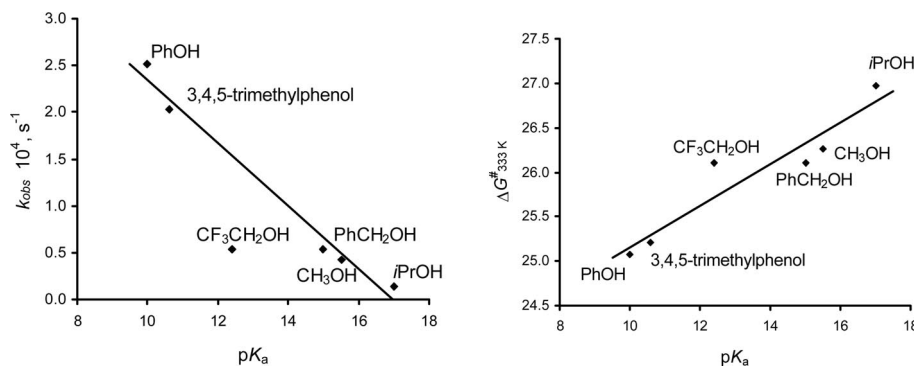


Figure 7. Correlations between the reaction rate constants k_{obs} (left) and the activation free energies $\Delta G^\ddagger_{333\text{K}}$ (right) and the proton donors $\text{p}K_{\text{a}}$ for the reaction of $[\text{WH}(\text{CO})(\text{NO})(\text{PMe}_3)_3]$ with acids in $[\text{D}_8]\text{toluene}$ at 333 K. Calculated from the $t_{1/2}$ data in ref.^[66]



The *large positive* activation entropy suggests that the transition state is dissociative in nature. It explains also why the reaction does not occur at low temperatures: the contribution of the entropic term raises the activation free energy to a greater extent at lower temperatures, so that the barrier becomes too high to be overcome.

While solvent effects on hydrogen bonding and proton transfer – a topic which deserves a separate review – is well appreciated in organic chemistry,^[72,73] studies aimed at understanding how the reaction medium may influence proton transfer to transition metal hydrides are scarce. The solvent polarity (dielectric permittivity) is greater at lower temperatures, assisting proton transfer. A change of solvent may, obviously, have the same effect. Thus, the high dielectric permittivity of the Freon mixture $\text{CDCl}_2\text{F}/\text{CDF}_3$ (2:1) at low temperatures has been reported to allow the proton transfer to $[\text{Cp}^*\text{RuH}_3(\text{PCy}_3)]$ by $\text{R}^\text{F}\text{OH}$ $\{\text{R}^\text{F}\text{OH} = (\text{CF}_3)_2\text{CHOH}$ or $(\text{CF}_3)_3\text{COH}\}$, yielding $[\text{Cp}^*\text{Ru}(\text{H})_2(\eta^2\text{-H}_2)(\text{PCy}_3)]^+[\text{OR}^\text{F}]^-$, whereas no reaction occurs for the same mixture in toluene.^[74] For the hydrides listed in Table 1 the proton transfer activation free energies ΔG^\ddagger in hexane (dielectric permittivity $\epsilon = 1.8$ ^[72]) are systematically higher than those in the more polar dichloromethane ($\epsilon = 8.93$ at 298 K^[72]), see Figures 3 and 4. Theoretical studies for the protonation of $[\text{CpRuH}(\text{CO})(\text{PCy}_3)]$,^[29] $[\text{Cp}^*\text{FeH}(\text{dppe})]$ ^[26]

So far we have discussed only how the *nonspecific* interaction with the environment affects the proton transfer kinetics and thermodynamics. However *specific* properties of the medium (e.g., the solvent ability to serve as hydrogen-bond donor or acceptor) could as well greatly influence the position of the proton transfer equilibrium and the stability of the $M(\eta^2-H_2)^+$ complexes. Hence, the proton transfer equilibrium position is very different in THF and CH_2Cl_2 ; the greater proton accepting ability of the former dampens the proton donating strength of the acid, thwarting the hydrogen bond formation and the proton transfer reaction relative to the similarly polar CH_2Cl_2 .^[47,50,70] In toluene, possessing weak hydrogen bond accepting properties and lower polarity, the proton transfer equilibrium is shifted further towards the neutral hydrogen-bonded species in comparison with CH_2Cl_2 .^[70]

Calculations show that the intervention of a second proton donor molecule in hydrogen bonding, $M-H\cdots H-A\cdots H-A$ strengthens the dihydrogen bond with the ensuing decrease of the proton transfer barrier and a shift of the equilibrium to the right.^[26,29,30] The same, but obviously weaker, effect is caused by CH acids such as dichloromethane.^[50] These theoretical findings are confirmed by the experiment. Indeed kinetic data show the participation of two HA mole-

cules in protonation reaction yielding $[M(\eta^2-H_2)]^+[28,32]$ while UV/Vis titration experiments confirm the involvement of the homoconjugated anions, $[AHA]^-$, into the product ion pair.^[24,26,50,59] The second-order dependence of the rate constants on the acid concentration was also found for the protonation of the hydride cluster $[W_3S_4H_3(dmpe)_3]^+$ {dmpe = 1,2-bis(dimethylphosphanyl)ethane} in CH_2Cl_2 .^[75] However, a first order dependence on the acid concentration was found in neat MeCN or MeCN/ H_2O .^[76] On the basis of a theoretical study the effect was attributed to the unfavourable disruption of the acid–solvent H-bonds in MeCN and water upon the interaction of the acid with the tungsten hydride cluster.^[75] As exemplified for the $[PP_3RuH_2]/$ substituted phenols system,^[50] proton transfer is better assisted by a protic solvent (CH_3OH) rather than an aprotic one (CH_3CN) under comparable medium polarity, because of the additional hydrogen bonding of CH_3OH with the solutes.

Proton accepting/coordinating solvents may not only hamper the hydride-proton donor interaction and disfavor proton transfer, but also crucially affect the stability of the proton transfer products. For example, a fast equilibrium between the dihydrogen bonded adduct, $Cp^*Mo(dppe)H_3 \cdots HOCCF_3$, the ion paired proton transfer product, $Cp^*Mo(dppe)H_4^+ \cdots OOCF_3$, and the separated ions is established upon interaction of the Mo trihydride complex with CF_3COOH in different solvents. In low polarity, weakly coordinating solvents (benzene/toluene) the acid excess stabilizes $Cp^*Mo(dppe)H_4^+$ against H_2 loss via the separation of charged species by forming the less basic homoconjugate anion, $[CF_3COO(HOCCF_3)_n]^-$. This is not possible in THF or MeCN, which bind the excess acid, thus the hydrogen bonded ion pair $Cp^*Mo(dppe)H_4^+ \cdots OOCF_3$ evolves to $[Cp^*Mo(dppe)H_2(O_2CCF_3)]$ via replacement of H_2 by the more basic trifluoroacetate ligand.

A unique example of the solvent effect on the structure of a dihydrido cation was found for compound $[Cp^*MoH_2(CO)(PMe_3)_2]^+[BF_4]^-$, which exists as a dihydrogen complex in THF and as a classical dihydride in CH_2Cl_2 .^[77] Theoretical calculations show that the solvent effect on the classical/non-classical equilibrium energetics can be described as operating through a second-order non-covalent interaction: solvent \cdots anion \cdots cation. The stronger $CH \cdots FBF_3$ interaction for CH_2Cl_2 relative to THF weakens the anion–cation interaction, thus allowing the cation isomerization to the classical form.

To conclude this section, we shall consider the origin of the entropy changes accompanying hydrogen bond formation and proton transfer. The dihydrogen bond formation entails a substantial entropy loss as does a regular hydrogen bond.^[78,79] This entropy loss originates from the loss of rotational and translational degrees of freedom in the complex in comparison to the individual acid/base molecules.^[80,81] Yet, hydrogen bond formation induces only slight changes in the orientation of the solvent dipoles at the solute site.^[80,82] This *nonspecific* interaction with the medium is smaller for lower polarity solvents, making hydrogen bonds stronger in nonpolar media. *Specific* interac-

tions – binding of a second HA molecule or a protic (hydrogen bond donating) solvent molecule – also have a strengthening effect due to the cooperative enhancement of a proton donor strength.^[29,50,83]

On the other hand, the proton transfer step occurs as an intracomplex (intramolecular) conversion of an $MH \cdots HA$ or $MH \cdots HA \cdots HA$ species into a $[M(\eta^2-H_2)]^+ \cdots [A]^-$ or $[M(\eta^2-H_2)]^+ \cdots [AHA]^-$ species and, in principle, should not be associated with a great entropy loss. However, it involves a charge separation and thus entails substantial modulation of the solute-solvent interaction. The ion pair formation causes ordering of the electric dipoles of the solvent around this species. The ensuing increase of the local electric field leads, in turn, to an energetic stabilization and assists the proton transfer.^[82] However, it requires also an entropy decrease. As a consequence a more negative proton transfer enthalpy is associated to a more negative entropy (Figure 8). The experimentally determined ΔS^\ddagger values for these systems are rather large and negative reflecting probably ordering of both the reacting complex and the solvent around it. Thus, despite the different origin of the negative entropy, both dihydrogen bonding and proton transfer equilibria shift to the right as the temperature decreases, gearing “low temperature assisted proton transfer”.^[46]

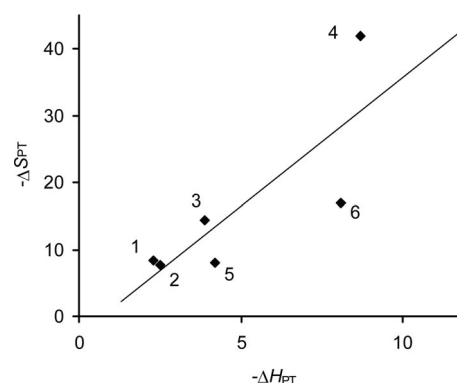


Figure 8. Enthalpy and entropy correlation for the proton transfer step determined for the reaction of $(CF_3)_3COH$ with [(triphos)- $Re(CO)_2H$]^[44] (1), CF_3CH_2OH with PP_3OsH_2 ^[47] (2), $[Cp^*MoH_3(dppe)]^{[25]}$ (3), and $(CF_3)_2CHOH$ with [(triphos) $Ru(CO)H_2$]^[45] (4), $[Cp^*FeH(dppe)]^{[26]}$ (5), $[Cp^*RuH(dppe)]^{[24]}$ (6).

When the temperature is lowered, ordering of solvent dipoles also occurs, which is responsible for the solvent polarity increase.^[84] This phenomenon is obviously more pronounced for polar solvents than for non-polar ones. For example, the dielectric permittivity (taken here as a measure of solvent polarity) of toluene remains almost constant between room temperature and 190 K ($\epsilon = 2.47$ at 240 K and 2.71 at 180 K^[85]) whereas that of CH_2Cl_2 changes from 8.93 at 298 K to 15.53 at 190 K.^[86] This solvent polarity change causes a local dielectric field increase around the solute, inducing the proton shift toward the base in a hydrogen bonded complex and favouring the charge separation.^[82,84] These concerted events are reflected in the temperature dependence of the reaction free energy and in the entropy changes determined for each step.

Conclusions

The reactivity of transition metal hydride complexes can be tuned by varying the ligands electronic and/or steric properties. For a given complex it can be further attenuated by interplay of secondary interactions such as hydrogen bonding and temperature effects. This is (intuitively) appreciated but there are not many explicit examples. The present microreview gathers such reports on the transition metal hydrides interaction with proton donors to reveal the physico-chemical (thermodynamic and kinetic) origin of these effects. Thus, temperature lowering assists reversible proton transfer due to (a) an increased stability of the hydrogen bonded intermediate and (b) a decreased activation free energy for proton transfer. Both are due to the reduced impact of the entropy term on the free energy. Another consequence of the temperature lowering is a solvent polarity (dielectric permittivity) increase, further favoring proton transfer. When proton transfer yielding an (η^2 -H₂) complex is followed by its isomerization to a classical dihydride or by hydrogen elimination, both processes featuring greater activation free energies than that of proton transfer and a positive activation entropy, the low temperature can be used to suppress these transformations. Fine-tuning the [M(η^2 -H₂)]⁺[A][−] ion pair stability can provide additional support in governing the reactivity of the non-classical hydride species.

Acknowledgments

The authors highly appreciate the long time fruitful partnership with Profs. A. Lledos (UAB, Barcelona), M. Peruzzini (ICCOM CNR, Florence) and R. Poli (LCC CNRS, Toulouse) within several bilateral and European programs. They thank also Dr. O. Filippov for very helpful discussions during this manuscript preparation. The financial support from the Russian Foundation for Basic Research (grant number 08-03-00464), Division of Chemistry and Material Sciences of RAS (Russia) is gratefully acknowledged.

- [1] R. H. Morris, *Coord. Chem. Rev.* **2008**, *252*, 2381–2394.
- [2] N. K. Szymczak, D. R. Tyler, *Coord. Chem. Rev.* **2008**, *252*, 212–230.
- [3] G. J. Kubas, *Chem. Rev.* **2007**, *107*, 4152–4205.
- [4] A. Weller, S. J. S. Mcindoe, *Eur. J. Inorg. Chem.* **2007**, 4411–4423.
- [5] *Recent Advances in Hydride Chemistry* (Eds.: M. Peruzzini, R. Poli), Elsevier, Amsterdam, **2001**, pp. 580.
- [6] M. Besora, A. Lledos, F. Maseras, *Chem. Soc. Rev.* **2009**, *38*, 957–966.
- [7] N. V. Belkova, E. S. Shubina, L. M. Epstein, *Acc. Chem. Res.* **2005**, *38*, 624–631.
- [8] N. V. Belkova, L. M. Epstein, E. S. Shubina, *ARKIVOC* **2008**, *iv*, 120–138.
- [9] L. Brammer, *Dalton Trans.* **2003**, 3145–3157.
- [10] V. I. Bakhmutov, *Eur. J. Inorg. Chem.* **2005**, 245–255.
- [11] R. H. Crabtree in *Encyclopedia of Supramolecular Chemistry* (Eds.: J. L. Atwood, J. W. Steed), Marcel Dekker, Inc., New York, **2004**, pp. 666–672.
- [12] R. Coustelcean, J. E. Jackson, *Chem. Rev.* **2001**, *101*, 1963–1983.
- [13] L. M. Epstein, E. S. Shubina, *Coord. Chem. Rev.* **2002**, *231*, 165–181.
- [14] L. M. Epstein, N. V. Belkova, E. I. Gutsul, E. S. Shubina, *Pol. J. Chem.* **2003**, *77*, 1371–1383.
- [15] W. K. Fung, X. Huang, M. L. Man, S. M. Ng, M. Y. Hung, Z. Lin, C. P. Lau, *J. Am. Chem. Soc.* **2003**, *125*, 11539–11544.
- [16] J.-W. Handgraaf, E. J. Meijer, *J. Am. Chem. Soc.* **2007**, *129*, 3099–3103.
- [17] A. Urakawa, F. Jutz, G. Laurenczy, A. Baiker, *Chem. Eur. J.* **2007**, *13*, 3886–3899.
- [18] X. Yang, M. B. Hall, *J. Am. Chem. Soc.* **2009**, *131*, 10901–10908.
- [19] E. S. Shubina, N. V. Belkova, A. N. Krylov, E. V. Vorontsov, L. M. Epstein, D. G. Gusev, M. Niedermann, H. Berke, *J. Am. Chem. Soc.* **1996**, *118*, 1105–1112.
- [20] V. I. Bakhmutov, *Dihydrogen Bond: Principles, Experiments and Applications*, John Wiley & Sons, Inc., Hoboken, New Jersey, **2008**, pp. 258.
- [21] L. M. Epstein, N. V. Belkova, E. S. Shubina, in: *Recent Advances in Hydride Chemistry* (Eds.: M. Peruzzini, R. Poli), Elsevier, Amsterdam, **2001**, pp. 391–418.
- [22] A. V. Iogansen, *Theor. Exp. Khim.* **1971**, *7*, 302–311.
- [23] A. V. Iogansen, *Theor. Exp. Khim.* **1971**, *7*, 312–317.
- [24] N. V. Belkova, P. A. Dub, M. Baya, J. Houghton, *Inorg. Chim. Acta* **2007**, *360*, 149–162.
- [25] N. V. Belkova, P. O. Revin, M. Besora, M. Baya, L. M. Epstein, A. Lledós, R. Poli, E. S. Shubina, E. V. Vorontsov, *Eur. J. Inorg. Chem.* **2006**, 2192–2209.
- [26] N. V. Belkova, E. Collange, P. Dub, L. M. Epstein, D. A. Lemenovskii, A. Lledós, O. Maresca, F. Maseras, R. Poli, P. O. Revin, E. S. Shubina, E. V. Vorontsov, *Chem. Eur. J.* **2005**, *11*, 873–888.
- [27] For example $\log K_{\text{AHA}} = 4.8$ for PFTB and 4.5 for CH₃COOH in acetonitrile, where the anions are rather poorly solvated: A. Kuejtt, I. Leito, I. Kaljurand, L. Soovaeli, V. M. Vlasov, L. M. Yagupolskii, I. A. Koppel, *J. Org. Chem.* **2006**, *71*, 2829–2838.
- [28] N. V. Belkova, M. Besora, M. Baya, P. A. Dub, L. M. Epstein, A. Lledós, R. Poli, P. O. Revin, E. Shubina, *Chem. Eur. J.* **2008**, *14*, 9921–9934.
- [29] N. V. Belkova, M. Besora, L. M. Epstein, A. Lledós, F. Maseras, E. S. Shubina, *J. Am. Chem. Soc.* **2003**, *125*, 7715–7725.
- [30] E. V. Bakhmutova, V. I. Bakhmutov, N. V. Belkova, M. Besora, L. M. Epstein, A. Lledós, G. I. Nikonov, E. S. Shubina, J. Tomas, E. V. Vorontsov, *Chem. Eur. J.* **2004**, *10*, 661–671.
- [31] A. Rossin, E. I. Gutsul, N. V. Belkova, L. M. Epstein, L. Gonsalvi, A. Lledos, K. A. Lyssenko, M. Peruzzini, E. S. Shubina, F. Zanobini, *Inorg. Chem.* **2010**, *49*, 4343–4354.
- [32] N. V. Belkova, P. O. Revin, L. M. Epstein, E. V. Vorontsov, V. I. Bakhmutov, E. S. Shubina, E. Collange, R. Poli, *J. Am. Chem. Soc.* **2003**, *125*, 11106–11115.
- [33] J. Zheng, M. D. Fayer, *J. Am. Chem. Soc.* **2007**, *129*, 4328–4335.
- [34] N. V. Belkova, L. M. Epstein, A. I. Krylova, E. G. Faerstein, E. S. Shubina, *Russ. Chem. Bull.* **2007**, *56*, 870–874.
- [35] N. V. Belkova, A. V. Ionidis, L. M. Epstein, E. S. Shubina, S. Gruendemann, N. S. Golubev, H. H. Limbach, *Eur. J. Inorg. Chem.* **2001**, 1753–1761.
- [36] S. Bolano, L. Gonsalvi, P. Barbaro, A. Albinati, S. Rizzato, E. Gutsul, N. Belkova, L. Epstein, E. Shubina, M. Peruzzini, *J. Organomet. Chem.* **2006**, *691*, 629–637.
- [37] P. A. Dub, O. A. Filippov, N. V. Belkova, J.-C. Daran, L. M. Epstein, E. S. Shubina, R. Poli, *Dalton Trans.* **2010**, *39*, 2008–2015.
- [38] N. V. Belkova, E. S. Shubina, A. V. Ionidis, L. M. Epstein, H. Jacobsen, A. Messmer, H. Berke, *Inorg. Chem.* **1997**, *36*, 1522–1525.
- [39] A. Messmer, H. Jacobsen, H. Berke, *Chem. Eur. J.* **1999**, *5*, 3341–3349.
- [40] A. Rossin, L. Gonsalvi, A. D. Phillips, O. Maresca, A. Lledos, M. Peruzzini, *Organometallics* **2007**, *26*, 3289–3296.

- [41] F. A. Jalon, B. R. Manzano, A. Caballero, M. C. Carrion, L. Santos, G. Espino, M. Moreno, *J. Am. Chem. Soc.* **2005**, *127*, 15364–15365.
- [42] J. Baur, H. Jacobsen, P. Burger, G. Artus, H. Berke, L. Dahlenburg, *Eur. J. Inorg. Chem.* **2000**, 1411–1422.
- [43] K. Abdur-Rashid, T. P. Fong, B. Greaves, D. G. Gusev, J. G. Hinman, S. E. Landau, A. J. Lough, R. H. Morris, *J. Am. Chem. Soc.* **2000**, *122*, 9155–9171.
- [44] N. V. Belkova, E. V. Bakhmutova, E. S. Shubina, C. Bianchini, M. Peruzzini, V. I. Bakhmutov, L. M. Epstein, *Eur. J. Inorg. Chem.* **2000**, 2163–2165.
- [45] V. I. Bakhmutov, E. V. Bakhmutova, N. V. Belkova, C. Bianchini, L. M. Epstein, D. Masi, M. Peruzzini, E. S. Shubina, E. V. Vorontsov, F. Zanobini, *Can. J. Chem.* **2001**, *79*, 479–489.
- [46] J. A. Ayllon, C. Gervaux, S. Sabo-Etienne, B. Chaudret, *Organometallics* **1997**, *16*, 2000–2002.
- [47] E. Gutsul, N. Belkova, M. Sverdllov, L. Epstein, E. Shubina, V. Bakhmutov, T. Gribanova, R. Minyaev, C. Bianchini, M. Peruzzini, F. Zanobini, *Chem. Eur. J.* **2003**, *9*, 2219–2228.
- [48] N. V. Belkova, E. I. Gutsul, E. S. Shubina, L. M. Epstein, *Z. Phys. Chem.* **2003**, *217*, 1525–1538.
- [49] G. Orlova, S. Scheiner, *J. Phys. Chem. A* **1998**, *102*, 4813–4818.
- [50] N. V. Belkova, T. N. Gribanova, E. I. Gutsul, R. M. Minyaev, C. Bianchini, M. Peruzzini, F. Zanobini, E. S. Shubina, L. M. Epstein, *J. Mol. Struct.* **2007**, *844*, 115–131.
- [51] S. Feracin, T. Buergi, V. I. Bakhmutov, I. Eremenko, E. V. Vorontsov, A. B. Vimenits, H. Berke, *Organometallics* **1994**, *13*, 4194–4202.
- [52] F. Maseras, A. Lledós, E. Clot, O. Eisenstein, *Chem. Rev.* **2000**, *100*, 601–636.
- [53] O. A. Filippov, N. V. Belkova, L. M. Epstein, E. S. Shubina, manuscript in preparation.
- [54] A. A. H. Van Der Zeijden, C. Sontag, W. Bosch, V. Shklover, H. Berke, D. Nanz, W. Von Philipsborn, *Helv. Chim. Acta* **1991**, *74*, 1194–1204.
- [55] M. Baya, P. A. Dub, J. Houghton, J.-C. Daran, R. Poli, N. V. Belkova, E. S. Shubina, L. M. Epstein, A. Lledós, *Inorg. Chem.* **2009**, *48*, 209–220.
- [56] M. Baya, O. Maresca, R. Poli, Y. Coppel, F. Maseras, A. Lledós, N. V. Belkova, P. A. Dub, L. M. Epstein, E. S. Shubina, *Inorg. Chem.* **2006**, *45*, 10248–10262.
- [57] E. T. Papish, F. C. Rix, N. Spetseris, J. R. Norton, R. D. Williams, *J. Am. Chem. Soc.* **2000**, *122*, 12235–12242.
- [58] P. A. Dub, N. V. Belkova, K. A. Lyssenko, G. A. Silantsev, L. M. Epstein, E. S. Shubina, J.-C. Daran, R. Poli, *Organometallics* **2008**, *27*, 3307–3311.
- [59] P. A. Dub, N. V. Belkova, O. A. Filippov, G. A. Silantsev, J.-C. Daran, L. M. Epstein, R. Poli, E. S. Shubina, *Eur. J. Inorg. Chem.* **2010**, 1489–1500.
- [60] M. S. Chinn, D. M. Heinekey, *J. Am. Chem. Soc.* **1990**, *112*, 5166–5175.
- [61] M. G. Basallote, M. Besora, C. E. Castillo, M. J. Fernandez-Trujillo, A. Lledós, F. Maseras, M. A. Manez, *J. Am. Chem. Soc.* **2007**, *129*, 6608–6618.
- [62] E. S. Shubina, N. V. Belkova, E. V. Bakhmutova, E. V. Vorontsov, V. I. Bakhmutov, A. V. Ionidis, C. Bianchini, L. Marvelli, M. Peruzzini, L. M. Epstein, *Inorg. Chim. Acta* **1998**, *280*, 302–307.
- [63] N. V. Belkova, E. S. Shubina, E. I. Gutsul, L. M. Epstein, I. L. Eremenko, S. E. Nefedov, *J. Organomet. Chem.* **2000**, *610*, 58–70.
- [64] N. V. Belkova, A. V. Ionidis, L. M. Epstein, E. S. Shubina, S. Gruendemann, N. S. Golubev, H. H. Limbach, *Eur. J. Inorg. Chem.* **2001**, 1753–1761.
- [65] G. Orlova, S. Scheiner, *J. Phys. Chem. A* **1998**, *102*, 260–269.
- [66] N. Avramovic, J. Hock, O. Blacque, T. Fox, H. W. Schmalle, H. Berke, *J. Organomet. Chem.* **2010**, *695*, 382–391.
- [67] B. Pleune, R. Poli, J. C. Fetting, *Organometallics* **1997**, *16*, 1581–1594.
- [68] J. Andrieu, N. V. Belkova, M. Besora, E. Collange, L. M. Epstein, A. Lledós, R. Poli, P. O. Revin, E. S. Shubina, E. V. Vorontsov, *Russ. Chem. Bull.* **2003**, *52*, 2679–2682.
- [69] N. V. Belkova, P. O. Revin, M. Besora, M. Baya, L. M. Epstein, A. Lledós, R. Poli, E. S. Shubina, E. V. Vorontsov, *Eur. J. Inorg. Chem.* **2006**, 2192–2209.
- [70] P. A. Dub, M. Baya, J. Houghton, N. V. Belkova, J. C. Daran, R. Poli, L. M. Epstein, E. S. Shubina, *Eur. J. Inorg. Chem.* **2007**, 2813–2826.
- [71] F. J. Safarowicz, D. J. Bierdeman, J. B. Keister, *J. Am. Chem. Soc.* **1996**, *118*, 11805–11812.
- [72] C. Reichardt, *Solvents and Solvent Effects in Organic Chemistry*, WILEY-VCH, Weinheim, **2003**, p. 653.
- [73] J. L. Cook, C. A. Hunter, C. M. R. Low, A. Perez-Velasco, J. G. Vinter, *Angew. Chem. Int. Ed.* **2007**, *46*, 3706–3709.
- [74] S. Gründeman, S. Ulrich, H.-H. Limbach, N. S. Golubev, G. S. Denisov, L. M. Epstein, S. Sabo-Etienne, B. Chaudret, *Inorg. Chem.* **1999**, *38*, 2550–2551.
- [75] A. G. Algarra, M. G. Basallote, M. Feliz, M. J. Fernández-Trujillo, R. Llusar, V. S. Safont, *Chem. Eur. J.* **2006**, *12*, 1413–1426.
- [76] M. G. Basallote, M. Feliz, M. J. Fernández-Trujillo, R. Llusar, V. S. Safont, S. Uriel, *Chem. Eur. J.* **2004**, *10*, 1463–1471.
- [77] P. A. Dub, N. V. Belkova, O. A. Filippov, J.-C. Daran, L. M. Epstein, A. Lledós, E. S. Shubina, R. Poli, *Chem. Eur. J.* **2010**, *16*, 189–201.
- [78] E. M. Arnett, L. Joris, E. Mitchell, T. S. S. R. Murty, T. M. Gorrie, P. v. R. Schleyer, *J. Am. Chem. Soc.* **1970**, *92*, 2365–2377.
- [79] M. C. S. Lopes, H. W. Thompson, *Spectrochim. Acta A* **1968**, *24*, 1367–1383.
- [80] P. E. Blatz, J. A. Tompkins, *J. Am. Chem. Soc.* **1992**, *114*, 3951–3956.
- [81] M. I. Page, W. P. Jencks, *Proc. Natl. Acad. Sci. USA* **1971**, *112*, 1678–1683.
- [82] N. S. Golubev, I. G. Shenderovich, S. N. Smirnov, G. S. Denisov, H. H. Limbach, *Chem. Eur. J.* **1999**, *5*, 492–497.
- [83] C. A. Hunter, H. L. Anderson, *Angew. Chem. Int. Ed.* **2009**, *48*, 7488–7499.
- [84] I. G. Shenderovich, A. P. Burtsev, G. S. Denisov, N. S. Golubev, H.-H. Limbach, *Magn. Reson. Chem.* **2001**, *39*, S91–S99.
- [85] T. W. Richards, J. W. Shipley, *J. Am. Chem. Soc.* **1919**, *41*, 2002–2012.
- [86] S. O. Morgan, H. H. Lowry, *J. Phys. Chem.* **1930**, *34*, 2385–2432.

Received: May 17, 2010
Published Online: July 13, 2010

Copper(I) Trinuclear Phosphorescent Complexes with Tuneable Optical and Photophysical Properties

Inmaculada Andrés-Tomé,^[a] Christopher J. Winscom,^[a] and Paolo Coppo^{*[a]}

Dedicated to Professor Luisa De Cola on the occasion of her 50th birthday

Keywords: Luminescence / Copper / OLEDs / Alkyne ligands / Phosphane ligands

Novel Cu^I trinuclear complexes carrying a range of alkynyl ligands with different electronic structure have been prepared. They have high quantum yields of photoluminescence. The energy, as well as the lifetime of the triplet state emission, can be tuned to a large extent by careful choice of

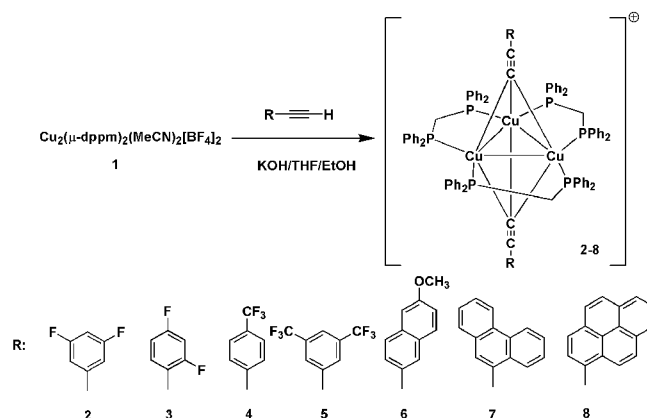
the alkynyl ligand, making these complexes suitable candidates for application either in optoelectronic devices or in time-resolved and gated luminescence detection. The nature of the excited state has been identified as a metal-to-ligand charge transfer (MLCT) state.

Introduction

Phosphorescent Cu^I coordination complexes have attracted increasing interest for various applications ranging from organic light emitting devices (OLEDs) to biological sensors.^[1] Copper is potentially more attractive than other well-established phosphorescent metal complexes, based on rare iridium(III), ruthenium(II) or osmium(II), in view of its wide availability. Among the drawbacks of copper(I) complexes, there is the relatively low quantum yield of photoluminescence as compared with those of iridium(III) cyclometallated coordination species. Trinuclear Cu^I coordination complexes with phosphane and conjugated alkynyl ligands have been investigated as potential phosphorescent soluble materials, and very effective synthetic protocols have been developed.^[2] A range of alkynyl-coordinated trinuclear Cu^I complexes have been reported over the years with emission ranging along the visible spectrum, but the photoluminescence efficiency has so far been elusive, relative to other transition metals.^[3] In this work, we report on new alkynyl-bridged coordination complexes based on copper(I) diphenylphosphanyl, showing high quantum yields of photoluminescence, over a tuneable emission range within the visible region, and phosphorescence lifetimes ranging from 10⁻⁵ up to 10⁻³ seconds.

Results and Discussion

Synthesis of coordination complexes **2–8** was performed according to the procedure published by Yam et al.^[3] The complexes, purified by recrystallisation in diethyl ether/hexanes mixtures, were obtained in yields varying from as low as 7% up to 98%. Such a large difference in the yields could be due to steric hindrance of the large CF₃ groups for complexes **4** and **5** and to the bulky pyrene units for complex **8**. In all cases sub-millimeter, needle-shaped crystals were obtained, unsuitable for single-crystal X-ray diffraction. We therefore assumed the crystal structure to be consistent with previous reports on similar complexes.^[2b,4] Solution NMR spectrometry of these complexes in deuterated chloroform confirmed their structure and composition as drawn in Scheme 1. Interestingly, ¹⁹F NMR spectroscopy revealed



[a] Wolfson Centre for Materials Processing and Centre for Phosphors and Display Materials, Brunel University, Kingston Lane, UB8 3PH, Uxbridge, United Kingdom
Fax: +44-18-9526-9737

E-mail: paolo.coppo@brunel.ac.uk

Supporting information for this article is available on the WWW under <http://dx.doi.org/10.1002/ejic.201000514>.

Scheme 1. Synthetic procedure for the preparation of complexes **2–8**.

that the complexes retain the original BF_4 counterion, in spite of being prepared in the presence of a large excess of OH^- . Integration of the signal for complexes **2–5** confirmed an almost quantitative retention of the counterion. NMR spectra could not be recorded for complex **8**, because of its low stability in solution. All complexes are readily soluble in common organic solvents, such as dichloromethane, tetrahydrofuran and toluene, and they can be processed in combination with PMMA to obtain luminescent polymer films. The complexes were prepared with the aim to investigate two separate effects. On the one hand, complexes **2–5** carry electron-withdrawing substituents on the phenyl ring, which have proved to contribute significantly to a shift of the emission energy towards higher frequencies, as in the case of cyclometallated iridium(III) complexes.^[5] Complexes **6–8** on the other hand, were prepared with the aim to extend the π -conjugated system on the alkynyl ligand. An MLCT excited state centred on larger aromatic systems is expected to be stabilised, resulting in improved quantum yield of photoluminescence and extended lifetime. Additionally, a significant shift of the emission towards lower frequencies is to be expected for these complexes, in accordance with the literature on other transition-metal systems.^[6]

The UV/Vis absorption spectra were recorded in aerated dichloromethane solutions. Complexes **2–5** have absorption spectra in which the MLCT transition bands (ca. 325–350 nm) overlap with the stronger bands, characteristic of the conjugated system π - π^* intraligand transitions centred at approximately 250–280 nm. The molar extinction coefficients were measured in 10^{-5} M solutions and were found to be in the range of 3 – 5×10^4 , compatible with this assignment. The absorption spectra of complexes **5–8** present a further set of structured features, which, in view of their wavelength maxima (350–420 nm) and molar extinction coefficient (2 – 3×10^4), can be assigned to MLCT transition bands. Consistent with other high-quantum-yield organometallic phosphorescent complexes, the low-energy absorption into the $^3\text{MLCT}$ excited state is expected to be sufficiently allowed to be detectable with an extinction coefficient in the range 10^2 – 10^3 , and we conclude that it is located in the long-wavelength wing of this absorption, since no longer-wavelength absorption features are observed. The bulk of the low-energy absorption, which is into the $^1\text{MLCT}$ state, is centred at slightly shorter wavelength. This implies a relatively small singlet–triplet energy gap, that is, a small HOMO–LUMO exchange integral consistent with the long-range metal-to-ligand charge displacement of an MLCT transition. The wavelength associated with the MLCT band is, as expected, consistent with the degree of conjugation of the alkynyl ligand for these complexes.

The inset in Figure 1 presents both the emission and the absorption spectra of complex **8**, the most structured example, as a frequency representation. These spectra have been first subjected to Multiple Even Derivative Sharpening (MEDS). This is a technique that cumulatively improves the resolution whilst suppressing the extraneous features that accompany higher-derivative representations, and it has been successfully applied to absorption spectra of photo-

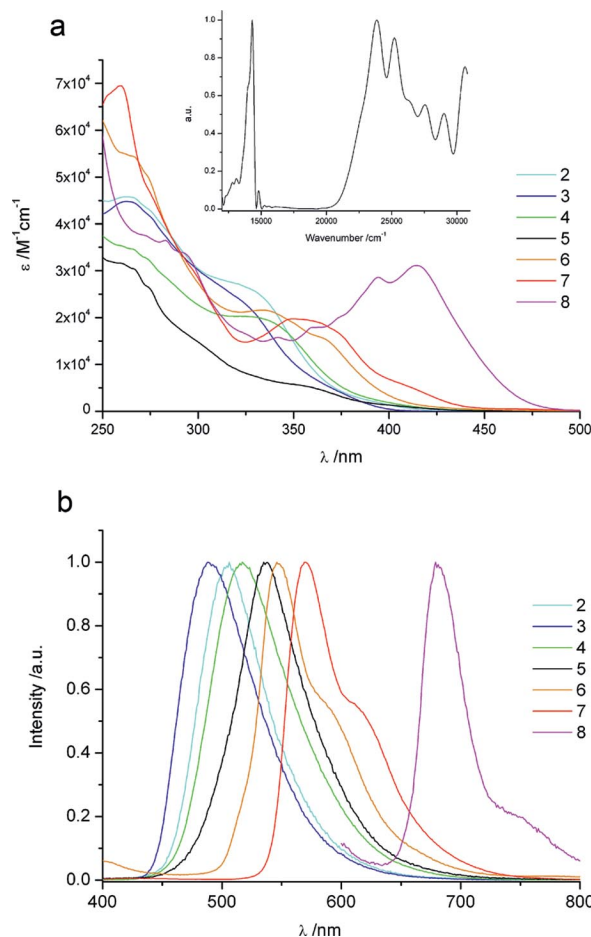


Figure 1. (a) Absorption spectra and molar extinction coefficients of complexes **2–8**. Inset: MEDS-sharpened absorption and emission spectra of complex **8** in wavenumber units (cm^{-1}). (b) Emission spectra of complexes **2–8** in degassed dichloromethane solutions.

graphic dyes.^[7a,7b] Repetitive incremental improvements [Equation (1)] are applied.

$$S_{\text{new}}(\lambda) = N \{ c_0 S + c_2 (d^2 S / d\lambda^2) + c_4 (d^4 S / d\lambda^4) + \dots + c_{2n} (d^{2n} S / d\lambda^{2n}) \} \quad (1)$$

In Equation (1), S and S_{new} are the old and improved spectra, N is a normalising constant, and the coefficients of the linear combination c_0, c_2, \dots, c_{2n} are chosen to provide near-cancellation of the higher-derivative features in the wings of a fundamental lineshape. Typical resolution enhancements factors of 1.3 – $2.0 \times$ can be safely achieved without introduction of artefacts. Finally, the spectra have been converted from wavelength to frequency representation. (In passing, we mention that frequency conversion followed by MEDS yields the same end result.) Comparing these enhanced emission and absorption spectra for complex **8** in the frequency domain clearly shows that the vibrational progressions are distinctly different in each case. Dominant vibrational modes have associated normal coordinates with a strong representation in those structural regions of the molecule where the greatest geometrical change occurs in going from the initial to the final electronic state. In the example (complex **8**), the geometrical change in go-

ing from the ground state to the excited state in absorption is thus not mirrored by the geometrical change in the reverse situation in emission from the excited state to the ground state. This provides clear supporting evidence that another geometrical change occurs whilst in the excited state, consistent with the Stokes shift behaviour discussed below. UV/Vis absorption spectra of complexes **2–8** in PMMA films do not show significant variations, when compared to the solution ones (see Supporting Information).

Emission spectra for complexes **2–8** were recorded in dilute dichloromethane solutions. Attempts to record spectra in acetonitrile resulted in irreproducible results, possibly due to poor stability in such a highly nucleophilic solvent. Air-saturated dichloromethane solutions at room temperature do not show appreciable luminescence, clearly indicating the triplet nature of the emission. Conversely, thoroughly degassed solutions show broad, unstructured emission spectra, characteristic of MLCT excited states decays. Large Stokes shifts were observed for complexes **5–8**, consistent with a spatial rearrangement of the metal cluster in the excited state. Charge transfer from Cu^I to the alkynyl ligand results in a geometrically relaxed Cu^{II}-like excited state.^[8] Complex **8**, in particular, shows a Stokes shift, measured between a maximum centred in the high-wavelength wing of the MLCT absorption band and the emission maximum of approximately 200 nm, as an indication of a large rearrangement occurring in the charge transfer state. Complexes **2–5** show emission λ_{max} values in the range 490–527 nm. The effect of electron-withdrawing groups on the phenyl ring does not contribute to a hypsochromic shift in the emission spectrum, as 490 nm is the maximum of the emission in an analogous trinuclear complex with an unsubstituted ethynylbenzene ligand. This result is somewhat surprising, as fluorine-containing ligands are known to shift the emission dramatically in iridium(III) cyclometallated complexes, up to 60 nm towards lower wavelengths.^[5] It is likely that in the case of ethynylbenzene ligands, the substitutions are too far from the metal centre to produce any major effect. In contrast, complexes **4** and **5**, bearing CF₃ groups, appear significantly lower in the emission energy. The excited-state lifetime of degassed solutions of complexes **2–5** range from 35 to 105 μs , which is consistent with existing literature on similar complexes.^[3] Single-exponential decays were observed for all the complexes measured (see Table 1). Quantum yields were measured for these complexes, with quinine sulfate in 1 N H₂SO₄ as standard reference. The effect of fluorine atoms on the ring appear to be beneficial, as all the quantum yields for complexes **2–5** appear to greatly exceed that measured for an unsubstituted ethynyl benzene trinuclear complex. Complex **5** in particular has a quantum yield of 57%, which is comparable with those of the best iridium(III) cyclometallated coordination complexes and offers a promising prospect with regard to applications in light-emitting devices. The trifluoromethyl groups are likely to provide greater shielding towards solvent quenching of the excited state. Complexes **6–8**, in which a large π -conjugated system is attached to the ethynyl functionality, show emissions ranging

from 547 to 680 nm. As expected, the presence of an extended conjugated system results in a large energy shift towards higher wavelengths, tailing in the near-infrared region for complex **8**. Interestingly, the excited-state lifetimes for these complexes are one order of magnitude longer, when compared to those of complexes **2–5**. Complex **7** in particular, shows an emission lifetime of approximately 1 ms, comparable with that of lanthanides, like Eu³⁺. Such extended lifetime is an indication of a stabilised excited state, consistent with the presence of a charge-transfer-type excited state. The quantum yields are, however, comparable with those of complexes **2–5**, implying that nonradiative relaxation has not increased in spite of the lower energy of these MLCT excited states.

Table 1. Maximum emission wavelength, quantum yield of photoluminescence (vs. quinine bisulfate) and lifetime of complexes **2–8** in degassed dichloromethane solutions.

Complex	λ_{max} /nm	Φ	τ / μs
2	507	0.240	105
3	490	0.017	35
4	519	0.144	67
5	527	0.574	88
6	547	0.273	525
7	570	0.199	976
8	678	N.A.	216

Conclusions

A wide range of emission colours can be achieved in trinuclear Cu^I coordination complexes by using alkynyl ligands with different electronic properties. Interestingly, even the lifetime of the emission can be tuned up to the millisecond region, by choosing a highly conjugated alkynyl ligand, for applications in time-resolved detection. The nature of the excited state in these complexes has been assigned to a MLCT State.

Experimental Section

Complexes **2–8** were prepared according to the literature, as shown in Scheme 1.^[3] To a tetrahydrofuran solution (40 mL) of complex **1** (0.87 mmol) was added the corresponding alkynyl ligand **R** (1.17 mmol) in portions, in the presence of an excess of KOH. The mixture was stirred at room temperature for 24 h under an inert atmosphere. The solutions were filtered and allowed to dry. The crude products were purified by dissolving them in a small amount of dichloromethane (5 mL) and precipitating them from mixtures of hexane and diethyl ether. The precipitation was repeated twice. The products were vacuum-filtered and allowed to dry in air. Yield: **2**: 98%, **3**: 72%, **4**: 30%, **5**: 34%, **6**: 93%, **7**: 63% and **8**: 7%.

Complex 2: ¹H NMR in CDCl₃: δ = 7.04–7.11 (m, 36 H), 6.95 (tt, J_1 = 8.9, J_2 = 2.3 Hz, 2 H), 6.86 (t, J = 7.5 Hz, 24 H), 6.77 (td, J_1 = 5.9, J_2 = 2.3 Hz, 4 H), 3.08 (s, 6 H) ppm. ¹⁹F NMR in CDCl₃: δ = –108.78, –154.69 ppm. ¹³C NMR in CDCl₃: δ = 163.20 (C-F), 132.62, 132.11, 130.19, 128.51, 113.90, 103.85, 27.54 ppm. C₉₁H₇₂BCu₃F₈P₆ (1704.84): calcd. C 64.11, H 4.26; found C 63.90, H 4.33.

Complex 3: ^1H NMR in CDCl_3 : $\delta = 7.13$ (dt, $J_1 = 8.7$, $J_2 = 2.3$ Hz, 2 H), 6.99–7.09 (m, 36 H), 6.92 (dt, $J_1 = 8.7$, $J_2 = 2.3$ Hz, 2 H), 6.79 (t, $J = 7.5$ Hz, 24 H), 3.12 (s, 6 H) ppm. ^{19}F NMR in CDCl_3 : $\delta = -105.36$, -107.04 , -154.31 ppm. ^{13}C NMR in CDCl_3 : $\delta = 162.86$ (C-F), 161.91 (C-F), 134.62, 132.71, 132.34, 129.88, 128.30, 111.90, 104.60, 27.34 ppm. $\text{C}_{91}\text{H}_{72}\text{BCu}_3\text{F}_6$ (1704.84): calcd. C 64.11, H 4.26; found C 64.02, H 4.35.

Complex 4: ^1H NMR in CDCl_3 : $\delta = 7.69$ (d, $J = 8.0$ Hz, 4 H), 7.37 (d, $J = 8.0$ Hz, 4 H), 7.05–7.11 (m, 36 H), 6.83 (t, $J = 7.5$ Hz, 24 H), 3.10 (s, 6 H) ppm. ^{19}F NMR in CDCl_3 : $\delta = -62.23$, -154.31 ppm. ^{13}C NMR in CDCl_3 : $\delta = 132.67$, 132.21, 131.31, 130.39, 130.11, 129.98, 129.10 (C-F), 128.46, 125.77, 27.60 ppm. $\text{C}_{93}\text{H}_{74}\text{BCu}_3\text{F}_{10}\text{P}_6$ (1768.88): calcd. C 63.15, H 4.22; found C 62.88, H 4.29.

Complex 5: ^1H NMR in CDCl_3 : $\delta = 8.01$ (s, 2 H), 7.45 (s, 4 H), 7.01–7.19 (m, 36 H), 6.90 (t, $J = 7.5$ Hz, 24 H), 3.11 (s, 6 H) ppm. ^{19}F NMR in CDCl_3 : $\delta = -62.15$, -151.25 ppm. ^{13}C NMR in CDCl_3 : $\delta = 133.27$, 132.27, 131.01, 130.06, 128.93, 128.68, 126.95, 125.24, 124.24, 123.94, 122.72, 121.51, 118.79, 26.28 ppm. $\text{C}_{95}\text{H}_{72}\text{BCu}_3\text{F}_{16}\text{P}_6$ (1904.87): calcd. C 59.90, H 3.81; found C 59.71, H 3.93.

Complex 6: ^1H NMR in CDCl_3 : $\delta = 8.05$ (d, $J = 8.3$ Hz, 2 H), 7.97 (d, $J = 8.3$ Hz, 2 H), 7.86 (s, 2 H), 7.68 (d, $J = 8.3$ Hz, 2 H), 7.58 (d, $J = 8.4$ Hz, 2 H), 7.36 (s, 2 H), 3.90 (s, 6 H), 3.09 (s, 6 H) ppm. $\text{C}_{101}\text{H}_{84}\text{BCu}_3\text{F}_4\text{O}_2\text{P}_6$ (1793.06): calcd. C 67.65, H 4.72; found C 67.38, H 4.84.

Complex 7: ^1H NMR in CDCl_3 : $\delta = 9.02$ (d, $J = 8.3$ Hz, 2 H), 8.93 (d, $J = 8.5$ Hz, 2 H), 8.77 (d, $J = 8.5$ Hz, 2 H), 8.00 (t, $J = 7.5$ Hz, 2 H), 7.92 (s, 2 H), 7.88 (t, $J = 7.5$ Hz, 2 H), 7.66 (d, $J = 8.0$ Hz, 2 H), 7.61 (t, $J = 7.5$ Hz, 2 H), 6.98–7.08 (m, 36 H), 6.69 (t, $J = 7.5$ Hz, 24 H), 3.17 (s, 6 H) ppm. ^{13}C NMR in CDCl_3 : $\delta = 132.77$, 132.12, 131.68, 131.33, 130.88, 130.31, 129.77, 128.96, 128.43, 128.10, 127.94, 127.84, 127.73, 127.53, 123.40, 121.99, 26.44 ppm. $\text{C}_{107}\text{H}_{84}\text{BCu}_3\text{F}_4\text{P}_6$ (1833.12): calcd. C 70.11, H 4.62; found C 69.70, H 4.77.

Supporting Information (see footnote on the first page of this article): lifetime decay curves; absorption spectra of the complexes in PMMA; emission spectra of the complexes in PMMA; details of ^1H NMR spectra.

Acknowledgments

Dr Peter Meadows and Dr Naoyuki Fujii (JEOL UK) are gratefully acknowledged for providing the NMR spectroscopic facilities for these studies.

- [1] a) Q. Zhang, J. Ding, Y. Cheng, L. Wang, Z. Xie, X. Jing, F. Wang, *Adv. Funct. Mater.* **2007**, *17*, 2983–2990; b) O. Moudam, A. Kaeser, B. Delavaux-Nicot, C. Duhayon, M. Holler, G. Accorsi, N. Armaroli, I. Ségué, J. Navarro, P. Destruel, J.-F. Nierengarten, *Chem. Commun.* **2007**, 3077–3079; c) Q. Zhang, Q. Zhou, Y. Cheng, L. Wang, D. Ma, X. Jing, F. Wang, *Adv. Funct. Mater.* **2006**, *16*, 1203–1208; d) N. Armaroli, G. Accorsi, M. Holler, O. Moudam, J.-F. Nierengarten, Z. Zhou, R. T. Wegh, R. Welter, *Adv. Mater.* **2006**, *18*, 1313–1316; e) Q. Zhang, Q. Zhou, Y. Cheng, L. Wang, D. Ma, X. Jing, F. Wang, *Adv. Mater.* **2004**, *16*, 432–436.
- [2] a) N. J. Long, C. K. Williams, *Angew. Chem. Int. Ed.* **2003**, *42*, 2586–2617; b) V. Wing-Wah Yam, W.-K. Lee, T.-F. Lai, *Organometallics* **1993**, *12*, 2383–2387; c) J. Diez, P. Gamasa, J. Gimeno, E. Lastra, A. Aguirre, S. Garcia-Granda, *Organometallics* **1993**, *12*, 2213–2220.
- [3] V. Wing-Wah Yam, W. Kit-Mai Fung, M.-T. Wong, *Organometallics* **1997**, *16*, 1772–1778.
- [4] V. Wing-Wah Yam, K. Kam-Wing Lo, K. Man-Chung Wong, *J. Organomet. Chem.* **1999**, *578*, 3–30.
- [5] a) P. Coppo, E. A. Plummer, L. De Cola, *Chem. Commun.* **2004**, 1774–1775; b) E. Orselli, G. S. Kottas, A. E. Konradsson, P. Coppo, R. Fröhlich, L. De Cola, A. van Dijken, M. Buchel, H. Börner, *Inorg. Chem.* **2007**, *46*, 11082–11093.
- [6] A. Tsuboyama, H. Iwawaki, M. Furugori, T. Mukaide, J. Kamatani, S. Igawa, T. Moriyama, S. Miura, T. Takiguchi, S. Okada, M. Hoshino, K. Ueno, *J. Am. Chem. Soc.* **2003**, *125*, 12971–12979.
- [7] a) C. K. Parmar, G. Rumbles, C. J. Winscom, *Phys. Chem. Chem. Phys.* **2005**, *7*, 1815–1823; b) C. K. Parmar, “Spectroscopic and Light Stability Behaviour of Photographic Dyes at Oil-Aqueous Interfaces” PhD Thesis, Imperial College, London, **2002**, pp. 28–31, pp. 69–76.
- [8] M. Ruthkosky, C. A. Kelly, F. N. Castellano, G. J. Meyer, *Coord. Chem. Rev.* **1998**, *171*, 309–322.

Received: May 10, 2010

Published Online: June 30, 2010

Reversible, Fine Performance Tuning of an Organometallic Molecular Wire by Addition, Ligand Replacement and Removal of Dicobalt Fragments

Yuya Tanaka,^[a] Takashi Koike,^[a] and Munetaka Akita*^[a]

Keywords: Metal–metal interactions / Mixed-valent compounds / Molecular devices / Molecular wires / Organometallic compounds

Communication between the two iron centres in (dithienylethyne)diyl complex **1** can be finely tuned by reversible addition to, ligand replacement at and removal of the C≡C moiety in **1** of dicobalt fragments $\text{Co}_2(\text{CO})_n(\text{PR}_3)_{6-n}$. Performance analysis reveals that disparate mechanisms are in oper-

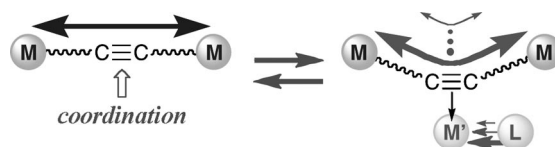
ation for the two systems. In the case of the dicobalt adducts, indirect communication via the dicobalt steppingstone can be finely tuned by controlling the electronic structure of the dicobalt unit.

Introduction

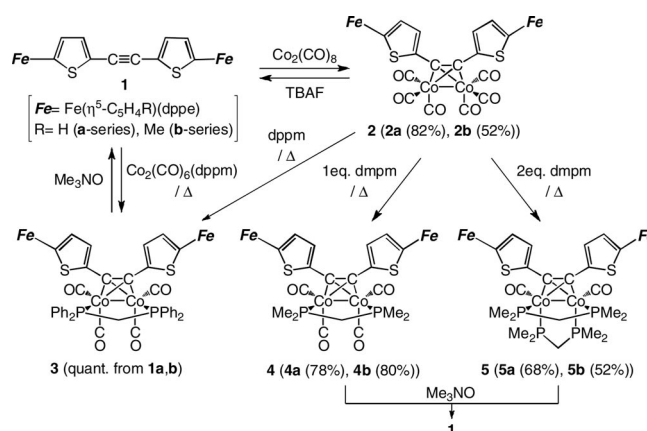
Downsizing is one of key issues in modern electronic science and industry,^[1] and, as one of effective bottom-up strategies for this issue, molecular electronics has attracted increasing attention. If functions of an electronic circuit can be represented by a combination of molecular components, one would be able to obtain a circuit miniaturized to a minimal level. A number of studies have been conducted toward this goal, and, in organic-based systems, π -conjugated systems play central roles as devices carrying electrons and holes.^[2] Furthermore, combination with metal fragments renders the systems more sophisticated, thanks to their unique properties such as redox and magnetic features. Organometallic molecular wires consisting of redox-active metal centres connected by a π -conjugated bridge have been studied extensively; as a result, many excellent molecular wires with strongly interacting metal centres (e.g. polyyne diyl complexes) have been developed so far.^[3] In addition to the most basic component, that is, wires, fine tuning of the electronic communication between two or more remote redox-active sites is demanded to develop molecular parts such as switches, resistors and diodes.^[4] Recently, efficient ON/OFF-type *switches* based on photo-, pH- and ionochromic linkers have been developed by several research groups including our group.^[5–7]

Herein we describe reversible, fine tuning of the performance of an acetylene-based diiron molecular wire (Scheme 1). To achieve the desired functions, the molecule should be stable in at least three different states that can be interconverted to each other. We have chosen “coordina-

tion” to control the communication between the two metal centres (Scheme 1) and picked up an acetylene-based diiron molecular wire, **1** (Scheme 2), in which (i) the communication may be controlled by addition of dicobalt species to the C≡C moiety and (ii) the effects brought about by the dicobalt fragment can be further finely tuned by introducing appropriate ligands to it. The present study has also revealed that different communication mechanisms operate for **1** and its dicobalt adducts.



Scheme 1. Reversible, fine tuning of metal–metal interaction.



Scheme 2. Synthesis of dicobalt adducts of **1**.

[a] Chemical Resources Laboratory, Tokyo Institute of Technology, R1-27, 4259 Nagatsuta, Midori-ku, Yokohama 226-8503, Japan Fax: +81-45-924-5230

E-mail: makita@res.titech.ac.jp

Supporting information for this article is available on the WWW under <http://dx.doi.org/10.1002/ejic.201000661>.

Results and Discussion

A diiron complex with the (dithienylethyne)diyl bridge, $[Fe-Th-C\equiv C-Th-Fe]$ (**1**) ($\{Fe = Fe(\eta^5-C_5H_4R)(dppe)\}$; $R = H$ (**a**-series), Me (**b**-series); $Th =$ thiophene-2,5-diyl}, was prepared by lithiation of bis(thien-2-yl)ethyne followed by metalation with $I-Fe(\eta^5-C_5H_4R)(CO)_2$ and photochemical ligand substitution with $dppe$.^[8] (The **b**-series derivatives were prepared in order to avoid the solubility problem.) X-ray crystallographic analysis of **1b** (Figure 1) reveals the coplanar conformation of the two thiophene rings and an $Fe\cdots Fe$ separation of 12.7 Å.^[9] Cobalt adducts **2** and **3** were obtained by reaction of **1** with $[Co_2(CO)_8]$ and $[Co_2(CO)_6(dppm)]$, respectively, in thf at room temperature.^[10] Ligand replacement of **2** with bidentate phosphanes $[R'_2PCH_2PR'_2]$; $R' = Ph(dppm)$, $Me(dmpm)$ gave the mono- (**3**, **4**) and disubstituted (**5**) products. All complexes show single sets of NMR spectroscopic signals for the $\eta^5-C_5H_4R$ (1H) and $dppe$ ligands (^{31}P) at room temperature, indicating symmetrical structures for **1–5** and the occurrence of fluxional behaviour of the ligands attached to the Co centres in **3–5**.

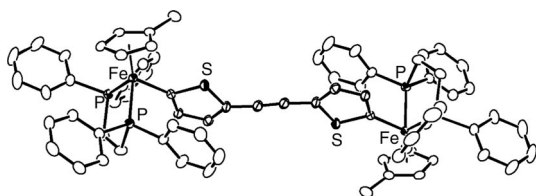


Figure 1. An ORTEP view of **1b** drawn with thermal ellipsoids at the 30% probability level. Hydrogen atoms are omitted for clarity.

Electron densities at the Fe and Co centres are estimated by CV and IR spectroscopic measurements. Two Fe-centred redox waves appear in the range -1200 to -400 mV (Table 1).^[11] Attachment of the $Co_2(CO)_6$ fragment to **1a** causes slight anodic shifts of $E_{1/2}^{Fe1}$ and $E_{1/2}^{Fe2}$ (the first and second redox potential for the iron centres, respectively), whereas ligand replacement of the resultant adduct **2a** by the electron-donating diphosphane ligands causes significant cathodic shifts of $E_{1/2}^{Fe1}$ and $E_{1/2}^{Fe2}$ (increasing order of the electron densities at the Fe centres: **2a** < **3a** < **4a** < **5a**) in accord with the increasing order of the electron densities at the dicobalt centres estimated on the basis of

the shifts of the CO vibrations to lower energies [ν_{CO} (KBr): 2067, 2033, 2001 (**2a**), 2009, 1984, 1957 (**3a**), 2001, 1972, 1945 (**4a**), 1898 (**5a**) cm^{-1}] as well as the cathodic shifts of the Co-centred redox processes ($E_{1/2}^{Co}$).

Communication performance of the obtained complexes is evaluated on the basis of IVCT bands (MMCT appearing in the near IR region) of *1e*-oxidized monocationic species.^[12] In particular, the V_{ab} coupling value, which is derived from the spectral parameters of the IVCT bands, represents the extent of electronic interaction between the two redox-active metal centres.^[12c] A high-performance organometallic molecular wire shows a large V_{ab} value associated with an intense, sharp IVCT band (with a large ϵ_{max} and a small $\nu_{1/2}^{exp}$).^[12a] Prior to the determination of the V_{ab} value, it is essential to classify the compound into one of three classes (Robin–Day Classes I–III), because different equations are applied to obtain the V_{ab} value (see footnotes [c,d] of Table 1); two V_{ab} values for Class II and III compounds are shown in Table 1.^[13] For the Robin–Day classification, solvent dependency and half-height width of the IVCT band are critical factors.^[12c] For a high-performance Class III compound, (1) the absorption maximum (ν_{max}) of the IVCT band is little affected by the solvent polarity, and (2) the half-height width thereof ($\nu_{1/2}^{exp}$) is narrower than the value predicted on the basis of the Hush theory ($\nu_{1/2}^{calc}$). Comparison of the performances of compounds belonging to different classes should be made with care by taking into account the above-mentioned factors. Monocationic complexes **1a**⁺, **3a**⁺, **4a**⁺ and **5a**⁺ were obtained by chemical 1e-oxidation of the corresponding neutral complexes with 1 equiv. of $[FeCp_2][PF_6]$, whereas the thermodynamically less stable **2a**⁺ was generated in situ by comproportionation of the isolable neutral (**2a**) and dicationic species (**2a**²⁺).^[8]

Complex **1a**⁺ shows intense NIR bands in the region 3000–8000 cm^{-1} (Figure 2a), which are attributed to the Fe-to-Fe IVCT bands, as noted for the related $Fe(\eta^5-C_5R_5)(dppe)$ complexes.^[3a,14] These NIR bands have been successfully deconvoluted into three Gaussian curves, of which the most intense, lowest energy band (band I; $\nu_{max} = 4240$ cm^{-1}) is used for the determination of V_{ab} .^[3a,14] Because (1) ν_{max} of this IVCT band is little affected by the solvent polarity (less than 100 cm^{-1})^[8,12c,15] and (2) the half-height width of this band ($\nu_{1/2}^{exp} = 1220$ cm^{-1}) is signifi-

Table 1. Electrochemical and NIR data for complexes **1a–5a**.^[a]

Complex	$E_{1/2}^{Fe1}$ /mV	$E_{1/2}^{Fe2}$ /mV	$E_{1/2}^{Co}$ /mV	$\Delta E^{Co/Fe2}$ /mV	ν_{max} / cm^{-1}	ϵ_{max} / $M^{-1}cm^{-1}$	$\nu_{1/2}^{exp}$ / cm^{-1}	$\nu_{1/2}^{calc[d]}$ / cm^{-1}	$V_{ab}^{II[c]}$ / cm^{-1}	$V_{ab}^{III[d]}$ / cm^{-1}
1a	−620	−432	—	—	4240	22320	1220	3130	551	2120
2a	−595	−483	>400 [e]	>883	7650	1900	2646	4204	550	3825
3a	−736	−571	21	592	8295	5120	3562	4377	1091	4148
4a	−755	−567	−112	455	7660	5380	3086	4206	1000	3830
5a	−1039	−681	−312	369	6060	10660	2550	3741	1138	3030

[a] The CV data are for the neutral species, and the NIR spectroscopic data are for the corresponding monocationic species. Conditions for electrochemical measurements: [complex] = $\approx 1.0 \times 10^{-3}$ M, $[NBu_4^+PF_6^-] = 0.1$ M at 293 K, scan rate = 100 mV/sec. $E_{1/2}$ values are referenced against the $FeCp_2/[FeCp_2]^+$ couple. $E_{1/2}^{Fe1}$, $E_{1/2}^{Fe2}$ and $E_{1/2}^{Co}$ are the first and second redox potentials for the iron centres and the redox potential for the dicobalt centre, respectively. $\Delta E^{Co/Fe2}$ is the difference between $E_{1/2}^{Co}$ and $E_{1/2}^{Fe2}$. [b] $\nu_{1/2}^{calc}$. (in cm^{-1}) = $(2310 \cdot \nu_{max})^{1/2}$. [c] V_{ab}^{II} (estimated as a Class II compound) = $2.06 \times 10^{-2} (\nu_{max} - \epsilon_{max} \cdot \nu_{1/2}^{exp})^{1/2} \cdot r^{-1}$ (r : M \cdots M distance).^[9] [d] V_{ab}^{III} (estimated as a Class III compound) = $(1/2) \cdot \nu_{max}$. [e] The $E_{1/2}^{Co}$ process overlaps with the $Fe^{III}-Fe^{III}/Fe^{III}-Fe^{IV}$ process.

cantly narrower than the predicted value ($\nu_{1/2}^{\text{calc}} = 3130 \text{ cm}^{-1}$),^[13] it is concluded that complex **1a**⁺ falls in the Robin–Day Class III (fully delocalized system) with an V_{ab} value of 2120 cm^{-1} , and thus the two metal centres therein strongly interact with each other.

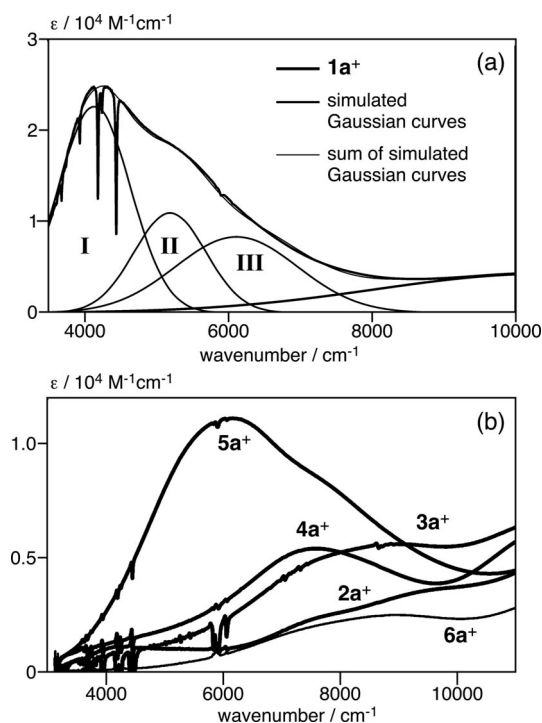


Figure 2. (a) NIR spectrum for **1a**⁺ and its deconvoluted Gaussian curves and (b) NIR spectra for **2a**⁺–**6a**⁺ (observed in CH_2Cl_2).

Cobalt adducts **2a**⁺–**5a**⁺ exhibit IVCT bands that are remarkably different from those of **1a**⁺ (Figure 2b; the absorptions at greater than 10000 cm^{-1} are LMCT bands), because of the different IVCT mechanisms (see below). For example, the IVCT bands for **2a**⁺–**5a**⁺ are considerably weaker than those of **1a**⁺, and the absorption maxima (ν_{max}) are shifted to higher energies. The order of the solvent dependency is determined to be as follows: **3a**⁺ > **4a**⁺ > **5a**⁺^[8] (**2a**⁺ can not be examined because of its low stability).

Compound **5a**⁺ has been assigned to Class IIB, although the little solvent dependency and the half-height width ($\nu_{1/2}^{\text{exp}}$) of the IVCT band narrower than $\nu_{1/2}^{\text{calc}}$ suggest its assignment to Class III. One debatable point is the considerably large $\nu_{1/2}^{\text{exp}}$ value (2550 cm^{-1}) compared to those of typical Class III compounds (e.g. **1a**⁺: 1220 cm^{-1}). Recently, this type of compounds has been categorized into the subclass “Class IIB”, as discussed by Brunshwig et al.,^[12b] that is, the electronic coupling is underestimated by the Hush treatment ($V_{\text{ab}}^{\text{II}}$) and overestimated by the Class III treatment ($V_{\text{ab}}^{\text{III}}$).^[14a]

The solvent-dependent species **2a**⁺–**4a**⁺ belong to Class II (Table 1). Complex **2a**⁺ shows the smallest $V_{\text{ab}}^{\text{II}}$ value (550 cm^{-1}). Although the $V_{\text{ab}}^{\text{II}}$ values for **3a**⁺ (1091 cm^{-1}) **4a**⁺ (1000 cm^{-1}) and **5a**⁺ (1138 cm^{-1}) are comparable, a monotonous increase of ϵ_{max} and a monotonous decrease of

$\nu_{1/2}^{\text{exp}}$ are noted for the series **2a**⁺–**5a**⁺ with the only exception of $\nu_{1/2}^{\text{exp}}$ of **2a**⁺. Because high performance is associated with an intense, sharp IVCT band (with a large ϵ_{max} and a small $\nu_{1/2}^{\text{exp}}$) leading to a large V_{ab} value, the two factors (ϵ_{max} and $\nu_{1/2}^{\text{exp}}$) are also considered to be criteria for the classification. The monotonous changes of ϵ_{max} and $\nu_{1/2}^{\text{exp}}$ and the Class III performance of **1a**⁺ discussed above (with by far the largest ϵ_{max} and smallest $\nu_{1/2}^{\text{exp}}$ values) reveal the order of the wire-like performance as follows: **1a**⁺ (Class III) >> **5a**⁺ (Class IIB) > **4a**⁺ > **3a**⁺ > **2a**⁺ (Class IIA). This order turns out to be consistent with that estimated on the basis of the ESR parameters for **1a**⁺–**5a**⁺,^[16,17] and can furthermore be correlated to the increasing order of the electron densities at the Co centres discussed above.

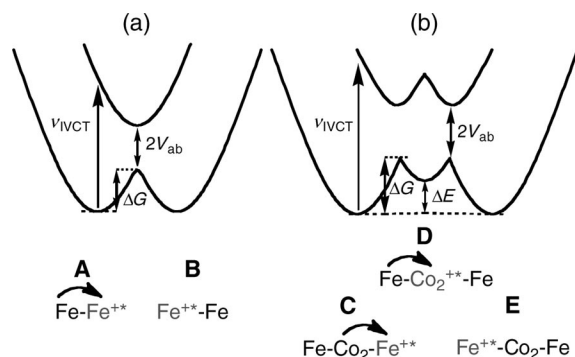
Thus, the communication between the two iron centres can be controlled by coordination of the dicobalt species to the $\text{C}\equiv\text{C}$ moiety in **1** and can be further tuned by introduction of a phosphane ligand with the appropriate electron-donating ability.

The attached dicobalt fragments in **2**–**5** can be removed upon treatment with NBu_4F or $\text{O}\leftarrow\text{NMe}_3$ (Scheme 2).^[20] Thus, the dicobalt fragment can be attached to and removed from **1** in a reversible manner. In other words, the wire-like performance of the organometallic molecular wire **1** can be controlled by addition, ligand substitution and removal of the dicobalt unit.

The significantly different features of the IVCT bands observed for **1a**⁺ and **2a**⁺–**5a**⁺ suggest disparate mechanisms operating for the two systems. The IVCT band for **1a**⁺ arises from the Fe-to-Fe MMCT, because **1a**⁺ contains the two iron centres as the unique redox-active sites. On the other hand, two pathways are feasible for the dicobalt adducts **2a**⁺–**5a**⁺, that is, the direct Fe–Fe MMCT as observed for **1a**⁺ and the indirect Fe–Co–Fe MMCT, where the dicobalt unit works like a steppingstone. Of the two mechanisms, it turns out that the latter process is at work for **2a**⁺–**5a**⁺, because monocationic species $[(\mu-\eta^2:\eta^2\text{-Fe}-\text{Th}-\text{C}\equiv\text{C}-\text{Th}-\text{H})\text{Co}_2(\text{CO})_4(\text{dppm})]$ (**6a**), a monoiron derivative of **3a**, for which *direct Fe–Fe transition is not feasible but Fe–Co transition is feasible*, has a NIR absorption band that is close in shape to that of **3a**⁺ (Figure 2b). It should be also noted that (1) ϵ_{max} of the monoiron species **6a**⁺ is about half of that of the diiron species **3a**⁺ (Figure 2b) and (2) the transition is characterized as an IVCT band as revealed by the linear relationship between ν_{max} and $(1/n^2 - 1/D_s^2)$ observed in solvents with different polarities (n and D_s are denoted by the optical and statistical dielectric constants of the solvent).^[8,21]

Electron transfer process of dinuclear species has been interpreted in terms of the diagram involving two overlapping potential energy curves.^[22] A simplified diagram for a Class II dinuclear species is shown in Scheme 3a. Photochemical excitation of the ground state A by absorption of the IVCT transition energy (ν_{IVCT}) and subsequent thermal relaxation following the potential curve finally lead to B to accomplish the electron transfer between the two iron centres. For the three-component dicobalt adducts **2**–**5**,

electron transfer can be explained by the potential energy curve diagrams shown in Scheme 3b.^[23] The IVCT transition from the ground state C followed by thermal relaxation in a manner similar to the dinuclear system leads to the intermediary state D. Subsequent thermally induced electronic transition from the other iron centre to the dicobalt unit leads to the other ground state E to accomplish the electron transfer between the two iron centres via the dicobalt unit. In this context, the energy gap (ΔE) is a key factor for the determination of V_{ab} , because a diminution of ΔE brings about an increase in the electronic coupling V_{ab} . ΔE can be experimentally estimated by the CV data, that is, ΔE is equivalent to the difference of the redox potentials for the iron and cobalt centres ($\Delta E^{\text{Co/Fe}2}$).^[24] As summarized in Table 1, the order of the $\Delta E^{\text{Co/Fe}2}$ values are **2a** > **3a** > **4a** > **5a**. Thus a compound with a small $\Delta E^{\text{Co/Fe}2}$ value gives a large V_{ab} value (**5a** > **4a** > **3a** > **2a**), in accord with the experimental results described above. As a result of these electronic effects, the communication performance (V_{ab}) of the dicobalt adducts can be finely tuned by choosing a ligand with appropriate electron-donating ability. ΔE can be correlated to the densities at the dicobalt unit, which can be estimated by $E_{1/2}^{\text{Co}}$ and ν_{CO} as discussed above; in other words, an electron-donating ligand induces better communication between the two metal centres.



Scheme 3. Energy diagrams for (a) di- and (b) tricomponent systems of Class II. V_{ab} : electronic coupling; ν_{IVCT} : IVCT transition energy; ΔE : energy gap between the Fe and Co centres; ΔG : thermal electron-transfer barrier.

Conclusions

We have succeeded in fine tuning the communication between the two metal centres in the organometallic molecular wire **1** by attachment and removal of an appropriate dicobalt fragment (Scheme 1). It is notable that: (1) the wire-like performance of the derivatives varies in the range from Robin–Day Class IIA (**2**) to Class III (**1**); and (2) **1** and the cobalt adducts **2–5** can be interconverted in a reversible and facile manner. In the case of the dicobalt adducts, the indirect communication via the dicobalt steppingstone can be finely tuned by controlling the electronic structure of the dicobalt unit.

CCDC-775289 (**1b**) contains the supplementary crystallographic data for this paper. These data can be obtained free of charge from

The Cambridge Crystallographic Data Centre via www.ccdc.cam.ac.uk/data_request/cif.

Supporting Information (see footnote on the first page of this article): Full synthetic and spectroscopic details of **1–5**.

Acknowledgments

The financial support from the Japanese government (Grants-in-Aid for Scientific Research: Nos. 18065009, 20044007 and 50167839; M. A.) and the Japan Society for the Promotion of Science (Y. T.) are gratefully acknowledged. We are also grateful to Dr. F. Paul (University of Rennes 1) for the helpful discussion on the ESR analysis.

- [1] J. Jortner, M. A. Ratner, *Molecular Electronics*, Blackwell Science, Oxford, **1997**; A. Aviram, M. Ratner, *Ann. NY Acad. Sci.* **1998**, 852; M. Ratner, *Nature* **2000**, 404, 137; B. L. Feringa (Ed.), *Molecular Switches*, Wiley-VCH, Weinheim, **2001**; J. M. Tour, *Acc. Chem. Res.* **2000**, 33, 791; N. Robertson, G. A. Mc Gowan, *Chem. Soc. Rev.* **2003**, 32, 96; M. A. Reed, T. Lee (Eds.), *Molecular Nanoelectronics*, American Scientific Publishers, Stevenson Ranch, CA, **2003**; M. C. Petty, *Molecular Electronics: From Principles to Practice*, Wiley, New York, **2008**; K. Szacilowski, *Chem. Rev.* **2008**, 108, 3481.
- [2] V. Coropceanu, J. Cornil, D. A. S. Filho, Y. Olivier, R. Silbey, J.-L. Brédas, *Chem. Rev.* **2007**, 107, 926.
- [3] a) F. Paul, C. Lapinte, *Coord. Chem. Rev.* **1998**, 178–180; F. Paul, C. Lapinte, *Coord. Chem. Rev.* **1998**, 427; b) M. I. Bruce, P. J. Low, *Adv. Organomet. Chem.* **2004**, 50, 231; c) S. Szafert, J. A. Gladysz, *Chem. Rev.* **2006**, 106, PR1; d) T. Ren, *Chem. Rev.* **2008**, 108, 4185–4207; e) M. Akita, T. Koike, *Dalton Trans.* **2008**, 3523; f) P. F. H. Schwab, M. D. Levin, J. Michl, *Chem. Rev.* **1999**, 99, 1863; g) P. F. H. Schwab, J. R. Smith, J. Michl, *Chem. Rev.* **2005**, 105, 1197.
- [4] C. Joachim, J. K. Gimzewski, A. Aviram, *Nature* **2000**, 408, 541; M. Irie, *Chem. Rev.* **2000**, 100, 1685.
- [5] S. Fraysee, C. Coudret, J.-P. Launay, *Eur. J. Inorg. Chem.* **2000**, 1581; G. Guirado, C. Christophe, J.-P. Launay, *J. Phys. Chem. C* **2007**, 111, 2770; Y. Tanaka, T. Koike, M. Akita, *Chem. Commun.* **2007**, 1169; K. Motoyama, T. Koike, M. Akita, *Chem. Commun.* **2008**, 5812; Y. Liu, C. Lagrost, K. Costuas, N. Touchar, H. Le Bozec, S. Rigaut, *Chem. Commun.* **2008**, 6117; Y. Lin, J. Yuan, M. Hu, J. Cheng, J. Yin, S. Jin, S. H. Liu, *Organometallics* **2009**, 28, 6402.
- [6] H. Tannai, K. Tsuge, Y. Sasaki, *Inorg. Chem.* **2005**, 44, 5206; C. D. Pietro, S. Campagna, M. T. Gandolfi, R. Ballardini, S. Fnni, W. R. Browne, J. G. Vos, *Inorg. Chem.* **2002**, 41, 2871; M. Haga, M. M. Ali, S. Koseki, K. Fujimoto, A. Yoshimura, K. Nozaki, T. Ohno, K. Nakajima, D. J. Stufkens, *Inorg. Chem.* **1996**, 35, 3335.
- [7] Y. Ie, T. Kawabata, T. Kaneda, Y. Aso, *Chem. Lett.* **2006**, 35, 1366.
- [8] See Supporting Information.
- [9] Crystallographic data for **1b**: $\text{C}_{78}\text{H}_{74}\text{Cl}_8\text{Fe}_2\text{P}_4\text{S}_2$ (**1b**·4CH₂Cl₂), $M_r = 1594.67$; triclinic space group $P\bar{1}$; $a = 9.3537(13)$ Å, $b = 12.1333(15)$ Å, $c = 17.988(2)$ Å; $\alpha = 81.632(6)^\circ$; $\beta = 84.916(6)^\circ$; $\gamma = 67.604(5)^\circ$; $V = 1866.1(4)$ Å³; $Z = 1$; $\rho_{\text{calcd.}} = 1.419$ g cm⁻³; $\mu = 0.860$ mm⁻¹; $\lambda = 0.71073$ Å; $T = -60$ °C; total data collected = 15426; $R1 = 0.0538$ [5126 observed reflections with $F_o^2 > 2\sigma(F_o^2)$]; $wR2 = 0.1520$ for 424 variables and all 7796 unique reflections.
- [10] Preliminary X-ray crystallographic structure analysis of **3b** revealed the equatorial coordination of the dppm ligand as well as the value of 7.34 Å (r for the dicobalt adducts; Table 1) for the average Fe...Co separation.
- [11] K_C (comproportionation constant) values are as follows: ΔE (in mV)/ $K_C = 188/1.5 \times 10^3$ (**1a**), $112/79$ (**2a**), $165/6.1 \times 10^2$ (**3a**), $189/1.5 \times 10^3$ (**4a**), and $358/1.1 \times 10^6$ (**5a**).

- [12] a) N. S. Hush, *Prog. Inorg. Chem.* **1967**, 8, 391; b) B. S. Brunshwig, C. Creutz, N. Sutin, *Chem. Soc. Rev.* **2002**, 31, 168; c) K. D. Demadis, C. M. Hartshorn, T. J. Meyer, *Chem. Rev.* **2001**, 101, 2655.
- [13] C. Creutz, H. Taube, *J. Am. Chem. Soc.* **1969**, 91, 3988.
- [14] a) S. I. Ghazala, F. Paul, L. Toupet, T. Roisnel, P. Hapiot, C. Lapinte, *J. Am. Chem. Soc.* **2006**, 128, 2463; b) F. de Montigny, G. Argouarch, K. Costuas, J.-F. Halet, T. Roisnel, L. Toupet, C. Lapinte, *Organometallics* **2005**, 24, 4558; c) Y. Tanaka, J. A. Shaw-Taberlet, F. Justaud, O. Cador, T. Roisnel, M. Akita, J.-R. Hamon, C. Lapinte, *Organometallics* **2009**, 28, 4656.
- [15] S. Stang, F. Paul, C. Lapinte, *Organometallics* **2000**, 19, 1035.
- [16] P. Hamon, F. Justaud, O. Cador, P. Hapiot, S. Rigaut, L. Toupet, L. Ouahab, H. Stueger, J.-R. Hamon, C. Lapinte, *J. Am. Chem. Soc.* **2008**, 130, 17372; T.-Y. Dong, D. N. Hendrickson, C. G. Pierpont, M. F. Moore, *J. Am. Chem. Soc.* **1986**, 108, 963.
- [17] The extent of delocalization of the radical centre over the metal- π -conjugated system can also be estimated on the basis of ESR parameters. Complex **1** displays three components of g tensors expected for pseudo-octahedral d^5 low spin Fe^{III} complexes, indicating that the radical cation is mainly localized on the iron centre on the ESR measurement time scale (ca. 10^{-9} s). The cobalt adducts show a couple of slightly broad g tensors, which also arise from Fe^{III} . The isotropic g value (g_{iso}) and the anisotropy tensor (Δg) are measures for the delocalization. The g_{iso} value is an indicator of the metal character of the SOMO,^[18] and Δg decreases as the rate of the intramolecular electron transfer increases in a homologous series of mixed-valence compounds.^[19,3a] The tendencies of the two parameters ($1\text{a}^+ < 5\text{a}^+ < 4\text{a}^+ < 3\text{a}^+ < 2\text{a}^+$) are in accord with the result obtained from the NIR spectroscopic data. $\Delta g = 0.213$ (2a^+) > 0.130 (3a^+) > 0.113 (4a^+) > 0.091 (5a^+) > 0.084 (1a^+); $g_{\text{iso}} = 2.092$ (2a^+) > 2.068 (3a^+) > 2.057 (4a^+) > 2.052 (5a^+) > 2.042 (1a^+).
- [18] F. D. Montigny, G. Argouarch, K. Costuas, J.-F. Halet, T. Roisnel, L. Toupet, C. Lapinte, *Organometallics* **2005**, 24, 4558.
- [19] T.-Y. Dong, D. N. Hendrickson, C. G. Pierpont, M. F. Moore, *J. Am. Chem. Soc.* **1986**, 108, 963.
- [20] a) D. S. Davis, S. C. Shadinger, *Tetrahedron Lett.* **1999**, 40, 7749; b) G. B. Jones, J. M. Wright, T. M. Rush, G. W. Plourde II, T. F. Kelton, J. E. Mathews, R. S. Huber, J. P. Davidson, *J. Org. Chem.* **1997**, 62, 9379.
- [21] M. J. Powers, T. J. Meyer, *J. Am. Chem. Soc.* **1978**, 100, 4393.
- [22] R. A. Marcus, N. Sutin, *Biochim. Biophys. Acta* **1985**, 811, 265.
- [23] D. M. D'Alessandro, F. R. Keene, *Chem. Rev.* **2006**, 106, 2270; Y. Zhu, O. Clot, M. O. Wolf, G. P. A. Yap, *J. Am. Chem. Soc.* **1998**, 120, 1812; B. W. Pfennig, A. B. Bocarsly, *J. Phys. Chem.* **1992**, 96, 226.
- [24] Because, in general, $E_{1/2}^{\text{Fe}^{\text{I}}}$ is significantly influenced by the wire-like performance, $E_{1/2}^{\text{Fe}^{\text{II}}}$, which is hardly affected by the wire-like performance, is used instead.

Received: June 16, 2010

Published Online: July 16, 2010

Molybdenum Dithiolene Complexes as Structural Models for the Active Sites of Molybdenum(IV) Sulfide Hydrodesulfurization Catalysts

Neilson Nguyen,^[a] Daniel J. Harrison,^[a] Alan J. Lough,^[b] Antonio G. De Crisci,^[a] and Ulrich Fekl^{*[a]}

Keywords: Molybdenum / Sulfur / Desulfurization / Heterogeneous catalysis

The removal of sulfur (as H₂S) from organosulfur species in petroleum feedstocks (hydrodesulfurization, HDS) is carried out on an enormous scale by using heterogeneous catalysts based on MoS₂ (usually doped with Co). Partially hydrogenated thiophenes are postulated intermediates in the MoS₂-catalyzed hydrodesulfurization of thiophene. The present contribution describes new molecular models for the proposed active sites in HDS catalysis. The models are derived from a mixed-ligand (push–pull) molybdenum trisdithiolene {[Mo(tfd)₂(bdt)]; tfd = S₂C₂(CF₃)₂, bdt = S₂C₆H₄}; selective intraligand alkyne binding converts the bdt group to a labile Mo-chelating benzodithiin, which can be substituted with a variety of weak donor ligands. The complexes [Mo(tfd)₂-(dht)₂] and [Mo(tfd)₂(tht)₂] (dht = 2,5-dihydrothiophene; tht =

tetrahydrothiophene) were synthesized and crystallographically characterized. The Mo(tfd)₂ substructures closely resemble the presumed active site in MoS₂ HDS catalysts. The coordination geometries at molybdenum are approximately trigonal prismatic, and the metal bears two strongly bound dithiolene (tfd) groups and two comparatively weakly bound thioether ligands (dht or tht). Competitive binding experiments establish that tht binds more strongly to the Mo center than dht ($K_{\text{eq}} = 6.5 \pm 0.5$). Preliminary reactivity studies reveal that [Mo(tfd)₂(dht)₂] decomposes to [Mo(tfd)₃], thiophene, and unidentified species upon heating. Further, [Mo(tfd)₂(tht)₂] induces the isomerization of 1,4-cyclohexadiene to 1,3-cyclohexadiene at elevated temperatures.

Introduction

As high-grade petroleum reserves dwindle, lower and lower grades of petroleum resources must be brought into service to meet the continually growing energy demands. Environmental concerns require that the sulfur content of low-grade petroleum be reduced before use.^[1] Hydrodesulfurization (HDS) processes – the removal of sulfur from organosulfur species as H₂S – utilize catalysts based on molybdenum(IV) sulfide (MoS₂; most commonly encountered as the hexagonal molybdenite, usually modified with cobalt for HDS applications) and hydrogen gas as a feedstock. As a greater and greater efficiency is being demanded of hydrodesulfurization techniques, the search for better catalysts has intensified. Of special interest is the desulfurization of thiophenes, which are less reactive in HDS than noncyclic thioethers and much-less reactive than thiols.^[2,3] Thus, the removal of sulfur from thiophenes and related “stubborn” (*refractory*) compounds (*deep desulfurization*) is a formidable challenge. While some noble metal catalysts show excel-

lent activity in deep desulfurization,^[4] the high activity of those metals is offset by their cost. Developing increasingly active Mo-based catalysts is thus a worthwhile goal, and we focus here on molecular coordination compounds of molybdenum. Heterogeneous MoS₂-based HDS catalysis has been investigated by experimental surface techniques as well as by computational (DFT) studies on cluster models.^[5–7] However, small molecular (soluble) models mimicking the active sites in molybdenite HDS catalysts are rare.^[8] Small molecule models should be useful for understanding the mechanism of HDS catalysis and could lead to the development of better catalysts.^[6] It is thought that exposed (coordinatively unsaturated) edges of MoS₂ sheets are the active sites and that the internal centers are inactive.^[9] A fragment of the molybdenite structure is shown in Figure 1, which shows internal sites, edge sites, and key metric parameters.

As shown in Figure 1, the molybdenum edge sites possess pyramidal structures, with molybdenum at the apex of a square pyramid and four sulfur atoms forming the base of the pyramid. Current evidence suggests that thiophene coordinates to the molybdenum edge sites. The coordinated thiophene then undergoes hydrogenation to 2,5-dihydrothiophene and, finally, desulfurization (through cycloreversion) of the organic moiety produces 1,3-butadiene and a terminal metal sulfide (Scheme 1).^[13] Reduction of the metal sulfide with H₂ releases H₂S and regenerates the unsaturated Mo center.

[a] University of Toronto,
3359 Mississauga Road N, Mississauga, Ontario L5L 1C6,
Canada
Fax: +1-905-828-5425
E-mail: ulrich.fekl@utoronto.ca

[b] X-ray Crystallography Lab, University of Toronto,
80 St. George St., Toronto, Ontario M5S 3H6, Canada

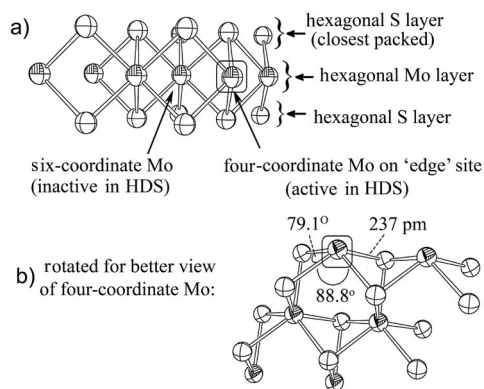
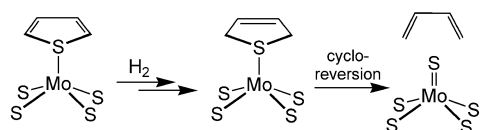


Figure 1. Views of exposed molybdenum sites in hexagonal MoS_2 ; (a) standard orientation, in which the hexagonal layers are oriented horizontally; (b) rotated to highlight the geometry^[10] of the edge sites. The picture was generated with ORTEP^[11] by using MoS_2 coordinates^[12] from the literature.



Scheme 1. Desulfurization of thiophene at a MoS_2 edge site.

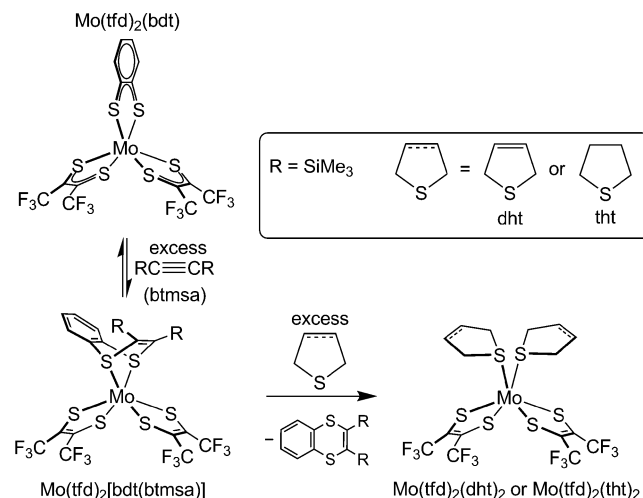
Accurate structural models of MoS_2 -based HDS catalysts should have the square-pyramidal structure (with Mo at the apex and four sulfur donors forming the basal plane) as seen for the edge sites in molybdenite. Additionally, the model should incorporate vacant (or labile) sites to bind organosulfur substrates (e.g. thiophene derivatives). While many examples of molybdenum^[14–18] (or tungsten^[19]) complexes bearing four sulfur donors are known, they usually contain additional strongly bound ligands, such as thiolates or phosphanes, which cannot be displaced by thioether groups or other weakly coordinating sulfur donors. However, they do show catalytic activity toward nitrate and formate reduction, and in that area, are showing promise as models for enzymes. On the other hand, the few truly four-coordinate MoS_4 complexes {e.g. $[\text{Mo}(\text{SR})_4]$, $\text{R} = 2,4,6$ -triisopropylbenzene} are extremely electrophilic toward small donor molecules and form a variety of MoS_4L complexes, where $\text{L} = (\text{e.g.})$ alkyne, MeCN , $t\text{BuNC}$, CO .^[20] However, these four-coordinate MoS_4 complexes have tetrahedral rather than pyramidal geometry at the metal, which makes them less desirable as model complexes for the molybdenite edge sites. Monosulfided molybdenum^[21] or tungsten^[19] species with dithiolene ligands [$^-\text{SM}(\text{S}_2\text{C}_2\text{R}_2)_2^-$] have also been produced, and they may be regarded to be excellent models for the intermediate obtained after butadiene loss (right-hand side of Scheme 1). Schrauzer et al. produced thioether complexes on tungsten-based dithiolenes by methylation of one of the dithiete ligands.^[22] $[\text{Mo}(\text{CO})_2(\text{S}_2\text{C}_2\text{Me}_2)_2]$ complexes are known and offer both the square-pyramidal MoS_4 structure as well as labile CO groups.^[19,23] While CO is a labile ligand in such complexes (as we also confirmed experimentally, see below), we pro-

vide here an alternative approach to the opening up of two labile sites at “ S_4Mo ”.

The first coordination sphere of neutral molybdenum trisdithiolenes resembles the environment of the internal (non-edge sites) molybdenum atoms in molybdenite – in both cases, the metal geometry is approximately trigonal prismatic with six sulfur-donor ligands. Our group has previously reported that mixed-ligand molybdenum trisdithiolenes $[\text{Mo}(\text{tfd})_2(\text{bdt})]$ and $[\text{Mo}(\text{bdt})_2(\text{tfd})]$ with $\text{tfd} = \text{S}_2\text{C}_2(\text{CF}_3)_2$, $\text{bdt} = \text{S}_2\text{C}_6\text{H}_4$ react with ethylene through the sulfur atoms of one bdt ligand (i.e. intraligand alkene addition) to form a metal-chelating dihydrobenzodithiin moiety.^[24] The weakly bound dihydrobenzodithiin can be substituted with a variety of nucleophiles, which allows access to new molybdenum bis- and trisdithiolene complexes. In this paper we extend this versatile method to create molybdenum bisdithiolenes with thioether ligands (partially hydrogenated thiophenes), which provide structural models for postulated intermediates in MoS_2 -based HDS catalysis.

Results and Discussion

The syntheses of our structural models exploits the ligand-based reactivity of $[\text{Mo}(\text{tfd})_2(\text{bdt})]$: treatment of the trisdithiolene with bis(trimethylsilyl)acetylene (btmsa)^[25] gave $[\text{Mo}(\text{tfd})_2\{\text{bdt}(\text{btmsa})\}]$, which was subjected to ligand substitution with excess dht or tht ($\text{dht} = 2,5$ -dihydrothiophene; $\text{tht} = \text{tetrahydrothiophene}$) to yield $[\text{Mo}(\text{tfd})_2(\text{dht})_2]$ or $[\text{Mo}(\text{tfd})_2(\text{tht})_2]$, respectively, upon loss of the metal-coordinated benzodithiin (Scheme 2, see experimental section for details). The resulting complexes were characterized by multinuclear NMR spectroscopy, elemental analysis, and X-ray crystallography. However, this approach failed to produce any complexes with *thiophene* ligand.



Scheme 2. Syntheses of $[\text{Mo}(\text{tfd})_2(\text{dht})_2]$ and $[\text{Mo}(\text{tfd})_2(\text{tht})_2]$ from $[\text{Mo}(\text{tfd})_2(\text{bdt})]$.

Figure 2 shows the crystallographically determined structures of $[\text{Mo}(\text{tfd})_2(\text{dht})_2]$ and $[\text{Mo}(\text{tfd})_2(\text{tht})_2]$. Crystallographic data are summarized in the Exp. Sect. (Table 3).

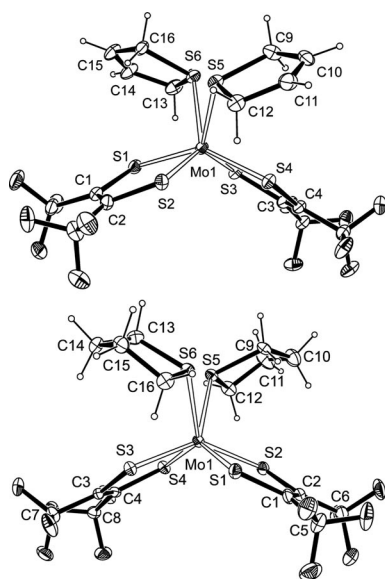


Figure 2. Top: structure of $[\text{Mo}(\text{tfd})_2(\text{dht})_2]$. Bottom: structure of $[\text{Mo}(\text{tfd})_2(\text{tht})_2]$. Non-hydrogen atoms are displayed by using 30% thermal ellipsoids.

The structures of $[\text{Mo}(\text{tfd})_2(\text{dht})_2]$ and $[\text{Mo}(\text{tfd})_2(\text{tht})_2]$ (Figure 2) are, expectedly, quite similar. In each case, the molybdenum centers are coordinated by six sulfur atoms. Two adjacent (*cis*) coordination sites are occupied by thioether ligands (dht or tht); these labile sites will possibly allow access to mechanisms utilizing two coordination sites on the same Mo atom. In $[\text{Mo}(\text{tfd})_2(\text{dht})_2]$, the π bonds of the dht ligands do not interact with the metal (i.e. dht binds in an $\eta^1\text{-S}$ fashion), consistent with experimental (NEXAFS) data for dht adsorbed on a sulfided molybdenum surface.^[26] The “locked” conformation of the thioether ligands is likely enforced by crystal packing. NMR spectroscopy (^{19}F) indicates apparent C_{2v} symmetry for $[\text{Mo}(\text{tfd})_2(\text{dht})_2]$ and $[\text{Mo}(\text{tfd})_2(\text{tht})_2]$, which indicates interconversion between ring conformers in solution. The crystal structure determinations for $[\text{Mo}(\text{tfd})_2(\text{dht})_2]$ and $[\text{Mo}(\text{tfd})_2(\text{tht})_2]$ have yielded detailed information on the sulfur environment in such species, which is very consistent across the two structures. Key structural data are summarized in Table 1. The Mo–S(tfd) bond lengths (Table 1) for $[\text{Mo}(\text{tfd})_2(\text{dht})_2]$ and $[\text{Mo}(\text{tfd})_2(\text{tht})_2]$ [average 2.335(1) Å and 2.333(1) Å, respectively] are marginally shorter than the analogous Mo–S(tfd)

Table 1. Selected structural data for $[\text{Mo}(\text{tfd})_2(\text{dht})_2]$ and $[\text{Mo}(\text{tfd})_2(\text{tht})_2]$.

		[Mo(tfd) ₂ (dht) ₂]			[Mo(tfd) ₂ (tht) ₂]
Bond lengths (Å)					
Mo–S(tfd)	Mo1–S1	2.336(2)	Mo1–S1	2.331(1)	
	Mo1–S2	2.329(2)	Mo1–S2	2.336(1)	
	Mo1–S3	2.337(2)	Mo1–S3	2.324(1)	
	Mo1–S4	2.337(2)	Mo1–S4	2.343(1)	
Mo–S(thioether)	Mo1–S5	2.520(2)	Mo1–S5	2.513(1)	
	Mo1–S6	2.520(2)	Mo1–S6	2.523(1)	
	Bond angles [°]				
S–Mo–S (tfd)	S1–Mo1–S2	81.28(6)	S1–Mo1–S2	81.50(5)	
	S3–Mo1–S4	81.76(6)	S3–Mo1–S4	81.55(5)	
S–Mo–S (thioether)	S5–Mo1–S6	75.20(6)	S5–Mo1–S6	73.85(4)	
S–Mo–S (<i>trans</i> S)	S1–Mo1–S4	142.11(6)	S3–Mo1–S2	139.92(5)	
	S1–Mo1–S5	127.77(6)	S1–Mo1–S4	138.83(5)	
	S3–Mo1–S2	137.21(6)	S3–Mo1–S5	130.58(5)	
	S3–Mo1–S5	136.69(6)	S1–Mo1–S5	133.30(5)	
	S6–Mo1–S2	134.27(6)	S2–Mo1–S6	128.73(5)	
	S6–Mo1–S4	129.85(6)	S4–Mo1–S6	135.44(5)	
Nonbonded distances [Å]					
S–S (trigonal face) inter-tfd	S1–S3	3.170(2)	S1–S3	3.117(2)	
	S2–S4	3.132(2)	S2–S4	3.167(2)	
tfd–thioether	S3–S6	3.239(2)	S3–S6	3.277(2)	
	S1–S6	3.233(2)	S1–S6	3.151(2)	
	S2–S5	3.150(2)	S2–S5	3.268(2)	
	S4–S5	3.242(2)	S4–S5	3.232(2)	
S–S (prism edge) inter-tfd	S1–S2	3.038(2)	S1–S2	3.047(2)	
	S3–S4	3.059(2)	S3–S4	3.048(2)	
inter-thioether	S5–S6	3.075(2)	S5–S6	3.026(2)	
Nonbonded angles (trigonal face) [°]					
S–S–S	S3–S1–S6	60.77(6)	S3–S1–S6	63.04(5)	
	S1–S3–S6	60.58(6)	S1–S3–S6	58.99(5)	
	S1–S6–S3	58.65(6)	S1–S6–S3	57.97(5)	
	S4–S2–S5	62.14(6)	S4–S2–S5	60.29(5)	
	S2–S4–S5	59.21(6)	S2–S4–S5	61.4(5)	
	S2–S5–S4	58.64(6)	S2–S5–S4	58.3(5)	
interplanar angle	S1–S3–S6 to S2–S4–S5	0.59(11)	S1–S3–S6 to S2–S4–S5	0.57(8)	

bonds in $[\text{Mo}(\text{bdt})_2(\text{tfd})]^{[24]}$ and $[\text{Mo}(\text{tfd})_3]^{[27]}$ [average 2.367(1) Å and 2.355(4) Å, respectively]. Particularly striking is the fact that the thioether ligands are apparently very weakly bonded, with Mo–S bond lengths that are much longer, by almost 0.2 Å, than the Mo–S(tfd) bonds. Indeed, the Mo–S(thioether) bond lengths (thioether = dht or tht, 2.51–2.52 Å) are among the longest molybdenum–sulfur bonds known.

There are few examples of structurally characterized Mo–thioether complexes available for comparison. The most similar one is the ethylene adduct $[\text{Mo}(\text{tfd})_2\{\text{bdt}(\text{CH}_2\text{CH}_2)\}]$, with an average distance of 2.523 Å to the sulfur atoms on the dihydrobenzodithiin ligand.^[24] The closest non-dithiolene-based Mo^{IV} system is an octahedral molybdenum “S₄-crown” thioether complex, with slightly shorter Mo–S(thioether) distances (2.469–2.498 Å).^[28]

Computed Mo–S distances for dht and tht bound to a Mo₃S₉ catalyst model fragment are 2.53 Å and 2.50 Å, respectively.^[29] Thus, $[\text{Mo}(\text{tfd})_2(\text{dht})_2]$ and $[\text{Mo}(\text{tfd})_2(\text{tht})_2]$ can be regarded as being structurally very similar to the active sites they are modelling.

In both compounds, the coordination geometry at molybdenum is very close to trigonal prismatic. Figure 3 shows the bond angles used to corroborate this statement. By using the three largest S–M–S_{trans} angles (Figure 3a) to position the structures on the scale ranging from perfect octahedron (0%) to perfect trigonal prism (100%),^[30] $[\text{Mo}(\text{tfd})_2(\text{dht})_2]$ and $[\text{Mo}(\text{tfd})_2(\text{tht})_2]$ were found to have 92% and 94% trigonal-prismatic character, respectively.^[31] The largest deviations^[32] in the SMS_{trans} angles were ca. 14° {for $[\text{Mo}(\text{tfd})_2(\text{dht})_2]$ } and ca. 11° {for $[\text{Mo}(\text{tfd})_2(\text{tht})_2]$ }. The triangular faces of the trigonal prisms contain S–S–S (formally nonbonded) angles very close to 60° (Figure 3b) – the largest deviation is ca. 3° in both cases (Table 1). This observation is surprising insofar as the large difference between the Mo–S(tfd) and Mo–S(thioether) bond lengths could be expected to lead to a more distorted MoS₆ substructure.

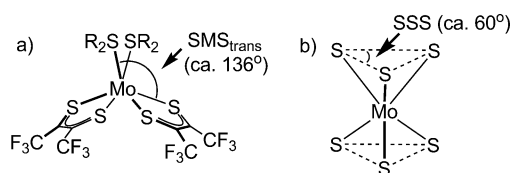


Figure 3. Bond angles used for analysis; (a) example for S–M–S_{trans} angle, (b) example for S–S–S (nonbonding) angle.

Trigonal-prismatic geometry, which maximizes ligand–metal and interligand π interactions,^[33] is quite common for high-valent (oxidized) metal trisdithiolenes (e.g. neutral group six trisdithiolenes). Reduced analogues, on the other hand, usually exhibit distortion toward octahedral geometries, thereby relieving ligand–ligand repulsion in these comparatively electron-rich systems. To illustrate, the metal geometry in neutral $[\text{Mo}(\text{tfd})_3]$ is very close to trigonal prismatic^[27] (99% by using the S–M–S_{trans} angle criterion, see above),^[31] while dianionic $[\text{Mo}(\text{tfd})_3]^{2-}$ has considerably

more octahedral character^[27] (70% trigonal prismatic).^[32] In general, trigonal-prismatic structures are more likely for complexes with low d electron counts (i.e. d^n , $n \leq 2$).^[34] This has been explicitly discussed for MoS₂ by using crystal field theory.^[35] Analogous effects have been shown computationally and experimentally for $[\text{Mo}(\text{butadiene})_3]$ complexes^[36] and computationally for $\text{M}(\text{CH}_3)_6^n$ complexes ($\text{M} = \text{Ti}, \text{Zr}, \text{Hf}, \text{V}, \text{Nb}, \text{Ta}, \text{Cr}, \text{Mo}, \text{W}, \text{Tc}, \text{Re}, \text{Ru}, \text{Os}$; $n = -2, -1, 0, +1$).^[37] The two complexes synthesized for the present study – $[\text{Mo}(\text{tfd})_2(\text{dht})_2]$ and $[\text{Mo}(\text{tfd})_2(\text{tht})_2]$ – are charge neutral and formally Mo^{IV} (d^2) species, with two ene–dithiolate donors and two neutral thioether ligands. Similarly, neutral group VI metal trisdithiolenes, such as $[\text{Mo}(\text{tfd})_3]$, can be reasonably formulated as a d^2 species, with two dianionic dithiolene ligands and one neutral, weakly donating dithioketone ligand.^[38] The trigonal-prismatic geometries observed at the metals in $[\text{Mo}(\text{tfd})_2(\text{dht})_2]$ and $[\text{Mo}(\text{tfd})_2(\text{tht})_2]$ can, therefore, be rationalized on the basis of low d electron counts and neutral charge states for both complexes, with analogy to group VI metal trisdithiolenes. The observed trigonal prismatic geometries mimic the environment of the Mo centers in molybdenum(IV) sulfide.

The S–Mo–S angles involving the thioether ligands are very acute {75.2° for $[\text{Mo}(\text{tfd})_2(\text{dht})_2]$ and 73.9° for $[\text{Mo}(\text{tfd})_2(\text{tht})_2]$ }. The S–Mo–S angles in the dithiolene chelate rings are much wider (ca. 82°) for both complexes. Interestingly, there are many examples in the literature of Mo (or W) bisdithiolene complexes with various non-dithiolene ligands that also exhibit this acute non-dithiolene ligand angle and wider dithiolene ligand bite angles. Relevant examples are summarized in Table 2. Despite a large variation in non-dithiolene ligands (which are of variable steric demand), the non-dithiolene and the dithiolene bite angles remain remarkably consistent.

This narrow non-dithiolene ligand angle is intriguing. A similar observation was made by Holm and co-workers^[39] when narrow C–M–C bond angles for $\text{M}(\text{CO})_2(\text{S}_2\text{C}_2\text{Me}_2)_2$ were observed: 83.5° for $\text{M} = \text{Mo}$ and 84.1° for $\text{M} = \text{W}$. These bond angles became smaller even more upon stepwise reduction (monoanion, dianion), down to 72.3° for the dianions. CO is, of course, a very special ligand because of its π -acceptor properties, and Fomitchev, Lim and Holm^[39] concluded that the observed effect is “suggestive of a weak bonding interaction between the carbonyl ligands”. For those ligands that are not π acceptors, ligands such as dht and tht in this work, alternative explanations are needed. The lowest-lying empty orbitals of the $\text{Mo}(\text{tfd})_2$ fragment points toward an explanation. Using density functional theory (DFT), we found that both a pseudo-tetrahedral structure and the pyramidal structure that is relevant here are minima on the hypersurface for $\text{Mo}(\text{tfd})_2$, as confirmed by geometry optimization and subsequent frequency analysis (no imaginary frequency). The pyramidal structure (uphill relative to the pseudo-tetrahedral structure by 12.3 kcal/mol) has two low-lying empty orbitals (LUMO and NLUMO), shown in Figure 4, that contain some p-orbital contribution from the sulfur atoms but are largely metal-based and correspond roughly to $d_{x^2-y^2}$ (LUMO) and d_{yz}

Table 2. A comparative sampling of bite angles (°) in bisdithiolenes with various ligands [mnt = S₂C₂(CN)₂].

	Non-dithiolene bite angle [°]	Dithiolene bite angle (av.) [°]	Trigonal-prismatic character ^[31] [%]	Deviation ^[32] [°]	Ref.
[Et ₄ N] ₂ [Mo ₂ (SCH ₂ CH ₂ OH) ₂ (mnt) ₄]	68	83	82	25	[15]
[Et ₄ N] ₂ [Mo ₂ (SPh) ₂ (mnt) ₄]	67	82	96	12	[15]
[Et ₄ N] ₂ [W ₂ (SCH ₂ Ph) ₂ (mnt) ₄]	68	83	95	10	[15]
[Et ₄ N] ₂ [W ₂ (SCH ₂ CH ₃) ₂ (mnt) ₄]	67	82	87	21	[15]
[Et ₄ N] ₂ [W ₂ (SCH ₂ CH ₂ OH) ₂ (mnt) ₄]	68	83	92	18	[15]
[Et ₄ N] ₂ [W ₂ (SPh) ₂ (mnt) ₄]	66	82	93	14	[15]
[Et ₄ N] ₂ [Mo ₂ (SCH ₂ Ph) ₂ (mnt) ₄]	67	83	91	20	[15]
[Et ₄ N] ₂ [Mo ₂ (SCH ₂ CH ₃) ₂ (mnt) ₄]	68	82	86	22	[15]
[Et ₄ N] ₂ [Mo(NCS) ₂ (mnt) ₂]	66	86	88	23	[16]
[Ph ₄ P] ₂ [W(SPh) ₂ (mnt) ₂]·0.5(CH ₃) ₂ CHOH	72	82	98	7	[15]
[Et ₄ N][Mo(PPh ₃)(NCS)(mnt) ₂]	76	83	83	21	[16]
[Et ₄ N][Mo(PPh ₃)(SC ₆ H ₄ -4-Me)(mnt) ₂]	77	82	93	10	[16]
[Ph ₃ PNPPh ₃][Mo(PPh ₃)(SC ₆ H ₄ -2-COOH)(mnt) ₂]	76	82	73	29	[16]
[Et ₄ N][Mo(SPh)(PPh ₃)(mnt) ₂]·CH ₂ Cl ₂	77	82	90	17	[17]
[PPh ₄][Mo(PPh ₃)(SCH ₂ CH ₃)(mnt) ₂]·CH ₂ Cl ₂	76	83	74	28	[18]
[PPh ₄][Mo(PPh ₃)(SCH ₂ Ph)(mnt) ₂]	77	81	94	14	[18]
[Et ₄ N][Mo(PPh ₃)(Br)(mnt) ₂]	78	83	81	23	[18]
[Mo(tfd) ₂ {bdt(CH ₂ CH ₂) ₂ }]	72	82	86	20	[24]
[Mo(tfd) ₂ (dht) ₂]	75	82	92	14	this work
[Mo(tfd) ₂ (tht) ₂]	74	82	94	11	this work

(NLUMO), where the labeling assumes that we define the paper plane to be the *xy* plane with *y* being vertical and *x* horizontal. The system will be “frustrated” every time a Lewis acid/Lewis base adduct is formed with *two* added lone-pair donors L: an L–Mo–L bond angle close to 90° would optimize overlap with the NLUMO, which, however, leads to poor overlap with the LUMO. Good overlap with the orbital that is the LUMO in Mo(tfd)₂ necessitates a narrow L–Mo–L bond angle.

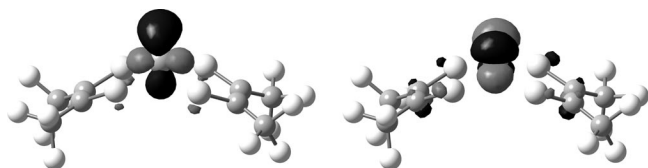


Figure 4. DFT-computed (B3LYP/SDD, see Experimental Section) low-lying molecular orbitals (Kohn–Sham orbitals; left: LUMO, –0.205 eV; right: NLUMO, –0.185 eV; plotted at 0.06 isovalue) of geometry-optimized (local minimum but not global minimum) pyramidal Mo(tfd)₂. Note the similarity of the free pyramidal fragment to the Mo(tfd)₂ substructure in [Mo(tfd)₂(dht)₂] and [Mo(tfd)₂(tht)₂], shown in Figure 2 in a similar orientation.

While the narrow bite angle described above is a deviation from a perfect trigonal-prismatic geometry, the “trigonal” planes in [Mo(tfd)₂(dht)₂] and [Mo(tfd)₂(tht)₂] are almost perfectly parallel.

If the S1–S3–S6 and S2–S4–S5 faces of both complexes are taken to define planes, the angle between the two planes is 0.59° and 0.57° for [Mo(tfd)₂(dht)₂] and [Mo(tfd)₂(tht)₂], respectively (i.e. essentially parallel as in a true triangular prism). In each triangular face, the sulfur atoms are essentially closest packed. A diagram showing the van der Waals spheres for the sulfur atoms of [Mo(tfd)₂(dht)₂] is shown in Figure 5 (the structure of the tht complex leads to a virtually identical picture). Visually, the impression of a very

symmetrical arrangement of closest-packed sulfur atoms (Figure 5A) is striking, which is quantitatively re-enforced by the very consistent nonbonded distances (Table 1).

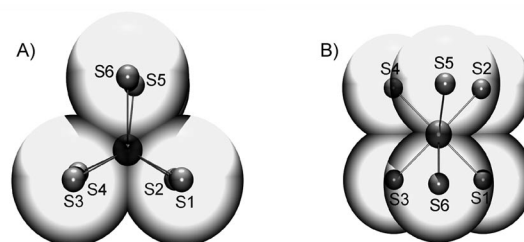


Figure 5. View of the sulfur environment of [Mo(tfd)₂(dht)₂], by using the van der Waals radii for the sulfur atoms; A: view perpendicular to S2–S3–S6 “close-packed” plane; B: view onto S5–S6 edge.

While the preference for trigonal-prismatic (instead of octahedral) geometry is electronic in origin (as is the acuteness of one S–Mo–S angle), the resulting structure is surprisingly consistent with a closest-packing model in which the two closest-packed “S₃” triangles are stacked on top of another and in which the central Mo is dislocated from the center toward the more donating sulfur atoms. In both [Mo(tfd)₂(dht)₂] and [Mo(tfd)₂(tht)₂], the sulfur atoms are found in a geometric arrangement very similar to that observed for molybdenum inside solid MoS₂, including the overlapping Van der Waals radii for adjacent sulfur centers.

Reactivity

The new complexes show some interesting and promising reactivity at slightly elevated temperatures (60–120 °C), which, unfortunately, is accompanied by decomposition. [Mo(tfd)₂(dht)₂] and [Mo(tfd)₂(tht)₂] are stable for days at room temperature in nonpolar/noncoordinating solvents

(e.g. C_6D_6), but rapidly react with coordinating solvents such as thf and acetonitrile (color change to green or red, respectively, observed immediately upon dissolution). Both complexes are somewhat unstable in chloroform, decaying within a few days at room temperature, and within 1 h at 60 °C. The decomposition products were identified by ^{19}F / 1H NMR as $[Mo(tfd)_3]$ and free thioethers (dht or tht). Presumably molybdenum metal is also deposited, as a faint darkening of the NMR tubes can be observed; this film is insoluble in organic solvents but dissolves in inorganic acids. The complexes are considerably more stable in C_6D_6 : only minor decomposition was observed after heating either complex to 60 °C for 1 d.

The complexes are sufficiently stable (in $CDCl_3$) to determine the relative binding constant of dht vs. tht with respect to coordination to the $Mo(tfd)_2$ fragment. We found that tht binds more strongly by a factor of 6.5(5) at a temperature of ca. 22 °C (Figure 6). The lesser binding affinity for dht, relative to that for tht, is likely because of the electron-withdrawing alkene group in dht, which can be expected to decrease the σ -donor ability of the thioether ligand. Substitution of dht with *thiophene* was not observed at any concentration of thiophene in $CDCl_3$ or with neat thiophene. These results can be compared to a recent computational paper by Joshi et al. in which the adsorption energies of various sulfur-containing molecules onto MoS_2 is reported.^[40] The lowest binding energies for an unsaturated molybdenum edge structure with tht and dht were found to be -1.67 eV and -1.60 eV, respectively, which corresponds to an energy difference of -6.75 kJ/mol. Our experimentally determined equilibrium constant corresponds to a difference in binding free energy of $-4.6(2)$ kJ/mol (for tht vs. dht), quite consistent with the calculated value. Joshi et al. also calculated the binding energy of thiophene to be -1.04 eV, compared with -1.60 eV for dht (difference: -0.56 eV or -54 kJ/mol). This energy difference would yield

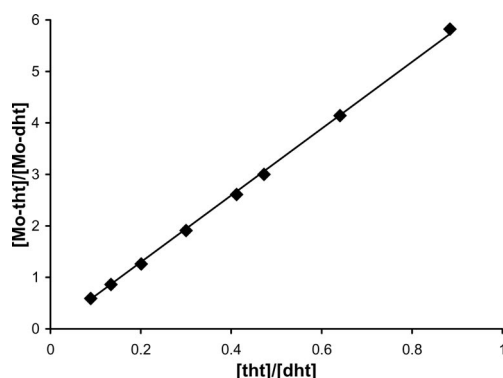


Figure 6. Determination of the equilibrium constant for the binding of tht vs. dht at 22 °C in $CDCl_3$, according to the equation: $Mo-dht + tht \rightleftharpoons Mo-tht + dht$. The model, predicting a linear dependence of the ratio $[Mo-tht]/[Mo-dht]$ vs. the ratio of free thioethers ($[tht]/[dht]$), fits the data very well ($R^2 = 0.9991$). No cooperativity is observed, and the two labile sites behave independently in this process. The slope yields $K_{eq} = 6.5 \pm 0.5$ (tht binds more strongly, by a factor of close to seven, than dht). See Experimental Section for details.

an equilibrium constant (at 22 °C) of 3.7×10^9 in favor of dht binding and thus explains the inability of thiophene to displace dht.

When $[Mo(tfd)_2(dht)_2]$ was heated in deuterated chloroform (60 °C, 1 h), thiophene (12%, relative to original concentration) was identified by 1H NMR spectroscopy as one of the decomposition products. $[Mo(tfd)_3]$ was also observed, as well as a smaller percentage of unidentified decomposition products (by ^{19}F NMR spectroscopy). It therefore appears that the dht ligands in the $[Mo(tfd)_2(dht)_2]$ complex are dehydrogenated to thiophene, although free hydrogen gas was not observed in the 1H NMR spectrum. These reactions were not catalytic when excess dht was present. At the temperatures accessible to this system (before decomposition occurs), we have not been able to reproducibly demonstrate desulfurization. Butadiene, which would be expected to form upon desulfurization of dht (Scheme 1), was not observed in any of the reactions we screened. Performing of the same reaction after an atmosphere of hydrogen was sealed into the tubes produced no change in the product type or distribution. All hydrogen reactions were done under a pressure of 1 atm; greater pressures may be needed to observe any reactivity. Many proposed HDS mechanisms invoke the action of the surrounding sulfur atoms,^[41,42] and/or multiple metal centers,^[43,44] in MoS_2 to facilitate the hydrodesulfurization of thiophene. Such pathways may not be accessible at the relatively low temperatures we tried (60–120 °C, as necessitated by the temperature-sensitivity of our model complexes; cf. 300–400 °C for industrial HDS processes^[2]). It will be the goal of future studies (with more temperature-stable analogs) to investigate whether a HDS cycle can be achieved with a single molybdenum center or whether the participation of more than one metal is required.^[44]

However, we observed the isomerization of 1,4-cyclohexadiene to 1,3-cyclohexadiene at 110 °C in $[D_{12}]$ cyclohexane in the presence of $[Mo(tfd)_2(tht)_2]$. Performing of the same reaction with $[Mo(tfd)_2(bdt)]$ did not yield any isomerized diene.

Finally, we would like to address the question of how the lability of carbon monoxide (which binds weakly to molybdenum bisdithiolenes, see Introduction) relates to the lability of thioethers. When a slow stream of carbon monoxide is bubbled through a solution of $[Mo(tfd)_2(dht)_2]$ in C_6D_6 for a total of 4 h, a new complex is observed by 1H and ^{19}F NMR spectroscopy [ca. 70–90% conversion, as determined by ^{19}F NMR spectroscopy, with 3,5-bis(trifluoromethyl)bromobenzene internal standard]. The new species is assigned as $[Mo(tfd)_2(dht)(CO)]$: NMR integration of the dht protons yields that only one dht molecule is bound per molybdenum. In addition, the amount of free dht observed matches the dht bound to the new complex, in accord with expectations from mass balance. When a large excess of dht was added, the equilibrium shifted back to $[Mo(tfd)_2(dht)_2]$. Thus, carbon monoxide and thioethers have a similar binding strength when coordination to $Mo(tfd)_2$ fragments is involved. Some metal bisdithiolene complexes containing carbonyls are already known,^[19,23] and it may be

come useful knowledge for future syntheses that CO and thioethers can be of comparable lability in such systems.

Conclusions

The molecular compounds $[\text{Mo}(\text{tfd})_2(\text{dht})_2]$ and $[\text{Mo}(\text{tfd})_2(\text{tht})_2]$ were synthesized and characterized as structural models for the hydrodesulfurization catalyst molybdenum disulfide. X-ray crystallography shows that they are excellent models for the proposed active site of molybdenum disulfide. Preliminary investigations show some intriguing reactivity consistent with transfer dehydrogenation, yet temperature-sensitivity hampers full exploration of this avenue. It may be anticipated that molecular compounds for actual HDS catalysis will have to be designed to be more robust at high-temperature conditions, which will likely necessitate departure from a close structural model. Additionally, it may be necessary to consider models containing more than one metal site (e.g. homo- or heterodimetallic complexes of Mo). The new complexes are useful, however, to test equilibria at room temperature, as demonstrated with a dht/tht competition on a sulfur-ligated Mo^{IV} center.

Experimental Section

$[\text{Mo}(\text{tfd})_2(\text{bdt})]$ was prepared by literature methods.^[24] Grubbs' second generation catalyst, tetrahydrothiophene (tht) (99%) and bis-(trimethylsilyl)acetylene (btmsa) (99%) were obtained from Sigma Aldrich. Tetrahydrothiophene was redistilled and dried with molecular sieves (3 Å) before use. Bis(trimethylsilyl)acetylene was used directly. Solvents were dried on a MBraun Solvent Purification System (MB-SPS). NMR spectroscopic data were collected on a Bruker Avance III 400 MHz spectrometer. ^1H and $^{13}\text{C}\{^1\text{H}\}$ spectra were referenced to the CDCl_3 solvent peaks, ($\delta = 7.26$ ppm and 77.23 ppm, respectively). ^1H spectra were also referenced to the C_6D_6 solvent peaks where applicable ($\delta = 7.16$ ppm). ^{19}F was referenced to an external capillary of neat trifluoroacetic acid ($\delta = -78.5$ ppm). Elemental analysis was performed by Chemisar Laboratories, Guelph, Ontario, Canada. DFT calculations were performed on a Desktop PC by using Gaussian 03W Rev D.01^[45] on closed-shell singlets (charge-neutral molecules) with the B3LYP^[46] functional and SDD basis set (ECP) for molybdenum. The SDD basis set is the combination of the Dunning/Huzinaga double- ζ basis set^[47] on lighter elements with the Stuttgart–Dresden relativistic effective core potential^[48] (RECP) on heavier elements.^[49] To improve the accuracy of the calculation, d functions were added to all sulfur atoms [as polarization functions; d coefficients from the 6-311G(d,p) basis set]. No symmetry restrictions were used, and default convergence criteria were employed.

Synthesis of $[\text{Mo}(\text{tfd})_2(\text{tht})_2]$: In air: $[\text{Mo}(\text{tfd})_2(\text{bdt})]$ (51.3 mg, 74.5 μmol) was dissolved in dry hexanes (10 mL) along with tetrahydrothiophene (63.4 μL , 719 μmol) and btmsa (80.4 μL , 360 μmol), and the mixture was left to stand. Brown crystals slowly came out of solution over ca. 1 h, and the solution turned red-purple. After 18 h, the crystals were recovered by filtration and washed three times with 5 mL portions of hexane. The crystals were dried in vacuo to give $[\text{Mo}(\text{tfd})_2(\text{tht})_2]$ (39 mg, 54 μmol , 72%). The crystals were stored under inert atmosphere and were found to be stable at room temperature. X-ray quality crystals were obtained directly from the hexane reaction mixture. ^1H NMR (400 MHz, CDCl_3): $\delta = 2.28$ (m, 8 H, tht), 3.54 (m, 8 H, tht) ppm. ^{19}F NMR (376 MHz, CDCl_3): $\delta = -54.9$ [s, 12 F, $(\text{CF}_3)_2 \times 2$] ppm. $^{13}\text{C}\{^1\text{H}\}$

NMR (100 MHz, CDCl_3): $\delta = 30.109$ (s, C_β , tht), $\delta = 42.31$ (s, C_α , tht) ppm. $\text{C}_{16}\text{H}_{16}\text{F}_{12}\text{MoS}_6$ (724.59): calcd. C 26.52, H 2.23, S 26.55; found C 26.82, H 1.97, S 26.23.

Synthesis of 2,5-Dihydrothiophene: Grubbs' second generation catalyst, 1,3-bis(2,4,6-trimethylphenyl)-2-(imidazolidinylidene)(dichlorophenylmethylene)(tricyclohexylphosphane)ruthenium, (75 mg, 88.3 μmol) was added to diallyl sulfide (75 mL of a 0.1 M solution) in dry chloroform (7.5 mmol). The solution was stirred under a stream of argon for 24 h. The volatiles were vacuum transferred to a new container and heated to 70 °C until the volume was reduced to ca. 1 mL. The solution was vacuum-distilled a second time to a new container and stored under nitrogen. NMR spectroscopy showed the sample to consist of ca. 70% 2,5-dihydrothiophene and ca. 30% chloroform. Volumes used were adjusted for actual 2,5-dihydrothiophene content.

Synthesis of $[\text{Mo}(\text{tfd})_2(\text{dht})_2]$: The procedure for $[\text{Mo}(\text{tfd})_2(\text{tht})_2]$ was repeated but with $[\text{Mo}(\text{tfd})_2(\text{bdt})]$ (52.4 mg, 76.1 μmol), 2,5-dihydrothiophene solution (50 μL), and btmsa (50 μL , 224 μmol). The crystals were dried in vacuo to give $[\text{Mo}(\text{tfd})_2(\text{dht})_2]$ (24.4 mg, 33.8 μmol , or 44%). The crystals were stored under an inert atmosphere and were stable at room temperature. X-ray quality crystals were obtained directly from the hexane solution. ^1H NMR (400 MHz, CDCl_3): $\delta = 4.35$ [m, 8 H, $(\text{CH}_2) \times 4$], 5.99 [m, 4 H, $(\text{CH}) \times 4$] ppm. ^{19}F NMR (376 MHz, CDCl_3): $\delta = -54.96$ [s, 12 F, $(\text{CF}_3)_2 \times 2$] ppm. ^{13}C NMR (100 MHz, CDCl_3): $\delta = 48.78$ (s, CH_2), $\delta = 126.62$ (s, CH) ppm. $\text{C}_{16}\text{H}_{16}\text{F}_{12}\text{MoS}_6$ (720.56): calcd. C 26.67, H 1.68, S 26.70; found C 26.89, H 1.49, S 26.04.

Attempted Synthesis of $[\text{Mo}(\text{tfd})_2(\text{thiophene})_2]$: $[\text{Mo}(\text{tfd})_2(\text{bdt})]$ (2 mg) was placed into an NMR tube with C_6D_6 (500 μL), btmsa (ca. 10 μL), and thiophene (ca. 5 μL), and 3,5-bis(trifluoromethyl)bromobenzene (ca. 3 μL) as an internal standard. After 2 h only unreacted $[\text{Mo}(\text{tfd})_2(\text{bdt})]$ and btmsa along with a smaller quantity of the $[\text{Mo}(\text{tfd})_2\{\text{bdt}(\text{btmsa})\}]$ adduct {20% yield relative to unreacted $[\text{Mo}(\text{tfd})_2(\text{bdt})]$ } were identified by NMR spectroscopy and integration. No new products could be detected. The procedure for $[\text{Mo}(\text{tfd})_2(\text{tht})_2]$ was also repeated but by substituting tht with thiophene. After 24 h, the solution remained green and no crystals were observed.

Thermal Decomposition of $[\text{Mo}(\text{tfd})_2(\text{dht})_2]$: $[\text{Mo}(\text{tfd})_2(\text{dht})_2]$ (2.5 mg, 3.5 μmol) was placed in an NMR tube with CDCl_3 (600 μL), and 3,5-bis(trifluoromethyl)bromobenzene (ca. 5 μL) as an internal standard. The mixture was heated to 60 °C for 20 h. Thiophene {12% yield relative to starting $[\text{Mo}(\text{tfd})_2(\text{dht})_2]$ } was identified in the products by using NMR spectroscopy and integration.

Noncatalytic Dehydrogenation of dht with $[\text{Mo}(\text{tfd})_2(\text{dht})_2]$: $[\text{Mo}(\text{tfd})_2(\text{dht})_2]$ (0.7 mg, 0.967 μmol) was placed in an NMR tube with dht (600 μL of a 0.062 M solution) in CDCl_3 along with 3,5-bis(trifluoromethyl)bromobenzene (ca. 5 μL) as an internal standard. The tube was heated to 60 °C for 24 h and then to 120 °C for 5 h. Thiophene was identified by NMR spectroscopy in a 43% yield based on the reagent $\text{Mo}(\text{tfd})_2(\text{dht})_2$.

Hydrogen Reactivity: Both the thermal decomposition and the noncatalytic dehydrogenation experiments were repeated, but before heating, the NMR tubes were thoroughly degassed by freeze-pump-thaw cycling. Hydrogen at atmospheric pressure was admitted to the tubes (ca. 1 mL) and then sealed. Heating proceeded as described previously. No new products or significant changes in product distribution were observed by NMR spectroscopy.

Isomerization of 1,4-Cyclohexadiene: $[\text{Mo}(\text{tfd})_2(\text{tht})_2]$ (0.5 mg, 0.69 μmol) and 1,4-cyclohexadiene (5 μL , 52.9 μmol) were added

to C₆D₁₂ (500 µL) in an NMR tube and sealed. The contents were heated to 110 °C for 24 h. ¹H NMR spectroscopy revealed isomerization to 1,3-cyclohexadiene (35% by NMR integration).

Reaction with Carbon Monoxide to Produce [Mo(tfd)₂(dht)(CO)]: [Mo(tfd)₂(dht)₂] (2 mg, 2.77 µmol) was added to C₆D₆ (400 µL) in an NMR tube along with 3,5-bis(trifluoromethyl)bromobenzene (ca. 5 µL) as an internal standard. Carbon monoxide gas was gently bubbled into the solution for a total of 4 h with occasional refilling of the solvent to make up for evaporation losses. The yellowish-brown solution turned bright orange, and a new complex was identified by ¹⁹F NMR spectroscopy and integration {70–90% yield relative to [Mo(tfd)₂(dht)₂]}. ¹H NMR spectroscopy and integration showed an equal amount of free dht and bound dht on this complex {excluding dht bound to known [Mo(tfd)₂(dht)₂]}. The sample was degassed by freeze-pump-thaw cycling, and dht (300 µL of a 0.067 M solution) in C₆D₆ (20 µmol) was added, followed by shaking. After 2 h, NMR integration revealed 85% [Mo(tfd)₂(dht)₂] and 15% [Mo(tfd)₂(dht)(CO)], which indicates that the equilibrium shifted back to the starting materials. ¹H NMR (400 MHz, C₆D₆): δ = 2.66 [m, 8 H, (CH₂)₄], 4.60 [m, 4 H, (CH)₄] ppm. ¹⁹F NMR (376 MHz, C₆D₆): δ = −54.92 [s, 12 F, (CF₃)₂×2] ppm.

Determination of *K*_{eq} (Preferred Binding of tht Over dht): A stock solution of dht in CDCl₃ was prepared by adding diallyl sulfide (200 µL) to CDCl₃ (16 mL) and Grubb's catalyst (10 mg). After 24 h, the reaction was checked for completion by NMR spectroscopy, and the volatiles were purified by vacuum transfer. The concentration of the stock solution was approximately 0.097 M. The method used for the determination of the equilibrium constant is based on relative ratios (by NMR integration) and not on absolute amounts. [Mo(tfd)₂(tht)₂] (2 mg) was added to CDCl₃ (400 µL) in an NMR tube. The NMR spectra were recorded at 22 °C. After each spectrum, a small amount of dht in CDCl₃ was added. The ratios of the various species were determined by NMR integration: Mo-bound tht ("Mo–tht"), Mo-bound dht ("Mo–dht"), free dht, and free tht were independently observed and quantified by NMR

integration. An excellent fit was obtained for the simple model Mo–dht + tht ⇌ Mo–tht + dht, which demonstrates that the two labile sites at Mo have a very similar preference for binding tht vs. dht, i.e. no cooperativity is observed. The equilibrium constant (for the reaction as written, Mo–tht as the product of the reaction) is equal to ([Mo–tht]/[Mo–dht])([tht]/[dht])^{−1}, and a straight line was indeed obtained from plotting the ratio [Mo–tht]/[Mo–dht] against the ratio [tht]/[dht] (Figure 5). The slope yields *K*_{eq} = 6.5(5); tht binds more strongly than dht by that factor. A similar experiment was performed with thiophene (NMR, 20 °C). No substitution was observed at any concentration including neat thiophene.

CCDC-762433 and CCDC-762434 for [Mo(tfd)₂(tht)₂] and [Mo(tfd)₂(dht)₂] (Table 3), respectively, contain the supplementary crystallographic data for this paper. These data can be obtained free of charge from The Cambridge Crystallographic Data Centre via www.ccdc.cam.ac.uk/data_request/cif.

Acknowledgments

Funding by the Natural Science and Engineering Research Council (NSERC) of Canada is gratefully acknowledged, along with an Early Researcher Award (Province of Ontario) to U. F.

Table 3. Crystal data and structure refinement for [Mo(tfd)₂(dht)₂] and [Mo(tfd)₂(tht)₂].

	[Mo(tfd) ₂ (dht) ₂]	[Mo(tfd) ₂ (tht) ₂]
Empirical formula	C ₁₆ H ₁₂ F ₁₂ Mo ₁ S ₆	C ₁₆ H ₁₆ F ₁₂ Mo ₁ S ₆
Formula mass	720.56	724.59
Crystal size [mm]	0.08 × 0.06 × 0.02	0.24 × 0.16 × 0.10
Crystal system	triclinic	monoclinic
Space group	P $\bar{1}$	P2 ₁ /c
<i>a</i> [Å]	8.3184(3)	12.0316(5)
<i>b</i> [Å]	12.1554(8)	25.0104(6)
<i>c</i> [Å]	12.9245(9)	8.4960(4)
<i>α</i> [°]	76.092(3)	90
<i>β</i> [°]	90.074(4)	109.275(1)
<i>γ</i> [°]	69.878(3)	90
<i>V</i> [Å ³]	1186.03(12)	2413.27(16)
<i>Z</i>	2	4
<i>T</i> [K]	150(2)	150(1)
<i>λ</i> [Å]	0.71073	0.71073
<i>R</i> (000)	708	1432
Data/restraints/ parameters	4826/0/317	5440/0/316
<i>D</i> _{calc.} [mgm ^{−3}]	2.018	1.994
<i>μ</i> [mm ^{−1}]	1.181	1.161
Reflections (collected)	7732	13879
Reflections (unique)	4826	5440
GOF	1.164	1.041
<i>R</i> 1 [<i>I</i> > 2σ(<i>I</i>)]	0.0553	0.0516
<i>wR</i> 2 (all data)	0.1465	0.1358

- [1] T. V. Choudhary, S. Parrott, B. Johnson, *Environ. Sci. Technol.* **2008**, 42, 1944–1947.
- [2] C. Song, *Catal. Today* **2003**, 86, 211–263.
- [3] I. V. Babich, J. A. Moulijn, *Fuel* **2003**, 82, 607–631.
- [4] Y. Sun, R. Prins, *Angew. Chem. Int. Ed.* **2008**, 47, 8478–8481.
- [5] B. Hinnemann, P. G. Moses, J. K. Nørskov, *J. Phys.: Condens. Matter* **2008**, 20, 064236–064244.
- [6] P. Raybaud, *Appl. Catal. A: Gen.* **2007**, 322, 76–91.
- [7] M. Sun, J. Adjaye, A. E. Nelson, *Appl. Catal. A: Gen.* **2004**, 263, 131–143.
- [8] M.-G. Choi, L. M. Daniels, R. J. Angelici, *Inorg. Chem.* **1991**, 30, 3647–3651.
- [9] P. G. Moses, B. Hinnemann, H. Topsøe, J. K. Nørskov, *J. Catal.* **2007**, 248, 188–203.
- [10] This simple picture is based on the structure of bulk material and neglects surface reconstruction.
- [11] *ORTEP-3 for Windows, Version 1.08* (based on Johnson, C. K.; Burnett, M. N. *ORTEP-3 Version 1.0.3*): L. J. Farrugia, *J. Appl. Crystallogr.* **1997**, 30, 565.
- [12] a) B. Schönfeld, J. J. Huang, S. C. Moss, *Acta Crystallogr., Sect. B* **1983**, 39, 404–407; b) R. G. Dickinson, L. Pauling, *J. Am. Chem. Soc.* **1923**, 45, 1466–1471.
- [13] D. L. Sullivan, J. G. Ekerdt, *J. Catal.* **1998**, 178, 226–233.
- [14] D. Sellmann, B. Hadawi, F. Knoch, M. Moll, *Inorg. Chem.* **1995**, 34, 5963–5972.
- [15] A. Majumdar, K. Pal, K. Nagarajan, S. Sarkar, *Inorg. Chem.* **2007**, 46, 6136–6147.
- [16] A. Majumdar, K. Pal, S. Sarkar, *Dalton Trans.* **2009**, 1927–1938.
- [17] A. Majumdar, K. Pal, S. Sarkar, *J. Am. Chem. Soc.* **2006**, 128, 4196–4197.
- [18] A. Majumdar, K. Pal, S. Sarkar, *Inorg. Chem.* **2008**, 47, 3393–3401.
- [19] S. Groysman, R. H. Holm, *Inorg. Chem.* **2007**, 46, 4090–4102.
- [20] E. Roland, E. C. Walborsky, J. C. Dewan, R. R. Schrock, *J. Am. Chem. Soc.* **1985**, 107, 5795–5797.
- [21] H. Sugimoto, T. Sakurai, H. Miyake, K. Tanaka, H. Tsukube, *Inorg. Chem.* **2005**, 44, 6927–6929.
- [22] G. N. Schrauzer, H. N. Rabinowitz, *J. Am. Chem. Soc.* **1969**, 91, 6522–6524.
- [23] B. S. Lim, J. P. Donahue, R. H. Holm, *Inorg. Chem.* **2000**, 39, 263–273.

- [24] D. J. Harrison, A. J. Lough, N. Nguyen, U. Fekl, *Angew. Chem. Int. Ed.* **2007**, *46*, 7644–7647.
- [25] A variety of alkenes may also be used to labilize the bdt ligand. See ref.^[24] and D. J. Harrison, U. Fekl, *Chem. Commun.* **2009**, 7572–7574.
- [26] H. Xu, P. Uvdal, C. M. Friend, J. Stöhr, *Surf. Sci.* **1993**, *289*, L599–L603.
- [27] K. Wang, J. M. McConnachie, E. I. Stiefel, *Inorg. Chem.* **1999**, *38*, 4334–4341.
- [28] T. Yoshida, T. Adachi, K. Matsumura, K. Kawazu, K. Baba, *Chem. Lett.* **1991**, *20*, 1067–1070.
- [29] X.-Q. Yao, Y.-W. Li, H. Jiao, *THEOCHEM* **2005**, *726*, 81–92.
- [30] C. L. Beswick, J. M. Schulman, E. I. Stiefel, *Prog. Inorg. Chem.* **2004**, *52*, 55–110.
- [31] The degree of trigonal prismatic character by the S–M–S_{trans} criterion is determined by first taking the individual “corner” sulfur atoms on one triangular face of a trigonal prism and then measuring the S–M–S angles to all the sulfur atoms on the opposite triangular face. Nine angles are obtained this way. The average of the three largest angles is used to determine the degree of octahedral vs. trigonal prismatic character using S–M–S_{trans}. The S–M–S_{trans} values for a perfect octahedron and a perfect trigonal prism are 180° and 136°, respectively. Small chelate bite angles may constrain S–M–S_{trans} from reaching the octahedral limit, so a correction is applied (ϵ_{corr}). ϵ_{corr} is found by $\epsilon_{\text{corr}} = 90^\circ + \text{S–M–S}_{\text{intra}}$, where S–M–S_{intra} is the average of the three smallest angles S–M–S angles that correspond to the sulfur atoms on the same chelating ligand (chelate “bite”). Finally the degree of prismatic character on the scale ranging from perfect octahedron (0%) to perfect trigonal prism (100% TP) is found by using %TP = $[1 - (\text{S–M–S}_{\text{trans}} - 136^\circ)/(\epsilon_{\text{corr}} - 136^\circ)] \times 100\%$. This criterion is paraphrased from ref.^[30] but inversely scaled so that trigonal prismatic character is 100% while octahedral is 0%.
- [32] For some sense of distortion, the largest deviation is found by removing the S–M–S_{intra} angles from the previous set of nine angles found in ref.^[31] and by taking the difference between the smallest and largest angles in the remaining six.
- [33] M. L. Kirk, R. L. McNaughton, M. E. Helton, *Prog. Inorg. Chem.* **2004**, *52*, 111–212.
- [34] For complexes with purely σ donor ligands, the t_{1u} orbitals (in an octahedral field) experience net stabilization upon distortion to trigonal-prismatic geometry, while the t_{2g} orbitals (in an octahedral field) are destabilized. See: S. K. Kang, H. Tang, T. A. Albright, *J. Am. Chem. Soc.* **1993**, *115*, 1971–1981. Thus, for complexes with higher d electron counts (d^n , $n > 2$), the stabilization of the t_{1u} orbitals is off set by the destabilization of electrons in the t_{2g} orbitals, usually favoring octahedral geometry.
- [35] R. Huisman, R. De Jonge, C. Haas, F. Jellinek, *J. Solid State Chem.* **1971**, *3*, 56–66.
- [36] M. Kaupp, T. Kopf, A. Murso, D. Stalke, C. Strohmann, J. R. Hanks, F. G. N. Cloke, P. B. Hitchcock, *Organometallics* **2002**, *21*, 5021–5028.
- [37] M. Kaupp, *Chem. Eur. J.* **1998**, *4*, 1678–1686.
- [38] A variety of resonance forms can be envisioned for neutral group VI metal trisdithiolenes: the most reasonable contributors, in light of computational and spectroscopic evidence, have metal oxidation states of IV or V (singlet diradical character for the latter case). For early MO calculations on metal trisdithiolenes, see: a) E. I. Stiefel, R. Eisenberg, R. Rosenberg, H. B. Gray, *J. Am. Chem. Soc.* **1966**, *88*, 2956–2966. For more recent discussions on the electronic structures of metal trisdithiolenes, see: b) K. Ray, T. Petrenko, K. Wieghardt, F. Neese, *Dalton Trans.* **2007**, 1552–1566; c) R. R. Kapre, E. Bothe, T. Weyhermüller, S. DeBeer George, K. Wieghardt, *Inorg. Chem.* **2007**, *46*, 5642–5650; d) A. L. Tenderholt, R. K. Szilagy, R. H. Holm, K. O. Hodgson, B. Hedman, E. I. Solomon, *Inorg. Chem.* **2008**, *47*, 6382–6392.
- [39] D. V. Fomitchev, B. S. Lim, R. H. Holm, *Inorg. Chem.* **2001**, *40*, 645–654.
- [40] Y. V. Joshi, P. Ghosh, P. S. Venkataraman, W. N. Delgass, K. T. Thomson, *J. Phys. Chem. C* **2009**, *113*, 9698–9709.
- [41] H. Kwart, G. C. A. Schuit, B. C. Gates, *J. Catal.* **1980**, *61*, 128–134.
- [42] K. F. McCarty, G. L. Schrader, *J. Catal.* **1987**, *103*, 261–269.
- [43] R. A. Sánchez-Delgado, “Organometallic Modeling of the Hydrodesulfurization and Hydrodenitrogenation Reactions” in *Catalysis by Metal Complexes*, D. Reidel, Dordrecht, Holland, **2004**, vol. 24, pp. 95–137.
- [44] T. M. Brunier, M. G. B. Drew, P. C. H. Mitchell, *J. Chem. Soc. Faraday Trans.* **1992**, *88*, 3225–3232.
- [45] M. J. Frisch, G. W. Trucks, H. B. Schlegel, G. E. Scuseria, M. A. Robb, J. R. Cheeseman, J. A. Montgomery Jr., T. Vreven, K. N. Kudin, J. C. Burant, J. M. Millam, S. S. Iyengar, J. Tomasi, V. Barone, B. Mennucci, M. Cossi, G. Scalmani, N. Rega, G. A. Petersson, H. Nakatsuji, M. Hada, M. Ehara, K. Toyota, R. Fukuda, J. Hasegawa, M. Ishida, T. Nakajima, Y. Honda, O. Kitao, H. Nakai, M. Klene, X. Li, J. E. Knox, H. P. Hratchian, J. B. Cross, V. Bakken, C. Adamo, J. Jaramillo, R. Gomperts, R. E. Stratmann, O. Yazyev, A. J. Austin, R. Cammi, C. Pomelli, J. W. Ochterski, P. Y. Ayala, K. Morokuma, G. A. Voth, P. Salvador, J. J. Dannenberg, V. G. Zakrzewski, S. Dapprich, A. D. Daniels, M. C. Strain, O. Farkas, D. K. Malick, A. D. Rabuck, K. Raghavachari, J. B. Foresman, J. V. Ortiz, Q. Cui, A. G. Baboul, S. Clifford, J. Cioslowski, B. B. Stefanov, G. Liu, A. Liashenko, P. Piskorz, I. Komaromi, R. L. Martin, D. J. Fox, T. Keith, M. A. Al-Laham, C. Y. Peng, A. Nanayakkara, M. Challacombe, P. M. W. Gill, B. Johnson, W. Chen, M. W. Wong, C. Gonzalez, and J. A. Pople, *Gaussian 03, Revision D.01 and E.01*, Gaussian, Inc., Wallingford CT, 2004.
- [46] A. D. Becke, *J. Chem. Phys.* **1993**, *98*, 5648–5652.
- [47] T. H. Dunning Jr., P. J. Hay, *Modern Theoretical Chemistry* (Eds.: H. F. Schaefer Editor), Plenum, New York, **1976**, vol. 3, p. 1.
- [48] P. J. Hay, W. R. Wadt, *J. Chem. Phys.* **1985**, *82*, 270–283.
- [49] M. Dolg, “Effective Core Potentials” In *Modern Methods and Algorithms of Quantum Chemistry*, John von Neuman Institute for Computing, Jülich, **2000**, vol. 1, p. 479.

Received: March 8, 2010

Published Online: July 6, 2010

Structure and Dynamics of Lanthanide(III) Complexes with an *N*-Alkylated do3a Ligand ($H_3do3a = 1,4,7,10$ -Tetraazacyclododecane-1,4,7-triacetic Acid): A Combined Experimental and DFT Study

Martín Regueiro-Figueroa,^[a] David Esteban-Gómez,^[a] Andrés de Blas,^[a] Teresa Rodríguez-Blas,^{*[a]} and Carlos Platas-Iglesias^{*[a]}

Keywords: Lanthanides / Macrocyclic ligands / Density functional calculations / X-ray diffraction

Lanthanide(III) complexes with 10-benzyl-1,4,7-tris(carboxymethyl)-1,4,7,10-tetraazacyclododecane (H_3L) have been investigated as model compounds of *N*-alkylated Ln^{III} -do3a complexes ($H_3do3a = 1,4,7,10$ -tetraazacyclododecane-1,4,7-triacetic acid) with potential application in molecular imaging. The X-ray structures of the $[Ln(L)(H_2O)]_4 \cdot 18H_2O$ complexes ($Ln = Eu$ or Tb) show that the metal ion is directly bound to the seven donor atoms of the ligand, with the nine-coordination sphere completed by an oxygen atom of an inner-sphere water molecule and an oxygen atom of a carboxylate group from a neighboring $[Ln(L)]$ unit. This results in the formation of tetrameric units through the sharing of carboxylic groups between adjacent $[Ln(L)(H_2O)]$ complexes. Luminescence lifetime measurements recorded in H_2O and D_2O provide a number of coordinated water molecules (q) of 1.2, which indicates that the major species that exists in solution contains one inner-sphere water molecule. The confor-

mational properties of the $[Ln(L)(H_2O)]$ complexes ($Ln = Gd$ or Lu) have been investigated by using density functional theory (DFT) calculations (B3LYP model). Our results indicate that the $\Delta(\lambda\lambda\lambda\lambda)$ conformation is more stable than the $\Delta(\delta\delta\delta\delta)$ one for both complexes. The interconversion between these two isomers may proceed either through the inversion of the five-membered rings formed upon coordination of the 1,4,7,10-tetraazacyclododecane (cyclen) unit, or through the stepwise rotation of the three acetate pendant arms. According to our calculations, the activation free energy for the arm-rotation process ($5.6 \text{ kcal mol}^{-1}$) is much lower than that of the ring-inversion path ($14.6 \text{ kcal mol}^{-1}$), which in turn is very similar to those determined experimentally for $Ln^{III}(\text{dota})$ complexes. Thus, a low energy barrier for the arm-rotation process appears to be responsible for the relatively fast isomer interconversion observed for $Ln^{III}(\text{N-alkylated do3a})$ complexes.

Introduction

Lanthanide coordination chemistry in aqueous solution has experienced a fast development in the last two decades,^[1] mainly promoted by the successful biomedical application of lanthanide chelates both in diagnostics^[2] and therapy.^[3] Among the different ligands used for lanthanide complexation in water, macrocyclic systems based on 1,4,7,10-tetraazacyclododecane (cyclen) play an essential role. The most important and widely studied representative of this group is $H_4\text{dota}$ (1,4,7,10-tetraazacyclododecane-1,4,7,10-tetraacetic acid), which forms lanthanide complexes of exceptionally high thermodynamic stability and kinetic inertness.^[4] Lanthanide complexes of the heptadentate ligand $H_3\text{do3a}$ (1,4,7,10-tetraazacyclododecane-1,4,7-triacetic acid) have been also extensively studied.^[5,6] Furthermore, $H_3\text{do3a}$ can be easily derivatized on its sec-

ondary amine nitrogen atom for different purposes. This property, together with the remarkable stability and kinetic inertia to metal dissociation,^[5] has led to a widespread use of $Ln^{III}(\text{do3a})$ derivatives in molecular imaging, generally as unsymmetrically substituted derivatives targeted with biologically,^[7] chemically,^[8,9] or photochemically^[10] active moieties.

It is well known that in nonacoordinated $Ln^{III}(\text{dota})$ -like complexes, the four ethylenediamine groups adopt *gauche* conformations that give rise to two macrocyclic ring conformations: $(\delta\delta\delta\delta)$ and $(\lambda\lambda\lambda\lambda)$. Furthermore, there are two possible orientations of the pendant arms (absolute configuration Δ or Λ), thereby resulting in four possible stereoisomers, which exist as two enantiomeric pairs. These stereoisomers differ by the layout of the four acetate arms and adopt either a square-antiprismatic (SAP) or twisted-square-antiprismatic (TSAP) geometry.^[11] The two structures display a different orientation of the two square planes formed by the four cyclen nitrogen atoms and the four binding oxygen atoms, thereby making an angle of around 40° in SAP-type structures, whereas this situation is reversed and reduced to around -30° in TSAP-type derivatives.^[1] However, whereas the solution structure of Ln^{III} -

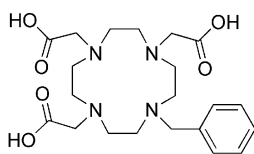
[a] Departamento de Química Fundamental, Universidade da Coruña, Alejandro de la Sota 1, 15008 A Coruña, Spain
Fax: +34-981-167-065
E-mail: cplatas@udc.es

Supporting information for this article is available on the WWW under <http://dx.doi.org/10.1002/ejic.201000334>.

(dota) complexes is well understood,^[10] little is known about the solution structure of Ln^{III}(do3a)-like complexes, as *N*-alkylated complexes of do3a often show poorly defined, exchange-broadened NMR spectra.^[12]

Several theoretical investigations of Ln^{III}(dota) or Ln^{III}-(dota)-like complexes based on molecular mechanics,^[13] Hartree–Fock,^[14] density functional theory (DFT),^[15] or molecular dynamics^[16] have been reported in the literature. Cosentino et al.^[17] have reported a conformational characterization of Ln^{III}(dota) complexes by using HF and DFT calculations. In subsequent works, we have used a similar computational approach based on HF and/or B3LYP calculations to obtain information at the molecular level on lanthanide complexes with both macrocyclic^[18] and acyclic ligands,^[19] as well as to predict the ¹³C NMR spectra of diamagnetic La³⁺ and Lu³⁺ complexes. In a recent paper, we reported a detailed DFT study on the structure and dynamics of Ln^{III}(dota) complexes and their analogues that contain methylphosphonate pendant arms.^[20] This work provides a general example of how the dynamics of complexes with multidentate ligands can be better understood with the aid of DFT calculations.

With the aim of obtaining a deeper understanding of the structure and dynamics of Ln^{III}(do3a)-like complexes in solution, herein we report several complexes of the model ligand 10-benzyl-1,4,7-tris(carboxymethyl)-1,4,7,10-tetraazacyclododecane (H₃L, Scheme 1). Luminescence emission lifetimes have been used to determine the number of inner-sphere water molecules in solution. Density functional theory (DFT) calculations performed at the B3LYP level have been used to obtain information on the solution structure of the complexes, as well as on the mechanisms responsible for the interconversion between the different stereoisomers. Finally, the X-ray structures of the Eu^{III} and Tb^{III} analogues are also reported.

H₃L

Scheme 1.

Results and Discussion

Synthesis

Ligand H₃L·2CF₃COOH was prepared in 57% overall yield by *N*-alkylation^[21] of do3a(*t*BuO)₃ with 1-(bromomethyl)benzene and subsequent deprotection of the *tert*-butyl esters with trifluoroacetic acid. The ligand was derivatized to form several charge-neutral lanthanide complexes. Compounds of formula [Ln(L)]·2H₂O (Ln = La, Eu, Gd, Tb, or Lu) were obtained in 78–87% yields by reaction of the ligand with equimolar amounts of the corresponding

lanthanide triflate in 2-propanol and in the presence of triethylamine. The high-resolution ESI-MS of the complexes evidenced peaks that correspond to [LnL + H]⁺ species. In the case of the Eu complex, the isotopic distribution that corresponded to the presence of the ¹⁵¹Eu and ¹⁵³Eu isotopes unambiguously confirms the formation of the desired complex.^[22] The IR spectra of the complexes are very similar and point to a similar structure of the five complexes in the solid state. The ¹H NMR spectra of solutions of La^{III}, Eu^{III}, and Lu^{III} complexes recorded in D₂O at 298 K (pD = 7.0) show broad signals for the proton nuclei of the do3a core (Figure S1 in the Supporting Information), as usually observed for *N*-alkylated Ln^{III} complexes of do3a.^[12] Lowering the temperature to 277 K in D₂O, or to 186 K in [D₃]MeOD, did not provide better resolved spectra. This behavior is attributed to a relatively fast interconversion between the SAP and TSAP isomers on the NMR spectroscopic timescale.

Assessment of the Hydration State

Luminescence lifetime measurements have been widely used for quantifying the number of inner-sphere water molecules in lanthanide complexes.^[23] Although ions that emit in the near-infrared region (such as Yb^{III}) have also been used for this purpose,^[24] Tb^{III} and Eu^{III} are most commonly applied for lifetime measurements, because they emit in the visible region of the spectrum and show longer emission lifetimes. Unfortunately, the [Eu(L)] complex does not show Eu^{III}-centered emission upon excitation through the benzyl chromophore at 254 nm. However, the emission spectrum of the Tb^{III} analogue recorded at pH = 7.4 [(3-morpholino-propane)sulfonic acid (MOPS) 0.1 M] shows the typical ⁵D₄→⁷F_J transitions with maxima at 621.2 (*J* = 3), 586.2 (*J* = 4), 545.4 (*J* = 5), and 489.7 nm (*J* = 6), together with residual emission of the ligand-centered singlet state at 351 nm (Figure S2 in the Supporting Information). The emission lifetimes (τ_{obsd.}) of the Tb(⁵D₄) excited level were measured in solutions of the complex in D₂O and H₂O, and were used to calculate the number of coordinated water molecules (*q*) according to Equations (1)^[25] and (2).^[26]

$$q = 4.2\Delta k_{\text{obsd.}} \quad (1)$$

$$q = 5.0(\Delta k_{\text{obsd.}} - 0.06) \quad (2)$$

In these equations, Δ*k*_{obsd.} = *k*_{obsd.}(H₂O) – *k*_{obsd.}(D₂O) and *k*_{obsd.} = 1/τ_{obsd.} (*k*_{obsd.} = observed rate constant). The measured emission lifetimes of the complexes in H₂O and D₂O amount to 1.39 and 2.34 ms, respectively, which correspond to *q* = 1.2. Average hydration numbers of 1.3–1.4 have been previously obtained for different Tb^{III} complexes with do3a-like binding sites.^[27] However, these *q* values are lower than those reported for [Ln(do3a)(H₂O)_{*q*}] (Ln = Eu or Tb), for which *q* = 1.8 has been observed.^[28] These results show that *N*-alkylation of Ln^{III}(do3a) complexes favor lower hydration numbers in aqueous solution. This is in agreement with previous results, which showed that the in-

roduction of a bulk substituent at the secondary nitrogen atom of the do3a ligand causes a stabilization of the species with a lower q value.^[29] In some instances, this effect could be partially related to the aggregation of the complexes in solution. Indeed, a hydration of $q = 1$ was established for xylene-cored Gd^{III}(do3a) derivatives as a result of the formation of aggregates in aqueous solution.^[30] However, an analogous Eu^{III} complex that contained a benzyl linker was found to present a hydration equilibrium between $q = 0$ and $q = 1$ species.^[31] These results taken together show that different scenarios can occur for similar systems. We thus conclude that the major form of the [Tb(L)] complex in aqueous solution contains one inner-sphere water molecule, but the presence of a hydration equilibrium cannot be ruled out on the basis of luminescence lifetime measurements.

Solid-State Structure of [Ln(L)] Complexes (Ln = Eu, Tb)

The relatively low solubility of the complexes of **L** in water at room temperature (ca. 1 mM) allowed us to obtain crystals of formula $[\{\text{Ln}(\text{L})(\text{H}_2\text{O})\}_4] \cdot 18\text{H}_2\text{O}$ (Ln = Eu or Tb) by slow concentration of aqueous solutions of the corresponding complexes. Figure 1 shows a view of the structure of the complexes, whereas bond lengths and angles of

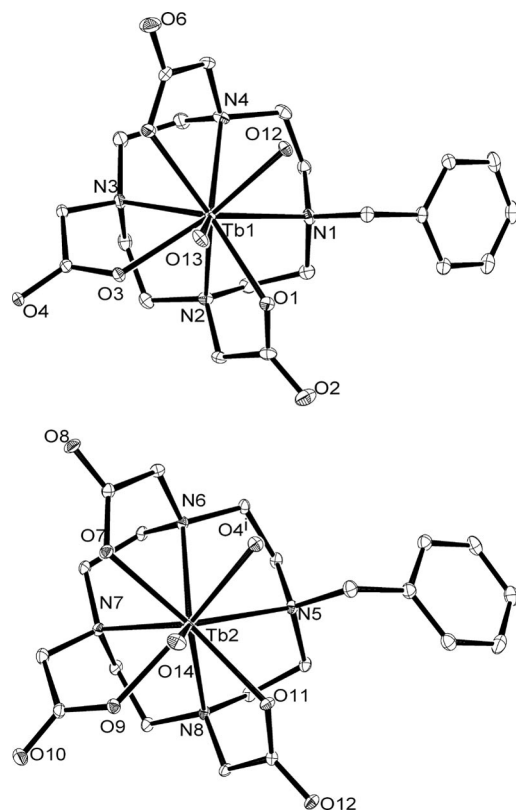


Figure 1. View of the [Tb(L)(H₂O)] complex entities present in crystals of $[\{\text{Tb}(\text{L})(\text{H}_2\text{O})\}_4] \cdot 18\text{H}_2\text{O}$. O12 and O4 correspond to oxygen atoms of a carboxylate group from a neighboring complex unit. The ORTEP plots are at the 30% probability level.

the metal coordination environments are given in Table 1. In both complexes, the metal ion is directly bound to the seven donor atoms of the ligand, with the nine-coordination sphere completed by an oxygen atom of a coordinated water molecule and an oxygen atom of a carboxylate group of a neighboring [Ln(L)] unit. This results in the formation of a tetrameric unit through the sharing of carboxylic groups between adjacent complexes (Figure 2). Several examples of lanthanide complexes forming oligomeric or polymeric units due to the presence of bridging bidentate carboxylate groups have been reported in the literature.^[32,33] The four metal centers are placed on the vertexes of a rhomb with sides of ca. 6.30 Å and angles of ca. 108 and 72°. The metal ions placed at opposite sides of the rhomb are related by an inversion center. As a result, in each centrosymmetric tetrameric unit, there are two different sets of bond lengths and angles of the metal-coordination environment, as the asymmetric unit contains half of the tetrameric unit (Figure 2).

Table 1. Bond lengths [Å] and angles [°] of the metal-coordination environment in $[\{\text{Ln}(\text{L})(\text{H}_2\text{O})\}_4] \cdot 18\text{H}_2\text{O}$ (Ln = Eu, Tb) complexes.

	Eu		Tb	
Ln1–O1	2.326(4)	2.296(2)	Ln2–O9	2.358(3)
Ln1–O3	2.386(3)	2.373(2)	Ln2–O11	2.377(3)
Ln1–O12	3.393(4)	2.374(2)	Ln2–O7	2.387(4)
Ln1–O5	2.402(4)	2.377(2)	Ln2–O4	2.411(3)
Ln1–O13	2.543(4)	2.520(2)	Ln2–O14	2.409(4)
Ln1–N4	2.635(5)	2.622(2)	Ln2–N6	2.634(4)
Ln1–N2	2.671(5)	2.647(2)	Ln2–N7	2.671(4)
Ln1–N3	2.690(5)	2.676(2)	Ln2–N8	2.688(4)
Ln1–N1	2.766(5)	2.763(2)	Ln2–N5	2.745(4)
$\omega^{[a]}$	39.1	40.6	$\omega^{[a]}$	41.0
$\phi^{[b]}$	2.95	2.43	$\phi^{[b]}$	3.68
Ln1–P _O	0.759	0.756	Ln2–P _O	0.737
Ln1–P _N	1.691	1.652	Ln2–P _N	1.648

[a] Mean twist angle [°] of the upper and lower planes. [b] Angle between the least-squares planes defined by the oxygen (P_O) and nitrogen (P_N) atoms.

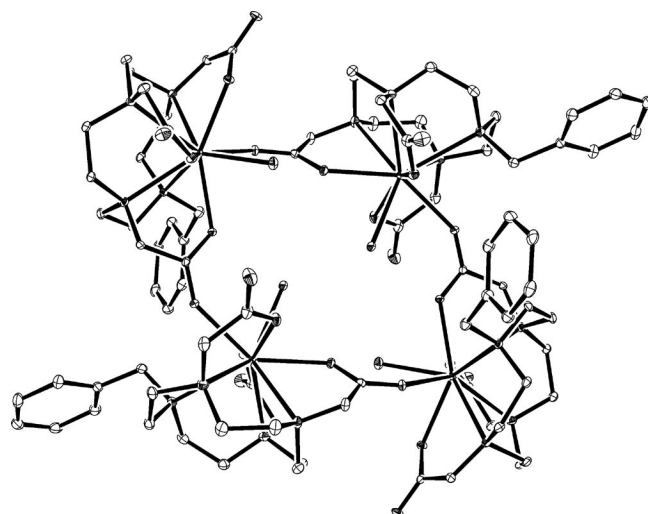


Figure 2. View of the tetrameric unit present in crystals of $[\{\text{Tb}(\text{L})(\text{H}_2\text{O})\}_4] \cdot 18\text{H}_2\text{O}$.

The distances between the metal ions and the donor atoms of the ligand decrease along the lanthanide series from Eu to Tb, as usually observed for Ln^{III} complexes as a consequence of the lanthanide contraction.^[34] Three of the distances between the oxygen atoms of the carboxylate groups and the metal ion are very similar, whereas the fourth one (Ln1–O1) is substantially shorter. With regards to the distances between the metal ion and the oxygen atoms of coordinated water molecules, we notice that the Ln1–O13 distances are ca. 0.12 Å longer than the Ln2–O14 ones. This is attributed to the fact that the inner-sphere water molecule that contains O14 is involved in strong hydrogen-bonding interactions with a second-sphere water molecule [Tb: H141...O24 1.83(2) Å, O14...O24 2.645(4) Å, O14–H141...O24 165(4)°]. This hydrogen-bonding interaction polarizes the inner-sphere water molecule, thereby strengthening the water–ion interaction. The observed Ln–N and Ln–O bond lengths are very similar to those found for the [Ln(dota)(H₂O)][–] complexes (Ln = Eu, Gd).^[6,35]

The coordination polyhedron around the lanthanide atom may be considered to be comprised of two nearly parallel planes: the four amine nitrogen atoms define the lower plane (P_N), whereas the four oxygen atoms of carboxylate groups coordinated to the metal ion define the upper plane (P_O). The inner-sphere water molecule caps the upper plane. The angles between these nearly parallel planes range between 2.43 and 3.68° (ϕ ; Table 1). The lanthanide ion is placed at ca. 0.75 Å from the upper plane (P_O), and at ca. 1.65 Å from the plane delineated by the four amine nitrogen atoms of the macrocycle. Inspection of the X-ray structures shows that both the $\Delta(\lambda\lambda\lambda\lambda)$ and $\Lambda(\delta\delta\delta\delta)$ isomers are present in each tetrameric unit (racemate). This conformation results in a monocapped SAP geometry around the metal ion, as the mean twist angles ω ^[36] between the two P_N and P_O parallel squares amount to ca. 39–41° (Table 1). These values are very similar to those observed in the solid state for the respective isomers of dota complexes.^[6,35] A $\Delta(\lambda\lambda\lambda\lambda)$ [or $\Lambda(\delta\delta\delta\delta)$] conformation has been previously observed in the solid state for Gd(do3a).^[6]

DFT Calculations

Luminescence-lifetime measurements performed on the Tb^{III} complex of **L** indicate that the major species in solution is octacoordinated and contains one inner-sphere water molecule ($q = 1$). Thus, to obtain information on the solution structure of the Ln^{III} complexes of **L**, the [Ln(L)(H₂O)] systems (Ln = Gd or Lu) were characterized by means of DFT calculations performed at the B3LYP level. In these calculations, we used the effective core potential (ECP) of Dolg et al.^[37] and the related [5s4p3d]-GTO valence basis set for the lanthanide, whereas the remaining atoms were described by using the 6-31G(d) basis set. This ECP includes 46 + 4fⁿ electrons in the core, thus leaving the outermost 11 electrons to be treated explicitly. The Cartesian coordinates of the [Ln(L)(H₂O)] systems optimized in vacuo are given in the Supporting Information.

As expected, our calculations on the [Gd(L)(H₂O)] system provide the $\Delta(\lambda\lambda\lambda\lambda)$ and $\Lambda(\delta\delta\delta\delta)$ isomers as minimum-energy conformations (Table 2). The mean distances between the Gd^{III} ion and the donor atoms of the carboxylate groups, as well as the average Gd–N distances, are in good agreement with those observed in the solid state for the Eu^{III} and Tb^{III} complexes (Table 1). The distance between Gd and the oxygen atom of the coordinated water molecule is slightly shorter for the $\Delta(\lambda\lambda\lambda\lambda)$ isomer (2.50 Å) than for the $\Lambda(\delta\delta\delta\delta)$ one (2.52 Å), which is in line with a higher steric compression around the inner-sphere water molecule in the latter form.^[38] A similar situation is observed for the Lu^{III} analogue. The Gd–O_w distances are close to that normally assumed in the analysis of ¹⁷O NMR spectroscopic relaxation data (2.50 Å),^[39] and those obtained experimentally for different Gd^{III} complexes by using electron nuclear double resonance (ENDOR) spectra (2.4–2.5 Å).^[40] In both $\Delta(\lambda\lambda\lambda\lambda)$ and $\Lambda(\delta\delta\delta\delta)$ conformations, the distances between the Ln^{III} ions and the donor atoms of the ligand decrease along the lanthanide series, as usually observed for Ln^{III} complexes as a consequence of the lanthanide contraction.^[34]

Table 2. Average bond lengths [Å] and twist angles [°] obtained from DFT calculations on the [Ln(L)(H₂O)] (Ln = Gd, Lu) systems.^[a]

	Gd		Lu	
	$\Delta(\lambda\lambda\lambda\lambda)$	$\Lambda(\delta\delta\delta\delta)$	$\Delta(\lambda\lambda\lambda\lambda)$	$\Lambda(\delta\delta\delta\delta)$
Ln–O _{COO}	2.29(5)	2.29(4)	2.21(5)	2.21(5)
Ln–N	2.73(7)	2.74(9)	2.66(9)	2.67(10)
Ln–O _w	2.499	2.522	2.410	2.435
ω ^[b]	34.1	21.6	36.4	24.2

[a] Mean values are provided with standard deviations within parentheses. O_{COO}: coordinated oxygen atoms of acetate groups; O_w: oxygen atom of inner-sphere water molecules. [b] Mean twist angle [°] of the upper and lower planes, for which the upper plane is described by three coordinated oxygen atoms of acetate groups.

In the [Ln(L)(H₂O)] complexes, the coordination polyhedron around the lanthanide ion cannot be described as SAP or TSAP, because one of the positions of the upper plane is vacant, with the water molecule placed well above the plane described by the three bound oxygen atoms of the acetate groups. Table 2 shows the mean twist angles ω ^[36] formed between the planes described by the three oxygen atoms of the acetate groups coordinated to the metal ion, and the three nitrogen atoms attached to acetate groups. The values obtained for the $\Delta(\lambda\lambda\lambda\lambda)$ and $\Lambda(\delta\delta\delta\delta)$ conformations are somewhat smaller than those observed for the respective isomers of Ln^{III}(dota) complexes.^[6,35,41]

For the Gd^{III} complex, the relative free energy of the $\Delta(\lambda\lambda\lambda\lambda)$ isomer with respect to the $\Lambda(\delta\delta\delta\delta)$ one amounts to –0.68 kcal mol^{–1}. Analogous calculations performed on Ln^{III}(dota)-like complexes that contained methylphosphonate pendant arms showed that the calculated relative free energies of the two isomers deviate from the experimental values by 0.2–1.1 kcal mol^{–1}.^[20] Thus, the major form of the [Gd(L)(H₂O)] complex in solution most likely corresponds to the $\Delta(\lambda\lambda\lambda\lambda)$ [or $\Lambda(\delta\delta\delta\delta)$] isomer, which is in line

with the solid-state structures described above. This is also in agreement with previous observations that showed that increasing the steric hindrance around the lanthanide ion favors the $\Delta(\delta\delta\delta\delta)$ isomer.^[42] In the present case, the heptadentate nature of the ligand, together with the absence of bulky groups around the metal ion, results in a low steric hindrance around the lanthanide atom, and thus the $\Delta(\lambda\lambda\lambda\lambda)$ form is stabilized with respect to the $\Delta(\delta\delta\delta\delta)$ one. The $\Delta(\lambda\lambda\lambda\lambda)$ conformation has also been identified as the major form in solution for several $\text{Yb}^{\text{III}}(\text{do3a})$ derivatives.^[43] The $\Delta(\lambda\lambda\lambda\lambda)$ isomer is further stabilized on decreasing the ionic radius of the lanthanide atom from Gd^{III} to Lu^{III} , the relative free energy of the $\Delta(\lambda\lambda\lambda\lambda)$ isomer with respect to the $\Delta(\delta\delta\delta\delta)$ one amounting to $-1.72 \text{ kcal mol}^{-1}$ for the Lu^{III} complex. This is also in line with NMR spectroscopic studies performed on $\text{Ln}^{\text{III}}(\text{dota})$ complexes, which have shown that the abundance of the $\Delta(\delta\delta\delta\delta)$ isomer progressively decreases upon moving to the right across the lanthanide series.^[11] We have shown recently that this is because the $\Delta(\lambda\lambda\lambda\lambda)$ isomer provides a stronger interaction between the ligand and the metal ion than the $\Delta(\lambda\lambda\lambda\lambda)$ one, an effect that is magnified across the lanthanide series as the charge density of the metal ion increases.^[20]

The interconversion between the SAP and TSAP isomers has been investigated experimentally for several $[\text{Ln}(\text{dota})\text{-(H}_2\text{O)}]^-$ and $\text{Eu}^{\text{III}}(\text{dota-tetraamide})$ complexes.^[44,45] These studies have concluded that the $\text{SAP} \leftrightarrow \text{TSAP}$ interconversion process may proceed along different pathways (Figure 3): (i) the inversion of the five-membered chelate rings formed upon coordination of the cyclen moiety, which leads to a $(\delta\delta\delta\delta) \leftrightarrow (\lambda\lambda\lambda\lambda)$ conformational change; or (ii) the rotation of the pendant arms, which results in a $\Delta \leftrightarrow \Lambda$ configurational change. Either process alone interconverts SAP and TSAP geometries, whereas the combination of the two processes exchanges enantiomeric pairs (Figure 3). The $\text{TSAP} \leftrightarrow \text{SAP}$ interconversion process has also been investigated on the $[\text{Lu}(\text{dota})]^-$ system by using $\text{HF}^{[17]}$ and $\text{DFT}^{[20]}$ calculations. With the aim of obtaining a deeper understanding of the $\text{TSAP} \leftrightarrow \text{SAP}$ interconversion process that occurs in $\text{Ln}^{\text{III}}(\text{do3a})$ derivatives, we have performed a detailed investigation of the arm rotation and cyclen inversion processes on the $[\text{Lu}(\text{L})(\text{H}_2\text{O})]$ system (Figure 3).

According to our results obtained on $\text{B3LYP/6-31G}^*\text{-op}$ -optimized geometries, the inversion of the cyclen moiety in the $[\text{Lu}(\text{L})(\text{H}_2\text{O})]$ complex is a four-step process. In each of these steps, one five-membered chelate ring changes its configuration from λ to δ and passes through a transition state (TS) in which the chelate ring adopts a nearly planar conformation with the NCCN moiety in eclipsed disposition. A similar result has been previously reported for the $[\text{Lu}(\text{dota})]^-$ system on the basis of $\text{HF/3-21G}^{[17]}$ and $\text{B3LYP/6-31G(d)}^{[20]}$ calculations. Due to the symmetry properties of the $[\text{Lu}(\text{L})(\text{H}_2\text{O})]$ complex (C_1 point group), the first step of the ring-inversion process may proceed through any of the four five-membered chelate rings of the cyclen moiety (Figure 4). Thus, the inversion of the first chelate ring leads to four possible intermediates through four different transi-

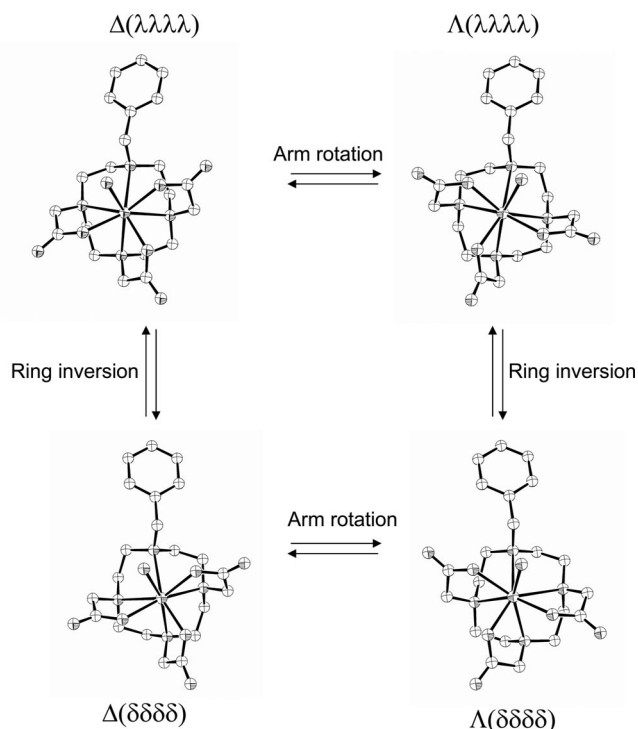


Figure 3. Optimized geometries of the four isomers of $[\text{Lu}(\text{L})(\text{H}_2\text{O})]$ and their interconversion pathways. Symbols Δ and Λ refer to the helicity of the pendant arms, δ and λ to that of the macrocycle.

tion states (TS). Symmetry considerations show that the inversion of a second chelate ring leads to the formation of six potential intermediates; however, there are up to 12 transition states that connect intermediates $\text{I}_{1\text{R}}$ and $\text{I}_{2\text{R}}$ (Figure 4). Inversion of a third chelate ring gives rise to the formation of four new intermediates ($\text{I}_{3\text{R}}$, Figure 4) through 12 possible TSs. Finally, the inversion of the fourth chelate ring converts intermediates $\text{I}_{3\text{R}}$ into the $\Delta(\delta\delta\delta\delta)$ isomer.

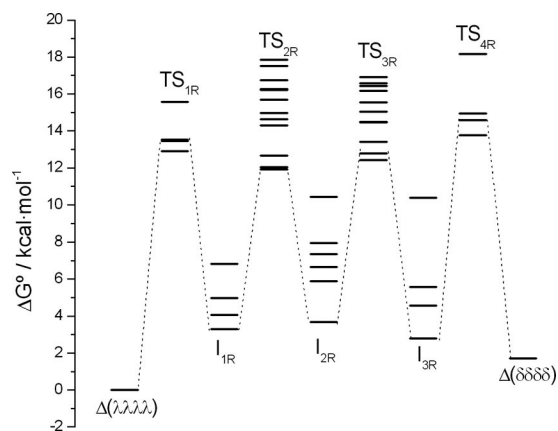


Figure 4. In vacuo relative free energies of minima, intermediates (I), and transition states (TS) involved in the ring-inversion processes of $[\text{Lu}(\text{L})(\text{H}_2\text{O})]$. The minimum-energy pathway is highlighted by connecting the corresponding intermediates and transition states with dotted lines.

The energies of intermediates and transition states calculated for the lowest-energy pathway of the ring-inversion process are given in Table 3. By assuming the rate-determining step to be the passage between I_{3R} and the $\Delta(\delta\delta\delta\delta)$ form, the barrier for the ring inversion path is the one associated to TS_{4R} , which amounts 14.6 kcal mol⁻¹. This value is very similar to those obtained experimentally for the [Yb(dota)]⁻ (14.6 kcal mol⁻¹) and [Lu(dota)]⁻ (15.8 kcal mol⁻¹) complexes.^[44]

Table 3. Relative free energies [kcal mol⁻¹] of minima, intermediates (I), and transition states (TS) involved in the ring inversion and arm-rotation interconversion processes of [Lu(L)(H₂O)]^[a]

	Ring inversion ^[b]		Arm rotation	
	$\Delta(\lambda\lambda\lambda\lambda)$	0.00	$\Delta(\lambda\lambda\lambda\lambda)$	0.00
TS_{1R}	$\Delta(\lambda\lambda\lambda X)$	13.45	TS_{1A}	4.18
I_{1R}	$\Delta(\lambda\lambda\lambda\delta)$	3.29	I_{1A}	2.87
TS_{2R}	$\Delta(\lambda X\lambda\delta)$	11.92	TS_{2A}	4.57
I_{2R}	$\Delta(\lambda\delta\lambda\delta)$	3.68	I_{2A}	3.04
TS_{3R}	$\Delta(\lambda\delta X\delta)$	12.78	TS_{3A}	5.60
I_{3R}	$\Delta(\lambda\delta\delta\delta)$	2.78	$\Lambda(\lambda\lambda\lambda\lambda)$	1.72
TS_{4R}	$\Delta(X\delta\delta\delta)$	14.59		
	$\Delta(\delta\delta\delta\delta)$	1.72		

[a] Subscripts R and A refer to intermediates and transition states responsible for the ring-inversion and arm-rotation processes, respectively. [b] A nearly planar conformation with the NCCN moiety in eclipsed disposition is denoted as X; only the energies of minima and transition states that provide the lowest energy path are given.

Our calculations indicate that the arm-rotation process responsible for the $\Delta(\lambda\lambda\lambda\lambda) \leftrightarrow \Lambda(\lambda\lambda\lambda\lambda)$ interconversion is a three-step process that involves the stepwise rotation of each of the three acetate pendant arms (Figure 5). Indeed, the rotation of one of the acetate groups of the SAP form leads to the formation of intermediate I_{1A} . In this process, the NCCO dihedral angle changes from 37.2° in the $\Delta(\lambda\lambda\lambda\lambda)$ form to -30.6° in I_{1A} . Subsequent rotation of a second acetate pendant group provides intermediate I_{2A} through transition state TS_{2A} . Finally, rotation of the third acetate group provides the $\Lambda(\lambda\lambda\lambda\lambda)$ form of the complex through transition state TS_{3A} (Figure 5). By assuming the rate-determining step to be the passage between the last intermediate, I_{2A} , and the $\Lambda(\lambda\lambda\lambda\lambda)$ form, the barrier for the arm-rotation path is the one associated to TS_{3A} , which amounts only to 5.6 kcal mol⁻¹. This value is much smaller than that calculated for the ring-inversion pathway (14.6 kcal mol⁻¹). Thus, we conclude that a low energy barrier for the arm-rotation process is responsible for the relatively fast interconversion between the $\Delta(\lambda\lambda\lambda\lambda)$ and $\Delta(\delta\delta\delta\delta)$ forms of Ln^{III}(do3a)-like complexes.

The low energy barrier calculated for the arm-rotation process can be easily rationalized by looking at the geometries of energy minima and transition states shown in Figure 5. The $\Delta(\lambda\lambda\lambda\lambda) \leftrightarrow \Lambda(\lambda\lambda\lambda\lambda)$ interconversion process starts with the rotation of one of the acetate pendant arms in the vicinity of the benzyl group. The absence of donor atoms in the benzyl group facilitates the rotation of the acetate arm, which is accompanied by a displacement of the inner-sphere water molecule from its original position over

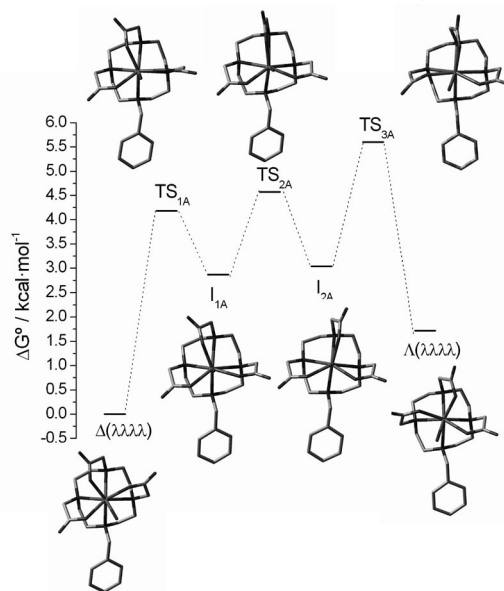


Figure 5. In vacuo relative free energies of minima, intermediates (I), and transition states (TS) involved in the arm-rotation processes of [Lu(L)(H₂O)].

the *N*-benzyl group to an axial position over the Lu^{III} ion. The rotation of the first acetate arm decreases the steric hindrance for the rotation of the acetate arm attached to the adjacent nitrogen atom, and finally the rotation of the second acetate facilitates the rotation of the third one. The last rotation process is accompanied by a displacement of the inner-sphere water molecule (Figure 5).

We would like to point out that the investigation of the ring-inversion and arm-rotation pathways of [Lu(L)(H₂O)] did not consider the possible effect of water-exchange kinetics on these interconversion processes. By using the Eyring formula $1/\tau = k_B T/h \exp(-\Delta G^\ddagger/RT)$ and $\Delta G^\ddagger = 5.6$ and 14.6 kcal mol⁻¹ for the arm-rotation and ring-inversion processes (k_B = Boltzmann constant; T = temperature; h = Planck constant; ΔG^\ddagger = change in Gibbs free energy; R = gas constant), respectively, we obtained $\tau = 2 \times 10^{-9}$ s (arm rotation) and $\tau = 8 \times 10^{-3}$ s (ring inversion). The residence time of inner-sphere water molecules in [Gd(do3a)(H₂O)₉] was determined to be 91 ns.^[28] From these data, it is clear that the ring-inversion and water-exchange processes occur on different timescales, and that many water-exchange events occur between two ring-inversion processes. According to our calculations, the arm rotation process is very fast, and will occur with a rate comparable to, or even faster than the water exchange of inner-sphere water molecules. Thus, we cannot discard the possibility that these two processes could be coupled, as they appear to take place on a similar timescale.

Conclusion

The detailed investigation of the structure and dynamics of lanthanide(III) complexes with 10-benzyl-1,4,7-tris(carboxymethyl)-1,4,7,10-tetraazacyclododecane (**H₃L**) shows

that: (i) the major form of the complexes in aqueous solution contains one inner-sphere water molecule, with *N*-alkylation responsible for such a low hydration number; (ii) the $\Delta(\lambda\lambda\lambda\lambda)$ [or $\Lambda(\delta\delta\delta\delta)$] conformation is favored over the $\Lambda(\delta\delta\delta\delta)$ [or $\Lambda(\lambda\lambda\lambda\lambda)$] one; (iii) the energy barrier associated with the ring-inversion process is similar to that observed for $\text{Ln}^{\text{III}}(\text{dota})$ complexes; and (iv) a low energy barrier for the arm-rotation process appears to be responsible for the relatively fast isomer interconversion observed by ^1H NMR spectroscopy in solution. We believe that these conclusions can be extended to other *N*-alkylated $\text{Ln}^{\text{III}}(\text{do3a})$ complexes, and therefore the results reported in this paper increase the current understanding of the structure and dynamics of this important family of complexes with potential application in different molecular-imaging modalities.

Experimental Section

Solvents and Starting Materials: All chemicals were purchased from commercial sources and used without further purification, unless otherwise stated.

Physical Methods: ^1H and ^{13}C NMR spectra were recorded at 25 °C with a Bruker Avance 500 MHz spectrometer. For measurements in D_2O , *tert*-butyl alcohol was used as an internal standard with the methyl signal calibrated at $\delta = 1.2$ (^1H) and 31.2 ppm (^{13}C). High-resolution ESI-TOF mass spectra were recorded with an LC-Q-q-TOF Applied Biosystems QSTAR Elite spectrometer in the positive mode. IR spectra were recorded with a Bruker Vector 22 spectrophotometer equipped with a Golden Gate Attenuated Total Reflectance (ATR) accessory (Specac). Excitation and emission spectra were recorded with a Perkin–Elmer LS-50B spectrometer. Luminescence lifetimes were calculated from the monoexponential fitting of the average decay data, and they are averages of at least 3–5 independent determinations.

Computational Methods: All calculations were performed by employing hybrid DFT with the B3LYP exchange–correlation functional,^[46,47] and the Gaussian 03 package (Revision C.01).^[48] Relativistic effects were considered through the use of relativistic effective core potentials (RECP). Different computational studies on Ln^{III} complexes have shown that the 4f orbitals do not participate in bonding because of their contraction into the core.^[49] Thus, full geometry optimizations of the $[\text{Gd}(\text{L})(\text{H}_2\text{O})]$ and $[\text{Lu}(\text{L})(\text{H}_2\text{O})]$ systems were performed in vacuo by using the RECP of Dolg et al. and the related $[\text{5s}4\text{p}3\text{d}]-\text{GTO}$ valence basis set for the lanthanide,^[37] and the 6-31G(d) basis set for C, H, N, and O atoms. The RECP of Dolg et al. includes 46 + 4fⁿ electrons in the core for the lanthanide, thus leaving the outermost 11 electrons to be treated explicitly, which is in line with the nonparticipation of 4f electrons in bonding. Thus, this RECP treats $[\text{Kr}]4\text{d}^{10}4\text{f}^n$ as a fixed core, whereas only the $5\text{s}^25\text{p}^65\text{d}^16\text{p}^0$ shell is explicitly taken into account. Symmetry constraints were not imposed during the optimizations. The default values for the integration grid (“fine”) and the self-consistent field (SCF) energy convergence criteria (10^{-6}) were used. The stationary points found on the potential energy surfaces as a result of the geometry optimizations were tested to represent energy minima rather than saddle points by means of frequency analysis. The relative free energies of the different conformations calculated for each system include non-potential-energy contributions (that is, zero-point energy and thermal terms) obtained by frequency analysis. The interconversion between the isomers of

$[\text{Lu}(\text{L})(\text{H}_2\text{O})]$ was investigated in vacuo by means of the synchronous transit-guided quasi-Newton method.^[50] The nature of the saddle points and intermediates was characterized by frequency analysis. The one imaginary mode in the transition state corresponded to the direction of motion consistent with the particular conformational change. The energy barriers calculated in vacuo include non-potential-energy contributions (that is, zero-point energies and thermal terms) obtained by frequency analysis.

X-ray Crystal Structures: Three-dimensional X-ray data were collected with a Bruker X8 APEXII CCD diffractometer. Data were corrected for Lorentz and polarization effects and for absorption by semiempirical methods^[51] based on symmetry-equivalent reflections. Complex scattering factors were taken from the program SHELX97^[52] running under the WinGX program system^[53] as implemented on a Pentium computer. Both structures were solved by Patterson methods (DIRDIF99^[54]) and refined^[52] by full-matrix least squares on F^2 . Hydrogen atoms were included in calculated positions and refined in riding mode in both compounds, except those of water molecules, which were located in a difference electron-density map if possible; some others were located with CALC-H₂^[55] and finally, some of the water hydrogen atoms were placed in dummy positions; in any case, the positional parameters were fixed. Refinement converged with anisotropic displacement parameters for all non-hydrogen atoms after imposing 70 restraints for the Tb complex and 120 restraints for the Eu complex. Crystal data and details on data collection and refinement are summarized in Table 4. CCDC-770914 ($[\{\text{Eu}(\text{L})(\text{H}_2\text{O})\}_4] \cdot 18\text{H}_2\text{O}$) and -770913 ($[\{\text{Tb}(\text{L})(\text{H}_2\text{O})\}_4] \cdot 18\text{H}_2\text{O}$) contain the supplementary crystallographic data for this paper. These data can be obtained free of charge from The Cambridge Crystallographic Data Centre via www.ccdc.cam.ac.uk/data_request/cif.

Table 4. Crystal data and structure refinement for $[\{\text{Ln}(\text{L})(\text{H}_2\text{O})\}_4] \cdot 18\text{H}_2\text{O}$ complexes (Ln = Eu, Tb) complexes.

	Eu	Tb
Empirical formula	$\text{C}_{84}\text{H}_{160}\text{Eu}_4\text{N}_{16}\text{O}_{46}$	$\text{C}_{84}\text{H}_{160}\text{Tb}_4\text{N}_{16}\text{O}_{46}$
M_r [g mol ^{−1}]	2738.12	2765.96
Crystal system	monoclinic	monoclinic
T [K]	100.0(2)	100.0(2)
λ [Å]	0.71073	0.71073
Space group	$P2_1/n$	$P2_1/n$
a [Å]	17.7200(4)	17.5474(6)
b [Å]	17.6458(4)	17.6594(6)
c [Å]	18.5248(3)	18.4854(7)
β [°]	112.438(1)	112.478(1)
V [Å ³]	5353.9(2)	5293.0(3)
Z	2	2
ρ_{calcd} [g cm ^{−3}]	1.698	1.735
μ [mm ^{−1}]	2.409	2.739
R_{int}	0.0691	0.0323
Reflections measured	13336	13142
Reflections observed	9357	11501
R_1 [a]	0.0461	0.0253
wR_2 (all data) [b]	0.1156	0.0588

[a] $R_1 = \frac{\sum \|F_o\| - |F_c|}{\sum \|F_o\|}$. [b] $wR_2 = \frac{\{\sum [w(\|F_o\|^2 - |F_c|^2)]\}^{1/2}}{\sum [w(F_o^4)]^{1/2}}$.

10-Benzyl-1,4,7-tris(carboxymethyl)-1,4,7,10-tetraazacyclododecane Difluoroacetate ($\text{H}_3\text{L} \cdot 2\text{CF}_3\text{COOH}$): This compound was prepared by using a synthetic procedure different to that reported previously.^[56] 1-(Bromomethyl)benzene (0.100 g, 0.585 mmol) and Na_2CO_3 (0.250 g, 2.359 mmol) were added to a solution of do3a(*t*-BuO)₃ (0.300 g, 0.583 mmol) in acetonitrile (25 mL). The mixture was heated to reflux with stirring under argon for a period of 24 h,

and then the excess amount of Na_2CO_3 was filtered off, and the filtrate was concentrated to dryness. The residue was partitioned between H_2O and CH_2Cl_2 (20:10), the organic phase was separated, dried with MgSO_4 , filtered, and the solvents were evaporated to dryness. The crude ester intermediate was purified by column chromatography on Al_2O_3 with a CH_2Cl_2 /5% MeOH mixture as eluent to give a yellow oil, which was dissolved in a CH_2Cl_2 /TFA (1:1) mixture (5 mL) and stirred at room temperature for 24 h. The mixture was concentrated to dryness, and the resulting oil was dissolved in methanol (ca. 1 mL). Addition of diethyl ether resulted in the formation of a white solid that was collected by filtration and dried under vacuum. Yield: 0.220 g, 57%. $\text{C}_{21}\text{H}_{32}\text{N}_4\text{O}_6 \cdot 2\text{CF}_3\text{COOH}$ (664.55): calcd. C 45.18, H 5.16, N 8.43; found C 45.33, H 5.14, N 8.65. MS (ESI+): $m/z = 437$ [$\text{C}_{21}\text{H}_{33}\text{N}_4\text{O}_6$] $^+$. IR (ATR): $\tilde{\nu} = 1675$ (C=O) cm^{-1} . ^1H NMR (D_2O , pD = 2.3, 500 MHz, 25 °C, TMS): $\delta = 7.48\text{--}7.44$ (m, 5 H, ArH), 4.39–3.14 (m, 24 H, CH_2) ppm. ^{13}C NMR (D_2O , pD = 2.3, 125.8 MHz, 25 °C, TMS): $\delta = 175.1$ and 171.5 (C=O), 132.3 and 131.2 (Ar), 59.2, 57.1, 55.0, 52.5, 50.9 and 49.9 (CH_2) ppm.

General Procedure for the Preparation of the $[\text{Ln}(\text{L})]\cdot 2\text{H}_2\text{O}$ Complexes: A mixture of $\text{H}_3\text{L}\cdot 2\text{CF}_3\text{COOH}$ (0.100 g, 0.150 mmol), triethylamine (0.076 g, 0.751 mmol), and $\text{Ln}(\text{OTf})_3$ (0.150 mmol, Ln = La, Eu, Gd, Tb, or Lu) in 2-propanol (10 mL) was heated to reflux for 24 h. The reaction mixture was allowed to cool to room temperature and then concentrated to dryness. Addition of water (1 mL) resulted in the formation of a white precipitate that was isolated by filtration and dried under vacuum.

$[\text{La}(\text{L})]\cdot 2\text{H}_2\text{O}$: Yield: 0.075 g, 82%. $\text{C}_{21}\text{H}_{33}\text{LaN}_4\text{O}_8$ (608.41): calcd. C 41.46, H 5.47, N 9.21; found C 41.23, H 5.35, N 8.93. HRMS (ESI+): calcd. for [$\text{C}_{21}\text{H}_{30}\text{LaN}_4\text{O}_6$] $^+$ 573.1223; found 573.1224. IR (ATR): $\tilde{\nu} = 1575$ (C=O) cm^{-1} .

$[\text{Eu}(\text{L})]\cdot 2\text{H}_2\text{O}$: Yield: 0.072 g, 78%. $\text{C}_{21}\text{H}_{33}\text{EuN}_4\text{O}_8$ (621.47): calcd. C 40.58, H 5.35, N 9.02; found C 40.23, H 5.04, N 8.65. HRMS (ESI+): calcd. for [$\text{C}_{21}\text{H}_{30}\text{EuN}_4\text{O}_6$] $^+$ 587.1372; found 587.1390. IR (ATR): $\tilde{\nu} = 1583$ (C=O) cm^{-1} .

$[\text{Gd}(\text{L})]\cdot 2\text{H}_2\text{O}$: Yield: 0.082 g, 87%. $\text{C}_{21}\text{H}_{33}\text{GdN}_4\text{O}_8$ (626.76): calcd. C 40.24, H 5.31, N 8.94; found C 39.95, H 5.17, N 8.48. HRMS (ESI+): calcd. for [$\text{C}_{21}\text{H}_{30}\text{GdN}_4\text{O}_6$] $^+$ 592.1400; found 592.1428. IR (ATR): $\tilde{\nu} = 1590$ (C=O) cm^{-1} .

$[\text{Tb}(\text{L})]\cdot 2\text{H}_2\text{O}$: Yield: 0.079 g, 84%. $\text{C}_{21}\text{H}_{33}\text{N}_4\text{O}_8\text{Tb}$ (628.43): calcd. C 40.14, H 5.29, N 8.92; found C 40.08, H 5.12, N 8.70. HRMS (ESI+): calcd. for [$\text{C}_{21}\text{H}_{30}\text{N}_4\text{O}_6\text{Tb}$] $^+$ 593.1413; found 593.1418. IR (ATR): $\tilde{\nu} = 1583$ (C=O) cm^{-1} .

$[\text{Lu}(\text{L})]\cdot 2\text{H}_2\text{O}$: Yield: 0.076 g, 79%. $\text{C}_{21}\text{H}_{33}\text{LuN}_4\text{O}_8$ (644.48): calcd. C 39.14, H 5.16, N 8.69; found C 39.23, H 5.04, N 8.65. HRMS (ESI+): calcd. for [$\text{C}_{21}\text{H}_{30}\text{LuN}_4\text{O}_6$] $^+$ 609.1567; found 609.1575. IR (ATR): $\tilde{\nu} = 1598$ (C=O) cm^{-1} .

Supporting Information (see footnote on the first page of this article): ^1H NMR spectra of the La^{III} and Lu^{III} complexes, excitation and emission spectra of $[\text{Tb}(\text{L})(\text{H}_2\text{O})_q]$, and optimized Cartesian coordinates for the $[\text{Gd}(\text{L})(\text{H}_2\text{O})]$ and $[\text{Lu}(\text{L})(\text{H}_2\text{O})]$ systems.

Acknowledgments

The authors thank the Ministerio de Educación y Ciencia (MEC), the Fondo Europeo de Desarrollo Regional (FEDER) (CTQ2006-07875/PPQ and CTQ2009-10721), and the Xunta de Galicia (INCITE09EIR103013ES) for financial support. The authors are indebted to the Centro de Supercomputación de Galicia (CESGA) for providing the computer facilities. M. R.-F.

thanks the Ministerio de Educación y Ciencia (FPU program) for a predoctoral fellowship.

- [1] D. Parker, R. S. Dickins, H. Puschmann, C. Crossland, J. A. K. Howard, *Chem. Rev.* **2002**, 102, 1977–2010.
- [2] a) *Lanthanide Probes in Life, Chemical and Earth Sciences: Theory and Practice* (Eds.: J.-C. G. Bünzli, G. R. Choppin), Elsevier, Amsterdam, **1989**; b) P. Caravan, J. J. Ellinson, T. J. McMurry, R. B. Lauffer, *Chem. Rev.* **1999**, 99, 2293; c) *The Chemistry of Contrast Agents in Medical Magnetic Resonance Imaging* (Eds.: A. E. Merbach, É. Tóth), Wiley, New York, **2001**; d) L. M. De Leon-Rodriguez, A. J. M. Lubag, C. R. Malloy, G. V. Martinez, R. J. Gillies, A. D. Sherry, *Acc. Chem. Res.* **2009**, 42, 948–957; e) K. W.-Y. Chan, W.-T. Wong, *Coord. Chem. Rev.* **2007**, 251, 2428–2451.
- [3] a) S. Liu, *Adv. Drug Deliv. Rev.* **2008**, 60, 1347–1370; b) F. Roesch, *Radiochim. Acta* **2007**, 95, 303–311; c) W. A. Volkert, T. J. Hoffman, *Chem. Rev.* **1999**, 99, 2269–2292; d) M. F. Tweedle, *Acc. Chem. Res.* **2009**, 42, 958–968.
- [4] a) X. Wang, T. Jin, V. Comblin, A. Lopez-Mut, E. Merciny, J.-F. Desreux, *Inorg. Chem.* **1992**, 31, 1095–1099; b) E. Toth, E. Brucher, I. Lazar, I. Toth, *Inorg. Chem.* **1994**, 33, 4070–4076.
- [5] a) K. Kumar, C. A. Chang, L. C. Francesconi, D. D. Dischino, M. F. Malley, J. Z. Gougoutas, M. F. Tweedle, *Inorg. Chem.* **1994**, 33, 3567–3575; b) K. Kumar, C. A. Chang, M. F. Tweedle, *Inorg. Chem.* **1993**, 32, 587–593; c) K. Kumar, M. F. Tweedle, *Inorg. Chem.* **1993**, 32, 4193–4199.
- [6] C. A. Chang, L. C. Francesconi, M. F. Malley, K. Kumar, J. Z. Gougoutas, M. F. Tweedle, D. W. Lee, L. J. Wilson, *Inorg. Chem.* **1993**, 32, 3501–3508.
- [7] a) L. M. Urbanczyk-Pearson, F. J. Femia, J. Smith, G. Parigi, J. A. Duimstra, A. L. Eckermann, C. Luchinat, T. J. Meade, *Inorg. Chem.* **2008**, 47, 56–68; b) C. Carrera, G. Digilio, S. Baroni, D. Burgio, S. Consol, F. Fedeli, D. Longo, A. Mortillaro, S. Aime, *Dalton Trans.* **2007**, 4980–4987; c) J. A. Duimstra, F. J. Femia, T. J. Meade, *J. Am. Chem. Soc.* **2005**, 127, 12847–12855.
- [8] M. Regueiro-Figueroa, K. Djanashvili, D. Esteban-Gómez, T. Chauvin, E. Toth, A. de Blas, T. Rodríguez-Blas, C. Platas-Iglesias, *Inorg. Chem.* **2010**, 49, 4212–4223.
- [9] a) E. L. Que, E. Gianolio, S. L. Baker, A. P. Wong, S. Aime, C. J. Chang, *J. Am. Chem. Soc.* **2009**, 131, 8527–8536; b) M. P. Lowe, D. Parker, O. Reany, S. Aime, M. Botta, G. Castellano, E. Gianolio, R. Pagliarini, *J. Am. Chem. Soc.* **2001**, 123, 7601–7609; c) L. M. Manus, D. J. Mastarone, E. A. Waters, X.-Q. Zhang, E. A. Schultz-Sikma, K. W. MacRenaris, D. Ho, T. J. Meade, *Nano Lett.* **2010**, 10, 484–489; d) E. Gianolio, R. Napolitano, F. Fedeli, F. Arena, S. Aime, *Chem. Commun.* **2009**, 6044–6046; e) S. Lacerda, M. P. Campello, F. Marques, L. Gano, V. Kubicek, P. Fouskova, E. Toth, I. Santos, *Dalton Trans.* **2009**, 4509–4518.
- [10] a) T. Koullourou, L. S. Natrajan, H. Bhavsar, S. J. A. Pope, J. Feng, J. Narvainen, R. Shaw, E. Scales, R. Kauppinen, A. M. Kenwright, S. Faulkner, *J. Am. Chem. Soc.* **2008**, 130, 2178–2179.
- [11] a) S. Aime, M. Botta, M. Fasano, M. P. M. Marques, C. F. G. C. Geraldes, D. Pubanz, A. E. Merbach, *Inorg. Chem.* **1997**, 36, 2059–2068; b) S. Hoeft, K. Roth, *Chem. Ber.* **1993**, 126, 869–873; c) S. Aime, M. Botta, G. Ermondi, *Inorg. Chem.* **1992**, 31, 4291–4299.
- [12] M. Jauregui, W. S. Perry, C. Allain, L. R. Vidler, M. C. Willis, A. M. Kenwright, J. S. Snaith, G. J. Stasiuk, M. P. Lowe, S. Faulkner, *Dalton Trans.* **2009**, 6283–6285.
- [13] a) E. S. Henriques, C. F. G. C. Geraldes, M. J. Ramos, *Mol. Phys.* **2003**, 101, 2319–2333; b) R. S. Ranganathan, N. Raju, H. Fan, X. Zhang, M. F. Tweedle, J. F. Desreux, V. Jacques, *Inorg. Chem.* **2002**, 41, 6856–6866; c) C. A. Chang, Y.-L. Liu, C.-Y. Chen, X.-M. Chou, *Inorg. Chem.* **2001**, 40, 3448–3455; d) R. Fossheim, H. Dugstad, S. G. Dahl, *Eur. J. Med. Chem.* **1995**, 30, 539–546; e) R. Fossheim, S. G. Dahl, *Acta Chem. Scand.* **1990**, 44, 698–706.

- [14] a) E. S. Henriques, M. Bastos, C. F. G. C. Geraldies, M. J. Ramos, *Int. J. Quantum Chem.* **1999**, 73, 237–248; b) U. Cosentino, G. Moro, D. Pitea, A. Villa, P. C. Fantucci, A. Maiocchi, F. Uggeri, *J. Phys. Chem. A* **1998**, 102, 4606–4614.
- [15] a) B. A. Hess Jr., A. Kedzierski, L. Smentek, D. J. Bornhop, *J. Phys. Chem. A* **2008**, 112, 2397–2407; b) O. V. Yazyev, L. Helm, V. G. Malkin, O. L. Malkina, *J. Phys. Chem. A* **2005**, 109, 10997–11005; c) L. Smentek, B. A. Hess Jr., J. P. Cross, H. C. Manning, D. J. Bornhop, *J. Chem. Phys.* **2005**, 123, 244302; d) K. H. Chalmers, E. De Luca, N. H. M. Hogg, A. M. Kenwright, I. Kuprov, D. Parker, M. Botta, J. I. Wilson, A. M. Blamire, *Chem. Eur. J.* **2010**, 16, 134–148.
- [16] a) O. V. Yazyev, L. Helm, *Eur. J. Inorg. Chem.* **2008**, 201–211; b) F. Yerly, A. Borel, L. Helm, A. E. Merbach, *Chem. Eur. J.* **2003**, 9, 5468–5480; c) A. Borel, L. Helm, A. E. Merbach, *Chem. Eur. J.* **2001**, 7, 600–610.
- [17] U. Cosentino, A. Villa, D. Pitea, G. Moro, V. Barone, A. Maiocchi, *J. Am. Chem. Soc.* **2002**, 124, 4901–4909.
- [18] a) A. Roca-Sabio, M. Mato-Iglesias, D. Esteban-Gomez, E. Toth, A. de Blas, C. Platas-Iglesias, T. Rodríguez-Blas, *J. Am. Chem. Soc.* **2009**, 131, 3331–3341; b) M. del C. Fernandez-Fernandez, R. Bastida, A. Macias, P. Perez-Lourido, C. Platas-Iglesias, L. Valencia, *Inorg. Chem.* **2006**, 45, 4484–4496; c) M. Gonzalez-Lorenzo, C. Platas-Iglesias, F. Avecilla, S. Faulkner, S. J. A. Pope, A. de Blas, T. Rodríguez-Blas, *Inorg. Chem.* **2005**, 44, 4254–4262; d) C. Nuñez, R. Bastida, A. Macias, M. Mato-Iglesias, C. Platas-Iglesias, L. Valencia, *Dalton Trans.* **2008**, 3841–3850; e) C. Nuñez, M. Mato-Iglesias, R. Bastida, A. Macias, P. Perez-Lourido, C. Platas-Iglesias, L. Valencia, *Eur. J. Inorg. Chem.* **2009**, 1086–1095; f) M. Gonzalez-Lorenzo, C. Platas-Iglesias, M. Mato-Iglesias, D. Esteban-Gomez, A. de Blas, T. Rodríguez-Blas, *Polyhedron* **2008**, 27, 1415–1422.
- [19] a) C. Platas-Iglesias, M. Mato-Iglesias, K. Djanashvili, R. N. Muller, L. Vander Elst, J. A. Peters, A. de Blas, T. Rodríguez-Blas, *Chem. Eur. J.* **2004**, 10, 3579–3590; b) M. Mato-Iglesias, T. Rodríguez-Blas, C. Platas-Iglesias, M. Starck, P. Kadjane, R. Ziessel, L. Charbonniere, *Inorg. Chem.* **2009**, 48, 1507–1518; c) L. Charbonniere, S. Mameri, P. Kadjane, C. Platas-Iglesias, R. Ziessel, *Inorg. Chem.* **2008**, 47, 3748–3762; d) M. Mato-Iglesias, C. Platas-Iglesias, K. Djanashvili, J. A. Peters, E. Toth, E. Balogh, R. N. Muller, L. Vander Elst, A. de Blas, T. Rodríguez-Blas, *Chem. Commun.* **2005**, 4729–4731; e) M. Mato-Iglesias, E. Balogh, C. Platas-Iglesias, E. Toth, A. de Blas, T. Rodríguez-Blas, *Dalton Trans.* **2006**, 5404–5415.
- [20] M. Purgel, Z. Baranyai, A. de Blas, T. Rodríguez-Blas, I. Bányai, C. Platas-Iglesias, I. Tóth, *Inorg. Chem.* **2010**, 49, 4370–4382.
- [21] A. Barge, L. Tei, D. Upadhyaya, F. Fedeli, L. Beltrami, R. Stefania, S. Aime, G. Cravotto, *Org. Biomol. Chem.* **2008**, 6, 1176–1184.
- [22] P. Kadjane, C. Platas-Iglesias, R. Ziessel, L. J. Charbonniere, *Dalton Trans.* **2009**, 5688–5700.
- [23] W. D. Horrocks Jr., D. R. Sudnick, *Acc. Chem. Res.* **1981**, 14, 384–392.
- [24] R. S. Dickens, S. Aime, A. S. Batsanov, A. Beeby, M. Botta, J. I. Bruce, J. A. K. Howard, C. S. Love, D. Parker, R. D. Peacock, H. Puschmann, *J. Am. Chem. Soc.* **2002**, 124, 12697–12705.
- [25] W. D. Horrocks Jr., D. R. Sudnick, *J. Am. Chem. Soc.* **1979**, 101, 334–340.
- [26] A. Beeby, I. M. Clarkson, R. S. Dickens, S. Faulkner, D. Parker, L. Royle, A. S. de Sousa, J. A. G. Williams, M. Woods, *J. Chem. Soc. Perkin Trans. 2* **1999**, 493–504.
- [27] S. Faulkner, S. J. A. Pope, *J. Am. Chem. Soc.* **2003**, 125, 10526–10527.
- [28] a) E. Toth, O. M. Ni Dhubhghaill, G. Besson, L. Helm, A. E. Merbach, *Magn. Reson. Chem.* **1999**, 37, 701–708; b) X. Zhang, C. A. Chang, H. G. Brittain, J. M. Garrison, J. Telsner, M. F. Tweedle, *Inorg. Chem.* **1992**, 31, 5597–5600.
- [29] F. A. Dunand, S. Aime, S. G. Crich, G. B. Giovenzana, A. E. Merbach, *Magn. Reson. Chem.* **2002**, 40, 87–92.
- [30] J. Costa, E. Balogh, V. Turcay, R. Tripier, M. Le Baccon, F. Chuburu, H. Handel, L. Helm, E. Toth, A. E. Merbach, *Chem. Eur. J.* **2006**, 12, 6841–6851.
- [31] A. Mishra, P. Fouskova, G. Angelovski, E. Balogh, A. K. Mishra, N. K. Logothetis, E. Toth, *Inorg. Chem.* **2008**, 47, 1370–1381.
- [32] a) M. B. Inoue, M. Inoue, Q. Fernando, *Inorg. Chim. Acta* **1995**, 232, 203–206; b) S. I. Kang, R. S. Ranganathan, J. E. Emswiler, K. Kumar, J. Z. Gougoutas, M. F. Malley, M. F. Tweedle, *Inorg. Chem.* **1993**, 32, 2912–2918.
- [33] M. Mato-Iglesias, A. Roca-Sabio, Z. Palinkas, D. Esteban-Gomez, C. Platas-Iglesias, E. Toth, A. de Blas, T. Rodríguez-Blas, *Inorg. Chem.* **2008**, 47, 7840–7851.
- [34] M. Seitz, A. G. Oliver, K. N. Raymond, *J. Am. Chem. Soc.* **2007**, 129, 11153–11160.
- [35] M. R. Spirllet, J. Rebizant, J. F. Desreux, M. F. Loncin, *Inorg. Chem.* **1984**, 23, 359–363.
- [36] C. Piguet, J.-C. G. Bünzli, G. Bernardinelli, C. G. Bochet, P. Froidevaux, *J. Chem. Soc., Dalton Trans.* **1995**, 83–97.
- [37] M. Dolg, H. Stoll, A. Savin, H. Preuss, *Theor. Chim. Acta* **1989**, 75, 173–194.
- [38] M. Woods, Z. Kovacs, S. Zhang, A. D. Sherry, *Angew. Chem. Int. Ed.* **2003**, 42, 5889–5892.
- [39] a) H. D. Powell, O. M. Ni Dhubhghaill, D. Pubanz, L. Helm, Y. Lebedev, W. Schlaepfer, A. E. Merbach, *J. Am. Chem. Soc.* **1996**, 118, 9333–9346; b) Z. Palinkas, A. Roca-Sabio, M. Mato-Iglesias, D. Esteban-Gomez, C. Platas-Iglesias, A. De Blas, T. Rodríguez-Blas, E. Toth, *Inorg. Chem.* **2009**, 48, 8878–8889.
- [40] A. M. Raitsimring, A. V. Astashkin, D. Baute, D. Goldfarb, P. Caravan, *J. Phys. Chem. A* **2004**, 108, 7318–7323.
- [41] S. Aime, A. Barge, F. Benetollo, G. Bombieri, M. Botta, F. Uggeri, *Inorg. Chem.* **1997**, 36, 4287–4289.
- [42] S. Aime, A. Barge, J. I. Bruce, M. Botta, J. A. K. Howard, J. M. Moloney, D. Parker, A. S. de Sousa, M. Woods, *J. Am. Chem. Soc.* **1999**, 121, 5762.
- [43] M. P. Placidi, L. S. Natrajan, D. Sykes, A. M. Kenwright, S. Faulkner, *Helv. Chim. Acta* **2009**, 92, 2427–2438.
- [44] a) V. Jacques, J. F. Desreux, *Inorg. Chem.* **1994**, 33, 4048–4053; b) S. Aime, A. Barge, M. Botta, M. Fasano, J. D. Ayala, G. Bombieri, *Inorg. Chim. Acta* **1996**, 246, 423–429.
- [45] M. Woods, S. Aime, M. Botta, J. A. K. Howard, J. M. Moloney, M. Navet, D. Parker, M. Port, O. Rousseaux, *J. Am. Chem. Soc.* **2000**, 122, 9781–9792.
- [46] A. D. Becke, *J. Chem. Phys.* **1993**, 98, 5648–5652.
- [47] C. Lee, W. Yang, R. G. Parr, *Phys. Rev. B* **1988**, 37, 785–789.
- [48] M. J. Frisch, G. W. Trucks, H. B. Schlegel, G. E. Scuseria, M. A. Robb, J. R. Cheeseman, J. A. Montgomery Jr., T. Vreven, K. N. Kudin, J. C. Burant, J. M. Millam, S. S. Iyengar, J. Tomasi, V. Barone, B. Mennucci, M. Cossi, G. Scalmani, N. Rega, G. A. Petersson, H. Nakatsuji, M. Hada, M. Ehara, K. Toyota, R. Fukuda, J. Hasegawa, M. Ishida, T. Nakajima, Y. Honda, O. Kitao, H. Nakai, M. Klene, X. Li, J. E. Knox, H. P. Hratchian, J. B. Cross, V. Bakken, C. Adamo, J. Jaramillo, R. Gomperts, R. E. Stratmann, O. Yazyev, A. J. Austin, R. Cammi, C. Pomelli, J. W. Ochterski, P. Y. Ayala, K. Morokuma, G. A. Voth, P. Salvador, J. J. Dannenberg, V. G. Zakrzewski, S. Dapprich, A. D. Daniels, M. C. Strain, O. Farkas, D. K. Malick, A. D. Rabuck, K. Raghavachari, J. B. Foresman, J. V. Ortiz, Q. Cui, A. G. Baboul, S. Clifford, J. Cioslowski, B. B. Stefanov, G. Liu, A. Liashenko, P. Piskorz, I. Komaromi, R. L. Martin, D. J. Fox, T. Keith, M. A. Al-Laham, C. Y. Peng, A. Nanayakkara, M. Challacombe, P. M. W. Gill, B. Johnson, W. Chen, M. W. Wong, C. Gonzalez, J. A. Pople, *Gaussian 03*, Revision C.01, Gaussian, Inc., Wallingford CT, **2004**.
- [49] a) L. Maron, O. Eisenstein, *J. Phys. Chem. A* **2000**, 104, 7140–7143; b) C. Boehme, B. Coupez, G. Wipff, *J. Phys. Chem. A* **2002**, 106, 6487–6498.

- [50] a) C. Peng, P. Y. Ayala, H. B. Schlegel, M. J. Frisch, *J. Comput. Chem.* **1996**, *17*, 49–56; b) C. Peng, H. B. Schlegel, *Isr. J. Chem.* **1994**, *33*, 449–454.
- [51] G. M. Sheldrick, *SADABS*, Version 2.10, University of Göttingen, Germany, **2004**.
- [52] SHELX: G. M. Sheldrick, *Acta Crystallogr., Sect. A* **2008**, *64*, 112–122.
- [53] WinGX MS-Windows system of programs for solving, refining, and analyzing single-crystal X-ray diffraction data for small molecules: L. J. Farrugia, *J. Appl. Crystallogr.* **1999**, *32*, 837–838.
- [54] DIRDIF99: P. T. Beurskens, G. Beurskens, R. de Gelder, S. García-Granda, R. O. Gould, R. Israel, J. M. M. Smits, *The DIRDIF-99 Program System*, Technical Report of the Crystallography Laboratory, University of Nijmegen, The Netherlands, **1999**.
- [55] M. Nardelli, *J. Appl. Crystallogr.* **1999**, *32*, 563–571.
- [56] D. D. Dischino, E. J. Delaney, J. E. Emswiler, G. T. Gaughan, J. S. Prasad, S. K. Srivastava, M. F. Tweedle, *Inorg. Chem.* **1991**, *30*, 1265–1269.

Received: March 26, 2010
Published Online: June 23, 2010

Ruthenium vs. Osmium Complexes as Catalysts for Atom Transfer Radical Addition Reactions

Mariano A. Fernández-Zúmel,^[a] Gregor Kiefer,^[a] Katrin Thommes,^[a] Rosario Scopelliti,^[a] and Kay Severin^{*[a]}

Keywords: ATRA / ATRC / Osmium / Radical reactions / Ruthenium

The catalytic activity of $[\text{Cp}^*\text{OsBr}_2(\text{PPh}_3)]$ in conjunction with Mg has been evaluated for atom transfer radical addition (ATRA) and cyclization (ATRC) reactions. The Os complex enabled these reactions to be performed with similar efficiency as that of the analogous Ru complex $[\text{Cp}^*\text{RuCl}_2(\text{PPh}_3)]$. The olefin complex $[\text{Cp}^*\text{OsBr}(\text{H}_2\text{C}=\text{CHPh})(\text{PPh}_3)]$

was obtained by reduction of $[\text{Cp}^*\text{OsBr}_2(\text{PPh}_3)]$ with Mg in the presence of an excess of styrene, whereas an analogous Ru complex was not observed. Kinetic investigations suggest that olefin complexes of Os can form under catalytic conditions.

Introduction

Halogenated compounds can be coupled to olefins by an atom transfer radical addition mechanism. Pioneering studies in this area were performed by Kharasch and his group in the 1940s,^[1] and reactions of this type are commonly referred to as “Kharasch reactions”.^[2] Modern, transition-metal-catalyzed versions of this reaction have found numerous applications in organic synthesis.^[2,3] Copper^[4] and ruthenium complexes^[5,6] typically show the best catalytic performance for ATRA reactions. One of the most active catalysts described so far is the half-sandwich complex $[\text{Cp}^*\text{RuCl}_2(\text{PPh}_3)]$ (**1**), which is used in conjunction with either AIBN or Mg.^[6] This catalytic system enables turnover numbers of 1000 or above to be obtained for a number of substrates. Furthermore, it has been successfully applied to atom transfer radical cyclization (ATRC) reactions, which are particularly interesting from a synthetic point of view.^[6a]

The metal-catalyzed atom transfer radical polymerization (ATRP) of olefins is mechanistically closely related to ATRA reactions.^[3b] For the former reaction, it was reported that the Os^{II} complex $[\text{Cp}^*\text{OsBr}(\text{P}i\text{Pr}_3)]$ is a more active catalyst than its Ru analogue $[\text{Cp}^*\text{RuCl}(\text{P}i\text{Pr}_3)]$.^[7] This finding suggested that Os complexes could also be beneficial for ATRA and ATRC reactions. Below we report the results of a study in which we have compared the catalytic activity of the complex $[\text{Cp}^*\text{RuCl}_2(\text{PPh}_3)]$ (**1**) with that of its Os analogue $[\text{Cp}^*\text{OsBr}_2(\text{PPh}_3)]$ (**2**). Furthermore, we demonstrate that olefin complexes are readily formed in the

case of Os, whereas the analogous Ru complexes are significantly less stable. The implication of this finding for the mechanism of the reaction is discussed.

Results and Discussion

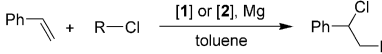
First, we have evaluated the catalytic performance of the complexes $[\text{Cp}^*\text{RuCl}_2(\text{PPh}_3)]$ (**1**) and $[\text{Cp}^*\text{OsBr}_2(\text{PPh}_3)]$ (**2**) for different intermolecular ATRA reactions. Complex **2** is not a perfect analogue of **1**, because – apart from the metal – the halide coligand has also been changed from chloride to bromide. The synthetic chemistry of organometallic Os–Br complexes is much more developed than the chemistry of Os–Cl complexes (the reduction of OsO_4 is more facile with HBr than with HCl).

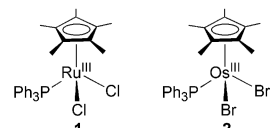
The halogenated compounds used in our study were ethyl trichloroacetate, ethyl dichloroacetate, and chloroform, and the olefinic reaction partner was styrene. The reactions were performed with substrate concentrations of $[\text{styrene}] = [\text{R}-\text{Cl}] = 500 \text{ mM}$ in neat toluene with catalyst concentrations of 0.1 and 0.02 mol-%. All reactions were carried out in the presence of an excess of Mg powder. It should be noted that these conditions are not necessarily the optimum conditions for these reactions (faster conversions can be achieved with higher substrate concentrations),^[6a] but the goal of this study was to evaluate the relative performance of the Ru and the Os catalyst. The results of the reactions are summarized in Table 1.

For the addition of ethyl dichloroacetate to styrene at room temp. we found that reactions with the Ru complex **1** were faster than with the Os complex **2**: after 24 h, we observed a full conversion of styrene in the case of complex **1**, whereas a conversion of only 57% was recorded for reactions with complex **2** (Table 1, Entries 1 and 2). At 60 °C,

[a] Institut des Sciences et Ingénierie Chimiques, École Polytechnique Fédérale de Lausanne (EPFL)
1015 Lausanne, Suisse
Fax: +41-21-693-9305
E-mail: kay.severin@epfl.ch

Table 1. ATRA reactions of chlorinated compounds to styrene catalyzed by complex **1** or **2** in the presence of Mg.^[a]





Entry	Cat.	RCl	Temp. [°C]	[RCl]/[Cat]	Yield (Conv.) [%]
1	1	CCl ₂ HCO ₂ Et	r.t.	1000:1	84 (>99)
2	2	CCl ₂ HCO ₂ Et	r.t.	1000:1	42 (57)
3	1	CCl ₂ HCO ₂ Et	60	1000:1	84 (>99)
4	2	CCl ₂ HCO ₂ Et	60	1000:1	84 (>99)
5	1	CCl ₂ HCO ₂ Et	60	5000:1	14 (31)
6	2	CCl ₂ HCO ₂ Et	60	5000:1	16 (39)
7	1	CCl ₃ CO ₂ Et	60	1000:1	55 (83)
8	2	CCl ₃ CO ₂ Et	60	1000:1	24 (45)
9	1	CCl ₃ CO ₂ Et	60	5000:1	17 (31)
10	2	CCl ₃ CO ₂ Et	60	5000:1	3 (14)
11	1	CHCl ₃	60	1000:1	28 (47)
12	2	CHCl ₃	60	1000:1	31 (47)

[a] Reaction conditions: [RCl] = 500 mM; [styrene] = 500 mM; [Ru/Os] = 0.50 or 0.10 mM (0.1 or 0.02 mol-%), [Mg] = 100 mg (4.1 mmol), toluene, reaction time 24 h. The data represent averaged values of two independent experiments. Yields and styrene conversions were determined by GC using mesitylene as the internal standard.

however, the differences in reactivity were much less pronounced, and comparable yields and conversions were obtained for reactions with 0.1 and 0.02 mol-% of catalyst (Table 1, Entries 3–6). Apparently, the Os complex **2** benefits more from the enhanced reaction temperature. A possible explanation is that the reduction of the Os^{III} precursor **2** to a catalytically active Os^{II} species by Mg is relatively slow at room temp. This assumption is substantiated by the following observation: when a toluene solution of the Ru^{III} complex **1** is added to a flask containing Mg, a rapid color change from orange to yellow is observed at room temp. within minutes. In the case of the Os^{III} complex **2**, however, a change in color proceeds slowly within the first hour.

For the reaction of ethyl trichloroacetate with styrene, we found that the Ru complex **1** gave superior results, even at 60 °C (Table 1, Entries 7–10). However, the differences in reactivity were not very pronounced. Comparable yields and conversions were observed for reactions with chloroform as the substrate (Table 1, Entries 11 and 12). For all reactions investigated, the yields were lower than the conversions. This is likely to be a result of the formation of oligomers, a common problem in ATRA reactions.^[4,5]

Next, we tested the performance of the catalysts **1** and **2** in atom transfer radical cyclization (ATRC) reactions. We used two trichloroethyl ethers and three dichloroacetamides as representative substrates. The cyclizations were performed at 60 °C with 1.0 mol-% of the complexes **1** or **2** in the presence of Mg. The results are summarized in Table 2. In most cases the Ru complex **1** gave better results in terms

of yield. On the other hand, the diastereoselectivity was higher for the Os-catalyzed reactions, in particular for the substrate 1-(2,2,2-trichloroethoxy)-3-phenylprop-2-ene (Entry 2). It should be noted, however, that the stereoselectivity was found to change during the course of the reaction. When ATRC reactions with 1-(2,2,2-trichloroethoxy)-3-phenylprop-2-ene were examined after 40 min, both the Ru- and the Os-catalyzed reactions showed a diastereoselectivity of 19:1 (the yields at that point were 61 % and 20 %, respectively). These results suggest that epimerization processes are occurring, which are more pronounced for reactions with the “faster” Ru catalyst.

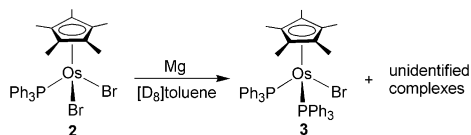
Table 2. ATRC reactions catalyzed by complex **1** or **2** in the presence of Mg.^[a]

Entry	Substrate	Product	Cat.	Yield (Conv.) [%]
1			1	87 (100)
			2	92 (100)
2			1	88 (99) [6:1] ^[c]
			2	78 (91) [15:1] ^[c]
3			1	86 (96) [3.4:1] ^[c]
			2	71 (88) [3.4:1] ^[c]
4 ^[b]			1	58 (73) [4:1] ^[c]
			2	27 (57) [5:1] ^[c]
5			1	91 (100) [2.4:1] ^[c]
			2	81 (83) [2.6:1] ^[c]

[a] Reaction conditions: [substrate] = 100 mM; [Ru/Os] = 1.0 mM (1.0 mol-%), [Mg] = 100 mg (4.1 mmol), [D₈]toluene, 60 °C, reaction time: 24 h. Yields and conversions were determined by NMR spectroscopy using mesitylene as the internal standard. [b] 2.5 mol-% of catalyst was used. [c] Diastereoselectivity.

For ATRA reactions with the catalyst precursor [Cp*₂RuCl₂(PPh₃)] (**1**) it is assumed that the reaction starts by Mg-induced reduction to give an Ru^{II} complex that can reversibly abstract a halogen atom from the substrate.^[8] A likely candidate for the active Ru^{II} catalyst is the 16e[−] complex [Cp*₂RuCl(PPh₃)], but attempts to prepare this complex on a preparative scale have failed.^[9] However, it was possible to stabilize a structurally related complex by using a sterically very demanding cyclopentadienyl ligand.^[10] In the case of Os, the synthesis and the structure of the 16e[−] complex [Cp*₂OsBr(PiPr₃)] has been reported,^[11] but, to the best of our knowledge, an analogous PPh₃ complex is not known. We wanted to explore the Mg-induced reduction of complex **2** in more detail. Thus, a [D₈]toluene suspension of **2** (0.025 mmol in 1 mL of solvent) was mixed with an excess of Mg. After 24 h, the Mg was filtered off, and the solution was investigated by NMR spectroscopy. The major

diamagnetic species in solution (36% yield, as determined with the internal standard mesitylene) was found to be the known complex $[\text{Cp}^*\text{OsBr}(\text{PPh}_3)_2]$ (**3**) (Scheme 1).^[12]



Scheme 1. Reduction of complex **2** by Mg.

The reduction of complex **2** with Mg apparently induced a ligand transfer of PPh_3 . We have not tried to optimize this synthetic procedure since complex **3** is more conveniently obtained by reaction of $[\text{Cp}^*\text{OsBr}_2]$ with PPh_3 .^[12] However, we have performed a single-crystal X-ray analysis of **3** (Figure 1). For comparison, we have also examined the solid-state structure of the precursor **2** (Figure 2).

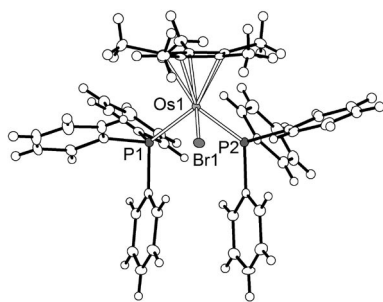


Figure 1. Molecular structure of complex **3** with ellipsoids at the 50% probability level. Only one of the two independent molecules in the unit cell is shown. Selected bond lengths [Å] and angles [°]: Os1–Br1 2.5934(4), Os1–P1 2.3370(9), Os1–P2 2.3313(9); P2–Os1–P1 96.51(3), P2–Os1–Br1 88.61(2), P1–Os1–Br1 93.98(2).

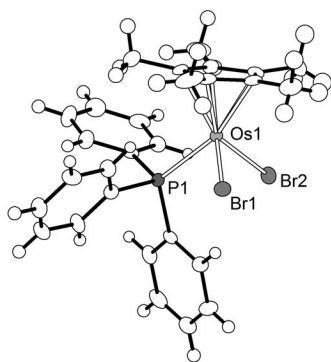
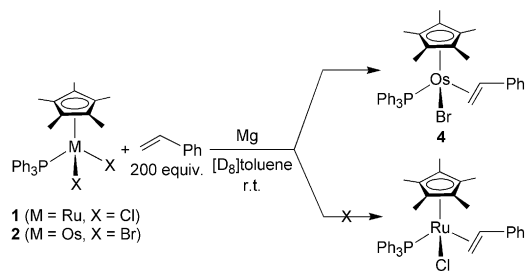


Figure 2. Molecular structure of complex **2** with ellipsoids at the 50% probability level. Selected bond lengths [Å] and angles [°]: Os1–Br1 2.5110(9), Os1–Br2 2.4955(8), Os1–P1 2.3379(1); P1–Os1–Br1 88.49(5), P1–Os1–Br2 88.50(5), Br2–Os1–Br1 97.81(3).

Both complexes show the expected three-legged piano-stool geometry. The Os–Br and Os–P bond lengths observed for **3** (Figure 1) are very similar to those found for the analogous complex $[\text{Cp}^*\text{OsBr}(\text{PPh}_3)_2]$ ($\text{Cp} = \eta^5\text{-cyclopentadienyl}$).^[13] The Os–Br bond lengths [2.5110(9) and 2.4955(8) Å] of the Os^{III} complex **2** are shorter than that

found for the Os^{II} complex **3** [2.5934(4) Å]. A similar shortening has been observed for the analogous Ru complexes $[\text{Cp}^*\text{RuCl}_2(\text{PPh}_3)]$ [Ru–Cl 2.4042(5) and 2.3775(5) Å]^[6a] and $[\text{Cp}^*\text{RuCl}(\text{PPh}_3)_2]$ [Ru–Cl 2.4583(6) Å].^[14]

We have also investigated the reduction of the complexes **1** and **2** with Mg in the presence of an excess of styrene (Scheme 2). This experiment was performed to evaluate the possibility that the hypothetical intermediates $[\text{Cp}^*\text{MX}(\text{PPh}_3)]$ are stabilized by coordination to the olefinic substrate. As before, the reactions were performed in deuterated toluene to allow in situ NMR analyses. For reactions with the Os complex **2**, we observed the formation of a new complex **4** with a ^{31}P NMR signal at $\delta = 7.4$ ppm. In the ^1H NMR spectrum, this complex showed three well-defined signals at $\delta = 5.71$ (dd), 2.91 (ddd), and 2.47 (ddd) ppm, which suggests the presence of coordinated styrene (the signals of “free” styrene can be observed at $\delta = 6.82$, 5.86, and 5.35 ppm). The description of **4** as an olefin complex with the formula $[\text{Cp}^*\text{OsBr}(\text{H}_2\text{C}=\text{CHPh})(\text{PPh}_3)]$ was also supported by the ^{13}C NMR spectroscopic data. For reactions with the Ru complex **1** we did not find evidence for the formation of a diamagnetic styrene complex (the ^1H NMR spectrum showed no signals between $\delta = 2$ and 3 ppm). It is interesting to note that olefin complexes of the formula $[\text{Cp}^*\text{RuCl}(\text{H}_2\text{C}=\text{CHR})(\text{PPh}_3)]$ ($\text{R} = \text{CN}$, COCH_3) have been prepared by reaction of $[\text{Cp}^*\text{RuCl}(\text{PPh}_3)_2]$ with the respective olefin in thf .^[15] We have attempted a similar reaction with styrene: complex $[\text{Cp}^*\text{RuCl}(\text{PPh}_3)_2]$ (0.020 mm) was mixed with styrene (0.050 mm) in $[\text{D}_8]\text{thf}$, and an ^1H NMR spectrum was recorded after 4 h. As before, we did not observe signals corresponding to an olefin complex. These results suggest that the hypothetical styrene complex $[\text{Cp}^*\text{RuCl}(\text{H}_2\text{C}=\text{CHPh})(\text{PPh}_3)]$ is significantly less stable than complexes with electron-deficient olefins such as acrylonitrile or 3-buten-2-one, a finding that is in line with what has been observed for other late-transition-metal complexes.^[16]



Scheme 2. Reduction of the complexes **1** and **2** by Mg in the presence of an excess of styrene.

The facile formation of the styrene complex $[\text{Cp}^*\text{OsBr}(\text{H}_2\text{C}=\text{CHPh})(\text{PPh}_3)]$ (**4**) has potential implications for the mechanism of Os-catalyzed ATRA reactions since olefin complexes are possible intermediates, which could inhibit the reaction.^[17] To investigate this issue in more detail, we have performed a kinetic study of the Os-catalyzed ATRA reaction of ethyl trichloroacetate with styrene. The reactions were performed with a fixed concentra-

tion of $[\text{Cl}_3\text{CCO}_2\text{Et}] = 100 \text{ mM}$ and $[\mathbf{2}] = 0.50 \text{ mM}$ in the presence of Mg powder. The styrene concentrations were varied from 12.5 mM to 3.2 M, and the initial rate of the reaction was calculated from the yields obtained at nine different times within the first 25 min. For comparison, we have performed reactions with the Ru complex **1** under otherwise identical conditions. The results are summarized in Figure 3.

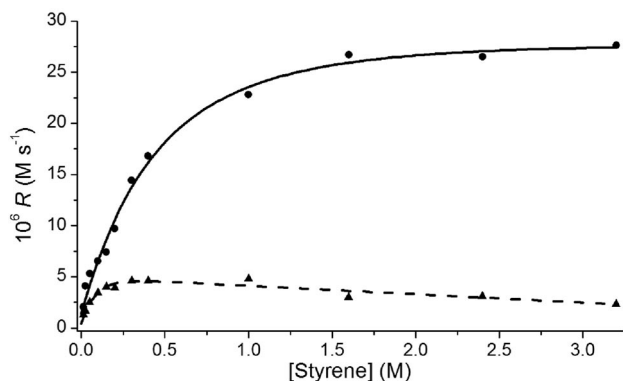


Figure 3. Observed initial reaction rates vs. initial styrene concentrations for the ATRA of ethyl trichloroacetate to styrene catalyzed by the Ru^{III} complex **1** (dots) or by the Os^{III} complex **2** (triangles) in the presence of Mg. Reaction conditions: [ethyl trichloroacetate] = 100 mM; [Ru/Os] = 0.50 mM, [Mg] = 100 mg, toluene, 60 °C. Yields were determined by GC using mesitylene as the internal standard.

For reactions with the Ru catalyst **1** one observes a nearly linear correlation between the initial reaction rate and the styrene concentration for $[\text{styrene}] \leq 200 \text{ mM}$. This result is in line with what we observed previously for kinetic studies carried out at 35 °C.^[8] At higher styrene concentrations, however, the reaction rates level off with saturation occurring at $[\text{styrene}] \approx 2 \text{ M}$. Such a saturation is expected because the high styrene/ $\text{Cl}_3\text{CCO}_2\text{Et}$ ratio favors oligomeric side products.^[18] Reactions with the Os complex **2** were slower than those with the Ru complex **1**. Importantly, the reaction rates started to level off at much lower styrene concentrations, and concentrations of above 1 M led to a decrease in the rate.

In addition, we have investigated the catalytic activity of the isolated styrene complex **4**, using the addition of ethyl dichloroacetate to styrene ($[\text{styrene}] = 500 \text{ mM}$, $[\text{Cl}_2\text{HCCO}_2\text{Et}] = 500 \text{ mM}$, $[\mathbf{4}] = 0.50 \text{ mM}$) as a test reaction.^[19] The initial rate of the reaction was found to be $1.3(\pm 0.2) \times 10^{-5} \text{ M s}^{-1}$, which is lower than that observed for reactions with the catalyst precursor **2** $[2.4(\pm 0.3) \times 10^{-5} \text{ M s}^{-1}]$.

The results suggest that Os-catalyzed ATRA reactions of halogenated compounds with styrene can be inhibited by the formation of olefin complexes, in particular when the reactions are performed with high concentrations of styrene. One should point out, however, that we have only indirect evidence for the relevance of styrene complexes under catalytic conditions, and alternative explanations for the observed data cannot be ruled out.

Conclusions

We have studied the catalytic activity of the Os complex $[\text{Cp}^*\text{OsBr}_2(\text{PPh}_3)]$ (**2**) in conjunction with Mg for intra- and intermolecular atom transfer radical reactions. It was found that the complex is a potent catalyst, which enables the ATRA and ATRC reactions to be performed in an efficient manner. However, under the conditions studied, its activity was either similar or lower than that of $[\text{Cp}^*\text{RuCl}_2(\text{PPh}_3)]$ (**1**). It is thus not justified to use a more expensive and toxic Os complex for these types of reactions. The isolation of $[\text{Cp}^*\text{OsBr}(\text{H}_2\text{C}=\text{CHPh})(\text{PPh}_3)]$ (**4**) shows that olefin complexes are more likely to form in reactions with Cp^*Os catalysts, and this should be considered for future studies with Os-catalyzed polymerization reactions.^[7,20]

Experimental Section

General: The complexes $[\text{Cp}^*\text{RuCl}_2(\text{PPh}_3)]$ (**1**),^[21] $[\text{Cp}^*\text{RuCl}(\text{PPh}_3)_2]$,^[22] and $[\text{Cp}^*\text{OsBr}_2(\text{PPh}_3)]$ (**2**),^[23] were prepared according to literature procedures. The substrates 1-(2,2,2-trichloroethoxy)-2-phenylprop-2-ene,^[5a] 1-(2,2,2-trichloroethoxy)-3-phenylprop-2-ene,^[24] *N*-allyl-2,2-dichloro-*N*-phenylacetamide,^[25] *N*-allyl-2,2-dichloro-*N*-(4-tolylsulfonyl)acetamide,^[26] and *N,N*-diallyl-2,2-dichloroacetamide^[26] for the ATRC reactions were also prepared according to published procedures. Mg powder (>99%) was purchased from Fluka and was agitated by means of a stirring bar under dry dinitrogen for 10 d before use. All ATRA, ATRC, and synthesis reactions were performed in a glove box under dinitrogen. The solvents were collected under dinitrogen from an Innovative Technologies SPS-400-5 solvent system. The commercially available substrates were distilled from appropriate drying agents and stored under dinitrogen. GC measurements were made with a Varian Chrompack CP3-380 apparatus (Chrompack CP-SIL8CB column; 30 m; 250 μm) coupled to an FID detector. The NMR spectra (¹H, ¹³C, ³¹P) were recorded at room temp. with a Bruker AVANCE DPX 400 spectrometer. Chemical shifts are relative to solvent signals as internal references; $\delta(^{31}\text{P})$ are relative to external H_3PO_4 (85% in D_2O). Microanalyses (C, H, N) were performed with an EA 1110 CHN Carlo Erba instrument.

General Procedure for the ATRA Reactions: An aliquot of a stock solution of complex **1** or **2** in toluene (400 μL of a 1.25 mM stock solution) was added to a 1.5 mL vial containing Mg powder (100 mg). The total volume was increased to 800 μL with toluene, and the resulting mixture was stirred at room temp. or 60 °C for 10 min. The reaction was then initiated by addition of 200 μL of a freshly prepared stock solution containing styrene, the chlorinated compound, and mesitylene as an internal standard. The solution was stirred at room temp. or 60 °C, and samples (25 μL) were removed at given times from the reaction mixtures, diluted with non-deoxygenated acetone (500 μL), and analyzed by GC chromatography.

General Procedure for the ATRC Reactions: An aliquot of a stock solution of complex **1** or **2** in $[\text{D}_8]\text{toluene}$ (800 μL of a 1.25 mM stock solution) was added to a 1.5 mL vial that contained Mg powder (100 mg). The resulting mixture was stirred at 60 °C for 10 min. The reaction was then initiated by addition of 200 μL of a freshly prepared stock solution containing the substrate and mesitylene as an internal standard in $[\text{D}_8]\text{toluene}$. For *N*-allyl-2,2-dichloro-*N*-(4-tolylsulfonyl)acetamide, a 1.5 mL vial was charged with 2.5 μmol of the solid catalysts **1** (or **2**), 100 mg of Mg, and 800 μL of $[\text{D}_8]$ -

toluene, and the mixture stirred at 60 °C for 10 min, before 200 μL of a freshly prepared stock solution containing the substrate and mesitylene as an internal standard in $[\text{D}_8]\text{toluene}$ was added. After 24 h, the reaction mixture was analyzed by ^1H NMR spectroscopy.

Reduction of Complexes 1 and 2 with or without Styrene: Complex 1 or 2 (5.0 μmol) and Mg powder (100 mg) were suspended in $[\text{D}_8]\text{-toluene}$ (1.0 mL). If styrene was used, 200 equiv. (1 mmol, 114.6 μL) of it were added. The resulting reaction mixtures were stirred at room temp. for 2 h, and the liquid phase was analyzed by ^1H NMR and ^{31}P NMR spectroscopy.

Synthesis of Complex 4: Styrene (800 μL , 6.99 mmol) was added to a suspension of complex 2 (33 mg, 44 μmol) and Mg (300 mg) in toluene (15 mL). The mixture was stirred at 35 °C for 15 h and then filtered through a glass frit. Solvents and excess styrene were removed under vacuum to give complex 4 as a yellow solid. Yield: 27 mg (ca. 75%). ^1H NMR (400 MHz, C_6D_6): δ = 1.23 (d, J = 1.4 Hz, 15 H, C_5Me_5), 2.47 (ddd, J = 15.7, J = 7.7, J = 2.6 Hz, 1 H, $\text{CH}=\text{CH}_2$), 2.91 (ddd, J = 10.2, J = 2.8, J = 2.6 Hz, 1 H, $\text{CH}=\text{CH}_2$), 5.71 (dd, J = 10.2, J = 7.7 Hz, 1 H, $\text{CH}=\text{CH}_2$), 6.98–8.18 (m, 20 H, aromatic) ppm. $^{31}\text{P}\{^1\text{H}\}$ NMR (162 MHz, C_6D_6): δ = 7.4 ppm. $^{13}\text{C}\{^1\text{H}\}$ NMR (101 MHz, C_6D_6): δ = 8.98 (s, C_5Me_5), 21.0 (d, J = 4.4 Hz, $\text{CH}=\text{CH}_2$), 41.8 (d, J = 2.9 Hz, $\text{CH}=\text{CH}_2$), 92.1 (d, J = 2.9 Hz, C_5Me_5), 124.8–136.9 (m), 145.9 (s) ppm. Attempts to characterize complex 4 by elemental analysis were unfortunately not successful. We assume that the styrene ligand is partially removed during the drying procedure.

Crystallographic Analyses: Single crystals of complex 2 were obtained by slow vapor diffusion of pentane into a benzene solution of 2. Single crystals of complex 3 were obtained by slow diffusion of hexane at -18 °C into a toluene solution, which was obtained after reduction of complex 2 with Mg and filtration. Intensity data for 2 were collected with an Oxford Diffraction KM-4 CCD dif-

fractometer, whereas in the case of 3 a Bruker APEX II CCD was employed, both having kappa geometry and using graphite-monochromatized Mo- K_α radiation (λ = 0.71073 Å) at low temperature. A summary of the crystallographic data, the data-collection parameters, and the refinement parameters are given in Table 3. Data reduction was carried out with CrysAlis PRO^[27] (2) and EvalCCD^[28] (3) and then corrected for absorption.^[29] Structure solution and refinement were performed with the SHELXTL software package.^[30] The structures were refined by using the full-matrix least-squares routines on F^2 . All non-hydrogen atoms were refined with anisotropic displacement parameters. Hydrogen atoms were included in the models in calculated positions by using the riding model. CCDC-772348 (2) and -772349 (3) contain the supplementary crystallographic data for this paper. These data can be obtained free of charge from The Cambridge Crystallographic Data Centre via www.ccdc.cam.ac.uk/data_request/cif.

Acknowledgments

This work was supported by the Swiss National Science Foundation and by the Ecole Polytechnique Fédérale de Lausanne (EPFL). We thank Dr. E. Solari for help with the crystallographic measurements.

Table 3. Crystallographic data for the complexes 2 and 3.

	Complex 2	Complex 3
Empirical formula	$\text{C}_{28}\text{H}_{30}\text{Br}_2\text{OsP}$	$\text{C}_{46}\text{H}_{45}\text{BrOsP}_2$
M_r [g mol^{-1}]	747.51	929.87
Crystal size [mm]	$0.32 \times 0.28 \times 0.17$	$0.31 \times 0.16 \times 0.37$
Crystal system	monoclinic	monoclinic
Space Group	$P2_1/n$	$P2_1/c$
a [Å]	8.7145(2)	17.349(2)
b [Å]	32.4584(8)	10.7211(10)
c [Å]	18.2551(6)	20.5972(17)
α [°]	90	90
β [°]	91.504(3)	101.101(8)
γ [°]	90	90
V [Å ³]	5161.8(2)	3759.4(7)
Z	8	4
$\rho_{\text{calcd.}}$ [g cm^{-3}]	1.924	1.643
T [K]	140(2)	100(2)
μ [mm^{-1}]	8.114	4.573
θ range [°]	2.64–27.88	3.36–27.51
Reflections collected	12237	86119
Independent reflections	12237	8624
Absorption corrections	semi-empirical	semi-empirical
Max./min. transmissions	1.00000/0.19163	1.0000/0.7237
Data/restraints/parameters	12237/0/579	8624/0/451
Goodness of fit on F^2	1.125	1.242
Final R indices [$I > 2\sigma(I)$]	$R_1 = 0.0517$, $wR_2 = 0.1318$	$R_1 = 0.0297$, $wR_2 = 0.0494$
R indices (all data)	$R_1 = 0.0600$, $wR_2 = 0.1354$	$R_1 = 0.0430$, $wR_2 = 0.0531$
Max. peak/hole [e Å^{-3}]	4.944/−2.163	0.778/−0.657

- a) M. S. Kharasch, E. V. Jensen, W. H. Urry, *Science* **1945**, 102, 128; b) M. S. Kharasch, W. H. Urry, E. V. Jensen, *J. Am. Chem. Soc.* **1945**, 67, 1626.
- a) K. Severin, *Curr. Org. Chem.* **2006**, 10, 217–224; b) R. A. Gossage, L. A. van de Kuil, G. van Koten, *Acc. Chem. Res.* **1998**, 31, 423–431.
- a) W. T. Eckenhoff, T. Pintauer, *Catal. Rev.* **2010**, 52, 1–59; b) T. Pintauer, K. Matyjaszewski, *Chem. Soc. Rev.* **2008**, 37, 1087–1097; c) L. Delaude, A. Demonceau, A. F. Noels, *Top. Organomet. Chem.* **2004**, 11, 155–171; d) H. Nagashima in *Ruthenium in Organic Synthesis* (Ed.: S.-I. Murahashi), Wiley-VCH, Weinheim, **2004**, pp. 333–343; e) A. J. Clark, *Chem. Soc. Rev.* **2002**, 31, 1–11; f) K. I. Kobrakov, A. V. Ivanov, *J. Heterocycl. Chem.* **2001**, 37, 529–539; g) J. Iqbal, B. Bhatia, N. K. Nayyar, *Chem. Rev.* **1994**, 94, 519–564; h) F. Minisci, *Acc. Chem. Res.* **1975**, 8, 165–171.
- For selected examples, see: a) J. Muñoz-Molina, T. R. Belderrain, P. J. Pérez, *Inorg. Chem.* **2010**, 49, 642–645; b) M. Patazzoli, F. Roncaglia, V. Giangiordano, P. Davoli, F. Prati, F. Ghelfi, *Synthesis* **2010**, 694–700; c) T. Pintauer, W. T. Eckenhoff, C. Ricardo, M. N. C. Balili, A. B. Biernesser, S. T. Noonan, M. T. Taylor, *Chem. Eur. J.* **2009**, 15, 38–41; d) C. Ricardo, T. Pintauer, *Chem. Commun.* **2009**, 3029–3031; e) A. J. Clark, P. Wilson, *Tetrahedron Lett.* **2008**, 49, 4848–4850; f) J. M. Muñoz-Molina, T. R. Belderrain, P. J. Pérez, *Adv. Synth. Catal.* **2008**, 350, 2365–2372; g) J. A. Bull, M. G. Hutchings, C. Luján, P. Quayle, *Tetrahedron Lett.* **2008**, 49, 1352–1356; h) W. T. Eckenhoff, S. T. Garrity, T. Pintauer, *Eur. J. Inorg. Chem.* **2008**, 563–571; i) R. N. Ram, N. Kumar, *Tetrahedron Lett.* **2008**, 49, 799–802; j) J. A. Bull, M. G. Hutchings, P. Quayle, *Angew. Chem. Int. Ed.* **2007**, 46, 1869–1872; k) W. T. Eckenhoff, T. Pintauer, *Inorg. Chem.* **2007**, 46, 5844–5846; l) A. J. Clark, J. V. Geden, S. Thom, P. Wilson, *J. Org. Chem.* **2007**, 72, 5923–5926; m) J. M. Muñoz-Molina, A. Caballero, M. M. Díaz-Requejo, S. Trofimenko, T. R. Belderrain, P. J. Pérez, *Inorg. Chem.* **2007**, 46, 7725–7730; n) C. V. Stevens, E. Van Meenen, K. G. R. Masschelein, Y. Eeckhout, W. Hooghe, B. D'hondt, V. N. Nemykin, V. V. Zhdankin, *Tetrahedron Lett.* **2007**, 48, 7108–7111; o) D. Yang, Y.-L. Yan, B.-F. Zheng, Q. Gao, N.-Y. Zhu, *Org. Lett.* **2006**, 8, 5757–5760.
- For selected examples, see: a) K. Thommes, G. Kiefer, R. Scopelliti, K. Severin, *Angew. Chem. Int. Ed.* **2009**, 48, 8115–8119; b) J. Wolf, K. Thommes, O. Briel, R. Scopelliti, K. Severin,

- Organometallics* **2008**, *27*, 4464–4474; c) R. J. Lundgren, M. A. Rankin, R. McDonald, M. Stradiotto, *Organometallics* **2008**, *27*, 254–258; d) B. Dutta, E. Solari, R. Scopelliti, K. Severin, *Organometallics* **2008**, *27*, 423–429; e) Y. Borguet, A. Richel, S. Delfosse, A. Leclerc, L. Delaude, A. Demonceau, *Tetrahedron Lett.* **2007**, *48*, 6334–6338; f) Y. Motoyama, S. Hanada, K. Shimamoto, H. Nagashima, *Tetrahedron* **2006**, *62*, 2779–2788; g) L. Quebatte, E. Solari, R. Scopelliti, K. Severin, *Organometallics* **2005**, *24*, 1404–1406; h) Y. Motoyama, S. Hanada, S. Niibayashi, K. Shimamoto, N. Takaoka, H. Nagashima, *Tetrahedron* **2005**, *61*, 10216–10226; i) L. Quebatte, M. Haas, E. Solari, R. Scopelliti, Q. T. Nguyen, K. Severin, *Angew. Chem. Int. Ed.* **2005**, *44*, 1084–1088; j) L. Quebatte, R. Scopelliti, K. Severin, *Eur. J. Inorg. Chem.* **2005**, 3353–3358; k) L. Quebatte, R. Scopelliti, K. Severin, *Angew. Chem. Int. Ed.* **2004**, *43*, 1520–1524; l) B. T. Lee, T. O. Schrader, B. Martin-Matute, C. R. Kauffman, P. Zhang, M. L. Snapper, *Tetrahedron* **2004**, *60*, 7391–7396; m) O. Tutusaus, S. Delfosse, A. Demonceau, A. F. Noels, C. Viñas, F. Teixidor, *Tetrahedron Lett.* **2003**, *44*, 8421–8425; n) O. Tutusaus, C. Viñas, R. Núñez, F. Teixidor, A. Demonceau, S. Delfosse, A. F. Noels, I. Mata, E. Molins, *J. Am. Chem. Soc.* **2003**, *125*, 11830–11831; o) B. de Clercq, F. Verpoort, *Tetrahedron Lett.* **2002**, *43*, 4687–4690; p) F. Simal, L. Włodarczak, A. Demonceau, A. F. Noels, *Eur. J. Org. Chem.* **2001**, *14*, 2689–2695; q) F. Simal, L. Włodarczak, A. Demonceau, A. F. Noels, *Tetrahedron Lett.* **2000**, *41*, 6071–6074.
- [6] a) K. Thommes, B. Içli, R. Scopelliti, K. Severin, *Chem. Eur. J.* **2007**, *13*, 6899–6907; b) L. Quebatte, K. Thommes, K. Severin, *J. Am. Chem. Soc.* **2006**, *128*, 7440–7441.
- [7] a) W. A. Braunecker, W. C. Brown, B. C. Morelli, W. Tang, R. Poli, K. Matyjaszewski, *Macromolecules* **2007**, *40*, 8576–8585; b) W. A. Braunecker, Y. Itami, K. Matyjaszewski, *Macromolecules* **2005**, *38*, 9402–9404.
- [8] M. A. Fernández-Zúmel, K. Thommes, G. Kiefer, A. Sienkiewicz, K. Pierzchala, K. Severin, *Chem. Eur. J.* **2009**, *15*, 11601–11607.
- [9] T. Braun, G. Münch, B. Windmüller, O. Gevert, M. Laubender, H. Werner, *Chem. Eur. J.* **2003**, *9*, 2516–2530.
- [10] B. Dutta, E. Solari, S. Gauthier, R. Scopelliti, K. Severin, *Organometallics* **2007**, *26*, 4791–4799.
- [11] P. B. Glaser, T. D. Tilley, *Eur. J. Inorg. Chem.* **2001**, 2747–2750.
- [12] C. L. Gross, G. S. Girolami, *Organometallics* **1996**, *15*, 5359–5367.
- [13] G. J. Parkins, M. I. Bruce, B. W. Skelton, A. H. White, *Inorg. Chim. Acta* **2006**, *359*, 2644–2649.
- [14] D. C. Smith Jr., C. M. Haar, L. Luo, C. Li, M. E. Cucullu, C. H. Mahler, S. P. Nolan, *Organometallics* **1999**, *18*, 2357–2361.
- [15] C. S. Yi, J. R. Torres-Lubian, N. Liu, A. L. Rheingold, I. A. Guzei, *Organometallics* **1998**, *17*, 1257–1259.
- [16] For some examples, see: a) J. Vicente, J. Gil-Rubio, J. Guerrero-Leal, D. Bautista, *Organometallics* **2005**, *24*, 5634; b) E. Lindner, R. M. Jansen, H. A. Mayer, W. Hiller, R. Fawzi, *Organometallics* **1989**, *8*, 2355.
- [17] For a discussion of the role of olefin complexes in Cu-catalyzed ATRP reactions, see: a) W. A. Braunecker, K. Matyjaszewski, *J. Mol. Catal. A* **2006**, *254*, 155–164; b) W. A. Braunecker, N. V. Tsarevsky, T. Pintauer, R. R. Gil, K. Matyjaszewski, *Macromolecules* **2005**, *38*, 4081–4088; c) W. A. Braunecker, T. Pintauer, N. V. Tsarevsky, G. Kickelbick, K. Matyjaszewski, *J. Organomet. Chem.* **2005**, *690*, 916–924.
- [18] The formation of side products can be taken into account by determining the conversion of styrene in addition to the yield of the product. However, it was not possible to calculate the conversion accurately because of the very high styrene/ $\text{Cl}_3\text{CCO}_2\text{Et}$ ratios used in this study (up to 32:1).
- [19] As stated in the Experimental Section, we failed to obtain a satisfactory elemental analysis of complex **4**. The concentration of the catalyst precursor **4** is thus not very precise ($\pm 10\%$).
- [20] In the case of Ru, an acrylonitrile complex has successfully been used as a catalyst precursor in ATRP reactions: A. Saenz-Galindo, H. M. Textle, A. R. Jasso, J. R. Torres-Lubián, *J. Polym. Science A* **2005**, *44*, 676–680.
- [21] T. Arliguie, C. Border, B. Chaudret, J. Devillers, R. Poilblanc, *Organometallics* **1989**, *8*, 1308–1314.
- [22] Synthesis of $[\text{Cp}^*\text{RuCl}(\text{PPh}_3)_2]$: M. S. Chinn, D. M. Heinekey, *J. Am. Chem. Soc.* **1990**, *112*, 5166–5175.
- [23] C. L. Gross, G. S. Girolami, *Organometallics* **2006**, *25*, 4792–4798.
- [24] R. N. Ram, I. Charles, *Chem. Commun.* **1999**, 2267–2268.
- [25] T. Sato, Y. Wada, M. Nishimoto, H. Ishibashi, M. Ikeda, *J. Chem. Soc. Perkin Trans. 1* **1989**, *5*, 879–886.
- [26] H. Nagashima, N. Ozaki, M. Ishii, K. Seki, M. Washiyama, K. Itoh, *J. Org. Chem.* **1993**, *58*, 464–470.
- [27] *CrysAlis PRO*, Oxford Diffraction Ltd., Abingdon OX14 1RL, Oxfordshire, UK, **2008**.
- [28] A. J. M. Duisenberg, L. M. J. Kroon-Batenburg, A. M. M. Schreurs, *J. Appl. Crystallogr.* **2003**, *36*, 220–229.
- [29] R. H. Blessing, *Acta Crystallogr., Sect. A* **1995**, *51*, 33–38.
- [30] G. M. Sheldrick, University of Göttingen, Germany, **1997**; *SHELXTL*, version 6.1.4, Bruker AXS Inc., Madison, Wisconsin 53719, USA, **2003**.

Received: April 8, 2010

Published Online: July 2, 2010

Synthesis, Characterization, and Catalytic Studies of (Aryloxy)magnesium Complexes

Jolanta Ejfler,^[a] Katarzyna Krauzy-Dziedzic,^[a] Sławomir Szafert,^[a]
Lucjan B. Jerzykiewicz,^[a] and Piotr Sobota*^[a]

Keywords: Aminophenolates / Magnesium / Lactides / Polymerization / Structure elucidation

The reaction of MgBu_2 with 1 equiv. of four-coordinating (*R*)- or *rac*-*N,N*-bis(3,5-di-*tert*-butylbenzyl-2-hydroxy)tetrahydrofurfurylamine (*R/rac*-bpthfa- H_2) gave dinuclear homoleptic $[\text{Mg}(\mu\text{-}R/rac\text{-bpthfa})]_2$ (*R/rac*-**2c**) as white powders in 54–67 % yields. Analogous reactions of MgBu_2 with 2 equiv. of two-coordinating *N*-(3,5-di-*tert*-butylbenzyl-2-hydroxy)-*N*-methylcyclohexanamine (tbpca- H ; **1e**- H) and (*S*)-*N*-(3,5-di-*tert*-butylbenzyl-2-hydroxy)-*N*, α -dimethylbenzylamine (*S*-tbpmpa- H ; *S*-**1f**- H) gave white crystals of homoleptic mononuclear compounds of general formula $[\text{Mg}(\text{L})_2]$ (**2e** and *S*-**2f**) in 87–89 % yields. The resulting aminophenolates were

characterized by spectroscopic methods and, in the case of *R*-**2c** and *S*-**2f**, by X-ray crystallography. The new complexes *R/rac*-**2c**, **2e**, and *S*-**2f**, as well as the previously described homo- and heteroleptic tetranuclear $[\text{Mg}(\text{ddbfo})_2]_4$ (**2a**), $[\text{Mg}(\text{thffo})_2]_4$ (**2b**), $[\text{Mg}_4(\mu_3\text{-OMe})_2(\mu, \eta^2\text{-ddbfo})_2(\mu, \eta^1\text{-ddbfo})_2(\eta^1\text{-ddbfo})_2(\text{MeOH})_5]\cdot\text{CH}_3\text{OH}\cdot\text{thf}$ (**3a**· $\text{CH}_3\text{OH}\cdot\text{thf}$) and $[\text{Mg}_4(\mu_3, \eta^2\text{-thffo})_2(\mu, \eta^2\text{-thffo})_2(\text{Ph}_3\text{SiO})_2]$ (**4b**), were tested in the polymerization of lactide to reveal good activity only in the case of mononuclear four-coordinate species grafted with an external donor, benzyl alcohol.

Introduction

The potential of magnesium alkoxides and aryloxides has been explored systematically in a variety of chemical processes. Among others, numerous catalytic, noncatalytic, organic, and organometallic reactions, as well as syntheses of advanced materials are noteworthy.^[1] Recently, magnesium complexes have also gained considerable attention as initiators in the syntheses of biodegradable polymers.^[2] Two important classes of these polymers are polyesters and, in particular, polylactides (PLAs) due to their wide application in biomedical and pharmaceutical fields.^[3] Although many strategies have been developed for the preparation of PLAs, the most effective is the ring-opening polymerization (ROP) of lactides initiated by metal alkoxides.^[4] Among the known initiators, candidates of primary importance are monomeric complexes with nontoxic and life-essential metals such as magnesium.^[2,5]

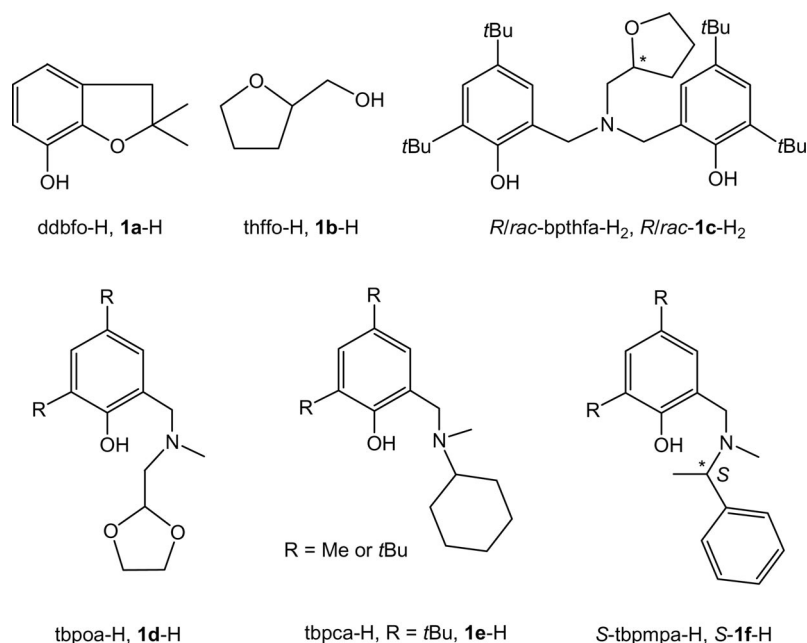
To date, only a few examples of heteroleptic magnesium compounds that are active as initiators in the ROP of cyclic esters have been described.^[2] Recently, interest has also been directed towards homoleptic compounds able to act as initiators for the ROP in the presence of exterior alcohol, which is extremely interesting from the perspective of polymer chain modification.^[6] However, only a few magnesium alkoxides and aryloxides have a structure proven by X-ray analysis, which is highly desirable to design well-defined “single-site” initiators.

Some of our previous research has already included the synthesis of magnesium alkoxides and aryloxides, where we utilized variety of oxido ligands, including commercially available 2,3-dihydro-2,2-dimethyl-7-benzofuranol (ddbfo- H ; **1a**- H) and tetrahydrofurfuryl alcohol (thffo- H ; **1b**- H), as well as aminophenolato ligands bpthfa- H_2 (**1c**- H_2),^[7] tbpca- H (**1d**- H),^[2b] and tbpca- H (**1e**- H),^[2b] which are shown in Scheme 1.

It has been shown that reactions of sterically undemanding bidentate **1a**- H or **1b**- H with MgBu_2 or magnesium turnings yield tetranuclear compounds $[\text{Mg}(\text{ddbfo})_2]_4$ (**2a**)^[8a] and $[\text{Mg}(\text{thffo})_2]_4$ (**2b**),^[8b] which have open dicubane geometry. Both molecules possess two five-coordinate magnesium atoms of trigonal-bipyramidal geometry and two six-coordinate octahedral metal centers. The most interesting feature of these compounds is the presence of coordinatively unsaturated metal sites which can react easily with methanol or Ph_3SiOH to form heteroleptic tetrameric magnesium complexes $[\text{Mg}_4(\mu_3\text{-OMe})_2(\mu, \eta^2\text{-ddbfo})_2(\mu, \eta^1\text{-ddbfo})_2(\eta^1\text{-ddbfo})_2(\text{MeOH})_5]\cdot\text{CH}_3\text{OH}\cdot\text{thf}$ (**3a**· $\text{CH}_3\text{OH}\cdot\text{thf}$)^[8a] and $[\text{Mg}_4(\mu_3, \eta^2\text{-thffo})_2(\mu, \eta^2\text{-thffo})_2(\text{Ph}_3\text{SiO})_2]$ (**4b**).^[8b]

Higher dentate or more bulky bidentate ligands form less aggregated structures that are usually dimeric and perform well as initiators in the ROP of lactides. A few important examples include $[(\text{EDBP})\text{Mg}(\text{Et}_2\text{O})]$, $[(\text{EDBP})\text{Mg}(\text{thf})]_2$ [EDBP = 2,2'-ethylenebis(4,6-di-*tert*-butylphenoxido)],^[2a] and a series of dimeric $[(\text{L})\text{Mg}(\mu\text{-OBz})]_2$ compounds $\{\text{L} = \text{NNO-ketimate}^{[2d,2i]}$ or 2,4-di-*tert*-butyl-6-[1-(3,5-di-*tert*-butyl-2-phenoxy)ethyl]phenyl benzenesulfonate $\}$,^[2h] which

[a] Department of Chemistry, University of Wrocław, 14 F. Joliot-Curie, 50-383 Wrocław, Poland



Scheme 1. Some of the precursors of alkoxido and aryloxy ligands.

were all designed by Lin and co-workers. Another interesting example, prepared by Cheng et al., is a compound formed in situ from $[(\text{BDI})\text{MgN}(\text{TMS})_2]$ {BDI = 2-[(2,6-diisopropylphenyl)amino]-4-[(2,6-diisopropylphenyl)imino]-2-pentene} and paclitaxel, a potent chemotherapeutic agent, that is most probably a monomeric species and allows incorporation of the agent into the polylactide chain to form an interesting drug-delivery system.^[2g]

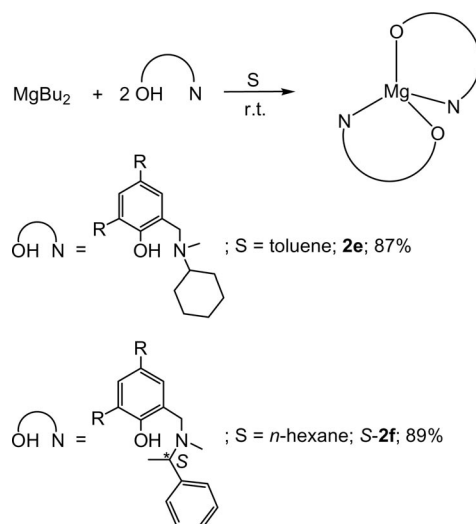
In this paper, we report the preparation of a series of homoleptic magnesium complexes with aryloxy and aminophenolato ligands. The ligands have been varied from two- to four-dentate in order to evaluate the resulting structural motifs. The additional donor arm on the nitrogen atom in the aminophenolato ligands, which could readily involve dynamic behavior in solution, may be an important factor for catalytic applications. Preliminary results of the activity of the compounds in the ROP of lactides are also reported.

Results and Discussion

Synthesis and Characterization of Complexes

The aminophenolato bidentate ligands **1e-H** and **S-1f-H** appear to be well suited for the synthesis of monomeric magnesium complexes. The latter was prepared by Mannich condensation from (–)-(S)- α ,4-dimethylbenzylamine, para-formaldehyde, and 2,4-di-*tert*-butylphenol in refluxing methanol in 54% unoptimized yield as described in the Experimental Section. As already described, the reaction of **1e-H** performed in a mixture of solvents (hexane/thf) gave monomeric octahedral $[\text{Mg}(\text{tbpca})_2(\text{thf})_2]$ (**5**).^[2b] It has also been demonstrated that the reaction of MgBu_2 with **1d-H** in toluene gave the six-coordinate complex $[\text{Mg}(\text{tbpoa})_2]$.^[2b]

As shown in Scheme 2 ligands **1e-H** or **S-1f-H** were treated with 0.5 equiv. of MgBu_2 in toluene or hexanes to form monomeric tetrahedral compounds $[\text{Mg}(\text{tbpca})_2]$ (**2e**) and $[\text{Mg}(\text{tbpmpa})_2]$ (**S-2f**) in 87 and 89% yields, respectively.

Scheme 2. Synthesis of monomeric magnesium complexes **2e** and **S-2f**.

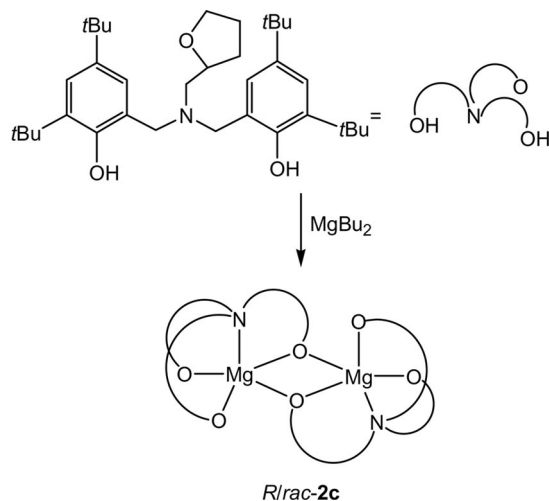
The new complexes **2e** and **S-2f** were isolated as colorless solids, which are readily soluble in hydrocarbons, CH_2Cl_2 , and thf. Their structures were confirmed by elemental analysis and NMR spectroscopy, as well as X-ray crystallography for **S-2f**.

The ^1H NMR spectra were routine. The spectrum for **2e** shows one set of resonances for the aryl protons at $\delta = 7.66$ and 7.08 ppm, two singlets from the *tert*-butyl groups at $\delta = 1.78$ and 1.56 ppm, and a signal arising from the *N*-methyl protons at $\delta = 2.02$ ppm. The methylene protons from the

phenyl-CH₂-N linker appear as broad singlets at δ = 4.12 and 3.44 ppm. For *S*-**2f**, the signals of the aminophenolato ligands are broad indicating a fluxional process on the NMR timescale. The aryl protons of the phenolate ring appear as broadened singlets at δ = 7.69 and 6.96 ppm. The methine and methyl protons of the chiral amine substituents also show broad resonances at δ = 3.54 and 1.84 ppm, respectively. The signal of the methylene protons from the phenyl-CH₂-N linker appears at δ = 4.21 ppm.

Attempts to introduce alcohols into the monomeric (aminophenolato)magnesium complexes **2e** and *S*-**2f** were unsuccessful. The reactions between **2e** or *S*-**2f** and EtOH or benzyl alcohol were monitored by NMR spectroscopy, which indicated the synthesis of a mixture of products (presumably due to a reversible reaction), but, after a few days and after a careful workup, the isolated products were identified as the homoleptic starting complexes.

In the next stage of our investigation, the chiral and racemic aminobis(phenolato) ligands *R*-**1c**-H₂ and *rac*-**1c**-H₂ containing additional N,O-donor atoms (going from two- to four-dentate ligands) were used. Their reactions with 1 equiv. of MgBu₂ in toluene at room temperature cleanly afforded the dimeric magnesium complexes [Mg(*R*-bpthfa)]₂ (*R*-**2c**) and [Mg(*rac*-bpthfa)]₂ (*rac*-**2c**) by butane elimination, as presented in Scheme 3. The complexes were isolated in good yields (54–67%) as colorless crystals, soluble in hydrocarbons and chlorinated solvents. Compounds *R/rac*-**2c** contain unsaturated five-coordinate metal centers, are unreactive towards alcohols, and remain stable even in hot ethanol. Similarly to **2e** and *S*-**2f**, incorporation of alkoxido ligands and formation of heteroleptic products were not observed.



Scheme 3. Synthesis of dimeric complexes *R/rac*-**2c**.

The ¹H NMR spectra of the complexes *R/rac*-**2c** are identical and show one set of resonances for 1 equiv. of the coordinated bis(phenoxido) ligand, which could be assigned in detail on the basis of 2D ¹H-¹H COSY, ¹H, and ¹³C NMR experiments. Complementary investigations of these compounds indicated that the NMR features were essentially unchanged in C₆D₅CD₃, CDCl₃, and CD₃OD up to 60 °C.

X-ray Crystallographic Studies

Colorless, needle-shaped crystals of *R*-**2c**·2C₆H₅CH₃·CH₂Cl₂ were obtained by crystallization from a CH₂Cl₂/toluene mixture. The detailed structure was determined as outlined in the Experimental Section. Key metrical parameters are listed in Table 1, and the structure is shown in Figure 1.

Table 1. Selected bond lengths [Å] and angles [°] for *R*-**2c**·2C₆H₅CH₃·CH₂Cl₂.

Atoms	Distance	Atoms	Distance
Mg(1)–Mg(2)	3.008(3)	Mg(1)–O(1)	2.027(4)
Mg(1)–O(2)	1.907(4)	Mg(1)–O(3)	2.058(4)
Mg(1)–O(4)	2.014(4)	Mg(1)–N(1)	2.208(5)
Mg(2)–O(1)	1.993(4)	Mg(2)–O(4)	2.018(4)
Mg(2)–O(5)	1.922(4)	Mg(2)–O(6)	2.090(4)
Mg(2)–N(2)	2.205(5)		
Atoms	Angle	Atoms	Angle
O(1)–Mg(1)–O(2)	162.86(19)	O(1)–Mg(1)–O(3)	95.31(15)
O(1)–Mg(1)–O(4)	76.36(15)	O(1)–Mg(1)–N(1)	86.65(16)
O(2)–Mg(1)–O(3)	100.49(18)	O(2)–Mg(1)–O(4)	95.80(16)
O(2)–Mg(1)–N(1)	89.35(17)	O(3)–Mg(1)–O(4)	138.32(17)
O(3)–Mg(1)–N(1)	80.73(16)	O(4)–Mg(1)–N(1)	137.85(18)
O(1)–Mg(2)–O(4)	77.05(14)	O(1)–Mg(2)–O(5)	94.65(16)
O(1)–Mg(2)–O(6)	140.29(18)	O(1)–Mg(2)–N(2)	136.41(19)
O(4)–Mg(2)–O(5)	163.93(19)	O(4)–Mg(2)–O(6)	95.88(15)
O(4)–Mg(2)–N(2)	86.87(16)	O(5)–Mg(2)–O(6)	99.17(17)
O(5)–Mg(2)–N(2)	89.98(17)	O(6)–Mg(2)–N(2)	80.86(16)
Mg(1)–O(1)–Mg(2)	96.88(15)	Mg(1)–O(4)–Mg(2)	96.52(15)

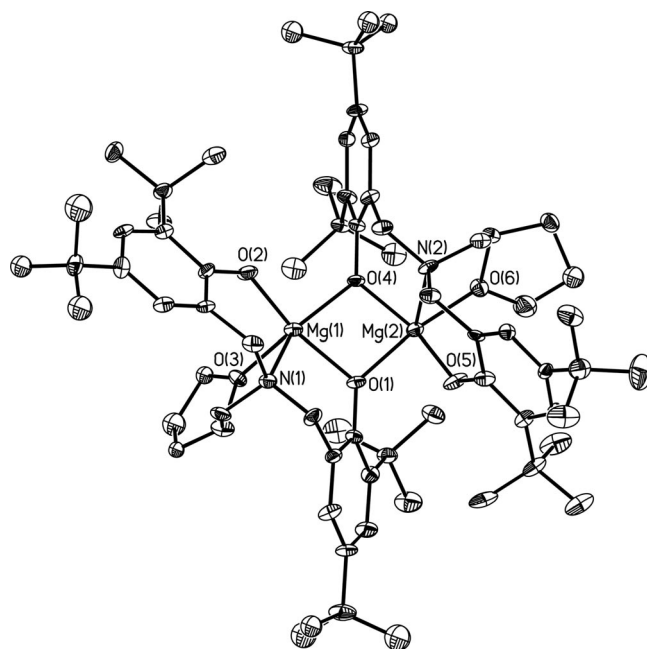


Figure 1. ORTEP view of *R*-**2c**·2C₆H₅CH₃·CH₂Cl₂ (H and disordered atoms are omitted for clarity; the displacement ellipsoids are drawn at 40% probability level).

The X-ray analysis shows *R*-**2c**·2C₆H₅CH₃·CH₂Cl₂ to be a homoleptic molecular dimer. The two magnesium centers are identically coordinated, each surrounded by two bridging oxygen atoms of two phenoxido ligands coming from

separate aminobis(phenolato) ligands, one terminal phenoxido oxygen atom, one nitrogen atom, and one oxygen atom from the tetrahydrofuran ring.

The pentacoordinate magnesium atoms are in an almost identical arrangement, that is between trigonal-bipyramidal and square-pyramidal geometry with a τ parameter of 0.41 for Mg(1) and 0.39 for Mg(2).^[9] In both cases the nitrogen atom resides in the apical position.

Although complexes with pentacoordinate magnesium are quite commonly observed, only two examples of the crystallographically characterized species with a coordination environment similar to **R-2c** (MgO_4N comprising two bridging phenoxido groups) were found in the CCDC.^[10] The Mg_2O_2 central core in **R-2c**· $2\text{C}_6\text{H}_5\text{CH}_3$ · CH_2Cl_2 is a distorted rhombohedron with four different Mg–O distances of 2.027(4) [Mg(1)–O(1)], 2.014(4) [Mg(1)–O(4)], 1.993(4) [Mg(2)–O(1)], and 2.018(4) Å [Mg(2)–O(4)]. The distances are similar to those found in the magnesium dimer with bis(α,α -diarylprolinol) [$\text{Mg}_2(\text{L})_2$] [Mg–O 1.991(6), 2.031(6), 1.979(6), and 2.016(6) Å].^[10a]

The terminal Mg–O_{aryloxy} distances in **R-2c**· $2\text{C}_6\text{H}_5\text{CH}_3$ · CH_2Cl_2 are 1.907(4) and 1.922(4) Å and are typical. Also typical are the Mg–O–C bond angles for the terminal aryloxy ligands, which are 134.3(3) and 134.9(3)°, and suggest a very small π -character in the Mg–O_{aryloxy} bonds.

Light pink blocks of **S-2f** were obtained by slow concentration of a hexane solution. The detailed structure was determined as outlined in Table 1 and described in the Experimental Section. The structure is depicted in Figure 2, and selected bond lengths and angles are listed in the caption.

The X-ray analysis shows **S-2f** to be a molecular monomer with the four-coordinate magnesium center surrounded by two pairs of N,O atoms from two aminophenolato ligands forming a distorted tetrahedron. Although such coordination seems typical for magnesium, to our surprise, only one monomeric four-coordinate magnesium aminophenolato was found in the CCDC.^[11]

The distances Mg(1)–O(1) and Mg(1)–O(2) in **S-2f** are 1.892(3) and 1.900(3) Å, respectively, and are similar to those found in [$\text{Mg}(2,6\text{-}t\text{Bu}_2\text{C}_6\text{H}_4\text{O})_2(\text{tmeda})$] [tmeda = *N,N,N',N'*-tetramethylethylenediamine; Mg–O 1.8803(8) and 1.8817(9) Å]. The Mg(1)–N(1) and Mg(1)–N(2) distances in **S-2f** of 2.176(4) and 2.166(3) Å are a little shorter than those in [$\text{Mg}(2,6\text{-}t\text{Bu}_2\text{C}_6\text{H}_4\text{O})_2(\text{tmeda})$] [Mg–N 2.2625(11) and 2.2695(11) Å].

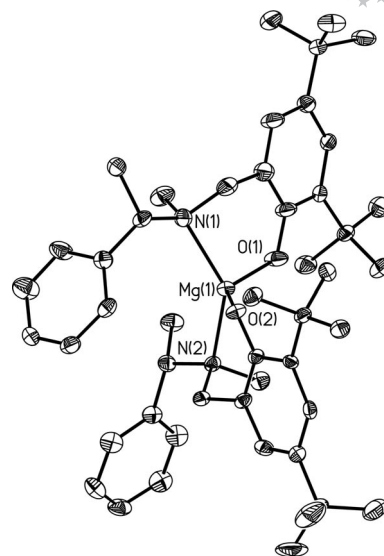


Figure 2. View of **S-2f** (H atoms are omitted for clarity; the displacement ellipsoids are drawn at 40% probability level). Selected bond lengths [Å] and angles [°]: Mg(1)–O(1) 1.892(3), Mg(1)–O(2) 1.900(3), Mg(1)–N(1) 2.176(4), Mg(1)–N(2) 2.166(3); O(1)–Mg(1)–O(2) 125.77(15), O(1)–Mg(1)–N(1) 92.68(13), O(1)–Mg(1)–N(2) 105.32(13), O(2)–Mg(1)–N(1) 105.69(14), O(2)–Mg(1)–N(2) 95.71(13), N(1)–Mg(1)–N(2) 136.07(14), Mg(1)–O(1)–C(11) 129.9(3), Mg(1)–O(2)–C(41) 124.5(2).

Lactide Polymerization

Previous research in our group has shown that zinc complexes that incorporate **1e–H** are effective initiators for the ROP of lactide.^[12] In addition, the monomeric hexacoordinate magnesium complex **5**^[2b] was proved to initiate the polymerization of L-lactic acid (L-LA) in high conversion within 30 min to afford PLA with a moderate M_w of 8600 and a polydispersity index (PDI) of 1.12. In this case, the NMR end-group analysis of the isolated PLA indicated the presence of hydroxy and aminophenolate ester end groups. Biocompatible metals such as Zn and Mg are of great interest in this process because of the propensity for trace amounts of the catalyst to be incorporated within the polymer.^[2d] Therefore, preliminary research exploring the use of the above described and characterized aryloxy magnesium complexes as initiators for the ROP of lactide. The tetrameric complexes **2a–b**, **3a**, and **4b**, as well as dimeric **R/rac-2c** were tested and proved to be essentially inactive.

Table 2. Polymerization of L-lactide with initiators (**I**) **2e**, **S-2f**, **2e**/BnOH, and **S-2f**/BnOH.^[a]

Entry	I	[I]/[L-LA]/[BnOH]	<i>t</i> (min)	$10^{-3} M_n^{[b]}$	$10^{-3} M_n$	Conv. ^[c]	PDI ^[b]
1	2e	1:100:0	5 d	–	–	–	–
2	2e	1:50:1	1 min	6.88	7.02	96%	1.09
3	2e	1:100:1	5 min	15.58	13.37	92%	1.10
4	S-2f	1:100:0	5 d	–	–	–	–
5	S-2f	1:50:1	1 min	7.20	6.59	90%	1.02
6	S-2f	1:100:1	10 min	14.82	13.80	95%	1.08

[a] General polymerization conditions: solvent: toluene (10 mL), $T = 25^\circ\text{C}$, $[\text{I}] = 0.025$. [b] Conversion determined by ^1H NMR spectroscopy. [c] Determined by GPC, PDI calibrated with polystyrene standards.

Monomeric tetrahedral aminophenolate compounds **2e** and *S*-**2f** were tested next. Although they both showed no activity they become extremely active when an external donor was added as described in Table 2.

Polymerization of L-LA initiated by **2e** in the presence of BnOH was very effective, and high conversion was achieved within 5 min for [**2e**]/[L-LA]/BnOH (1:100:1) (Figure 3).

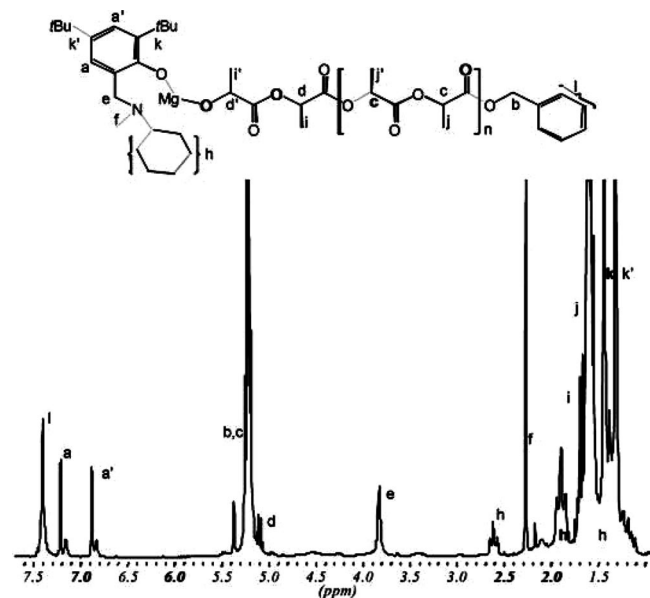


Figure 3. ^1H NMR spectrum of a living oligomer in the ROP of L-LA initiated by **2e** in the presence of BnOH.

The predictable molecular weights and narrow PDIs of the obtained PLAs indicate a well-controlled polymerization process. The ^1H NMR spectrum of PLA in CD_2Cl_2 prepared by using [**2e**]/[L-LA]/[BnOH] in 1:10:1 ratio showed one benzyl ester and one hydroxy chain end suggesting that the initiation occurred through the insertion of the benzyloxy group into L-lactide (Figure 4).

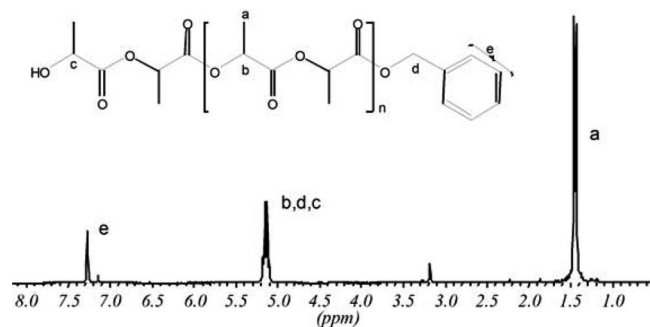


Figure 4. ^1H NMR spectrum of PLA synthesized with the **2e**/BnOH initiator.

Similar results were obtained for the polymerization of L-LA initiated with *S*-**2f** in the presence of BnOH performed at room temperature in toluene. A high conversion was achieved within 10 min for [*S*-**2f**]/[L-LA]/[BnOH] (1:100:1). The ^1H and ^{13}C NMR spectra of the PLAs obtained in the presence of *S*-**2f** showed that the polymer

chains at one end are terminated by benzyl ester with no sign of transesterification products (the OH proton was not observed) (Figure 5).

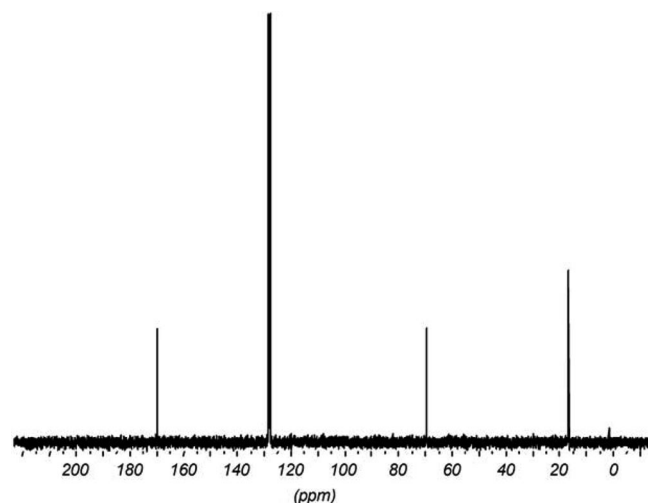


Figure 5. ^{13}C NMR spectrum of PLA synthesized with the *S*-**2f**/BnOH initiator.

All of the initiator systems exhibit molecular weights in close agreement with calculated values, and narrow PDIs are characteristic for well-controlled living propagation.

Conclusions

We have synthesized a new chiral aminophenolato ligand *S*-**1f-H** and four new magnesium aminophenolates *R*/*rac*-**2c**, **2e**, and *S*-**2f**. The compounds were characterized by spectroscopic methods and, in case of *R*-**2c** and *S*-**2f**, by X-ray crystallography, thereby enriching the library of well-defined magnesium aminophenolates. As expected, the compound with the tetracoordinate *R*-bpthfa ligand appeared to be dimeric with five-coordinate magnesium atoms, whereas the compound with the dicoordinate *S*-tbmpa was monomeric with tetrahedral geometry around the metal atom.

All of the new compounds, as well as few polynuclear magnesium species **2a–b**, **3a**, and **4b** synthesized previously, were tested in the polymerization of L-lactide, and all of them proved to be essentially inactive. Nevertheless, in the case of **2e** and *S*-**2f**, grafting with benzyl alcohol led to greatly enhanced polymerization activities resulting in high activity initiators, which gave 92–95% conversion after 5–10 min, and exclusively linear polymers with low PDI values, 1.08–1.10. These results clearly support the advantage of monomeric magnesium species over polynuclear analogs in lactide polymerization.

Experimental Section

General Materials and Experimental Procedures: All the reactions and operations were performed under N_2 by using standard Schlenk techniques. Reagents were purified by standard methods: thf was distilled from CuCl , predried with NaOH, and then dis-

tilled from Na/benzophenone. $\text{C}_6\text{H}_5\text{CH}_3$ was distilled from Na; CH_2Cl_2 and CD_2Cl_2 were distilled from P_2O_5 ; hexanes were distilled from Na; methanol was distilled from Mg; C_6D_6 and $\text{C}_6\text{D}_5\text{CD}_3$ were distilled from CaH_2 . L-LA (98%; Aldrich) was sublimed and recrystallized from toluene prior to use. MgBu_2 (Aldrich; 1.0 M solution in hexanes) and (–)-(*S*)- α ,4-dimethylbenzylamine (Aldrich, 98%) were used as received. BnOH (Aldrich; >99%) was distilled prior to use. Ligands (tbpc-H), *R*/*rac*-bpthfa- H_2 were prepared according to literature procedures.^[2b,7] ^1H and ^{13}C NMR spectra were recorded in the temperature range 298–351 K with Bruker ESP 300E or 500 MHz spectrometers. Chemical shifts are reported in ppm and referenced to the signals of residual protons in deuterated solvents. The weights and number-average molecular weights of the PLAs were determined by gel permeation chromatography (GPC) using an HPLC-HP 1090 II with a DAD-UV/Vis and RI detector HP 1047A, and polystyrene calibration. Microanalyses were conducted with an ARL Model 3410 + ICP spectrometer (Fisons Instruments) and a VarioEL III CHNS (in-house).

Ligand and Complex Synthesis. *S*-1f-H: To a mixture of 2,4-di-*tert*-butylphenol (7.88 g, 38.20 mmol) and (–)-(*S*)- α ,4-dimethylbenzylamine (5.60 mL, 38.06 mmol) in methanol (50 mL) was added a 1.5 molar excess of formaldehyde (4.32 mL, 58.01 mmol, 37% solution in water). The solution was then stirred and heated under reflux for 5 d. The solvent was removed to give a yellow oil. Cold methanol was added (10 mL), and the mixture was stirred for 1 h and cooled to -15°C . After 1 d, colorless crystals of *S*-1f-H had formed. Yield 7.21 g (54%). $\text{C}_{24}\text{H}_{35}\text{NO}$ (353.55): calcd. C 81.53, H 9.98, N 3.96; found C 81.62, H 10.12, N 4.11. ^1H NMR (C_6D_6 , 298 K): δ = 7.58 (d, J_{HH} = 2.42 Hz, 1 H, ArH), 7.30–7.14 (m, 5 H, Ph), 6.93 (d, J_{HH} = 2.42 Hz, 1 H, ArH), 3.60 (br. s, 2 H, NCH_2Ar), 3.50 (q, J_{HH} = 6.82 Hz, 2 H, CH), 1.93 (s, 3 H, NCH_3), 1.82 [s, 9 H, $\text{C}(\text{CH}_3)_3$], 1.44 [s, 9 H, $\text{C}(\text{CH}_3)_3$], 1.20 (d, J_{HH} = 6.82 Hz, 3 H, CH_3) ppm. ^{13}C NMR (76 MHz, C_6D_6 , 298 K): δ = 19.6 (CHCH_3), 29.6 [$\text{C}(\text{CH}_3)_3$], 31.9 [$\text{C}(\text{CH}_3)_3$], 33.8 [$\text{C}(\text{CH}_3)_3$], 35.2 [$\text{C}(\text{CH}_3)_3$], 36.3 (NCH_3), 58.9 (CH_2), 62.1 (CHCH_3), 121.1, 121.6, 122.6, 122.8, 123.4, 123.9, 135.7, 140.2, 140.6, 154.1, 155.0 (12 C, 2Ar) ppm.

[Mg(*R*-1c)]₂ (*R*-2c): To a solution of *R*-1c- H_2 (0.86 g, 1.61 mmol) in toluene (15 mL) was added MgBu_2 (1.61 mL, 1.61 mmol) dropwise. The mixture was stirred for 24 h, and the solution was concentrated to dryness. *n*-Hexane was added (25 mL), and the suspension was stirred for 2 h. The resulting white powder was collected by filtration, washed with *n*-hexanes (20 mL) and dried in vacuo to yield *R*-2c (0.96 g, 54%, 0.86 mmol). Crystals suitable for X-ray determination were obtained after recrystallization with *n*-hexane/ CH_2Cl_2 . $\text{C}_{70}\text{H}_{106}\text{Mg}_2\text{N}_2\text{O}_6$ (1120.23): calcd. C 75.05, H 9.54, N 2.50; found C 74.78, H 9.47, N 2.41. ^1H NMR (C_6D_6 , 298 K): δ = 7.47 (d, J_{HH} = 2.5 Hz, 2 H, ArH), 7.41 (d, J_{HH} = 2.5 Hz, 2 H, ArH), 7.10 (d, J_{HH} = 2.6 Hz, 2 H, ArH), 6.92 (d, J_{HH} = 2.6 Hz, 2 H, ArH), 4.65–4.73, 4.74–4.80 (2 m, 4 H, $\text{CHOCH}_2\text{C}_2\text{H}_4$), 4.58–4.63 (m, 2 H, $\text{CHOCH}_2\text{C}_2\text{H}_4$), 3.19–3.26, 3.48–3.53 (2 m, 8 H, CH_2Ar), 3.04–3.13 (m, 4 H, NCH_2), 2.55–2.60, 2.63–2.72 (2 m, 8 H, $\text{CHOCH}_2\text{C}_2\text{H}_4$), 1.48, 1.54, 1.56, 1.88 [4 s, 72 H, $\text{C}(\text{CH}_3)_3$] ppm. ^{13}C NMR (76 MHz, C_6D_6 , 298 K): δ = 28.7, 31.7 (4 C, $\text{CHOCH}_2\text{C}_2\text{H}_4$), 29.8, 31.1, 31.9, 32.1 [24 C, $\text{C}(\text{CH}_3)_3$], 33.8, 33.9, 35.0, 35.1 [8 C, $\text{C}(\text{CH}_3)_3$], 55.5 (2 C, NCH_2), 65.2, 64.4 (4 C, CH_2Ar), 68.9 (2 C, $\text{CHOCH}_2\text{C}_2\text{H}_4$), 78.8 (2 C, $\text{CHOCH}_2\text{C}_2\text{H}_4$), 121.5, 123.4 [4 C, *o*-C(Ar)- CH_2N], 123.9, 125.1 [4 C, *m*-C(Ar)], 125.4, 127.1 [4 C, *m*-C(Ar)], 137.0, 137.2 [4 C, *o*-C(Ar) $\text{C}(\text{CH}_3)_3$], 138.9, 139.7 [4 C, *p*-C(Ar) $\text{C}(\text{CH}_3)_3$] ppm.

[Mg(*rac*-1c)]₂ (*rac*-2c): *rac*-1c-H (2.53 g, 4.72 mmol) and MgBu_2 (4.72 mL, 4.72 mmol) were allowed to react according to a pro-

cedure analogous to that of *R*-2c described above. A similar workup gave *rac*-2c in 67% yield (3.52 g, 3.14 mmol). $\text{C}_{70}\text{H}_{106}\text{Mg}_2\text{N}_2\text{O}_6$ (1120.23): calcd. C 75.05, H 9.54, N 2.50; found 75.14, H 9.37, N 2.34.

[Mg(1e)]₂ (2e): To a solution of 1e-H (1.32 g, 4.00 mmol) in toluene (10 mL) was added MgBu_2 (2 mL, 2.00 mmol) dropwise. The reaction mixture was stirred for 24 h, and the solvent was removed to give a yellow oil. *n*-Hexane was added (20 mL), and colorless crystals precipitated at room temperature after 1 d. They were collected by filtration, washed with *n*-hexane (10 mL), and dried in vacuo to yield 2e (2.40 g, 87%, 3.50 mmol). $\text{C}_{44}\text{H}_{72}\text{MgN}_2\text{O}_2$ (685.37): calcd. C 77.11, H 10.59, N 4.09; found C 76.68, H 10.31, N 3.98. ^1H NMR (C_6D_6 , 298 K): δ = 7.66 (s, 2 H, ArH), 7.08 (s, 2 H, ArH), 4.12 (br. s, 2 H, NCH_2Ar), 3.44 (s, 2 H, NCH_2Ar), 2.27–2.39 (m, 2 H, C_6H_{11}), 2.02 (s, 6 H, NCH_3), 1.78 [s, 18 H, $\text{C}(\text{CH}_3)_3$], 1.60–1.70 (m, 10 H, C_6H_{11}), 1.56 [m, 18 H, $\text{C}(\text{CH}_3)_3$], 1.30–1.47 (m, 10 H, C_6H_{11}) ppm. ^{13}C NMR (76 MHz, C_6D_6 , 298 K): δ = 25.2 (10 C, C_6H_{11}), 25.5 (10 C, C_6H_{11}), 29.4 [6 C, $\text{C}(\text{CH}_3)_3$], 31.0 (2 C, NCH_3), 31.5 [6 C, $\text{C}(\text{CH}_3)_3$], 33.3 [2 C, $\text{C}(\text{CH}_3)_3$], 34.7 [2 C, $\text{C}(\text{CH}_3)_3$], 59.4 (2 C, C_6H_{11}), 60.3 (2 C, NCH_2Ar) 62.3, 136.8, 134.6, 125.0, 123.5, 121.0 (24 C, Ar) ppm.

[Mg(*S*-1f)]₂ (*S*-2f): To a solution of *S*-1f-H (1.36 g, 2.00 mmol) in *n*-hexane (10 mL) was added MgBu_2 (2.00 mL, 2.00 mmol) dropwise. The reaction mixture was stirred for 24 h, and the solvent was removed to yield a pink oil. *n*-Hexane was added (20 mL) and, after additional stirring at room temperature for 24 h, a pink solid precipitated from the solution. The powder was collected by filtration, washed with *n*-hexane (10 mL), and dried in vacuo to yield *S*-2f (1.68 g, 89%, 2.30 mmol). $\text{C}_{48}\text{H}_{68}\text{MgN}_2\text{O}_2$ (729.35): calcd. C 79.05, H 9.40, N 3.84; found C 78.95, H 9.53, N 3.94. ^1H NMR (300 MHz, C_6D_6 , 298 K): δ = 7.69 (br. s, 2 H, ArH), 7.16–7.21 (m, 5 H, ArH), 6.96 (br. s, 2 H, ArH), 4.21 (br. s, 4 H, NCH_2Ar), 3.54 (br. s, 2 H, CHCH_3), 1.93 (s, 6 H, NCH_3), 1.84 (br. s, 6 H, CHCH_3), 1.82 [s, 18 H, $\text{C}(\text{CH}_3)_3$], 1.45 [m, 18 H, $\text{C}(\text{CH}_3)_3$] ppm. ^{13}C NMR (76 MHz, C_6D_6 , 298 K): δ = 29.6 [6 C, $\text{C}(\text{CH}_3)_3$], 29.7 [6 C, $\text{C}(\text{CH}_3)_3$], 31.9 [2 C, $\text{C}(\text{CH}_3)_3$], 34.7 [2 C, $\text{C}(\text{CH}_3)_3$], 35.7 [2 C, $\text{C}(\text{CH}_3)_3$], 36.4 (2 C, NCH_3), 59.2 (CH_2), 61.3 (CH), 156.3, 155.1, 141.6, 140.3, 131.2, 129.4, 124.0, 123.5, 122.8, 122.9, 122.1, 121.5, 121.3 (24 C, Ar) ppm.

Polymerization Procedure: In a Schlenk flask under argon, a complex I was treated with L-LA, $[\text{I}]/[\text{L-LA}] = 1:100$ in toluene (10 mL). The reaction mixture was stirred at the desired temperature for the prescribed time. At certain time intervals, aliquots of about 1 mL were removed for the determination of the conversion by ^1H NMR spectroscopy. After the reaction was complete, it was quenched with methanol; the solution was concentrated in vacuo, and the polymer was precipitated with an excess of cold methanol. A white product was collected by filtration and dried in vacuo.

Details of X-ray Data Collection and Reduction: X-ray diffraction data were collected with a KUMA KM4 CCD (ω -scan technique) diffractometer equipped with an Oxford Cryosystem-Cryostream cooler.^[13] The space groups were determined from systematic absences and subsequent least-squares refinement. Lorentz and polarization corrections were applied. The structures were solved by direct methods and refined by full-matrix least squares on F^2 by using the SHELXTL package.^[14] Non-hydrogen atoms were refined with anisotropic thermal parameters. Hydrogen-atom positions were calculated and added to the structure-factor calculations, but were not refined (Table 3). The *t*Bu groups, C(17)–C(110), C(27)–C(210), and C(47)–C(410), and both tetrahydrofuran rings in 2e are disordered and were solved with two positions for each moiety. The

Table 3. Summary of crystallographic data for *R*-2c·2C₆H₅CH₃·CH₂Cl₂ and *S*-2f.

	<i>R</i> -2c·2C ₆ H ₅ CH ₃ ·CH ₂ Cl ₂	<i>S</i> -2f
Empirical formula	C ₈₅ H ₁₂₄ Cl ₂ Mg ₂ N ₂ O ₆	C ₄₈ H ₆₈ MgN ₂ O ₂
Formula mass	1389.38	729.35
Crystal system	monoclinic	orthorhombic
Space group	<i>P</i> 2 ₁	<i>P</i> 2 ₁ 2 ₁ 2 ₁
Temperature [K]	120(2)	100(2)
Cell dimensions		
<i>a</i> [Å]	15.3323(10)	10.859(5)
<i>b</i> [Å]	14.3051(10)	19.999(5)
<i>c</i> [Å]	18.5068(14)	20.399(5)
β [°]	93.379(6)	90
<i>V</i> [Å ³]	4052.0(5)	4430(3)
<i>Z</i>	2	4
<i>D</i> _{calcd.} [g/cm ³]	1.139	1.094
μ [mm ⁻¹]	0.147	0.078
Crystal dimensions [mm]	0.45 × 0.24 × 0.18	0.35 × 0.20 × 0.19
Radiation (λ [Å])	Mo- <i>K</i> _α (0.71073)	Mo- <i>K</i> _α (0.71073)
Reflections measured	31 061	41 850
Range/indices (<i>h</i> , <i>k</i> , <i>l</i>)	−18, 18; −17, 16; −22, 22	−13, 13; −24, 23; −25, 25
θ limit [°]	3.00–25.06	2.74–26.11
Total no. of unique data	12756	8678
No. of observed data [<i>I</i> > 2σ(<i>I</i>)]	7125	5522
No. of variables	842	486
No. of restraints	17	0
Absolute structure parameter	0.05(13)	−0.1(4)
<i>R</i> _{int}	0.0962	0.1254
$R = \Sigma F_o - F_c /\Sigma F_o $ (all, observed)	0.1450, 0.0796	0.1417, 0.0762
$wR_2 = \Sigma[w(F_o^2 - F_c^2)^2]/\Sigma w(F_o^4)^{1/2}$ (all, observed)	0.1759, 0.1543	0.1653, 0.1447
GOOF	0.969	0.994
Data completeness	0.997	0.993
Absorption correction (<i>T</i> _{min} , <i>T</i> _{max})	0.947, 0.975	0.929, 0.966
$\Delta\rho$ (max, min) [e/Å ³]	0.54, −0.49	0.41, −0.24

FVAR parameter was also refined separately for each group, and these additional parameters are contained within the supplementary crystallographic data for this paper (CCDC-743616 and -743617); these data can be obtained free of charge from The Cambridge Crystallographic Data Centre via www.ccdc.cam.ac.uk/data_request/cif.

Acknowledgments

The authors would like to thank the Polish State Committee for Scientific Research (Grants N204 261234 and N205 4036 33) for support of this research.

- [1] a) S. Kanemasa, M. Nishiuchi, E. Wada, *Tetrahedron Lett.* **1992**, 33, 1357; b) H. R. Kim, J. H. Song, S. Y. Rhie, E. K. Ryu, *Synth. Commun.* **1995**, 25, 1801; c) L. Crombie, D. E. Games, A. W. G. James, *J. Chem. Soc. Perkin Trans. 1* **1996**, 22, 2715; d) F. Luderer, H. Reinke, H. Oehme, *J. Organomet. Chem.* **1996**, 510, 181; e) E. P. Moore Jr., in *Polypropylene Handbook*, Hanser/Gardner Publications, Cincinnati, **1996**; f) S. G. Hegde, D. C. Myles, *Synth. Commun.* **1997**, 27, 2111; g) P. Sobota, J. Utko, J. Ejfler, L. B. Jerzykiewicz, *Organometallics* **2000**, 19, 4929; h) H. O. Davies, A. C. Jones, T. J. Leedham, M. J. Crosbie, P. J. Wright, N. M. Boag, J. R. Thompson, *Chem. Vap. Deposition* **2000**, 6, 71; i) W. Teng, M. Guino, J. Hitzbleck, U. English, K. Ruhlandt-Senge, *Inorg. Chem.* **2005**, 44, 9531; j) W. L. Leong, S. K. Batabyal, S. Kasapis, J. J. Vittal, *Chem. Eur. J.* **2008**, 14, 8822.
- [2] a) M.-L. Shueh, Y.-S. Wang, B.-H. Huang, C.-Y. Kuo, C.-C. Lin, *Macromolecules* **2004**, 37, 5155; b) J. Ejfler, M. Kobyłka, L. B. Jerzykiewicz, P. Sobota, *Dalton Trans.* **2005**, 2047; c) M.-L. Shueh, B.-T. Ko, T. Athar, C.-C. Lin, T.-M. Wu, S.-F. Hsu, *Organometallics* **2006**, 25, 4144; d) H.-Y. Tang, H.-Y. Chen, J.-H. Huang, C.-C. Lin, *Macromolecules* **2007**, 40, 8855; e) L. F. Sánchez-Barba, A. Garcés, M. Fajardo, C. Alonso-Moreno, J. Fernández-Baeza, A. Otero, A. Antiñolo, J. Tejada, A. Lara-Sánchez, M. I. Lopez-Sólera, *Organometallics* **2007**, 26, 6403; f) B. Lian, C. M. Thomas, O. L. Casagrande Jr., T. Roisnel, J.-F. Carpentier, *Polyhedron* **2007**, 26, 3817; g) R. Tong, J. Cheng, *Angew. Chem. Int. Ed.* **2008**, 47, 4830; h) J. Wu, Y.-Z. Chen, W.-C. Hung, C.-C. Lin, *Organometallics* **2008**, 27, 4970; i) W.-C. Hung, C.-C. Lin, *Inorg. Chem.* **2009**, 48, 728; j) C. A. Wheaton, P. G. Hayes, B. J. Ireland, *Dalton Trans.* **2009**, 4832; k) R. H. Platel, L. M. Hodgson, C. K. Williams, *Polym. Rev.* **2008**, 48, 11; l) V. Poirier, T. Roisnel, J.-F. Carpentier, Y. Sarazin, *Dalton Trans.* **2009**, 9820.
- [3] a) P. U. Rokkanen, O. Böstman, E. Hirvensalo, E. A. Mäkelä, E. K. Partio, H. Päätilä, S. Vainionpää, K. Vihtonen, P. Törmälä, *Biomaterials* **2000**, 21, 2607; b) R. Haag, F. Kratz, *Angew. Chem. Int. Ed.* **2006**, 45, 1198; c) Z. Zhang, S.-S. Feng, *Biomaterials* **2006**, 27, 262; d) J. Cheng, B. A. Teplý, I. Sherifi, J. Sung, G. Luther, F. X. Gu, E. Levy-Nissenbaum, A. F. Radovic-Moreno, R. Langer, O. C. Farokhzad, *Biomaterials* **2007**, 28, 869; e) K. Kurokawa, K. Yamashita, Y. Doi, H. Abe, *Biomacromolecules* **2008**, 9, 1071; f) K. Numata, A. Finne-Wistrand, A.-C. Albertsson, Y. Doi, H. Abe, *Biomacromolecules* **2008**, 9, 2180; g) A. P. Dove, *Chem. Commun.* **2008**, 6446; h) M. Florczak, A. Duda, *Angew. Chem. Int. Ed.* **2008**, 47, 9088; i) L. S. Nair, C. T. Laurencin, *Prog. Polym. Sci.* **2007**, 32, 762.
- [4] a) B. J. O'Keefe, M. A. Hillmyer, W. B. Tolman, *J. Chem. Soc., Dalton Trans.* **2001**, 2215; b) O. Dechy-Cobaret, B. Martin-

- Vaca, D. Bourissou, *Chem. Rev.* **2004**, *104*, 6147; c) J. Wu, T. L. Yu, C. T. Chen, C.-C. Lin, *Coord. Chem. Rev.* **2006**, *250*, 602.
- [5] a) M. Chisholm, J. C. Gallucci, K. Phomphrai, *Inorg. Chem.* **2004**, *43*, 6717; b) L. E. Breyfogle, C. K. Williams, V. G. Young, M. A. Hillmyer, W. B. Tolman, *Dalton Trans.* **2006**, 928; c) D. J. Darensbourg, W. Choi, C. P. Rizhters, *Macromolecules* **2007**, *40*, 3521; d) M. H. Chisholm, J. C. Gallucci, G. Yaman, *Inorg. Chem.* **2007**, *46*, 8676; e) Z. Zheng, G. Zhao, R. Fablet, M. Bouyahyi, C. M. Thomas, T. Roisnel, O. Casagrande Jr., J.-F. Carpentire, *New J. Chem.* **2008**, *32*, 2279; f) D. J. Darensbourg, W. Choi, O. Karroonnirun, N. Bhuvanesh, *Macromolecules* **2008**, *41*, 3493.
- [6] a) A. Kowalski, A. Duda, S. Penczek, *Macromolecules* **2000**, *33*, 689; b) S. Sosnowski, S. Słomkowski, A. Lorenc, H. R. Kircheldorf, *Colloid Polym. Sci.* **2002**, *280*, 107; c) T. Zou, S.-X. Cheng, R.-X. Zhuo, *Colloid Polym. Sci.* **2005**, *283*, 1091; d) C. M. Silvernail, L. J. Yao, L. M. R. Hill, M. A. Hillmyer, W. B. Tolman, *Inorg. Chem.* **2007**, *46*, 6565; e) M. G. Davidson, C. T. O'Hara, M. D. Jones, C. G. Keir, M. F. Mahon, G. Kociok-Köhn, *Inorg. Chem.* **2007**, *46*, 7686; f) A. D. Celiz, O. A. Scherman, *Macromolecules* **2008**, *41*, 4115.
- [7] S. Groysman, I. Goldberg, M. Kol, E. Genizi, Z. Goldsmid, *Inorg. Chim. Acta* **2003**, *345*, 137.
- [8] a) P. Sobota, J. Utko, K. Sztajnowska, J. Ejfler, J. B. Jerzykiewicz, *Inorg. Chem.* **2000**, *39*, 235; b) P. Sobota, J. Utko, J. Ejfler, J. B. Jerzykiewicz, *Organometallics* **2000**, *19*, 4929.
- [9] A. W. Addison, T. N. Rao, J. Reedijk, J. van Rijn, G. C. Verschoor, *J. Chem. Soc., Dalton Trans.* **1984**, 1349.
- [10] a) Y. Xiao, Z. Wang, K. Ding, *Macromolecules* **2006**, *39*, 128; b) B. Courcot, D. Firley, B. Fraisse, P. Becker, J.-M. Gillet, P. Pattison, D. Chernyshov, M. Sghaier, F. Zouhiri, D. Desmaele, J. d'Angelo, F. Bonhomme, S. Geiger, N. E. Ghermani, *J. Phys. Chem. B* **2007**, *111*, 6042.
- [11] K. W. Henderson, G. W. Honeyman, A. R. Kennedy, R. E. Mulvey, J. A. Parkinson, D. C. Sherrington, *Dalton Trans.* **2003**, 1365.
- [12] J. Ejfler, S. Szafert, K. Mierzwicki, L. B. Jerzykiewicz, P. Sobota, *Dalton Trans.* **2008**, 6556.
- [13] *CrysAlisRED Software*, Oxford Diffraction, Wrocław, Poland, **1995–2004**.
- [14] G. M. Sheldrick, *Acta Crystallogr., Sect. A* **2008**, *64*, 112.

Received: December 14, 2009
Published Online: July 6, 2010

Syntheses, Crystal Structures, and the Phase Transformation of Octacyanometallate-Based $\text{Ln}^{\text{III}}\text{--W}^{\text{V}}$ Bimetallic Assemblies with Two-Dimensional Corrugated Layers

Ai-Hua Yuan,^{*,[a,b]} Peter D. Southon,^[a] David J. Price,^[a] Cameron J. Kepert,^{*,[a]} Hu Zhou,^[b] and Wen-Yan Liu^[b]

Keywords: Octacyanometallates / Lanthanides / Solid-state structures / Tungsten / Layered compounds / Phase transformation

The reactions between $\text{Ln}(\text{NO}_3)_3 \cdot n\text{H}_2\text{O}$ and $(\text{Bu}_3\text{NH})_3[\text{W}(\text{CN})_8] \cdot \text{H}_2\text{O}$ have led to two series of octacyanometallate-based complexes: $\text{Ln}(\text{H}_2\text{O})_5[\text{W}(\text{CN})_8]$ [$\text{Ln} = \text{La}$ (1), Pr (2), Nd (3), Eu (4), Gd (5)] and $\text{Ln}(\text{H}_2\text{O})_4[\text{W}(\text{CN})_8]$ [$\text{Ln} = \text{Ho}$ (6), Er (7), Tm (8), Lu (9)]. The crystal structures of 1–9 have two-

dimensional corrugated layers in which the Ln^{III} and W^{V} centres are linked in an alternating fashion. Thermogravimetric (TG) and powder XRD results reveal the presence of a phase transformation in the $\text{Ln}^{\text{III}}\text{--W}^{\text{V}}$ system with increasing atomic number of the Ln^{III} atoms.

Introduction

In the past few years, $[\text{M}(\text{CN})_8]^{3-/4-}$ ($\text{M} = \text{Mo}$, W , and Nb) anions have become attractive building blocks that can adopt three different spatial configurations [square antiprism (D_{4d}), dodecahedron (D_{2d}) and bicapped trigonal prism (C_{2v})] depending on their surroundings, such as ligands and other metal ions.^[1] In recent studies, investigations of octacyanometallate-based bimetallic systems has mainly focused on second- and third-row transition metals. The exploration of cyano-bridged 3d–nd ($n = 4$ or 5) systems based on $[\text{M}(\text{CN})_8]^{3-/4-}$ anions and transition metal cations has resulted in a wide variety of coordination networks from 0D ionic complexes and discrete molecules, 1D chains, 2D layers and 3D networks. Due to their flexible molecular structures, multifarious magnetic properties as varied as those of the hexacyanometallates, such as photo-induced magnetism,^[2] relatively high magnetic phase transition temperature^[3] and single-molecule magnetism,^[4] are observed in octacyanometallate-based assemblies.

Recently, the investigation of octacyanometallate-based bimetallic systems has been extended to the first-row lanthanide ions. As lanthanide ions often have higher coordination numbers, mixed d–f complexes using 4d or 5d metal ions can have very complicated topologies and magnetic behaviours that are different from those of 3d–4f complexes.

A better understanding of the property–structure relationships of such materials relies on the synthesis and evaluation of new lanthanide–transition metal complexes. However, synthesis of complexes containing octacyanometallates and lanthanide ions is challenging due to the tendency of the rare earth metal ions to adopt high coordination numbers and their ability to easily adapt to a given environment. To the best of our knowledge, there are limited examples of octacyano- and lanthanide-based assemblies^[5] to date, and these complexes have presented interesting properties such as long-range magnetic ordering, cooling-rate-dependent ferromagnetism and luminescence.

For the reasons noted above, we have tried to prepare lanthanide-containing octacyanometallate-based bimetallic assemblies using $[\text{W}(\text{CN})_8]^{3-}$ and Ln^{3+} as building blocks. In the present work, two series of heterobimetallic 4f–5d complexes, $\text{Ln}(\text{H}_2\text{O})_5[\text{W}(\text{CN})_8]$ [$\text{Ln} = \text{La}$ (1), Pr (2), Nd (3), Eu (4), Gd (5)] and $\text{Ln}(\text{H}_2\text{O})_4[\text{W}(\text{CN})_8]$ [$\text{Ln} = \text{Ho}$ (6), Er (7), Tm (8), Lu (9)] have been synthesized and characterized structurally. It should be noted here that TG and powder XRD results revealed the presence of phase transformations in the $\text{Ln}\text{--W}$ system with increasing atomic number of the Ln^{III} atoms (from La to Lu).

Results and Discussion

Crystal Structures of 1–9

The structures of 1–9 have been determined by single-crystal X-ray diffraction (Table S1). 1–5 are isostructural, have tetragonal geometries and crystallize in the space group $P4/nmm$, except for 1, which belongs to $P4/ncc$. The crystal structures of 1–5 consist of 2D cyano-bridged corru-

[a] School of Chemistry, The University of Sydney, Sydney NSW 2006, Australia
E-mail: c.kepert@chem.usyd.edu.au

[b] School of Material Science and Engineering, Jiangsu University of Science and Technology, Zhenjiang 212003, China
E-mail: aihuayuan@163.com

Supporting information for this article is available on the WWW under <http://dx.doi.org/10.1002/ejic.201000320>.

gated layers, in which Ln^{III} and W^V centres are linked in an alternating fashion (Figure 1a). In the structures of **1–5**, the [W(CN)₈] moiety exhibits a slightly distorted dodecahedral geometry (*D*_{2d}) with four bridging and four terminal cyano ligands. The W–C bonds are in the range of 2.132 to 2.168 Å and the W–C1–N1 bonds are nearly linear with angles ranging from 175.3 to 179.0° (Table S2). It is worth noting that half of the coordinated cyanide groups in **2–5** are bidentate, establishing physical links (μ-CN) with neighbouring Ln^{III} centres, while the other half are terminal, exhibiting statistical disorder over two crystallographic positions (occupancy of 50% each) for the uncoordinated nitrogen atom. In the structures of **1–5** the Ln^{III} atom is nine-coordinate, ligated by four cyano nitrogen atoms and five oxygen atoms from five water molecules, {LnN₄O₅}, describing a slightly distorted monocapped square antiprism geometry with the O1 atom in a capping position (Figure 2). The sites of one face are finished by four cyano nitrogen atoms with Ln–N_{cyanide} distances ranging from 2.504 to 2.647 Å, while those of the other face by four oxygen atoms with Ln–O distances ranging from 2.467 to 2.620 Å. Four cyanide bridges are close to linear with bond angles of C1–N1–Ln in the range of 165.3 to 176.7°. The geometry of the Ln atom for **1–5** is different from the tricapped trigonal prism found for related complexes Ln(H₂O)₅[W(CN)₈] (Ln = Sm, Eu, Gd, Tb).^[5f,5j]

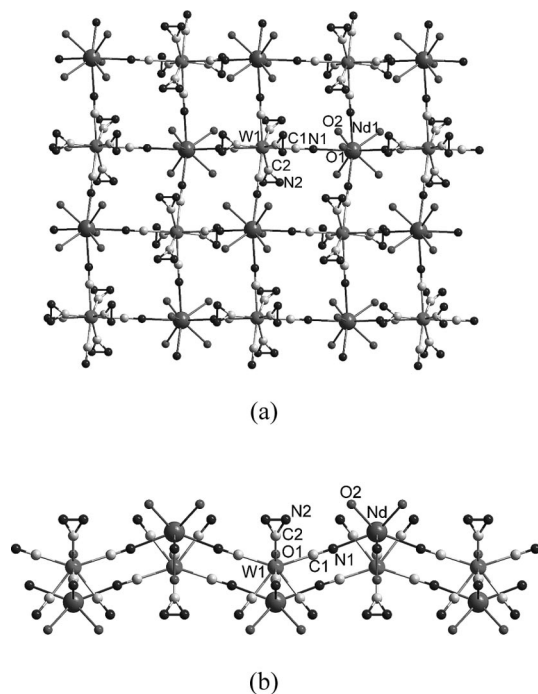


Figure 1. Projection of 2D corrugated layers for **1–5**: (a) in the *ab* plane and (b) along the *c* axis. Note: four terminal cyanide groups in **1** exhibit order, which is different from those in **2–5**.

As shown in Figure 1a, the Ln^{III} and the [W(CN)₈]^{3–} units form 12-membered Ln₂W₂(CN)₄ squares with the Ln^{III} and W^V atoms occupying the vertices. The side view of the 2D corrugated layer is shown in Figure 1b. The average distances of the closest intramolecular Ln^{III}–W,

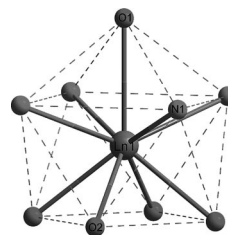


Figure 2. Coordination environment of **1–5**.

Ln^{III}–Ln, and W^V–W distances are 5.832, 8.652 and 7.823 Å, respectively. The average Ln^{III}–W, Ln^{III}–Ln and W^V–W distances between neighbouring aligned layers are 7.644, 7.123 and 7.123 Å, respectively. The 2D layers are linked by relatively strong O–H⁺–N hydrogen bonds between H₂O molecules and terminal cyano ligands, connecting the O(1 W) coordinated molecules from one layer to the terminal C2N2 cyanide groups of another layer with *d*_{O...N} of 2.781, 2.586, 2.626, 2.606 and 2.614 Å for **1–5**, respectively. It is worth mentioning that the degree of disorder in the structures of complexes **4** and **5** is superior to that of those reported in the literature.^[5j]

Similar to **1–5**, the structures of **6–9** are tetragonal and crystallize in the space group *P4/nmm*. The crystal structures consist of 2D cyano-bridged corrugated layers in which Ln^{III} and W^V ions are linked in an alternating fashion (Figure 3a). The side view of the 2D corrugated layer is shown in Figure 3b. The central geometry around W^V adopts a slightly distorted dodecahedral geometry (*D*_{2d}). The W^V atom is coordinated by eight CN groups, four of which are bridging and four are terminal. For **6–9** the

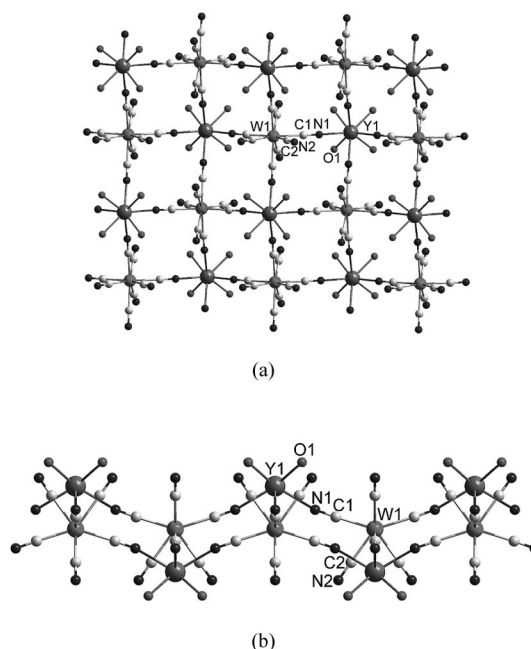


Figure 3. Projection of 2D corrugated layers for **6–9**: (a) in the *ab* plane and (b) along the *c* axis.

average W–C bond length is 2.167 Å and the bridging W–C–N angles remain almost linear with maximum deviation from linearity of 2.4°.

In contrast to that in **1–5**, the Ln atom is eight coordinate and is surrounded by four cyano nitrogen atoms and four oxygen atoms from four water molecules. The coordination sphere of the Ln^{III} centre, {LnN₄O₄}, displays a slightly distorted square antiprism geometry (Figure 4). The sites of both faces are finished by four cyano nitrogen atoms and four oxygen atoms, respectively. The average Ln–N and Ln–O bond lengths both slightly decrease from **6** to **9** (on going from the Ho to Lu) because of systematic ionic radii contraction. The Ln–C1–N1 units are bent slightly with angles ranging from 167.8 to 169.6°. For **6–9**, the closest intramolecular Ln···W, Ln···Ln, and W···W distances are 5.806, 8.620 and 7.781 Å, respectively, and the shortest intermetallic distances between one layer and its closest neighbour (Ln···W, Ln···Ln and W···W) are 7.595, 7.761 and 7.761 Å, respectively. The O atom of one coordinated water molecule and the N2 atom of terminal CN group in neighbouring layers are connected through the relatively strong O–H···N hydrogen bonds with an average *d*_{O···N} distance of 7.761 Å.

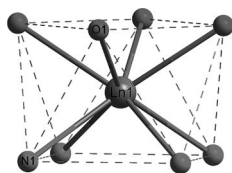


Figure 4. Coordination environment of **6–9**.

In summary, the structures of **1–9** comprise neutral corrugated layers consisting of 12-membered Ln₂W₂(CN)₄ puckered squares, which is similar to the 12-membered Ru₂Ln₂(CN)₄ squares observed in [{Ru(bpy)(CN)₄}₃{Ln(H₂O)₄}₂]_x·*x*H₂O (Ln = Nd, Gd; *x* = 11 or 10, respectively).^[6]

The Phase Transformation in the Ln–W System

Powder samples of [Ln(H₂O)_{*n*}][W(CN)₈] (Ln = La, Pr, Nd, Sm, Eu, Gd, Tb, Ho, Er, Tm, Lu) were prepared by mixing aqueous solutions of (Bu₃NH)₃[W(CN)₈] and Ln(NO₃)₃·*n*H₂O. Powder XRD patterns (Figure S2) are in correspondence with those simulated from single-crystal structures, which reveals that the as-synthesized products are the expected materials. It is worth mentioning here that the powder XRD pattern of Tb(H₂O)₅[W(CN)₈] corresponds closely with that simulated from the single-crystal structure of Tb(H₂O)₅[Mo(CN)₈]^[5j] reported previously, indicating that the two complexes are isostructural.

Powder XRD patterns of [Ln(H₂O)_{*n*}][W(CN)₈] are shown in Figure 5. With increasing atomic number of Ln^{III} atoms from La to Tb, the diffraction patterns remain unchanged, which shows that the Ln–W systems (Ln = La, Ce, Pr, Nd, Sm, Eu, Gd, Tb) have the same lattice structure. Combining the powder data with the single-crystal struc-

tural analysis, we can speculate that the *n* value in [Ce(H₂O)_{*n*}][W(CN)₈] is five. With increasing atomic number (to Dy), some changes in the diffraction patterns were observed. A few peaks attributed to [Ln(H₂O)₅][W(CN)₈] disappear or reduce in intensity and some new peaks attributed to another uncertain phase emerge, which indicates the phase transformation. With atomic number increasing from Ho to Lu, [Ln(H₂O)₄][W(CN)₈] (Ln = Ho, Er, Tm, Lu) have the same lattice structures, which have been confirmed by single-crystal structures. We can conclude that a phase transformation occurs from [Ln(H₂O)₅][W(CN)₈] (Ln = La to Tb) to [Ln(H₂O)₄][W(CN)₈] (Ln = Ho to Lu) via [Dy(H₂O)_{*x*}][W(CN)₈] with increasing atomic number.

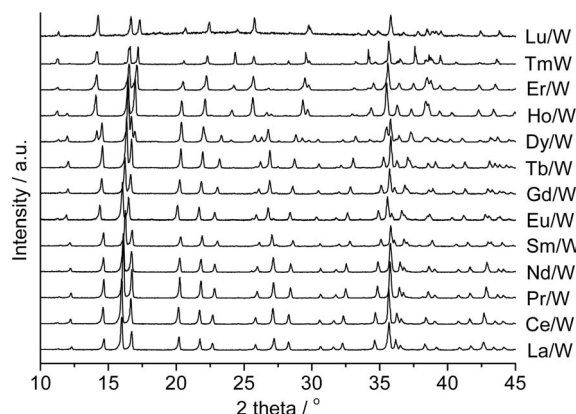


Figure 5. Powder XRD patterns of Ln(H₂O)_{*n*}[W(CN)₈].

TGA (Figure S3) and variable temperature powder XRD (Figures S4 and S5) results show that [Ln(H₂O)₅][W(CN)₈] (Ln = Sm, Eu, Gd, Tb) change reversibly to [Ln(H₂O)₄][W(CN)₈] with the loss of the first coordinated water molecule followed by the collapse of the framework structure with the loss of the remaining four coordinated water molecules on heating. Here we take complex **4** as an example. The TG result (Figure 6) reveals that one coordinated water molecule is lost at approximately 55 °C. The remaining four water molecules are lost gradually along with the collapse of framework, which can be confirmed by

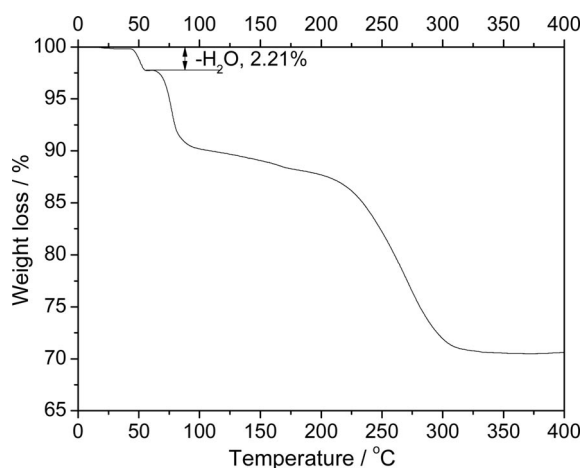


Figure 6. TG curve of **4**.

a variable temperature powder XRD experiment (Figure 7). In addition, the structure changes after **4** converts to [Eu(H₂O)₄][W(CN)₈], which reveals that the loss of the coordinated water molecule has an important impact on the structure of the framework. Interestingly, the process of this change is reversible (Figure 8). However, for [Ln(H₂O)₅][W(CN)₈] (Ln = La, Ce, Pr, Nd) and [Ln(H₂O)₄][W(CN)₈] (Ln = Ho, Er, Tm, Lu) the structures collapse directly when the coordinated water molecules are lost (Figures S3 and S4).

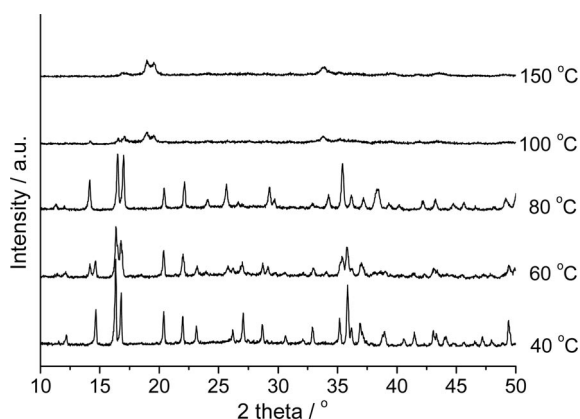


Figure 7. Variable temperature powder XRD patterns of **4**.

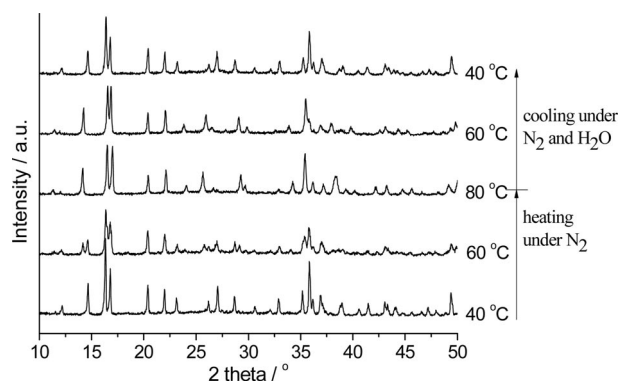


Figure 8. Variable temperature powder XRD patterns of **4** with sorption and desorption of water.

Conclusions

Two series of octacyanometallate-based complexes, Ln(H₂O)₅[W(CN)₈] [Ln = La(**1**), Pr(**2**), Nd(**3**), Eu(**4**), Gd(**5**)] and Ln(H₂O)₄[W(CN)₈] [Ln = Ho(**6**), Er(**7**), Tm(**8**), Lu(**9**)], have been synthesized and characterized structurally. The crystal structures of **1–9** have two-dimensional corrugated layers, in which the Ln^{III} and W^V centres are linked in an alternating fashion. TG and powder XRD results reveal the presence of a phase transformation in the Ln–W system with increasing atomic number of the Ln^{III} atoms.

Experimental Section

Materials: All chemicals and solvents were of analytical grade. (Bu₃NH)₃[W(CN)₈] was prepared according to the literature method.^[7] TG analysis revealed that the octacyanometallate precursor did not contain crystallized water molecules (Figure S1).

Syntheses of 1–9: Single crystals of **1–9** were prepared in the dark by slow diffusion of an acetonitrile solution (20 mL) containing Ln(NO₃)₃·*n*H₂O [Ln = La(**1**), Pr(**2**), Nd(**3**), Eu(**4**), Gd(**5**), Ho(**6**), Er(**7**), Tm(**8**), Lu(**9**)] (0.05 mmol) and (Bu₃NH)₃[W(CN)₈] (0.05 mmol). Orange crystals were formed over two to six weeks. **1:** C₈H₁₀LaN₈O₅W (620.97): calcd. C 15.47, H 1.62, N 18.05; found C 15.39, H 1.68, N 18.06. **2:** C₈H₁₀N₈O₅PrW (622.98): calcd. C 15.42, H 1.62, N 17.99; found C 15.52, H 1.55, N 18.02. **3:** C₈H₁₀N₈NdO₅W (626.31): calcd. C 15.34, H 1.61, N 17.89; found C 15.37, H 1.60, N 17.81. **4:** C₈H₁₀EuN₈O₅W (634.03): calcd. C 15.16, H 1.59, N 17.67; found C 15.13, H 1.66, N 17.72. **5:** C₈H₁₀GdN₈O₅W (639.32): calcd. C 15.03, H 1.58, N 17.53; found C 15.11, H 1.56, N 17.49. **6:** C₈H₈HoN₈O₄W (628.98): calcd. C 15.28, H 1.28, N 17.82; found C 15.31, H 1.26, N 17.86. **7:** C₈H₈ErN₈O₄W (631.31): calcd. C 15.22, H 1.28, N 17.75; found C 15.34, H 1.26, N 17.79. **8:** C₈H₈N₈O₄TmW (632.99): calcd. C 15.18, H 1.27, N 17.70; found C 15.14, H 1.30, N 17.65. **9:** C₈H₈LuN₈O₄W (639.02): calcd. C 15.04, H 1.26, N 17.54; found C 15.00, H 1.21, N 17.45. Powder samples were prepared by mixing aqueous solutions of (Bu₃NH)₃[W(CN)₈] (15 mL, 0.15 mmol) and Ln(NO₃)₃·2H₂O (Ln = La, Ce, Pr, Nd, Sm, Eu, Gd, Tb, Dy, Ho, Er, Tm, Lu) (15 mL, 0.15 mmol). C₈H₁₀N₈O₅WLa: C, 15.35; H, 1.59; N, 18.15. C₈H₁₀N₈O₅WCe: C, 15.43; H, 1.69; N, 18.10. C₈H₁₀N₈O₅WPr: C, 15.45; H, 1.66; N, 17.91. C₈H₁₀N₈O₅WNd: C, 15.40; H, 1.65; N, 17.97. C₈H₁₀N₈O₅WSm: C, 15.28; H, 1.62; N, 17.81. C₈H₁₀N₈O₅WEu: C, 15.15; H, 1.69; N, 17.64. C₈H₁₀N₈O₅WGd: C, 15.08; H, 1.59; N, 17.42. C₈H₁₀N₈O₅WTb: C, 15.04; H, 1.55; N, 17.54. C₈H₉N₈O_{4.5}WDy: C, 15.12; H, 1.42; N, 17.69. C₈H₈N₈O₄WHo: C, 15.32; H, 1.29; N, 17.86. C₈H₈N₈O₄WER: C, 15.18; H, 1.21; N, 18.88. C₈H₈N₈O₄WTm: C, 15.15; H, 1.27; N, 17.66. C₈H₈N₈O₄WLu: C, 15.10; H, 1.33; N, 17.51. Powder XRD patterns (Figure S2) of as-synthesized products correspond fully to those simulated from single-crystal structures (Figure S2), which reveals that highly pure products have been obtained.

Physical Measurements: Thermogravimetric (TG) analyses were carried out with a TA Instruments Hi-Res TGA 2950 analyzer to identify the approximate temperatures of guest water loss and thermal decomposition. The temperature was increased at a rate of 1 K/min from 294 K to 1053 K under a dry dinitrogen atmosphere with a 60 mL/min flow. Powder XRD patterns were collected with Cu-K_α radiation using a Shimadzu XRD-6000 diffractometer equipped with an Anton-Paar HTK 1200 stage for atmosphere and temperature control. Dehydration measurements were run under flowing dry dinitrogen with a heating rate of 1 K/min. For rehydration measurements the dinitrogen flow was saturated with water vapour by diverting the flow through a water bubbler.

X-ray Crystallographic Analysis: Diffraction data for **1–9** were collected with a Bruker Smart 1000 CCD equipped with Mo-K_α (λ = 0.71073 Å) radiation. Diffraction data analysis and reduction were performed with SMART, SAINT, and XPREP.^[8] Correction for Lorentz, polarization and absorption effects were performed with SADABS.^[9] Structures were solved by using the Patterson method with SHELXS-97^[10] and refined with SHELXL-97.^[11] All non-hydrogen atoms were refined with anisotropic thermal parameters. The H atoms bound to coordinated water molecules were located from difference maps and refined with a riding model. The crystallographic data and experimental details for the structural analyses

of 1–9 are summarized in Table S1. Selected bond lengths and angles are listed in Table S2. CCDC-716068 (1), -729451 (2), -698970 (3), -698971 (4), -698972 (5), -698973 (6), -698974 (7), -698975 (8) and -698976 (9) contain the supplementary crystallographic data for this paper. These data can be obtained free of charge from The Cambridge Crystallographic Data Centre via www.ccdc.cam.ac.uk/data_request/cif.

Supporting Information (see footnote on the first page of this article): Additional room-temperature powder XRD patterns, TG curves, variable-temperature powder XRD patterns and tables of crystallographic data and bond lengths and angles.

Acknowledgments

This work is supported by the Australian Research Council (DP0664834 and FF0561456), the University Natural Science Foundation of Jiangsu Province, China (No. 07KJB150030) and the Jiangsu Government Scholarship for Overseas Studies (China).

- [1] a) P. Przychodzeń, T. Korzeniak, R. Podgajny, B. Sieklucka, *Coord. Chem. Rev.* **2006**, *250*, 2234–2260; b) B. Sieklucka, R. Podgajny, P. Przychodzeń, T. Korzeniak, *Coord. Chem. Rev.* **2005**, *249*, 2203–2221; c) J. Larionova, S. Willemin, B. Donnadieu, B. Henner, C. Guérin, B. Gillon, A. Goujon, *J. Phys. Chem. Solids* **2004**, *65*, 677–691; d) B. Sieklucka, R. Podgajny, P. Przychodzeń, R. Kania, *C. R. Chim.* **2002**, *5*, 639–649; e) R. Garde, C. Desplanches, A. Bleuzen, P. Veillet, M. Verdager, *Mol. Cryst. Liq. Cryst.* **1999**, *334*, 587–595.
- [2] a) S. I. Ohkoshi, S. Ikeda, T. Hozumi, T. Kashiwagi, K. Hashimoto, *J. Am. Chem. Soc.* **2006**, *128*, 5320–5321; b) C. Mathonière, R. Podgajny, P. Guionneau, C. Labrugere, B. Sieklucka, *Chem. Mater.* **2005**, *17*, 442–449; c) T. Hozumi, K. Hashimoto, S. Ohkoshi, *J. Am. Chem. Soc.* **2005**, *127*, 3864–3869; d) J. M. Herrera, V. Marvaud, M. Verdager, J. Marrot, M. Kalisz, C. Mathonière, *Angew. Chem. Int. Ed.* **2004**, *43*, 5468–5471; e) Y. Arimoto, S. Ohkoshi, Z. J. Zhong, H. Seino, Y. Mizobe, K. Hashimoto, *J. Am. Chem. Soc.* **2003**, *125*, 9240–9241.
- [3] a) W. Kosaka, K. Imoto, Y. Tsunobuchi, S. Ohkoshi, *Inorg. Chem.* **2009**, *48*, 4604–4606; b) D. Pinkowicz, R. Podgajny, M. Bałanda, M. Makarewicz, B. Gawel, W. Łasocha, B. Sieklucka, *Inorg. Chem.* **2008**, *47*, 9745–9747; c) J. M. Herrera, P. Franz, R. Podgajny, M. Pilkington, M. Biner, S. Decurtins, H. Stoeckli-Evans, A. Neels, R. Garde, Y. Dromzée, M. Julve, B. Sieklucka, K. Hashimoto, S. Ohkoshi, M. Verdager, *C. R. Chim.* **2008**, *11*, 1192–1199; d) W. Kosaka, K. Hashimoto, S. Ohkoshi, *Bull. Chem. Soc. Jpn.* **2008**, *81*, 992–994; e) R. Podgajny, D. Pinkowicz, T. Korzeniak, W. Nitek, M. Rams, B. Sieklucka, *Inorg. Chem.* **2007**, *46*, 10416–10425; f) S. Ohkoshi, Y. Tsunobuchi, H. Takahashi, T. Hozumi, M. Shiro, K. Hashimoto, *J. Am. Chem. Soc.* **2007**, *129*, 3084–3085; g) H. Higashikawa, K. Okuda, J. Kishine, N. Masuhara, K. Inoue, *Chem. Lett.* **2007**, *36*, 1022–1023; h) J. R. Withers, D. F. Li, J. Triplet, C. Ruschman, S. Parkin, G. B. Wang, G. T. Yee, S. M. Holmes, *Inorg. Chem.* **2006**, *45*, 4307–4309; i) Y. Song, S. Ohkoshi, Y. Arimoto, H. Seino, Y. Mizobe, K. Hashimoto, *Inorg. Chem.* **2003**, *42*, 1848–1856; j) Z. J. Zhong, H. Seino, Y. Mizobe, M. Hidai, M. Verdager, S. Ohkoshi, K. Hashimoto, *Inorg. Chem.* **2000**, *39*, 5095–5101.
- [4] a) J. H. Lim, J. H. Yoon, H. C. Kim, C. S. Hong, *Angew. Chem. Int. Ed.* **2006**, *45*, 7424–7426; b) Y. Song, P. Zhang, X. M. Ren, X. F. Shen, Y. Z. Li, X. Z. You, *J. Am. Chem. Soc.* **2005**, *127*, 3708–3709.
- [5] a) I. V. Typilo, O. A. Sereda, H. Stoeckli-Evans, R. E. Gladyshevskii, D. I. Semenyshyn, *Russ. J. Coord. Chem.* **2009**, *35*, 920–924; b) I. V. Typilo, O. A. Sereda, D. I. Semenyshyn, H. Stoeckli-Evans, R. E. Gladyshevskii, *Pol. J. Chem.* **2009**, *83*, 339–344; c) O. A. Sereda, G. Stöckli-Evans, I. V. Typilo, D. I. Semenyshyn, R. E. Gladyshevskii, *Russ. J. Coord. Chem.* **2009**, *35*, 15–18; d) S. L. Ma, S. Ren, Y. Ma, D. Z. Liao, *J. Chem. Sci.* **2009**, *121*, 421–427; e) S. L. Ma, S. Ren, *J. Inorg. Organomet. Polym.* **2009**, *19*, 382–388; f) E. Chelebaeva, J. Larionova, Y. Guari, R. A. S. Ferreira, L. D. Carlos, F. A. A. Paz, A. Trifonov, C. Guérin, *Inorg. Chem.* **2009**, *48*, 5983–5995; g) S. Tanase, M. Evangelisti, L. J. de Jongh, J. M. M. Smits, R. de Gelder, *Inorg. Chim. Acta* **2008**, *361*, 3548–3554; h) S. Tanase, L. J. de Jongh, F. Prins, M. Evangelisti, *ChemPhysChem* **2008**, *9*, 1975–1978; i) S. L. Ma, Y. Ma, D. Z. Liao, S. P. Yan, Z. H. Jiang, G. L. Wang, *Chin. J. Inorg. Chem.* **2008**, *24*, 1290–1293; j) E. Chelebaeva, J. Larionova, Y. Guari, R. A. S. Ferreira, L. D. Carlos, F. A. A. Paz, A. Trifonov, C. Guérin, *Inorg. Chem.* **2008**, *47*, 775–777; k) P. Przychodzeń, R. Pełka, K. Lewiński, J. Supel, M. Rams, K. Tomala, B. Sieklucka, *Inorg. Chem.* **2007**, *46*, 8924–8938; l) F. Prins, E. Pasca, L. J. de Jongh, H. Kooijman, A. L. Spek, S. Tanase, *Angew. Chem. Int. Ed.* **2007**, *46*, 6081–6084; m) W. Kosaka, K. Hashimoto, S. Ohkoshi, *Bull. Chem. Soc. Jpn.* **2007**, *80*, 2350–2356; n) Z. X. Wang, X. F. Shen, J. Wang, P. Zhang, Y. Z. Li, E. N. Nfor, Y. Song, S. Ohkoshi, K. Hashimoto, X. Z. You, *Angew. Chem. Int. Ed.* **2006**, *45*, 3287–3291; o) S. Tanase, F. Prins, J. M. M. Smits, R. de Gelder, *CrystEngComm* **2006**, *6*, 863–865; p) P. Przychodzeń, K. Lewiński, R. Pełka, M. Bałanda, K. Tomala, B. Sieklucka, *Dalton Trans.* **2006**, 625–628; q) S. Ikeda, T. Hozumi, K. Hashimoto, S. Ohkoshi, *Dalton Trans.* **2005**, 2120–2123; r) T. Hozumi, S. Ohkoshi, Y. Arimoto, H. Seino, Y. Mizobe, K. Hashimoto, *J. Phys. Chem. B* **2003**, *107*, 11571–11574.
- [6] G. M. Davies, S. J. A. Pope, H. Adams, S. Faulkner, M. D. Ward, *Inorg. Chem.* **2005**, *44*, 4656–4665.
- [7] L. D. C. Bok, J. G. Leipoldt, S. S. Basson, *Z. Anorg. Allg. Chem.* **1975**, *415*, 81–83.
- [8] SMART, SAINT and XPREP: Area Detector Control and Data Integration and Reduction Software, Bruker Analytical X-ray Instruments Inc., Madison, Wisconsin, USA, **1995**.
- [9] G. M. Sheldrick, *SADABS: Empirical Absorption and Correction Software*, University of Göttingen, Göttingen, Germany, **1999**.
- [10] G. M. Sheldrick, *SHELXS-97: Programs for Crystal Structure Solution*, University of Göttingen, Göttingen, Germany, **1997**.
- [11] G. M. Sheldrick, *SHELXL-97: Programs for the Refinement of Crystal Structures*, University of Göttingen, Göttingen, Germany, **1997**.

Received: March 21, 2010
Published Online: July 1, 2010

Synthesis and Reaction Chemistry of Heterodi- and Heterotrimetallic Transition-Metal Complexes Based on 1-(Diphenylphosphanyl)-1'-terpyridylferrocene

Alexander Hildebrandt,^[a] Nora Wetzold,^[a] Petra Ecorchard,^[a] Bernhard Walfort,^[a] Tobias Rüffer,^[a] and Heinrich Lang*^[a]

Keywords: Heterometallic complexes / Metallocenes / Solid-state structures / Terpyridine / N,P ligands

The reaction of $[\text{Fe}(\eta^5\text{-C}_5\text{H}_4\text{PPh}_2)(\eta^5\text{-C}_5\text{H}_4\text{terpy})]$ (**5**; terpy = 2,2':6',2''-terpyridin-4'-yl) with diverse transition-metal compounds including $[\text{PtCl}_2(\text{Et}_2\text{S})_2]$, $[\text{Pd}(\text{cod})\text{X}_2]$, $[\text{AuCl}(\text{tht})]$, $[\text{CuBr}]$, $[\text{Mo}(\text{CO})_4(\text{nbd})]$, and $[\{\text{RhCl}(\text{cod})\}_2]$ ($\text{X} = \text{Cl}, \text{Br}$; tht = tetrahydrothiophene; nbd = norbornadiene; cod = cyclooctadiene) to afford heterobi- and trimetallic complexes and a coordination polymer is reported. The following compounds were prepared: $[\text{Fe}(\eta^5\text{-C}_5\text{H}_4\text{PPh}_2\{\text{PtCl}_2(\text{SEt}_2)\})(\eta^5\text{-C}_5\text{H}_4\text{terpy})]$ (**7**), *trans*- $[\text{PtCl}_2\{(\text{Ph}_2\text{P}-\eta^5\text{-C}_5\text{H}_4)(\eta^5\text{-C}_5\text{H}_4\text{terpy})\text{Fe}\}_2]$ (**9**), $[\text{Fe}(\eta^5\text{-C}_5\text{H}_4\text{PPh}_2\text{PdCl}_2)(\eta^5\text{-C}_5\text{H}_4\text{terpy})]$ (**12**), $[\text{Fe}(\eta^5\text{-C}_5\text{H}_4\text{PPh}_2(\text{Cl}_3\text{Pd}^-))(\eta^5\text{-C}_5\text{H}_4\text{terpy}\{(\text{dmsO})_2\text{ClNi}^+\})]$ (**14**), *trans*- $[\text{PdX}_2\{(\text{Ph}_2\text{P}-\eta^5\text{-C}_5\text{H}_4)(\eta^5\text{-C}_5\text{H}_4\text{terpy})\text{Fe}\}_2]$ (**16a**, $\text{X} = \text{Cl}$; **16b**, $\text{X} = \text{Br}$), $[\text{Mo}(\text{CO})_4\{(\eta^5\text{-C}_5\text{H}_4\text{PPh}_2)(\eta^5\text{-C}_5\text{H}_4\text{terpy})\text{Fe}\}_2]$ (**17**), $[\text{Fe}(\eta^5\text{-C}_5\text{H}_4\text{Ph}_2\text{P}(\text{CuBr}))(\eta^5\text{-C}_5\text{H}_4\text{terpy})]_n$ (**19**), $[\text{Fe}(\eta^5\text{-C}_5\text{H}_4\text{Ph}_2\text{P}(\text{AuCl}))(\eta^5\text{-C}_5\text{H}_4\text{terpy})]$ (**22**), $[\text{Fe}(\eta^5\text{-C}_5\text{H}_4\text{Ph}_2\text{P}$

$\{\text{Rh}(\text{cod})\text{Cl}\})(\eta^5\text{-C}_5\text{H}_4\text{terpy})]$ (**23**), $[\text{Ru}\{(\eta^5\text{-C}_5\text{H}_4\text{Ph}_2\text{P}(\text{AuCl}))(\eta^5\text{-C}_5\text{H}_4\text{terpy})\text{Fe}\}_2\text{Cl}_2]$ (**25**), and $[\text{Fe}(\eta^5\text{-C}_5\text{H}_4\text{PPh}_2\text{PdCl}_2)\{(\eta^5\text{-C}_5\text{H}_4\text{-CH=CHC}(\text{O})(\text{py}))\}]$ (**26**). The molecular structures of **5**, **9**, **12**, **14**, **16b**, **22**, and **26** in the solid state are reported. They show typical features of related phosphanylferrocenes and terpyridylferrocenes. Characteristic of **12** is a C–H activation as a result of the close distance of palladium to the terpyridyl moiety. Complexes **12**, **26**, and $[\text{PdCl}_2(\text{dppf})]$ [dppf = 1,1'-bis(diphenylphosphanyl)ferrocene], for comparison, were used in preliminary studies as catalysts in the carbon–carbon coupling of iodobenzene with *tert*-butyl acrylate to give (*E*)-*tert*-butyl cinnamate. The conversion amounts to 80 % with a turnover number of 160 and turnover frequency of 48 h^{-1} .

Introduction

In recent years, ferrocene-based organometallics have received remarkable attention because such molecules are in general very robust and show a reversible redox character.^[1] They are of interest in many fields of chemistry including organic synthesis, molecular recognition, material sciences, and homogeneous catalysis.^[2] Whereas symmetrically substituted ferrocenes with nitrogen,^[3] phosphorus,^[4] oxygen,^[5] or sulfur^[6] donor groups at the cyclopentadienyl rings are well studied, less is known about sandwich compounds that bear two different coordination functionalities.^[7] The latter type of molecules, with their asymmetric 1,1'-substitution pattern, are of great interest in, for example, homogeneous catalysis due to their hemilabile coordination sites.^[8] In this respect, the work of Gibson et al.,^[8a,9] Gimeno et al.,^[10] Keim et al.,^[11] Long et al.,^[7a,8a,9] and others^[12] must be mentioned, who recently reported about the systematic synthesis, reaction behavior, and characterization of P/S, P/O,

and N/O hemilabile ligand systems. First reports about the use of such asymmetric 1,1'-disubstituted ferrocenes in homogeneous catalysis were reported as well.^[7–9] One of the reports implied a chiral thioether–phosphanylferrocene, which was used in Pd-catalyzed allylic substitution of 1,3-diphenylpropenyl acetate with malonate and nitrogen nucleophiles.^[13] The use of ferrocenes that contain unsymmetrical P/S or P/O ligands at the cyclopentadienyl rings as catalytic active species in combination with palladium(0) and palladium(II) reagents, respectively, were also tested by Gibson and Long in the Suzuki–Miyaura carbon–carbon cross-coupling reaction of 4-bromotoluene with phenyl boronic acid to produce 4-methylbiphenyl.^[8a] Within this reaction the yield was doubled, when compared with the symmetrical 1,1'-bis(diphenylphosphanyl)ferrocene.

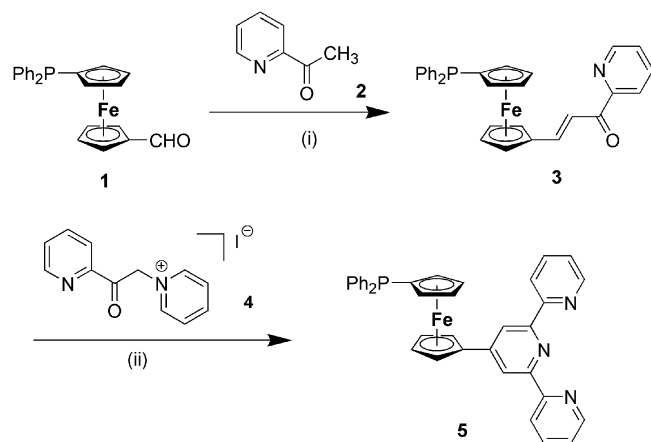
These studies have prompted us to prepare 1-(diphenylphosphanyl)-1'-terpyridylferrocene and to use this compound for the synthesis of transition-metal complexes of higher nuclearity. We chose this molecule as starting compound because the diphenylphosphanyl group should preferentially bind to soft and the terpyridyl unit to hard transition-metal-complex fragments.^[14] The application of the appropriate Fe–Pd-containing molecules in the Heck–Mizoroki reaction of iodobenzene with *tert*-butyl acrylate to give

[a] Technische Universität Chemnitz, Fakultät für Naturwissenschaften, Institut für Chemie, Lehrstuhl für Anorganische Chemie, Straße der Nationen 62, 09111 Chemnitz, Germany
Fax: +49-371-531-21219
E-mail: heinrich.lang@chemie.tu-chemnitz.de

(*E*)-*tert*-butyl cinnamate is reported as well. The molecular structures of seven compounds in the solid state are discussed.

Results and Discussion

To synthesize asymmetric 1,1'-substituted ferrocene-based heterodi- and heterotrimetallic FeM (M = Mo, Pd, Pt, Rh, Cu, Au), Fe₂M (M = Mo, Pd, Pt), Au₂Fe₂Ru, and PdFeNi complexes, we chose [Fe(η^5 -C₅H₄PPh₂)(η^5 -C₅H₄terpy)] (**5**; terpy = 2,2':6',2''-terpyridin-4'-yl) as the key starting molecule, which is accessible by the reaction sequence shown in Scheme 1 including an aldol condensation [reaction (i)] and a Michael addition with subsequent ring closure [reaction (ii)]. Whereas molecules **1** and **5** are orange-colored, complex **3** is purple, most probably resulting from the α,β -unsaturated carbonyl pyridyl unit. Ferrocenes **3** and **5** could be isolated as solid materials that dissolve in common polar organic solvents. The unsymmetrical sandwich compound **5** is stable in the solid state and in solution, whereas it rapidly decomposes on exposure to light and hence should best be stored in the dark.



Scheme 1. Synthesis of **5** from **1**: (i) dichloromethane/ethanol mixture (1:5 v/v); NaOH, 25 °C, 2.5 h; (ii) ethanol, [H₄N]OAc, 100 °C, 3 h.

The molecular structure of **5** in the solid state was determined by single-crystal X-ray structure analysis, thus confirming the structural assignment made from spectroscopic characterization (see Exp. Section). Single crystals of this compound were obtained by diffusion of *n*-pentane into a saturated solution of **5** in dichloromethane at room temperature. The molecular structure of **5** and selected bond distances [Å] and angles [°] are presented in Figure 1. The crystal and structure refinement data are summarized in Table 3 (see Exp. Section).

Ferrocene **5** represents a unsymmetrical 1,1'-disubstituted sandwich molecule in which a diphenylphosphanyl and a terpyridyl ligand are bonded to individual cyclopentadienyl rings. They are rotated by 85.0(3)° to each other (Figure 1). The C₅H₄ rings are inclined by 3.0(3)° and are

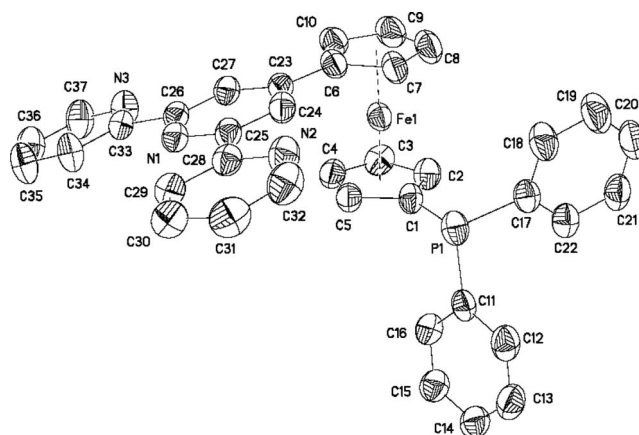
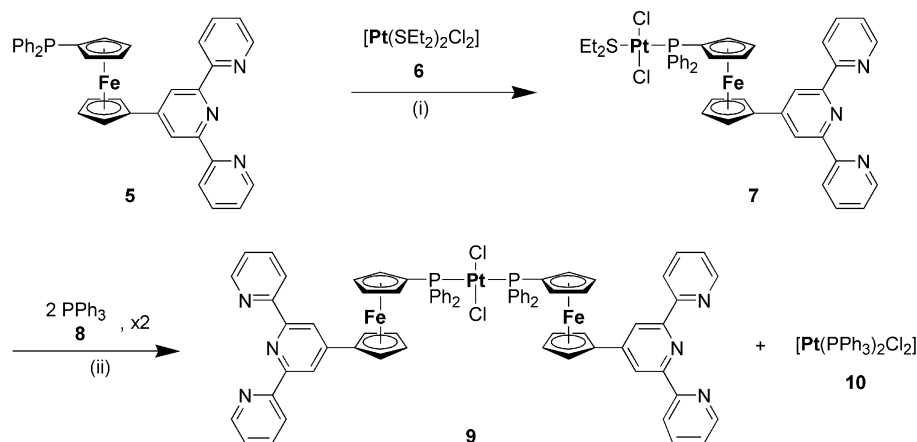


Figure 1. ORTEP diagram of **5**. Thermal ellipsoids are shown at the 50% probability level. The hydrogen atoms are omitted for clarity. Selected bond distances [Å] and angles [°]: Fe1–D1 1.647(3), Fe1–D2 1.648(3), P1–C1 1.814(5), P1–C11 1.836(6), P1–C17 1.829(5), C6–C23 1.479(6); P1–C1–C2 130.6(4), P1–C1–C5 123.2(4), C11–P1–C17 102.3(2), C1–P1–C17 100.7(2); D1: centroid of C1–C5, D2: centroid of C6–C10.

staggered by 9°. The geometry at P1 is distorted tetrahedral with angles in the range of 100.7(2)–102.3(2)° (Figure 1). The 2,2':6',2''-terpyridyl group adopts, as expected, a *trans*–*trans* conformation about the interannular C25–C28 and C26–C33 bonds.^[15] In addition, the terpy group is nearly planar [root mean-square deviation (RMSD) from planarity = 0.068 Å]. The interplanar angle between the cyclopentadienyl ring C6–C10 and N1, C23–C27 is 11.1(3)°, thereby showing that both groups are not coplanar to each other (Figure 1). The bonds and angles about the ferrocene, diphenylphosphanyl, and terpyridyl building blocks are similar to those typically found for this type of fragments.^[16] As a guide to the coordination properties of **5**, we treated it with diverse transition-metal complexes including [PtCl₂(Et₂S)₂], [Pd(cod)X₂], [Mo(CO)₄(nbd)], [CuBr], [AuCl(tht)], and [{RhCl(cod)}₂] (X = Cl, Br; nbd = norbornadiene; tht = tetrahydrothiophene; cod = cyclooctadiene-1,5-ene).

The appropriate FePt compound [Fe(η^5 -C₅H₄PPh₂){PtCl₂(SEt₂)}(η^5 -C₅H₄terpy)] (**7**) was formed by treatment of **5** with equimolar amounts of [PtCl₂(SEt₂)₂] (**6**) in dichloromethane as solvent at ambient temperature (Scheme 2). Exclusive coordination of the diphenylphosphanyl group to platinum is observed. Since unsymmetrical substituted **7** possesses with the Et₂S donor group a labile ligand,^[17] we treated it with a further equivalent of **5**. After appropriate workup, the expected trimetallic Fe₂Pt complex **9** (Scheme 2) could be isolated as an orange solid in 89% yield (see Exp. Section). The latter molecule was also formed when **7** was treated with triphenylphosphane. The in situ formed unsymmetrical complex [{Pt(Cl)₂(PPh₃)}-Fe(η^5 -C₅H₄PPh₂)(η^5 -C₅H₄terpy)] rapidly exchanges its ligands to give **9** and the respective [Pt(PPh₃)₂Cl₂] species, a common feature of [Pt(L)(L')Cl₂] complexes (L, L' = 2-electron donors).



Scheme 2. Synthesis of **7** and **9** from **5** and **6**: (i) 25 °C, 10 min, dichloromethane; (ii) 25 °C, 30 min, tetrahydrofuran.

The identities of **7** and **9** have been confirmed by elemental analysis, ^1H and $^{31}\text{P}\{^1\text{H}\}$ NMR spectroscopy, and ESI-TOF mass spectrometry (**9**). The molecular structure of **9** in the solid state was additionally measured by single-crystal X-ray structure determination (Figure 2).

The $^{31}\text{P}\{^1\text{H}\}$ NMR spectrum of **5** displays a resonance signal at $\delta = -18.3$ ppm due to the presence of the noncoordinating Ph_2P unit. The P-coordination of the diphenylphosphane moiety to a $[\text{PtCl}_2(\text{SEt}_2)]$ fragment in **7** or a PtCl_2 unit in **9** is best reflected by a significant shift to lower field (**7**, $\delta = 14.9$ ppm; **9**, $\delta = 10.0$ ppm). The signals thereby show a characteristic coupling with ^{196}Pt ($I = 1/2$, 25.3% abundance) giving doublets with typical $^1J_{^{31}\text{P},^{196}\text{Pt}}$ coupling constants of 3690 (**7**) and 2630 Hz (**9**). These values are in agreement with the coupling data found in other square-planar platinum–diphosphanyl complexes with *trans* geometry.^[18]

The formation of **7** is also confirmed by ^1H NMR spectroscopy since two new resonances for the $[\text{PtCl}_2(\text{SEt}_2)]$ coordination fragment can be observed at $\delta = 1.08$ (CH_3) and 2.50 ppm (CH_2) with $^3J_{\text{H,H}} = 7.2$ Hz. On replacement of SEt_2 by a second $[\text{Fe}(\eta^5\text{-C}_5\text{H}_4\text{PPh}_2)(\eta^5\text{-C}_5\text{H}_4\text{terpy})]$ unit,

these two resonances disappear and the progress of the reaction can therefore easily be controlled by ^1H NMR spectroscopy.

The formation of **9** is additionally evidenced from ESI-TOF mass spectrometric investigations, which indicate the presence of the molecular ion $[\text{M} + \text{H}]^+$ at a mass-to-charge ratio (m/z) of 1468.90 (see Exp. Section).

Single crystals of **9** were obtained from slow diffusion of *n*-pentane into a saturated solution of **9** in dichloromethane at 25 °C. The molecular structure of **9** is shown in Figure 2. The crystal and structural refinement data are summarized in Table 3 (see Exp. Section). Compound **9**, as the 2:1 adduct of **5** and PtCl_2 , crystallized in the monoclinic centrosymmetric space group $P2_1/c$ with crystallographically imposed inversion symmetry at Pt1. The platinum atom is coordinated by two chlorido and two phosphorus atoms in a precisely planar geometry. For compound **9**, an identical rotation of the Ph_2P versus terpyridyl moieties, as discussed for **5**, has been observed. The cyclopentadienyl rings are inclined by $3.8(3)^\circ$ and staggered by approximately $3\text{--}5^\circ$. Due to the Pt–P bond the angles around P1 are more open

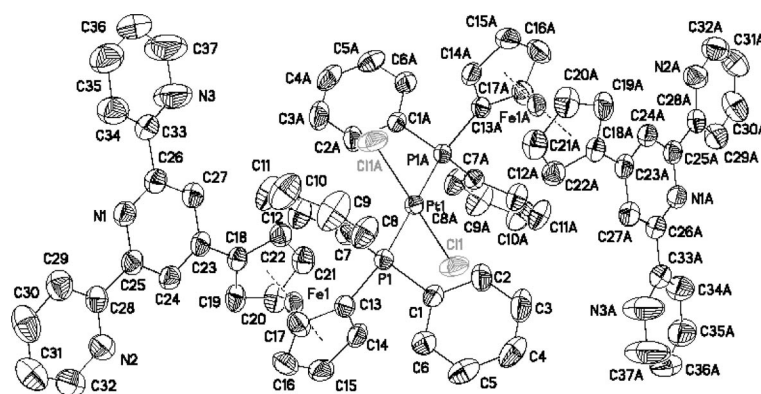


Figure 2. ORTEP diagram (50% probability level) of the molecular structure of **9**. The hydrogen atoms are omitted for clarity. Symmetry transformations used to generate equivalent atoms labeled with A: $-x, -y, -z + 1$. Selected bond distances [Å] and angles [°]: Fe1–D1 1.650(2), Fe1–D2 1.653(2), P1–C1 1.827(3), P1–C13 1.803(4), P1–C7, C18–C23 1.473(5); Pt1–Cl1 2.301(1), Pt1–P1 2.322(1); C7–P1–C1 104.52(15), C13–P1–C1 102.14(16), C11–Pt1–P1 88.47(4) C1–P1–Pt1 112.15(11); D1: centroid of C13–C17, D2: centroid of C18–C22.

relative to **5** and range from 104.5(2)–116.7(1)°. This is in a good agreement with the observations made in similar systems.^[7a]

A further possibility to prepare heterodi- (FePd) and heterotrimetallic (Fe₂M; M = Mo, Pd) transition-metal complexes based on **5** is given by the reactions depicted in Scheme 3. In this respect, we treated **5** with the palladium source [PdCl₂(cod)] in an equimolar amount, whereby dark orange **12** was formed in good yield (see Exp. Section). In **12**, the square-planar coordination geometry of the palladium(II) ion is set up by two *trans*-oriented chlorido ligands, the diphenylphosphanyl group, and one pyridyl ligand of the terpyridyl moiety. When molecule **12** was further treated with a third transition-metal salt such as [NiCl₂(dme)] (**13**; dme = dimethoxyethane) in tetrahydrofuran, a dark red precipitate was formed. After appropriate workup, and addition of dimethyl sulfoxide (dmsO), zwitterionic heterotrimetallic **14** could be isolated in which a [PdCl₃(Ph₂P)][−] fragment and a [Ni(Cl)(dmsO)₂(terpy)]⁺ ion are connected by the Fe(η⁵-C₅H₄)₂ sandwich backbone (Scheme 3). A somewhat different reaction behavior was found when **5** was treated with [ML_nL'] [**11a**, M = Pd, L = Cl, L' = cod, *n* = 2; **11b**, M = Pd, L = Br, L' = cod, *n* = 2; **15**, M = Mo, L = CO, L' = nbd, *n* = 4] in a 2:1 molar ratio (Scheme 3). Treatment of **5** with **11a** or **11b** exclusively gave *trans*-[PdL₂{(η⁵-C₅H₄Ph₂P)(η⁵-C₅H₄terpy)Fe₂}] (**16a**, L = Cl; **16b**, L = Br), which could be isolated as an orange solid material in 84% yield (Scheme 3, Exp. Section). Complex [Mo(CO)₄{(η⁵-C₅H₄PPh₂)(η⁵-C₅H₄terpy)Fe₂}] (**17**) was prepared by combining **5** with **15**, whereby nbd was concomitantly eliminated from **15** (Scheme 3).

Complexes **16** and **17** are barely soluble in common organic solvents (dichloromethane, tetrahydrofuran). Compound **14** is, due to its zwitterionic nature, only moderately soluble in dmsO. Due to the insufficient solubility of **16** and **17**, no ¹³C{¹H} NMR spectra could be obtained. As a re-

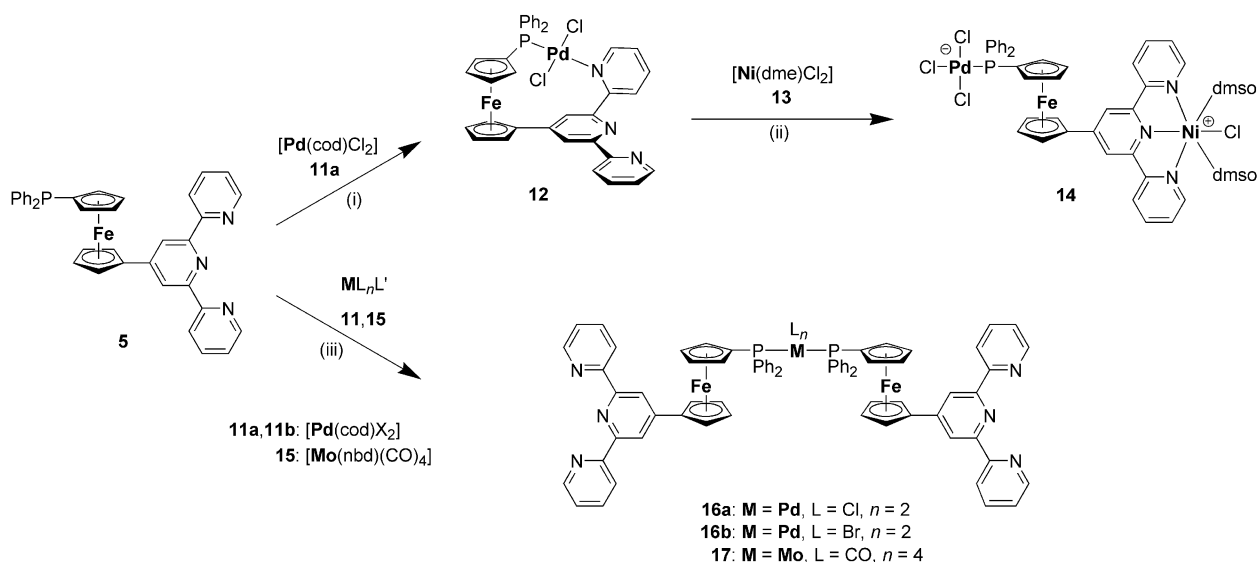
sult of the paramagnetic character of **14** (octahedral-coordinated Ni^{II}), no standard NMR spectroscopic measurements could be performed.

As expected, **16** and **17** show different spectral features from **12** because in **12** the terpyridyl moiety asymmetrically coordinates with one of its pyridyl units to the Pd^{II} ion. That is why for the terpyridyl ligand two sets of signals are found in the ¹H and ¹³C{¹H} NMR spectra (Exp. Section). It is noteworthy that the hydrogen atom at C24 (see X-ray structure determination, Figure 3) is found at δ = 10.46 ppm and is significantly shifted to lower field when compared with the chemical shift of the hydrogen atom bonded to C26 (δ = 8.61 ppm). An explanation for this behavior is the close proximity (2.55 Å) of the respective hydrogen atom to palladium, which could be confirmed by X-ray structure analysis (vide infra). For all other species, the expected signal and coupling patterns are observed (Exp. Section). A representative ¹H NMR spectrum of **12** is depicted in Figure 3; for comparison the ¹H NMR spectrum of **5** is presented as well.

From ³¹P{¹H} NMR spectroscopic studies it is clear that the diphenylphosphanyl groups in **12**, **16**, and **17** are datively bonded to the transition metals palladium and molybdenum, respectively, since a distinct downfield shift is observed (δ = 14–26 ppm) relative to **5** (δ = −18.3 ppm; see Exp. Section).

Less information can be obtained from IR spectroscopic studies of **12**, **14**, **16a**, and **16b**, whereas the metal carbonyl building block in **17** shows the characteristic strong absorptions typical for a [Mo(CO)₄] fragment (ν_{CO} = 2018, 1900, 1867, 1812 cm^{−1}), thereby indicating a *cis* coordination^[19] of the two bulky [Fe(η⁵-C₅H₄PPh₂)(η⁵-C₅H₄terpy)] moieties.

Figures 4, 5, and 6 highlight the solid-state structures and selected bond lengths [Å] and angles [°] of **12** (Figure 4), **14** (Figure 5), and **16b** (Figure 6). X-ray-quality single crystals of these molecules could be grown by diffusion



Scheme 3. Synthesis of **12**, **14**, **16**, and **17** from **5**: (i) dichloromethane, 30 min, 25 °C; (ii) tetrahydrofuran, 1 min, 25 °C, recrystallization from dmsO; (iii) dichloromethane, 10 min, 25 °C.

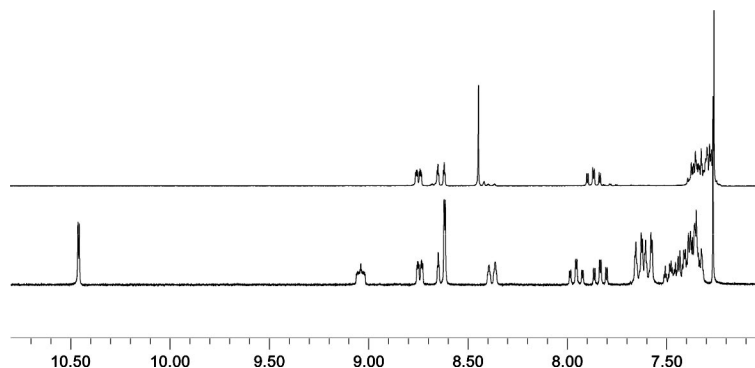


Figure 3. ^1H NMR spectra of **5** (top) and **12** (below) (in CDCl_3 , 25 $^\circ\text{C}$, 250 MHz).

of *n*-hexane into solutions of **12** or **16b** in chloroform, whereas crystals of **14** were obtained by diffusion of diethyl ether into a mixture of dmsol/dichloromethane in a ratio of 70:30 (v/v) at ambient temperature. The crystal and structure refinement data of **12**, **14**, and **16b** are summarized in Table 3 (see Exp. Section).

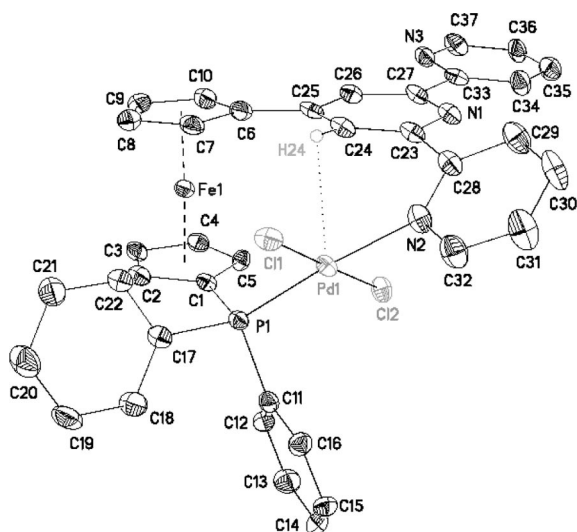


Figure 4. ORTEP diagram of **12**. Thermal ellipsoids are shown at the 50% probability level. All hydrogen atoms, except H24, and the disordered tetrahydrofuran molecule as noncoordinating packing solvent have been omitted for clarity. Selected bond lengths [\AA], angles [$^\circ$], and torsion angles [$^\circ$]: Fe1–D1 1.663(3), Fe1–D2 1.661(3), Pd1–P1 2.2413(16), Pd1–N2 2.146(6), Pd1–C11 2.3101(16), Pd1–C12 2.3128(16), P1–C1 1.803(6), C6–C25 1.468(9); C1–P1–Pd1 116.4(2), N2–Pd1–P1 175.44(17), C11–Pd1–C12 177.87(6), P1–Pd1–C11 94.97(6), Pd1–N2–C28 124.2(5); N1–C23–C28–N2 $-140.8(6)$, N1–C27–C33–N3 $-177.3(6)$; D1: centroid of C1–C5, D2: centroid of C6–C10.

Crystallographic data of **12** reveal an almost square-planar geometry about the Pd^{II} center. The sum of the angles around Pd1 is essentially 360° with *trans*-oriented chlorido ligands. The Pd1–C11 and Pd1–C12 bond lengths of 2.3101(16) and 2.3128(16) \AA , respectively, are comparable with bond separations observed for other palladium dichloride molecules that feature phosphane and/or pyridyl ligands.^[20] As expected, the Pd1–P1 distance [2.2413(16) \AA] is shorter than in *trans*-bis(phosphanyl)palladium(II) complexes (i.e., 2.325 \AA),^[20b] whereas the respective Pd1–N2

separation found in **12** [2.146(6) \AA] is long compared to distances that involve Pd–N bonds that are *trans* oriented (i.e., 2.007 \AA).^[21] This can be explained by the *trans* influence.^[22] The two noncoordinated pyridyl rings of the terpy unit are found to be in-plane-bonded with the cyclopentadienyl ring C6–C10 (RMSD 0.070 \AA) (Figure 4). The pyridyl ring coordinated to Pd1 is twisted by about $36.9(9)^\circ$ from this plane. The unusual chemical shift of the hydrogen atom bonded to C24 can be explained by the short Pd1–H24 distance, which is with 2.55 \AA shorter than the sum of palladium and hydrogen van der Waals radii (2.8 \AA).^[23]

The overall structural features of **14** are similar to those of related structurally characterized molecules containing (diphenylphosphanyl)ferrocene, terpyridylferrocene, palladium chloride, and nickel chloride.^[20,21,24] Complex **14** consists of a 1-(diphenylphosphanyl)-1'-terpyridylferrocene centrality with a distorted square-planar Pd1, C11–C13, P1 fragment and a distorted octahedrally coordinated Ni^{II} ion (Ni1, C14, O1, O2, N1–N3) (Figure 5). The C11–Pd1–C13 angle [$170.78(8)^\circ$] is reduced from 180° as a result of the steric demand of the organometallic $[\text{Fe}(\eta^5\text{-C}_5\text{H}_4\text{PPh}_2)(\eta^5\text{-C}_5\text{H}_4\text{terpy}\{\text{NiCl}(\text{dmsol})_2\})]$ building block. As expected, the Pd1–C12 bond length of 2.399(3) \AA is longer than the appropriate Pd1–C11 [2.296(2) \AA] and Pd1–C13 separations [2.297(3) \AA] that are *trans*-oriented to ligands with a *trans* influence weaker than phosphorus.^[22] The cyclopentadienyl rings of the ferrocenyl moiety are rotated by around 3° , which verifies an almost eclipsed conformation. The Fe–D distances (D is the centroid of the respective cyclopentadienyls) are characteristic^[25] and indicate that the iron atoms are almost equidistant from the cyclopentadienyl rings and correspond to those bond lengths found for other ferrocenes.^[20b] The coordination sphere about Ni1 is set up by a terpy (N1–N3) and one dmsol (O2) ligand in equatorial positions, and C14 as well as the second dmsol solvent molecule localized in axial positions (Figure 5). The Ni1–O2 bond [2.052(5) \AA] is shorter than the Ni1–O1 distance [2.105(6) \AA], thus indicating the *trans* influence of pyridyl and chloride ligands, respectively (Figure 5). The best planes of the terpy group and the cyclopentadienyl C6–C10 ring are rotated by $11.7(4)^\circ$ to each other. The bond lengths and bond angles about the phosphanyl and terpy substituents are close to those reported for analogous transition-metal building blocks.^[20,21,25]

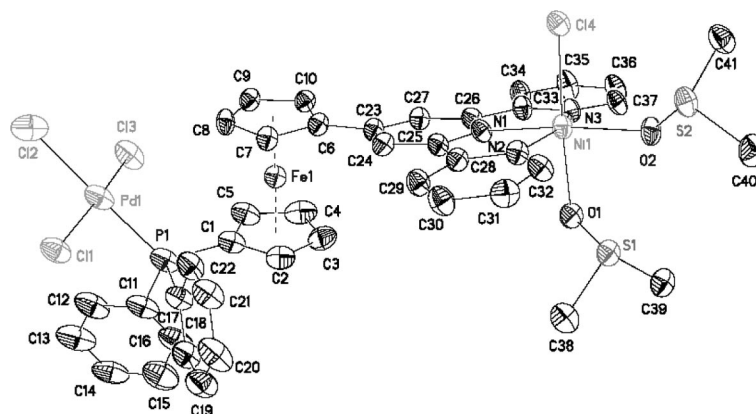


Figure 5. ORTEP diagram of **14**. Thermal ellipsoids are shown at the 50% probability level. The hydrogen atoms and the disordered dichloromethane molecule as noncoordinating packing solvent are omitted for clarity. Selected bond lengths [Å], angles [°], and torsion angles [°]: Fe1–D1 1.6541(7), Fe1–D2 1.6552(8), Pd1–P1 2.252(3), Pd1–Cl1 2.296(2), Pd1–Cl3 2.297(3), Pd1–Cl2 2.399(3), P1–C1 1.803(10), C6–C23 1.457(11); Ni1–N1 1.987(6), Ni1–N2 2.124(6), Ni1–N3 2.106(6), Ni1–O1 2.105(6), Ni1–O2 2.052(5), Ni1–Cl4 2.390(2); P1–Pd1–Cl1 89.68(10), Cl1–Pd1–Cl3 170.78(8), P1–Pd1–Cl2 176.08(8), N1–Ni1–O2 171.5(2), N3–Ni1–N2 156.8(2), O1–Ni1–Cl4 176.31(16), N3–Ni1–Cl4 90.31(19); N1–C26–C33–N3 –0.2(11), N1–C25–C28–N2 4.1(10), C7–C6–C23–C24 –8.1(13); D1: centroid of C1–C5, D2: centroid of C6–C10.

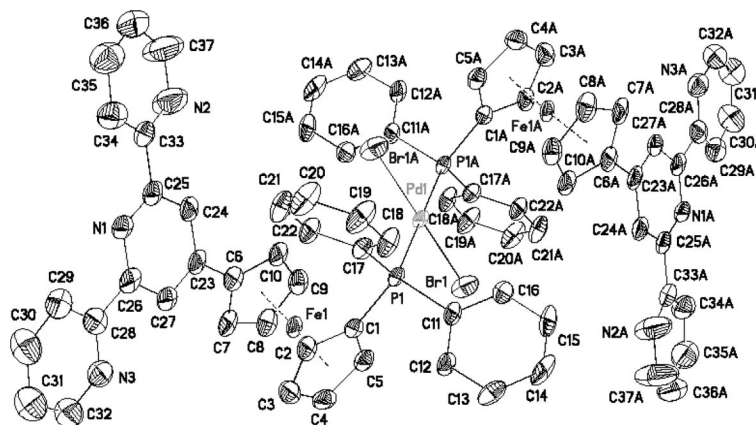


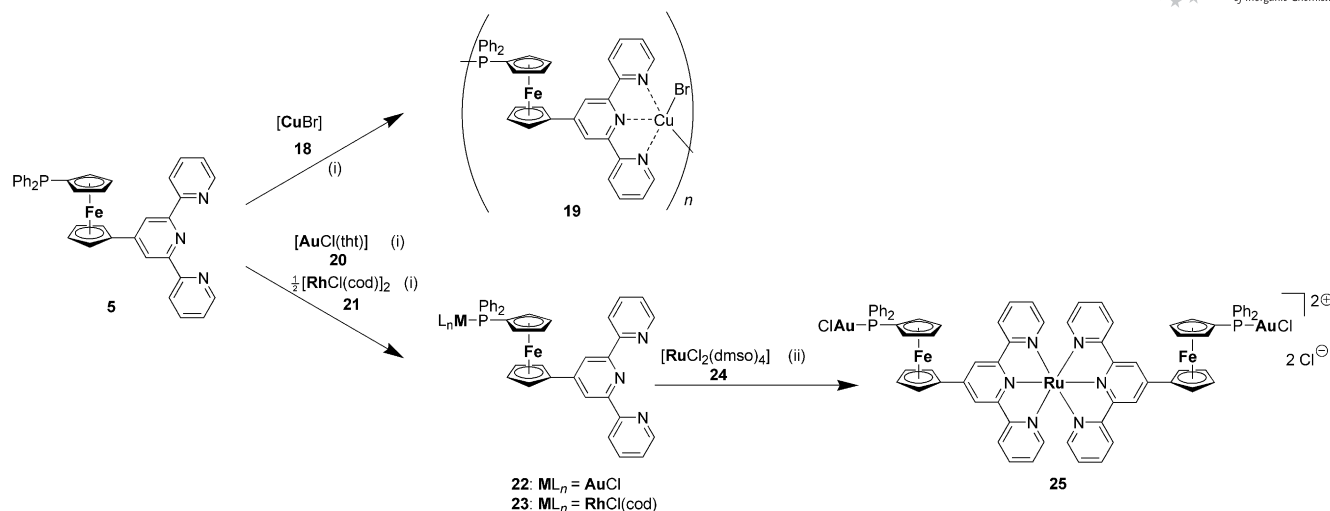
Figure 6. ORTEP diagram of **16b**. Thermal ellipsoids are shown at the 50% probability level (symmetry transformations used to generate equivalent atoms: $-x, -y, -z + 1$; center of inversion on Pd1). The hydrogen atoms are omitted for clarity. Selected bond lengths [Å], angles [°], and torsion angles [°]: Fe1–D1 1.646(3), Fe1–D2 1.643(3), Pd1–P1 2.3304(17), Pd1–Br1 2.3969(8), P1–C1 1.785(6), C6–C23 1.466(10); P1–Pd1–Br1 88.77(4), Cl1–P1–Pd1 115.7(2); C7–C6–C23–C24, N1–C25–C28–N3 175.5(5), N1–C26–C33–N2 –173.6(8); D1: centroid of C1–C5, D2: centroid of C6–C10.

The single-crystal X-ray structure analysis of **16b** shows nearly the same structural features as discussed for **5** and **9** (see Figures 1 and 2). Complex **16b** crystallized in the monoclinic centrosymmetric space group $P2_1/c$ with crystallographically imposed inversion symmetry at Pd1. The platinum atom is coordinated in a planar geometry by two bromides and two phosphorus atoms. The cyclopentadienyl rings are inclined by 3.7(5)° and staggered by 3–5°.

Treatment of a solution of **5** in tetrahydrofuran with the copper(I) salt [CuBr] (**18**) resulted in the formation of coordination polymer **19** in virtually quantitative yield (Scheme 4, Exp. Section). Elemental analysis of **19** is in good agreement with the proposed composition. The $^{31}\text{P}\{^1\text{H}\}$ NMR spectrum of **19** is indicative of the coordination of the diphenylphosphanyl group to copper(I) because a typical chemical shift from $\delta = -18.3$ (**5**) to -14.9 ppm (**19**) is found.^[26] A broad signal is observed that is attributed to

the two isotopes of copper (^{63}Cu , ^{65}Cu).^[27] Coordination of the terpy group to copper(I) was proven by ^1H NMR spectroscopy. The signals for the terpy ligand are shifted to a lower field than that of the starting material **5** [$\text{C}_5\text{H}_2\text{N}$: $\delta = 8.46$ ppm (**5**); 8.53 ppm (**19**)] (see Exp. Section). Due to this, we postulate that **19** is polymerically constructed. On addition of dmsO, complex **19** was transformed to a species of composition $[\text{Fe}(\eta^5\text{-C}_5\text{H}_4\text{Ph}_2\text{P}\{\text{CuBr}(\text{dmsO})_n\})(\eta^5\text{-C}_5\text{H}_4\text{terpy})]$, which affirms the postulation of a coordination polymer.

Organometallic **5** as a multitopic molecule with the Lewis basic diphenylphosphanyl and terpyridyl units to allow mono-, bi-, and/or tridentate coordination of different organometallic coordination fragments (vide supra) was also treated with tetrahydrothiophene gold(I) chloride (**20**) in tetrahydrofuran as solvent at 25 °C (Scheme 4). Within this reaction the weakly bonded tht ligand is replaced by



Scheme 4. Reaction chemistry of **5** towards $[CuBr]$, $[AuCl(tht)]$, and $[RhCl(cod)]_2$: (i) tetrahydrofuran, 2 h, 25 °C; (ii) ethanol, 12 h, reflux.

the stronger donor/acceptor group PPh_2 . After appropriate workup, pale yellow $[Fe\{\eta^5-C_5H_4Ph_2P(AuCl)\}(\eta^5-C_5H_4terpy)]$ (**22**) was obtained in high yield (Exp. Section). Heterobimetallic (FeRh) **23** could be prepared by treatment of **5** with $[RhCl(cod)]_2$ (**21**) in a 1:1 molar ratio in tetrahydrofuran (Scheme 4).

Compounds **22** and **23** were characterized by elemental analysis and IR and NMR spectroscopy. NMR spectroscopic properties of both complexes correlate with their formulation as heterodimetallic FeM complexes ($M = Au, Rh$). The identity of **22** was further confirmed by single-crystal X-ray diffraction studies.

For compound **22**, X-ray quality crystals could be obtained by slow diffusion of *n*-pentane into a solution of **22** in dichloromethane at ambient temperature. The molecular structure of **22** is presented in Figure 7 together with selected bond lengths [Å] and angles [°]. The crystal and structure refinement data are summarized in Table 4 (Exp. Section).

Molecule **22** crystallized in the triclinic space group $P\bar{1}$. The structure of **22** shows a linear geometry around Au1 set up by the Ph_2P and Cl ligands, and Fe1 as part of a sandwich structure. Geometrical parameters within the Ph_2PAuCl fragment and the ferrocenyl-terpy building block are similar to those reported previously in comparable molecules.^[16,28] As observed for **5**, also in **22** the terpyridyl moiety adopts a *trans-trans* conformation. In contrast to **5**, the terpyridyl moiety is not planar. Calculated interplanar angles between the C_5H_4N groups range from 7.7(2) (N1, C23–C27 vs. N3, C33–C37) to 20.6(2)° (N1, C23–C27 vs. N2, C28–C32).

Coordination of the terpyridyl donor group in **22** to ruthenium using $[RuCl_2(dmsO)_4]$ as the ruthenium source gave pentametallic (Au_2Fe_2Ru) **25**. In this molecule, two units of **22** are bridged through the coordination of their terpyridyl moieties to the centered ruthenium(II) ion, which was proven by 1H NMR spectroscopy [C_5H_2N : $\delta = 8.35$ ppm (**22**), 9.67 ppm (**25**)].

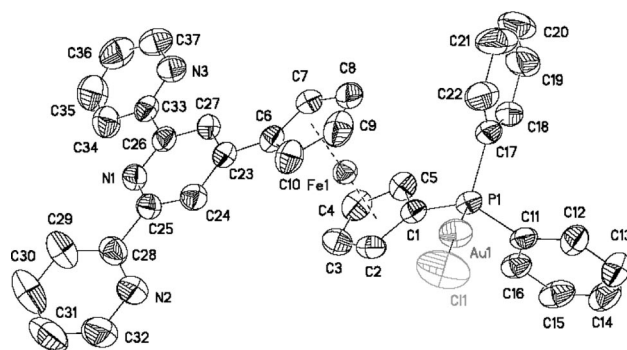
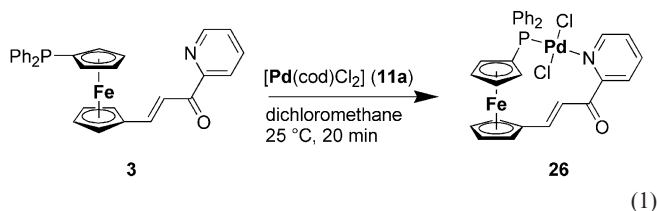


Figure 7. ORTEP diagram of **22**. Thermal ellipsoids are shown at the 50% probability level. The hydrogen atoms are omitted for clarity. Selected bond lengths [Å], angles [°], and torsion angles [°]: Fe1–D1 1.631(1), Fe1–D2 1.644(1), Au1–Cl1 2.2616(9), Au1–P1 2.2154(7), P1–C1 1.773(3), C6–C23 1.470; P1–Au1–Cl1 178.29(4), Au1–P1–C1 113.78(9); N1–C26–C33–N3 172.2(2), N1–C25–C28–N2 161.2(3), C7–C6–C23–C24 170.1(3); D1: centroid of C1–C5, D2: centroid of C6–C10.

For catalytic purposes, we treated **3** with equimolar amounts of **11a** [Reaction (1)]. The PdFe molecule **26** formed in this way was obtained as a deep purple solid.



Characterization of **26** is based on elemental analysis, spectroscopy (NMR, IR) and mass spectrometry (ESI-TOF) (see Exp. Section) as well as single X-ray structure analysis (Figure 8, Table 1).

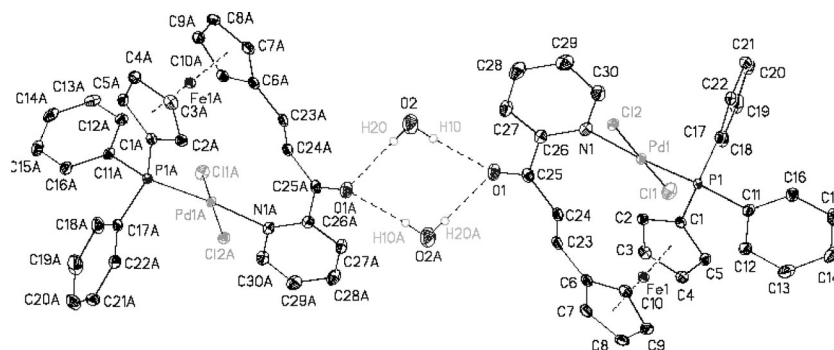


Figure 8. ORTEP diagram (50% probability level) of the molecular structure of **26** forming a solvent-bridged centrosymmetric dimer in the solid state, due to the formation of hydrogen bonds. All carbon-bonded hydrogen atoms have been omitted for clarity. Symmetry operations used to generate equivalent atoms are labeled with A: $-x + 2, -y + 2, -z$. Selected bond lengths [Å] and angles [°]: Fe1–D1 1.634(4), Fe1–D2 1.648(4), Pd1–P1 2.2443(5), Pd1–N1 2.1337(13), Pd1–Cl1 2.2935(4), Pd1–Cl2 2.3073(4), C6–C23 1.453(2), C23–C24 1.341(2), P1–Pd1–N1 175.03(4), Cl1–Pd1–Cl2 175.379(15), Cl1–Pd1–P1 88.14(4), Cl2–Pd1–N1 87.85(4); D1: centroid of C1–C5, D2: centroid of C6–C10.

Table 1. Bond lengths [Å] and angles [°] of the intermolecular hydrogen bonds of **26** (D: donor, A: acceptor).

D–H...A	D–H [Å]	H...A [Å]	D...A [Å]	D–H...A [°]
O2–H1O...O1	0.82(5)	2.09(5)	2.907(3)	176(4)
O2A–H2OA...O1	0.75(5)	2.21(5)	2.958(3)	175(6)

Crystallization of **26** was carried out in untreated solvents; it resulted in the presence of water in the solid-state structure. Compound **26** crystallized as a centrosymmetric dimer in which two water molecules bridge two molecules of **26** by the formation of intermolecular hydrogen bonds by molecular recognition.

The PdCl₂NP coordination setup is almost planar, as the sum of all angles around Pd1 is 359.9(5)°, with *trans*-oriented chlorido ligands. The Pd1–Cl1 and Pd1–Cl2 bond lengths of 2.2935(4) and 2.3073(4) Å are comparable with distances of related complexes.^[20b]

In a preliminary study, heterobimetallic transition-metal complexes **12** and **26** were screened for their catalytic activities in the Heck–Mizoroki reaction.^[29] The results obtained (rate of conversion, kinetic studies) are summarized in Table 2 and Figure 9. To test the productivity of these two organometallic species, we treated iodobenzene (**27**) with *tert*-butyl acrylate (**28**) to give (*E*)-*tert*-butyl cinnamate (**29**) in toluene and acetonitrile mixtures of ratio 1:1 (v/v) at 80 °C in presence of EtN_iPr₂ as a base and as reducing agent with a catalyst loading of 0.5 mol-% [see reaction (2), Table 2, Figure 9]. In addition to these studies, reactions

with the conventional [PdCl₂(dppf)] system [dppf = 1,1'-bis(diphenylphosphanyl)ferrocene] (**30**) were carried out so that direct comparison might be achieved.

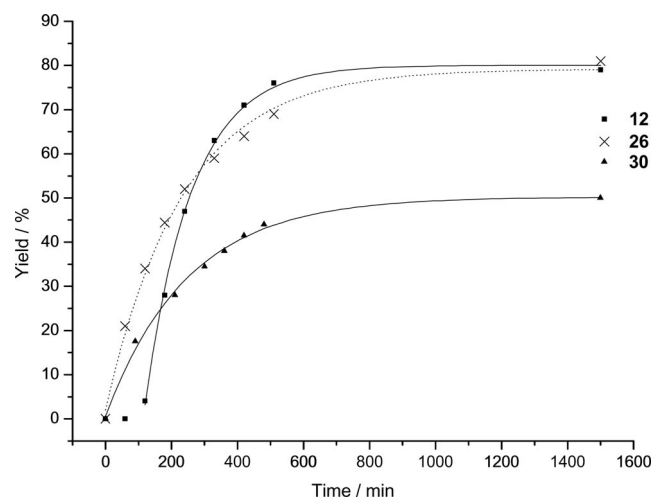


Figure 9. Kinetic investigations of **12**, **26**, and **30** (for comparison) in the Heck–Mizoroki carbon–carbon cross-coupling of **27** with **28** (0.5 mol-% catalyst, 80 °C).

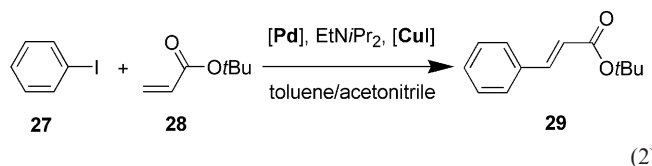


Table 2. Conditions of the Heck–Mizoroki carbon–carbon cross-coupling reaction of **27** with **28** by complexes **12**, **26**, and **30** for comparison (conc. 0.5 mol-%, 80 °C, 25 h).

Compound	Yield of 29 [%] ^[a]	TON ^[b]	TOF [h ^{−1}] ^[b]
12	79	158	48
26	81	162	42
30	50	100	23

[a] Yields have been measured by ¹H NMR spectroscopy with acetylferrocene as internal standard. [b] TON = turnover number. Turnover frequencies (TOFs) are determined after one hour.

As summarized in Table 2 and Figure 9, the maximum possible conversion amounts to 80%. As a consequence of these data, it can be concluded that a higher productivity is obtained with catalysts possessing hemilabile ligands as given in complexes **12** and **26** when compared to an analogous symmetrical diphosphane such as dppf.

Conclusion

A new ligand system based on a ferrocenyl backbone that features a terpyridyl and a diphenylphosphanyl donor group is described using consecutive synthesis methodologies. A series of novel heterobi- and heterotrimetallic complexes including $[\text{Fe}(\eta^5\text{-C}_5\text{H}_4\text{Ph}_2\{\text{PtCl}_2(\text{SEt}_2)\})(\eta^5\text{-C}_5\text{H}_4\text{terpy})]$, *trans*- $[\text{PtCl}_2\{(\eta^5\text{-C}_5\text{H}_4\text{Ph}_2\text{P})(\eta^5\text{-C}_5\text{H}_4\text{terpy})\}\text{Fe}_2]$, $[\text{Fe}\{\eta^5\text{-C}_5\text{H}_4\text{PPh}_2(\text{Cl}_2\text{Pd})\}(\eta^5\text{-C}_5\text{H}_4\text{terpy})]$, $[\text{Fe}\{\eta^5\text{-C}_5\text{H}_4\text{PPh}_2(\text{Cl}_3\text{Pd})\}(\eta^5\text{-C}_5\text{H}_4\text{terpy})\{(\text{dmsO})_2\text{-ClNi}^+\}]$, *trans*- $[\text{PdX}_2\{(\eta^5\text{-C}_5\text{H}_4\text{Ph}_2\text{P})(\eta^5\text{-C}_5\text{H}_4\text{terpy})\}\text{Fe}_2]$ ($\text{X} = \text{Cl}, \text{Br}$), $[\text{Mo}(\text{CO})_4\{(\eta^5\text{-C}_5\text{H}_4\text{PPh}_2)(\eta^5\text{-C}_5\text{H}_4\text{terpy})\}\text{Fe}_2]$, $[\text{Fe}\{\eta^5\text{-C}_5\text{H}_4\text{Ph}_2\text{P}(\text{CuBr})\}(\eta^5\text{-C}_5\text{H}_4\text{terpy})]$, $[\text{Fe}\{\eta^5\text{-C}_5\text{H}_4\text{Ph}_2\text{P}(\text{AuCl})\}(\eta^5\text{-C}_5\text{H}_4\text{terpy})]$, $[\text{Fe}(\eta^5\text{-C}_5\text{H}_4\text{Ph}_2\text{P}\{\text{Rh}(\text{cod})\text{Cl}\})\text{Fe}_2]$, $[\text{Ru}\{(\eta^5\text{-C}_5\text{H}_4\text{Ph}_2\text{P}(\text{AuCl}))(\eta^5\text{-C}_5\text{H}_4\text{terpy})\}\text{Fe}_2]\text{Cl}_2$, and $[\text{Fe}\{\eta^5\text{-C}_5\text{H}_4\text{PPh}_2(\text{PdCl}_2)\}\{\eta^5\text{-C}_5\text{H}_4\text{-CH=CHC}(\text{O})(\text{py})\}]$ have been synthesized by treatment of $[\text{PtCl}_2(\text{Et}_2\text{S})_2]$, $[\text{Pd}(\text{cod})\text{X}_2]$, $[\text{AuCl}(\text{tht})]$, $[\text{CuBr}]$, $[\text{Mo}(\text{CO})_4(\text{nbd})]$, and $[\{\text{Rh}(\text{cod})\text{Cl}\}_2]$ with $[\text{Fe}(\eta^5\text{-C}_5\text{H}_4\text{PPh}_2)(\eta^5\text{-C}_5\text{H}_4\text{terpy})]$ and $[\text{Fe}(\eta^5\text{-C}_5\text{H}_4\text{PPh}_2)\{\eta^5\text{-C}_5\text{H}_4\text{-CH=CHC}(\text{O})(\text{py})\}]$, respectively. Seven compounds have been structurally characterized by single-crystal X-ray diffraction analysis. The appropriate molecules show typical features known for related phosphanylferrocenes and terpyridylferrocenes.^[16] The phosphanyl and terpyridyl groups are oppositely oriented except for complex **12**, due to the chelating P/N coordination. A carbon–hydrogen bond activation could be observed for **12** as a result of the close distance of the palladium atom to the terpyridyl moiety. Complex **24** is to the best of our knowledge the first zwitterionic heteromultimetallic system set up by organometallic and metal–organic parts. For catalytic applications, two palladium complexes with hemilabile P/N ligands of type $[\text{Fe}(\eta^5\text{-C}_5\text{H}_4\text{PPh}_2)(\eta^5\text{-C}_5\text{H}_4\text{terpy})]$ and $[\text{Fe}(\eta^5\text{-C}_5\text{H}_4\text{PPh}_2)\{\eta^5\text{-C}_5\text{H}_4\text{-CH=CHC}(\text{O})(\text{py})\}]$ were synthesized. They show good activity ($\text{TON} = 160$, $\text{TOF} = 48 \text{ h}^{-1}$) as catalysts in the Heck–Mizoroki reaction [see reaction (2), Table 2, Figure 9] relative to $[\text{PdCl}_2(\text{dppf})]$ [$\text{dppf} = 1,1'$ -bis(diphenylphosphanyl)ferrocene]. However, catalysts reported by, for example, Fu et al.,^[30] Herrmann et al.,^[31] and Reetz et al.,^[32] are more active than **12** and **26** and can even be used for less-reactive aryl halides under mild conditions.

Experimental Section

General Data: All reactions were carried out under an atmosphere of nitrogen using standard Schlenk techniques. Tetrahydrofuran, toluene, *n*-hexane, and *n*-pentane were purified by distillation from sodium/benzophenone ketyl; dichloromethane and chloroform were purified by distillation from calcium hydride. Diethylamine and diisopropylamine were distilled from KOH; absolute methanol was obtained by distillation from magnesium.

Instruments: Infrared spectra were recorded with a Perkin–Elmer FTIR spectrometer Spectrum 1000. NMR spectra were recorded with a Bruker Avance 250 spectrometer [^1H NMR at 250.12 MHz and $^{13}\text{C}\{^1\text{H}\}$ NMR at 62.86 MHz] in the Fourier transform mode. Chemical shifts are reported in δ units (parts per million) downfield

from tetramethylsilane ($\delta = 0.00$ ppm) with the solvent as the reference signal (CDCl_3 : ^1H NMR, $\delta = 7.26$ ppm; $^{13}\text{C}\{^1\text{H}\}$ NMR, $\delta = 77.16$ ppm).^[19] $^{31}\text{P}\{^1\text{H}\}$ NMR spectra were recorded at 101.255 MHz in CDCl_3 with $\text{P}(\text{OMe})_3$ as external standard [$\delta = 139.0$ ppm, relative to H_3PO_4 (85%) with $\delta = 0.00$ ppm]. ESI-TOF mass spectra were recorded with a Mariner biospectrometry workstation 4.0 (Applied Biosystems). Microanalyses were performed with a C,H,N-analyzer FlashAE 1112 (Thermo Company). Melting points of analytical pure samples (sealed off in nitrogen-purged capillaries) were determined with a Gallenkamp MFB 595010 M melting point apparatus.

Reagents: $[\text{PdCl}_2(\text{cod})]$,^[33] $[\text{PdBr}_2(\text{cod})]$,^[33] $[\text{PtCl}_2(\text{SEt}_2)_2]$,^[34] $[\text{Mo}(\text{CO})_4(\text{nbd})]$,^[35] $[\text{NiCl}_2(\text{dme})]$,^[36] $[\text{AuCl}(\text{tht})]$,^[37] $[\{\text{RhCl}(\text{cod})\}_2]$,^[38] pyridylacetylpyridinium iodide,^[39] and 1-(diphenylphosphanyl)-1'-formylferrocene^[40] were prepared according to published procedures. All other chemicals were purchased from commercial suppliers and were used as received.

Synthesis of 3: Compound **1** (1.36 g, 3.34 mmol) was dissolved in dichloromethane (30 mL) and ethanol (150 mL). Acetylpyridine (**2**) (0.46 mL, 4.31 mmol) was added in a single portion to this mixture. After 5 min of stirring, an NaOH solution (12 mL, 2 M) was slowly dropped into the reaction mixture. Stirring was continued for 2.5 h at 25 °C. The solution changed from orange to purple. The reaction mixture was evaporated to 50 mL and water (200 mL) was added. This solution was extracted twice with dichloromethane (200 mL portions). The organic phases were combined and dried with MgSO_4 and all volatile materials were removed in an oil-pump vacuum. The obtained crude material was purified by column chromatography on silica gel (column size: 4×15 cm, chloroform). With chloroform the starting material **1** could be eluted (100 mg, 0.25 mmol), whereas with ethyl acetate the title compound **3** was obtained. All volatiles were removed under reduced pressure. Compound **3** was isolated as a dark purple solid; yield 1.2 g (2.4 mmol, 70% based on **1**). $\text{C}_{30}\text{H}_{24}\text{FeNOP}$ (501.34): calcd. C 71.87, H 4.83, N 2.79; found C 71.60, H 5.05, N 2.71; m.p. 131 °C. IR (KBr): $\tilde{\nu} = 1433$ (m, ν_{PC}), 1468 (m, ν_{PC}), 1577 (s, $\nu_{\text{C}=\text{C}}$), 1594 (s, $\nu_{\text{C}=\text{C}}$), 1663 (s, ν_{CO}) cm^{-1} . ^1H NMR (CDCl_3): $\delta = 4.14$ (m, 2 H, C_5H_4), 4.38 (pt, $J = 1.9$ Hz, 2 H, C_5H_4), 4.40 (pt, $J = 1.8$ Hz, 2 H, C_5H_4), 4.56 (pt, $J = 1.9$ Hz, 2 H, C_5H_4), 7.27–7.4 (m, 10 H, C_6H_5), 7.47 (ddd, $^3J = 7.6$, 4.6 Hz, $^4J = 1.0$ Hz, 1 H, $\text{C}_5\text{H}_4\text{N}$), 7.72 (d, $^3J = 15.8$ Hz, 1 H, $\text{C}_5\text{H}_4\text{N}$), 7.77 (d, $^3J = 15.8$ Hz, 1 H, $\text{C}_5\text{H}_4\text{N}$), 7.86 (ddd, $^3J = 7.6$, 7.8 Hz, $^4J = 1.8$ Hz, 1 H, $\text{C}_5\text{H}_4\text{N}$), 8.17 (ddd, $^3J = 7.8$ Hz, $^4J = 1.0$ Hz, $^5J = 0.9$ Hz, 1 H, $\text{C}_5\text{H}_4\text{N}$), 8.73 (ddd, $^3J = 4.6$ Hz, $^4J = 1.8$ Hz, $^5J = 0.9$ Hz, 1 H, $\text{C}_5\text{H}_4\text{N}$) ppm. $^{13}\text{C}\{^1\text{H}\}$ NMR (CDCl_3): $\delta = 70.4$ (C_5H_4), 73.0 (C_5H_4), 73.3 (d, $^3J_{\text{CP}} = 4$ Hz, C_5H_4), 74.4 (d, $^2J_{\text{CP}} = 14$ Hz, $\text{C}_i\text{-C}_5\text{H}_4$), 77.9 ($\text{C}_i\text{-C}_5\text{H}_4$), 80.3 (C_5H_4), 118.8 (CO-CH=CH-), 123.0 ($\text{C}_5\text{H}_4\text{N}$), 126.7 ($\text{C}_5\text{H}_4\text{N}$), 128.4 ($^3J_{\text{CP}} = 7$ Hz, $m\text{-C}_6\text{H}_5$), 128.8 ($p\text{-C}_6\text{H}_5$), 133.6 (d, $^2J_{\text{CP}} = 20$ Hz, $o\text{-C}_6\text{H}_5$), 137.0 ($\text{C}_5\text{H}_4\text{N}$), 138.8 (d, $^1J_{\text{CP}} = 10$ Hz, $\text{C}_i\text{-C}_6\text{H}_5$), 146.4 (CO-CH=CH-), 148.9 ($\text{C}_5\text{H}_4\text{N}$), 154.8 ($\text{C}_5\text{H}_4\text{N}$), 188.6 (CO-CH=CH-) ppm. $^{31}\text{P}\{^1\text{H}\}$ NMR (CDCl_3): $\delta = -18.5$ ppm. ESI-TOF-MS: $m/z = [\text{M} + \text{H}]^+ 502.17$.

Synthesis of 5: Compound **3** (2.9 g, 5.78 mmol), ammonium acetate (5.0 g, 64.87 mmol), and **4** (2.2 g, 6.93 mmol) were dissolved in degassed ethanol (20 mL) and heated for 3 h to reflux. An orange solid precipitated. The reaction mixture was allowed to cool to 25 °C. The orange solid was filtered off and washed twice with ice-cooled ethanol (25 mL portions); the residue was dried in an oil-pump vacuum; yield 1.67 g (2.77 mmol, 48% based on **3**). $\text{C}_{37}\text{H}_{28}\text{FeN}_3\text{P}$ (601.46): calcd. C 73.89, H 4.69, N 6.99; found C 73.39, H 4.80, N 6.82; m.p. 186 °C. IR (KBr): $\tilde{\nu} = 1433$ (m, ν_{PC}),

1468 (m, ν_{PC}), 1576 (s, $\nu_{\text{C}=\text{C}}$), 1584 (s, $\nu_{\text{C}=\text{C}}$), 1602 (s, $\nu_{\text{C}=\text{C}}$) cm^{-1} . ^1H NMR (CDCl_3): δ = 4.06 (pq, J = 1.9 Hz, 2 H, C_5H_4), 4.24 (pt, J = 1.9 Hz, 2 H, C_5H_4), 4.34 (pt, J = 1.9 Hz, 2 H, C_5H_4), 4.88 (pt, J = 1.9 Hz, 2 H, C_5H_4), 7.26–7.4 (m, 12 H, $\text{C}_6\text{H}_5/5\text{-C}_5\text{H}_4\text{N}$), 7.88 (ddd, 3J = 7.9, 8.0 Hz, 4J = 1.8 Hz, 2 H, $\text{C}_5\text{H}_4\text{N}$), 8.46 (s, 2 H, $\text{C}_5\text{H}_2\text{N}$), 8.64 (ddd, 3J = 8 Hz, 4J = 1.0, 5J = 0.9 Hz, 2 H, $\text{C}_5\text{H}_4\text{N}$), 8.75 (ddd, 3J = 4.8 Hz, 4J = 1.8 Hz, 5J = 0.9 Hz, 2 H, $\text{C}_5\text{H}_4\text{N}$) ppm. $^{13}\text{C}\{^1\text{H}\}$ NMR (CDCl_3): δ = 68.4 (C_5H_4), 71.8 (C_5H_4), 73.8 (d, $^3J_{\text{CP}}$ = 4 Hz, C_5H_4), 74.5 (d, $^2J_{\text{CP}}$ = 14 Hz, C_5H_4), 77.9 (*Ci*- C_5H_4), 82.4 (*Ci*- C_5H_4), 117.9 (3- $\text{C}_5\text{H}_2\text{N}$), 121.4 ($\text{C}_5\text{H}_4\text{N}$), 123.8 ($\text{C}_5\text{H}_4\text{N}$), 128.4 (d, $^3J_{\text{CP}}$ = 7 Hz, *m*- C_6H_5), 128.8 (*p*- C_6H_5), 133.5 (d, $^2J_{\text{CP}}$ = 20 Hz, *o*- C_6H_5), 138.9 ($\text{C}_5\text{H}_4\text{N}$), 139.2 (d, $^1J_{\text{CP}}$ = 10 Hz, *Ci*- C_6H_5), 149.1 ($\text{C}_5\text{H}_4\text{N}$), 150.1 (4- $\text{C}_5\text{H}_2\text{N}$), 156.5 ($\text{C}_5\text{H}_4\text{N}$), 158.1 (2- $\text{C}_5\text{H}_2\text{N}$) ppm. $^{31}\text{P}\{^1\text{H}\}$ NMR (CDCl_3): δ = -18.3 ppm. ESI-MS: m/z = $[\text{M} + \text{H}]^+$ 602.24.

Synthesis of 7: Compound **5** (200 mg, 0.33 mmol) dissolved in dichloromethane (25 mL) was slowly dropped into a solution of $[\text{PtCl}_2(\text{SEt}_2)_2]$ (**6**) (148.5 mg, 0.33 mmol) in dichloromethane (20 mL). After 10 min of stirring, the solvent was evaporated to 5 mL and diethyl ether (30 mL) was added. Compound **7** crystallized as orange needles at -30 °C. The crystals were washed with diethyl ether (40 mL) and dried in an oil-pump vacuum; yield 172 mg (0.18 mmol, 55% based on **5**). $\text{C}_{41}\text{H}_{38}\text{Cl}_2\text{FeN}_3\text{PPtS}$ (957.63): calcd. C 51.42, H 4.00, N 4.39; found C 51.50, H 3.82, N 4.39; m.p. 189.3 °C (dec.). IR (KBr): $\tilde{\nu}$ = 1435 (m, ν_{PC}), 1468 (m, ν_{PC}), 1567 (s, $\nu_{\text{C}=\text{C}}$), 1583 (s, $\nu_{\text{C}=\text{C}}$), 1600 (s, $\nu_{\text{C}=\text{C}}$), 2928 (w, ν_{CH}), 2966 (w, ν_{CH}) cm^{-1} . ^1H NMR (CDCl_3): δ = 1.08 (t, 3J = 7.2 Hz 6 H, SCH_2CH_3), 2.50 (q, 3J = 7.2 Hz 4 H, SCH_2CH_3), 4.32 (pq, J = 1.9 Hz, 2 H, C_5H_4), 4.35 (pt, J = 1.9 Hz, 2 H, C_5H_4), 4.70 (pt, J = 1.8 Hz, 2 H, C_5H_4), 4.90 (pt, J = 1.8 Hz, 2 H, C_5H_4), 7.36 (ddd, 3J = 7.7, 1.2 Hz, 4J = 1.2 Hz, 2 H, $\text{C}_5\text{H}_4\text{N}$), 7.4–7.7 (m, 12 H, $\text{C}_6\text{H}_5/5\text{-C}_5\text{H}_4\text{N}$), 7.88 (ddd, 3J = 7.7, 7.8 Hz, 4J = 1.8 Hz, 2 H, $\text{C}_5\text{H}_4\text{N}$), 8.46 (s, 2 H, $\text{C}_5\text{H}_2\text{N}$), 8.64 (ddd, 3J = 7.8 Hz, 4J = 1.2 Hz, 5J = 0.9 Hz, 2 H, $\text{C}_5\text{H}_4\text{N}$), 8.75 (ddd, 3J = 4.8 Hz, 4J = 1.8 Hz, 5J = 0.9 Hz, 2 H, $\text{C}_5\text{H}_4\text{N}$) ppm. $^{31}\text{P}\{^1\text{H}\}$ NMR (CDCl_3): δ = 4.9 (J_{PPt} = 3690 Hz) ppm.

Synthesis of 9: Compound **5** (100 mg, 0.17 mmol) was dissolved in dichloromethane (10 mL), and $[\text{PtCl}_2(\text{SEt}_2)_2]$ (**6**) (37 mg, 0.08 mmol) was added in a single portion. After 10 min of stirring, the reaction solution was evaporated to 5 mL and *n*-hexane (30 mL) was added. Molecule **9** crystallized as orange needles at -30 °C. The crystals were washed with *n*-hexane (40 mL) and dried in an oil-pump vacuum; yield 108 mg (0.073 mmol, 89% based on **5**). $\text{C}_{74}\text{H}_{56}\text{Cl}_2\text{Fe}_2\text{N}_6\text{P}_2\text{Pt}$ (0.5 C_6H_{14}) (1511.99): calcd. C 61.17, H 4.20, N 5.56; found C 61.07, H 4.43, N 5.18; m.p. 153 °C (dec.). IR (KBr): $\tilde{\nu}$ = 1439 (m, ν_{PC}), 1468 (m, ν_{PC}), 1567 (s, $\nu_{\text{C}=\text{C}}$), 1584 (s, $\nu_{\text{C}=\text{C}}$), 1602 (s, $\nu_{\text{C}=\text{C}}$) cm^{-1} . ^1H NMR (CDCl_3): δ = 4.22 (m, 4 H, C_5H_4), 4.61 (m, 4 H, C_5H_4), 4.91 (m, 4 H, C_5H_4), 5.08 (m, 4 H, C_5H_4), 7.33 (ddd, 3J = 7.9, 4.8 Hz, 4J = 1.0 Hz, 4 H, $\text{C}_5\text{H}_4\text{N}$), 7.38–7.7 (m, 24 H, $\text{C}_6\text{H}_5/5\text{-C}_5\text{H}_4\text{N}$), 7.86 (ddd, 3J = 7.9, 8.0 Hz, 4J = 1.8 Hz, 4 H, $\text{C}_5\text{H}_4\text{N}$), 8.47 (s, 4 H, $\text{C}_5\text{H}_2\text{N}$), 8.62 (ddd, 3J = 8 Hz, 4J = 1.0 Hz, 5J = 0.9 Hz, 4 H, $\text{C}_5\text{H}_4\text{N}$), 8.73 (ddd, 3J = 4.8 Hz, 4J = 1.8 Hz, 5J = 0.9 Hz, 4 H, $\text{C}_5\text{H}_4\text{N}$) ppm. $^{31}\text{P}\{^1\text{H}\}$ NMR (CDCl_3): δ = 10.0 (J_{PPt} = 2629 Hz) ppm. ESI-MS: m/z = $[\text{M} + \text{H}]^+$ 1469.90.

Synthesis of 12: Compound **5** (500 mg, 0.83 mmol) was dissolved in dichloromethane (25 mL) and $[\text{PdCl}_2(\text{cod})]$ (**11a**) (237 mg, 0.83 mmol) was added in a single portion at 25 °C. After 30 min of being stirred in the dark, the solution was filtered through Celite and the filtrate was evaporated to 5 mL. The product precipitated by addition of diethyl ether (30 mL). The solid was filtered off,

washed twice with *n*-hexane (20 mL), and dried in an oil-pump vacuum; yield 485 mg (0.62 mmol, 74% based on **5**). $\text{C}_{37}\text{H}_{28}\text{Cl}_2\text{FeN}_3\text{PPd}$ (0.5 CH_2Cl_2) (821.25): calcd. C 55.17, H 3.53, N 5.08; found C 55.47, H 3.62, N 4.97; m.p. 188 °C (dec.). IR (KBr): $\tilde{\nu}$ = 1434 (m, ν_{PC}), 1471 (m, ν_{PC}), 1585 (s, $\nu_{\text{C}=\text{C}}$), 1595 (s, $\nu_{\text{C}=\text{C}}$) cm^{-1} . ^1H NMR (CDCl_3): δ = 4.32 (br. s, 2 H, C_5H_4), 4.66 (br. s, 2 H, C_5H_4), 4.7 (pt, J = 1.8 Hz, 2 H, C_5H_4), 5.30 (s, 1 H, CH_2Cl_2) 5.77 (br. s, 2 H, C_5H_4), 7.3–7.51 (m, 8 H, $\text{C}_6\text{H}_5/\text{C}_5\text{H}_4\text{N}$), 7.55–7.66 (m, 4 H, C_6H_5), 7.83 (ddd, 3J = 7.9, 7.8 Hz, 4J = 1.8 Hz, 1 H, $\text{C}_5\text{H}_4\text{N}$), 7.95 (ddd, 3J = 7.9, 7.8 Hz, 4J = 2.0 Hz, 1 H, $\text{C}_5\text{H}_4\text{N-Pd}$), 8.37 (ddd, 3J = 7.8 Hz, 4J = 1 Hz, 5J = 0.8 Hz, 1 H, $\text{C}_5\text{H}_4\text{N-Pd}$), 8.61 (d, 4J = 1.3 Hz, 1 H, $\text{C}_5\text{H}_2\text{N}$), 8.63 (ddd, 3J = 7.8 Hz, 4J = 1 Hz, 5J = 1 Hz, 1 H, $\text{C}_5\text{H}_4\text{N}$), 8.74 (ddd, 3J = 4.8 Hz, 4J = 1.8 Hz, 5J = 0.8 Hz, 1 H, $\text{C}_5\text{H}_4\text{N}$), 9.04 (ddd, 3J = 3.7 Hz, 4J = 2 Hz, 5J = 1 Hz, 1 H, $\text{C}_5\text{H}_4\text{N-Pd}$), 10.46 (d, 4J = 1.3 Hz, 1 H, $\text{C}_5\text{H}_2\text{N}$) ppm. $^{31}\text{P}\{^1\text{H}\}$ NMR (CDCl_3): δ = 23.5 ppm. ESI-TOF-MS: m/z = $[\text{M} + \text{H}]^+$ 780.05.

Synthesis of 14: Compound **12** (100 mg, 0.13 mmol) was dissolved in tetrahydrofuran (50 mL) and $[\text{NiCl}_2(\text{dme})]$ (**13**) (28.3 mg, 0.13 mmol) was added in a single portion. After a few seconds, a red solid started to precipitate. The solid was filtered off and washed twice with diethyl ether. After drying the precipitate in an oil-pump vacuum it was dissolved in dimethyl sulfoxide (10 mL). Next, *n*-hexane (40 mL) was added, at which point **14** precipitated in the form of red crystals that were washed twice with *n*-hexane (30 mL); yield 112 mg (0.107 mmol, 81% based on **12**). $\text{C}_{41}\text{H}_{40}\text{Cl}_4\text{FeN}_3\text{NiO}_2\text{PPdS}_2$ (1064.65): calcd. C 46.25, H 3.79, N 3.96; found C 46.52, H 3.65, N 4.05. Mp. 215 °C (dec.). IR (KBr): $\tilde{\nu}$ = 1432 (m, ν_{PC}), 1472 (m, ν_{PC}), 1547 (s, $\nu_{\text{C}=\text{C}}$), 1570 (s, $\nu_{\text{C}=\text{C}}$), 1602 (s, $\nu_{\text{C}=\text{C}}$) cm^{-1} .

Synthesis of 16a: Compound **16a** was prepared as described for the synthesis of **9**. Instead of $[\text{PtCl}_2(\text{SEt}_2)_2]$ (**6**), $[\text{PdCl}_2(\text{cod})]$ (**11a**) (23 mg, 0.08 mmol) was used; yield 96 mg (0.07 mmol, 84% based on **5**); m.p. 140 °C (dec.). IR (KBr): $\tilde{\nu}$ = 1438 (m, ν_{PC}), 1467 (m), 15767 (s, $\nu_{\text{C}=\text{C}}$), 1584 (s, $\nu_{\text{C}=\text{C}}$), 1602 (s, $\nu_{\text{C}=\text{C}}$) cm^{-1} . ^1H NMR (250 MHz, CDCl_3): δ = 4.23 (m, 4 H, C_5H_4), 4.64 (m, 4 H, C_5H_4), 4.91 (m, 4 H, C_5H_4), 5.00 (m, 4 H, C_5H_4), 7.26–7.7 (m, 24 H, $\text{C}_6\text{H}_5/\text{C}_5\text{H}_4\text{N}$), 7.86 (ddd, 3J = 7.9, 8.0 Hz, 4J = 1.8 Hz, 4 H, $\text{C}_5\text{H}_4\text{N}$), 8.47 (s, 4 H, $\text{C}_5\text{H}_2\text{N}$), 8.62 (ddd, 3J = 8 Hz, 4J = 1.0 Hz, 5J = 0.9 Hz, 4 H, $\text{C}_5\text{H}_4\text{N}$), 8.73 (ddd, 3J = 4.8 Hz, 4J = 1.8 Hz, 5J = 0.9 Hz, 4 H, $\text{C}_5\text{H}_4\text{N}$) ppm. $^{31}\text{P}\{^1\text{H}\}$ NMR (CDCl_3): δ = 14.3 ppm. ESI-MS: m/z = $[\text{M} + \text{H}]^+$ 1379.24.

Synthesis of 16b: Compound **16b** was prepared as described for the synthesis of **9**. Instead of $[\text{PtCl}_2(\text{SEt}_2)_2]$ (**6**), $[\text{PdBr}_2(\text{cod})]$ (**11b**) (30 mg, 0.08 mmol) was used; yield 103 mg (0.07 mmol, 84% based on **5**). $\text{C}_{74}\text{H}_{56}\text{Br}_2\text{Fe}_2\text{N}_6\text{P}_2\text{Pd}$ (0.5 C_6H_{14}) (1509.07): calcd. C 61.16, H 4.20, N 5.56; found C 61.10, H 4.39, N 5.35; m.p. 240 °C (dec.). IR (KBr): $\tilde{\nu}$ = 1467 (s, ν_{PC}), 1533 (m, $\nu_{\text{C}=\text{C}}$) cm^{-1} . ^1H NMR (CDCl_3): δ = 4.27 (pt, J = 1.8 Hz, 4 H, C_5H_4), 4.63 (pt, J = 1.8 Hz, 4 H, C_5H_4), 4.37 (pt, J = 1.8 Hz, 4 H, C_5H_4), 5.07 (pt, J = 1.8 Hz, 4 H, C_5H_4), 7.39–7.55 (m, 20 H, C_6H_5), 7.67–7.75 (m, 4 H, $\text{C}_5\text{H}_4\text{N}$), 7.87 (dt, 3J = 7.5, 3.0 Hz, 4 H, $\text{C}_5\text{H}_4\text{N}$), 8.49 (s, 4 H, $\text{C}_5\text{H}_2\text{N}$), 8.62 (d, 3J = 3.0 Hz, 4 H, $\text{C}_5\text{H}_4\text{N}$), 8.75 (d, 3J = 4.79 Hz, 4 H, $\text{C}_5\text{H}_4\text{N}$) ppm. $^{31}\text{P}\{^1\text{H}\}$ NMR (CDCl_3): δ = 13.4 ppm. ESI-MS: m/z = $[\text{M} + \text{K}]^+$ 1507.03.

Synthesis of 17: Compound **17** was prepared as described for **9**. Instead of $[\text{PtCl}_2(\text{SEt}_2)_2]$ (**6**), $[\text{Mo}(\text{CO})_4(\text{nbd})]$ (**15**) (24 mg, 0.08 mmol) was used; yield 68 mg (0.05 mmol, 59% based on **5**); m.p. 153 °C (dec.). IR (KBr): $\tilde{\nu}$ = 1438 (m, ν_{PC}), 1468 (m, ν_{PC}), 1567 (s, $\nu_{\text{C}=\text{C}}$), 1584 (s, $\nu_{\text{C}=\text{C}}$), 1602 (s, $\nu_{\text{C}=\text{C}}$), 1812 (s, ν_{CO}), 1867 (s, ν_{CO}), 1900 (s, ν_{CO}), 2018 (s, ν_{CO}) cm^{-1} . ^1H NMR (CDCl_3): δ = 4.07 (m, 4 H, C_5H_4), 4.12 (m, 4 H, C_5H_4), 4.21 (pt, J = 1.8 Hz, 4 H,

C₅H₄), 4.63 (pt, $J = 1.8$ Hz, 4 H, C₅H₄), 7.17–7.24 (m, 20 H, C₆H₅), 7.34 (ddd, $^3J = 7.5$, 4.7 Hz, $^4J = 1$ Hz, 4 H, C₅H₄N), 7.86 (ddd, $^3J = 7.5$, 7.9 Hz, $^4J = 1.8$ Hz, 4 H, C₅H₄N), 8.33 (s, 4 H, C₅H₂N), 8.61 (ddd, $^3J = 7.9$ Hz, $^4J = 1$ Hz, $^5J = 0.8$ Hz, 4 H, C₅H₄N), 8.73 (ddd, $^3J = 4.7$ Hz, $^4J = 1.8$ Hz, $^5J = 0.8$ Hz, 4 H, C₅H₄N) ppm. $^{31}\text{P}\{^1\text{H}\}$ NMR (CDCl₃): $\delta = 25.9$ ppm. ESI-MS: $m/z = [\text{M} + \text{H}]^+$ 1411.20.

Synthesis of $[\{\text{CuBr}(\mathbf{5})\}_n]$ (19**):** Compound **5** (100 mg, 0.17 mmol) was dissolved in tetrahydrofuran (20 mL) and [CuBr] (**18**) (24 mg, 0.17 mmol) was added in a single portion. After two hours of stirring at 25 °C, the [CuBr] had been consumed and the solution was evaporated to 5 mL. Next *n*-hexane (30 mL) was added, at which point a red-orange material precipitated. The solid was filtered off and washed twice with *n*-hexane (30 mL portions) and was then dried in an oil-pump vacuum; yield 120 mg (0.16 mmol, 95% based on **5**). C₃₇H₂₈BrCuFeN₃P (744.91): calcd. C 59.66, H 3.79, N 5.64; found C 59.16, H 4.02, N 5.49; m.p. 180 °C (dec.). IR (KBr): $\tilde{\nu} = 1473$ (s, ν_{PC}), 1535 (m, $\nu_{\text{C}=\text{C}}$) cm⁻¹. ^1H NMR (CDCl₃): $\delta = 4.21$ (pt, $J = 1.8$ Hz, 2 H, C₅H₄), 4.37 (pt, $J = 1.8$ Hz, 2 H, C₅H₄), 4.43 (pt, $J = 1.9$ Hz, 2 H, C₅H₄), 4.36 (pt, $J = 1.9$ Hz, 2 H, C₅H₄), 7.13–7.32 (m, 12 H, C₆H₅/C₅H₄N), 7.83 (pt, $^3J = 7.9$ Hz, 2 H, C₅H₄N), 8.53 (s, 2 H, C₅H₄N), 8.64 (d, $^3J = 7.9$ Hz, 2 H, C₅H₄N), 8.32 (d, $^3J = 4.33$ Hz, 2 H, C₅H₄N) ppm. $^{31}\text{P}\{^1\text{H}\}$ NMR (CDCl₃): $\delta = -14.9$ ppm. ESI-MS: $m/z = [\text{M} - \text{Br}]^+$ 664.13.

Synthesis of **22:** Compound **22** was prepared as described for the synthesis of **19**. In this respect [AuCl(tht)] (**20**) (55 mg, 0.17 mmol) was used; yield 131 mg (0.16 mmol, 93% based on **5**). C₃₇H₂₈AuClFeN₃P(C₆H₁₄) (920.05): calcd. C 56.13, H 4.60, N 4.57; found C 55.92, H 4.43, N 4.35; m.p. 135 °C (dec.). IR (KBr): $\tilde{\nu} = 1471$ (s, ν_{PC}), 1531 (m, $\nu_{\text{C}=\text{C}}$) cm⁻¹. ^1H NMR (CDCl₃): $\delta = 4.36$ (pt, $J = 1.8$ Hz, 2 H, C₅H₄), 4.42 (pt, $J = 1.8$ Hz, 2 H, C₅H₄), 4.59 (pt, $J = 1.9$ Hz, 2 H, C₅H₄), 4.91 (pt, $J = 1.9$ Hz, 2 H, C₅H₄), 7.30–7.47 (m, 10 H, C₆H₅), 7.55 (ddd, $^3J = 7.40$ Hz, $^3J = 4.9$ Hz, 2 H, C₅H₄N), 7.87 (dt, $^3J = 7.40$, 3.0 Hz, 2 H, C₅H₄N), 8.35 (s, 2 H, C₅H₂N), 9.62 (d, $^3J = 7.9$ Hz, 2 H, C₅H₄N), 9.75 (dd, $^3J = 4.9$ Hz, $^4J = 1.3$ Hz, 2 H, C₅H₄N) ppm. $^{31}\text{P}\{^1\text{H}\}$ NMR (CDCl₃): $\delta = 27.2$ ppm. ESI-MS: $m/z = [\text{M} - \text{Cl}]^+$ 798.14.

Synthesis of **23:** Compound **23** was prepared as described for the synthesis of **19**. In this case, $[\{\text{RhCl}(\text{cod})\}_2]$ (**21**) (42 mg, 0.09 mmol) was used; yield 137 mg, 0.16 mmol, 95% based on **5**; m.p. 194 °C (dec.). IR (KBr): $\tilde{\nu} = 1473$ (s, ν_{PC}), 1535 (m, $\nu_{\text{C}=\text{C}}$) cm⁻¹. ^1H NMR (CDCl₃): $\delta = 2.40$ (m, 8 H, cod), 4.28 (pt, $J = 1.8$ Hz, 2 H, C₅H₄), 4.69 (pt, $J = 1.8$ Hz, 2 H, C₅H₄), 4.74 (pt, $J = 1.9$ Hz, 2 H, C₅H₄), 5.15 (pt, $J = 1.9$ Hz, 2 H, C₅H₄), 5.60 (s, 4 H, cod), 7.25–7.31 (m, 10 H, C₆H₅), 7.54 (dpt, $^3J = 8.00$ Hz, $^4J = 2.0$ Hz, 2 H, C₅H₄N), 7.83 (ddd, $^3J = 7.90$ Hz, $^4J = 1.9$ Hz, 2 H, C₅H₄N), 8.55 (s, 2 H, C₅H₂N), 8.66 (d, $^3J = 3.0$ Hz, 2 H, C₅H₄N), 8.73 (dd, $^3J = 4.30$ Hz, $^4J = 1.8$ Hz, 2 H, C₅H₄N) ppm. $^{31}\text{P}\{^1\text{H}\}$ NMR (CDCl₃): $\delta = 22.1$ (d, $J_{\text{Rh,P}} = 151$ Hz) ppm. ESI-MS: $m/z = [\text{M} - \text{cod}]^+$ 739.07, $[\text{M}]^+$ 847.21.

Synthesis of **25:** Compound **22** (300 mg, 0.36 mmol) was dissolved in ethanol (50 mL) and [RuCl₂(dmsO)₄] (**24**) (87 mg, 0.18 mmol) was added in a single portion. The reaction mixture was heated to reflux for 12 h. After removing all volatiles in an oil-pump vacuum, the remaining solid was washed five times with *n*-hexane (10 mL portions) and dried in vacuo; yield 315 mg (0.17 mmol, 95% based on **22**). C₇₄H₅₆Au₂Cl₄Fe₂N₆P₂Ru (1839.73): calcd. C 48.31, H 3.07, N 4.57; found C 48.66, H 3.21, N 4.38%; m.p. 245 °C (dec.). IR (KBr): $\tilde{\nu} = 1431$ (m, ν_{PC}), 1609 (s, $\nu_{\text{C}=\text{C}}$) cm⁻¹. ^1H NMR (CDCl₃): $\delta = 4.21$ (pt, $J = 1.8$ Hz, 4 H, C₅H₄), 4.43 (pt, $J = 1.8$ Hz, 4 H,

C₅H₄), 5.29 (pt, $J = 1.9$ Hz, 4 H, C₅H₄), 5.43 (pt, $J = 1.9$ Hz, 4 H, C₅H₄), 7.06–7.43 (m, 20 H, C₆H₅), 7.54 (m, 4 H, C₅H₄N), 8.63 (dt, $^3J = 7.9$ Hz, $^3J = 3.0$ Hz, 4 H, C₅H₄N), 9.46 (d, $^3J = 3.0$ Hz, 4 H, C₅H₄N), 9.53 (dd, $^3J = 4.30$ Hz, $^4J = 1.8$ Hz, 4 H, C₅H₄N), 9.67 (s, 4 H, C₅H₂N) ppm. $^{31}\text{P}\{^1\text{H}\}$ NMR (CDCl₃): $\delta = 27.4$ ppm.

Synthesis of **26:** Compound **3** (500 mg, 1.0 mmol) was dissolved in dichloromethane (25 mL) and [PdCl₂(cod)] (**11a**) (285 mg, 1.0 mmol) was added in a single portion. After 20 min of stirring, the reaction mixture was evaporated to 5 mL and diethyl ether (30 mL) was added. A purple solid precipitated and was filtered off. The solid was washed twice with *n*-hexane (10 mL) and dried in an oil-pump vacuum; yield 612 mg (0.9 mmol, 90% based on **3**). C₃₀H₂₄Cl₂FeNOPPd·(0.5 CH₂Cl₂·H₂O) (730.14): calcd. C 50.17, H 3.59, N 1.92; found C 50.14, H 3.58, N 1.88; m.p. 215 °C (dec.). IR (KBr): $\tilde{\nu} = 1435$ (m, ν_{PC}), 1481 (m, ν_{PC}), 1586 (s, $\nu_{\text{C}=\text{C}}$), 1602 (s, $\nu_{\text{C}=\text{C}}$), 1667 (s, ν_{CO}) cm⁻¹. ^1H NMR (CDCl₃): $\delta = 4.63$ (m, 2 H, C₅H₄), 4.74 (m, 2 H, C₅H₄), 4.83 (m, 2 H, C₅H₄), 5.30 (s, 1 H, CH₂Cl₂), 5.38 (m, 2 H, C₅H₄), 7.3–7.68 (m, 10 H, C₆H₅), 7.63 (m, 1 H, C₅H₄N), 7.94 (m, 1 H, C₅H₄N), 7.95 (d, $^3J = 15.8$ Hz, 1 H, CO-CH=CH), 8.01 (d, $^3J = 15.8$ Hz, 1 H, CO-CH=CH), 8.84 (m, 1 H, C₅H₄N), 9.0 (m, 1 H, C₅H₄N) ppm. $^{13}\text{C}\{^1\text{H}\}$ NMR (CDCl₃): $\delta = 68.1$ (C₅H₄), 69.7 (C₅H₄), 70.8 (d, $^3J_{\text{C,P}} = 4$ Hz, C₅H₄), 72.8 (d, $^2J_{\text{C,P}} = 14$ Hz, C₅H₄), 76.3 (C*i*-C₅H₄), 81.5 (C*r*-C₅H₄), 122.3 (CO-CH=CH), 125.5 (C₅H₄N), 127.2 (C₅H₄N), 128.9 (d, $^3J_{\text{C,P}} = 7$ Hz, C₆H₅), 131.1 (C₆H₅), 134.0 (d, $^2J_{\text{C,P}} = 20$ Hz, C₆H₅), 139.1 (C₅H₄N), 144.8 (CO-CH=CH), 151.2 (d, $^1J_{\text{C,P}} = 10$ Hz, C*i*-C₆H₅), 151.4 (C₅H₄N), 156.9 (C₅H₄N), 188.2 (CO-CH=CH) ppm. $^{31}\text{P}\{^1\text{H}\}$ NMR (CDCl₃): $\delta = 22.1$ ppm. ESI-MS: $m/z = [\text{M} + \text{H}]^+$ 678.08.

Heck–Mizoroki Reaction of Iodobenzene (27**) with *tert*-Butyl Acrylate (**28**):** Iodobenzene (654 mg, 5.1 mmol), *tert*-butyl acrylate (672 mg, 5.2 mmol), Et₃NiPr₂ (672 mg, 5.2 mmol), and acetylferrocene (114 mg, 0.5 mmol) were dissolved in a toluene/acetonitrile mixture [20 mL, ratio 1:1 (v/v)] and loaded with 0.5 mol-% of the respective catalyst (**12**, **26**, or **30**). [CuI] (2 equiv.) was added in a single portion. The reaction suspension was stirred at 80 °C. Samples (1 mL) were taken every hour over a period of 9 h. An additional sample was taken after 25 h. The samples were subjected to chromatography on silica gel with diethyl ether as eluent. All volatiles were evaporated from the samples under reduced pressure. The conversions were determined by ^1H NMR spectroscopy with acetylferrocene as an internal standard.

Crystal data for **5**, **9**, **12**, **14**, **16b**, **22**, and **26** are presented in Table 3 (**5**, **9**, **12**, **14**) and Table 4 (**16b**, **22**, **26**). The data for **12**, **14**, and **26** were collected with an Oxford Gemini S diffractometer, whereas the data for **5**, **9**, **16b**, and **22** were collected with a Bruker Smart 1K CCD diffractometer with graphite-monochromatized Mo- K_{α} ($\lambda = 0.71073$ Å) for **5**, **9**, **12**, **16b**, **22**, and **26** or Cu- K_{α} radiation ($\lambda = 1.54184$ Å) for molecule **14** using oil-coated shock-cooled crystals. The structures were solved by direct methods using SHELXS-97^[41] or SIR-92^[42] and refined by full-matrix least-squares procedures on F^2 using SHELXL-97.^[43] All non-hydrogen atoms were refined anisotropically and a riding model was employed in the refinement of the hydrogen atom positions.

CCDC-775761 (for **5**), -775762 (for **9**), -775763 (for **12**), -775764 (for **14**), -775765 (for **16b**), -775766 (for **22**), and -775767 (for **26**) contain the supplementary crystallographic data for this paper. These data can be obtained free of charge from The Cambridge Crystallographic Data Centre via http://www.ccdc.cam.ac.uk/data_request/cif.

Table 3. Crystal and intensity collection data for **5**, **9**, **12**, and **14**.

	5	9	12	14
Formula weight	601.44	1468.88	850.85	1234.46
Chemical formula	C ₃₇ H ₂₈ FeN ₃ P	C ₇₄ H ₅₆ Cl ₂ Fe ₂ N ₆ P ₂ Pt	C ₄₁ H ₃₆ Cl ₂ FeN ₃ OPPd	C ₄₃ H ₄₄ Cl ₈ FeN ₃ NiOPPdS ₂
Crystal system	tetragonal	monoclinic	monoclinic	monoclinic
Space group	<i>P</i> 4 ₂ / <i>n</i>	<i>P</i> 2 ₁ / <i>c</i>	<i>P</i> 2 ₁ / <i>c</i>	<i>P</i> 2 ₁ / <i>c</i>
<i>a</i> [Å]	27.667(10)	13.113(4)	14.5568(7)	15.6337(7)
<i>b</i> [Å]	27.667(10)	17.246(4)	20.0956(6)	12.9595(3)
<i>c</i> [Å]	7.751(5)	14.707(5)	14.6087(6)	25.0932(2)
α [°]	90	90	90	90
β [°]	90	110.954(10)	116.427(5)	95.5010(10)
γ [°]	90	90	90	90
<i>V</i> [Å ³]	5933(5)	3106.0(15)	3826.9(3)	5060.59(14)
$\rho_{\text{calcd.}}$ [g cm ⁻³]	1.347	1.571	1.477	1.620
<i>F</i> (000)	2496	1472	1728	2488
Crystal size [mm]	0.3 × 0.03 × 0.02	0.2 × 0.2 × 0.1	0.6 × 0.5 × 0.3	0.3 × 0.1 × 0.1
<i>Z</i>	8	2	4	4
Index ranges	−23 ≤ <i>h</i> ≤ 23 0 ≤ <i>k</i> ≤ 33 0 ≤ <i>l</i> ≤ 9	−16 ≤ <i>h</i> ≤ 15 0 ≤ <i>k</i> ≤ 21 0 ≤ <i>l</i> ≤ 18	−17 ≤ <i>h</i> ≤ 17 −24 ≤ <i>k</i> ≤ 24 −18 ≤ <i>l</i> ≤ 18	−17 ≤ <i>h</i> ≤ 17 −14 ≤ <i>k</i> ≤ 13 −28 ≤ <i>l</i> ≤ 28
μ [mm ⁻¹]	0.594	2.895	1.066	10.807
<i>T</i> [K]	298	298	100	100
θ [°]	1.47 to 25.35	1.66 to 26.38	2.97 to 26.00	3.20 to 60.69
Total reflections	25251	34416	34308	35666
Unique reflections	6524	6598	7352	7547
<i>R</i> _{int} [%] ^[a]	7.04	4.45	2.55	3.83
Data/restraints/parameters	5441/0/380	6359/0/394	7352/122/497	7547/66/615
<i>R</i> ₁ ^[a] , <i>wR</i> ₂ ^[a] [<i>I</i> ≥ σ (<i>I</i>)]	0.0664, 0.1719	0.0279, 0.0521	0.0663, 0.1762	0.0670, 0.1931
<i>R</i> ₁ ^[a] , <i>wR</i> ₂ ^[a] (all data)	0.1393, 0.2299	0.0427, 0.0589	0.0778, 0.1831	0.0962, 0.2201
Goodness-of-fit on <i>F</i> ^{2[b]}	1.040	1.148	1.193	1.157
$\Delta\rho$ [e Å ⁻³]	0.405, −0.434	0.859, −0.811	3.103, −1.414	2.446, −1.902

[a] $R = [\Sigma(|F_o| - |F_c|)] / \Sigma|F_o|$; $wR_2 = \{\Sigma[w(F_o^2 - F_c^2)^2] / \Sigma(wF_o^4)\}^{1/2}$. $w = 1/[\sigma^2(F_o^2) + (0.0835P)^2 + 4.1728P]$, $P = (F_o^2 + 2F_c^2)/3$. [b] $S = [\Sigma w(F_o^2 - F_c^2)^2] / (n - p)^{1/2}$ (*n* = number of reflections, *p* = parameters used).

Table 4. Crystal and intensity collection data for **16b**, **22**, and **26**.

	16b	22	26
Formula weight	1469.11	833.85	689.43
Chemical formula	C ₇₄ H ₅₆ Br ₂ Fe ₂ N ₆ P ₂ Pd	C ₃₇ H ₂₈ AuClFeN ₃ P	C ₃₀ H _{25.20} Cl ₂ FeNO _{1.60} PPd
Crystal system	monoclinic	triclinic	triclinic
Space group	<i>P</i> 2 ₁ / <i>c</i>	<i>P</i> $\bar{1}$	<i>P</i> $\bar{1}$
<i>a</i> [Å]	12.879(3)	9.9416(14)	10.1183(9)
<i>b</i> [Å]	17.208(5)	12.6191(18)	11.1906(8)
<i>c</i> [Å]	14.573(4)	13.860(2)	13.5351(10)
α [°]	90	112.005(2)	90.340(6)
β [°]	110.185(4)	101.591(2)	99.045(7)
γ [°]	14.573(4)	91.244(2)	113.162(7)
<i>V</i> [Å ³]	3031.5(14)	1570.2(4)	1387.64(19)
$\rho_{\text{calcd.}}$ [g cm ⁻³]	1.609	1.764	1.650
<i>F</i> (000)	1480	816	692
Crystal size [mm]	0.3 × 0.1 × 0.1	0.3 × 0.2 × 0.2	0.4 × 0.3 × 0.2
<i>Z</i>	2	2	2
Index ranges	−16 ≤ <i>h</i> ≤ 15 0 ≤ <i>k</i> ≤ 21 0 ≤ <i>l</i> ≤ 188	−12 ≤ <i>h</i> ≤ 12 −15 ≤ <i>k</i> ≤ 15 −17 ≤ <i>l</i> ≤ 17	−12 ≤ <i>h</i> ≤ 12 −13 ≤ <i>k</i> ≤ 13 −16 ≤ <i>l</i> ≤ 16
μ [mm ⁻¹]	2.188	5.296	1.448
<i>T</i> [K]	298	298	100
θ [°]	1.68 to 26.46	1.63 to 26.41	2.91 to 26.05
Total reflections	21852	17961	13913
Unique reflections	6505	6400	5483
<i>R</i> _{int} [%] ^[a]	7.72	2.81	1.11
Data/restraints/parameters	6171/0/394	6400/0/397	5483/0/351
<i>R</i> ₁ ^[a] , <i>wR</i> ₂ ^[a] [<i>I</i> ≥ σ (<i>I</i>)]	0.0826, 0.2113	0.0217, 0.0519	0.0165, 0.0408
<i>R</i> ₁ ^[a] , <i>wR</i> ₂ ^[a] (all data)	0.1081, 0.2393	0.0282, 0.0544	0.0196, 0.0429
Goodness-of-fit on <i>F</i> ^{2[b]}	1.054	1.020	1.063
$\Delta\rho$ [e Å ⁻³]	2.771, −3.241	0.543, −0.597	0.442, −0.309

[a] $R = [\Sigma(|F_o| - |F_c|)] / \Sigma|F_o|$; $wR_2 = \{\Sigma[w(F_o^2 - F_c^2)^2] / \Sigma(wF_o^4)\}^{1/2}$. $w = 1/[\sigma^2(F_o^2) + (0.0835P)^2 + 4.1728P]$, $P = (F_o^2 + 2F_c^2)/3$. [b] $S = [\Sigma w(F_o^2 - F_c^2)^2] / (n - p)^{1/2}$ (*n* = number of reflections, *p* = parameters used).

Acknowledgments

We gratefully acknowledge the generous financial support by the Deutsche Forschungsgemeinschaft (DFG) and the Fonds der Chemischen Industrie.

- [1] For example: a) C. M. Casado, I. Cuadrado, M. Morán, B. Alonso, B. García, B. González, J. Losada, *Coord. Chem. Rev.* **1999**, 185–186, 53; b) G. Ferguson, C. Glidewell, G. Opromolla, C. M. Zakaria, P. Zanello, *J. Organomet. Chem.* **1996**, 517, 183; c) J. D. Carr, S. J. Coles, M. B. Hursthouse, J. H. R. Tucker, *J. Organomet. Chem.* **2001**, 637–639, 304; d) J. Sehnert, A. Hess, N. Metzler-Nolte, *J. Organomet. Chem.* **2001**, 637–639, 349; e) I. P. Beletskaya, A. V. Tsvetkov, G. V. Latyshev, V. A. Tafeenko, N. V. Lukashev, *J. Organomet. Chem.* **2001**, 637–639, 653; f) J. Diez, M. P. Gamasa, J. Gimeno, M. Lanfranchi, A. Tiripicchio, *J. Organomet. Chem.* **2001**, 637–639, 677; g) T. J. Colacot, H. Qian, R. Cea-Olivares, S. Hernandez-Ortega, *J. Organomet. Chem.* **2001**, 637–639, 691; h) B. Longato, R. Coppo, G. Pilloni, C. Corvaja, A. Toffoletti, G. Bandoli, *J. Organomet. Chem.* **2001**, 637–639, 710; i) U. Siemeling, U. Vorfeld, B. Neumann, H. G. Stammer, M. Fontani, P. Zanello, *J. Organomet. Chem.* **2001**, 637–639, 733.
- [2] For example: a) I. Manners, *Adv. Organomet. Chem.* **1995**, 37, 131; b) I. Manners, *Chem. Commun.* **1999**, 857; c) Y. Zhu, O. Clot, M. O. Wolf, G. P. A. Yap, *J. Am. Chem. Soc.* **1998**, 120, 1812; d) P. D. Beer, *Acc. Chem. Res.* **1998**, 31, 71; e) J. E. Kingston, L. Ashford, P. D. Beer, M. G. B. Drew, *J. Chem. Soc., Dalton Trans.* **1999**, 251; f) C. Valério, J. L. Fillaut, J. Rui, J. Guittard, J. C. Blais, D. Astruc, *J. Am. Chem. Soc.* **1997**, 119, 2588; g) J. D. Carr, S. J. Coles, W. W. Hassan, M. B. Hursthouse, M. A. Malik, J. H. R. Tucker, *J. Chem. Soc., Dalton Trans.* **1999**, 57; h) R. S. Ingram, M. J. Hostetler, R. W. Murray, *J. Am. Chem. Soc.* **1997**, 119, 9175; i) T. J. Colacot, *Chem. Rev.* **2003**, 103, 3101.
- [3] a) C. T. Carver, D. Benitez, K. L. Miller, B. N. Williams, E. Tkatchouk, W. A. Goddard, P. L. Diaconescu, *J. Am. Chem. Soc.* **2009**, 131, 10269; b) M. J. Monreal, P. L. Diaconescu, *Organometallics* **2008**, 27, 1703; c) A. Shafir, D. Fiedler, J. Arnold, *Chem. Commun.* **2003**, 2598.
- [4] G. Bandoli, A. Dolmella, *Coord. Chem. Rev.* **2000**, 209, 161.
- [5] a) S. Guo, R. Hauptmann, S. Losi, P. Zanello, J. J. Schneider, *J. Organomet. Chem.* **2009**, 694, 1022; b) S. Akabori, T. Kumagai, T. Shirahige, S. Sato, K. Kawazoe, C. Tamura, *Organometallics* **1987**, 10, 2107.
- [6] a) C. K. A. Gregson, N. J. Long, A. J. P. White, D. J. Williams, *Organometallics* **2004**, 23, 3675; b) V. C. Gibson, N. J. Long, C. K. Williams, V. Fontani, P. Zanello, *Dalton Trans.* **2003**, 3599.
- [7] a) R. C. J. Atkinson, V. C. Gibson, N. J. Long, A. J. P. White, D. J. Williams, *Organometallics* **2004**, 23, 2744; b) I. R. Butler, R. L. Davies, *Synthesis* **1996**, 1350.
- [8] a) V. C. Gibson, N. J. Long, A. J. P. White, C. K. Williams, D. J. Williams, M. Fontani, P. Zanello, *J. Chem. Soc., Dalton Trans.* **2002**, 3280; b) J. P. Wolfe, S. L. Buchwald, *Tetrahedron Lett.* **1997**, 38, 6359.
- [9] R. C. J. Atkinson, V. C. Gibson, N. J. Long, A. J. P. White, L. J. West, *Dalton Trans.* **2006**, 3597.
- [10] J. E. Aguado, S. Canales, M. C. Gimeno, P. G. Jones, A. Laguna, M. D. Villacampa, *Dalton Trans.* **2005**, 3005.
- [11] S. Y. Desjardins, K. J. Cavell, J. L. Hoare, B. W. Skelton, A. N. Sobolev, A. H. White, W. Keim, *J. Organomet. Chem.* **1997**, 544, 163.
- [12] For example: a) W. Simanko, W. Tesch, V. N. Sapunov, K. Merz, R. Schmid, K. Kirchner, *Organometallics* **1998**, 17, 5674; b) G. Ifime, C. Moreau-Bossuet, E. Manoury, G. G. A. Balavoine, *Chem. Commun.* **1996**, 527; c) L.-L. Lai, T.-Y. Dong, *J. Chem. Soc., Chem. Commun.* **1994**, 1078; d) I. R. Butler, S. C. Quayle, *J. Organomet. Chem.* **1998**, 552, 63.
- [13] O. G. Mancheno, J. Priego, S. Cabrera, R. G. Arrayás, T. Llamas, J. C. Carretero, *J. Org. Chem.* **2003**, 68, 3679.
- [14] R. G. Pearson, *J. Am. Chem. Soc.* **1963**, 85, 3533.
- [15] T.-Y. Dong, M. C. Lin, M. Y.-N. Chiang, J. Y. Wu, *Organometallics* **2004**, 23, 3921.
- [16] For example: a) R. Wang, X. Wang, E. B. Sundberg, P. Nguyen, G. P. G. Grant, C. Sheth, Q. Zhao, S. Herron, K. A. Kantardjieff, L. Li, *Inorg. Chem.* **2009**, 48, 9779; b) S. Hayami, K. Danjobara, Y. Shigeoyoshi, K. Inoue, Y. Ogawa, Y. Maeda, *Inorg. Chem. Commun.* **2005**, 8, 506; c) P. Štěpnička, I. Cisařová, R. Gyepes, *Eur. J. Inorg. Chem.* **2006**, 926; d) K. Rößler, T. Rüffer, B. Walfort, R. Packheiser, R. Holze, M. Zharnikov, H. Lang, *J. Organomet. Chem.* **2007**, 692, 1530.
- [17] P. Kapoor, K. Löfqvist, Å. Oskarsson, *J. Mol. Struct.* **1998**, 470, 39.
- [18] a) P. S. Braierman, R. J. Cross, B. B. Young, *J. Chem. Soc., Dalton Trans.* **1976**, 1306; b) H. A. Brune, J. Ertl, *Liebigs Ann. Chem.* **1980**, 928; c) H. A. Brune, J. Unsinn, H. G. Alt, G. Schmidtberg, K.-H. Spohn, *Chem. Ber.* **1984**, 117, 1606.
- [19] a) R. Packheiser, A. Jakob, P. Ecorchard, B. Walfort, H. Lang, *Organometallics* **2008**, 27, 1214; b) C. G. Barlow, G. C. Hollywell, *J. Organomet. Chem.* **1969**, 16, 439.
- [20] a) F. Liu, S. A. Pullarkat, Y. Li, S. Chen, M. Yuan, Z. Y. Lee, P.-H. Leung, *Organometallics* **2009**, 28, 3941; b) J. Kühnert, M. Düsek, J. Demel, H. Lang, P. Štěpnička, *Dalton Trans.* **2007**, 2802.
- [21] M. Mastalerz, H. J. E. Rivera, W. Hüggenberg, K. Merz, I. M. Oettel, G. Dyker, *CrystEngComm* **2008**, 10, 1120.
- [22] B. J. Coe, S. J. Glenwright, *Coord. Chem. Rev.* **2000**, 203, 5–80.
- [23] A. Bondi, *J. Phys. Chem.* **1964**, 68, 441.
- [24] Y. D. M. Champouret, J.-D. Maréchal, R. K. Chaggar, J. Fawcett, K. Singh, F. Maserasc, G. A. Solan, *New J. Chem.* **2007**, 31, 75.
- [25] E. O. Fischer, W. Pfab, *Z. Naturforsch., Teil B* **1952**, 7, 377.
- [26] H. Lang, M. Leschke, M. Melter, B. Walfort, K. Köhler, S. E. Schulz, *Z. Anorg. Allg. Chem.* **2003**, 629, 2371.
- [27] J. W. Diesveld, E. M. Menger, H. T. Edzes, W. S. Veeman, *J. Am. Chem. Soc.* **1980**, 102, 1935.
- [28] a) D. T. Hill, G. R. Girard, F. L. McCabe, R. K. Johnson, P. D. Stupik, J. H. Zhang, W. M. Reiff, D. S. Eggleston, *Inorg. Chem.* **1989**, 28, 3529; b) F. Canales, M. C. Gimeno, P. G. Jones, A. Laguna, C. Sarroca, *Inorg. Chem.* **1997**, 36, 5206.
- [29] a) R. F. Heck, J. P. Nolley, *J. Org. Chem.* **1972**, 37, 2320; b) I. P. Beletskaya, A. V. Cheprakov, *Chem. Rev.* **2000**, 100, 3009; c) N. T. S. Phan, M. Van Der Sluys, C. W. Jones, *Adv. Synth. Catal.* **2006**, 348, 609.
- [30] A. F. Littke, G. C. Fu, *J. Am. Chem. Soc.* **2001**, 123, 6989.
- [31] D. Frey, J. Schütz, E. Herdtweck, W. A. Herrmann, *Organometallics* **2005**, 24, 4416.
- [32] M. T. Reetz, G. Lohmar, R. Schwickardi, *Angew. Chem. Int. Ed.* **1998**, 37, 481.
- [33] D. Drew, J. R. Doyle, *Inorg. Synth.* **1990**, 28, 346.
- [34] G. B. Kauffman, D. O. Cowan, *Inorg. Synth.* **1990**, 28, 154.
- [35] H. Werner, R. Prinz, *Chem. Ber.* **1967**, 100, 265.
- [36] L. R. Nylander, S. F. Pavkovic, *Inorg. Chem.* **1959**, 9, 1970.
- [37] K. C. Dash, H. Schmidbaur, *Chem. Ber.* **1973**, 106, 1221.
- [38] A. van der Ent, A. L. Onderdelinden, *Inorg. Synth.* **1990**, 28, 90.
- [39] G. U. Priimov, P. Moore, P. K. Maritim, P. K. Butalanyi, N. W. Alcock, *J. Chem. Soc., Dalton Trans.* **2000**, 445.
- [40] M. E. Wright, *Organometallics* **1990**, 9, 853.
- [41] G. M. Sheldrick, *Acta Crystallogr., Sect. A* **1990**, 46, 467.
- [42] A. Altomare, G. Cascarano, C. Giacovazzo, A. Gualardi, *J. Appl. Crystallogr.* **1993**, 26, 343.
- [43] G. M. Sheldrick, *SHELXL-97, Program for Crystal Structure Refinement*, University of Göttingen, Germany, **1997**.

Received: April 1, 2010
Published Online: July 7, 2010

Interaction of Gold with Co-Condensed and Grafted HMS-SH Silica: A ^{29}Si $\{^1\text{H}\}$ CP-MAS NMR Spectroscopy, XRD, XPS and Au L_{III} EXAFS Study

Valeria La Parola,^[a] Alessandro Longo,^[a] Anna Maria Venezia,^{*,[a]} Alberto Spinella,^[b] and Eugenio Caponetti^[b,c]

Keywords: Mesoporous materials / Silica / Inorganic-organic hybrid composites / Gold / Sulfur

Hexagonal mesoporous silica (HMS) is functionalised with mercaptopropyl groups by adopting two different procedures; co-condensation and grafting. In both cases tetraethylorthosilicate (TEOS) and 3-mercaptopropyltriethoxysilane (3-MPTES) are used as the silicon and sulfur precursors, respectively. The obtained materials are analysed by several techniques such as N_2 sorption, TG-DTA, XRD, SAXS and solid state ^{29}Si $\{^1\text{H}\}$ CP-MAS NMR spectroscopy. By taking advantage of the chemical interaction between gold and

the $-\text{SH}$ groups, the effect of the thiol addition procedure on the supporting capability of the functionalised silica is evaluated by depositing gold through the incipient wet impregnation technique. The influence of the functionalisation method on the electronic structure of gold and on its surface distribution is determined by extended X-ray fine absorption spectra (EXAFS) of Au at the L_{III} edge and by X-ray photoelectron spectroscopy (XPS).

Introduction

Since their discovery, by Mobil researchers in the early 1990s,^[1] mesoporous template silicates (MTS) have found application in environmental and industrial processes. The so-called M14S materials, characterised by high surface area and by uniformly sized pores, are used as adsorbents and also as catalyst and sensor components. The pore sizes, larger than those in zeolites, can be adjusted in the nanometer range by appropriate choice of the surfactant templates, which makes these systems suitable to host large molecules. Many reviews have covered several aspects of these mesoporous materials related to their synthesis, surface modification and practical applications.^[2–4] Depending on the type of surfactants, either cationic, anionic or neutral, and also on the surfactant/ SiO_2 molecular ratio, different structures are obtained.^[5] The main problems associated with such materials, especially in the earlier syntheses, were their poor hydrothermal stability and lower reactivity relative to zeolites of the same chemical composition. The hydrothermal stability could be improved by adding salts or by using amphiphilic block copolymers as organic structure-directing agents.^[6,7] The reactivity of the materials is enhanced by the addition of functional groups.^[8] In particular, organic groups with a rather low reactivity, in addition to increasing

the surface hydrophobicity and avoiding surface hydrolysis, are used to tailor the pore sizes. The addition of more reactive groups such as alkylamines and alkylthiol is pursued for making innovative catalysts or for environmental applications.^[8,9]

These organic–inorganic nanocomposites can be prepared by following two procedures; grafting and co-condensation. The grafting method refers to post-synthesis modification of a mesoporous material by attachment of functional groups.^[8,10] The co-condensation procedure refers to a one-pot or single-step synthesis of mesoporous silicas, containing organically modified surfaces, through sol-gel.^[10,11] Although the single-step method generally provides a more uniform distribution of the organic groups at the surface and also in the structure, the post-synthesis grafting allows to obtain more hydrothermally stable materials, with a better defined structure and better pore-size control.^[8,12] Thiol-containing organic groups are certainly among the most interesting functional groups. Thiol-functionalised silicas (SiO_2-SH) are generally oxidised to sulfonic acid silica materials ($\text{SiO}_2-\text{SO}_3\text{H}$) and are used as acid catalysts for dehydration or esterification reactions.^[9,10,13] Thiol-functionalised nanoporous silicas are also used as adsorbents for the removal of heavy metals from both aqueous and nonaqueous waste streams, as they exploit the complexation between the ligand and the metal.^[11,14–18] With respect to this application, the distribution of the thiol groups over the porous structure of the silica supports is extremely important. Indeed, the more accessible the groups are, the more efficient the uptake of metal ions would be.^[15] The factors affecting the reactivity of thiol-functionalised mesoporous silica towards Hg^{II} have been

[a] Istituto per lo Studio dei Materiali Nanostrutturati (ISMN-CNR),
Via Ugo La Malfa 153, 90146 Palermo, Italy

E-mail: venezia@pa.ismn.cnr.it

[b] Centro Grandi Apparecchiature, Università di Palermo,
Via Marini 14, 90128 Palermo, Italy

[c] Dipartimento di Chimica Fisica, Università di Palermo, Parco d'Orleans II,
Viale delle Scienze pad. 17, 90128 Palermo, Italy

analysed and discussed in a recent paper.^[19] The adsorbing capacity of Hg^{II} was higher for the material obtained by co-condensation than for the grafted materials because of the larger amount of incorporated ligand. On the other hand, the mercury uptake of the grafted adsorbent was faster at the beginning of the process because of a higher concentration of binding sites at the pore entrance than that for the co-condensed materials.^[19] Thiol-functionalised silicas are also used in nanofabrication, such as in the preparation of cadmium sulfide or gold nanoparticles, when control of the particle size and shape is highly desirable for optimising the electronic and optical properties.^[20,21]

In the present study, the functionalisation of HMS with 3-mercaptopropyltriethoxysilane (3-MPTES) groups is exploited by keeping in mind the possible application of the obtained materials as supports for heterogeneous metal catalysts. The combination of the structural feature of a mesoporous support with the presence of reactive functional groups such as alkylthiols is meant to produce a high surface dispersion of the supported metal. To this purpose, thiol-functionalisation is carried out by using both methods, grafting and co-condensation. The subsequent anchoring of gold, a noble metal that has recently been highly investigated for catalytic applications,^[22] is achieved by incipient wet impregnation. By looking at the electronic and structural properties of the noble metal in the grafted and co-condensed functionalised silicas, the outcome of the two functionalisation procedures in terms of support structural changes and anchoring properties, both relevant for the preparation of catalysts, are compared.

Results and Discussion

Support Characterisation

The N_2 adsorption–desorption isotherms for HMS and the grafted and co-condensed functionalised HMS (HMS-SH_g and HMS-SH_c, respectively) are given in Figure 1 along with the corresponding pore size distribution shown in the inset. The isotherms are a mixture of type IV, characteristic of mesoporous compounds, and type II, indicating the presence of larger pores probably arising from textural porosity.^[23] In Table 1, the specific surface areas determined from BET analysis and the pore volumes and the average pore sizes derived from the nitrogen adsorption/desorption measurements are listed. As expected and in accord with the literature, the grafted HMS sample undergoes a decrease in the original surface area and pore size, which can be attributed to the partial blocking of the pores by the mercaptopropyl groups.^[10]

On the contrary and opposite to previous findings on analogous materials,^[14] the HMS functionalised by the co-condensation method has the same surface area and pore size of pure HMS. The discrepancy with the literature may arise from the different treatments applied here to the bare and the thiol co-condensed HMS. Indeed, in the former case the template was removed by calcination at 600 °C, whereas in the latter case, the template was removed by

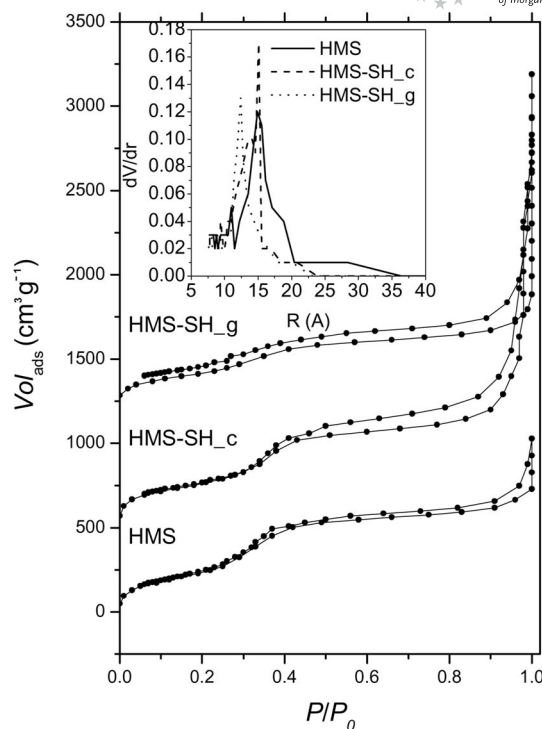


Figure 1. Nitrogen adsorption–desorption isotherm of siliceous HMS and of the grafted and co-condensed thiol-functionalised HMS. The isotherm of HMS-SH_c is offset by 600 cm³ g⁻¹ and that of HMS-SH_g by 1200 cm³ g⁻¹ for clarity. The inset shows the pore size distribution.

Table 1. Textural and structural data of HMS and thiol-modified HMS.

Sample	$S_{\text{BET}}^{\text{[a]}}$ (m² g⁻¹)	$V_p^{\text{[a]}}$ (cm³ g⁻¹)	$D_p^{\text{[a]}}$ (Å)	$d_{100}^{\text{[b]}}$ (Å)
HMS	981	1.3	30	42.3
HMS-SH_g	750	0.7	24	40.2
HMS-SH_c	980	1.0	30	38.5

[a] The specific surface area (S_{BET}), the pore volume (V_p) and the average pore size (D_p) were calculated from N_2 adsorption/desorption isotherms. [b] d_{100} spacing is the plane distance computed by means of Bragg's law.

chemical extraction in order to preserve the mercaptopropyl groups. This mild procedure may compensate for the possible area reduction that would arise from the presence of the mercaptopropyl groups.

Small angle X-ray scattering measurements were performed to check the long-range ordering of the mesoporous channel structure of the HMS materials. The SAXS patterns of pure and functionalised HMS are shown in Figure 2. The experimental intensities are plotted as a function of the transfer moment q (Å⁻¹) [$q = 4\pi\sin(\theta)/\lambda$]. As reported in the literature, the framework of pure HMS exhibits a single diffraction peak located at $q \approx 0.15$ Å⁻¹, which can be attributed to the (100) first-order reflection.^[15] As observed in Figure 2, the peaks in the curves of the thiol-functionalised silicas lie at higher q values relative to that of pure HMS. The shift corresponds to a contraction of the d_{100} spacing listed in Table 1 for the bare and the modified

silicas. As expected and in accord with the literature, the introduction of thiol groups by the co-condensation method produces a larger contraction of the framework lattice relative to that by post-synthesis surface functionalisation.^[10] The larger decrease in the lattice spacing may be attributed to the organophilic mercaptopropylsilane added directly in the synthesis mixture, which enables it to penetrate deeper within the hydrophobic core of the surfactant micelles.^[12]

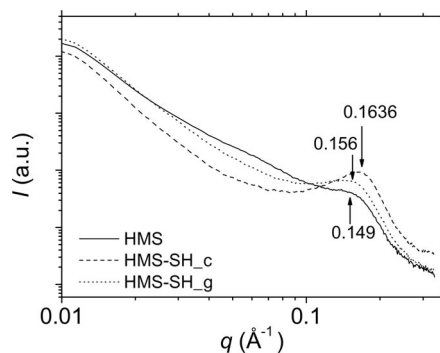


Figure 2. SAXS curves of pure HMS and of the functionalised HMS-SH_c and HMS-SH_g.

In order to confirm the presence of thiol groups in the HMS structure, solid-state ^{29}Si $\{^1\text{H}\}$ CP-MAS NMR spectra were collected. The experimental spectra with the corresponding fitted curves for the bare and the functionalised HMS are shown in Figure 3.

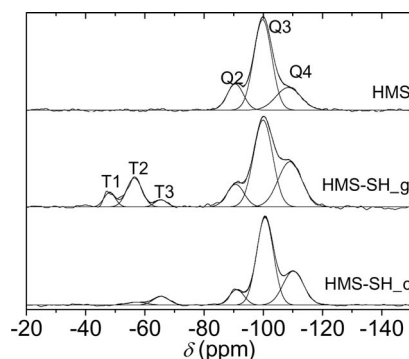


Figure 3. ^{29}Si $\{^1\text{H}\}$ CP-MAS NMR spectra of siliceous HMS and of functionalised HMS-SH_g and HMS-SH_c.

The spectrum of bare HMS exhibits three main peaks associated with the three different silicon atoms of the silica framework. Solid-state NMR spectroscopy allows to distinguish silicon atoms without hydroxy groups $\text{Si}-(\text{O}-\text{Si})_4$, silicon atoms bearing one hydroxy group $(\text{Si}-\text{O})_3-\text{Si}-\text{OH}$ and silicon atoms bearing two hydroxy groups $(\text{Si}-\text{O})_2-\text{Si}-(\text{OH})_2$ called germinal silanols. The first species is largely present in the bulk, whereas the second and third types of silicon atoms are present at the silica surface. The species are characterised by different chemical shifts. The peaks (arising from Q2 species) at -91.04 ppm, (Q3) at -100.6 ppm and (Q4) at -110.3 ppm are attributable to sili-

con atoms with geminal silanols, with single silanol and to silicon atoms involved only in siloxane bridges, respectively.^[24] The ^{29}Si $\{^1\text{H}\}$ CP-MAS NMR spectra of functionalised HMS contain the peaks discussed above for pure HMS and a new set of peaks in the range from -40 to -80 ppm. The peaks assigned to the Qn species maintain the same position but with different relative intensities. Since the ^{29}Si $\{^1\text{H}\}$ CP-MAS NMR technique is based on magnetisation transfer from the ^1H to ^{29}Si nuclei, the peak intensities are related to the total number of protons near the silicon atoms. As a consequence, a straight quantification of the different silicon groups is not possible. However, by assuming a similar chemical shift and the same cross-polarisation dynamic for bare and functionalised HMS, the relative intensities of the three different silicon contributions in the three samples can be estimated. Spectra deconvolution by means of three Gaussians, as shown in Figure 3, allowed the area of each peak in the set assigned to the Qn units for the three spectra to be obtained. The results of the fitting procedures are listed in Table 2.

Table 2. ^{29}Si $\{^1\text{H}\}$ CP-MAS NMR spectroscopic data for HMS and for mercaptopropyl-functionalised HMS samples: chemical shifts (ppm), corresponding relative peak areas for Qn [in parentheses (%)] and relative peak area ratio, calculated by the relative peak areas for Q4/(sum of relative peak areas of Q2 and Q3), obtained by curve deconvolution.

Samples	Q2	Q3	Q4	Q4/(Q2 + Q3)
HMS	-91.6 (16.2)	-100.6 (67.1)	-110.3 (16.7)	0.20
HMS-SH_g	-91.9 (12.3)	-100.7 (54.7)	-109.0 (33.0)	0.49
HMS-SH_c	-91.0 (9.3)	-101.3 (62.5)	-110.5 (28.2)	0.39

The increase in the signal assigned to Q4 arises from the direct involvement of the Q2 and Q3 units in the functionalisation process, which decreases their signal with respect to that of Q4.^[12] Such an effect is higher in the HMS-SH_g sample. As mentioned above, a new set of peaks (resulting from Tn species) in the range -40 to -80 ppm is evidence of HMS functionalisation by the mercapto groups. The peaks correspond to three different environments for the siloxane groups in the functionalised material:^[25] (i) T1 units bound to one siloxane and represented at -47.5 ppm, (ii) T2 units bound to two siloxanes and represented at -57.5 ppm and (iii) T3 units fully condensed and bound to three siloxanes and represented at -66.7 ppm. In the grafted sample, the most intense peaks are those related to T1 and T2, whereas in the co-condensed sample the most intense peak arises from T3 and no signal attributable to T1 is present. This suggests that the mercapto groups in the co-condensed sample, in contrast with those in the grafted sample, are preferentially incorporated in the wall surfaces.^[12] Moreover, in the spectrum of HMS-SH_c, the relative intensity of the Tn peaks with respect to the Qn peaks is much lower than that for the HMS-SH_g spectrum. As observed before, the cross-polarisation technique produces an enhancement of the signal from those ^{29}Si nuclei closer to ^1H .

The lower intensity of the (Tn) peaks observed in the case of the co-condensed sample may then be indicative of a more homogeneous functionalisation relative to the grafted sample, which gives rise to more distant mercapto groups and therefore less intense ^{29}Si signal.

The thermal stability and the loading of the organic functional groups in the mesoporous materials were determined by thermogravimetric analysis coupled with mass quadrupole analysis. For both co-condensed and grafted samples, similar plots of the weight loss as a function of temperature were obtained. As shown in Figure 4 for the HMS-SH_c sample, after an initial loss of solvent (toluene and ethanol), removal of H_2S in the range 320–430 °C occurs, followed by loss of propane in the temperature range 430–620 °C. From the percentage weight losses, the calculated weight ratio of propyl-SH/ SiO_2 was 0.13 for both samples.

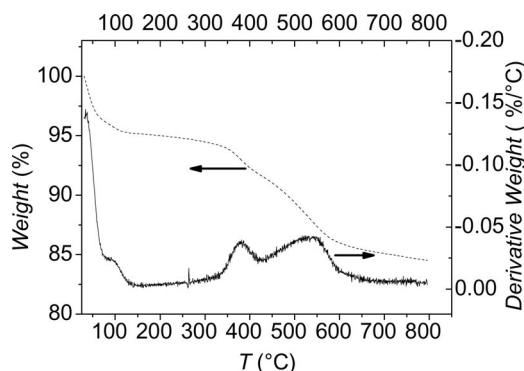


Figure 4. TGA (dashed line) and derivative TG (solid line) curves of HMS-SH_c.

Supported Gold Characterisation

The mercapto-functionalised ordered mesoporous silicas were used as supports for anchoring gold nanoparticles. The subsequent deposition of gold was indeed exploited as a way to (a) probe the presence of thiol groups on the basis of the strong Au–S interactions and (b) verify the suitability of the functionalised supports to disperse the metal and therefore to act as a possible hybrid carrier for catalytic application. The gold samples supported on the two differently functionalised silicas were characterised by SAXS, XRD, XPS and EXAFS techniques. The SAXS patterns in the region $0.01 < q < 0.4 \text{ \AA}^{-1}$ of the gold samples and of the corresponding functionalised supports are shown in Figure 5.

The persistence of the support (100) reflection upon gold deposition indicates that the structure of HMS-SH is preserved in both samples. However, the shallower profile with respect to the original support suggests that some de-structuring occurs upon gold deposition, to a larger extent in the sample of gold supported on the single-step prepared HMS-SH_c. As already suggested in the literature, the decrease in intensity of the first-order reflection, observed particularly in HMS-SH_c-Au, relative to the correspond-

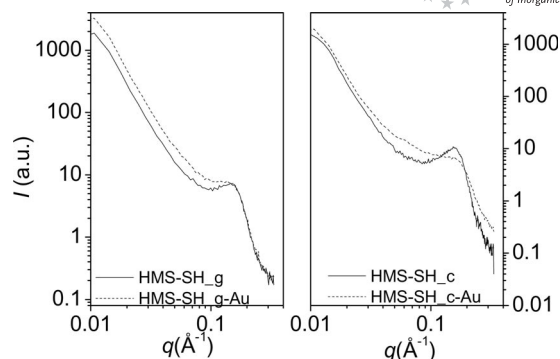


Figure 5. SAXS curves of supported gold samples and corresponding functionalised HMS-SH_c and HMS-SH_g supports.

ing support, could be attributed to the decreased scattering contrast caused by pore filling.^[26] The XRD patterns are given in Figure 6. They exhibit the two main reflections of metallic gold, (111) and (200) at 2θ values of ca. 38.1 and 44.3°, respectively. The formation of metallic gold achieved upon simple overnight drying at 120 °C is not too surprising.^[27] According to Bond and Thompson, chloroauric acid over silica is thermally unstable and metallic gold is formed without requiring any further reduction.^[22] The same behavior is observed here with an aqueous solution of AuCl_3 . In spite of the same amount of gold, the intensities of the Au-related peaks for the co-condensed support are much stronger with respect to those for the grafted sample. The difference is indicative of a higher dispersion of gold in the grafted sample. The crystalline sizes of the supported Au particles, as estimated from the Scherrer equation, are 40 and 21 Å in the co-condensed and grafted supports, respectively.

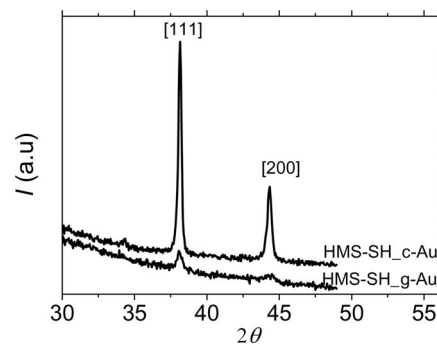


Figure 6. XRD pattern of mesoporous supported gold samples.

XPS investigation of the functionalised mesoporous silicas and the corresponding supported gold samples was carried out in order to check the surface distribution of the thiol groups and of the anchored gold and to determine their chemical state. The S 2p photoelectron peaks are shown in Figure 7, along with the intense Si 2s peak. A small downshift of the energy of less than 0.4 eV observed in the gold-containing samples, with respect to the corresponding supports alone, may be attributed to a charge compensation effect.

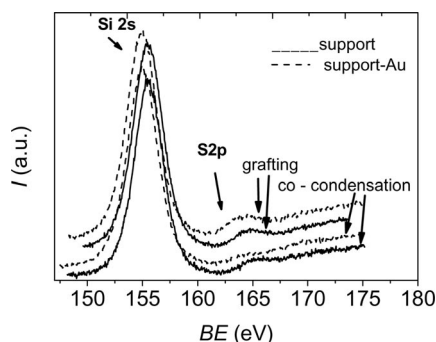


Figure 7. Si 2s and S 2p photoelectron peaks of the functionalised HMS and corresponding supported-gold samples.

In Figure 8, the Au 4f spectra of the two gold-containing samples are given. The rising signal observed at the high energy side of the Au 4f spectrum of the co-condensed sample results from the X-ray satellite peak of Si 2p, which, in this particular sample, is quite intense with respect to the gold signal.

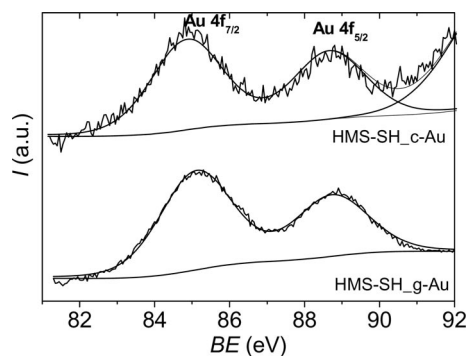


Figure 8. Au 4f photoelectron peaks in supported-gold functionalised HMS samples.

From the fitting of the experimental curves and the appropriate sensitivity factors, the Au/Si and S/Si atomic ratios were calculated. The XPS data of the gold samples are summarised in Table 3. The binding energy of the Au 4f_{7/2} at ca. 85 eV is typical of a slightly positively charged gold atom (Au⁺), whereas S 2s (at ca. 228 eV) and S 2p (at ca. 164 eV) are typical of sulfur atoms as in –SH groups.^[9,28] As obtained from the S/Si atomic ratio given in Table 3, the amount of surface sulfur in the gold sample derived from the co-condensed support is much lower than that from the grafted support, in spite of the same analytical concentration. This result is in agreement with the NMR spectra, which show correspondingly smaller peaks for the T_n units. The amount of surface gold is 4 times less in the co-condensed sample. The lower amount of gold may, in part, be due to the bigger Au particle sizes, as determined by XRD, and, in part, to the embedding of gold inside the pore structure, as probably driven by the co-condensed mercaptopropyl groups.

Table 3. Photoelectron binding energies and XPS-derived atomic ratios of the gold-containing samples.

Samples	Au 4f _{7/2} (eV)	S 2s (S2p) (eV)	Au/Si	S/Si
HMS-SH_c-Au	84.8	227.9 (163.9)	0.0025	0.001
HMS-SH_g-Au	85.1	228.1 (164.0)	0.01	0.02

The EXAFS spectra were collected at the Au L_{III} edge (11919 eV) to obtain information on the nearest neighbours of the absorbing Au atoms. The strong S–Au chemical bond (34 kcal/mol) should indeed provide a good opportunity to investigate S–Au interaction in SH-functionalised HMS matrices. The occurrence of such interactions could give an indication on the position of the thiol groups in the two differently functionalised materials.^[29]

The results are summarised in Table 4 and in Figure 9, which shows the Fourier transform of the EXAFS data (left panel) and the EXAFS signal (right panel). As observed in Figure 9, the sample obtained in a single-step by co-condensation exhibits similar features of the Au foil, which indicates that the local environment of gold is unaffected by the presence of the thiol group. This result suggests that the thiol groups, which are placed mostly inside the meso-

Table 4. Values of the nearest-neighbour distance of Au clusters (R_i), coordination number (N_i) and Debye-Waller factors (σ_i^2) at room temperature obtained from Fourier spectra and k space analysis.

Sample	R_i (± 0.02) (Å)	N_i (± 0.5)	σ_i^2 (± 0.0005) (Å ²)
HMS-SH_c-Au			
$i = 1$	2.87 ^[a]	11.8	0.0046
$i = 2$	4.05	5.9	0.0058
$i = 3$	4.98	23.4	0.0058
$i = 4$	5.73	11.6	0.0077
HMS-SH_g-Au			
$i = 1$ (Au–Au)	2.86 ^a	6.8	0.0113
$i = 2$ (Au–S)	2.29	2.0	0.0020

[a] The error for the first shell is (± 0.01).

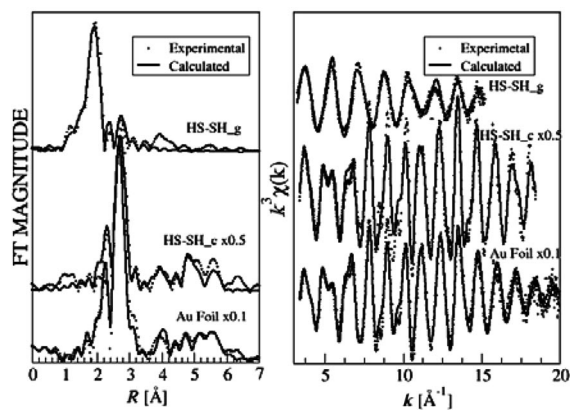


Figure 9. Au L_{III}-edge EXAFS analysis of gold samples supported on thiol functionalised HMS. Left panel: Fourier transform spectra uncorrected for the phase shift; right panel: EXAFS signals.

rous structure, in accord with the NMR spectroscopic data, are somehow inaccessible to the depositing gold. On the contrary, the sample of gold supported on the grafted functionalised silica exhibits distinctly the presence of Au–S distances in the second shell and Au–Au distances in the first shell. Therefore, it can be concluded that, by probing the nearest-neighbour interactions of gold, the two adopted procedures for the functionalisation of HMS afforded different localisation of the –SH groups. According to the EXAFS analysis, gold was successfully anchored to the –SH groups of the grafted functionalised HMS support, and in contrast, it grew as bigger metal particles in the co-condensed support.

Conclusions

A comparative study between the grafting and the direct synthesis of thiol-functionalised HMS materials, through the use of complementary surface and bulk techniques, has confirmed a direct relationship between the localisation of the –SH group and the two functionalisation procedures. In agreement with the literature and as shown by the N_2 adsorption–desorption isotherms, functionalisation by post-synthesis grafting of HMS led to a substantial decrease in the original surface area and pore sizes. The single-step procedure involving removal of templates by chemical extraction, rather than by calcination as for pure HMS, produced a functionalised material with similar textural properties as that of pure HMS. According to ^{29}Si $\{^1\text{H}\}$ CP-MAS NMR spectra and to XPS data, thiol-functionalisation occurred in both samples, however, the mercapto groups in the co-condensed sample are more homogeneously distributed along the pores, which are located deeper in the porous structure. In accord, as derived from the XPS analysis, much less sulfur was present at the surface of the co-condensed support relative to the grafted one. In the case of the gold supported co-condensed sample, XRD, XPS and EXAFS analysis confirmed the presence of big particles of metallic gold that do not interact with the thiol groups. On the other hand, and quite clearly, the EXAFS analyses evidenced Au–S bonding in the grafted sample, which corresponds to a better surface dispersion of the gold. On the basis of the above information, the localisation of the thiol groups in the two different cases can be visualised as in Figure 10. The different types of silanol groups, as discussed in the ^{29}Si $\{^1\text{H}\}$ CP-MAS NMR study, are pictured. In particular, T1, T2 and the fully condensed T3 are present in the grafted sample, whereas mainly T3 ones are present in the co-condensed sample. With regard to the gold distribution over the supports, it can be inferred that in the post-synthesis route, the –SH groups, spread over the outer surface, control the process of metal growth by interacting with gold. This limits the metal particle size and also prevents migration of gold inside the pores. In the direct synthesis, the thiols, more uniformly distributed inside the pores, do not exercise an effective ligand role, with the con-

sequent growth of big gold metal particles. On the basis of these results, the functionalisation by post-synthesis grafting appears more promising for catalytic purposes.

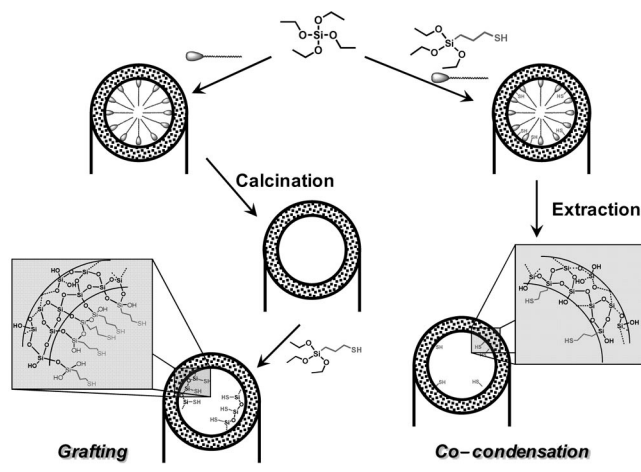


Figure 10. Schematic representation of mercapto-functionalisation by the grafting and co-condensation methods.

Experimental Section

Synthesis of Materials

Synthesis of Thiol-Functionalised HMS Silica – Grafting Procedure:

The mesostructured HMS material was synthesised according to a published procedure.^[14] Basically, HMS was assembled from 4:1 molar mixtures of tetraethyl orthosilicate (TEOS) (Aldrich) as the inorganic precursor and dodecylamine (DDA) (Aldrich) as the structure-directing surfactant in 9:1 (v/v) water/ethanol. DDA (ca. 49 mmol) was dissolved in ethanol (50 mL) and H_2O (450 mL). The surfactant solution was heated to 60 °C and TEOS (196 mmol) was added. The gel mixture thus obtained was kept, whilst stirring, in a closed Teflon vessel at 60 °C for 20 h. The reaction product was filtered, washed with distilled water and dried at room temperature for 24 h. The surfactant was removed by calcination in air at 600 °C for 4 h. The attainment of the ordered mesoporous structure was confirmed by SAXS and by the typical type IV N_2 adsorption–desorption isotherm.^[23,30] The obtained material was then activated by treating it overnight at 150 °C. The required amount of 3-MPTES (mmol SH/mmol SiO_2 = 0.09) was added to the activated oxide suspended in anhydrous toluene. Anhydrous conditions are indeed important to favour condensation with the surface silanol groups. The suspension was kept at 100 °C under reflux overnight. The product was vacuum filtered and washed with toluene and ethanol. Finally, it was washed with distilled water to hydrolyse the remaining ethoxy groups and then it was dried at 80 °C overnight. The propyl-SH/ SiO_2 weight ratio (0.13) was determined by TGA. The obtained sample was labelled as HMS-SH_g.

Synthesis of Thiol-Functionalised HMS Silica. Co-condensation Procedure:

The synthesis in this case was similar to that above. The only difference was that the required amount of 3-MPTES (mmol SH/mmol SiO_2 = 0.09) was added to the mixture of TEOS and DDA in water/ethanol directly. This technique, referred to as the direct addition pathway, was applied by Mercier and Pinnavaia to organoalkoxysilanes with short organic moieties, which replaced the equivalent amount of TEOS.^[31] In order to avoid the removal of the thiol-containing organic groups, after drying at room tem-

perature for 24 h, the resulting powder was washed by Soxhlet extraction over ethanol for 24 h. The propyl-SH/SiO₂ weight ratio (0.13) was determined by TGA. The sample was labelled as HMS-SH_c.

Synthesis of Gold-Containing Samples: The gold-containing samples were prepared by wet impregnation of the support with an aqueous solution of AuCl₃ (from Aldrich) followed by overnight drying at room temperature and overnight drying at 120 °C. Prior to gold impregnation, the supports were sieved, and only powders with particle sizes in the range 200–400 µm were used. Two samples, HMS-SH_c-Au and HMS-SH_g-Au, were prepared. The loading of gold, chosen with a ratio of 1:10 with respect to the anchored –SH groups, was 3 wt.-%, as ascertained by X-ray fluorescence analysis. Both samples were characterised by a mauve colour.^[22]

Characterisation: The microstructural properties of the materials were determined from N₂ adsorption–desorption isotherms at –196 °C by using a Sorptomat 1900 (Carlo Erba) instrument. Before the measurements, samples were heated in vacuo at 120 °C for 2 h. Specific surface areas were obtained according to the Brunauer–Emmett–Teller (BET) method. The pore size distributions were obtained by using the Barrett–Joyner–Hellenda (BJH) model applied to the desorption branch of the isotherms.^[23]

XRD patterns were measured with a Bruker goniometer by using Ni-filtered Cu-K α radiation. A proportional counter and 0.05° step sizes in 2 θ were used. The assignment of the crystalline phases was based on the JPDFS powder diffraction file cards.^[32] From the line broadening of the main reflection peaks, by using the Scherrer equation, Au particle sizes above the detection limits of 3 nm were determined.^[33] SAXS measurements were performed with a BRUKER AXS NANOSTAR instrument with step sizes of 0.02° in 2 θ .

X-ray fluorescence was performed with the Bruker S2 Ranger spectrophotometer.

Thermogravimetric analyses were performed on a TGA Q500 V20.8 Build 34 instrument. The sample (10 mg) was treated in flowing N₂ at 60 mL/min from room temperature to 800 °C with a heating rate of 10°/min. The weight loss was recorded with 1 point for second.

The X-ray photoelectron spectroscopy analyses were performed with a VG Microtech ESCA 3000 Multilab spectrometer, by using a non-monochromatised Al-K α source (1486.6 eV) run at 14 kV and 15 mA. Survey spectra were collected at a constant pass energy of 50 eV, individual peak energy regions were collected at a constant pass energy of 20 eV. Samples were mounted on a stub holder by using double-sided adhesive tape. The C 1s peak, set at 285.1 eV, arising from adventitious carbon, was used as reference for the binding energy values. Differential surface charging was ruled out by checking the reproducibility of XPS results in repeated scans under different X-ray exposures. The analysis of the peaks was performed with the software provided by VG manufacturer, on the basis of a non-linear least-square fitting routine by using a weighted sum of Lorentzian and Gaussian component curves after background subtraction, according to Shirley and Sherwood.^[34] Atomic concentrations were calculated from peak areas with the standard set of VG sensitivity factors. The binding energy values are quoted with a precision of ± 0.15 eV, and the atomic percentage with a precision of $\pm 10\%$.

²⁹Si cross-polarisation magic angle spinning nuclear magnetic resonance (²⁹Si {¹H} CP-MAS NMR) spectra were obtained at room temperature by means of a Bruker Avance II 400 MHz (9.4 T) spectrometer operating at 79.4 MHz for the ²⁹Si nucleus with a MAS

rate of 5 kHz, 4096 scans and a repetition delay of 8 s. A contact time of 8 ms was optimised on the samples through variable contact time (VCT) experiments in order to obtain the best signal to noise ratio. The relative area distribution of the signals did not change by varying the contact time. The optimisation of the Hartmann–Hahn condition was obtained by means of a Q8M8 (Si[(CH₃)₃]₈-Si₈O₂₀) standard.^[35] Samples were compressed in 4-mm zirconia rotors with Kel-F (PCTFE) caps. Deconvolution was performed by the Levenberg–Marquardt non-linear least-squares method, and Downhill Simplex algorithms were used for estimating peak parameters.

X-ray absorption spectra were recorded at the L_{III} Au absorption edge (11.920 KeV) at the BL 11.1 beamline of a ELETTRA Sincrotrone Trieste S.C.P.A. instrument, operating at an energy of 2.4 GeV with a 130 mA storage ring current. The beamline was equipped with a Si (1 1 1) double crystal monochromator with an energy resolution of 2×10^{-4} eV. In addition to those of the catalyst samples, EXAFS spectra were also acquired for the Au foil (internal standard reference for the energy calibration) and the AuCl₃ samples, as structural references for the Au clusters in the support matrix. EXAFS measurements of the reference samples and the Au/silica catalysts were performed in transmission mode by using two ionisation chambers filled with a N₂/Ar mixture at different compositions for the incident I₀ and transmitted I₁ beam. The samples were crushed by grinding in a mortar, pressed in self-supporting wafers and mounted in a sample holder suitable for EXAFS data collection. The measurements were then performed at liquid-nitrogen temperature (LN) to limit the thermal disorder effects, which damp the EXAFS oscillations, thus allowing the collection of very high-quality data, well above the instrumental noise, in a wide range of k photoelectron wave vectors ($k = [(2m_e/h^2)(E - E_0)]^{1/2}$, where m_e is the electron rest mass, E the photon energy and E_0 the edge energy). The data were extracted and analysed with the GNXAS package, which allowed the suitability of a given structural model to be assessed by simulation and the fitting to the data of the calculated EXAFS spectrum obtained by evaluation of the component single- and multiple-scattering path signals.^[36,37]

Acknowledgments

Support by the European Community, Network of Excellence (NoE) IDECAT (Integrated Design of Catalytic Nanomaterials for Sustainable Production) and the COST D36 action is acknowledged. NMR experimental data were provided by Centro Grandi Apparecchiature – UniNetLab – Università di Palermo, funded by P.O.R. Sicilia 2000-2006, Misura 3.15 Azione C Quota Regionale. The authors thank Dr. Diego Messina for the TGA measurements.

- [1] C. T. Kresge, M. E. Leonowicz, W. J. Roth, J. C. Vartuli, J. S. Beck, *Nature* **1992**, 359, 710–712.
- [2] A. Corma, *Chem. Rev.* **1997**, 97, 2373–2419.
- [3] A. Taguchi, F. Schuth, *Microporous Mesoporous Mater.* **2005**, 77, 1–45.
- [4] T. Linssen, K. Cassiers, P. Cool, E. F. Vansant, *Adv. Colloid Interface Sci.* **2003**, 103, 121–147.
- [5] J. C. Vartuli, K. D. Schmitt, C. T. Kresge, W. J. Roth, M. E. Leonowicz, S. B. McCullen, S. D. Hellring, J. S. Beck, J. L. Schlenker, D. H. Olson, E. W. Sheppard, *Chem. Mater.* **1994**, 6, 2317–2326.
- [6] R. Ryoo, S. Jun, *J. Phys. Chem. B* **1997**, 101, 317–320.
- [7] D. Zhao, J. Feng, Q. Huo, N. Melosh, G. H. Fredrickson, B. F. Chmelka, G. D. Stucky, *Science* **1998**, 279, 548–552.
- [8] A. Stein, B. J. Melde, R. C. Schroden, *Adv. Mater.* **2000**, 12, 1403–1419.

- [9] S. Shylesh, P. P. Samuel, Ch. Srilakshmi, R. Parisha, A. P. Singh, *J. Mol. Catal. A* **2007**, 274, 153–158.
- [10] A. Sayari, S. Hamoudi, *Chem. Mater.* **2001**, 13, 3151–3168.
- [11] J. Brown, R. Richer, L. Mercier, *Microporous Mesoporous Mater.* **2000**, 37, 41–48.
- [12] M. H. Lim, A. Stein, *Chem. Mater.* **1999**, 11, 3285–3295.
- [13] I. Diaz, F. Mohino, J. Pérez-Pariente, E. Sastre, *Appl. Catal. A* **2001**, 205, 19–30.
- [14] J. Brown, L. Mercier, T. J. Pinnavaia, *Chem. Commun.* **1999**, 69–70.
- [15] L. Mercier, T. J. Pinnavaia, *Adv. Mater.* **1997**, 9, 500–503.
- [16] E. F. S. Vieira, J. de A. Simoni, C. Airoidi, *J. Mater. Chem.* **1997**, 7, 2249–2252.
- [17] X. Cheng, X. Feng, J. Liu, G. E. Fryxell, M. Gong, *Separ. Sci. Technol.* **1999**, 34, 1121–1132.
- [18] S. J. L. Billinge, E. J. McKimmy, M. Shatnawi, H. Kim, V. Petkov, D. Wermeille, T. J. Pinnavaia, *J. Am. Chem. Soc.* **2005**, 127, 8492–8498.
- [19] C. Delacôte, F. O. M. Gaslain, B. Lebeau, A. Walcarius, *Talanta* **2009**, 79, 877–886.
- [20] H. Wellmann, J. Rathousky, M. Wark, A. Zukal, G. Schulz-Ekloff, *Microporous Mesoporous Mater.* **2001**, 44, 419–425.
- [21] Y. Guari, C. Thieuleux, A. Mehdi, C. Reyè, R. J. P. Corriu, S. Gomez-Gallardo, K. Philippot, B. Chaudret, *Chem. Mater.* **2004**, 15, 2017–2024.
- [22] G. C. Bond, D. T. Thompson, *Catal. Rev. Sci. Eng.* **1999**, 41, 319–388.
- [23] S. J. Gregg, K. S. Sing, *Adsorption, Surface Area and Porosity*, 2nd ed., Academic Press, San Diego, **1982**.
- [24] M. Luhmer, J. B. Espinose, H. Hommed, A. P. Legrand, *Magn. Reson. Imaging* **1996**, 14, 911–913.
- [25] X. Feng, G. E. Fryxell, L.-Q. Wang, A. Y. Kim, J. Liu, K. M. Kemner, *Science* **1997**, 276, 923–926.
- [26] N. Petkov, N. Stock, T. Bein, *J. Phys. Chem. B* **2005**, 109, 10737–10743.
- [27] A. M. Venezia, V. La Parola, V. Nicoli, G. Deganello, *J. Catal.* **2002**, 212, 56–62.
- [28] M. P. Casaletto, A. Longo, A. M. Venezia, A. Martorana, A. Prestianni, *Appl. Catal. A* **2006**, 302, 309–316.
- [29] C. S. S. R. Kumar, M. Aghasyan, H. Modrow, E. Doomes, C. Henk, J. Hormes, R. Tittsworth, *J. Nanopart. Res.* **2004**, 6, 369–376.
- [30] N. Marin-Astorga, G. Pecchi, T. J. Pinnavaia, G. Alvez-Manoli, P. Reyes, *J. Mol. Catal. A* **2006**, 247, 145–152.
- [31] L. Mercier, T. J. Pinnavaia, *Chem. Mater.* **2000**, 12, 188–196.
- [32] JCPDS Powder Diffraction File Int. Centre for Diffraction Data, Swarthmore, **1989**; File No. 42–1467.
- [33] H. P. Klug, *X-ray Diffraction Procedure for Polycrystalline and Amorphous Materials*, Wiley, New York, **1954**.
- [34] P. M. A. Sherwood in *Practical Surface Analysis* (Eds.: D. Briggs, M. P. Seah), Wiley, New York, **1990**, p. 181.
- [35] S. R. Hartmann, E. L. Hahn, *Phys. Rev.* **1962**, 128, 2042–2053.
- [36] A. Filippini, A. Di Cicco, C. R. Natoli, *Phys. Rev. B* **1995**, 52, 15122–15135.
- [37] A. Filippini, A. Di Cicco, *Phys. Rev. B* **1995**, 52, 15135–15149.

Received: April 18, 2010
Published Online: July 1, 2010

Reactions of 1,2,4-Trithiolane and Its 4-*S*-Oxide with Diphosphane Pt⁰ Complexes

Holm Petzold,^{*,[a,b]} Thomas Weisheit,^[a] Silvio Bräutigam,^[a] Helmar Görls,^[a]
Grzegorz Mloston,^{*,[c]} and Wolfgang Weigand^{*,[a]}

Dedicated to Professor Rolf Huisgen on the occasion of his 90th birthday

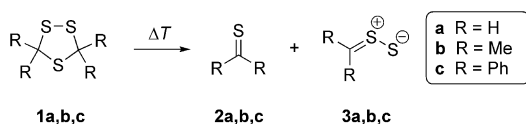
Keywords: 1,2,4-Trithiolanes / S ligands / Oxidative addition / Metallacycles / Reactive intermediates

Reactions of 1,2,4-trithiolanes with Pt⁰ complexes often proceed via an oxidative addition of the Pt⁰ complex fragment into the S–S bond and subsequent extrusion of a thioketone molecule by ring contraction. The six-membered intermediate **5a**, formed in the course of the reaction of the parent 1,2,4-trithiolane (**1a**) and Pt⁰ complex **4**, was detected by

means of low-temperature NMR spectroscopy. Stable derivatives of this type (compounds **9**, **11** and **12**) were isolated either by using (dppe)Pt⁰ complex **8** or 1,2,4-trithiolane 4-*S*-oxide (**10**). The molecular structures of platinum complexes **9**, **11** and **12**, as well as their unexpected stability, are discussed.

Introduction

1,2,4-Trithiolanes with the general structure **1** belong to the class of sulfur-rich heterocycles that are widely used as convenient precursors for the generation of the elusive thiosulfines (thiocarbonyl *S*-sulfides) **3**.^[1] Along with other intermediates of this type (thiocarbonyl ylides, thiocarbonyl *S*-oxides, thiocarbonyl *S*-imides, etc.) derived from thioketones **2**, they are considered to be so-called “sulfur-centred” 1,3-dipoles.^[1a] Huisgen and co-workers found that 3,3,5,5-tetraphenyl-1,2,4-trithiolane (**1c**) easily undergoes thermal [3+2]-cycloreversion (refluxing CHCl₃) to yield thiobenzophenone (**2c**) and diphenylthiosulfine (**3c**) (Scheme 1).^[1b]



Scheme 1. Thermal [3+2]-cycloreversion of 1,2,4-trithiolanes **1a–c**.

[a] Institut für Anorganische und Analytische Chemie, Friedrich-Schiller-Universität Jena, August-Bebel-Str. 2, 07743 Jena, Germany
Fax: +49-3641-948102
E-mail: wolfgang.weigand@uni-jena.de

[b] Institut für Chemie, TU-Chemnitz, Strasse der Nationen 62, 09111 Chemnitz, Germany

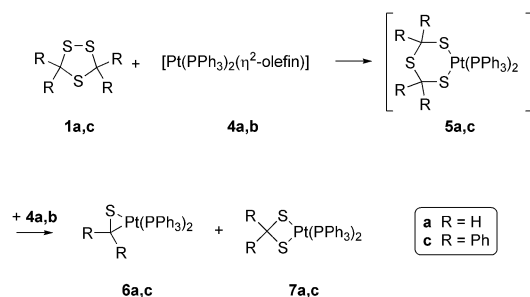
[c] Department of Organic and Applied Chemistry, University of Lodz, Tamka 12, 91-403 Lodz, Poland

Supporting information for this article is available on the WWW under <http://dx.doi.org/10.1002/ejic.200901229>.

In a recent paper, generation of parent thiosulfine **3a** from 1,2,4-trithiolane (**1a**) in the gas phase was reported.^[2a] The highly reactive intermediate **3a** was frozen in an argon matrix at 10 K and studied by means of spectroscopic methods (IR and UV/Vis spectroscopy). In addition, **3a** was transformed reversibly into the parent dithiirane H₂C(–S–S–) by selective irradiation with UV light.^[2a] Extension of this method to 3,3,5,5-tetramethyl-1,2,4-trithiolane (**1b**) revealed a smooth 1,4-H-shift in thiosulfine **3b** containing H-atoms at the β-position.^[3] In another case, the gas-phase thermolysis of a 1,2,4-trithiolane bearing two spiro-cyclobutanone rings at C(3) and C(5) yielded the ring-enlarged isomeric dithiolactone after the rearrangement of the initially formed dithiirane.^[4] These results are in good agreement with the initially postulated course of thiosulfine rearrangement,^[5] subsequently confirmed by calculations.^[1a] In addition to 1,2,4-trithiolane (**1a**), its regioisomers 1-*S*-oxide and 4-*S*-oxide were also studied in the gas phase. In both cases, thioformaldehyde *S*-oxide was found amongst the major products.^[2b]

In a series of papers, we have shown that 3,3,5,5-tetraphenyl-1,2,4-trithiolane (**1c**) reacts with [Pt(PPh₃)₂(η²-C₂H₄)] (**4a**) to yield a 1:1 mixture of thiobenzophenone complex **6c** and dithiolato complex **7c**.^[6] The mechanism of this reaction is not fully understood yet, but it seems likely that the conversion is initiated by the oxidative addition of the [Pt⁰(PPh₃)₂] fragment into the sulfur–sulfur bond to form an unstable six-membered platinacycle **5c**.^[6–8] Compound **5c** subsequently splits into **7c** and thiobenzophenone (**2c**), which then captures an additional equivalent of **4a** to afford complex **6c** (Scheme 2). The course of the reaction

depends on the phosphanes used for the preparation of complexes of type **4**. In the case of complexes containing a diphosphane unit exhibiting a small P–Pt–P angle, the reaction proceeds via [3+2]-cycloreversion of **1c** as the slowest, rate-determining step.^[9] In general, the oxidative addition of Pt⁰ complex fragments into the S–S bond of sulfur-rich heterocycles is attracting increasing interest with respect to the synthesis of thiolato, sulfenato and sulfinato complexes.^[7–10] In a recent paper, we showed that the reaction of [Pt(PPh₃)₂(η²-nb)] (**4b**) (nb = norbornene) with 3,5-(bis-spiro)cyclohexyl-1,2,4-trithiolane and its 1-*S*-oxide and 4-*S*-oxide regioisomers gives equimolar mixtures of dithiolato/thioketone, thiolato-sulfenato/thioketone and dithiolato/sulfine complexes, respectively.^[8]



Scheme 2. Reaction of 1,2,4-trithiolanes with [Pt(PPh₃)₂(η²-olefin)] (olefin = C₂H₄ or nb) (**4a,b**).

The aim of the present work was the synthesis and characterization of platinumacycles of type **5** derived from the parent 1,2,4-trithiolane (**1a**) and its 4-*S*-oxide **10**, which are postulated to appear as initial intermediates in the reaction pathway.

Results and Discussion

Pt⁰ complexes, [PtL₂(η²-C₂H₄)] (**4a**), [PtL₂(η²-nb)] (**4b**) (L = PPh₃) and [PtL₂(olefin)] (**8**) (L = 1/2 Ph₂PCH₂CH₂PPh₂, olefin = C₂H₄) were treated with 1,2,4-trithiolane (**1a**) or its 4-*S*-oxide **10**.

Reaction of the parent 1,2,4-trithiolane (**1a**) with Pt⁰ complex **4b** was performed in [D₈]toluene at low temperature in an NMR tube. Shortly after **1a** and **4b** were mixed at –50 °C, the recorded spectra showed only signals of the starting compounds. After a few minutes, and warming to –10 °C, a new, weak signal appeared in the ³¹P NMR spectrum at δ = 22.7 ppm. Further warming of the solution to 22 °C resulted in a higher intensity of this signal and the appearance of the characteristic ¹⁹⁵Pt satellites [¹J(P,Pt) = 2825 Hz]. Other new signals corresponding to an AB spin system [δ = 24.9/27.9 ppm, ¹J(P,Pt) = 3311/4348 Hz, ²J(P,P) = 17 Hz] as well as an A₂ system [δ = 21.5 ppm, ¹J(P,Pt) = 2890 Hz] were observed at 25 °C. The intensity of the signal localized at δ = 22.7 ppm decreased further after one day at 25 °C, and the two new spin systems became more intense.

The signal at δ = 21.5 ppm was assigned to the known dithiolato complex **7a**.^[11] In addition, this complex shows a characteristic triplet, with ¹⁹⁵Pt satellites [³J(Pt,H) =

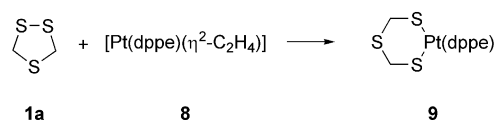
43.4 Hz and ⁴J(P,H) = 1.7 Hz], at δ = 5.54 ppm in the ¹H NMR spectrum. The AB spin system points to formation of thioformaldehyde complex **6a**, and the observed coupling constant fits well with other thiocarbonyl complexes of this type.^[6,8,9,12] The ¹H NMR spectrum shows a singlet at δ = 3.44 ppm with ²J(Pt,H) = 46.0 Hz.

In order to gain more information on the structure of the transient complex, related to the singlet localized at δ = 22.7 ppm, Pt⁰ complex **8** was treated with **1a**. After one hour at room temperature, the formation of a new product was detected by means of TLC. The ³¹P NMR spectrum exhibits an A₂ system localized at δ = 48.1 ppm with characteristic ¹⁹⁵Pt satellites [¹J(Pt,P) = 2757 Hz]. Interestingly, in the ¹H NMR spectrum a doublet at δ = 4.35 ppm [⁴J(P,H) = 8.4 Hz, ³J(Pt,H) = 54 Hz, 4 H], attributed to two equivalent CH₂ units, was also found. Elemental analysis and single-crystal X-ray diffraction confirmed the structure of complex **9** (Tables 1 and 2, Scheme 3). Unfortunately, complex **9** is disordered around S(2) in the solid state, and therefore bond lengths in that part of the molecule could not be determined precisely (Figure 1).

Table 1. Selected bond lengths [Å] and bond angles [°] for complexes **9**, **11** and **12**.

Complex	9 ^[a]	11	12
Pt–P(1)	2.2475(14)	2.2961(15)	2.2546(18)
Pt–P(2)	2.2458(14)	2.2897(14)	2.2476(19)
Pt–S(1)	2.3365(15)	2.3279(15)	2.3380(19)
Pt–S(3)	2.3474(16)	2.3537(15)	2.347(2)
S(1)–C(1)	—	1.830(7)	1.812(8)
C(1)–S(2)	—	1.798(7)	1.796(8)
S(2)–C(2)	—	1.824(7)	1.832(8)
C(2)–S(3)	—	1.783(7)	1.772(9)
S(2)–O(1)	—	1.493(5)	1.481(6)
P(1)–Pt–P(2)	86.49(5)	97.25(5)	86.02(7)
S(1)–Pt–S(3)	93.71(6)	90.82(5)	92.92(7)
P(1)–Pt–S(3)	175.57(5)	175.78(6)	175.66(8)
P(2)–Pt–S(1)	172.56(5)	174.58(5)	174.51(7)
P(1)–Pt–S(1)	89.85(5)	88.14(5)	89.49(7)
P(2)–Pt–S(3)	90.26(6)	83.85(5)	91.77(7)
Pt–S(1)–C(1)	—	107.7(2)	105.9(3)
S(1)–C(1)–S(2)	—	112.1(4)	110.9(4)
C(1)–S(2)–C(2)	—	97.4(3)	99.0(4)
S(2)–C(2)–S(3)	—	120.6(4)	121.5(5)
C(2)–S(3)–Pt	—	104.4(3)	105.3(3)

[a] C(1), S(2) and C(2) are disordered.



Scheme 3. Ring enlargement of 1,2,4-trithiolane (**1a**) after treatment with [Pt(dppe)(η²-C₂H₄)] (**8**).

Complex **9** is stable at room temperature and does not extrude thioformaldehyde. On the basis of ³¹P NMR spectroscopic data, we assumed that in the reaction of **1a** with **4b** the corresponding platinumacycle **5a** [δ = 22.7 ppm, ¹J(P,Pt) = 2825 Hz] would be formed analogously, but it spontaneously eliminated thioformaldehyde to yield complexes **6a**

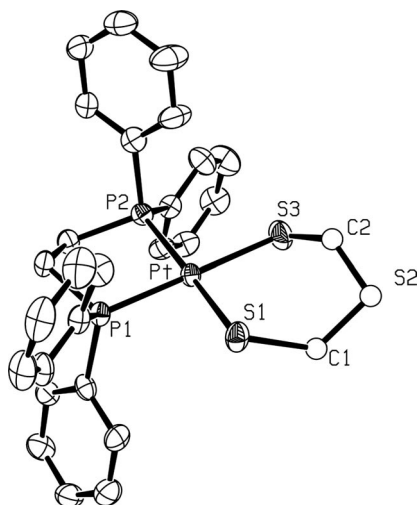
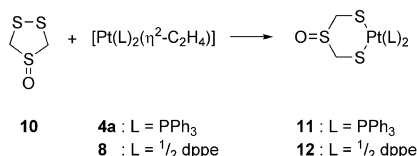


Figure 1. ORTEP drawing (with 50% probability ellipsoids) of the molecular structure of complex **9**. S2 and the adjacent carbon atoms are disordered. Therefore, the bond lengths and bond angles between C2, S2 and C1 are not reliable. Hydrogen atoms are omitted for clarity.

and **7a** with an additional equivalent of **4b**. According to literature data, Ni^{II} and Pd^{II} complexes analogous to **9** have been obtained by treatment of the corresponding dichlorido complexes [M(dppe)Cl₂] (M = Ni, Pd) with 1,3-dimercapto-2-thiapropane S(CH₂SH)₂.^[13] Moreover, the reaction of Fe₂(CO)₉ with spiro-cycloaliphatic substituted 1,2,4-trithiolanes of type **1** led to similar metallacycles containing even more crowded substituents, for example, the adamantane skeleton.^[14]

In contrast to **1a**, reaction of the “symmetrical” *S*-oxide **10** with complexes **4a** and **8** yielded a single product in each case (Scheme 4). The ³¹P NMR spectra of both products are very similar, exhibiting a singlet (δ = 26.3 ppm and 49.5 ppm, respectively) with ¹⁹⁵Pt satellites [¹J(P,Pt) = 2908 and 2790 Hz, respectively]. The ¹H NMR spectra show a characteristic AB system at δ = 3.91/4.19 ppm [²J(H,H) = 12.6 Hz] and δ = 4.01/4.25 ppm [²J(H,H) = 12.6 Hz], respectively. Finally, the FTIR spectra have intense absorption bands at 1032 and 1027 cm^{−1}, characteristic of sulfoxides (R₂SO). From these data, the complex structures were postulated as platinacycle **11** and **12**, respectively. Diffusion of pentane vapours into solutions of **11** in thf and **12** in chloroform yielded yellow crystals for both complexes, suitable for single-crystal X-ray diffraction analysis (Tables 1 and 2).



Scheme 4. Reactions of Pt⁰ complexes **4a** and **8** with 1,2,4-trithiolane 4-*S*-oxide (**10**).

Both complexes are distorted square planar (Figures 2 and 3). The P–Pt–P angles of 97.3(5)° in **11** and 86.02(7)° in **12** differ significantly. The bond lengths for Pt–S and Pt–P around the platinum atom correspond to the range expected for dithiolato Pt^{II} complexes.^[9–10]

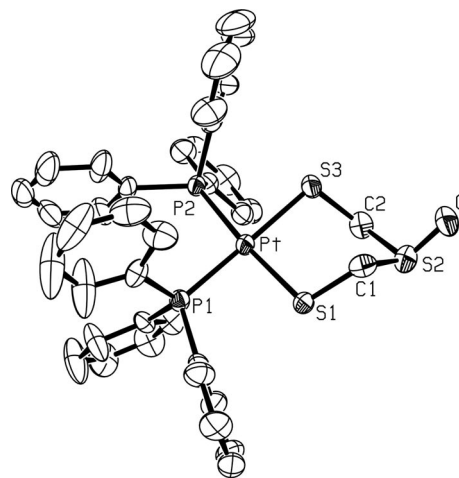


Figure 2. ORTEP drawing (with 50% probability ellipsoids) of the molecular structure of complex **11**. Hydrogen atoms are omitted for clarity.

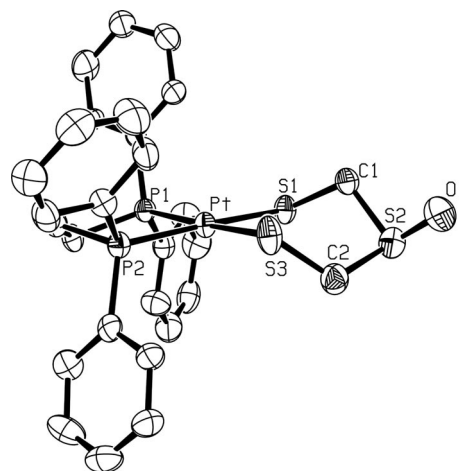
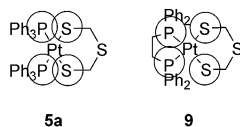


Figure 3. ORTEP drawing (with 50% probability ellipsoids) of the molecular structure of complex **12**. Hydrogen atoms are omitted for clarity.

The six-membered platinacycle adopts a distorted chair conformation. In contrast to starting compound **10**, the oxygen atom is located in the equatorial position in both **11** and **12**. The determined S–O bond length in **12** [1.481(6) Å] is similar to that found in **10** [1.496(2) Å]^[15]. The appearance of only one AB spin system for the CH₂ groups in the ¹H NMR spectra of **11** and **12** indicates a high flexibility for the ring system in solution.

It is still an open question why **5a** decomposes spontaneously to yield **6a** and **7a** whereas metallacycle **9** is stable at room temperature and can be isolated. A possible explanation is based on the assumption that there is a significant decrease in the intramolecular repulsion between the thiolato ligands and the phosphane ligands after replacement of

the two PPh₃ ligands by dppe (Scheme 5). Fragmentation of **5a** to thioformaldehyde (**2a**) and **7a** results in a smaller S–Pt–S angle in **7a** and therefore leads to a decrease in the repulsion between the sulfur and phosphorus atoms located around the platinum atom. This hypothesis finds additional support in the significantly larger intramolecular S...P distances S(1)...P(1) and S(3)...P(2) (3.238 Å and 3.256 Å, respectively) in **9**. Both distances are significantly longer than those found for **11** (3.216 Å and 3.103 Å, respectively).



Scheme 5. Schematic presentation of the intramolecular repulsion between the phosphane and thiolato ligands around the platinum centres in **5a** and **9**.

Alternatively, dissociation of one of the two phosphanes might form a free coordination site for the fragmentation reaction to form a thioformaldehyde dithiolato complex. Therefore, dissociation of one PPh₃ could be the key step for the fragmentation. In addition, the increased steric repulsion, as well as the chelate effect, would favour dissociation of one PPh₃ in **5a** and **11**. To gain more information on possible phosphane dissociation, we treated complex **11** with free dppe. Release of the intramolecular repulsion energy and the chelate effect should form **12** and free PPh₃ in the course of this reaction. Indeed, complex **12** was detected as the main product in this reaction. Formation of some unidentified products hampered the precise determination of the rate constant. However, the decay of **11** depends on the concentration of dppe in the solution, making a dissociative mechanism unlikely. The increased stability of **11** relative to **5a** might be explained by a different activation energy in one of the involved intermediates. It is not trivial to estimate the role of the oxidation of the sulfur atom on several intermediate steps during the fragmentation of **5a**. In general, it can be assumed that sulfenato ligands are weaker sigma donors than thiolato ligands. This is supported by the elongation of the Pt–S bond upon oxidation of the thiolato ligand.^[8,10c,10d,10g,10h] On the other hand, the sulfenato ligands showed a larger *trans* influence, indicating that they are stronger sigma donors. Moreover, it was found that oxidation of thiolato ligands to the sulfenato and sulfinato ligands can cause shortening of the metal–sulfur bond.^[16] More detailed investigation would be necessary to explain convincingly the enhanced stability of **11**.

Conclusions

In summary, stable derivatives of six-membered platinacycles of type **5** were synthesized, isolated and characterized. The fragmentation of **5a** into thioformaldehyde complex **6a** and dithiolato complex **7a** was confirmed by means of in situ NMR spectroscopy. The stability of the platinacycle **9** with respect to **5a** might be explained by re-

lease of the intramolecular ligand repulsion. Moreover, complexes **11** and **12** display an enhanced stability resulting from oxidation of the thioether function.

Experimental Section

All reactions were performed under an argon atmosphere by using the standard “Schlenk technique”. 1,2,4-Trithiolane (**1a**)^[17], its 4-S-oxide **10**^[15], as well as [Pt(PPh₃)₂(η²-C₂H₄)] (**4a**),^[18] [Pt(PPh₃)₂(η²-nb)] (**4b**)^[9a] and [Pt(dppe)(η²-C₂H₄)] (**8**),^[19] were prepared according to known protocols. The NMR spectra were recorded with Bruker DPX 400 and DPX 200 instruments. Chemical shifts refer to signals of the solvent or 85% H₃PO₄ (external standard) for ³¹P NMR spectra. The IR spectra were recorded with a PERKIN-ELMER system 2000 FTIR instrument. Elemental analyses were performed with a Vario EL III CHNS (Elementaranalysen GmbH Hanau) instrument.

³¹P{¹H} NMR In Situ Monitoring of the Reaction of **1a with **4b**:** Compound **1a** (4 mg, 0.0032 mmol) dissolved in [D₈]toluene (0.3 mL) was added dropwise to a cooled (–50 °C) solution of **4b** (26 mg, 0.032 mmol) in [D₈]toluene (0.6 mL) in a NMR tube. The NMR tube was immediately transferred into the NMR spectrometer, and the reaction was monitored from –50 °C to 25 °C. Selected spectra are presented in the Supporting Information.

X-ray Analysis: The intensity data were collected with a Nonius KappaCCD diffractometer, by using graphite-monochromated Mo-K_α radiation (λ = 0.71069 Å) at –90 °C. Data were corrected for Lorentz and polarization effects and for absorption effects.^[12–22] The structures were solved by direct methods (SHELXS)^[23] and refined by full-matrix least-squares techniques against |F_o|² (SHELXL-97)^[24]. All hydrogen atoms of the structures were included at calculated positions with fixed thermal parameters (1.2–1.5 times that of the related non-hydrogen atom). All non-disordered, non-hydrogen atoms were refined anisotropically.^[24] Complex **9** is disordered around S(2); this disorder could not be resolved. Therefore, bond lengths and bond angles in this part of the molecule are not discussed. ORTEP-3 for Windows^[25] was used for structure representations. More information on structure refinement is given in Table 2 and ref.^[26]

[Pt(dppe){(SCH₂)₂S}] (9**):** A solution of **8** (150 mg, 0.2 mmol) in toluene (20 mL) was added to **1a** (35 mg, 0.28 mmol) dissolved in thf (10 mL). The mixture was stirred for an additional 2 h. After that time, the volume of the solvent was reduced to ca. 3 mL. Addition of pentane (10 mL) resulted in the precipitation of the crude product as a yellow powder. The product was filtered off and washed with a small portion of pentane. Crystallization from thf/pentane yielded **9** as yellow plates (120 mg, 0.16 mmol, 82%). M. p. 130 °C (dec.); ¹H NMR (200 MHz, CDCl₃): δ = 7.76 (m, 8 H), 7.46 (m, 12 H), 4.35 [d, ³J(H,Pt) = 54 Hz, ⁴J(H,P) = 8.4 Hz, 4 H, –(S-CH₂)₂-S], 2.28 [d, ³J(H,Pt) = 25 Hz, ²J(H,P) = 18 Hz, 4 H, P-CH₂CH₂-P] ppm. ³¹P{¹H} NMR (81 MHz, CDCl₃): δ = 48.6 [s, ¹J(P,Pt) = 2757 Hz] ppm. IR (CsI): ν̄ = 3050, 2905, 1968, 1894, 1818, 1727, 1484, 1104, 821, 747, 715, 704, 690, 531, 485 (PC₃) cm^{–1}. C₂₈H₂₈OP₂PtS₃ (717.74): calcd. C 46.86, H 3.93, S 13.40; found C 46.65, H 3.94, S 13.70.

[Pt(PPh₃)₂{(SCH₂)₂S=O}] (11**):** Compound **4a** (145.0 mg, 0.20 mmol), dissolved in toluene (6 mL), was added to a stirred solution of **10** (13.6 mg, 0.10 mmol) in toluene (4 mL) at room temperature over a period of 30 min. The reaction mixture turned yellow, and a white precipitate was formed. The reaction mixture was stirred overnight, and the solid formed thereafter was filtered off.

Table 2. Data of single-crystal X-ray analyses of complexes **9**, **11** and **12**.

	9	11	12
Empirical formula	C ₂₈ H ₂₈ P ₂ PtS ₃	C ₃₈ H ₃₄ OP ₂ PtS ₃	C ₂₈ H ₂₈ OP ₂ PtS ₃ *2 CHCl ₃
Formula weight [g mol ⁻¹]	717.71	859.86	972.45
<i>T</i> [°C]	−90(2)	−90(2)	−90(2)
Crystal system	Monoclinic	Orthorhombic	Monoclinic
Space group	<i>P</i> 2 ₁ / <i>n</i>	<i>P</i> 2 ₁ 2 ₁ 2 ₁	<i>P</i> 2 ₁ / <i>c</i>
<i>a</i> [Å]	8.8320(2)	11.0546(3)	16.2108(4)
<i>b</i> [Å]	23.1538(4)	14.7560(4)	13.6271(4)
<i>c</i> [Å]	13.3482(2)	21.1438(5)	18.1346(4)
<i>α</i> [°]	90	90	90
<i>β</i> [°]	100.185(1)	90	114.684(2)
<i>γ</i> [°]	90	90	90
<i>V</i> [Å ³]	2686.62(9)	3449.01(16)	3639.99(16)
<i>Z</i>	4	4	4
<i>ρ</i> [g cm ⁻³]	1.774	1.656	1.775
<i>μ</i> [cm ⁻¹]	55.91	43.73	45.8
Reflections collected	16519	20809	14342
Reflections with <i>I</i> > 2σ(<i>I</i>)	4836	7050	5172
Independent reflections/ <i>R</i> _{int}	6118/0.0550	7763/0.0440	8316/0.0806
<i>wR</i> ₂ (all reflections <i>F</i> ²) ^[a]	0.0999	0.0871	0.1397
<i>R</i> ₁ [<i>I</i> > 2σ(<i>I</i>)] ^[a]	0.0395	0.0379	0.0544
<i>Goof</i> ^[b]	1.049	1.025	0.954
Extrema Δ <i>F</i> [e Å ⁻³]	1.663/−2.147	1.844/−1.366	1.754/−2.561
Flack parameter		−0.006(7)	
Absorption correction	multi-scan	multi-scan	multi-scan
<i>T</i> _{min/max}	0.8764/0.9064	0.2080/0.2891	0.8140/0.9456
CCDC no.	634395	634396	634397

[a] Definition of *R* indices: $R_1 = (\sum ||F_o| - |F_c||) / \sum |F_o|$, $wR_2 = \{\sum [w(F_o^2 - F_c^2)^2] / \sum [w(F_o^2)^2]\}^{1/2}$ with $w^{-1} = \sigma^2(F_o^2) + (aP)^2$. [b] *Goof* = $\{\sum [w(F_o^2 - F_c^2)^2] / (N_o - N_p)\}^{1/2}$.

The product was washed with a diethyl ether/pentane mixture and dried in vacuo to yield 62.0 mg (74.3%) of **11** as a colourless solid. M. p. 218 °C (dec.); ¹H{³¹P} NMR [*J*(H,P)] by comparison with ¹H NMR] (400 MHz, CD₂Cl₂): δ = 7.39 [d, ³*J*(H,H) = 8.4 Hz, 12 H], 7.33 [t, ³*J*(H,H) = 8.0 Hz, 4 H], 7.18 [dd, ³*J*(H,H) = 8.4 Hz, ³*J*(H,H) = 8.0 Hz, 12 H], 4.18 {d, ²*J*(H,H) = 12.8 Hz, ³*J*(H,Pt) = 54.9 Hz, [⁴*J*(H,P) = 6.0 Hz], 2 H, -(S-CHH)₂-S}, 3.89 {d, ²*J*(H,H) = 12.8 Hz, ³*J*(H,Pt) = 64.4 Hz, [⁴*J*(H,P) = 7.6 Hz], 2 H, -(S-CHH)₂-S}. ³¹P{¹H} NMR (81 MHz, CDCl₃): δ = 26.3 [s, ¹*J*(P,Pt) = 2908 Hz] ppm. ¹⁹⁵Pt{¹H} NMR (58 MHz, CD₂Cl₂): δ = 167 [t, ¹*J*(Pt,P) = 2920 Hz] ppm. IR (CsI): ν̄ = 1032 (s, S=O), 542, 525, 515, 495 (PC₃) cm⁻¹. C₂₈H₂₈OP₂PtS₃ (733.74): calcd. C 53.08, H 3.99, S 11.19; found C 52.50, H 3.85, S 10.60.

[Pt(dppe)]{(SCH₂)₂S=O} (**12**): 4-*S*-Oxide **10** (25 mg, 0.17 mmol) was dissolved in toluene (10 mL). To this solution was added dropwise **8** (100 mg, 0.16 mmol) dissolved in toluene (10 mL). The solution immediately turned light green, and a white precipitate was formed after a few minutes. The reaction mixture was stirred for an additional 30 min, and the volume of the solvent was reduced to ca. 3 mL. The yellow solid was separated by filtration and washed with a pentane/ether mixture to yield **12** as crude product. Crystallization from a chloroform/ether mixture yielded analytically pure complex **12** (60 mg, 50%) as yellow needles. M. p. 218 °C (dec.); ¹H{³¹P} NMR [*J*(H,P)] from comparison with ¹H NMR] (400 MHz, CD₂Cl₂): δ = 7.78 {d, ³*J*(H,H) = 7.2 Hz, [*J*(H,P) = 11.6 Hz], 4 H}, 7.71 {d, ³*J*(H,H) = 7.6 Hz, [*J*(H,P) = 12 Hz, 4 H}], 7.48 (m, 12 H), 4.25 {d, ²*J*(H,H) = 12.6 Hz, ³*J*(H,Pt) = 51.6 Hz, [⁴*J*(H,P) = 6.4 Hz], 2 H, -(S-CHH)₂-S}, 4.01 {d, ²*J*(H,H) = 12.6 Hz, ³*J*(H,Pt) = 59.6 Hz, [⁴*J*(H,P) = 7.2 Hz], 2 H, -(S-CHH)₂-S}, 2.35 {s, *J*(H,Pt) = 38.4 Hz, ²*J*(H,P) = 24 Hz}, 4 H, P-CH₂CH₂-P} ppm. ³¹P{¹H} NMR (81 MHz, CDCl₃): δ = 49.5 [s, ¹*J*(P,Pt) = 2790 Hz] ppm. IR (CsI): ν̄ = 3053, 2935, 2935, 1484, 1435, 1188, 1104, 1027 (s, S=O), 824, 748, 715, 705, 691, 531, 486 (PC₃) cm⁻¹.

C₂₈H₂₈OP₂PtS₃ (733.74): calcd. C 45.83, H 3.85, S 13.11; found C 46.47, H 4.02, S 12.54.

Supporting Information (see footnote on the first page of this article): Low-temperature ³¹P{¹H} NMR spectra for the reaction of **4b** with **1a** as well as data on the kinetic investigation for the reaction of **11** with dppe.

Acknowledgments

H. P. acknowledges financial support from Freistaat Thüringen and the Fonds der Chemischen Industrie as well as the Deutscher Akademischer Austausch Dienst (DAAD) (PKZ D/04/11451). The authors gratefully acknowledge the donation of K₂PtCl₄ by Heraeus GmbH. We are also grateful to Prof. Dr. K. Karagioshoff for recording ¹³C{¹H,³¹P} and ³¹P{¹H} NMR spectra. G. M. is grateful to the Alexander-von-Humboldt Foundation for financial support. We also thank a reviewer for his valuable remarks.

- [1] a) J. Fabian, A. Senning, *Sulfur Rep.* **1998**, *21*, 1–42; b) R. Huisgen, J. Rapp, *Tetrahedron* **1997**, *53*, 939–960.
- [2] a) G. Mloston, J. Romanski, H. P. Reisenauer, G. Maier, *Angew. Chem.* **2001**, *113*, 401–404; *Angew. Chem. Int. Ed.* **2001**, *40*, 393–396; b) G. Mloston, J. Romanski, M. L. McKee, H. P. Reisenauer, P. R. Schreiner, *Eur. J. Org. Chem.* **2010**, 2132–2137.
- [3] G. Maier, H. P. Reisenauer, J. Romanski, H. Petzold, G. Mloston, *Eur. J. Org. Chem.* **2006**, 3721–3729.
- [4] G. Mloston, J. Romanski, H. P. Reisenauer, H. Petzold, W. Weigand, P. R. Schreiner, *Eur. J. Org. Chem.* **2008**, 2998–3003.
- [5] A. Senning, *Angew. Chem.* **1979**, *91*, 1006–1008; *Angew. Chem. Int. Ed. Engl.* **1979**, *18*, 941–943.
- [6] W. Weigand, R. Wünsch, C. Robl, G. Mloston, H. Nöth, M. Schmidt, *Z. Naturforsch., Teil B* **2000**, *55*, 453–458.

- [7] W. Weigand, S. Bräutigam, G. Mloston, *Coord. Chem. Rev.* **2003**, *245*, 167–175.
- [8] H. Petzold, S. Bräutigam, H. Görls, W. Weigand, J. Romanski, G. Mloston, *Eur. J. Inorg. Chem.* **2007**, 5627–5632.
- [9] a) H. Petzold, H. Görls, W. Weigand, *J. Organomet. Chem.* **2007**, *692*, 2736–2742; b) T. Weisheit, H. Görls, H. Petzold, G. Mloston, W. Weigand, *Eur. J. Inorg. Chem.* **2009**, 3545–3551.
- [10] a) H. Petzold, S. Bräutigam, H. Görls, W. Weigand, M. Celeda, G. Mloston, *Chem. Eur. J.* **2006**, *12*, 8090–8095; b) T. Shigetomi, H. Soejima, Y. Nibu, K. Shioji, K. Okuma, Y. Yokomori, *Chem. Eur. J.* **2006**, *12*, 7742–7748; c) A. Ishii, M. Murata, H. Oshida, K. Matsumoto, J. Nakayama, *Eur. J. Inorg. Chem.* **2003**, 3716–3721; d) A. Ishii, M. Saito, M. Murata, J. Nakayama, *Eur. J. Org. Chem.* **2002**, 979–982; e) W. Weigand, R. Wünsch, *Chem. Ber.* **1996**, *129*, 1409–1419; f) A. Ishii, M. Ohishi, N. Nakata, *Eur. J. Inorg. Chem.* **2007**, 5199–5206; g) S. M. Aucott, P. Kilian, S. D. Robertson, A. M. Z. Slawin, J. D. Woollins, *Chem. Eur. J.* **2006**, *12*, 895–902; h) S. M. Aucott, H. L. Milton, S. D. Robertson, A. M. Z. Slawin, G. B. Walker, J. D. Woollins, *Chem. Eur. J.* **2004**, *10*, 1666–1676; i) W. Weigand, R. Wünsch, K. Polborn, *Inorg. Chim. Acta* **1998**, *273*, 106–110.
- [11] a) A. Shaver, R. D. Lai, P. H. Bird, W. Wickramasinghe, *Can. J. Chem.* **1985**, *63*, 2555–2558; b) V. W.-W. Yam, P. K.-Y. Yeung, K.-K. Cheung, *J. Chem. Soc., Chem. Commun.* **1995**, 267–269; c) S.-W. A. Fong, T. S. A. Hor, *J. Chem. Soc., Dalton Trans.* **1999**, 639–651.
- [12] H. Petzold, H. Görls, W. Weigand, J. Romanski, G. Mloston, *Heteroat. Chem.* **2007**, *18*, 584–590.
- [13] a) M. Schmidt, G. G. Hoffmann, *J. Organomet. Chem.* **1977**, *124*, C5–C8; b) M. Schmidt, G. G. Hoffmann, *Chem. Ber.* **1979**, *112*, 2190–2196.
- [14] a) J. Windhager, H. Görls, H. Petzold, G. Mloston, G. Linti, W. Weigand, *Eur. J. Inorg. Chem.* **2007**, 4462–4471; b) L. C. Song, Z. Y. Yang, Y. J. Hua, H. T. Wang, Y. Liu, Q.-M. Hu, *Organometallics* **2007**, *26*, 2106–2110; c) J. Windhager, M. Rudolph, S. Bräutigam, H. Görls, W. Weigand, *Eur. J. Inorg. Chem.* **2007**, 2748–2760.
- [15] H. Petzold, S. Bräutigam, H. Görls, W. Weigand, U. Uhlemann, R. Geßner, W. Kiefer, J. Popp, A. Majchrzak, G. Mloston, *Inorg. Chim. Acta* **2004**, *357*, 1897–1908.
- [16] a) P. Lugo-Mas, A. Dey, L. Xu, S. D. Davin, J. Benedict, W. Kaminsky, K. O. Hodgson, B. Hedman, E. I. Solomon, J. A. Kovacs, *J. Am. Chem. Soc.* **2006**, *128*, 11211–11221; b) T. Srisankandakumar, H. Petzold, P. C. A. Bruijninx, A. Habtemariam, P. J. Sadler, P. Kennepohl, *J. Am. Chem. Soc.* **2009**, *131*, 13355–13361; c) A. Dey, S. P. Jeffrey, M. Darensbourg, K. O. Hodgson, B. Hedman, E. I. Solomon, *Inorg. Chem.* **2007**, *46*, 4989–4996; d) H. Petzold, J. J. Xu, P. J. Sadler, *Angew. Chem. Int. Ed.* **2008**, *47*, 3008–3011.
- [17] K. Morita, S. Kobayashi, *Chem. Pharm. Bull.* **1967**, *15*, 988–993.
- [18] U. Nagel, *Chem. Ber.* **1982**, *115*, 1998–1999.
- [19] W. Weigand, G. Bosl, C. Robl, W. Amrein, *Chem. Ber.* **1992**, *125*, 1047–1051.
- [20] COLLECT, Data Collection Software; Nonius B. V., Netherlands, **1998**.
- [21] Z. Otwinowski, W. Minor, *Processing of X-ray Diffraction Data Collected in Oscillation Mode*, in *Methods in Enzymology*, vol. 276, Macromolecular Crystallography, Part A (Ed.: C. W. Carter, R. M. Sweet), pp. 307–326, Academic Press **1997**.
- [22] SORTAV, R. H. Blessing, *Acta Crystallogr., Sect. A* **1995**, *51*, 33–38.
- [23] G. M. Sheldrick, *Acta Crystallogr., Sect. A* **1990**, *46*, 467–473.
- [24] G. M. Sheldrick, *SHELXL-97*, University of Göttingen, Germany, **1997**.
- [25] *Ortep-3 for Windows*: L. J. Farrugia, *J. Appl. Crystallogr.* **1997**, *30*, 565–565.
- [26] CCDC-634395 (**9**), CCDC-634396 (**11**) and CCDC-634397 (**12**) contain the supplementary crystallographic data for this paper. These data can be obtained free of charge from The Cambridge Crystallographic Data Centre via www.ccdc.cam.ac.uk/data_request/cif.

Received: December 20, 2009
Published Online: June 23, 2010

Dinuclear Iridium(III) Complexes Linked by a Bis(β -diketonato) Bridging Ligand: Energy Convergence versus Aggregation-Induced Emission

Chang Hwan Shin,^[a] Jung Oh Huh,^[a] Sun Jong Baek,^[a] Sang Kyu Kim,^[a]
Min Hyung Lee,^{*[b]} and Youngkyu Do^{*[a]}

Keywords: Aggregation / Dimetallic complexes / Phosphorescence / Iridium / Platinum

Novel iridium(III)/iridium(III) and iridium(III)/platinum(II) dinuclear complexes, $[\{\text{Ir}(\text{ppyFF})_2\}_2(\mu_2\text{-L})]$ (**4**) and $[\{\text{Ir}(\text{ppyFF})_2\}(\mu_2\text{-L})\{\text{Pt}(\text{ppy})\}]$ (**5**) [ppyFF = 2-(2,4-difluorophenyl)pyridine, ppy = 2-phenylpyridine, L = 1,3-bis(3-phenyl-3-oxopropanoyl)benzene], linked by an L bridging ligand were prepared, and their photophysical properties were investigated in solution and in the solid state. The photophysical properties of mononuclear iridium(III) and platinum(II) complexes, $[\text{Ir}(\text{ppyFF})_2(\text{dbm})]$ (**1**) and $[\text{Pt}(\text{ppy})_2(\text{dbm})]$ (**2**) bearing a dibenzoylmethane (dbm) ligand were also compared. Whereas the UV/Vis absorption spectra of **4** and **5** show independent light absorption at each metal-centered moiety, the photoluminescence spectra of **4** and **5** display almost identical features, but very weak emissions in solution at both room temperature and 77 K. The weak emission in solution is found to mainly originate from a ^3LX state of the L bridging ligand,

which reflects the occurrence of efficient energy convergence from the triplet states of the $\text{Pt}(\text{ppy})$ and $\text{Ir}(\text{ppyFF})$ moieties to the ^3LX state of L . By contrast, intense orange-red emission, that is, aggregation-induced emission, is produced in the solid state of **4** and **5**. Inspection of the crystal-packing structures of **5** reveals that strong intermolecular π - π interactions between the adjacent pyridine rings of ppyFF ligands in the Ir-centered moieties are responsible for the emissive metal-to-ligand-ligand charge-transfer [$^3\text{M}(\text{LL})\text{CT}$] state of the solid-state dinuclear systems. The electrochemical properties of **4** and **5** further indicate that the first two reductions occur at the dbm moieties of the L bridging ligand linked to each metal center, which is consistent with the fact that the lowest-energy excited state of the L bridging ligand dominates the excited-state properties of **4** and **5** in solution.

Introduction

Luminescent solid materials have recently attracted great attention in the areas of optoelectronic device applications such as organic light-emitting diodes and sensors.^[1] Although the majority of organic dyes and luminescent metal complexes are highly emissive in their molecular state, aggregation into the solid state often has detrimental effects on their light-emitting properties like emission quenching, which may render them less suitable for many optical applications. Thus, it would be highly desirable to construct an emissive solid state or to enhance the light emission of molecular species by means of aggregation-induced emission (AIE).^[2] Although a number of AIEs of organic solid materials that constitute fluorescent emission have been reported, the solid-state emission based on heavy-metal ion

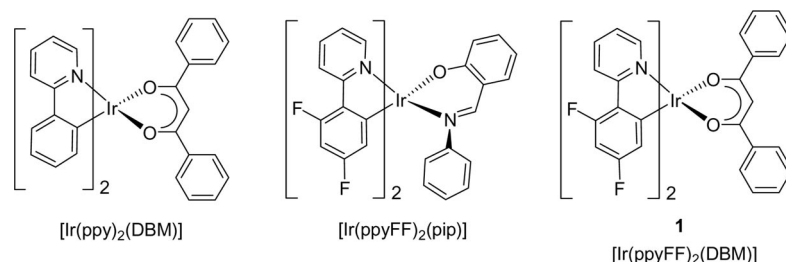
complexes may be of particular interest owing to the excellent emitting properties of molecular complexes^[3] such as the high quantum efficiency of their phosphorescent emission.^[4]

It has been well established in the square-planar platinum(II) complexes that $\text{Pt}^{\text{II}}\text{-Pt}^{\text{II}}$ interactions and/or π - π stacking of the ligands gives rise to the appearance of AIE or in some cases to the multiple AIEs induced by polymorphism.^[5] In contrast, the phosphorescent AIEs of iridium(III) systems have been relatively less investigated owing to the octahedral structure of the iridium(III) complex.^[6–11] Regarding the AIE phenomena, Zhao and Huang et al. demonstrated that the phosphorescent AIEs of heteroleptic iridium(III) complexes such as $[\text{Ir}(\text{ppy})_2(\text{dbm})]$ (ppy = 2-phenylpyridine, dbm = dibenzoylmethane)^[11] can be induced by the intermolecular excimer state, that is, the metal-to-ligand-ligand charge-transfer [$^3\text{M}(\text{LL})\text{CT}$] state (Scheme 1).^[8,9] Park and You et al. also suggested that the restricted intramolecular relaxation in the solid state is responsible for the AIE of the heteroleptic iridium(III) complexes such as $[\text{Ir}(\text{ppyFF})_2(\text{pip})]$ [pip = 2-(phenylimino-methyl)phenol] bearing an imine ancillary ligand^[10] although the proposed mechanism has been recently refuted by Chou and Chi et al.^[12] and Huang et al.^[8] Very recently, we have also reported that the dual phosphorescent emis-

[a] Department of Chemistry, KAIST,
Daejeon 305-701, Republic of Korea
Fax: +82-42-350-2810
E-mail: ykdo@kaist.ac.kr

[b] Department of Chemistry and Energy Harvest-Storage
Research Center,
University of Ulsan, Ulsan 680-749, Republic of Korea
Fax: +82-52-259-2348
E-mail: lmh74@ulsan.ac.kr

Supporting information for this article is available on the
WWW under <http://dx.doi.org/10.1002/ejic.201000275>.



Scheme 1.

sion from a solid-state iridium(III) complex could be achievable through the crystal-packing polymorphism induced by the modification of π - π interactions between the cyclometalated ligands of $[\text{Ir}(\text{ppyFF})_2(\text{dbm})]$ (**1**) [ppyFF = 2-(2,4-difluorophenyl)pyridine].^[7] These examples of the iridium(III) systems reveal that the very weakly emissive or nonemissive ^3LX excited state of the ancillary ligand can be switched into emissive states if a proper manipulation of the crystal-packing structure is allowed in the solid state.

In a continuous effort to develop novel AIE, we turned our attention to the dinuclear iridium(III) systems bearing photoactive cyclometalated ligands, as the multinuclearity could lead to facile modulation of π - π stacking and/or metal-metal interactions in the solid state. Furthermore, whereas the earlier investigations of phosphorescence have been extensively directed toward mononuclear Ir^{III} complexes,^[13–15] there have been few reports on the photophysical properties of dinuclear Ir^{III} complexes.^[16] Since the solid-state AIE derived from dinuclear complexes could also be useful for the development of color-tunable emitters for full-color and white-light display applications,^[17] it would be intriguing to investigate the photophysical properties

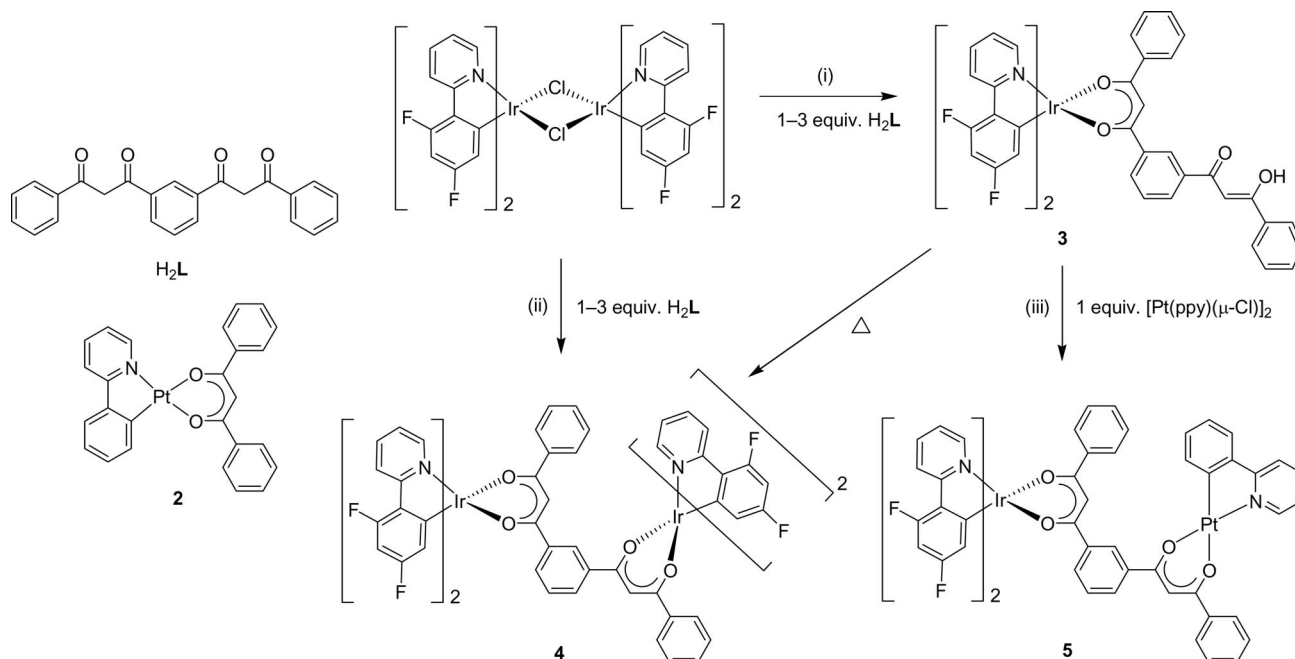
and AIE of dinuclear complexes. In this regard, we designed novel Ir^{III}/Ir^{III} homodinuclear and Ir^{III}/Pt^{II} heterodinuclear complexes that are linked by means of a bridging ligand comprising two β -diketonato binding sites. As noted in previous reports, a β -diketonato ligand such as dbm can act as an energy-converging unit through its low-energy ^3LX excited state in the mononuclear systems. By the same analogy, we chose 1,3-bis(3-phenyl-3-oxopropanoyl)benzene (H_2L),^[18,19] which possesses two β -diketonato binding sites connected by a 1,3-phenylene spacer as the bridging ligand.

In the present study, the synthesis and characterization of neutral Ir^{III}/Ir^{III} homodinuclear and Ir^{III}/Pt^{II} heterodinuclear complexes linked by a bis(β -diketonato) bridging ligand (**L**) are described to investigate the electronic energy convergence from the metal centers to the bridging ligand in the molecular state, as well as the solid-state AIE.

Results and Discussion

Synthesis and Crystal Structure

The mononuclear platinum complex $[\text{Pt}(\text{ppy})(\text{dbm})]$ (**2**) was obtained in good yield (68%) according to the analo-



Scheme 2. Reaction conditions: (i) 2-ethoxyethanol, Na_2CO_3 , 25 °C, 24 h, 45%; (ii) 2-ethoxyethanol, Na_2CO_3 , 130 °C, 24 h, 70%; (iii) 2-ethoxyethanol, Na_2CO_3 , 25 °C, 24 h, 40%.

gous method applied to the synthesis of **1**. The synthesis of mono- and diiridium complexes of $[\text{Ir}(\text{ppyFF})_2(\text{HL})]$ (**3**) and $[\{\text{Ir}(\text{ppyFF})_2\}_2(\mu_2\text{-L})]$ (**4**) was achieved through the reaction of the H_2L ligand and a dimeric precursor, $[\{\text{Ir}(\text{ppyFF})_2(\mu\text{-Cl})\}_2]$, by varying the reaction temperature and the stoichiometry of the reactants according to the procedures outlined in Scheme 2. It is noteworthy that the reaction temperature plays an important role in the syntheses of **3** and **4**. When $[\{\text{Ir}(\text{ppyFF})_2(\mu\text{-Cl})\}_2]$ was treated with H_2L (1–3 equiv.) at room temperature, monosubstituted β -diketonato complex **3** was the sole product. In contrast, the same reaction at 130 °C gave disubstituted **4** as the major product. This result may indicate that **4** is a thermodynamic product of the reaction between $[\{\text{Ir}(\text{ppyFF})_2(\mu\text{-Cl})\}_2]$ and H_2L . Indeed, **3** was slowly changed to **4** upon heating of the solution. The reaction between **3** and the $[\{\text{Pt}(\text{ppy})_2(\mu\text{-Cl})\}_2]$ precursor at room temperature afforded an orange solid of heterodinuclear complex $[\{\text{Ir}(\text{ppyFF})_2\}_2(\mu_2\text{-L})\{\text{Pt}(\text{ppy})_2\}]$ (**5**) linked by an **L** bridge in 40% yield. All the complexes were characterized by ^1H and ^{13}C NMR spectroscopy, MALDI-TOF mass spectrometry, and elemental analysis. In particular, an X-ray diffraction study was performed on single crystals of **5**.

The molecular structure of **5** and selected interatomic distances and angles are shown in Figure 1. The structure of **5** clearly shows the heterodinuclear connectivity between the Ir- and Pt-centered moieties by means of the **L** bridging ligand. The Ir-centered moiety adopts a Λ -configuration and bears two ppyFF ligands with a *trans* disposition of pyridine rings. In the Pt-centered moiety, the N3–Pt–C16 angle of 81.6(3)° and the O2–Pt–O1 angle of 91.42(18)° indicate a distorted square-planar geometry around the Pt center similar to that of the reported cyclometalated Pt complexes.^[20] When compared to the dihedral angle between the phenyl rings in dbm of **1** (20.25°),^[7] the dbm fragment at the Ir center of **5** forms a much larger angle of 53.97° probably due to the steric hindrance exerted by the adjacent ppy ligand of the Pt-centered moiety. In addition, the planes defined by O3–Ir–O4 and O1–Pt–O2 are linked to the central phenylene plane of the **L** bridging ligand by a relatively small dihedral angle of 18.74 and 10.68°, respectively, which indicates the presence of electronic conjugation between the planes. This feature may suggest that efficient electronic interactions can occur between the metal-centered moieties and the **L** bridging ligand through a π -orbital overlap.^[21] It seems that Ir and Pt atoms do not interact with each other as judged by the large Ir...Pt separation of 9.926 Å.

Photophysical Properties and Solid-State Emission

The absorption spectra of the complexes were recorded in degassed solutions of chloroform at room temperature (Figure 2 and Table 1). The intense high-energy bands below the 300 nm region can be assigned to singlet spin-allowed $\pi\text{-}\pi^*$ ligand-centered (^1LC) transitions of ppy and ppyFF ligands.^[15,20,22] The broad bands in the region rang-

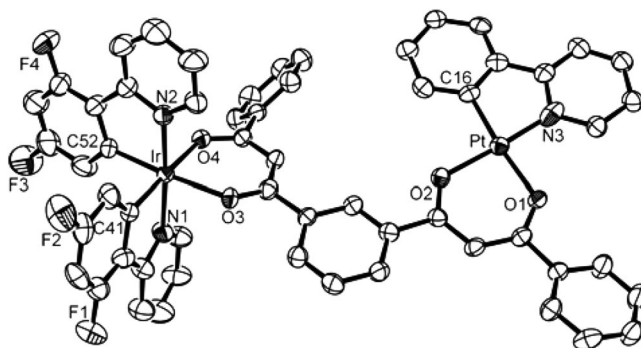


Figure 1. Molecular structure of **5** (50% thermal ellipsoid). Hydrogen atoms and solvent molecules (THF) are omitted for clarity. Selected bond lengths [Å] and angles [°]: Ir–C41 1.992(7), Ir–C52 1.994(6), Ir–N1 2.043(5), Ir–N2 2.045(5), Ir–O4 2.120(5), Ir–O3 2.145(4), Pt–N3 1.911(8), Pt–C16 1.982(6), Pt–O2 2.034(5), Pt–O1 2.039(4); C41–Ir–N1 82.1(2), C52–Ir–N2 81.2(3), O4–Ir–O3 87.95(17), N3–Pt–C16 81.6(3), C16–Pt–O2 94.9(2), N3–Pt–O1 92.1(2), O2–Pt–O1 91.42(18).

ing from 350 to 400 nm are caused by $\pi\text{-}\pi^*$ transitions (^1LX) on the β -diketonato bridging ligands (**L** and dbm).^[19] Whereas the lower energy absorption in 400–500 nm is weak for **2**, the Ir-centered species **1**, **4**, and **5** exhibit more intense bands with two shoulders in this region. The weak shoulder at 437 nm is assignable to the spin-allowed MLCT transition ($^1\text{MLCT}$), and the other one at 465 nm, which tails to 500 nm, can be assigned to the spin-forbidden MLCT transition ($^3\text{MLCT}$). These features of $^1\text{MLCT}$ and $^3\text{MLCT}$ transitions are very similar to those of the reported phosphorescent Ir complexes.^[15,23] In particular, the absorption spectrum of **4** shows an identical absorption band with an intensity twice that of the spectrum of **1**. Heterodinuclear **5** also exhibits an absorption feature corresponding to the sum of the independent spectra of **1** and **2**. These results indicate that the electronic transition at each metal-centered moiety in **4** and **5** is not affected by the **L** bridging ligand.

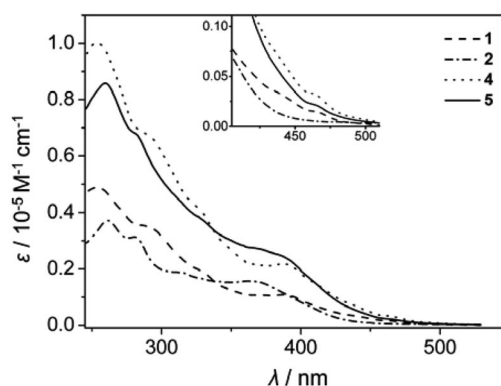


Figure 2. Absorption spectra of **1**, **2**, **4**, and **5** in CHCl_3 at room temperature. Inset: enlarged absorption spectra.

The room-temperature photoluminescence (PL) spectra of solutions of **1**, **2**, **4**, and **5** in degassed chloroform are shown in Figure 3, and the photophysical data are summarized in Table 1. The selective excitation at a wavelength of

Table 1. Photophysical data.

	Absorption ^[a] λ_{abs} [nm] (ϵ [$10^{-4} \text{ M}^{-1} \text{ cm}^{-1}$])	λ_{max} [nm]	Emission at 293 K ^[b]			Emission at 77 K ^[b]		
			Solution ^[a] τ [ns]	Φ_{em} ^[c]	Solid λ_{max} [nm]	τ [ns]	λ_{max} [nm]	τ [μ s]
1	254 (4.88), 290 (3.51), 330 (1.88), 388 (1.08), 437 (0.34), 465 (0.15)	611	23	3.0×10^{-2}	605 ^[d]	n.d. ^[e]	555	1.3
2	261 (3.72), 280 (3.12), 314 (1.88), 365 (1.56)	540	180	2.3×10^{-1}	548, 570	n.d.	495, 527, 555 (sh)	4.9
4	253 (10.0), 290 (6.75), 328 (4.07), 388 (2.17), 435 (0.76), 465 (0.31)	615	22	3.0×10^{-2}	597	67	570	1.3
5	259 (8.58), 281 (6.81), 327 (3.83), 369 (2.72), 388 (2.43), 437 (0.58), 465 (0.21)	615	22	2.3×10^{-2}	597	56	570	1.4

[a] In degassed CHCl_3 . [b] $\lambda_{\text{ex}} = 388 \text{ nm}$. [c] $[\text{Ir}(\text{ppy})_3]$ ($\Phi_{\text{em}} = 0.40$) was used as a standard. [d] For the orange-red crystals of **1**. [e] Not determined.

388 nm provides the most feasible quantitative explanation of the electronic energy relaxation since the Ir- and Pt-centered moieties are estimated to absorb nearly an equal quantity of light at that wavelength, as judged from the similar absorption coefficients of mononuclear complexes **1** and **2** ($\epsilon_1 = 10804 \text{ M}^{-1} \text{ cm}^{-1}$; $\epsilon_2 = 11319 \text{ M}^{-1} \text{ cm}^{-1}$). As reported earlier, the very weak emission band at 611 nm in **1** could be assignable to the major contribution from the ^3LX state of the dbm ligand.^[7,9] Moreover, although weak in intensity, the observation of the emission band of **1** ($\Phi_{\text{em}} = 0.03$) with a relatively short emission lifetime ($\tau = 23 \text{ ns}$ for **1**) may further indicate the possible involvement of the $^3\text{MLCT}$ state, thus leading to the proper description of the lowest-energy excited state of **1** in solution as the mixed $^3\text{MLCT}$ – ^3LX state. The absence of a $^3\text{MLCT}$ band is likely due to the large π – π^* energy gap of the ppyFF ligand, which causes the LUMO to be located mostly at the dbm ligand, thus allowing the ^3LX state of the dbm ligand to dominate the lowest-lying excited state. Chou and Chi et al. very recently demonstrated that all higher-energy excited states of relevant heteroleptic Ir^{III} complexes are strongly coupled with each other.^[12] In contrast, **2** exhibits an intense emission band at 540 nm with high quantum efficiency ($\Phi_{\text{em}} = 0.23$), which indicates that the emission from an excited state of the Pt(ppy) moiety is not quenched despite the presence of the dbm moiety in **2** (vide infra). The emission spectrum of homodinuclear complex **4** exhibits a very weak emission band at 615 nm with low quantum efficiency ($\Phi_{\text{em}} = 0.03$) indicative of inefficient phosphorescence. This feature is in fact very similar to that observed in the mononuclear complex **1** ($\lambda_{\text{em}} = 611 \text{ nm}$, $\Phi_{\text{em}} = 0.03$),^[7] which suggests that the observed weak emission in **4** is dominated by the L-based triplet excited state (^3LX). Interestingly, heterodinuclear **5** also exhibits a weak emission band at 615 nm with low quantum efficiency ($\Phi_{\text{em}} = 0.023$) as observed in **4**. The characteristic emission band around 540 nm that appeared in the mononuclear Pt complex **2** is not observed in the emission spectrum of **5**, pointing to the quenching of the Pt(ppy)-based emission. One order of magnitude decrease in quantum efficiency ($\Phi_{\text{em}} = 0.23$ for **2** vs. 0.023 for **5**) and a much reduced emission lifetime of **5** relative to that of **2** ($\tau = 180 \text{ ns}$ for **2** vs. 22 ns for **5**) are in agreement with this observation. Further-

more, a comparison of the emission intensities for **1** and **5** at the same molar concentration reveals that the 615 nm-band intensity of **5** is increased 1.5-fold. This result may suggest that the internal conversion of the T_n state, which is contributed mainly by the Pt(ppy) moiety, into an energy state of 615 nm, that is, the T_1 state, dominated by the ^3LX state of the L bridging ligand, effectively takes place in **5**.

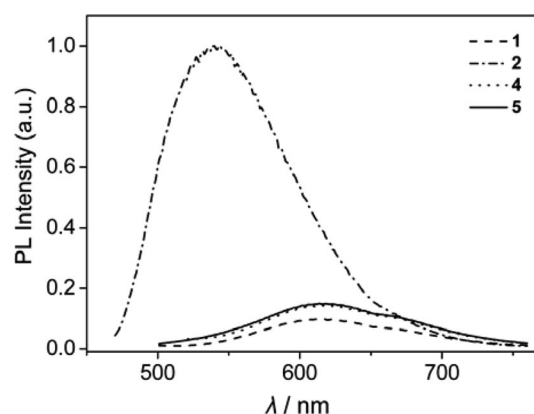


Figure 3. Emission spectra of **1**, **2**, **4**, and **5** in CHCl_3 ($1.0 \times 10^{-5} \text{ M}$; $\lambda_{\text{ex}} = 388 \text{ nm}$) at room temperature.

To clarify the electronic energy convergence, low-temperature PL experiments were performed in chloroform rigid matrices at 77 K. The emission spectra of **2**, **4**, and **5** are displayed in Figure 4, and that of **1** is shown for comparison. The mononuclear Pt complex **2** shows a structured band at 495 nm with a long emission lifetime of $4.9 \mu\text{s}$, thus confirming that the emission is originated from a mixed MLCT – $^3\text{LC}(\text{ppy})$ excited state^[20] (Figure 4a). In addition, the weak shoulder around 555 nm that was not observed in the room-temperature spectrum could be attributed to a dbm-based excited state (^3LX) as similarly found in **1** ($\lambda_{\text{em}} = 555 \text{ nm}$ at 77 K).^[7,9]

This result indicates that the lowest-energy excited state of **2** could be described as a mixed MLCT – $^3\text{LC}(\text{ppy})$ – $^3\text{LX}(\text{dbm})$ state presumably due to a small difference in energy between these states. In contrast, the emission band of the Pt(ppy) moiety in heterodinuclear **5** is completely quenched at 77 K, only giving rise to a 570 nm band. This feature is actually similar to that observed at room tempera-

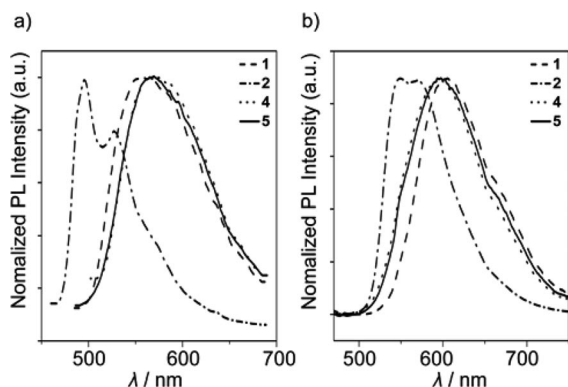


Figure 4. Emission spectra ($\lambda_{\text{ex}} = 388 \text{ nm}$) of **1**, **2**, **4**, and **5** in (a) a CHCl_3 rigid matrix at 77 K and (b) the solid state. The solid-state spectrum of **1** was taken from an orange polymorph reported in the literature.^[10]

ture. Since the emission spectra of an equimolar mixture of **1** and **2** contain all of the emission bands derived from the Pt complex **2** (Figure S1 in the Supporting Information), this finding signifies the occurrence of an efficient $T_n \rightarrow T_1$ internal conversion from the Pt(pppy) moiety to the **L** bridging ligand in **5**. Moreover, the shapes of emission bands and the maximum emission wavelength of the dinuclear complexes **4** and **5** are virtually identical, and the maximum peak positions are also redshifted by 15 nm in comparison with mononuclear **1**. This feature further indicates that the lowest-excited state of **4** and **5** is mainly involved with the

^3LX state of the **L** bridging ligand, the energy level of which would be lower than that of dbm probably owing to a longer conjugation length. Consequently, as depicted in the schematic energy-level diagram of **5** (Figure 5), all these results together with the electrochemical data (vide infra) may suggest that in the given molecular dinuclear Ir^{III} systems linked by the bis(β -diketonato) **L** bridging ligand, energy convergence effectively takes place from the T_n states contributed by metal-centered moieties to the T_1 state dominated by the **L** bridging ligand, which thus plays the role of an energy “collector” or a “converging unit”.

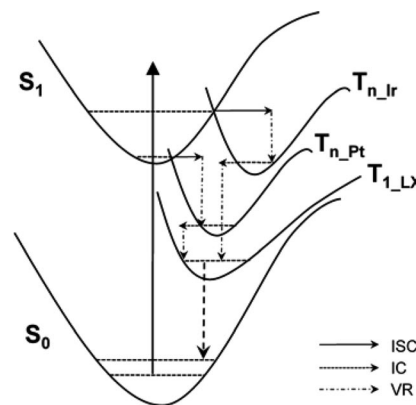


Figure 5. Schematic energy-level diagram and proposed emission processes of **5** in solution. IC: internal conversion; ISC: intersystem crossing; VR: vibrational relaxation.

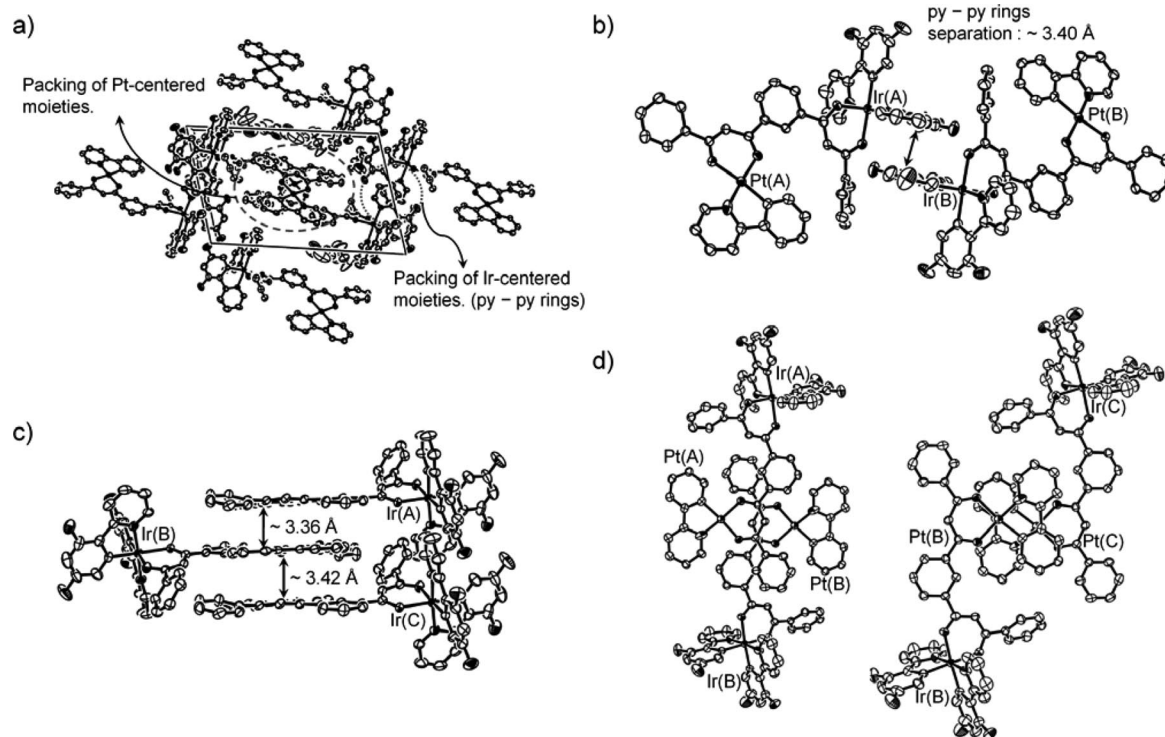


Figure 6. Crystal-packing structures of **5**. (a) Overall packing structure. (b) π - π interaction between Ir-centered moieties. (c) Extended π - π stacking structure between Pt-centered moieties. (d) Top views showing two kinds of π - π interaction between Pt-centered moieties: left, $\text{Pt(A)L} \cdots \text{Pt(B)L}$ interactions; right, $\text{Pt(B)(ppy)} \cdots \text{Pt(C)(ppy)}$ interactions.

Unlike the very weak luminescence of **4** and **5** in solution, the intense orange-red emission (i.e., AIE) centered at 597 nm is observed in the solid state (Figure 4b and Figure S2 in the Supporting Information). This feature is in accord with those observed in solid-state iridium complexes such as [Ir(ppy)₂(dbm)]^[9] and **1**.^[7] To elucidate the origin of the AIE, the crystal-packing structures of heterodinuclear **5** were examined. The packing structures illustrated in Figure 6 clearly show that each metal-centered moiety forms π – π interactions in the crystal (Figure 6a). One is the effective overlap between the ppyFF ligands of the Ir-centered moieties in adjacent molecules (Figure 6b), and the other is π – π stacking of the Pt-centered moieties (Figure 6c). In the Ir-centered moieties, the interplanar separation between the adjacent pyridine rings of ppyFF ligands is estimated to be approximately 3.40 Å, comparable to those observed in mononuclear [Ir(ppy)₂(dbm)] (3.37 Å)^[9] and **1** (3.40 Å),^[7] which reflects the presence of sufficiently strong π – π interactions. The Pt-centered moieties, on the other hand, pack as an extended π – π stacking structure consisting of two kinds of alternating π – π interactions, that is, Pt(A)L...Pt(B)L and Pt(B)(ppy)...Pt(C)(ppy) interactions (Figure 6c and d). This feature is quite different from the isolated ppyFF...ppyFF interactions observed in the Ir-centered moieties. Along with the apparent incorporation of Pt centers into the stacking structures, this could be ascribed to the planar geometry of the Pt moiety. Whereas a direct Pt...Pt interaction appears absent as judged by the long separations [6.575 Å in Pt(A)L...Pt(B)L and 4.299 Å in Pt(B)(ppy)...Pt(C)(ppy)], the short interplanar separations of approximately 3.36 and 3.42 Å, respectively, indicate the presence of strong π – π interactions between the Pt-centered moieties.^[20] Therefore, it can be suggested that in the solid state of **5**, the strong π – π interactions between the adjacent ppyFF ligands induce the ppyFF-centered triplet excited state, that is, the ³M(LL)CT state, which is lower in energy than ³LX of the L bridging ligand. As a result, the ³M(LL)CT state dominates the lowest-energy excited state leading to the intense emission. Furthermore, the essentially identical emission features observed for both **4** and **5** in terms of emission wavelength (λ_{em} = 597 nm) and lifetime (τ = 67 ns for **4** and 56 ns for **5**) imply the quenching of the Pt(ppy)-based emission in the solid state of **5** (Figure 4b). We attribute this to the extended π – π stacking structure comprised of alternating Pt(A)L...Pt(B)L and Pt(B)(ppy)...Pt(C)(ppy) interactions. Although the Pt(B)(ppy)...Pt(C)(ppy) interactions may lead to an emissive ³M(LL)CT excited state, the energy of such a state appears to be efficiently converged into the weakly emissive triplet state (³LLX) formed by adjacent Pt(A)L...Pt(B)L interactions.

Electrochemical Properties

The electrochemical properties of the complexes were examined by cyclic voltammetry (Table 2 and Figure 7). The mononuclear Ir complex **1** shows reversible oxidation at 0.73 V, whereas Pt complex **2** exhibits an irreversible oxi-

dation feature with an onset potential of 0.48 V. In the case of heterodinuclear **5**, two successive oxidations are observed. Whereas the irreversible first oxidation ascribable to the Pt-centered moiety in **5** occurs at a potential identical to that of **2**, the reversible second oxidation potential of the Ir-centered moiety (0.78 V) is slightly higher than that of **1**. This result indicates a stabilization of the filled d orbitals of the Ir center in **5** due to the electron-withdrawing effect caused by the first oxidation of the linked Pt moiety as similarly found in an Ru^{II}/Os^{II} system.^[24] In contrast, **4** undergoes a single two-electron reversible oxidation process consistent with identical environments of both Ir-centered moieties and thereby simultaneous oxidation. Hence, the increase of the Ir-centered oxidation potential in **4** (0.76 V) relative to the potential of **1** is less apparent than that in **5**.

Table 2. Electrochemical data.^[a]

Complexes	Oxidation		$E_{\text{red}}^{\text{1st}}$ [V]	Reduction	
	$E_{\text{ox}}^{\text{2nd}}$ [V] (Ir ^{III} /Ir ^{IV})	$E_{\text{ox}}^{\text{1st}}$ [V] (Pt ^{II} /Pt ^{III})		$E_{\text{red}}^{\text{2nd}}$ [V]	$E_{\text{red}}^{\text{3rd}}$ [V]
1	0.73	–	–2.16	–2.77 ^[b]	–
2	–	0.48 ^[b]	–2.00	–2.58	–
4	0.76 ^[c]	–	–2.06	–2.27	–2.68 ^[b]
5	0.78	0.48 ^[b]	–1.94	–2.23	–2.64 ^[b]

[a] Conditions: 10^{–3} M in CH₃CN, 0.1 M [nBu₄N][PF₆], scan rate 50 mV s^{–1}, redox potential reported versus $E_{1/2}$ (ferrocene/ferrocenium). [b] Irreversible redox. [c] Single two-electron wave.

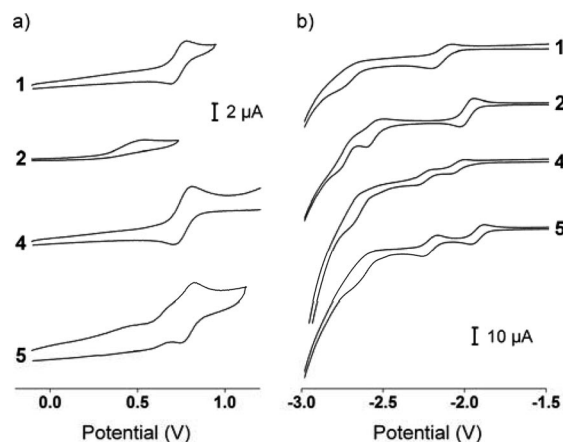
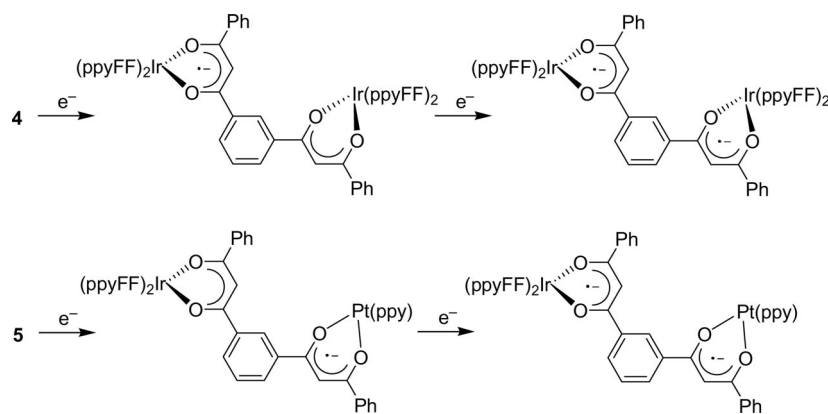


Figure 7. Cyclic voltammograms of **1**, **2**, **4**, and **5** showing (a) oxidation and (b) reduction.

However, mononuclear **1** undergoes a two-step reduction process with first and second reduction potentials of –2.16 and –2.77 V, respectively. Since the second reduction potential falls in the typical range observed for Ir–ppy derivatives^[13] and it is known that the LUMO of the [Ir(ppy)₂(dbm)] complex is distributed mainly on the dbm ligand,^[9] the first and second reductions of **1** can be assigned to the dbm and ppyFF ligand-based reduction. In the case of **2**, two-step reduction processes take place at a less negative potential (–2.00 and –2.58 V) than those observed for **1**, but the reduction features are quite similar to those of **1**.

Scheme 3. First and second reduction processes in **4** and **5**.

Moreover, $[(ppy)Pt(O^{\cap}O)]^{[20]}$ ($O^{\cap}OH$ = acetylacetone, dipivaloylmethane) and $[Pt(ppy)_2]^{[25]}$ complexes are reported to have a ppy ligand-based reduction at around -2.4 to -2.5 V. Although the second reduction potential of **2** is slightly more negative than the reported values, presumably due to the already reduced state of **2**, these results indicate that the first and second reductions of **2** are the dbm and ppy ligand-based reductions, respectively. The dinuclear complexes **4** and **5** undergo a three-step reduction process with a comparable reduction potential at each reduction step. The first and third reductions could be assignable to the reduction at the dbm moiety in the **L** bridging ligand and at the ppyFF or ppy ligand in the metal-centered moieties, respectively. The second reduction, which exhibits a reversible feature, has its potential close to the first reduction potentials of **1** and **2**, which suggests that the second reduction also occurs at the dbm moiety in the **L** bridging ligand. Furthermore, the first reduction potentials of **4** and **5** show an anodic shift, to a similar extent, with respect to those of **1** and **2**, respectively, implying that the LUMO localized on the dbm moiety of the **L** bridging ligand has a lower energy than that of the monomeric dbm complexes. This feature is in accord with the extended conjugation in the **L** bridging ligand. In addition to the anodic shift of the first reduction potential of **5** (-1.94 V) with respect to that of **4** (-2.06 V), as similarly shown in **1** and **2**, these findings indicate that the initial two reduction processes in **4** and **5** involve the first reduction at the dbm moiety of the **L** bridging ligand linked to the Ir and Pt centers, respectively, and is followed by the second reduction at the dbm moiety linked to the remaining Ir centers in the first reduced state of **4** and **5** (Scheme 3). These reduction behaviors are also in good agreement with the fact that the **L** bridging ligand dominates the lowest-energy excited state of **4** and **5** in solution.

Conclusion

Novel Ir^{III}/Ir^{III} homodinuclear and Ir^{III}/Pt^{II} heterodinuclear complexes linked by a bis(β -diketonato) bridging ligand (**L**) were synthesized and characterized. According to the photophysical results in solution, it was found that the

lowest-energy excited state of dinuclear complexes receives its major contribution from the 3LX state of the **L** bridging ligand, and hence the absorbed energy was efficiently converged into the energy acceptor, the **L** bridging ligand between Ir^{III}/Ir^{III} - and Ir^{III}/Pt^{II} -based luminophores. In contrast to the weak luminescence in solution, intense emission (i.e., aggregation-induced emission) was produced in the solid state. It is suggested from the crystal-packing structures that strong π - π intermolecular interactions between adjacent pyridine rings of ppyFF ligands in the Ir-centered moieties are responsible for the emissive $^3M(LL)CT$ state of the solid-state dinuclear systems. The electrochemical properties of **4** and **5** further indicate that the first two reductions occur at the dbm moieties of the **L** bridging ligand linked to each metal center, which supports evidence that the **L** bridging ligand dominates the lowest excited state of **4** and **5** in solution.

Experimental Section

General: All manipulations were performed under nitrogen by using standard Schlenk and glove-box techniques. Anhydrous-grade solvents (Aldrich) were purified by passing them through an activated alumina (Acros, 50–200 micron) column. All reagents were used without any further purification after being purchased from Aldrich (dimethyl isophthalate, acetophenone, 2-phenylpyridine, 2-bromopyridine, 2,4-difluorophenylboronic acid, dibenzoylmethane, 2-ethoxyethanol), Fluka (anhydrous Na_2CO_3), and Strem [iridium(III) chloride hydrate, potassium tetrachloroplatinate]. The compounds 2-(2,4-difluorophenyl)pyridine,^[13] 1,3-bis(3-oxo-3-phenylpropanoyl)benzene (H_2L),^[19] $[Ir(ppyFF)_2(\mu-Cl)]_2$,^[13] $[Pt(ppy)(\mu-Cl)]_2$,^[20] and $[Ir(ppyFF)_2(dbm)]$ (**1**)^[7] were prepared according to modified literature procedures. Deuterated solvents (Cambridge Isotope Laboratories) were dried with activated molecular sieves (5 Å). 1H and ^{13}C NMR spectra of the compounds were recorded with a Bruker Spectrospin 400 spectrometer at ambient temperature. All chemical shifts are reported in δ with reference to the residual peaks of $CDCl_3$ for proton ($\delta = 7.24$ ppm) and carbon ($\delta = 77.0$ ppm) chemical shifts. Elemental analyses (EA) were carried out with an EA1110-FISONS (CE Instruments) instrument by the Environmental Analysis Laboratory at KAIST. MALDI-TOF MS were measured with a Voyager DE-STR 4700 proteomics analyzer at the Korea Basic Science Center (KBSC).

UV/Vis and PL spectra were obtained with a Jasco V-530 spectrophotometer and a Spex Fluorog-3 luminescence spectrometer, respectively. Solution PL experiments were performed by using HPLC-grade chloroform. All solutions in chloroform were degassed by several freeze-pump-thaw cycles using a diffusion pump. The emission quantum yields of the complexes were calculated by using degassed *fac*-[Ir(ppy)₃] in toluene ($\Phi = 0.40$) as a reference. Low-temperature measurements were recorded in 5 mm diameter quartz tubes that were placed in a quartz-walled Dewar flask filled with liquid nitrogen (77 K). Emission lifetimes were determined by using a third-harmonic generator of an Nd:YAG laser (Spectra-Physics LAB170, 10 Hz). A laser beam collected through a fused silica window was applied to excite the sample, and the delay time (310 μ s) between the flash lamp and Q-switch was used to reduce the laser output power. The final power of the laser beam to the pump samples was about 100 μ J pulse⁻¹. A monochromator (Dongwoo Optron, DM150i) and a general photomultiplier tube (PMT; Hamamatsu, R928) were employed to select the wavelength of the emission and to detect the strength of the emission. The signals from the PMT were spread on an oscilloscope (Lecroy waverunner 104Xi, 1 GHz bandwidth) and recorded. Cyclic voltammetry was performed by using an AUTOLAB/PGSTAT12 model system with a three-electrode cell configuration consisting of platinum working and counter electrodes and an Ag/AgNO₃ (0.1 M in acetonitrile) reference electrode at room temperature. Anhydrous acetonitrile was used as the solvent, and 0.1 M tetrabutylammonium hexafluorophosphate was used as the supporting electrolyte. The redox potentials were recorded at a 50 mV s⁻¹ scan rate and reported against the ferrocene/ferrocenium (Cp₂Fe/Cp₂Fe⁺; Cp = cyclopentadienyl) redox couple that was used as an internal standard.

Synthesis of [Pt(ppy)(dbm)] (2): [Pt(ppy)(μ -Cl)]₂ (0.45 g, 0.58 mmol), dibenzoylmethane (0.39 g, 1.74 mmol), and Na₂CO₃ (0.62 g, 5.8 mmol) were mixed in 2-ethoxyethanol (30 mL) at room temperature. The mixture was stirred and heated at reflux overnight. After cooling to room temperature, water (30 mL) was added, and the mixture was then filtered to give a dark crude product, which was washed with water (30 mL) and diethyl ether (30 mL). The pure complex was obtained by flash chromatography on a silica column by using dichloromethane as the eluent to yield **2** (0.45 g) as a yellow solid in 68% yield. ¹H NMR (400.13 MHz, CDCl₃): δ = 9.11 (d, $J_{\text{H,H}}$ = 5.7 Hz, 1 H), 8.02–8.08 (m, 4 H), 7.75–7.82 (m, 2 H), 7.63 (d, $J_{\text{H,H}}$ = 8.0 Hz, 1 H), 7.53–7.56 (m, 2 H), 7.45–7.50 (m, 5 H), 7.25 (td, $J_{\text{H,H}}$ = 7.3, 0.9 Hz, 1 H), 7.10–7.16 (m, 2 H), 6.75 (s, 1 H) ppm. ¹³C NMR (100.62 MHz, CDCl₃): δ = 179.92, 178.94, 168.49, 147.28, 144.77, 140.27, 139.30, 138.88, 138.24, 130.90, 130.87, 130.74, 129.36, 128.63, 128.57, 127.11, 126.98, 123.74, 123.08, 121.35, 118.47, 97.55 ppm. MALDI-TOF MS: m/z = 571.80 [M⁺]. C₂₆H₁₉NO₂Pt (572.51): calcd. C 54.55, H 3.35, N 2.45; found C 54.49, H 3.19, N 2.44.

Synthesis of [Ir(ppyFF)₂(HL)] (3): [Ir(ppyFF)₂(μ -Cl)]₂ (1.22 g, 1.0 mmol), H₂L (1.11 g, 3.0 mmol), and Na₂CO₃ (1.06 g, 10 mmol) were mixed in 2-ethoxyethanol (30 mL) and stirred at room temperature for 24 h. Addition of water (30 mL) followed by filtration and flash column chromatography (eluent; ethyl acetate/hexane, 1:4) yielded **3** as an orange solid (0.85 g, 45%). ¹H NMR (400.13 MHz, CDCl₃): δ = 16.83 (br., 1 H), 8.51 (d, $J_{\text{H,H}}$ = 6.2 Hz, 2 H), 8.3 (t, $J_{\text{H,H}}$ = 1.7 Hz, 1 H), 8.26 (d, $J_{\text{H,H}}$ = 8.3 Hz, 2 H), 8.07 (d, $J_{\text{H,H}}$ = 8.1 Hz, 1 H), 7.90–7.93 (m, 3 H), 7.75–7.81 (m, 4 H), 7.4–7.60 (m, 5 H), 7.33 (t, $J_{\text{H,H}}$ = 7.2 Hz, 2 H), 7.08–7.13 (m, 2 H), 6.73 (s, 1 H), 6.63 (s, 1 H), 6.35–6.43 (m, 2 H), 5.75–5.80 (m, 2 H) ppm. ¹³C NMR (100.62 MHz, CDCl₃): δ = 186.07, 185.58, 185.34, 184.79, 180.01, 177.93, 165.19, 164.29, 162.47, 160.90, 159.05, 151.37, 151.16, 147.99, 141.17, 140.48, 138.28, 137.90, 135.76,

135.23, 130.81, 129.15, 128.76, 128.37, 127.28, 126.97, 126.71, 126.27, 125.40, 122.82, 122.56, 122.35, 121.88, 121.68, 115.39, 115.21, 97.61, 97.27, 96.91, 95.14, 93.13 ppm. MALDI-TOF MS: m/z = 941.99 [M⁺]. C₄₆H₂₉F₄IrN₂O₄ (941.94): calcd. C 58.65, H 3.10, N 2.97; found C 59.49, H 3.09, N 2.91.

Synthesis of [Ir(ppyFF)₂]₂(μ -L)] (4): [Ir(ppyFF)₂(μ -Cl)]₂ (0.61 g, 0.5 mmol), H₂L (0.19 g, 0.5 mmol), and Na₂CO₃ (0.53 g, 5.0 mmol) were mixed in 2-ethoxyethanol (30 mL), and the mixture was heated at 130 °C for 24 h. Workup followed by flash column chromatography (eluent: dichloromethane) yielded **4** as an orange solid (0.53 g, 70%). ¹H NMR (400.13 MHz, CDCl₃): δ = 8.46–8.51 (m, 4 H), 8.23 (t, $J_{\text{H,H}}$ = 6.8 Hz, 4 H), 8.15 (d, $J_{\text{H,H}}$ = 19 Hz, 1 H), 7.81–7.86 (m, 2 H), 7.67–7.74 (m, 8 H), 7.44 (t, $J_{\text{H,H}}$ = 7.0 Hz, 2 H), 7.30–7.35 (t, $J_{\text{H,H}}$ = 7.7 Hz, 4 H), 7.26 (dd, $J_{\text{H,H}}$ = 10.1, 1.8 Hz, 1 H), 7.07 (t, $J_{\text{H,H}}$ = 6.2 Hz, 2 H), 7.00–7.04 (m, 2 H), 6.51 (s, 2 H), 6.32–6.42 (m, 4 H), 5.70–5.79 (m, 4 H) ppm. ¹³C NMR (100.62 MHz, CDCl₃): δ = 179.50, 178.77, 178.67, 165.28, 164.66, 164.35, 164.19, 162.55, 160.98, 160.80, 159.11, 158.94, 151.59, 151.19, 147.89, 141.06, 140.50, 138.26, 137.85, 130.61, 129.15, 128.75, 128.51, 128.33, 127.15, 126.93, 126.38, 122.51, 121.64, 121.00, 115.31, 115.09, 97.62, 97.27, 96.90, 95.13 ppm. MALDI-TOF MS: m/z = 1514.15 [M⁺]. C₆₈H₄₀F₈Ir₂N₄O₄ (1513.49): calcd. C 53.96, H 2.66, N 3.70; found C 53.57, H 2.57, N 3.73.

Synthesis of [Ir(ppyFF)₂]₂(μ -L)]Pt(ppy)] (5): Compound **3** (0.43 g, 0.46 mmol), [Pt(ppy)(μ -Cl)]₂ (0.18 g, 0.23 mmol), and Na₂CO₃ (0.49 g, 4.6 mmol) were mixed in 2-ethoxyethanol (30 mL) and stirred at room temperature for 24 h. Workup followed by flash column chromatography (eluent: ethyl acetate/hexane, 1:4) yielded **5** as an orange solid (0.23 g, 40%). ¹H NMR (400.13 MHz, CDCl₃): δ = 9.07 (d, $J_{\text{H,H}}$ = 5.6 Hz, 0.5 H), 9.02 (d, $J_{\text{H,H}}$ = 5.5 Hz, 0.5 H), 8.53–8.59 (m, 2.5 H), 8.43 (s, 0.5 H), 8.26 (d, $J_{\text{H,H}}$ = 8.4 Hz, 2 H), 8.09–8.11 (m, 1 H), 7.96–8.00 (m, 3 H), 7.86 (d, $J_{\text{H,H}}$ = 7.6 Hz, 1 H), 7.81 (d, $J_{\text{H,H}}$ = 7.6 Hz, 1 H), 7.72–7.76 (m, 4 H), 7.56 (t, $J_{\text{H,H}}$ = 7.7 Hz, 2 H), 7.40–7.48 (m, 5 H), 7.32 (t, $J_{\text{H,H}}$ = 7.6 Hz, 2 H), 7.24 (t, J = 7.5 Hz, 0.5 H), 7.07–7.12 (m, 4 H), 6.90 (t, $J_{\text{H,H}}$ = 7.5 Hz, 0.5 H), 6.76 (s, 0.5 H), 6.67 (t, $J_{\text{H,H}}$ = 7.4 Hz, 1.5 H), 6.36–6.43 (m, 2 H), 5.78–5.83 (m, 2 H) ppm. ¹³C NMR (100.62 MHz, CDCl₃): δ = 180.06, 179.63, 179.01, 178.58, 177.92, 168.35, 165.24, 163.85, 162.05, 161.31, 159.47, 151.46, 151.25, 148.03, 147.21, 147.00, 144.77, 141.06, 140.62, 140.41, 140.04, 139.19, 138.78, 138.22, 138.05, 131.00, 130.84, 130.67, 130.57, 129.43, 128.96, 128.75, 128.62, 128.46, 127.03, 126.89, 125.10, 123.66, 123.12, 122.67, 122.48, 121.79, 121.36, 118.45, 115.32, 115.15, 97.52, 97.20, 97.02, 95.19, 95.07 ppm. MALDI-TOF MS: m/z = 1289.78 [M⁺]. C₅₇H₃₆F₄Ir₂N₄O₄Pt (1290.20): calcd. C 53.06, H 2.81, N 3.26; found C 53.86, H 2.73, N 3.28.

X-ray Crystallography: Single crystals of **5** suitable for X-ray diffraction studies were obtained by slow cooling of solutions of **5** in THF/hexane. Crystals were coated with Paratone oil, and diffraction data were measured at 100 K with synchrotron radiation (λ = 0.74999 Å) by a 4AMXW ADSC Quantum-210 detector equipped with a silicon double-crystal monochromator at the Pohang Accelerator Laboratory in Korea. The reflection data were collected as π -scan frames with a width of 1° per frame and an exposure time of 1 s per frame. HKL2000 (version 0.98.698)^[26] was used for data collection, cell refinement, reduction, and absorption correction. The structure was solved by direct methods and refined by full-matrix least-squares methods using the SHELXTL program package with anisotropic thermal parameters for all non-hydrogen atoms. Hydrogen atoms were placed in their geometrically calculated positions and refined riding on the corresponding carbon atoms with isotropic thermal parameters.

Crystal Data for 5-(thf)₃: C₆₉H₆₀F₄IrN₃O₇Pt, $M_r = 1506.49$, $\lambda = 0.74999$ Å (synchrotron radiation), triclinic, $P\bar{1}$, $a = 10.599(2)$ Å, $b = 13.534(3)$ Å, $c = 21.654(4)$ Å, $\alpha = 72.87(3)^\circ$, $\beta = 78.33(3)^\circ$, $\gamma = 79.76(3)^\circ$, $V = 2883.8(10)$ Å³, $Z = 2$, $\rho_{\text{calcd.}} = 1.735$ g cm⁻³, $\mu = 4.801$ mm⁻¹, $F(000) = 1484$, $T = 100$ K, measured reflections = 12793 in $h(0/14)$, $k(-17/18)$, $l(-27/29)$, unique reflections = 12793, $R_{\text{int}} = 0.000$, refined parameters = 766, $R_1 = 0.0626$, $wR_2 = 0.1829$ [$I > 2\sigma(I)$] and GOF on $F^2 = 1.008$, ρ_{final} (max./min.) = 2.150/−4.541 e Å⁻³.

CCDC-756977 (5) contains the supplementary crystallographic data for this paper. These data can be obtained free of charge from The Cambridge Crystallographic Data Centre via www.ccdc.cam.ac.uk/data_request/cif.

Supporting Information (see footnote on the first page of this article): Emission spectrum of a mixture of 1 and 2 in solution and MALDI-TOF MS spectra of complexes.

Acknowledgments

We gratefully acknowledge the Korea Research Foundation (no. KRF-2008-313-C00454 for Y. D.) and the Priority Research Centers Program of the National Research Foundation of Korea (no. 2009-0093818 for M. H. L.) for financial support and the Pohang Accelerator Laboratory (PAL) for beam-line use (grant 2008-2041-05).

- [1] P.-T. Chou, Y. Chi, *Chem. Eur. J.* **2007**, *13*, 380–395; E. Holder, B. M. W. Langeveld, U. S. Schubert, *Adv. Mater.* **2005**, *17*, 1109–1121; H. Yersin, *Top. Curr. Chem.* **2004**, *241*, 1–26; L. S. Hung, C. H. Chen, *Mater. Sci. Eng., R* **2002**, *39*, 143–222; S. Wang, *Coord. Chem. Rev.* **2001**, *215*, 79–98.
- [2] Z. Ning, Z. Chen, Q. Zhang, Y. Yan, S. Qian, Y. Cao, H. Tian, *Adv. Funct. Mater.* **2007**, *17*, 3799–3807; H. Zhang, Z. Zhang, K. Ye, J. Zhang, Y. Wang, *Adv. Mater.* **2006**, *18*, 2369–2372; H. J. Tracy, J. L. Mullin, W. T. Klooster, J. A. Martin, J. Haug, S. Wallace, I. Rudloe, K. Watts, *Inorg. Chem.* **2005**, *44*, 2003–2011; W. Lu, B.-X. Mi, M. C. W. Chan, Z. Hui, C.-M. Che, N. Zhu, S.-T. Lee, *J. Am. Chem. Soc.* **2004**, *126*, 4958–4971; J. Luo, Z. Xie, J. W. Y. Lam, L. Cheng, H. Chen, C. Qiu, H. S. Kwok, X. Zhan, Y. Liu, D. Zhu, B. Z. Tang, *Chem. Commun.* **2001**, 1740–1741.
- [3] L. Flamigni, A. Barbieri, C. Sabatini, B. Ventura, F. Barigelli, *Top. Curr. Chem.* **2007**, *281*, 143–203; J. A. G. Williams, *Top. Curr. Chem.* **2007**, *281*, 205–268; B. Ma, P. I. Djurovich, M. E. Thompson, *Coord. Chem. Rev.* **2005**, *249*, 1501–1510; W.-S. Huang, J. T. Lin, C.-H. Chien, Y.-T. Tao, S.-S. Sun, Y.-S. Wen, *Chem. Mater.* **2004**, *16*, 2480–2488.
- [4] C. Adachi, M. A. Baldo, S. R. Forrest, M. E. Thompson, *Appl. Phys. Lett.* **2000**, *77*, 904–906.
- [5] J. S. Field, L. P. Ledwaba, O. Q. Munro, D. R. McMillin, *CrysEngComm* **2008**, *10*, 740–747; Y. Sun, K. Ye, H. Zhang, J. Zhang, L. Zhao, B. Li, G. Yang, B. Yang, Y. Wang, S.-W. Lai, C.-M. Che, *Angew. Chem. Int. Ed.* **2006**, *45*, 5610–5613; V. W.-W. Yam, K. H.-Y. Chan, K. M.-C. Wong, N. Zhu, *Chem. Eur. J.* **2005**, *11*, 4535–4543; T. J. Wadas, Q.-M. Wang, Y.-j. Kim, C. Flaschenreim, T. N. Blanton, R. Eisenberg, *J. Am. Chem. Soc.* **2004**, *126*, 16841–16849; V. W.-W. Yam, K. M.-C. Wong, N. Zhu, *J. Am. Chem. Soc.* **2002**, *124*, 6506–6507; R. Büchner, J. S. Field, R. J. Haines, C. T. Cunningham, D. R. McMillin, *Inorg. Chem.* **1997**, *36*, 3952–3956; W. B. Connick, R. E. Marsh, W. P. Schaefer, H. B. Gray, *Inorg. Chem.* **1997**, *36*, 913–922; J. A. Baile, M. G. Hill, R. E. Marsh, V. M. Miskowski, W. P. Schaefer, H. B. Gray, *Inorg. Chem.* **1995**, *34*, 4591–4599; R. H. Herber, M. Croft, M. J. Coyer, B. Bilash, A. Sahiner, *Inorg. Chem.* **1994**, *33*, 2422–2426.
- [6] Y.-C. Chiu, C.-H. Lin, J.-Y. Hung, Y. Chi, Y.-M. Cheng, K.-W. Wang, M.-W. Chung, G.-H. Lee, P.-T. Chou, *Inorg. Chem.* **2009**, *48*, 8164–8172; Y.-C. Chiu, J.-Y. Hung, Y. Chi, C.-C. Chen, C.-H. Chang, C.-C. Wu, Y.-M. Cheng, Y.-C. Yu, G.-H. Lee, P.-T. Chou, *Adv. Mater.* **2009**, *21*, 2221–2225.
- [7] C. H. Shin, J. O. Huh, M. H. Lee, Y. Do, *Dalton Trans.* **2009**, 6476–6479.
- [8] K. Huang, H. Wu, M. Shi, F. Li, T. Yi, C. Huang, *Chem. Commun.* **2009**, 1243–1245.
- [9] Q. Zhao, L. Li, F. Li, M. Yu, Z. Liu, T. Yi, C. Huang, *Chem. Commun.* **2008**, 685–687.
- [10] Y. You, H. S. Huh, K. S. Kim, S. W. Lee, D. Kim, S. Y. Park, *Chem. Commun.* **2008**, 3998–4000.
- [11] C. Yi, Q.-Y. Cao, C.-J. Yang, L.-Q. Huang, J. H. Wang, M. Xu, J. Liu, P. Qiu, X.-C. Gao, Z.-F. Li, P. Wang, *Inorg. Chim. Acta* **2006**, *359*, 4355–4359.
- [12] Y. Chi, P.-T. Chou, *Chem. Soc. Rev.* **2010**, *39*, 638–655; H.-S. Duan, P.-T. Chou, C.-C. Hsu, J.-Y. Hung, Y. Chi, *Inorg. Chem.* **2009**, *48*, 6501–6508.
- [13] A. B. Tamayo, B. D. Alleyne, P. I. Djurovich, S. Lamansky, I. Tsyba, N. N. Ho, R. Bau, M. E. Thompson, *J. Am. Chem. Soc.* **2003**, *125*, 7377–7387.
- [14] A. Tsuboyama, H. Iwawaki, M. Furugori, T. Mukaide, J. Kamatani, S. Igawa, T. Moriyama, S. Miura, T. Takiguchi, S. Okada, M. Hoshino, K. Ueno, *J. Am. Chem. Soc.* **2003**, *125*, 12971–12979; V. V. Grushin, N. Herron, D. D. LeCloux, W. J. Marshall, V. A. Petrov, Y. Wang, *Chem. Commun.* **2001**, 1494–1495; S. Lamansky, P. Djurovich, D. Murphy, F. Abdel-Razzaq, R. Kwong, I. Tsyba, M. Bortz, B. Mui, R. Bau, M. E. Thompson, *Inorg. Chem.* **2001**, *40*, 1704–1711.
- [15] S. Lamansky, P. Djurovich, D. Murphy, F. Abdel-Razzaq, H. E. Lee, C. Adachi, P. E. Burrows, S. R. Forrest, M. E. Thompson, *J. Am. Chem. Soc.* **2001**, *123*, 4304–4312.
- [16] M. E. Thompson, B. Ma, P. Djurovich, *US Pat. Pub.* 2005/0164031 A1, **2005**.
- [17] X. Yang, Z. Wang, S. Madakuni, J. Li, G. E. Jabbour, *Adv. Mater.* **2008**, *20*, 2405–2409; Y.-S. Park, J.-W. Kang, D. M. Kang, J.-W. Park, Y.-H. Kim, S.-K. Kwon, J.-J. Kim, *Adv. Mater.* **2008**, *20*, 1957–1961; E. L. Williams, K. Haavisto, J. Li, G. E. Jabbour, *Adv. Mater.* **2007**, *19*, 197–202; X.-M. Yu, H.-S. Kwok, W.-Y. Wong, G.-J. Zhou, *Chem. Mater.* **2006**, *18*, 5097–5103; J.-H. Jou, M.-C. Sun, H.-H. Chou, C.-H. Li, *Appl. Phys. Lett.* **2006**, *88*, 141101–141103; B. W. D'Andrade, R. J. Holmes, S. R. Forrest, *Adv. Mater.* **2004**, *16*, 624–628; P. T. Furuta, L. Deng, S. Garon, M. E. Thompson, J. M. J. Fréchet, *J. Am. Chem. Soc.* **2004**, *126*, 15388–15389; I. Tanaka, M. Suzuki, S. Tokito, *Jpn. J. Appl. Phys.* **2003**, *42*, 2737–2740; B. W. D'Andrade, M. E. Thompson, S. R. Forrest, *Adv. Mater.* **2002**, *14*, 147–151.
- [18] J. K. Clegg, D. J. Bray, K. Gloe, K. Gloe, K. A. Jolliffe, G. A. Lawrance, L. F. Lindoy, G. V. Meehan, M. Wenzel, *Dalton Trans.* **2008**, 1331–1340; J. K. Clegg, D. J. Bray, K. Gloe, K. Gloe, M. J. Hayter, K. A. Jolliffe, G. A. Lawrance, G. V. Meehan, J. C. McMurtrie, L. F. Lindoy, M. Wenzel, *Dalton Trans.* **2007**, 1719–1730; M. M. Castano-Briones, A. P. Bassett, L. L. Meason, P. R. Ashton, Z. Pikramenou, *Chem. Commun.* **2004**, 2832–2833.
- [19] A. P. Bassett, S. W. Magennis, P. B. Glover, D. J. Lewis, N. Spencer, S. Parsons, R. M. Williams, L. De Cola, Z. Pikramenou, *J. Am. Chem. Soc.* **2004**, *126*, 9413–9424.
- [20] J. Brooks, Y. Babayan, S. Lamansky, P. I. Djurovich, I. Tsyba, R. Bau, M. E. Thompson, *Inorg. Chem.* **2002**, *41*, 3055–3066.
- [21] S. Welter, F. Lafolet, E. Cecchetto, F. Vergeer, L. De Cola, *ChemPhysChem* **2005**, *6*, 2417–2427.
- [22] A. Sarkar, S. Chakravorti, *J. Lumin.* **1995**, *65*, 163–168.
- [23] M. G. Colombo, A. Hauser, H. U. Güdel, *Top. Curr. Chem.* **1994**, *171*, 143–171.

- [24] F. Barigelletti, L. Flamigni, V. Balzani, J.-P. Collin, J.-P. Sauvage, A. Sour, E. C. Constable, A. M. W. C. Thompson, *J. Am. Chem. Soc.* **1994**, *116*, 7692–7699.
- [25] C. Cornioley-Deuschel, A. von Zelewsky, *Inorg. Chem.* **2002**, *41*, 3354–3358.
- [26] Z. Otwinowski, W. Minor in *Methods in Enzymology* (Eds.: C. W. Carter, R. M. Sweet), Academic Press, New York, **1997**, pp. 307–326.

Received: March 10, 2010
Published Online: July 1, 2010

A Hydroscopic Self-Catenated Net Formed by Borromean Layers Interlocked by Ferrocenyl Bridging Ligands

Xianju Shi,^[a] Weiyin Wang,^[a] Hongwei Hou,^{*[a]} and Yaoting Fan^[a]

Keywords: Structure elucidation / Coordination polymers / Layered compounds / Cadmium / Bridging ligands / Adsorption / Reversible hydration

Reaction of a flexible tripodal ligand, 1,3,5-tris(1,2,4-triazol-1-ylmethyl)-2,4,6-trimethylbenzene (ttmb), and an organo-metallic carboxylate 1,1'-bis(3-carboxy-1-oxopropyl)ferrocene (H₂bfc) with Cd(Ac)₂·2H₂O yields a trinodal, self-catenated 3D layer pillar complex {[Cd₃(bfc)₃(ttmb)₂(H₂O)₄]·8H₂O}_n (**1**), which is formed by connecting 2D hexagonal Cd^{II}-ttmb Borromean layers through ferrocenyl bridges in

both inter- and intralayers. The complex can undergo a dehydrated and rehydrated process in a single-crystal-to-single-crystal manner without affecting the overall framework. The amorphous sample of **1** can be regenerated by water to the crystalline material again. In addition, the nitrogen adsorption property of **1** was also investigated.

Introduction

The assembly of entangled coordination polymers showing topological complexity, structural integrity, and aesthetic beauty, such as polycatenation, polythreading and polyknotting (self-catenation), especially of those with undiscovered intriguing topologies has been appealing to chemists because of their promising applications as molecular devices or functional materials.^[1] Among the numerous reported novel entanglements of individual motifs, the Borromean system, which contains nontrivial three-ring links (three rings are interlocked without being interpenetrated), represents one of the most fascinating patterns and has long been regarded as an exceptionally challenging synthetic target.^[2]

To date, only a handful of coordination polymer systems comprising the entangled Borromean topology have been documented.^[3] Examination of these systems indicates that various supramolecular interactions play important roles in the formation and stabilization of this kind of linkage. We also noticed that such linkages mostly occur in low-dimensional architectures, the rarely reported 3D entanglements were all constructed through *n*-Borromean link.^[4,3a,3h,3i] Two-dimensional Borromean weaves interlocked together by ligand-supported coordination interactions to form 3D entangled frameworks have not been reported before. It is expected that the connections will increase the mechanical strength of the solid materials, since the whole entangle-

ment cannot be unraveled without breaking those strong chemical links in addition to the bonds of the Borromean rings. However, as a result of such a linkage, a real Borromean arrangement no longer exists, but the presence of this arrangement will make a significant contribution to enriching the topological types of coordination polymers.

It is well proven that complexes possessing particular structural features will likely exhibit distinctive properties. Given the fact that the entangled framework is flexible and can endure some structural expansion or contraction in response to diverse external stimuli, they have recently been regarded as potential materials in selective adsorption of guest molecules.^[5]

Therefore, the construction of novel flexible frameworks and the investigation of the framework stability is important in the search for a new generation of adsorption materials.

Herein, we present the first example of a trinodal self-catenated 3D layer pillar complex {[Cd₃(bfc)₃(ttmb)₂(H₂O)₄]·8H₂O}_n **1**, which contains 2D Cd^{II}-ttmb Borromean layers that are interlocked by ferrocenyl bridging ligands [H₂bfc = 1,1'-bis(3-carboxy-1-oxopropyl)ferrocene, ttmb = 1,3,5-tris(1,2,4-triazol-1-ylmethyl)-2,4,6-trimethylbenzene]. Maintenance of the framework upon removal and reintroduction of water molecules was investigated by using a combination of thermogravimetric analysis (TGA) and powder X-ray diffraction (PXRD). The results indicate that the partially dehydrated crystal of **1** can rehydrate spontaneously and rapidly in air to the nascent state, with identical cell parameters as those of the as-synthesized compound, and that the amorphous sample of **1** can once again be regenerated by water to the crystalline material, which is consistent with the presence of a flexible framework.

[a] Department of Chemistry, Zhengzhou University, Zhengzhou, Henan 450052, P. R. China
Fax: +86-371-67761744
E-mail: houghw@zzu.edu.cn

Supporting information for this article is available on the WWW under <http://dx.doi.org/10.1002/ejic.201000395>.

Results and Discussion

Crystal Structure of $\{[\text{Cd}_3(\text{bfc}s)_3(\text{tttmb})_2(\text{H}_2\text{O})_4] \cdot 8\text{H}_2\text{O}\}_n$ (**1**)

A single-crystal X-ray diffraction study reveals that the asymmetric unit of **1** contains three crystallographically independent Cd^{II} ions, three $\text{bfc}s^{2-}$ ligands, two tttmb ligands, and four coordinated water molecules. As can be seen from Figure 1a, Cd1, as well as Cd2, is coordinated in a distorted pentagonal-bipyramidal geometry, which is defined by five O atoms from two chelate carboxylate groups and one water molecule in the equatorial plane and two N atoms from two tttmb ligands in the apical position. Cd3 is in an octahedral geometry and coordinates to O12 and O19 from two monodentate carboxylate groups, O21 and O22 from two water molecules, and N15 and N18 from two tttmb ligands. The corresponding bond lengths and bond angles are listed in Table 1. The tttmb molecule is capable of bending and rotating freely, owing to its three flexible methylene groups. On coordinating to the Cd^{II} ions, one triazole ring lies outside the trimethylbenzene plane, and the other two triazole rings lie in the reverse orientation outside the trimethylbenzene plane to form a capital “Y”. In such a *cis,trans,trans* conformation, each tttmb ligand connects to three Cd^{II} ions to form an $(\text{ML})_6$ type network involving six tttmb and six Cd^{II} ions in a basic hexagonal ring, which adopts a chair conformation. The ring diameters, defined as the distance between two symmetry-related opposing Cd^{II} ions, range from 25.0350(51) to 26.6822(43) Å. Adjacent rings share edges and vertices to form a 2D (6, 3) undulated honeycomb (hcb) net, as shown in Figure 1b.

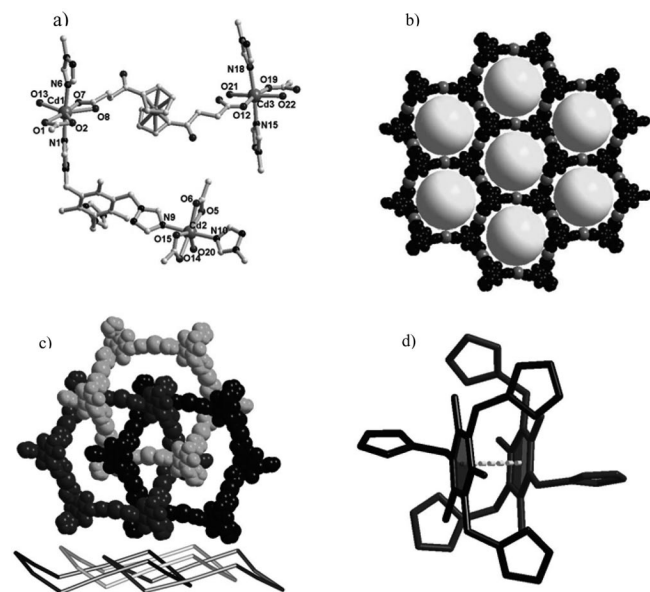


Figure 1. (a) Perspective drawing of **1** showing the local coordination environment around the Cd^{II} center. Hydrogen atoms and solvent molecules are omitted for clarity. (b) View of the 2D (6, 3) hcb network based on the $(\text{ML})_6$ -type hexagonal ring, which involves six tttmb ligands and six Cd^{II} ions. (c) The Borromean entangled rings from three adjacent networks isolated by removing $\text{bfc}s^{2-}$ groups. (d) Two adjacent tttmb ligands highlighting the π - π interactions (fragmented cylinder) between benzene rings.

Table 1. Selected bond lengths [Å] and angles [°] for complex **1**.^[a]

Cd1–N1	2.294(6)	Cd1–O13	2.326(5)
Cd1–N6#1	2.334(7)	Cd1–O8	2.402(5)
Cd1–O1	2.430(6)	Cd1–O2	2.456(6)
Cd1–O7	2.473(6)	Cd2–N9	2.329(6)
Cd2–O6	2.340(6)	Cd2–N10	2.335(6)
Cd2–O20	2.357(8)	Cd2–O15	2.415(6)
Cd2–O14	2.427(6)	Cd2–O5	2.521(6)
Cd3–O19	2.272(8)	Cd3–O12	2.304(6)
Cd3–N15	2.308(7)	Cd3–N18#2	2.298(6)
Cd3–O22	2.418(6)	Cd3–O21	2.444(8)
N1–Cd1–O13	97.6(2)	N1–Cd1–N6#1	175.0(2)
O13–Cd1–N6#1	87.4(2)	N1–Cd1–O8	95.4(2)
N6#1–Cd1–O8	81.7(2)	N1–Cd1–O1	84.3(2)
N6#1–Cd1–O1	95.4(2)	N1–Cd1–O2	90.3(2)
N6#1–Cd1–O2	85.5(2)	N1–Cd1–O7	91.9(2)
N6#1–Cd1–O7	89.6(2)	N9–Cd2–O6	90.4(2)
N9–Cd2–N10	175.2(2)	O6–Cd2–N10	87.0(2)
N9–Cd2–O20	88.3(3)	N10–Cd2–O20	96.4(3)
N9–Cd2–O15	85.6(2)	N10–Cd2–O15	90.5(2)
N9–Cd2–O14	92.9(2)	N10–Cd2–O14	87.0(2)
N9–Cd2–O5	87.2(2)	N10–Cd2–O5	94.4(2)
O19–Cd3–N15	87.7(3)	O12–Cd3–N15	86.3(2)
O19–Cd3–N18#2	93.4(3)	O12–Cd3–N18#2	93.2(2)
N15–Cd3–N18#2	174.3(2)	N15–Cd3–O22	93.2(2)
N18#2–Cd3–O22	92.5(2)	N15–Cd3–O21	83.3(3)
N18#2–Cd3–O21	91.3(3)		

[a] Symmetry transformations used to generate equivalent atoms in complex (**1**): #1 $-x + 3/2, y - 1/2, -z + 3/2$; #2 $-x + 1/2, y + 1/2, -z + 3/2$.

Further structure analyses reveal that there are three identical Cd^{II} - tttmb hcb networks entangled in one layer. Any two of the three parallelly interlocked networks are actually non-catenated and non-interpenetrated, but the appearance of the third network causes an inseparable interweaving, which is characteristic of Borromean topology (Figure 1c). The formation of this puzzling entanglement can be attributed to the large hcb voids and the corrugation of the single sheet. In the three entangled networks, there exist π - π interactions (face-to-face distance: 3.42 Å) between the adjacent central phenyl rings of tttmb (Figure 1d).

Notably, in addition to the weak π - π interactions, the three Cd^{II} - tttmb hcb networks are connected together through coordination interactions supported by bridging ferrocenyl carboxylate $\text{bfc}s^{2-}$, with $\text{Cd} \cdots \text{Cd}$ distances of 7.959(1) or 7.057(1) Å (Figure 2a). This is in contrast to known examples in which the Borromean interweaving takes place with the aid of various supramolecular forces^[3] or without any intermolecular interactions.^[6] However, upon connection through the $\text{bfc}s^{2-}$ ligands, the threefold entangled networks are held together more firmly, and it is no longer a Borromean entanglement.

Interestingly, stretched $\text{bfc}s^{2-}$ ligands exist, which connect the 2D layers together, to form a 3D layer pillar framework (Figure 2b). The $\text{Cd} \cdots \text{Cd}$ distance separated by such a bridging ligands is 18.118(4) Å, which is obviously longer than the length of the intralayer $\text{bfc}s^{2-}$ ligands. The whole 3D framework of **1** therefore can simply be regarded as resulting from connecting 2D Cd^{II} - tttmb Borromean layers through inter- and intralayer $\text{bfc}s^{2-}$ bridges. Topology

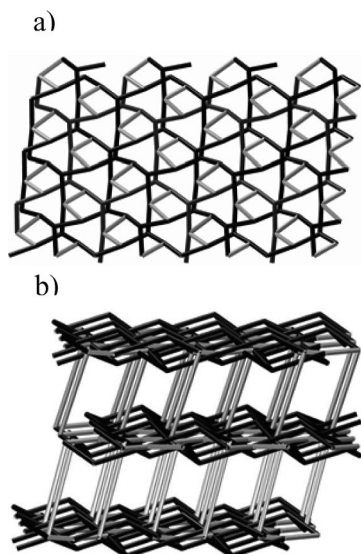


Figure 2. (a) Topological representation of the 2D connected "Borromean layer" structure. (b) The 3D layer pillar framework of **1**.

analysis performed by the program OLEX^[7] indicates that, in this adopted topological model, both kinds of ttmb ligands act as 3-connected nodes with a Schäfli symbol of $(6\cdot7^2)$; Cd1 and Cd3 are 4-connected nodes with the symbol $(6\cdot7\cdot8^4)$, while Cd2 is also a 4-connected node, but with a different symbol $(6^2\cdot7\cdot8^2\cdot9)$. By considering the stoichiometry, the whole net can be defined as a trinodal (3,4)-connected $(6\cdot7^2)_2(6\cdot7\cdot8^4)_2(6^2\cdot7\cdot8^2\cdot9)$ topological type. After further inspection of the structure, we found that some of the eight-membered shortest rings are catenated by other eight-membered short rings within this single network (Figure 3), so this net is an unusual self-catenated one. To the best of our knowledge, most of the reported self-catenated polymers are built on 4-, 5-, 6-, 8-, (3,5)-, or (3,6)-connected nodes;^[8] the (3,4)-connected self-catenated 3D polymers are very rare.^[9]

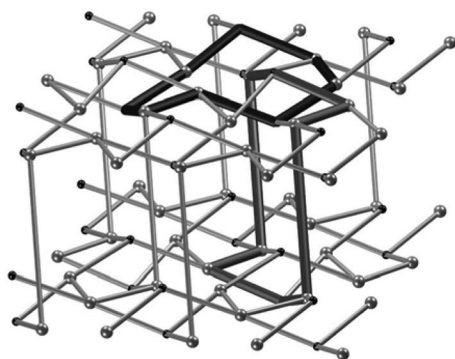


Figure 3. Schematic representation of the (3,4)-connected self-catenated 3D framework highlighting the catenated eight-membered shortest rings (thick stick).

Reversible Dehydrated and Rehydrated Studies

In view of the existence of abundant coordinated and guest water molecules in this entangled complex, we further

investigated the maintaining of the framework upon removal and reintroduction of water molecules, using a combination of TGA and PXRD. TGA of the as-synthesized sample shows a gradual weight loss of about 9.03% before 130 °C (Figure 4a, A), which indicates the release of solvent and coordinated water molecules (calculated 8.88%). The treatment of dichloromethane-immersed **1** at 110 °C under vacuum for one day led to the formation of the partially dehydrated **1a**, and the transparency of the single-crystal was still retained. The loss of water molecules was evidently proven by the TGA curve (Figure 4a, B). Noticeably, when **1a** was exposed to air, it rehydrated rapidly to afford **1b** without loss of crystallinity, and the single-crystal could be recollected with virtually identical cell parameters to the nascent solid.^[10] During the monitoring time (one hour), the increase in the weight of activated **1a** was about 4.48% (Figure 4a, lower left), which corroborates that the partially dehydrated framework responds with high affinity towards

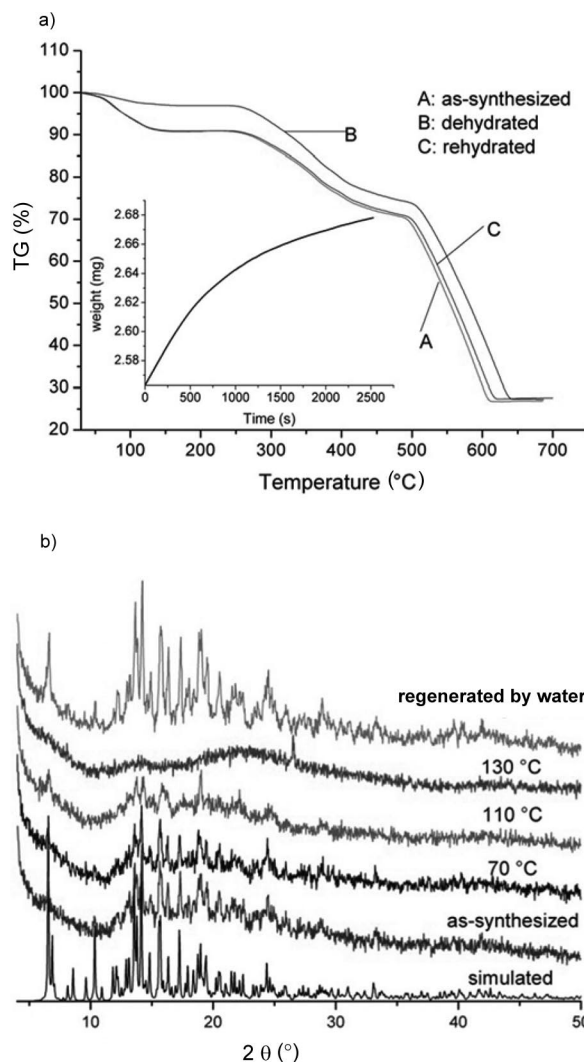


Figure 4. (a) Reversible dehydrated process for **1** as demonstrated by the TGA curves, A: as-synthesized **1**; B: dehydrated **1a**; C: rehydrated **1b**. Lower left: weight increase vs. time elapsed. (b) PXRD patterns of **1** in the different states.

water molecules. Three days later, the TGA curve of the air-exposed sample **1b** was investigated (Figure 4a, C), and it is almost identical to that of the as-synthesized **1**, which suggests that the mass has reverted back close to the original value.^[11] This result demonstrates that the transformation from **1** to **1b** is a single-crystal-to-single-crystal process in which the overall framework is not affecting (Figure S1).^[12]

Furthermore, the PXRD patterns were recorded for **1** after heating the dichloromethane-immersed crystalline samples to 70, 110, and 130 °C under vacuum, respectively. The phase purity of the bulk samples is supported by its PXRD pattern, which is in agreement with that simulated from the single-crystal X-ray diffraction data. As can be seen in Figure 4b, the PXRD patterns for the samples heated at 70 and 110 °C are similar to that of the as-synthesized sample, which indicates that the obvious phase transformation does not take place at such temperatures. When the sample was heated at 130 °C, the long-range order of the structure was lost and a phase transformation was observed, which may result from the dissociation of coordinated water molecules from the metal centers.^[13] Excitingly, this amorphous sample resulting from the loss of water can rejuvenate and regenerate to **1** when it is soaked in water for three days, which can be attributed to the readsorption and recoordination of water molecules.^[14] Such a transformation triggered by the removal and addition of water molecules can be characterized as a “crystal-to-crystal” process through an amorphous phase. Moreover, we used methanol instead of water to suspend the amorphous sample, and as a result, we obtained a broadened and weakened PXRD pattern in comparison with that of the as-synthesized sample, as can be seen in Figure S2.

Nitrogen Adsorption Study

Considering that the framework of **1** can be maintained even after water molecules pass in and out, nitrogen adsorption of **1** was investigated at 77 K to validate whether gas molecules can be enter the cavities. The Brunauer–Emmett–Teller (BET) surface area of **1** is calculated to be 8.88 m²/g, and the N₂ adsorption capacity is about 20.28 cc/g at $P/P_0 = 0.98$ (Figure 5). A slight shift is observed in the

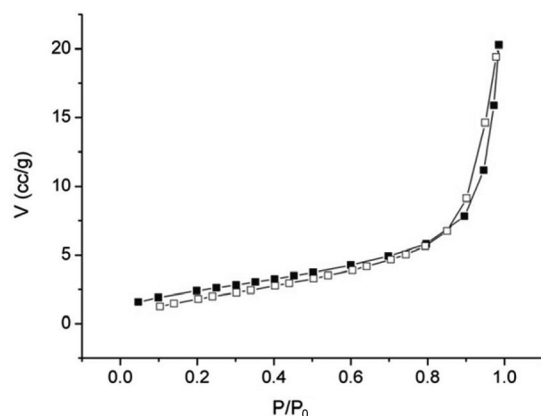


Figure 5. Nitrogen adsorption (filled) and desorption (open) isotherm of **1**.

PXRD pattern of the tested sample relative to that of the as-synthesized (Figure S3). This could be attributed to the dynamics and flexibility of the framework of **1**, a typical feature of the entangled framework in which subtle differences in the composition and guest content will lead to slightly different structures and thus PXRD patterns.^[15]

Conclusions

In conclusion, we present here an unprecedented infinite-layer pillar framework, which displays the following fascinating structure features: (a) they are formed by 2D hexagonal Borromean layers interlocked by bridging ligands; (b) they have a self-catenated 3D framework, which has a trinodal (3,4)-connected topology; (c) they form a rare 3D coordination polymer containing the organometallic ferrocene group.^[16] The complex exhibits a strong attachment to water molecules, because the partially dehydrated crystal of **1** can rehydrate spontaneously and rapidly in air to the nascent state with identical cell parameters to those of the as-synthesized **1**. Further the amorphous sample of **1** can be regenerated by water to the crystalline material again.

Experimental Section

Materials and Characterization: The ligands H₂bfc_s^[17] and ttmb^[18] were prepared according to literature methods. The other starting reagents and solvents employed were purchased from commercial sources and were used without further purification. The FTIR spectra were recorded from KBr pellets in the range 400–4000 cm^{−1} on a Bruker Tensor 27 spectrophotometer. Elemental analyses (C, H, and N) were carried out on a FLASH EA 1112 elemental analyzer. Thermal analyses were performed on a Netzsch STA 449C thermal analyzer from 30 to 700 °C at a heating rate of 10 °C min^{−1} in air. PXRD patterns were recorded by using Cu-K_α1 radiation on a PANalytical X'Pert PRO diffractometer. The sorption isotherm was measured at 77 K on a Quantachrome NOVA 1000e surface area and pore size analyzer.

Synthesis of {[Cd₃(bfc_s)₃(ttmb)₂(H₂O)₄]·8H₂O}_n (1**):** A MeOH/H₂O (v/v 2:1) solution (6 mL) containing H₂bfc_s (11.6 mg, 0.03 mmol) with a pH value of 7 (controlled by CH₃ONa) was added to a methanol solution (2 mL) of Cd(Ac)₂·2H₂O (8.0 mg, 0.03 mmol). A methanol solution (2 mL) of ttmb (7.3 mg, 0.02 mmol) was then added dropwise, and the mixture was homogenized and filtered. The resulting solution was allowed to stand in the dark at ambient temperature for one month. Finally, crimson crystals were obtained in 58% yield (14.1 mg). IR (KBr): $\tilde{\nu}$ = 3423 (m), 3117 (m), 1665 (s), 1562 (s), 1421 (s), 1258 (m), 1220 (m), 1009 (w), 879 (w), 675 (m), 533 (w), 481 (w) cm^{−1}. C₉₀H₁₁₄Cd₃Fe₃N₁₈O₃₀ (2432.74): calcd. C 44.43, H 4.72, N 10.36; found C 44.08, H 4.75, N 10.17.

TGA and PXRD Measurements: A sample of **1** (15 mg), after being immersed in dichloromethane for 3 d, was heated at 110 °C under vacuum for 1 d. Part of this sample was then used for TGA analysis immediately (Figure 4a, B), and the residual sample was exposed to air. The TGA curve (Figure 4a, C) of the air-exposed sample was investigated after 3 d. The samples, after being immersed in dichloromethane for 3 d, were heated at different temperatures (70, 110, and 130 °C) under vacuum for 1 d prior to PXRD measurements.

Nitrogen Adsorption Measurement: The sample, after being immersed in dichloromethane for 3 d, was heated at 110 °C under vacuum for 1 d prior to measurement. The pretreated sample (212.8 mg), which was placed in a cylindrical quartz tube, was heated at 110 °C under vacuum (1.33 Pa) for 1.5 h to remove the guest molecules. The sample was then dosed with N₂ gas, and the isotherm was recorded at each equilibrium pressure by the static volumetric method. The surface area was estimated by using the Brunauer–Emmett–Teller (BET) equation.

Crystal Data Collection and Refinement: Single crystals of **1** and **1b** were selected for indexing and intensity data collection on a Rigaku Saturn 724 CCD diffractometer with graphite-monochromated Mo-K α radiation ($\lambda = 0.71073$ Å) at room temperature. The structure of **1** was solved by direct methods and expanded by using Fourier techniques. The non-hydrogen atoms were refined with anisotropic thermal parameters, and hydrogen atoms were located at geometrically calculated positions and refined with isotropic displacement parameters. All calculations were performed by using the SHELXL-97 crystallographic software package^[19] and refined by full-matrix least-squares methods based on F^2 . Crystallographic and refinement details for **1** are summarized in Table 2. CCDC-757672 contains the supplementary crystallographic data for this paper. These data can be obtained free of charge from The Cambridge Crystallographic Data Centre via www.ccdc.cam.ac.uk/data_request/cif.

Table 2. Crystal data and structure refinement for complex **1**.

Formula	C ₉₀ H ₁₁₄ Cd ₃ Fe ₃ N ₁₈ O ₃₀
F_w	2432.74
Temp (K)	293(2)
Wavelength (Å)	0.71073
Crystal system	monoclinic
Space group	$P2_1/n$
a (Å)	15.317(3)
b (Å)	25.035(5)
c (Å)	27.591(6)
α (°)	90
β (°)	102.38(3)
γ (°)	90
V (Å ³)	10334(4)
Z	4
D_c (g cm ⁻³)	1.548
Absorption coefficient (mm ⁻¹)	1.100
$F(000)$	4872
GOF on F^2	1.044
$R_1 [I > 2\sigma(I)]^{[a]}$	0.0737
wR_2 (all data) ^[b]	0.2076
$\Delta\rho_{\min}$ and $\Delta\rho_{\max}$ (e Å ⁻³)	−0.935 and 1.837

[a] $R_1 = \|F_o\| - \|F_c\|/\|F_o\|$. [b] $wR_2 = [w(F_o^2 - F_c^2)^2/w(F_o^2)^2]^{1/2}$.

Supporting Information (see footnote on the first page of this article): Single-crystal pictures and PXRD patterns of the methanol-immersed sample and the sample after N₂ adsorption.

Acknowledgments

This work was financially supported by the National Natural Science Foundation (Nos. 20671082 and 20971110), the Program for New Century Excellent Talents of Ministry of Education of China (NCET) and the Outstanding Talented Persons Foundation of

Henan Province. The Ministry of Science and Technology of China is thanked for the International Science Linkages Program (2009DFA50620).

- a) N. W. Ockwig, O. Delgado-Friedrichs, M. O'Keeffe, O. M. Yaghi, *Acc. Chem. Res.* **2005**, *38*, 176–182; b) J. S. Siegel, *Science* **2004**, *304*, 1256–1258; c) X. L. Wang, C. Qin, E. B. Wang, Y. G. Li, Z. M. Su, L. Xu, L. Carlucci, *Angew. Chem. Int. Ed.* **2005**, *44*, 5824–5827; d) L. Carlucci, G. Ciani, D. M. Proserpio, *Coord. Chem. Rev.* **2003**, *246*, 247–289; e) S. R. Batten, R. Robson, *Angew. Chem. Int. Ed.* **1998**, *37*, 1460–1494; f) S. R. Batten, *CrystEngComm* **2001**, *3*, 67–72.
- a) K. S. Chichak, S. J. Cantrill, A. R. Pease, S. H. Chiu, G. W. V. Cave, J. L. Atwood, J. F. Stoddart, *Science* **2004**, *304*, 1308–1312; b) A. J. Peters, K. S. Chichak, S. J. Cantrill, J. F. Stoddart, *Chem. Commun.* **2005**, 3394–3396; c) J. C. Loren, M. Yoshizawa, R. F. Haldimann, A. Linden, J. S. Siegel, *Angew. Chem. Int. Ed.* **2003**, *42*, 5702–5705; d) C. D. Pentecost, A. J. Peters, K. S. Chichak, G. W. V. Cave, S. J. Cantrill, J. F. Stoddart, *Angew. Chem. Int. Ed.* **2006**, *45*, 4099–4104; e) C. D. Meyer, C. S. Joiner, J. F. Stoddart, *Chem. Soc. Rev.* **2007**, *36*, 1705–1723; f) C. A. Schalley, *Angew. Chem. Int. Ed.* **2004**, *43*, 4399–4401.
- a) S. Muthu, J. H. K. Yip, J. J. Vittal, *J. Chem. Soc., Dalton Trans.* **2002**, 4561–4568; b) R. Liantinio, P. Metrangolo, F. Meyer, T. Pilati, W. Navarrini, G. Resnati, *Chem. Commun.* **2006**, 1819–1821; c) P. Byrne, G. O. Lloyd, N. Clarke, J. W. Steed, *Angew. Chem. Int. Ed.* **2008**, *47*, 5761–5764; d) M. P. Suh, H. J. Choi, S. M. So, B. M. Kim, *Inorg. Chem.* **2003**, *42*, 676–678; e) X. Q. Lu, M. Pan, J. R. He, Y. P. Cai, B. S. Kang, C. Y. Su, *CrystEngComm* **2006**, *8*, 827–829; f) Q. X. Yao, X. H. Jin, Z. F. Ju, H. X. Zhang, J. Zhang, *CrystEngComm* **2009**, *11*, 1502–1504; g) J. R. Li, L. Song, S. W. Du, *Inorg. Chem. Commun.* **2007**, *10*, 358–361; h) Y. B. Men, J. L. Sun, Z. T. Huang, Q. Y. Zheng, *Angew. Chem. Int. Ed.* **2009**, *48*, 2873–2876; i) M. L. Tong, X. M. Chen, B. H. Ye, L. N. Jiang, *Angew. Chem. Int. Ed.* **1999**, *38*, 2237–2240; j) L. Dobrzanska, H. G. Raubenheimer, L. J. Barhour, *Chem. Commun.* **2005**, 5050–5052; k) D. B. Leznoff, B. Y. Xue, R. J. Batchelor, F. W. B. Einstein, B. O. Patrick, *Inorg. Chem.* **2001**, *40*, 6026–6034.
- L. Carlucci, G. Ciani, D. M. Proserpio, *CrystEngComm* **2003**, *5*, 269–279.
- a) R. Kitaura, K. Seki, G. Akiyama, S. Kitagawa, *Angew. Chem. Int. Ed.* **2003**, *42*, 428–431; b) S. Kitagawa, R. Kitaura, S. Noro, *Angew. Chem. Int. Ed.* **2004**, *43*, 2334–2375; c) B. L. Chen, M. Eddaoudi, S. T. Hyde, M. O'Keeffe, O. M. Yaghi, *Science* **2001**, *291*, 1021–1023.
- a) X. L. Zhang, C. P. Guo, Q. Y. Yang, W. Wang, W. S. Liu, B. S. Kang, C. Y. Su, *Chem. Commun.* **2007**, 4242–4244; b) J. J. Jang, L. Li, T. Yang, D. B. Kuang, W. Wang, C. Y. Su, *Chem. Commun.* **2009**, 2387–2389.
- O. V. Dolomanov, A. J. Blake, N. R. Champness, M. Schröder, *J. Appl. Crystallogr.* **2003**, *36*, 1283–1284.
- a) M. H. Bi, G. H. Li, Y. C. Zou, Z. Shi, S. H. Feng, *Inorg. Chem.* **2007**, *46*, 604–606; b) H. L. Sun, S. Gao, B. Q. Ma, S. R. Batten, *CrystEngComm* **2004**, *6*, 579–583; c) F. Luo, Y. X. Che, J. M. Zheng, *Cryst. Growth Des.* **2006**, *6*, 2432–2434; d) X. L. Wang, C. Qin, E. B. Wang, Z. M. Su, *Chem. Eur. J.* **2006**, *12*, 2680–2691; e) X. Li, R. Cao, D. F. Sun, W. H. Bi, D. Q. Yuan, *Eur. J. Inorg. Chem.* **2004**, 2228–2231.
- Y. Qi, F. Luo, Y. X. Che, J. M. Zheng, *Cryst. Growth Des.* **2008**, *8*, 606–611.
- Cell parameters of **1b**: $a = 15.329(7)$, $b = 24.603(5)$, $c = 27.176(5)$ Å, $\beta = 101.00(4)^\circ$, $V = 10061(5)$ Å³, $Z = 4$, 41566 reflections collected, 23086 unique ($R_{\text{int}} = 0.1828$). Elemental analysis: C 45.03, H 4.64, N 10.54.
- B. D. Chandler, D. T. Cramb, G. K. H. Shimizu, *J. Am. Chem. Soc.* **2006**, *128*, 10403–10412.

- [12] M. C. Das, P. K. Bharadwaj, *J. Am. Chem. Soc.* **2009**, *131*, 10942–10949.
- [13] a) X. D. Guo, G. S. Zhu, Z. Y. Li, Y. Chen, X. T. Li, S. L. Qiu, *Inorg. Chem.* **2006**, *45*, 4065–4070; b) T. K. Maji, G. Mostafa, H. C. Changa, S. Kitagawa, *Chem. Commun.* **2005**, 2436–2438.
- [14] a) J. S. Zhou, J. W. Cai, L. Wang, S. W. Ng, *Dalton Trans.* **2004**, 1493–1497; b) K. Uemura, S. Kitagawa, M. Kondo, K. Fukui, R. Kitaura, H. C. Chang, T. Mizutani, *Chem. Eur. J.* **2002**, *8*, 3586–3600.
- [15] a) D. N. Dybtsev, H. Chun, K. Kim, *Angew. Chem. Int. Ed.* **2004**, *43*, 5033–5036; b) B. L. Chen, S. Q. Ma, E. J. Hurtado, E. B. Lobkovsky, H. C. Zhou, *Inorg. Chem.* **2007**, *46*, 8490–8492.
- [16] a) L. W. Mi, H. W. Hou, Z. Y. Song, H. Y. Han, H. Xu, Y. T. Fan, S. W. Ng, *Cryst. Growth Des.* **2007**, *7*, 2553–2561; b) J. Yang, J. F. Ma, Y. Y. Liu, S. L. Li, G. L. Zheng, *Eur. J. Inorg. Chem.* **2005**, 2174–2180.
- [17] P. J. Graham, R. V. Lindsey, G. W. Parshall, M. L. Peterson, G. M. Whitman, *J. Am. Chem. Soc.* **1957**, *79*, 3416–3421.
- [18] H. K. Liu, W. Y. Sun, H. L. Zhu, K. B. Yu, W. X. Tang, *Inorg. Chim. Acta* **1999**, *295*, 129–135.
- [19] G. M. Sheldrick, *SHELXL97, A Program for the Refinement of Crystal Structures from X-ray Data*; University of Göttingen, Göttingen, Germany, **1997**.

Received: April 9, 2010
Published Online: June 25, 2010

Investigation of the Zero-Field Splitting in Six- and Seven-Coordinate Mononuclear Mn^{II} Complexes with N/O-Based Ligands by Combining EPR Spectroscopy and Quantum Chemistry

Jordi Rich,^[a,b] Carmen E. Castillo,^[a,c] Isabel Romero,^[b] Montserrat Rodríguez,^[b] Carole Duboc,^{*[a]} and Marie-Noëlle Collomb^{*[a]}

Keywords: Manganese / EPR spectroscopy / Zero-field splitting / Electronic parameters / Density functional calculations

The electronic properties of a series of seven mononuclear Mn^{II} complexes with an N/O and N/Cl coordination sphere have been investigated by X- and Q-band EPR spectroscopy as well as by density functional theory (DFT). The [Mn(terpy)(CF₃CO₂)₂(H₂O)] (**1**), [Mn(pb)₂(CF₃SO₃)₂] (**2**), [Mn(pb)₂(NO₃)(H₂O)](NO₃) (**3**), [Mn(bpy)₂(CF₃CO₂)₂] (**4**) and [Mn(pb)₂-Cl₂] (**5**) complexes are six-coordinate, whereas [Mn(terpy)-(NO₃)₂(H₂O)] (**6**) and [Mn(bpea)(NO₃)₂] (**7**) are seven-coordinate [terpy = 2,2':6,2''-terpyridine, pb = (-)-pinene[5,6]bipyridine, bpy = 2,2'-bipyridine, bpea = *N,N*-bis(2-pyridylmethyl)ethylamine]. The X-ray structure of new complex **1** has also been resolved, whereas the structures of **2–7** have been already reported. The *D* values of the N/O-coordinated complexes **1–4**, **6** and **7** all fall into the narrow range of 0.035–0.086 cm⁻¹. Complex **5** exhibits a slightly larger *D* value of

0.146 cm⁻¹, in accordance with its N/Cl coordination sphere. The sign of *D* has been determined from the low-temperature Q-band EPR spectra for all complexes with the exception of **1** because of its large *E/D* ratio. The zero-field splitting (ZFS) parameters of **1–7** have been predicted by DFT calculations using two types of functionals, BP86 and B3LYP. The calculations were initiated from the crystal structures as well as from optimized structures in which only the positions of the hydrogen atoms were relaxed. The calculated *D* values show that B3LYP is not suited to predict the ZFS for Mn^{II} complexes with only N/O-based ligands, whereas with BP86 the quality of the prediction is satisfactory. Moreover, with BP86, the sign of *D* is correctly reproduced within the series when experimentally determined.

Introduction

In recent years, considerable attention has been paid to the precise determination of the zero-field splitting (ZFS) of transition-metal ion complexes with a total ground spin state $S > 1/2$.^[1–4] In fact, the ZFS is largely involved in the design of single-molecule magnets for which a large and negative axial ZFS (*D* parameter) represents an essential criterion for reaching their desired magnetic characteristics.^[5,6] Furthermore, for several transition-metal ions, it has been evidenced that the ZFS can probe their structural and electrostatic environment.^[1] This is particularly true in the case of the Mn^{II} ion. Indeed, magnetostructural correlations have been proposed^[7] based on the experimental in-

vestigation of a large number of mononuclear Mn^{II} complexes for which the structure has been resolved by X-ray diffraction and the ZFS precisely determined by EPR spectroscopy. When the Mn^{II} ion is coordinated to at least one halide ligand, the nature of the halide controls the ZFS with $D_I > D_{Br} > D_{Cl}$.^[8–18] On the other hand, for five- and six-coordinate complexes with only nitrogen- and/or oxygen-based ligands, the ZFS is governed by the coordination number of the Mn^{II} atom with $|D_5| > |D_6|$.^[19–21]

The rationalization of these experimental tendencies has required the understanding of the physical origin of the ZFS. This has been recently achieved by quantum chemistry in a DFT framework.^[14,20,22,23] A good prediction of *D* has been obtained since the two physical factors that contribute to the bilinear term in the ZFS have been quantified: the direct dipole–dipole interaction of unpaired electrons (SSC) and the spin–orbit coupling (SOC) of excited states into the ground state.^[23,24] For the halide complexes, the major contribution to *D* arises from a cross term between the metal- and halide-SOC contributions that explains the strong effect of the nature of the halide on *D*.^[14] In contrast, for the five- and six-coordinate N/O complexes, the physical origin of *D* is different since the major contribution is the SOC and SSC parts, respectively.^[20]

[a] Université Joseph Fourier Grenoble 1 / CNRS, Département de Chimie Moléculaire, UMR-5250, Institut de Chimie Moléculaire de Grenoble FR-CNRS-2607, Laboratoire de Chimie Inorganique Rédox, B. P. 53, 38041 Grenoble Cedex 9, France

[b] Departament de Química and Serveis Tècnics de Recerca (STR), Universitat de Girona, Campus de Montilivi, 17071 Girona, Spain

[c] Dept. de Ciencia de los Materiales e Ingeniería Metalúrgica y Química Inorgánica, Facultad de Ciencias, Universidad de Cádiz, 11510 Cádiz, Spain

A deeper analysis of the ZFS for this latter class of compounds shows that the relative ratio between the N- and O-based ligands seems not to affect the D magnitude.^[7] However, this conclusion is almost exclusively based on our previous investigation performed on theoretical simplified models because of the limited experimental data available on compounds in a mixed N/O environment.^[20] The large majority of mononuclear Mn^{II} complexes for which the D magnitude has been precisely determined by EPR spectroscopy are in N₆, N₅, O₆ and O₅ environments. Furthermore, the ZFS of only one seven-coordinate mononuclear complex has been investigated by EPR so far.^[25] The reported D value for this N₆O complex falls in the range of the six-coordinate N/O complexes, but the prediction of the D value by DFT was rather poor. Thus, additional experimental and theoretical data on the ZFS of these compounds are required to evaluate whether or not the ZFS can probe the ratio of N/O ligands and the coordination number of the Mn^{II} ion (6 vs. 7). These data should be also useful for the biochemical community since this type of coordination sphere reproduces those of the Mn^{II} ions contained at the active sites of several metalloenzymes.^[26–30]

Consequently, in this paper, we determine, through the help of X- and Q-band EPR spectroscopy, the spin Hamil-

tonian parameters (SHPs) of a series of mononuclear Mn^{II} complexes in various mixed coordination spheres (i.e., N₃O₃, N₂O₄, N₄Cl₂ and N₃O₄; Figure 1). The [Mn(terpy)-(CF₃CO₂)₂(H₂O)] (1), [Mn(pb)₂(CF₃SO₃)₂] (2), [Mn(pb)₂(NO₃)(H₂O)](NO₃)(3), [Mn(bpy)₂(CF₃CO₂)₂] (4) and [Mn(pb)₂Cl₂] (5) complexes are six-coordinate, whereas [Mn(terpy)(NO₃)₂(H₂O)] (6) and [Mn(bpea)(NO₃)₂] (7) are seven-coordinate [terpy = 2,2':6,2''-terpyridine, pb = (–)-pinene[5,6]bipyridine, bpy = 2,2'-bipyridine, bpea = *N,N*-bis(2-pyridylmethyl)ethylamine]. Complexes 2–7 were previously synthesized and structurally characterized,^[31–33] whereas complex 1 has been isolated in this work and its structure resolved by X-ray crystallography. Based on the X-ray structures, we have also predicted the ZFS of 1–7 by quantum chemistry using a DFT approach.

In our previous works performed on complexes that contained halide(s) or only N/O ligand(s), we have successfully used the BP86 functional to calculate the ZFS.^[14,20,22] However, an improvement in the prediction of the ZFS for mononuclear Mn^{II} dihalide complexes has been recently achieved with B3LYP.^[23] Therefore, in this work, the D values of 1–7 have been calculated with both functionals to evaluate their respective performance.

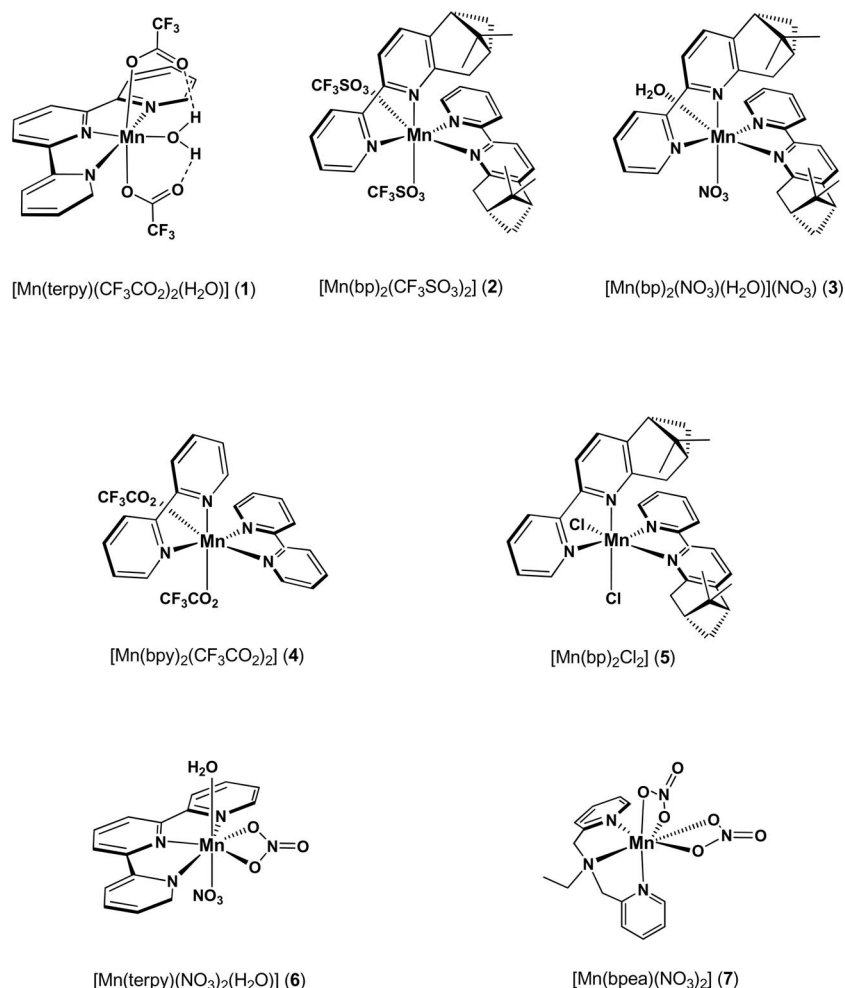


Figure 1. Schematic representation of complexes 1–7.

Results and Discussion

Synthesis and Crystal Structure of 1

Complex **1** was isolated from a mixture of an equimolar amount of $[\text{Mn}(\text{CF}_3\text{CO}_2)_2(\text{H}_2\text{O})_4]$ ^[34] and terpy in CH_3CN . Single crystals were obtained by slow diffusion of ethyl acetate into this solution and the structure was determined by X-ray diffraction. Figure 2 displays the ORTEP view of complex **1**. Table 1 provides the principal crystallographic data together with selected bond lengths and angles.

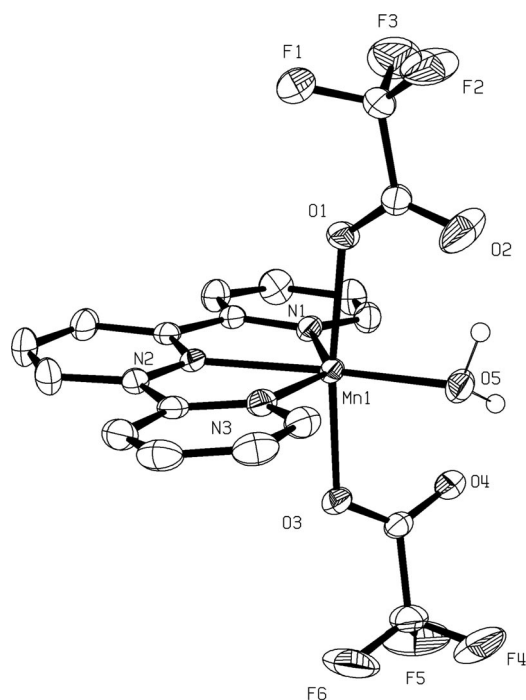


Figure 2. ORTEP diagram showing the molecular structure of complex **1**. Except for the hydrogen atoms of the water molecule that are discussed in the main text, the hydrogen atoms have been omitted for clarity.

Table 1. Selected bond lengths [Å] and angles [°] for **1**.

Mn1–O1	2.207(2)	Mn1–N1	2.269(2)
Mn1–O3	2.162(2)	Mn1–N2	2.233(2)
Mn1–O5	2.148(2)	Mn1–N3	2.275(2)
O1–Mn1–O3	173.30(6)	O3–Mn1–N1	93.26(7)
O1–Mn1–O5	85.93(6)	O3–Mn1–N2	94.09(6)
O1–Mn1–N1	88.87(7)	O3–Mn1–N3	92.10(7)
O1–Mn1–N2	92.61(6)	N1–Mn1–N2	71.63(7)
O1–Mn1–N3	90.04(7)	N1–Mn1–N3	142.67(7)
O3–Mn1–O5	87.56(6)	N2–Mn1–N3	71.15(7)

The Mn^{II} ion is six-coordinated by three nitrogen atoms of the terpy ligand and three oxygen atoms, one from the aqua ligand and the others from the two *trans*-trifluoroacetate anions in a distorted octahedral geometry. Both trifluoroacetate ions act as unidentate ligands. The main distortion of the resulting octahedral coordination sphere originates from the small $\text{N1}, \text{N3}–\text{Mn1}–\text{N2}$ angle of the terpy ligand. The $\text{Mn}–\text{N}$ distances fall in the same range as in other Mn^{II} -terpyridine complexes.^[13,33] The $\text{Mn}–\text{O}(\text{aqua or$

trifluoroacetate) bond lengths are comparable to those found in $[\text{Mn}(\text{CF}_3\text{CO}_2)_2(\text{H}_2\text{O})_4]$,^[34] **4**^[32] and $[\text{Mn}(\text{phen})(\text{CF}_3\text{CO}_2)(\text{H}_2\text{O})_3](\text{NO}_3)$.^[35]

The crystal structure of **1** is stabilized by intramolecular hydrogen bonds that involve the hydrogen atoms of the aqua ligand and both unbound oxygen atoms of the carboxylate ligands, O4 and O2. The hydrogen-bonding parameters are listed in Table 2. Similar intramolecular hydrogen-bonding interactions have been observed in $[\text{Mn}(\text{CF}_3\text{CO}_2)_2(\text{H}_2\text{O})_4]$.^[34]

Table 2. Hydrogen bonds [Å] and angles [°] for **1**.

D–H···A	D–H	H···A	D···A	D–H···A
O5–H12···O4	0.95	2.00	2.800(2)	140.2
O5–H13···O2	0.95	1.75	2.620(3)	151.1

X- and Q-Band EPR Spectroscopy Experiments

Powder X- and Q-band EPR spectra have been recorded on each complex over a temperature range between 5 K and room temperature (Figures 3, 4, 5 and 6). It clearly appears that the high-field limit condition is only reached at the Q-band frequency, which means that the D values of the complexes are generally smaller than the energy provided by the EPR spectrometer (i.e., 1.2 cm^{-1}). This is in accordance with the expected D values ($< 0.22 \text{ cm}^{-1}$) for such complexes.^[7] Such Q-band EPR-spectroscopy experiments have been already carried out on Mn^{II} complexes and in particular on a mononuclear Mn^{II} -containing enzyme.^[36] The Q-band EPR spectra recorded under such high-field conditions are easily analyzable, and a direct estimation of the D and E values can be afforded as described elsewhere.^[13] Actually, for high-spin Mn^{II} complexes, the shape of the EPR spectra only depends on the ZFS terms since the anisotropy of the Zeeman interaction is very small and leads to g values close to 2.^[37,38]

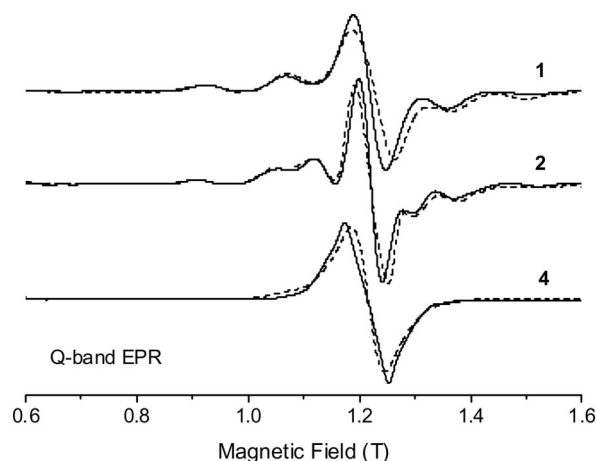


Figure 3. Experimental (solid line) and simulated (dashed line) Q-band EPR spectra recorded at room temperature on powder of complexes **1**, **2** and **4**. The parameters used for the simulation are: $g_{\text{iso}} = 2$; for **1**, $D = 0.068 \text{ cm}^{-1}$, $E/D = 0.308$; for **2**, $D = -0.071 \text{ cm}^{-1}$, $E/D = 0.070$; for **4**, $D = -0.035 \text{ cm}^{-1}$, $E/D = 0.154$.

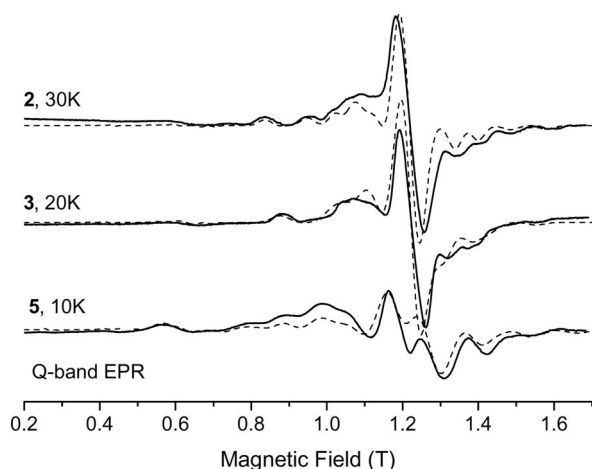


Figure 4. Experimental (solid line) and simulated (dashed line) Q-band EPR spectra recorded at low temperatures (10–30 K) on powder of complexes **2**, **3** and **5**. The parameters used for the simulation are: $g_{\text{iso}} = 2$; for **2**, $D = +0.087 \text{ cm}^{-1}$, $E/D = 0.138$; for **3**, $D = -0.078 \text{ cm}^{-1}$, $E/D = 0.077$; for **5**, $D = -0.150 \text{ cm}^{-1}$, $E/D = 0.113$.

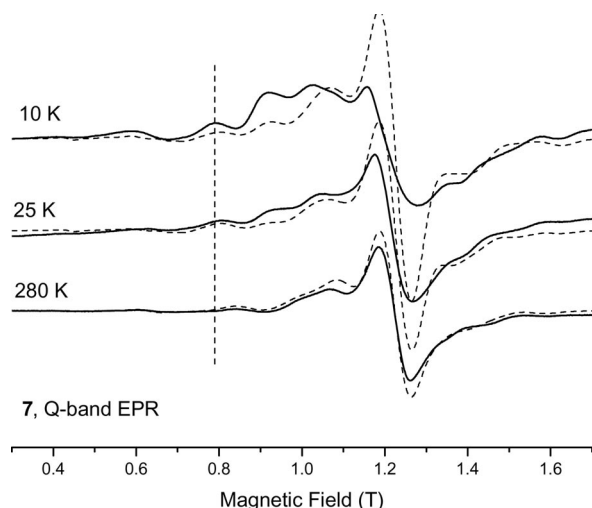


Figure 5. Experimental (solid line) and simulated (dashed line) Q-band EPR spectra recorded at different temperatures (10, 25 K and room temperature) on powder of complex **7**. The parameters used for the simulation are: $g_{\text{iso}} = 2$; at 10 K, $D = +0.095 \text{ cm}^{-1}$, $E/D = 0.152$; at 25 K, $D = +0.092 \text{ cm}^{-1}$, $E/D = 0.147$; at room temp. $D = +0.086 \text{ cm}^{-1}$, $E/D = 0.093$.

A comparable shape of the Q-band EPR spectra is observed for the whole series of complexes. Features are present around $g = 2$; these are associated with the $|^5/2, -1/2\rangle \rightarrow |^5/2, +1/2\rangle$ transitions along the x , y and z magnetic axes. The relative intensity of this central line varies as a function of the temperature and becomes prominent at room temperature to the detriment of the wings. Another common feature is the line located at 0.6 T ($g = 4$) observed at low temperature, which corresponds to the unique “forbidden” transition. On the other hand, the X-band EPR spectra (Figure 6) present a quite different shape depending on the complex and therefore seem to be very sensitive to the environment of the Mn^{II} ion. Nevertheless, the high-field limit condition not having been reached, their analysis

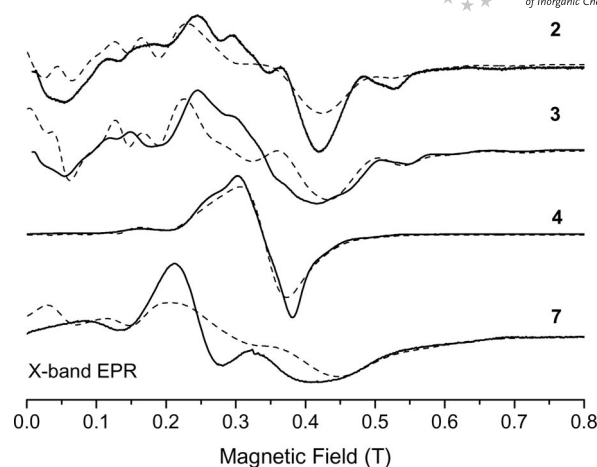


Figure 6. Experimental (solid line) and simulated (dashed line) X-band EPR spectra recorded at room temperature on powder of complexes **2**, **3**, **4** and **7**. The parameters used for the simulation are: $g_{\text{iso}} = 2$; for **2**, $|D| = 0.082 \text{ cm}^{-1}$, $E/D = 0.122$; for **3**, $|D| = 0.087 \text{ cm}^{-1}$, $E/D = 0.115$; for **4**, $|D| = 0.038 \text{ cm}^{-1}$, $E/D = 0.132$; for **7**, $|D| = 0.092 \text{ cm}^{-1}$, $E/D = 0.120$.

is rendered delicate because of the mixture that occurs between the Zeeman levels.

The variable-temperature study has pointed out an interesting effect. In Figure 5, the 10 K spectrum recorded on **7** presents a feature at 0.79 T that is shifted to 0.84 T at room temperature. A similar shift occurs for the 1.62 T transition at 10 K in the high-field wing that moves to 1.57 T at room temperature. These shifts are the signature of a slight decrease of the D value when the temperature increases and thus of small structural modifications of the Mn^{II} environment (see below). A similar behaviour has been observed for all complexes.

For neat-powder EPR spectra, the ^{55}Mn hyperfine interaction is never resolved, presumably because of the intermolecular dipole–dipole interactions together with the D strain that contribute to the broadening of the line. As a consequence, the accurate determination of the spin Hamiltonian parameters can be obtained by simulating the experimental EPR spectra using a full-matrix diagonalization procedure of the simplified Hamiltonian displayed in Equation (1).

$$H = \mu_B \hat{B} \cdot [g] \cdot \hat{S} + D(\hat{S}_z^2 - 1/3\hat{S}^2) + E(\hat{S}_x^2 - \hat{S}_y^2) \quad (1)$$

The first term represents the electronic Zeeman interaction. The last two terms define the second-order (bilinear) ZFS interaction with D and E representing the axial and rhombic parts, respectively. Table 3 summarizes all experimental D and E/D parameters at room temperature. The simulated EPR spectra nicely reproduce the experimental data even if a poorer quality of the simulations can be noticed in the case of the X-band EPR data (Figures 3, 4, 5 and 6). This may be attributed to the difficulty of precisely calculating the relative intensity of the transitions since they occur between mixed Zeeman levels.

Table 3. Experimental and calculated ZFS parameters (D in cm^{-1} and E/D) of complexes **1–7** at room temperature.

Complex	Coordination no.	sphere	$D_{\text{exptl.}}^{[a]}$	$D_{\text{calcd.}}^{[b]}$	$E/D_{\text{exptl.}}$	$E/D_{\text{calcd.}}$
[Mn(terpy)(CF ₃ CO ₂) ₂ (H ₂ O)] (1)	6	N ₃ O ₃	0.068	−0.041 (+0.405)	0.308	0.328
[Mn(pb) ₂ (CF ₃ SO ₃) ₂] (2)	6	N ₄ O ₂	−0.071	−0.029 (−0.108)	0.070	0.134
[Mn(pb) ₂ (NO ₃)(H ₂ O)](NO ₃) (3)	6	N ₄ O ₂	−0.074	−0.050 (+0.147)	0.122	0.292
[Mn(bpy) ₂ (CF ₃ CO ₂) ₂] (4)	6	N ₄ O ₂	−0.035	−0.087 (−0.307)	0.154	0.059
[Mn(pb) ₂ (Cl) ₂] (5)	6	N ₄ Cl ₂	−0.146	−0.180 (+0.173)	0.116	0.283
[Mn(terpy)(NO ₃) ₂ (H ₂ O)] (6)	7	N ₃ O ₄	−0.068	−0.090 (−0.077)	0.147	0.150
[Mn(bpea)(NO ₃) ₂] (7)	7	N ₃ O ₄	+0.086	+0.075 (+1.380)	0.093	0.094

[a] When determined, the sign of D is reported. [b] The basis used for the calculations is BP86; the results obtained with the B3LYP basis set are given in parentheses.

The sign of D has been unambiguously established from low-temperature Q-band EPR spectra for all complexes, except for **1**, because of its large E/D value of 0.308.^[39]

For the whole series of complexes, the D values are within the magnitude range of 0.035–0.146 cm^{-1} . The largest value has been observed for complex **5**, in which Mn^{II} is coordinated to two chloride anions. Previous studies have shown that the D magnitude is correlated to the nature of the halide in the case of the Mn^{II} ion, since a major contribution arises from the interference between metal- and halide-SOC contributions, proportional to $\zeta_{\text{Mn}}\zeta_{\text{X}}$. The D value of 0.146 cm^{-1} of **5** is in the range found for the other chlorido complexes (i.e., $0.110 < |D_{\text{Cl}}| < 0.319 \text{ cm}^{-1}$).^[7,17]

For the six-coordinate complexes **1–4** with only N- and O-based ligands, the D values are between 0.035 and 0.074 cm^{-1} , which is a very narrow range that falls between the previously reported values for such complexes (0.001–0.175 cm^{-1}).^[7] The N/O ratio of the coordination sphere of Mn^{II} seems to have no effect on D . Also, in agreement with previous observations done on six-coordinate Mn^{II} complexes with N₆, O₆ and N₅O coordination spheres, the E/D ratio can neither be rationalized in terms of the nature of the ligands, nor in terms of the N/O ratio.^[7]

The seven-coordinate complexes **6** and **7** display smaller D values (0.068 and 0.086 cm^{-1} , respectively) than that determined on the previously reported seven-coordinate mononuclear Mn^{II} complex ($D = 0.127 \text{ cm}^{-1}$).^[25] However, all of these D values are in the same range as observed for the six-coordinate N/O complexes, and thus significantly smaller than previously reported values for five-coordinate N/O complexes ($0.2500 < |D_{\text{S}}| < 0.3000$).^[20]

DFT Calculations

It has been previously shown that the DFT approach used here is suitable for mononuclear Mn^{II} complexes that contain either halide ligands,^[14,25] only N/O-based li-

gands^[20,25] or S-based ligands.^[40] In this work, DFT calculations have been performed on complexes **1–7**. The calculations were initiated from the crystal structures as well as from optimized structures in which only the positions of the hydrogen atoms were relaxed. Actually, the EPR parameters have not been calculated on fully optimized structures since they generally lead to a significant deterioration of the theoretical predictions.^[22,23,41,42] We have already demonstrated throughout several studies that D is very sensitive to small structural modifications.^[14,20] Therefore, the quality of the experimental structures is crucial for the success of the calculations. In particular, the position of the hydrogen atoms is not usually defined to high precision for structures resolved by X-ray diffraction experiments. The results obtained with the experimental structures are virtually indistinguishable from those where only the hydrogen atoms were optimized (less than 5% of difference between both the calculated D values). Thus, in Table 4, only a unique set of values corresponding to the optimized structures is reported.

Table 4. Spin–spin (D_{SSC}) and spin–orbit coupling (D_{SOC}) contributions to the D values together with the total D [cm^{-1}] obtained from DFT calculations.

Complex	D_{total}	D_{SOC}	$a \rightarrow a$	$\beta \rightarrow \beta$	$a \rightarrow \beta$	$\beta \rightarrow a$	D_{SSC}
1	−0.041	−0.039	+0.016	−0.007	−0.052	+0.004	−0.001
2	−0.029	+0.002	−0.019	−0.016	+0.028	+0.009	−0.031
3	−0.050	+0.020	−0.027	−0.030	+0.070	+0.006	−0.070
4	−0.087	−0.057	+0.001	+0.003	−0.057	−0.004	−0.031
5	−0.180	−0.177	−0.012	−0.048	−0.118	0.000	−0.003
6	−0.090	−0.062	−0.003	−0.012	−0.050	+0.003	−0.028
7	+0.075	+0.056	−0.001	−0.011	+0.060	+0.008	+0.019

Two physical factors contribute to the bilinear term in the ZFS: the direct dipole–dipole interaction of unpaired electrons (SSC) and the spin–orbit coupling (SOC) of excited states into the ground state.^[23,24] Systematic studies performed on Mn^{II} complexes have shown that the best approach to calculate the D_{SOC} part is provided by the cou-

pled perturbed SOC approach,^[43] whereas for the D_{SSC} contribution, slightly better predictions are reached with the DFT method based on the restricted open-shell Kohn–Sham (ROKS) reference determinants.^[22,44]

With respect to the functional, recent results have shown an improvement in the prediction of the ZFS of mononuclear Mn^{II} dihalide complexes with B3LYP compared to BP86.^[23] Thus, the D values have been calculated with both functionals. The results reported in Table 3 unambiguously show that B3LYP is not adapted to predict the ZFS for Mn^{II} complexes with only N/O-based ligands. This surprising result is additional proof of the extreme complexity of accurately predicting the ZFS of the Mn^{II} ion since the choice of the functional depends on the nature of the Mn^{II} coordination sphere.

With BP86, the quality of the prediction is satisfactory with discrepancies between the experimental and calculated D values ranging between 13 and 60%. However, the predicted magnitudes are alternatively under- or overestimated. For the six-coordinate complexes **1–5**, the best prediction is found for the chlorido complex with an overestimation of the calculated magnitude of 19%. This is in agreement with systematic studies performed for evaluating the performance of DFT to predict D in dihalide mononuclear Mn^{II} complexes.^[22,23] With regard to **1–4**, the trend is not reproduced [i.e., the smallest experimental D magnitude found for **4** (0.035 cm^{-1}) corresponds to the largest calculated D value (0.087 cm^{-1})].

In contrast to the previously reported seven-coordinate complex, for which the prediction of the D value was rather poor,^[25] the calculated D values obtained here for complexes **5** and **6** reproduce the experimental D and E/D values well.

The E/D values of the six-coordinate complexes are overestimated except for complex **4**, whereas for the seven-coordinate complexes they agree well with the experimental data. It has been previously shown that DFT is not reliable for predicting the sign of D for an E/D ratio larger than 0.2.^[22] This is partly due to the small magnitudes of both D and E (a few tenths and hundredths of wavenumbers, respectively) that prevent the prediction, with sufficient precision, of the relatively small differences between the axial tensor components. From Table 3, it can be seen that the sign of D is correctly reproduced by DFT within the series when experimentally determined.

Table 4 reports the SSC and SOC contributions to the **D** tensor for complexes **1–7**. In the six-coordinate series (**1–5**) the percentage of the SSC interaction is randomly distributed. Indeed, for complex **1** it represents only 2.5%, whereas for **2**, it represents 107%. However, for complexes **2–4**, D_{SSC} is far too large to be negligible and determines the sign of D in the cases of **2** and **3**. It was previously shown that the four classes of excitation of D_{SOC} present comparable magnitudes with partially cancelling signs in the case of halide complexes. A different behaviour is observed through the series of the six-coordinate N/O-based ligands. The dominant contribution to D_{SOC} arises from the $\alpha \rightarrow \beta$ excitation, whereas the $\beta \rightarrow \alpha$ one is negligible.

Independently of the sign, the D_{SSC} and D_{SOC} parts are comparable for both seven-coordinate complexes, **6** and **7**, with D_{SSC} corresponding to 31 and 25% of D , respectively. The major SOC contribution also originates from the $\alpha \rightarrow \beta$ excitation.

Conclusion

We have investigated by EPR spectroscopy and quantum chemistry the ZFS of a series of mononuclear Mn^{II} complexes including six- and seven-coordinate compounds with N/O-based ligands (**1–4**, **6** and **7**). The experimental D values all fall within a small magnitude range of $0.035\text{--}0.086\text{ cm}^{-1}$, which prevents the establishment of magneto correlations with the coordination number of the Mn^{II} ion (6 vs. 7) or with the N/O ratio of its coordination sphere. According to this work, and together with our previous investigations, we have confirmed that a good DFT prediction of the ZFS parameters requires precise calculations of the D_{SOC} and D_{SSC} contributions. More interestingly, this DFT study has also revealed that the choice of the functional is crucial to accurately predict the ZFS: B3LYP is the best functional in the case of halide complexes, whereas BP86 produces better results for complexes with only N/O-based ligands. This last result illustrates well the complexity of predicting the ZFS and the importance of such systematic studies.

Experimental Section

Materials: 2,2':6',2''-Terpyridine (terpy, 99.9%, Alfa Aesar) was used as supplied. Complexes **2–7**^[31–33] and $[\text{Mn}(\text{CF}_3\text{CO}_2)_2 \cdot (\text{H}_2\text{O})_4]$ ^[34] were prepared according to literature procedures.

Synthesis of $[\text{Mn}(\text{terpy})(\text{CF}_3\text{CO}_2)_2(\text{OH}_2)]$ (1**):** Solid terpy (100 mg, 0.429 mmol) was added to a stirred solution of $[\text{Mn}(\text{CF}_3\text{CO}_2)_2 \cdot (\text{H}_2\text{O})_4]$ (151 mg, 0.429 mmol) in CH_3CN (8 mL). CH_3CN (few mL) was then added until complete dissolution of terpy. The resulting pale yellow solution was stirred at room temperature for a few minutes and then filtered. Yellow crystals of **1** were obtained by diffusion of ethyl acetate into the solution in CH_3CN . Yield: 195 mg (85%). Selected IR bands: $\tilde{\nu} = 3350$ (vs), 1674 (s), 1595 (s), 1477 (m), 1453 (m), 1433 (m), 1316 (m), 1200 (s), 1118 (s), 1014 (m), 840 (m), 801 (m), 772 (s), 716 (m), 651 (m), 637 (m), 601 (w), 512 (w) 454 (w), 429 (w), 306 (w) cm^{-1} .

Physical Measurements: Powder X-band EPR spectra were recorded with a Bruker EMX, equipped with an ER-4192 ST Bruker cavity and an ER-4131 VT for the 100 K experiments. Powder Q-band EPR spectra were recorded with an ER-5106 QTW Bruker cavity and an Oxford Instruments ESR-900 continuous-flow helium cryostat for the Q-band for the 4.5 K experiments.

Crystal-Structure Determination of **1:** Diffraction data were collected with a Bruker AXS Enraf–Nonius Kappa CCD diffractometer, and the structure was solved by direct methods and refined with the TEXSAN software package.^[45] A pale yellow crystal of dimensions $0.40 \times 0.38 \times 0.25\text{ mm}$ was selected. The crystallographic data are summarized in Table 5. CCDC-768793 contains the supplementary crystallographic data for **1**. These data can be obtained free of charge from the Cambridge Crystallographic Data Center via www.ccdc.cam.ac.uk/data_request/cif.

Table 5. Principal crystallographic data and parameters for 1.

Empirical formula	C ₁₉ H ₁₃ F ₆ N ₃ MnO ₅
Formula mass	532.26
Crystal system	monoclinic
Space group	<i>P</i> 2 ₁ / <i>n</i>
<i>a</i> [Å]	11.244(2)
<i>b</i> [Å]	13.351(2)
<i>c</i> [Å]	14.061(3)
α [°]	90
β [°]	105.68(1)
γ [°]	90
<i>V</i> [Å ³]	2032.3(7)
<i>Z</i>	4
<i>T</i> [K]	150
λ [Å]	0.71073
$\rho_{\text{calcd.}}$ [mg m ⁻³]	1.739
μ [mm ⁻¹]	0.743
<i>F</i> (000)	1068
Reflections collected	19831
Independent reflections	5490 [<i>R</i> (int) = 3790]
Goodness-of-fit on <i>F</i>	1.979
<i>R</i>	0.0514
<i>wR</i> ^[a]	0.0678
Largest diff. peak/hole [e Å ⁻³]	0.84/−0.44

[a] $wR = 1/[\sigma^2(F_o + 0.0038|F_o|^2)]$.

Theoretical Calculations: All calculations were performed with the ORCA program package.^[46] The ZFS parameters were calculated on X-ray structures as well as from optimized structures in which only the positions of the hydrogen atoms were relaxed. For a discussion of this point, see the literature.^[22,23,41,42] The ZFS calculations based on DFT were performed with the hybrid B3LYP^[47] and the nonhybrid BP86^[48,49] functionals by using the TZVP basis set^[50] and taking advantage of the RI approximation with the auxiliary TZV/J Coulomb fitting basis sets.^[51] Four types of excitations were considered to calculate the *D*_{SOC} part.^[24] Qualitatively, they take the form of (1) excitation of a spin-down (β) electron from a doubly occupied MO (DOMO) to a singly occupied MO (SOMO) that leads to states of the same spin *S* as the ground state ($\beta \rightarrow \beta$); (2) excitation of a spin-up (α) electron from a SOMO to a virtual MO (VMO), which also gives rise to states of total spin *S* ($\alpha \rightarrow \alpha$); (3) excitations between two SOMOs that are accompanied by a spin-flip and that give rise to states of $S' = S - 1$ ($\alpha \rightarrow \beta$); and (4) “shell-opening” transitions from a DOMO to a VMO that lead to states of $S' = S + 1$ ($\beta \rightarrow \alpha$).

Acknowledgments

C. D. and M. N. C. thank the Agence Nationale pour la Recherche (grant no. ANR-JC09_435677) for financial support. I. R. and M. R. thank the Ministerio de Ciencia e Innovación (MICINN) of Spain through project CTQ2007-60476/PPQ. J. R. thanks the Universitat de Girona (UdG) for a predoctoral grant.

[1] R. Boca, *Coord. Chem. Rev.* **2004**, *248*, 757–815.

[2] F. Neese in *Calculation of NMR and EPR Parameters* (Eds.: M. B. M. Kaupp, V. G. Malkin), Wiley-VCH, Heidelberg, **2004**.

[3] F. Neese, E. I. Solomon in *In Magnetoscience – From Molecules to Materials*, vol. IV (Eds.: J. S. Miller, M. Drillon), Wiley-VCH, Weinheim, **2003**, p. 345.

[4] J. Krzystek, A. Ozarowski, J. Telser, *Coord. Chem. Rev.* **2006**, *250*, 2308–2324.

[5] D. Gatteschi, R. Sessoli, *Angew. Chem. Int. Ed.* **2003**, *42*, 268–297.

[6] D. Gatteschi, R. Sessoli, J. Villain in *Molecular Nanomagnets*, Oxford University Press, New York, **2006**.

[7] C. Duboc, M. N. Collomb, F. Neese, *Appl. Magn. Reson.* **2010**, *37*, 229–245.

[8] R. B. Birdy, M. Goodgame, *Inorg. Chim. Acta* **1981**, *50*, 183–187.

[9] C. J. H. Jacobsen, E. Pedersen, J. Villadsen, H. Weihe, *Inorg. Chem.* **1993**, *32*, 1216–1221.

[10] W. B. Lynch, R. S. Boorse, J. H. Freed, *J. Am. Chem. Soc.* **1993**, *115*, 10909–10915.

[11] R. M. Wood, D. M. Stucker, L. M. Jones, W. B. Lynch, S. K. Misra, J. H. Freed, *Inorg. Chem.* **1999**, *38*, 5384–5388.

[12] D. M. L. Goodgame, H. El Mkami, G. M. Smith, J. P. Zhao, E. J. L. McInnes, *Dalton Trans.* **2003**, 34–35.

[13] C. Mantel, C. Baffert, I. Romero, A. Deronzier, J. Pécaut, M. N. Collomb, C. Duboc, *Inorg. Chem.* **2004**, *43*, 6455–6463.

[14] C. Duboc, T. Phoeung, S. Zein, J. Pécaut, M. N. Collomb, F. Neese, *Inorg. Chem.* **2007**, *46*, 4905–4916.

[15] C. Duboc, T. Phoeung, D. Jouvenot, A. G. Blackman, L. F. McClintock, J. Pécaut, A. Deronzier, M. N. Collomb, *Polyhedron* **2007**, *26*, 5243–5249.

[16] C. Duboc, V. Astier-Perret, H. Y. Chen, J. Pécaut, R. H. Crabtree, G. W. Brudvig, M. N. Collomb, *Inorg. Chim. Acta* **2006**, *359*, 1541–1548.

[17] G. Berggren, P. Huang, L. Eriksson, M. F. Anderlund, *Appl. Magn. Reson.* **2009**, *36*, 9–24.

[18] The magnitude of *D* is between 0.9 and 1.2 cm⁻¹ for the iodo complexes, 0.5 and 0.7 cm⁻¹ for the bromido, and 0.16 and 0.30 cm⁻¹ for the chlorido derivatives, except for the *cis*-dihalide six-coordinate systems, which are characterized by significantly smaller *D* values ($|D_I| = 0.6$ cm⁻¹, $|D_{Br}| = 0.35$ cm⁻¹, $|D_{Cl}| = 0.12$ cm⁻¹).

[19] C. Mantel, C. Philouze, M. N. Collomb, C. Duboc, *Eur. J. Inorg. Chem.* **2004**, 3880–3886.

[20] C. Duboc, M. N. Collomb, J. Pécaut, A. Deronzier, F. Neese, *Chem. Eur. J.* **2008**, *14*, 6498–6509.

[21] $0.2500 < |D_S| < 0.3000$, $0.0008 < |D_Q| < 0.1750$ cm⁻¹.

[22] S. Zein, C. Duboc, W. Lubitz, F. Neese, *Inorg. Chem.* **2008**, *47*, 134–142.

[23] S. Zein, F. Neese, *J. Phys. Chem. A* **2008**, *112*, 7976–7983.

[24] F. Neese, *J. Am. Chem. Soc.* **2006**, *128*, 10213–10222.

[25] C. Hureau, S. Groni, R. Guillot, G. Blondin, C. Duboc, E. Anxolabéhère-Mallart, *Inorg. Chem.* **2008**, *47*, 9238–9247.

[26] A. F. Miller, *Curr. Opin. Chem. Biol.* **2004**, *8*, 162–168.

[27] T. A. Jackson, T. C. Brunold, *Acc. Chem. Res.* **2004**, *37*, 461–470.

[28] V. V. Barynin, M. M. Whittaker, S. V. Antonyuk, V. S. Lamzin, P. M. Harrison, P. J. Artymiuk, J. W. Whittaker, *Structure* **2001**, *9*, 725–738.

[29] K. N. Ferreira, T. M. Iverson, K. Maghlaoui, J. Barber, S. Iwata, *Science* **2004**, *303*, 1831.

[30] B. Loll, J. Kern, W. Saenger, A. Zouni, J. Biesiadka, *Nature* **2005**, *438*, 1040–1044.

[31] J. Rich, M. Rodríguez, I. Romero, L. Vaquer, X. Sala, A. Llobet, M. Corbella, M. N. Collomb, X. Fontrodona, *Dalton Trans.* **2009**, 8117–8126.

[32] M. Andruh, K. Hubner, M. Noltemeyer, H. W. Roesky, Z. *Naturforsch., Teil B* **1993**, *48*, 591–597.

[33] C. Baffert, I. Romero, J. Pécaut, A. Llobet, A. Deronzier, M. N. Collomb, *Inorg. Chim. Acta* **2004**, *357*, 3430–3436.

[34] Z. Olejnik, T. Lis, *Acta Crystallogr., Sect. C* **2000**, *56*, 1310–1311.

[35] X. F. Zhang, D. G. Huand, F. Chen, C. N. Chen, Q. T. Liu, *Chin. J. Struct. Chem.* **2003**, *22*, 525–528.

[36] S. K. Smoukov, J. Telser, B. A. Bernat, C. L. Rife, R. N. Armstrong, B. M. Hoffman, *J. Am. Chem. Soc.* **2002**, *124*, 2318–2326.

- [37] J. R. Pilbrow in *Transition Ion Paramagnetic Resonance*, Clarendon Press, Oxford, **1990**.
- [38] F. E. Mabbs, D. Collison in *Electron Paramagnetic Resonance of d Transition Metal Compounds*, Elsevier, Amsterdam, **1992**, chapter 12.
- [39] A. Abragam, B. Bleaney in *Electron Paramagnetic Resonance of Transition Ions*, Oxford University Press, New York, **1970**.
- [40] T. D. Tzima, G. Sioros, C. Duboc, D. Kovala-Demertzi, V. S. Melissas, Y. Sanakis, *Polyhedron* **2009**, *28*, 3257–3264.
- [41] Q. Scheifele, C. Riplinger, F. Neese, H. Weihe, A. L. Barra, F. Juranyi, A. Podlesnyak, P. L. W. Tregenna-Piggott, *Inorg. Chem.* **2008**, *47*, 439–447.
- [42] M. Bühl, C. Reimann, D. A. Pantazis, T. Bredow, F. Neese, *J. Chem. Theory Comput.* **2008**, *4*, 1449–1459.
- [43] F. Neese, *J. Chem. Phys.* **2007**, *127*, 164112.
- [44] S. Sinnecker, F. Neese, *J. Phys. Chem. A* **2006**, *110*, 12267–12275.
- [45] *Single Crystal Structure Analysis Software*, version 1.7, Molecular Structure Corporation, 3200 Research Forest Drive, The Woodlands, TX 77381, USA, **1995**.
- [46] F. Neese, University of Bonn, Bonn, Germany, **2007**.
- [47] A. D. Becke, *J. Chem. Phys.* **1993**, *98*, 1372–1377.
- [48] A. D. Becke, *Phys. Rev. A* **1988**, *38*, 3098–3100.
- [49] J. P. Perdew, *Phys. Rev. B* **1986**, *33*, 8822–8824.
- [50] A. Schäfer, C. Huber, R. Ahlrichs, *J. Chem. Phys.* **1994**, *100*, 5829–5835.
- [51] F. Weigend, *PhysChemChemPhys* **2006**, *8*, 1057–1065.

Received: April 2, 2010

Published Online: June 22, 2010

Mixed Disilyl-Substituted Cyclopentadiene Derivatives and Corresponding Zirconium, Molybdenum and Tungsten Compounds

Cristina E. Petrisor,^[a] Ghaita Chahboun,^[b] Mohamed Amin El Amrani,^[b] Eva Royo,^{*,[a]} and Tomás Cuenca^{*,[a]}

Keywords: Molybdenum / Tungsten / Zirconium / Cyclopentadienyl ligands

The mixed disilyl-substituted cyclopentadiene $C_5H_4[SiMe_2(CH=CHCH_3)](SiMe_3)$ (**2**) has been synthesized in a one-pot reaction by alkylation, deprotonation and silylation of $C_5H_5(SiMe_2Cl)$. The analogous olefin-tethered cyclopentadiene $C_5H_4[SiMe_2(CH_2CH=CH_2)](SiMe_3)$ (**3**) has been obtained through traditional metathesis routes from $Li[C_5H_4(SiMe_3)]$ and the chloroallylsilane $SiMe_2(CH_2CH=CH_2)Cl$. The corresponding mixed disilyl-substituted cyclopentadienyllithium salts $Li[C_5H_3-1-SiMe_2R-3-SiMe_3]$ [$R = CH=CHCH_3$ (*cis+trans*-**4**); $R = CH_2CH=CH_2$ (**5**)] were used to isolate the chiral zirconium compounds $[ZrX(\eta^5-C_5H_4SiMe_2-\eta^1-NtBu)-(\eta^5-C_5H_3-1-SiMe_2R-3-SiMe_3)]$ [$X = Cl$, $R = CH=CHCH_3$

(*cis+trans*-**6**); $R = CH_2CH=CH_2$ (**7**); $X = CH_3$, $R = CH=CHCH_3$ (*cis+trans*-**8**); $R = CH_2CH=CH_2$ (**9**)] and group 6 derivatives $[MH(\eta^5-C_5H_3-1-SiMe_2R-3-SiMe_3)(CO)_3]$ [$R = CH=CHCH_3$, $M = Mo$ (*cis+trans*-**10**), $M = W$ (*cis+trans*-**11**); $R = CH_2CH=CH_2$, $M = Mo$ (**12**) and $M = W$ (**13**)], which have been fully characterized. The behaviour of metal compounds **8–13** has been studied and compared with that previously reported for mono-substituted alkene-silylcyclopentadienyl systems $[Zr(CH_3)(\eta^5-C_5H_4SiMe_2-\eta^1-NtBu)[(\eta^5-C_5H_4SiMe_2)(CH_2CH=CH_2)]]$ and $[MH(\eta^5-C_5H_4SiMe_2-\eta^1-NtBu)[(\eta^5-C_5H_4SiMe_2)(CH_2CH=CH_2)]]$ ($M = Mo, W$).

Introduction

The possible metal-bonding modes, from σ -bonded (η^1 -) to π -bonded (η^n , $n = 2-5$), make cyclopentadienyl systems one of the most versatile ligands in organometallic chemistry. This versatility can be further enhanced when designing substituted cyclopentadienyl ligands with substituents that can act as potential coordinating groups. This approach opens access to ligand architectures that impart interesting properties to their metal species, including higher catalytic reactivity, the introduction of chirality, changes in solubility and their possible use as anchoring moieties to develop new supported single-site catalysts.^[1]

Recently, we reported the preparation and chemical behaviour of various allyldimethylsilyl- η^5 -cyclopentadienyl group 4, 5 and 6 metal compounds.^[2–7] Along with other tethered systems, those that incorporate olefinic functionalities provide an attractive means to elucidate metal-olefin interactions and reaction pathways pertinent to olefin poly-

merization and isomerization, and they could potentially facilitate the study of other olefin modification processes.^[2,4,6–9] In this regard, the higher flexibility and acidity of the silicon- versus the carbon-based spacer unit provide many advantages for a variety of purposes.^[10] We have a longstanding interest in silyl-substituted cyclopentadienyl metal compounds. Synthesis of *ansa*-dicyclopentadienyl^[11] and early transition-metal (amidosilyl)cyclopentadienyl compounds,^[5,6,12–15] comparative studies on the chemical behaviour of Si–Cl and M–Cl ($M =$ group 4 and 5 metals) bonds versus different organic reagents^[13,16] and studies on polynuclear systems with Si–O–M^[12,17,18] bonds are among our research topics.

A considerable number of modified silylcyclopentadienes have been prepared and used as precursors for the synthesis of a wide range of monosilyl- or disilylcyclopentadienyl metal compounds. While several chelating mixed disilylcyclopentadienyl ancillary ligands are known,^[5,15,19] reports of nonbridged disubstituted cyclopentadienyl metal compounds with different organosilyl substituents at the aromatic ring are scarce.^[20] Within this context, we were interested in the synthesis of mixed disilylcyclopentadienyl metal compounds through the introduction of different alkyl, alkenyl or alkynyl substituents into the silyl units of the cyclopentadiene system to test the chemical and structural properties of corresponding transition-metal cyclopentadienyl compounds.

Haloorganosilanes $SiCl_{4-x}R_x$ ($x = 1, 2$ or 3) have been extensively used to prepare a variety of silylcyclopentadiene

[a] Departamento de Química Inorgánica, Facultad de Ciencias, Universidad de Alcalá, 28871 Alcalá de Henares, Madrid, Spain
Fax: +34-918854683
E-mail: tomas.cuenca@uah.es
eva.royo@uah.es

[b] Université Abdelmalek Essaâdi, Faculté des Sciences, Département de Chimie – Laboratoire de Chimie Organique Appliquée, Mhannech II, B.P. 2121, Tétouan, Morocco
Supporting information for this article is available on the WWW under <http://dx.doi.org/10.1002/ejic.201000394>.

derivatives, which are generally formed through the metathesis reaction of the halosilane with the appropriate cyclopentadienyllithium, sodium, potassium or thallium salt (MCp).^[10] However, this process is limited by the commercial availability of the halosilane reagents. A different approach consists of alkylation of (halosilyl)cyclopentadienes with organolithium or -magnesium compounds. When (halosilyl)cyclopentadiene derivatives are treated with such reagents, alkylation at the silicon centre takes place together with deprotonation of the cyclopentadiene to afford the corresponding salt of the silyl-substituted ring.^[8,21] To the best of our knowledge, such procedure has been successful when tetraalkylcyclopentadiene compounds are used, and no examples of analogous reactions with halosilyl-non-alkylated-cyclopentadiene species have been reported to date. Alkenylmagnesium halides are widely commercially available due to their decreased tendency to add to C–C multiple bonds compared with organolithium species.^[22] With the aim of introducing alkenyl fragments into (halosilyl)cyclopentadiene derivatives, we decided to follow a similar approach and test the capability of Grignard reagents to alkenylate and deprotonate (halosilyl)cyclopentadiene derivatives.

Results and Discussion

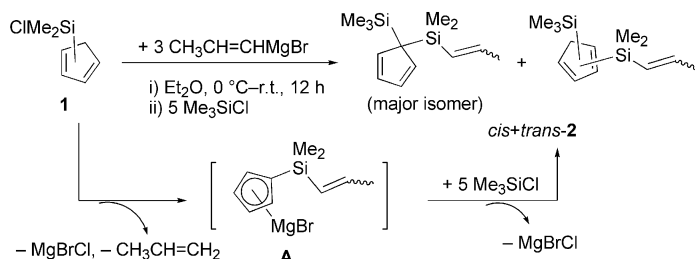
When (chlorodimethylsilyl)cyclopentadiene (**1**) was treated with *cis+trans*-1-propenylmagnesium bromide, [(*cis+trans*-CH₃CH=CH)MgBr] in a 1:3 molar ratio, the initially yellow solution gradually turned into an orange suspension. Quenching the reaction with an excess amount of SiClMe₃ afforded the disilylcyclopentadiene compound C₅H₄[SiMe₂(CH=CHCH₃)](SiMe₃) (*cis+trans*-**2**), MgClBr and CH₃CH=CH₂ (Scheme 1). Twelve isomers may exist for disubstituted cyclopentadiene compounds, in which interconversion occurs through alkylsilyl or hydrogen migrations in well-known rearrangement processes.^[23] As inferred from ¹H and ¹³C NMR spectra at room temperature, *cis+trans*-**2** is obtained as a mixture of isomers, the major product being the 5,5-disilyl-substituted isomer, which was

unambiguously identified by NMR spectroscopic techniques, and exists in solution as a mixture of *cis/trans* compounds in a molar ratio of approximately 1:2.

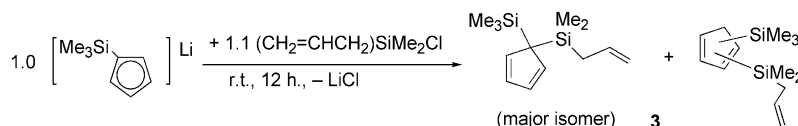
Scheme 1 illustrates the plausible way in which the formation of the compound *cis+trans*-**2** can occur. When the reaction of **1** with 1-propenylmagnesium bromide is carried out in 1:1 or 1:2 molar ratios, an unresolvable mixture of compounds is always obtained together with different amounts of the starting material **1**, as inferred by ¹H NMR spectroscopy. Two competitive processes, namely, the metathesis reaction between Si–Cl and Mg–C bonds and deprotonation of the cyclopentadiene ring by reaction with the Grignard derivative would afford the nonisolated intermediate species [C₅H₄(SiMe₂CH=CHCH₃)]MgBr (**A**). A variety of (silylcyclopentadienyl)magnesium compounds have been prepared by deprotonation of corresponding substituted cyclopentadienes with different Grignard compounds RMgX^[24] or R₂Mg^[25] (R = alkyl, X = Cl, Br). The addition of a onefold excess amount of (*cis+trans*-CH₃CH=CH)MgBr is always required to obtain pure *cis+trans*-**2** in good yield, probably because Grignard reagents are less effective Si–Cl bond alkylating agents than organolithium species.^[26] At this stage, the simple addition of an excess amount of Me₃SiCl in a one-pot reaction affords the pure mixed disilylcyclopentadiene compound *cis+trans*-**2**.

The similar disilyl-substituted cyclopentadiene C₅H₄[SiMe₂(CH₂CH=CH₂)](SiMe₃) (**3**) was prepared from the direct metathesis reaction of Li[C₅H₄(SiMe₃)] with commercially available allylchlorodimethylsilane. After convenient workup of the reaction mixture, derivative **3** was isolated in approximately 79% yield. The NMR spectroscopic study of **3** (¹H and ¹³C NMR spectroscopy) at room temperature allowed a full assignment of the resonances due to the major product, namely, the 5,5-disubstituted cyclopentadiene **3** (Scheme 2).

For both *cis+trans*-**2** and **3**, the ¹H NMR spectra show symmetrical A₂B₂ patterns for the cyclopentadiene protons (multiplets centred around δ = 6.72 and 6.53 ppm) that correspond to the major isomer, related to signals in the



Scheme 1.

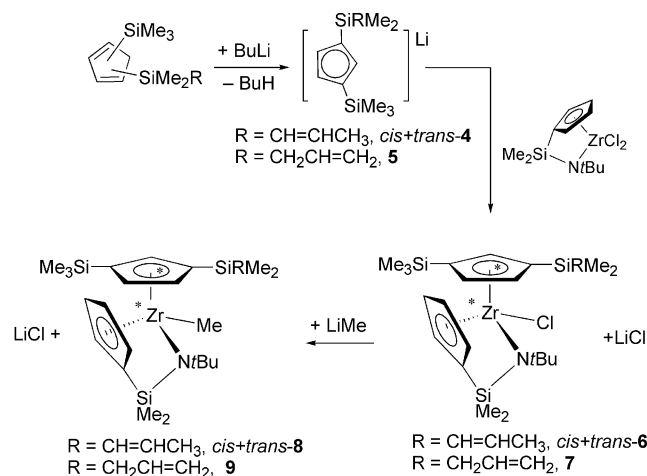


Scheme 2.

^1H , ^{13}C heteronuclear single quantum coherence (HSQC) NMR spectra at $\delta = 136.4$, 131.1 (*cis*-**2**), 136.3, 130.9 (*trans*-**2**) and 136.0, 131.1 ppm (**3**), respectively. For the quaternary carbon atoms, negative resonances in the attached proton test (APT) ^{13}C NMR spectra, with no associated protons in the 2D HSQC experiments, were observed at $\delta = 57.3$, 57.2 (*cis*+*trans*-**2**) and 57.0 ppm (**3**). Minor signals in the ^1H NMR spectra of *cis*+*trans*-**2** ($\delta = 3.10$, 3.00 ppm) and **3** ($\delta = 3.10$, 3.00 ppm) correlate, in HSQC experiments, with the negative resonances displayed in the APT ^{13}C NMR spectra of *cis*+*trans*-**2** ($\delta = 49.5$, 49.4, 49.3 ppm) and **3** ($\delta = 49.4$ ppm), which indicates the presence of $-\text{CH}_2$ units of minor 1,2-, 1,3-, or 1,4-disubstituted isomers.

Metalation of cyclopentadiene compounds *cis*+*trans*-**2** and **3** with *n*-butyllithium affords the corresponding lithium salts $\text{Li}[\text{C}_5\text{H}_3\text{-1-SiMe}_2\text{R-3-SiMe}_3]$ in which $\text{R} = \text{CH}=\text{CHCH}_3$ (*cis*+*trans*-**4**, molar ratio of around 1:2) and $\text{R} = \text{CH}_2\text{CH}=\text{CH}_2$ (**5**), respectively (Scheme 3), which can be isolated as white solids and fully characterized in solution by NMR spectroscopy. An unambiguous assignment of the regiochemistry of the silyl substituents by NMR spectroscopic techniques is not straightforward. It has been proposed^[27] that coupling constants of the AA'B pattern found for the C_5H_3 protons in ^1H NMR spectra can be used to distinguish between 1,2 ($J_{\text{A,B}} \approx J_{\text{A',B}} \geq 2.0\text{--}3.0$ Hz) and 1,3-disposition ($J_{\text{A,B}} \approx J_{\text{A',B}} \leq 2.0$ Hz) of the silyl fragments. Whereas cyclopentadienyl protons of *cis*+*trans*-**4** show broad resonances in the ^1H NMR spectra from which no coupling constants could be calculated, the set of signals for the C_5H_3 system for derivative **5** ($\delta = 6.87$ ppm, dd, both $J_{\text{H,H}}$ of around 1.6 Hz, and $\delta = 6.75$ ppm, 2 H, overlapped), agrees well with a 1,3-disposition of the silyl substituents. ^1H 2D NOESY experiments for *cis*+*trans*-**4** and **5** also confirm the 1,3-disposition of the silyl fragments at the cyclopentadienyl ring. Whereas NOE contacts are displayed between the three protons of the C_5H_3 and those of the $\text{Si}-\text{CH}_3$ (*cis*+*trans*-**4** and **5**) and $\text{Si}-\text{CH}_2$ (**5**) fragments, respectively, no NOE correlations are observed between the AA' and B signals of the AA'B system for the C_5H_3 protons. To the best of our knowledge, a 1,3-disposition is always preferred in all the reported nonchelating disilylmonocyclopentadienyl metal compounds with sterically demanding substituents.^[20]

Mixed disilyl-substituted cyclopentadienyl zirconium derivatives have been prepared by treatment of $[\text{ZrCl}_2(\eta^5\text{-C}_5\text{H}_4\text{SiMe}_2\eta^1\text{-NtBu})]$ with the cyclopentadienyllithium salts *cis*+*trans*-**4** and **5** in toluene to give yellow suspensions after around 16–18 h at room temperature. Evaporation of the solvent and extraction of the oily residues into hexane afforded yellow solutions from which yellow solids were isolated in approximately 90% yields and fully characterized as $[\text{ZrCl}(\eta^5\text{-C}_5\text{H}_4\text{SiMe}_2\eta^1\text{-NtBu})(\eta^5\text{-C}_5\text{H}_3\text{-1-SiMe}_2\text{R-3-SiMe}_3)]$, $\text{R} = \text{CH}=\text{CHCH}_3$, (*cis*+*trans*-**6**, molar ratio of around 1:2) and $\text{R} = \text{CH}_2\text{CH}=\text{CH}_2$ (**7**), respectively (Scheme 3). Alkylation of the $\text{Zr}-\text{Cl}$ bond present in *cis*+*trans*-**6** and **7** with LiMe in diethyl ether afforded the corresponding methyl derivatives $[\text{Zr}(\text{CH}_3)(\eta^5\text{-C}_5\text{H}_4\text{SiMe}_2\eta^1\text{-NtBu})(\eta^5\text{-C}_5\text{H}_3\text{-1-SiMe}_2\text{R-3-SiMe}_3)]$, $\text{R} = \text{CH}=\text{CHCH}_3$



Scheme 3.

(*cis*+*trans*-**8** in a molar ratio of around 2:3) and $\text{R} = \text{CH}_2\text{CH}=\text{CH}_2$ (**9**), respectively (Scheme 3).

The presence of a new stereogenic zirconium centre and the enantiotopic faces of the mixed-1,3-disilylcyclopentadienyl ring afforded two pairs of diastereomers **6a,b**, **7a,b**, **8a,b** and **9a,b**, which can be distinguished by NMR spectroscopy. Thus, ^1H and ^{13}C NMR spectra of compound *cis*+*trans*-**6** and *cis*+*trans*-**8** show a very complicated set of resonances due to the presence of two diastereomers (*cis*-**6a,b** and *trans*-**6a,b**; *cis*-**8a,b** and *trans*-**8a,b**) for each spatial *cis/trans* disposition of the alkene fragment. Unfortunately, the mixture could not be resolved and none of the different diastereomers could be isolated independently. However, TOCSY NMR spectroscopic experiments allow a full assignment of the proton signals displayed by the prop-1-enyl fragment. Table 1 summarizes the selected ^1H and ^{13}C NMR spectroscopic resonances assigned to the *cis*- and

Table 1. Selected ^1H and ^{13}C NMR spectroscopic shifts (δ in ppm, J values in Hz) of isomers *cis*-**6a,b**, *trans*-**6a,b**, *cis*-**8a,b** and *trans*-**8a,b**.

	Si-CH=	C-CH=	-CH ₃
<i>cis</i> - 6a,b ^[a]	5.72, 5.60, dq ^[c] <i>cis</i> $J = 14$, $^4J = 1$ 131.2, 130.8	6.60–6.38 overlapped 145.5, 144.8	1.77, 1.65, dd ^[c] $^3J = 7$, $^4J = 1$ 19.4, 18.8
<i>trans</i> - 6a,b ^[a]	5.74, 5.66, dq ^[c] <i>trans</i> $J = 18$, $^4J = 2$ 129.7, 129.5	6.09–5.90 overlapped 143.8, 143.2	1.89, 1.86, dd ^[c] $^3J = 6$, $^4J = 2$ 23.0, 22.9
<i>cis</i> - 8a,b ^[b]	5.79, dq <i>cis</i> $J = 13$, $^4J = 2$ 5.69, dq <i>cis</i> $J = 14$, $^4J = 2$ 130.3, 130.0	6.46–6.33 overlapped 145.3, 144.5	1.61, 1.60, dd ^[c] $^3J = 6$, $^4J = 2$ 19.3, 19.1
<i>trans</i> - 8a,b ^[b]	5.88, dq <i>trans</i> $J = 18$, $^4J = 1$ 5.80, dq <i>trans</i> $J = 19$, $^4J = 1$ 131.7, 131.1	6.10–5.97 overlapped 144.4, 143.8	1.71, 1.69, dd ^[c] $^3J = 6$, $^4J = 1$ 23.4, 23.3

[a] δ in ppm in $[\text{D}_1]\text{chloroform}$. [b] δ in ppm in $[\text{D}_6]\text{benzene}$. [c] $J_{\text{H,H}}$ coupling constants have the same values for both resonances. Full assignment of all resonances has been performed with the help of the bidimensional ^1H , ^1H COSY, TOCSY and ^1H , ^{13}C HSQC NMR spectroscopic methods.

trans-prop-1-enyl chains of each isomer. Analogously, ^1H and ^{13}C NMR spectra of compound **7** show two sets of signals due to diastereomers **7a** and **7b**. The ^1H NMR spectrum of derivative **9** displayed a single set of resonances due to overlapped proton signals of both diastereomers. This finding can be confirmed by ^{13}C NMR spectroscopic and bidimensional HSQC experiments, which indicate the formation of two different diastereomers, **9a** and **9b**. The asymmetry of all these zirconium compounds **6–9** is consistent with the ^1H and ^{13}C NMR spectra; it shows AA'B and AA'BB' proton systems for the cyclopentadienyl ligands together with five nonequivalent methylsilyl fragments, perfectly distinguishable for allyldimethylsilyl compounds **7** and **9**.

Recently, we prepared and studied group 6 hydrido-metal compounds that contained the monosubstituted (allyldimethylsilyl)cyclopentadienyl ligand.^[4] We were also interested in extending this chemistry to the synthesis of this type of disilyl-substituted cyclopentadienyl Mo and W carbonyl complexes. Traditional hydrogen-transfer reactions from the cyclopentadiene to the group 6 metal-carbonyl compounds $[\text{M}(\text{CO})_3(\text{NCCH}_3)_3]$ ($\text{M} = \text{Mo}, \text{W}$) take place under milder reaction temperatures by using THF as reaction solvent.

Treatment of *cis*+*trans*-**2** or **3** with equimolar amounts of $[\text{Mo}(\text{CO})_3(\text{NCCH}_3)_3]$ or $[\text{W}(\text{CO})_3(\text{NCCH}_3)_3]$ at room temperature gave the corresponding cyclopentadienyl hydrido compounds $[\text{MH}(\eta^5\text{-C}_5\text{H}_3\text{-1-SiMe}_2\text{R-3-SiMe}_3)(\text{CO})_3]$, in which $\text{R} = \text{CH=CHCH}_3$, $\text{M} = \text{Mo}$ (*cis*+*trans*-**10**), $\text{M} = \text{W}$ (*cis*+*trans*-**11**); $\text{R} = \text{CH}_2\text{CH=CH}_2$, $\text{M} = \text{Mo}$ (**12**), $\text{M} = \text{W}$ (**13**) (Scheme 4), which were isolated in around 53–60% yields and fully characterized. Compounds **10** and **11** were obtained as approximately 1:1 *cis*/*trans* mixtures of isomers, as inferred from the NMR spectroscopic study. For all of the compounds studied, ^1H and ^{13}C NMR spectroscopy show AA'B systems for cyclopentadienyl proton resonances and five nonequivalent carbon signals, respectively. Whereas cyclopentadienyl C_5H_3 protons of *cis*+*trans*-**10**, *cis*+*trans*-**11** and **13** show nonresolved resonances, the set of signals found for derivative **12** ($\delta = 5.22$, 1 H, dd, both $J_{\text{H,H}}$ of around 1.2 Hz, and $\delta = 5.03$ ppm, 2 H, overlapped), are consistent with a 1,3-disposition of the silyl substituents. Selected ^1H and ^{13}C NMR spectroscopic data assigned to the olefinic pendant unit for compounds **10–13** are shown in Table 2.

We have studied the intramolecular allyl to *trans*-prop-1-enyl selective isomerization that occurs in group 4 and 6 alkyl and hydrido-metal compounds that containing the

Table 2. Selected ^1H and ^{13}C NMR spectroscopic shifts (δ in ppm, $[\text{D}_6]\text{benzene}$, J values in Hz) of compounds *cis*-**10**, *cis*-**11**, *trans*-**11**, *trans*-**11** and **12**, **13**.^[a]

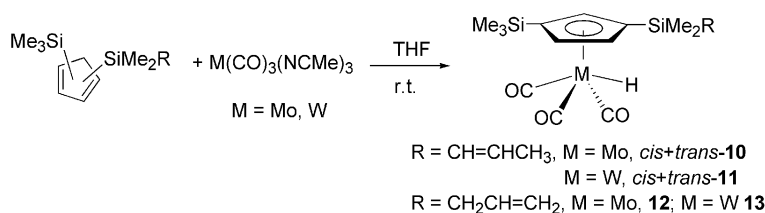
	Si-CH =	C-CH =	-CH ₃
<i>cis</i> - 10	5.55, d <i>cis</i> $J = 14$ 127.2	6.35, m <i>cis</i> $J = 14$, $^3J = 7$ 145.0	1.66, d, $^3J = 7$ 19.0
<i>trans</i> - 10	5.69, d <i>trans</i> $J = 20$ 129.0	6.01, m <i>trans</i> $J = 20$, $^3J = 6$ 145.5	1.59, d, $^3J = 6$ 22.3
<i>cis</i> - 11	5.55, dq <i>cis</i> $J = 12$, $^4J = 1$ 127.2	6.33, m <i>cis</i> $J = 12$, $^3J = 7$ 145.0	1.58, dd $^3J = 7$, $^4J = 1$ 19.2
<i>trans</i> - 11	5.67, dq <i>trans</i> $J = 18$, $^4J = 1$ 128.9	6.01, m <i>trans</i> $J = 18$, $^3J = 6$ 145.5	1.65, dd $^3J = 6$, $^4J = 1$ 22.5
	=CH	=CH ₂	Si-CH ₂
12	5.67, m <i>trans</i> $J = 17$ <i>cis</i> $J = 10$, $^3J = 8$ 134.8	4.89, d, <i>cis</i> $J = 10$ 4.86, d, <i>trans</i> $J = 17$ 114.9	1.51, d, $^3J = 8$ 25.4
13	5.65, m <i>trans</i> $J = 18$ <i>cis</i> $J = 11$, $^3J = 8$ 134.0	4.88 d, <i>cis</i> $J = 11$ 4.84 d, <i>trans</i> $J = 18$ 114.3	1.50, d, $^3J = 8$ 24.6

[a] Full assignment of all resonances has been performed with the help of the bidimensional ^1H , ^1H COSY, TOCSY and ^1H , ^{13}C HSQC NMR spectroscopic methods.

monosubstituted (allyldimethylsilyl)cyclopentadienyl ligand.^[4,6,7,28] To test the effect of the second trimethylsilyl substituent of the cyclopentadienyl ring, spectroscopic isomerization studies with the methyl derivatives **8**, **9** and the hydrido compounds **10–13** have been developed.

The allyl monosilyl-substituted zirconium complex $[\text{Zr}(\text{CH}_3)(\eta^5\text{-C}_5\text{H}_4\text{SiMe}_2\text{-}\eta^1\text{-NtBu})[(\eta^5\text{-C}_5\text{H}_4\text{SiMe}_2)(\text{CH}_2\text{CH=CH}_2)]$ isomerizes selectively and quantitatively to the *trans*-prop-1-enyl derivative $[\text{Zr}(\text{CH}_3)(\eta^5\text{-C}_5\text{H}_4\text{SiMe}_2\text{-}\eta^1\text{-NtBu})[(\eta^5\text{-C}_5\text{H}_4\text{SiMe}_2)(\text{CH=CHCH}_3)]$.^[7] In contrast, no *cis*- to *trans*-prop-1-enyl neither allyl to prop-1-enyl isomerization was detected for alkyl compounds *cis*+*trans*-**8** and **9**, respectively, at room temperature or after heating the solutions up to 120 °C over several weeks.

For the molybdenum derivatives, stirring *cis*+*trans*-**10** or **12** solutions at room temperature for more than 1 h affords, after evaporation of the solvent, oily residues in which decomposition products become prominent from ^1H and ^{13}C NMR spectra. A detailed investigation of the decomposition pathways of silyl-substituted cyclopentadienyl molybdenum hydrido species has been reported elsewhere.^[4]



Scheme 4.

Dehydrogenation processes of compound $[\text{MoH}\{\eta^5\text{-C}_5\text{H}_4\text{SiMe}_2(\text{CH}_2\text{CH}=\text{CH}_2)\}(\text{CO})_3]$ produce dimer $[\{\text{Mo}[\eta^5\text{-C}_5\text{H}_4\text{SiMe}_2(\text{CH}_2\text{CH}=\text{CH}_2)](\text{CO})_3\}_2]$, whereas the desilylation reactions favoured in THF solutions produce $[\text{MoH}(\eta^5\text{-C}_5\text{H}_5)(\text{CO})_3]$ and not-fully-characterized silane derivatives. In our present studies, separation or NMR spectroscopic characterization of the three possible dimers formed through dehydrogenation of species *cis*-**10** and *trans*-**10** is very difficult, as they always appear together with the already reported *trans*- $[\text{MoH}\{\eta^5\text{-C}_5\text{H}_4\text{SiMe}_2(\text{CH}=\text{CHCH}_3)\}(\text{CO})_3]$, $[\text{MoH}\{\eta^5\text{-C}_5\text{H}_4(\text{SiMe}_3)\}(\text{CO})_3]$, $[\text{MoH}(\eta^5\text{-C}_5\text{H}_5)(\text{CO})_3]$ and the corresponding dimer $[\{\text{Mo}(\eta^5\text{-C}_5\text{H}_5)(\text{CO})_3\}_2]$.^[4] Analogous desilylation and dehydrogenation transformations are observed when solutions of derivative **12** are studied at room temperature.

As described, tungsten cyclopentadienyl hydrido *cis*+*trans*-**11** is obtained from the synthesis reaction as a mixture of both isomers in a *cis*/*trans* ratio of around 1:1. Upon heating at 50 °C, the isomer ratio changed continuously toward the *trans*-**11** isomer. After about 24 h, a *cis*/*trans* ratio of around 1:10, inferred from ¹H NMR spectra, was reached, which then remained constant. This experimental results regarding the *cis*-to-*trans* prop-1-enyl isomerization agree well with the theoretically calculated lowest thermodynamic stability of the *cis* versus *trans* disposition of the pendant alkene unit in $[\text{MoH}(\eta^5\text{-C}_5\text{H}_4\text{SiMe}_2\text{-CH}=\text{CHCH}_3)(\text{CO})_3]$, in which *cis*-to-*trans* transformations have already been studied by computational methods.^[28] Regarding compounds **11** and **13**, no intramolecular prop-1-enyl to allyl nor allyl to prop-1-enyl isomerization, respectively, was observed, even after heating their THF solutions up to 140 °C for one week.

Conclusion

Alkylations of Si–Cl bonds of (halosilyl)cyclopentadiene derivatives have been performed and used for the synthesis of mixed disilyl-substituted cyclopentadiene systems attached to olefinic functionalities, from which metallation processes afford group 6 metal derivatives. Corresponding group 4 cyclopentadienyl metal compounds have been prepared by metathesis reactions and fully characterized. A thorough spectroscopic study allows for the unambiguous confirmation of the proposed structures for all the reported **3–13** compounds. Studies and comparison of the isomerization reactivity of the mixed disilyl-substituted cyclopentadienyl metal derivatives versus monosilylcyclopentadienyl compounds have been achieved. The results obtained establish that the presence of a second substituent on the cyclopentadienyl ring results in a lack of reactivity towards intramolecular isomerization of the olefin fragment when compared with the monosubstituted systems. Thus, under the reaction conditions used, only the tungsten hydrido compound suffered a *cis*-to-*trans* prop-1-enyl isomerization.

Experimental Section

General Information: All manipulations involving syntheses of metal complexes were performed at an argon/vacuum manifold

using standard Schlenk-line techniques under an argon atmosphere or in a glove box MBraun MOD System. Solvents were dried by conventional procedures and freshly distilled prior to use. $\text{C}_5\text{H}_5(\text{SiMe}_2\text{Cl})$,^[10,18] $\text{Li}[\text{C}_5\text{H}_4(\text{SiMe}_3)]$,^[10,18] $[\text{M}(\text{NCMe})_3(\text{CO})_3]$ ^[29] (*M* = Mo, W), and $[\text{ZrCl}_2(\eta^5\text{-C}_5\text{H}_4\text{SiMe}_2\text{-}\eta^1\text{-NtBu})]$ ^[30] were prepared according to previous reports. Commercially available reagents were used without further purification. NMR spectra were recorded with a Bruker 400 Ultrashield. ¹H and ¹³C chemical shifts are reported relative to tetramethylsilane. Coupling constants *J* are given in Hertz. IR spectra were measured with a Perkin–Elmer 883 IR spectrometer. Elemental analyses were performed in our laboratories (UAH) with a Perkin–Elmer 2400 CHNS/O Analyzer, Series II.

C₅H₄[SiMe₂(CH=CHCH₃)](SiMe₃) (*cis*+*trans*-2**):** A 0.5 M solution of *cis*+*trans*-1-propenylmagnesium bromide in THF (38 mL, 18.9 mmol) was added at 0 °C to a solution of 5-(chlorodimethylsilyl)cyclopentadiene (1.0 g, 6.3 mmol) in diethyl ether (10 mL). The reaction mixture was warmed to room temperature and stirred overnight. At this stage, chlorotrimethylsilane (4.0 mL, 31.5 mmol) was added to the resulting orange solution and the mixture stirred for a further 5 h. The solvent was removed under vacuum and the solid residue was extracted into hexane (2 × 10 mL); the resulting suspension was filtered and the solvent was completely removed from the orange solution to give an orange oil. Derivative **2** was obtained as a mixture of isomers from which major the product *cis*+*trans*-5,5-disilyl-substituted could be fully characterized; yield 1.10 g (4.6 mmol, 70%). $\text{C}_{13}\text{H}_{24}\text{Si}_2$ (236.50): calcd. C 66.02, H 10.23; found C 65.68, H 9.82. *cis*-**2**: ¹H NMR (400 MHz, CDCl₃, plus HSQC plus HMBC): δ = 6.72, 6.53 (both m, each 2 H, C₅H₄), 6.39 (dq, ^{cis}*J*_{H,H} = 14, ³*J*_{H,H} = 7 Hz, 1 H, =CHMe), 5.37 (d, ^{cis}*J*_{H,H} = 14 Hz, 1 H, =CHSi), 1.75 (d, ³*J*_{H,H} = 7 Hz, 3 H, =CCH₃), 0.09 [s, 6 H, Si(CH₃)₂], −0.04 [s, 9 H, Si(CH₃)₃] ppm. ¹³C NMR (100 MHz, CDCl₃, APT plus HSQC): δ = 143.8 (+, =CHMe), 136.4, 131.1 (+, C₅H₄), 128.8 (+, =CHSi), 57.3 (−, *ipso*-C₅H₄), 19.4 (+, =CCH₃), −0.3, −0.4 [+ , Si(CH₃)₂ + Si(CH₃)₃] ppm. ²⁹Si NMR (79 MHz, CDCl₃, HMBC): δ = −12.2 (Si–CH=), −6.0 [Si(CH₃)₃] ppm. *trans*-**2**: ¹H NMR (400 MHz, CDCl₃, plus HSQC plus HMBC): δ = 6.72, 6.53 (both m, each 2 H, C₅H₄), 6.06 (dq, ^{trans}*J*_{H,H} = 17, ³*J*_{H,H} = 5 Hz, 1 H, =CHMe), 5.64 (d, ^{trans}*J*_{H,H} = 17 Hz, 1 H, =CHSi), 1.82 (d, ³*J*_{H,H} = 5.0 Hz, 3 H, =CCH₃), 0.09 [s, 3 H, Si(CH₃)₂], −0.06 [s, 9 H, Si(CH₃)₃] ppm. ¹³C NMR (100 MHz, CDCl₃, APT plus HSQC): δ = 143.1 (+, =CHMe), 136.3, 130.9 (+, C₅H₄), 130.8 (+, =CHSi), 57.2 (−, *ipso*-C₅H₄), 22.9 (+, =CCH₃), −0.3, −0.4 [+ , Si(CH₃)₂ + Si(CH₃)₃] ppm. ²⁹Si NMR (79 MHz, CDCl₃, HMBC): δ = −10.8 (Si–CH=), −6.0 [Si(CH₃)₃] ppm.

C₅H₄[SiMe₂(CH₂CH=CH₂)](SiMe₃) (3**):** Allyl(chloro)dimethylsilane (3.0 mL, 20 mmol) was added to a suspension of (trimethylsilyl)cyclopentadienyllithium (2.30 g, 16 mmol) in hexane (20 mL). The reaction mixture was stirred at room temperature for 48 h. The resulting yellow suspension was filtered to remove the white LiCl solid and the solvent was completely removed from the resulting yellow solution to give an orange oil that was identified as pure derivative **3**, obtained as a mixture of isomers from which the major product $\text{C}_5\text{H}_4[5\text{-SiMe}_2(\text{CH}_2\text{CH}=\text{CH}_2)\text{-5-SiMe}_3]$ was fully characterized; yield 2.90 g (12.2 mmol, 76%). $\text{C}_{13}\text{H}_{24}\text{Si}_2$ (236.59): calcd. C 66.02, H 10.23; found C 65.98, H 9.83. ¹H NMR (400 MHz, CDCl₃, plus HSQC plus HMBC): δ = 6.73, 6.53 (both m, each 2 H, C₅H₄), 5.64 (m, ^{cis}*J*_{H,H} = 8, ^{trans}*J*_{H,H} = 16, ³*J*_{H,H} = 8 Hz, 1 H, =CH), 4.79 (d, ^{trans}*J*_{H,H} = 16 Hz, 1 H, =CH₂), 4.79 (d, ^{cis}*J*_{H,H} = 8 Hz, 1 H, =CH₂), 1.36 (d, ³*J*_{H,H} = 8.0 Hz, 2 H, Si–CH₂), 0.01, [s, 6 H, Si(CH₃)₂], −0.03 [s, 9 H, Si(CH₃)₃] ppm. ¹³C NMR (100 MHz, CDCl₃, APT plus HSQC): δ = 136.0 (+, C₅H₄), 135.6 (+, =CH), 131.1 (+, C₅H₄), 113.5 (−, =CH₂), 57.0 (−, *ipso*-C₅H₄), 22.9 (−, Si–

CH₂), −0.4 [+], Si(CH₃)₃], −2.4 [+], Si(CH₃)₂] ppm. ²⁹Si NMR (79 MHz, CDCl₃, HMBC): δ = −4.1 (Si–CH₂), −0.5 [Si(CH₃)₃] ppm.

Li[C₅H₃-1-SiMe₂(CH=CHCH₃)-3-SiMe₃] (*cis*+*trans*-4): *n*-Butyllithium (1.9 mL of a 1.6 M hexane solution, 3 mmol) was added dropwise to a solution of *cis*+*trans*-2 (0.6 g, 2.5 mmol) in diethyl ether (10 mL) at 0 °C. When the addition was finished, the reaction mixture was stirred at room temperature for a further 16 h. Solvent was removed under vacuum and hexane (2 × 3 mL) was then added to the orange residue. The resulting suspension was filtered off and the solvent was completely removed from the oily residue under vacuum to afford an orange foam, which was identified as pure derivative **4** obtained as a *cis* and *trans* isomer mixture in a 1:2 molar ratio; yield 0.60 g (2.4 mmol, 98%). *cis*-4: ¹H NMR (400 MHz, C₆D₆/C₅D₅N = 9:1, plus NOESY plus HSQC): δ = 6.87, 6.76, 6.76 (all br., each 1 H, C₅H₃), 6.38 (dq, ³J_{H,H} = 7, ^{cis}J_{H,H} = 12 Hz, 1 H, =CHMe), 5.97 (d, ^{cis}J_{H,H} = 12 Hz, 1 H, =CHSi), 1.79 (d, ³J_{H,H} = 7 Hz, 3 H, =CCH₃), 0.44 [s, 6 H, Si(CH₃)₂], 0.30 [s, 9 H, Si(CH₃)₃] ppm. ¹³C NMR (100 MHz, C₆D₆/C₅D₅N = 9:1, APT plus HSQC): δ = 142.2 (+, =CCH₃), 133.7 (+, =CHSi), 120.9, 116.3, 116.0 (+, C₅H₃), 115.6, 114.2 (−, *ipso*-C₅H₃), 20.0 (+, =CCH₃), 2.4 [+], −Si(CH₃)₂], 2.2 [+], −Si(CH₃)₃] ppm. ²⁹Si NMR (79 MHz, C₆D₆/C₅D₅N = 9:1, HMBC): δ = −22.9 (Si–CH=), −14.7 [Si(CH₃)₃] ppm. *trans*-4: ¹H NMR (400 MHz, C₆D₆/C₅D₅N = 9:1, plus NOESY plus HSQC): δ = 6.86, 6.74, 6.74 (all br., each 1 H, C₅H₃), 6.17 (dq, ³J_{H,H} = 6, ^{trans}J_{H,H} = 20 Hz, 1 H, =CHMe), 5.96 (d, ^{trans}J_{H,H} = 20 Hz, 1 H, =CHSi), 1.64 (d, ³J_{H,H} = 6 Hz, 3 H, =CCH₃), 0.38 [s, 6 H, −Si(CH₃)₂], 0.30 [s, 9 H, −Si(CH₃)₃] ppm. ¹³C NMR (100 MHz, C₆D₆/C₅D₅N = 9:1, APT plus HSQC): δ = 140.9 [+], =C(CH₃)], 135.3 (+, =CHSi), 120.9, 116.4, 116.0 (+, C₅H₃), 115.6, 113.6 (−, *ipso*-C₅H₃), 23.4 [+], =C(CH₃)], 2.2 [+], −Si(CH₃)₃], 0.8 [+], −Si(CH₃)₂] ppm. ²⁹Si NMR (79 MHz, C₆D₆/C₅D₅N = 9:1, HMBC): δ = −21.8 (Si–CH=), −14.7 [Si(CH₃)₃] ppm.

Li[C₅H₃-1-SiMe₂(CH₂CH=CH₂)-3-SiMe₃] (5): *n*-Butyllithium (7 mL of a 1.6 M hexane solution, 11.1 mmol) was added dropwise to a solution of **3** (2.2 g, 9.3 mmol) in diethyl ether (10 mL) at 0 °C. When the addition was complete, the reaction mixture was stirred at room temperature for a further 16 h. Solvent was removed under vacuum and hexane (2 × 3 mL) was then added to the brown residue. The resulting suspension was filtered off and the solid residue dried under vacuum to give a light orange solid, which was spectroscopically identified as pure derivative **5**; yield 1.80 g (7.4 mmol, 80%). ¹H NMR (400 MHz, C₆D₆/C₅D₅N = 9:1, plus NOESY plus HSQC): δ = 6.87 (dd, both ⁴J_{H,H} = 1.6 Hz, 1 H, C₅H₃), 6.75 (overlapped, 2 H, C₅H₃), 6.05 (m, ³J_{H,H} = 8, ^{cis}J_{H,H} = 10, ^{trans}J_{H,H} = 17 Hz, 1 H, =CH), 4.94 (d, ^{trans}J_{H,H} = 17 Hz, 1 H, =CH₂), 4.86 (d, ^{cis}J_{H,H} = 10 Hz, 1 H, =CH₂), 1.84 (d, ³J_{H,H} = 8 Hz, 2 H, Si–CH₂), 0.34 [s, 9 H, −Si(CH₃)₃], 0.33 [s, 6 H, −Si(CH₃)₂] ppm. ¹³C NMR (100 MHz, C₆D₆/C₅D₅N = 9:1, APT plus HSQC): δ = 138.2 (+, =CH), 120.8, 116.0, 115.9 (+, C₅H₃), 115.2, 113.0 (−, *ipso*-C₅H₃), 112.4 (+, =CH₂), 27.4 (+, Si–CH₂), 2.1, −0.3 [both +, −Si(CH₃)₃ + Si(CH₃)₂] ppm. ²⁹Si NMR (79 MHz, C₆D₆/C₅D₅N = 9:1, HMBC): δ = −12.4 (Si–CH₂), −13.1 [Si(CH₃)₃] ppm.

[ZrCl(η⁵-C₅H₄SiMe₂-η¹-N*r*Bu){η⁵-C₅H₃-1-SiMe₂(CH=CHCH₃)-3-SiMe₃}] (*cis*+*trans*-6): Toluene (5 mL) was added to a dry mixture of [ZrCl₂(η⁵-C₅H₄SiMe₂-η¹-N*r*Bu)] (0.2 g, 0.56 mmol) and **4** (0.18 g, 0.73 mmol). Stirring the reaction mixture for 18 h at room temperature gave a yellow suspension. The solvent was removed under vacuum and hexane (2 × 3 mL) was then added to the oily residue. The resulting suspension was filtered and the solvent was completely removed from the yellow solution to give a yellow oil that was identified as pure derivative **6**, obtained as a mixture of four diastereomers, *cis*-6a,b and *trans*-6a,b; yield 0.28 g (0.50 mmol,

91%). C₂₄H₄₂ClNSi₃Zr (555.53): calcd. C 51.88, H 7.63, N 2.52; found C 51.87, H 7.92, N 2.62. *cis*-6a,b + *trans*-6a,b: ¹H NMR (400 MHz, CDCl₃, plus TOCSY, plus HSQC): δ = 7.24–7.21, 6.70–6.51, 6.30–6.20, 5.88–5.80 (all m, 28 H, C₅H₄ + C₅H₃), 6.60–6.38 (overlapped, 2 H, CCH=, *cis*-6a,b), 6.09–5.90 (overlapped, 2 H, C–CH=, *trans*-6a,b), 5.74 (dq, ^{trans}J_{H,H} = 18, ⁴J_{H,H} = 2 Hz, 1 H, Si–CH=, *trans*-6a,b), 5.72 (dq, ^{cis}J_{H,H} = 14, ⁴J_{H,H} = 1 Hz, 1 H, Si–CH=, *cis*-6a,b), 5.66 (dq, ^{trans}J_{H,H} = 18, ⁴J_{H,H} = 2 Hz, 1 H, Si–CH=, *trans*-6a,b), 5.60 (dq, ^{cis}J_{H,H} = 14, ⁴J_{H,H} = 1 Hz, 1 H, Si–CH=, *cis*-6a,b), 1.89 (dd, ⁴J_{H,H} = 2, ³J_{H,H} = 6 Hz, 3 H, =CCH₃, *trans*-6a,b), 1.86 (dd, ⁴J_{H,H} = 2, ³J_{H,H} = 6 Hz, 3 H, =CCH₃, *trans*-6a,b), 1.77 (dd, ⁴J_{H,H} = 1, ³J_{H,H} = 7 Hz, 3 H, =CCH₃, *cis*-6a,b), 1.65 (dd, ⁴J_{H,H} = 1, ³J_{H,H} = 7 Hz, 3 H, =CCH₃, *cis*-6a,b), 1.32 [br., 36 H, NC(CH₃)₃], 0.55–0.23 [all s, 84 H, NSi(CH₃)₂ + Si(CH₃)₂ + Si(CH₃)₃] ppm. ¹³C NMR (100 MHz, CDCl₃, APT plus HSQC): δ = 145.5, 144.8, 143.8, 143.2 (+, C–CH=), 131.2, 130.8 (+, Si–CH=, *cis*-6a,b), 129.7, 129.5 (+, Si–CH=, *trans*-6a,b), 129.4, 129.4, 129.2, 129.2 (−, *ipso*-C₅H₄–C₅H₃), 128.5, 128.4, 128.3, 128.2, 128.1, 128.1, 128.0, 128.0, 127.8, 127.8 (+, C₅H₄/C₅H₃), 124.5, 124.5, 124.4, 124.3, 119.0, 118.9, 118.8, 118.7, 118.6 (+, C₅H₄/C₅H₃), 118.5, 118.5, 117.7, 117.6 (−, *ipso*-C₅H₄–C₅H₃), 117.2, 116.9, 116.8, 116.7, 116.6 (+, C₅H₄/C₅H₃), 112.6, 112.6, 112.5, 112.5 (−, *ipso*-C₅H₄–C₅H₃), 109.7, 109.6, 109.3 (+, C₅H₄/C₅H₃), 59.5 [br., −, N–C(CH₃)₃], 35.0 [+], N–C(CH₃)₃], 23.0, 22.9 (+, =C–CH₃, *trans*-6a,b), 19.4, 18.8 (+, =C–CH₃, *cis*-6a,b), 4.8–4.6, 2.3–2.0, 0.9–0.5, −0.6 to −1.3 [+], NSi(CH₃)₂ + Si(CH₃)₂ + Si(CH₃)₃] ppm. ²⁹Si NMR (79 MHz, CDCl₃, HMBC): δ = −7.7 [Si(CH₃)₃, *cis*-6a,b + *trans*-6a,b], −16.1 (Si–CH=, *cis*-6a,b + *trans*-6a,b), −24.8 (Si–N, *cis*-6a,b + *trans*-6a,b) ppm.

[ZrCl(η⁵-C₅H₄SiMe₂-η¹-N*r*Bu){η⁵-C₅H₃-1-SiMe₂(CH₂CH=CH₂)-3-SiMe₃}] (7): Toluene (5 mL) was added to a dry mixture of [ZrCl₂(η⁵-C₅H₄SiMe₂-η¹-N*r*Bu)] (0.2 g, 0.56 mmol) and **5** (0.16 g, 0.67 mmol). Stirring the reaction mixture for 16 h at room temperature gave a yellow suspension. The solvent was removed under vacuum and hexane (2 × 3 mL) was then added to the oily residue. The resulting suspension was filtered and the solvent was completely removed from the yellow solution under vacuum to give a yellow oil that was identified as pure derivative **7**, obtained as a mixture of two different stereoisomers, **7a** and **7b**; yield 0.29 g (0.52 mmol, 94%). for C₂₄H₄₂ClNSi₃Zr (555.53): calcd. C 51.88, H 7.63, N 2.52; found C 51.14, H 7.69, N 2.65. **7a+b**: ¹H NMR (400 MHz, CDCl₃, plus HSQC, plus HMBC): δ = 7.23, 6.68, 6.60, 6.51, 6.29, 5.82 (all m, 14 H, C₅H₄/C₅H₃), 5.74–5.58 (overlapped, 2 H, C–CH=), 4.82 (d, ^{cis}J_{H,H} = 10 Hz, 1 H, =CH₂), 4.81 (d, ^{cis}J_{H,H} = 11 Hz, 1 H, =CH₂), 4.77 (d, ^{trans}J_{H,H} = 18 Hz, 1 H, =CH₂), 4.75 (d, ^{trans}J_{H,H} = 17 Hz, 1 H, =CH₂), 1.66 (d, ³J_{H,H} = 8 Hz, 2 H, Si–CH₂), 1.61 (d, ³J_{H,H} = 8 Hz, 2 H, Si–CH₂), 1.31 [br., 18 H, N(CH₃)₃], 0.54 [s, 6 H, NSi(CH₃)₂], 0.44 [s, 3 H, Si(CH₃)₂], 0.42 [s, 6 H, NSi(CH₃)₂], 0.31 [s, 12 H, Si(CH₃)₃], 0.29, 0.23 [both s, each 3 H, Si(CH₃)₂], 0.22 [s, 9 H, Si(CH₃)₃] ppm. ¹³C NMR (100 MHz, CDCl₃, APT plus HSQC): δ = 135.2, 134.4 (+, CH=), 129.5 (−, *ipso*-C₅H₄–C₅H₃), 128.2, 128.1, 128.1, 128.0, 128.0, 127.7 (+, C₅H₄/C₅H₃), 127.4 (−, *ipso*-C₅H₄–C₅H₃), 124.5, 124.5, 118.9, 118.8 (+, C₅H₄/C₅H₃), 118.5 (−, *ipso*-C₅H₄–C₅H₃), 117.0, 116.9 (+, C₅H₄/C₅H₃), 116.4 (−, *ipso*-C₅H₄–C₅H₃), 114.1, 113.5 (−, =CH₂), 112.7, 112.6 (−, *ipso*-C₅H₄–C₅H₃), 109.4, 109.3 (+, C₅H₄/C₅H₃), 59.5 [br., −, N–C(CH₃)₃], 35.0, 34.9 [+], N–C(CH₃)₃], 25.9, 25.4 (−, Si–CH₂), 4.8, 4.8, 2.4, 2.3, 0.8, 0.5, −1.5, −1.7, −2.4, −2.6 [all +, NSi(CH₃)₂ + Si(CH₃)₂ + Si(CH₃)₃] ppm. ²⁹Si NMR (79 MHz, CDCl₃, HMBC): δ = −7.8 (Si–CH₂, **7a+b**), −7.4 [Si(CH₃)₃, **7a+b**], −24.7 (Si–N, **7a+b**) ppm.

[Zr(CH₃)(η⁵-C₅H₄SiMe₂-η¹-N*r*Bu){η⁵-C₅H₃-1-SiMe₂(CH=CHCH₃)-3-SiMe₃}] (*cis*+*trans*-8): Methyllithium (0.5 mL of a 1.5 M diethyl

ether solution, 0.74 mmol) was added dropwise to a solution of **6** (0.24 g, 0.5 mmol) in diethyl ether (10 mL) at 0 °C. When the addition was complete, the reaction mixture was stirred at room temperature for a further 2 h. The solvent was completely removed from the resulting brown suspension under vacuum and the solid residue was extracted into hexane (2 × 3 mL). Removal of the hexane from the brown solution gave a brown oil, which was identified as pure derivative **8**, obtained as a mixture of four diastereomers, *cis*-**8a,b** and *trans*-**8a,b**; yield 0.21 g (0.40 mmol, 90%). C₂₅H₄₅NSi₃Zr (535.11): calcd. C 56.11, H 8.48, N 2.62; found C 55.62, H 8.54, N 2.22. *cis*-**8a,b** + *trans*-**8a,b**: ¹H NMR (400 MHz, C₆D₆, plus TOCSY plus HSQC plus HMBC): δ = 6.97–6.91, 6.73, 6.68, 6.58, 6.09–5.99, 5.93–5.90 (all m, 28 H, C₅H₄/C₅H₃), 6.46–6.33 (overlapped, 2 H, C–CH=, *cis*-**8a,b**), 6.10–5.97 (overlapped, 2 H, C–CH=, *trans*-**8a,b**), 5.88 (dq, ^{trans}J_{H,H} = 18, ⁴J_{H,H} = 1 Hz, 1 H, Si–CH=, *trans*-**8a,b**), 5.80 (dq, ^{trans}J_{H,H} = 19, ⁴J_{H,H} = 1 Hz, 1 H, Si–CH=, *trans*-**8a,b**), 5.79 (dq, ^{cis}J_{H,H} = 13, ⁴J_{H,H} = 2 Hz, 1 H, Si–CH=, *cis*-**8a,b**), 5.69 (dq, ^{cis}J_{H,H} = 14, ⁴J_{H,H} = 2 Hz, 1 H, Si–CH=, *cis*-**8a,b**), 1.71 (dd, ⁴J_{H,H} = 1, ³J_{H,H} = 6 Hz, 3 H, =CCH₃, *trans*-**8a,b**), 1.69 (dd, ⁴J_{H,H} = 1, ³J_{H,H} = 6 Hz, 3 H, =CCH₃, *trans*-**8a,b**), 1.61 (dd, ⁴J_{H,H} = 2, ³J_{H,H} = 6 Hz, 3 H, =CCH₃, *cis*-**8a,b**), 1.60 (dd, ⁴J_{H,H} = 2, ³J_{H,H} = 6 Hz, 3 H, =CCH₃, *cis*-**8a,b**), 1.22, 1.21 (br., 36 H, *t*BuN), 0.56–0.20 [all s, 84 H, Si(CH₃)₂/Si(CH₃)₃], 0.17 (br., 12 H, Zr–Me) ppm. ¹³C NMR (100 MHz, C₆D₆, APT plus HSQC): δ = 145.3, 144.5 (+, C–CH=, *cis*-**8a,b**), 144.4, 143.8 (+, C–CH=, *trans*-**8a,b**), 131.7, 131.1 (+, Si–CH=, *trans*-**8a,b**), 131.1, 130.2 (–, *ipso*-C₅H₄/C₅H₃), 130.3, 130.0 (+, Si–CH=, *cis*-**8a,b**), 129.0, 129.0 (–, *ipso*-C₅H₄/C₅H₃), 127.2, 126.9, 126.7, 125.6, 125.5, 125.4, 124.3, 124.2 (+, C₅H₄/C₅H₃), 124.1 (–, *ipso*-C₅H₄/C₅H₃), 124.0 (+, C₅H₄/C₅H₃), 123.9, 122.5 (–, *ipso*-C₅H₄/C₅H₃), 121.7, 121.5, 121.4, 121.3, 117.8 (+, C₅H₄/C₅H₃), 116.9 (–, *ipso*-C₅H₄/C₅H₃), 116.8, 116.3, 116.2, 116.1, 116.1, 115.1, 114.9, 114.8, 114.6, 113.7 (+, C₅H₄/C₅H₃), 109.6, 109.5, 109.4, 109.4 (–, *ipso*-C₅H₄/C₅H₃), 108.9, 108.8, 108.5, 108.4 (+, C₅H₄/C₅H₃), 58.1 [br., –, N–C(CH₃)₃], 36.0 [br., +, N–C(CH₃)₃], 23.4, 23.3 (+, =C–CH₃, *trans*-**8a,b**), 19.7, 19.7, 19.6, 19.6 (+, Zr–CH₃), 19.3, 19.1 (+, =C–CH₃, *cis*-**8a,b**), 5.1–4.9, 3.0–2.9, 1.5–1.1, 0.1–0.6 [+], NSi(CH₃)₂ + Si(CH₃)₂ + Si(CH₃)₃] ppm. ²⁹Si NMR (79 MHz, C₆D₆, HMBC): δ = –7.3, –8.0 [Si(CH₃)₃, *cis*-**8a,b** + *trans*-**8a,b**], –15.5, –16.3 (Si–CH=, *cis*-**8a,b** + *trans*-**8a,b**), –24.3, –24.8 (Si–N, *cis*-**8a,b** + *trans*-**8a,b**) ppm.

[Zr(CH₃)₂(η⁵-C₅H₄SiMe₂η¹-*Nr*Bu){η⁵-C₅H₃-1-SiMe₂(CH₂CH=CH₂)-3-SiMe₃}] (**9**): Methyllithium (0.36 mL of a 1.5 M diethyl ether solution, 0.54 mmol) was added dropwise to a solution of **7** (0.15 g, 0.27 mmol) in diethyl ether (10 mL) at 0 °C. When the addition was complete, the reaction mixture was stirred at room temperature for a further 3 h. The solvent was removed from the resulting brown under vacuum and the solid residue extracted into hexane (2 × 3 mL). Removal of the hexane from the brown solution gave a brown oil, which was identified as pure derivative **9**, obtained as a mixture of two diastereomers, **9a** and **9b**; yield 0.11 g (0.21 mmol, 79%). C₂₅H₄₅NSi₃Zr (535.11): calcd. C 56.11, H 8.48, N 2.62; found C 55.96, H 9.17, N 3.05. **9a+b**: ¹H NMR (400 MHz, C₆D₆, plus HSQC): δ = 6.90, 6.65, 6.56, 5.99–5.96, 5.84–5.83 (all m, 14 H, C₅H₄/C₅H₃), 5.78–5.64 (overlapped, 2 H, C–CH=), 4.92 (d, ^{cis}J_{H,H} = 10 Hz, 1 H, =CH₂), 4.90 (d, ^{cis}J_{H,H} = 10 Hz, 1 H, =CH₂), 4.87 (d, ^{trans}J_{H,H} = 18 Hz, 1 H, =CH₂), 4.84 (d, ^{trans}J_{H,H} = 17 Hz, 1 H, =CH₂), 1.59 (overlapped, 4 H, Si–CH₂), 1.21 (s, 18 H, *t*BuN), 0.55, 0.45 [both s, each 6 H, N–Si(CH₃)₂], 0.27, 0.26 [both s, each 3 H, Si(CH₃)₂], 0.24, 0.20 [both s, each 9 H, Si(CH₃)₃], 0.16 (s, 6 H, Zr–CH₃), 0.17, 0.15 [both s, each 3 H, Si(CH₃)₂] ppm. ¹³C NMR (100 MHz, C₆D₆, APT plus HSQC): δ = 135.6, 135.3 (+, CH=), 127.0 (+, C₅H₄/C₅H₃), 126.9 (–, *ipso*-C₅H₄/C₅H₃), 126.7,

125.5, 125.5, 124.1 (+, C₅H₄/C₅H₃), 124.0 (–, *ipso*-C₅H₄/C₅H₃), 123.9 (+, C₅H₄/C₅H₃), 122.0 (–, *ipso*-C₅H₄/C₅H₃), 121.4, 121.4 (+, C₅H₄/C₅H₃), 116.7 (–, *ipso*-C₅H₄/C₅H₃), 116.1, 116.0, 114.8, 114.7 (+, C₅H₄/C₅H₃), 114.4, 114.2 (–, =CH₂), 109.5, 109.4 (–, *ipso*-C₅H₄/C₅H₃), 108.4, 108.3 (+, C₅H₄/C₅H₃), 58.0, 58.0 [–, NC(CH₃)₃], 36.0 [+], NC(CH₃)₃], 26.5, 26.4 (–, Si–CH₂), 19.3, 19.2 (+, Zr–CH₃), 5.1, 5.0, 3.0, 3.0, 1.3, 1.1, –0.9, –1.4, –1.8, –2.0 [+], NSi(CH₃)₂ + Si(CH₃)₂ + Si(CH₃)₃] ppm. ²⁹Si NMR (79 MHz, C₆D₆, HMBC): δ = –8.1 (Si–CH₂, **9a+b**), –8.4 [Si(CH₃)₃, **9a+b**], –25.3 (Si–N, **9a+b**) ppm.

[MoH{η⁵-C₅H₃-1-SiMe₂(CH=CHCH₃)-3-SiMe₃}(CO)₃] (*cis*+*trans*-**10**): A solution of *cis*+*trans*-**2** (0.13 g, 0.80 mmol) in THF (5 mL) was added to solid compound [Mo(CO)₃(NCCH₃)₃] (0.30 g, 1.0 mmol). Stirring the reaction mixture for 30 min at room temperature gave an orange suspension. The solvent was removed under vacuum and hexane (2 × 3 mL) was then added to the solid residue. The resulting suspension was filtered and the solvent was completely removed from the yellow solution under vacuum to give an orange oil, which was identified as a mixture of *cis*-**10** and *trans*-**10** in a molar ratio of approximately 1:1; yield 0.18 g (0.43 mmol, 53%). C₁₆H₂₄MoO₃Si₂ (416.47): calcd. C 46.14, H 5.81; found C 46.08, H 5.32. IR (THF): $\tilde{\nu}$ = 2015, 1951 (CO) cm^{–1}. *cis*+*trans*-**10**: ¹H NMR (400 MHz, C₆D₆, plus HSQC plus HMBC): δ = 6.35 (m, ^{cis}J_{H,H} = 14, ³J_{H,H} = 7 Hz, 1 H, =CHMe, *cis*-**10**), 6.01 (m, ^{trans}J_{H,H} = 20, ³J_{H,H} = 6 Hz, 1 H, =CHMe, *trans*-**10**), 5.69 (d, ^{trans}J_{H,H} = 20 Hz, 1 H, =CHSi, *trans*-**10**), 5.55 (d, ^{cis}J_{H,H} = 14 Hz, =CHSi, 1 H, *cis*-**10**), 5.29, 5.27, 5.12, 5.10, 5.04, 5.03 (all br., each 1 H, C₅H₃), 1.66 (d, ³J_{H,H} = 7 Hz, 3 H, =CCH₃, *cis*-**10**), 1.59 (d, ³J_{H,H} = 6 Hz, 3 H, =CCH₃, *trans*-**10**), 0.28, 0.21 [both s, each 6 H, Si(CH₃)₂], 0.09, 0.08 [both s, each 9 H, Si(CH₃)₃], –5.49, –5.49 (both s, each 1 H, Mo–H) ppm. ¹³C NMR (100 MHz, C₆D₆, APT plus HSQC): δ = 227.8 (–, CO), 145.0, 145.5 (both +, =CHMe), 129.0, 127.2 (both +, =CHSi), 104.6, 104.5, 104.0, 103.4 (all –, *ipso*-C₅H₃), 100.5, 100.5, 99.2, 99.1, 98.9, 98.8 (all +, C₅H₃), 22.3, 19.0 (both +, =CCH₃), –0.26 [+], Si(CH₃)₃], –1.5, –1.7 [+], Si(CH₃)₂] ppm. ²⁹Si NMR (79 MHz, C₆D₆, HMBC): δ = –16.2, –13.9 (Si–CH=, *cis*+*trans*-**10**), –5.3 [Si(CH₃)₃, *cis*+*trans*-**10**] ppm.

[W{η⁵-C₅H₃-1-SiMe₂(CH=CH-CH₃)-3-SiMe₃}(CO)₃] (*cis*+*trans*-**11**): A solution of *cis*+*trans*-**2** (0.13 g, 1.0 mmol) in THF (5 mL) was added to solid derivative [W(CO)₃(NCCH₃)₃] (0.40 g, 1.0 mmol). Stirring the reaction mixture at room temperature overnight gave an orange suspension. The solvent was removed under vacuum and hexane (2 × 3 mL) was then added to the solid residue. The resulting suspension was filtered and the solvent was completely removed from the orange solution under vacuum to give an orange oil, which was identified as pure **11**, obtained as a 1:1 *cis*/*trans* mixture of isomers, on which elemental analysis and IR have been conducted. Heating solutions of the mixture in THF permitted the major isomer *trans*-**11** to be isolated and allowed the assignment of NMR spectroscopic signals for each of the *cis* and *trans* isomers; yield 0.30 g (0.59 mmol, 60%). C₁₆H₂₄O₃Si₂W (504.37): calcd. C 38.10, H 4.80; found C 37.87, H 4.39. IR (THF): $\tilde{\nu}$ = 2016, 1930, 1924 (CO) cm^{–1}. *cis*-**11**: ¹H NMR (400 MHz, C₆D₆, plus HSQC plus HMBC-²⁹Si): δ = 6.33 (m, ^{cis}J_{H,H} = 12, ³J_{H,H} = 7 Hz, 1 H, =CHMe), 5.55 (dq, ^{cis}J_{H,H} = 12, ⁴J_{H,H} = 1 Hz, 1 H, =CHSi), 5.26, 5.09, 5.02 (all br., each 1 H, C₅H₃), 1.58 (dd, ³J_{H,H} = 7, ⁴J_{H,H} = 1 Hz, 3 H, =CCH₃), 0.28 [s, 6 H, Si(CH₃)₂], 0.09 [s, 9 H, Si(CH₃)₃], –7.17 (s, 1 H, Mo–H) ppm. ¹³C NMR (100 MHz, C₆D₆, APT plus HSQC): δ = 197.0 (–, CO), 145.0 (+, =CHMe), 127.2 (+, =CHSi), 103.5, 102.3 (–, *ipso*-C₅H₃), 98.2, 97.9, 97.8 (+, C₅H₃), 19.2 (+, =CCH₃), –0.1 [+], Si(CH₃)₃], –1.4 [+], Si(CH₃)₂] ppm. ²⁹Si NMR (79 MHz, C₆D₆, HMBC): δ = –13.6 (Si–CH=), –4.5 [Si(CH₃)₃] ppm. *trans*-**11**: ¹H NMR (400 MHz, C₆D₆, plus

HSQC plus HMBC- ^{29}Si): $\delta = 6.01$ (m, $^{trans}J_{\text{H,H}} = 18$, $^3J_{\text{H,H}} = 6$ Hz, 1 H, =CHMe), 5.67 (dq, $^{trans}J_{\text{H,H}} = 18$, $^4J_{\text{H,H}} = 1$ Hz, 1 H, =CHSi), 5.25, 5.07, 5.02 (all br., each 1 H, C_5H_3), 1.65 (dd, $^3J_{\text{H,H}} = 6$, $^4J_{\text{H,H}} = 1$ Hz, 3 H, =CCH $_3$), 0.22 [s, 6 H, Si(CH $_3$) $_2$], 0.10 [s, 9 H, Si(CH $_3$) $_3$], -7.18 (s, 1 H, W-H) ppm. ^{13}C NMR (100 MHz, C_6D_6 , APT plus HSQC): $\delta = 197.0$ (-, CO), 145.5 (+, =CHMe), 128.9 (+, =CHSi), 103.4, 102.9 (-, *ipso*- C_5H_3), 98.1, 97.9, 97.6 (+, C_5H_3), 22.5 (+, =CCH $_3$), -0.1 [+ , Si(CH $_3$) $_3$], -1.4 [+ , Si(CH $_3$) $_2$] ppm. ^{29}Si NMR (79 MHz, C_6D_6 , HMBC): $\delta = -15.9$ (Si-CH=), -4.5 [Si(CH $_3$) $_3$] ppm.

[MoH $\{\eta^5\text{-C}_5\text{H}_3\text{-1-SiMe}_2(\text{CH}_2\text{CH}=\text{CH}_2)\text{-3-SiMe}_3\}(\text{CO})_3$] (12): A solution of **3** (0.19 g, 0.8 mmol) in THF (5 mL) was added to solid compound [Mo(CO) $_3$ (NCCH $_3$) $_3$] (0.3 g, 1.0 mmol). Stirring the reaction mixture for 30 min at room temperature gave a red suspension. The solvent was removed under vacuum and hexane (2 \times 3 mL) was then added to the solid residue. The resulting suspension was filtered and the solvent was completely removed from the red solution under vacuum to give an orange oil; yield 0.27 g (0.65 mmol, 65%). $\text{C}_{16}\text{H}_{24}\text{MoO}_3\text{Si}_2$ (416.47): calcd. C 46.14, H 5.81; found C 46.16, H 5.33. IR (THF): $\tilde{\nu} = 2018, 1933$ (CO) cm^{-1} . ^1H NMR (400 MHz, C_6D_6 , plus HSQC plus HMBC- ^{29}Si): $\delta = 5.67$ (m, $^{trans}J_{\text{H,H}} = 17$, $^{cis}J_{\text{H,H}} = 10$, $^3J_{\text{H,H}} = 8$ Hz, 1 H, =CH), 5.22 (dd, $^4J_{\text{H,H}} = 1.2$, $^4J_{\text{H,H}} = 1.6$ Hz, 1 H, C_5H_3), 5.04 (second-order system, 2 H, C_5H_3), 4.89 (d, $^{cis}J_{\text{H,H}} = 10$ Hz, 1 H, =CH $_2$), 4.86 (d, $^{trans}J_{\text{H,H}} = 17$ Hz, 1 H, =CH $_2$), 1.51 (d, $^3J_{\text{H,H}} = 8$ Hz, 2 H, Si-CH $_2$), 0.09 [s, 15 H, Si(CH $_3$) $_2$ + Si(CH $_3$) $_3$], -5.53 (s, 1 H, Mo-H) ppm. ^{13}C NMR (100 MHz, C_6D_6 , APT plus HSQC): $\delta = 228.6$ (-, CO), 134.8 (+, =CH), 114.9 (-, =CH $_2$), 105.3, 103.5 (-, *ipso*- C_5H_3), 101.3, 99.9, 99.6 (+, C_5H_3), 25.4 (-, Si-CH $_2$), 0.6 [+ , Si(CH $_3$) $_3$], -1.6, -1.6 [both +, Si(CH $_3$) $_2$] ppm. ^{29}Si NMR (79 MHz, C_6D_6 , HMBC): $\delta = -6.3$ (Si-CH $_2$), -5.7 [Si(CH $_3$) $_3$] ppm.

[WH $\{\eta^5\text{-C}_5\text{H}_3\text{-1-SiMe}_2(\text{CH}_2\text{CH}=\text{CH}_2)\text{-3-SiMe}_3\}(\text{CO})_3$] (13): A solution of **3** (0.10 g, 0.43 mmol) in THF (5 mL) was added to solid compound [W(CO) $_3$ (NCCH $_3$) $_3$] (0.2 g, 0.51 mmol). Stirring the reaction mixture overnight at 50 $^\circ\text{C}$ gave an orange suspension. The solvent was removed under vacuum and hexane (2 \times 3 mL) was then added to the brown solid residue. The resulting suspension was filtered and the solvent was completely removed from the orange solution under vacuum to give an orange oil; yield 0.16 g (0.32 mmol, 60%). $\text{C}_{16}\text{H}_{24}\text{O}_3\text{Si}_2\text{W}$ (504.37): calcd. C 38.10, H 4.80; found C 38.13, H 4.62. IR (THF): $\tilde{\nu} = 2022, 1924$ (CO) cm^{-1} . ^1H NMR (400 MHz, C_6D_6 , plus HSQC plus HMBC): $\delta = 5.65$ (m, $^{trans}J_{\text{H,H}} = 18$, $^{cis}J_{\text{H,H}} = 11$, $^3J_{\text{H,H}} = 8$ Hz, 1 H, =CH), 5.20, 5.02, 5.00 (all br., each 1 H, C_5H_3), 4.88 (d, $^{cis}J_{\text{H,H}} = 11$ Hz, 1 H, =CH $_2$), 4.84 (d, $^{trans}J_{\text{H,H}} = 18$ Hz, 1 H, =CH $_2$), 1.50 (d, $^3J_{\text{H,H}} = 8$ Hz, 2 H, Si-CH $_2$), 0.09 [s, 15 H, Si(CH $_3$) $_2$ + Si(CH $_3$) $_3$], -7.22 (s, 1 H, W-H) ppm. ^{13}C NMR (100 MHz, C_6D_6 , APT plus HSQC): $\delta = 191.1$ (-, CO), 134.0 (+, =CH), 114.3 (-, =CH $_2$), 103.3, 101.7 (-, *ipso*- C_5H_3), 98.1, 97.8, 97.5 (+, C_5H_3), 24.6 (-, Si-CH $_2$), -0.1 [+ , Si(CH $_3$) $_3$], -2.8, -2.3 [both +, Si(CH $_3$) $_2$] ppm. ^{29}Si NMR (79 MHz, C_6D_6 , HMBC): $\delta = -5.7$ (Si-CH $_2$), -5.3 [Si(CH $_3$) $_3$] ppm.

General Procedure for Isomerization Experiments: Isomerization experiments were carried out by using a Young-valved NMR spectroscopy tube, which was charged with solutions of the corresponding derivatives **6–13** in [D_6]benzene. The reaction mixture was then warmed from 50 to 140 $^\circ\text{C}$ and the transformation was monitored by ^1H NMR spectroscopy. Under such conditions, only *cis*+*trans*-**11** isomerizes. Thus, after heating solutions of a 1:1 *cis*/*trans* mixture of compound **11** in [D_6]benzene or THF at 50 $^\circ\text{C}$ for 10–12 h, a final *cis*/*trans* ratio of approximately 1:10 is reached, which then remained constant.

Acknowledgments

Financial support from the Spanish Ministerio de Educación y Ciencia (MEC), project MAT2007-60997, Comunidad de Madrid (CM), project S-0505/PPQ/0328, and Universidad de Alcalá (UAH), project CCG08-UAH/PPQ-4026, is acknowledged. E. R. thanks Ministerio de Educación y Ciencia (MEC) for funding through Ramón y Cajal Program. C. E. P. and G. C. acknowledge UAH and Agencia Española de Cooperación Internacional (AECI), respectively, for fellowships.

- [1] P. Jutzi, T. Redeker, *Eur. J. Inorg. Chem.* **1998**, 663–674; H. Butenschon, *Chem. Rev.* **2000**, *100*, 1527–1564; U. Siemeling, *Chem. Rev.* **2000**, *100*, 1495–1526.
- [2] M. V. Galakhov, G. Heinz, P. Royo, *Chem. Commun.* **1998**, 17–18; G. Martinez, P. Royo, *Organometallics* **2005**, *24*, 4782–4787.
- [3] J. Cano, P. Gomez-Sal, G. Heinz, G. Martinez, P. Royo, *Inorg. Chim. Acta* **2003**, *345*, 15–26; P. Nicolas, P. Royo, M. V. Galakhov, O. Blacque, H. Jacobsen, H. Berke, *Dalton Trans.* **2004**, 2943–2951.
- [4] E. Royo, S. Acebrón, M. E. G. Mosquera, P. Royo, *Organometallics* **2007**, *26*, 3831–3839, and references cited therein.
- [5] C. Ramos, P. Royo, M. Lanfranchi, M. A. Pellinghelli, A. Tiripicchio, *Organometallics* **2007**, *26*, 445–454.
- [6] C. E. Petrisor, L. M. Frutos, O. Castaño, M. E. G. Mosquera, E. Royo, T. Cuenca, *Dalton Trans.* **2008**, 2670–2673 and references therein.
- [7] C. E. Petrisor, E. Gomez-Bengoia, E. Royo, T. Cuenca, *Organometallics* **2009**, *28*, 4165–4169.
- [8] W. J. Evans, J. C. Brady, J. W. Ziller, *J. Am. Chem. Soc.* **2001**, *123*, 7711–7712.
- [9] L. Lukesova, P. Stepnicka, K. Fejfarova, R. Gyepes, I. Cisarova, M. Horacek, J. Kubista, K. Mach, *Organometallics* **2002**, *21*, 2639–2653; L. Lukesova, M. Horacek, P. Stepnicka, R. Gyepes, I. Cisarova, J. Kubista, K. Mach, *J. Organomet. Chem.* **2004**, *689*, 1919–1929.
- [10] T. Cuenca, P. Royo, *Coord. Chem. Rev.* **1999**, *193–5*, 447–498, and references cited therein.
- [11] A. Cano, T. Cuenca, P. Gomez-Sal, B. Royo, P. Royo, *Organometallics* **1994**, *13*, 1688–1694.
- [12] S. Ciruelos, T. Cuenca, R. Gomez, P. Gomez-Sal, A. Manzanero, P. Royo, *Organometallics* **1996**, *15*, 5577–5585.
- [13] S. Ciruelos, A. Sebastian, T. Cuenca, P. Gomez-Sal, A. Manzanero, P. Royo, *J. Organomet. Chem.* **2000**, *604*, 103–115; G. Jimenez, P. Royo, T. Cuenca, E. Herdtweck, *Organometallics* **2002**, *21*, 2189–2195.
- [14] A. B. Vazquez, P. Royo, E. Herdtweck, *J. Organomet. Chem.* **2003**, *683*, 155–164; M. C. Maestre, C. Paniagua, E. Herdtweck, M. E. G. Mosquera, G. Jimenez, T. Cuenca, *Organometallics* **2007**, *26*, 4243–4251.
- [15] J. Cano, M. Sudupe, P. Royo, *J. Organomet. Chem.* **2007**, *692*, 4448–4459.
- [16] M. C. Maestre, M. E. G. Mosquera, H. Jacobsen, G. Jimenez, T. Cuenca, *Organometallics* **2008**, *27*, 839–849.
- [17] O. Buitrago, C. R. de Arellano, G. Jimenez, T. Cuenca, *Organometallics* **2004**, *23*, 5873–5876; O. Buitrago, G. Jimenez, T. Cuenca, *J. Organomet. Chem.* **2003**, *683*, 70–76; S. Ciruelos, T. Cuenca, R. Gomez, P. Gomez-Sal, A. Manzanero, P. Royo, *Polyhedron* **1998**, *17*, 1055–1064.
- [18] S. Ciruelos, T. Cuenca, P. Gomezsal, A. Manzanero, P. Royo, *Organometallics* **1995**, *14*, 177–185, and references cited therein.
- [19] P. B. Hitchcock, M. F. Lappert, S. Tian, *Organometallics* **2000**, *19*, 3420–3428; E. Ihara, M. Nodono, K. Katsura, Y. Adachi, H. Yasuda, M. Yamagashira, H. Hashimoto, N. Kanehisa, Y. Kai, *Organometallics* **1998**, *17*, 3945–3956; J. A. Pool, E. Lobkovsky, P. J. Chirik, *J. Am. Chem. Soc.* **2003**, *125*, 2241–2251.
- [20] C. H. Winter, X. X. Zhou, D. A. Dobbs, M. J. Heeg, *Organometallics* **1991**, *10*, 210–214; J. M. Smith, D. P. White, N. J. Co-

- ville, *Polyhedron* **1996**, *15*, 4541–4554; G. J. Pindado, M. Thornton Pett, M. Bochmann, *J. Chem. Soc., Dalton Trans.* **1997**, 3115–3127; J. A. Pool, C. A. Bradley, P. J. Chirik, *Organometallics* **2002**, *21*, 1271–1277; C. A. Bradley, S. Flores-Torres, E. Lobkovsky, H. D. Abruna, P. J. Chirik, *Organometallics* **2004**, *23*, 5332–5346; C. A. Bradley, I. Keresztes, E. Lobkovsky, V. G. Young, P. J. Chirik, *J. Am. Chem. Soc.* **2004**, *126*, 16937–16950; L. C. St'astna, K. Auerova, J. Kvicala, J. Cermak, *J. Organomet. Chem.* **2007**, *692*, 1974–1982; M. Gomez, P. Gomez-Sal, J. M. Hernandez, *Eur. J. Inorg. Chem.* **2006**, 5106–5114; M. Gomez, P. Gomez-Sal, J. M. Hernandez, *J. Organomet. Chem.* **2007**, *692*, 2291–2298.
- [21] C. M. Fendrick, L. D. Schertz, V. W. Day, T. J. Marks, *Organometallics* **1988**, *7*, 1828–1838.
- [22] C. Elschenbroich, *Organometallics*, 3rd ed., Wiley-VCH, Weinheim, Germany, **2006**.
- [23] A. Davison, P. E. Rakita, *Inorg. Chem.* **1970**, *9*, 289–294; Y. A. Ustynyuk, A. A. Zenkin, N. D. Antonova, I. M. Pribytkova, A. V. Kisin, *J. Organomet. Chem.* **1972**, *42*, 47–63; P. Jutzi, *Chem. Rev.* **1986**, *86*, 983–996.
- [24] C. P. Morley, P. Jutzi, C. Kruger, J. M. Wallis, *Organometallics* **1987**, *6*, 1084–1090; J. R. Stricklet, J. M. Power, U.S. Patent 5,359,105, Albermarle Corporation, **1994**; J. M. Pietryga, J. N. Jones, L. A. Mullins, R. J. Wiacek, A. H. Cowley, *Chem. Commun.* **2003**, 2510–2510, and references cited therein; R. J. Wiacek, C. L. B. Macdonald, J. N. Jones, J. M. Pietryga, A. H. Cowley, *Chem. Commun.* **2003**, 430–431, and references cited therein.
- [25] H. R. H. Damrau, A. Geyer, M. H. Prosenc, A. Weeber, F. Schaper, H. H. Brintzinger, *J. Organomet. Chem.* **1998**, *553*, 331–343; A. W. Duff, P. B. Hitchcock, M. F. Lappert, R. G. Taylor, J. A. Segal, *J. Organomet. Chem.* **1985**, *293*, 271–283.
- [26] H. Tsuji, A. Fukazawa, S. Yamaguchi, A. Toshimitsu, K. Tamao, *Organometallics* **2004**, *23*, 3375–3377.
- [27] J. Cano, Doctoral Thesis, Universidad de Alcalá (Alcalá de Henares, Spain), **2002**.
- [28] G. Chahboun, C. E. Petrisor, E. Gomez-Bengoa, E. Royo, T. Cuenca, *Eur. J. Inorg. Chem.* **2009**, 1514–1520.
- [29] F. Edelmann, P. Behrens, S. Behrens, U. Behrens, *J. Organomet. Chem.* **1986**, *310*, 333–355.
- [30] D. W. Carpenetti, L. Kloppenburg, J. T. Kupec, J. L. Petersen, *Organometallics* **1996**, *15*, 1572–1581; L. F. Braun, T. Dreier, M. Christy, J. L. Petersen, *Inorg. Chem.* **2004**, *43*, 3976–3987.

Received: April 9, 2010

Published Online: June 30, 2010